THE PETROLOGY OF SOME YOUNG VOLCANIC ROCKS FROM LOMBOK AND SUMBAWA, LESSER SUNDA ISLANDS

by

J.D. Foden, B.Sc. (ANU), B.Sc. Hons. (TAS.)

submitted in partial fulfilment of the
requirements for the degree of
Doctor of Philosophy

UNIVERSITY OF TASMANIA
HOBART

October 1979.

This thesis contains no material which has been accepted for the award of any other degree or diploma in any university, and to the best of my knowledge and belief, contains no copy or paraphrase of material previously published or written by another person, except when due reference is made in the text of the thesis.

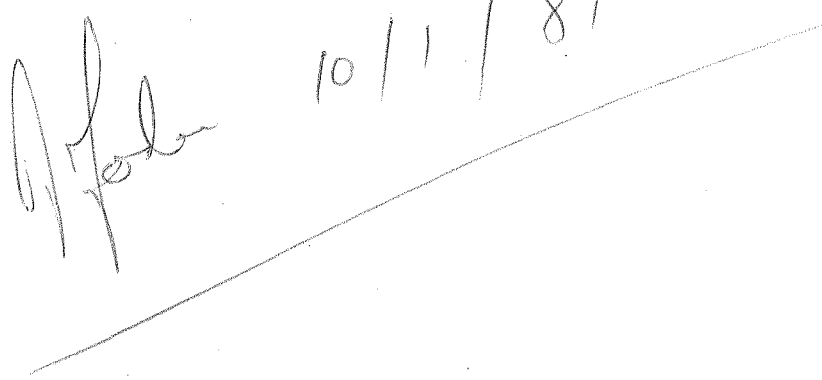

TABLE OF CONTENTS

Thesis Summary

Five volcanoes have been studied from the eastern Sunda arc, Indonesia: Rindjani on Lombok island and G. Sangenges, Tambora, Soromundi and Sangeang Api on Sumbawa island. Rindjani, Tambora and Sangeang Api are all active. G. Sangenges and Soromundi became inactive in the Quaternary. These volcanoes all occur 165-190 km above the active, north dipping Benioff Zone.

With respect to other parts of the Sunda arc, the Bali-Lombok-Sumbawa sector is unique in being flanked both to the north and south by oceanic crust. It is also part of the young (post Miocene) eastern Sunda arc, which is a much more recent feature than the western Sunda arc. These factors suggest that the lavas of these volcanoes have had minimal opportunity for contamination by differentiated crustal material.

The volcanoes of this sector of the arc have erupted a diverse range of lavas. They range from the ankaramite-high-Al basalt-andesite-dacite suite of Rindjani, through the moderately potassic *ne*-trachybasalt-trachyandesite suites from Sumbawan volcanoes, Tambora and Sangeang Api, to highly undersaturated, leucite-bearing types from G. Sangenges and Soromundi. The K_2O-content of these suites shows no correlation with the depth to the Benioff Zone.

Rindjani is a large, compound stratovolcano. Its lavas are similar to the calcalkaline suites erupted by many circum-Pacific volcanoes, though they show exceptional compositional diversity ranging from *ne*- to *Q*-normative.

The Sr-isotopic composition of all these lavas are the same (average 0.7039), which suggests a single source. Fractional crystallisation appears to play an important role in their differentiation, but cannot account for all aspects of geochemical differentiation. It seems likely that more than

one primary liquid must be involved. The andesites cannot be derived from the high-Al basalts by fractionation of the observed phenocryst assemblages, nor can the compositional range within the andesite group be modelled by mixtures of phenocrysts and groundmasses. The dacites may be liquids in equilibrium with the plagioclase-dominated phenocryst assemblages of the andesites and resemble their residual glasses.

For the andesites to be the products of fractional crystallisation of high-Al basalt parent magmas, constraints placed by variation in K_2O, Rb and Sr and K/Rb and Mg/Mg+Fe, suggest that such a connection may result from the crystallisation of an assemblage; amph+plag+mag$\pm$cpx$\pm$ol$\pm$apatite.

Phase relations in the system high-Al basalt + water suggest that optimum conditions under which the assemblage, amph+plag+mag may crystallise closest to the basalt liquidus, occur with 3% H_2O, between 7 and 10 kb and fO_2 between the NNO and HMN buffers. Under these conditions this assemblage may coexist up to about 1050-1060^{o}C, which is still 50^{o}C below the basalt liquidus. To yield andesitic differentiates, mantle derived parent basalts must cool markedly in the pressure-range 7-10 kb, a pressure corresponding to the probable depth to the Moho in this sector of the Sunda arc.

The elimination of amphibole from andesitic derivative magmas at low pressures and the rapid increase in the liquidus temperature of plagioclase, results in the replacement of this early amphibole-rich assemblage by a low-pressure plagioclase-rich assemblage. The dacites may represent the residual liquid formed as a result of this re-equilibration.

The suites from the other four volcanoes (G. Sangenges, Soromundi, Tambora and Sangeang Api) are almost all undersaturated. Like the Rindjani lavas, most of the *ne*-normative trachybasalts and trachyandesites from Tambora and Sangeang Api are plagiophyric, but are also distinguished by the presence of groundmass K-feldspar. Leucitites from Soromundi and

G. Sangenges are highly undersaturated and are plagioclase-poor or -free. Leucite occurs as phenocrysts and in the groundmasses.

Sangeang Api volcano has also erupted a suite of mafic to ultramafic nodules as xenoliths and blocks. These range from olivine-clinopyroxenites and magnetite clinopyroxenites to hornblende-anorthite gabbros.

Highly undersaturated, potassium-rich leucitic suites are unusual in island arcs and where they do occur are considered to be late-stage products and to be spatially most distant from the trench, above the deepest Benioff zone region. Yet in the Sunda arc, these rocks occur in a relatively young arc-sector, at a similar height above the Benioff zone to laterally adjacent calcalkaline suites.

The sequence from calcalkaline lavas, through *ne*-normative trachybasalts and trachyandesites to leucitites is marked by a progressive increase in K_2O, Rb, Sr, and LREE concentrations, increasing K_2O/Na_2O and decreasing K/Rb. The isotopic composition of Sr also becomes more radiogenic. By contrast, Zr, Ti, Nb and Hf and to a lesser extent P, show much less marked enrichment.

This between-suite variation must reflect variation in the composition of primary magmas, which in turn are considered to reflect a heterogeneous mantle-source which is variably enriched in K-type LIL incompatible elements.

Chapter 1

INTRODUCTION

1.1 Previous Work, Objectives and Scope

Although the nature and origin of the volcanic rocks of island arcs have long been the subject of debate by igneous petrologists, there is still no general agreement even about the full range of rock-types which may occur in island arcs, let alone their origin, or their relationship to tectonic setting.

Andesites have traditionally been believed to be the characteristic lava of island arcs, though as early as 1954, Rittman recognised that in the Sunda arc, coeval volcanoes erupted increasingly potassic lavas with increasing distance from the trench. Kuno (1966) recognised a similar pattern in Japan and also observed that volcanic rocks belonged to three distinct series: 1. the pigeonitic = tholeiitic series, 2. the hypersthenic = calcalkaline series and 3. the alkaline series, and that this sequence (1 to 2 t represented a progression towards the continent.

More recent studies, such as those of Jakeš and White (1969, 1972), Jakeš and Gill (1970) and Gill (1970) emphasised that basalts are also abundant, distinguished an arc tholeiite series and suggested that a spatial sequence of tholeiitic series-calcalkaline series-shoshonitic series, related to increasing distance from the trench and increasing height above the Benioff Zone, occurred also as a temporal sequence.

Most recently however, an even greater diversity of rock-types has been recognised, particularly very alkaline varieties (e.g. Johnson et al., 1976, Delong et al., 1975), as has the apparent transitional nature of the divisions between the previously defined suites. In addition several exceptions to the idealised temporal and spatial scheme described above, have been noted (e.g. Arculus and Johnson, 1978). Thus the generalized models for the evolution of arc-trench systems appear now to be too simplistic to account for the magmatic history of many individual arcs.

Thus in the past two decades, with the gathering of increasing amounts of new data, it has been recognised that the arc environment contains a diversity of volcanic rock-types as great or greater than that in other tectonic environments, rather than being monotonously andesitic.

The genesis of island arc magmas is the other major problem which has received considerable attention in the past few decades. In particular attempts have been made to account for the origin of andesites and for the origin of the compositional diversity of arc magmatism.

Although Bowen (1928) and Kuno (1968) regarded andesites as fractional crystallisation products of basaltic parents, more recently, particularly with the advent of plate tectonic theory and the recognition that island arcs may be underthrust by oceanic lithosphere (e.g. Isacks et al., 1968) many other theories have been proposed. A summary of these is presented by Ringwood (1974). Arguments about the origin of andesite variously suggest that these rocks are: 1. primary magmas, or 2. fractional crystallisation products of basalts, or 3. contaminated basalt, or 4. some combination of two or more of these factors.

The first of these suggestions includes two hypotheses: 1. that the andesites are primary melts of hydrous peridotite (e.g. Mysen and Kushiro and Nicholls and Ringwood, 1974), or that 2. andesites are primary melts derived by fusion of the upper portion of the subducted oceanic plate, either in the eclogite - (e.g. Green and Ringwood, 1968) or amphibolite-facies (e.g. Holloway and Burnham,, 1972). Fractional crystallisation mechanisms variously emphasise the roles of olivine-, amphibole- or magnetite-fractionation in the derivation of more silica-enriched liquids from basaltic parents. More complex models suggest that the liquids may have components derived from more than one source, subsequently also modified by fractional crystallisation.

In this thesis I seek to contribute to these debates in two ways:

1. By presenting detailed, new information on rocks from five active, or recently active volcanoes from a previously little-studied sector of the Sunda arc, a sector whose volcanoes have erupted a wide range of rock-types including unusual, highly alkaline varieties.
2. And to use these data, together with the results of some experimental work, to discuss arc magmatism and petrogenesis.

1.2 The Rationale Behind the Choice of Project and Locality

The islands of Lombok and Sumbawa in the central part of the Sunda arc were chosen as the location for this study for a number of reasons:

1. The Sunda arc is one of the largest arc systems on the earth's surface, one of the classical localities, as well as being easily accessible from Australia.
2. The segment of the arc chosen for study is tectonically and geologically reasonably simple (see chapter 2) compared to the arc sectors to the east and west and is a young feature uncomplicated by ancient basement.
3. This sector of the Sunda arc has not been the subject of any recent petrological research and as such the project is complementary to the work done by Whitford (1976) in the western part of the arc.
4. Although the young igneous rocks of this sector of the arc had received no recent attention, a few early Dutch reports, together with those invaluable primary sources; Part 1 of The Catalogue of Active Volcanoes of the World (Neumann van Padang, 1951) and The Geology of Indonesia (van Bemmelen, 1949), provided enough background information to indicate that some Sumbawan volcanoes had erupted lavas of unusual composition, including very alkaline leucite-bearing varieties. Furthermore reports that the eruption of the possibly alkaline volcano, Tambora, in 1815, was amongst the most violent and destructive in human history (e.g. Petroeschevsky, 1949) also suggested that an unusual and potentially interesting situation existed in Sumbawa.

By contrast, Rindjani, the large stratovolcano on the adjacent island of Lombok, proved to have erupted a "normal" series of calcalkaline lavas. Therefore, because volcanoes of this sector of the Sunda arc appeared to have erupted volcanic rocks of a very large compositional range, including very alkaline varieties, it seemed that this might be a good place to investigate the origin of the compositional diversity of island arc suites, particularly as in this arc sector this variation occurs in adjacent, active volcanoes at similar height above an active Benioff Zone.

5. Though no detailed geological mapping of either Lombok or Sumbawa has been carried out, reconnaissance surveys of Matrais et al., (1972) on Lombok and Sudrajat (1975) on Sumbawa, provided maps and gave some geological control to the sampling program.

In short this thesis is a detailed study of the petrology and geochemistry of lavas and some coarse-grained xenoliths, erupted by five Quaternary to Recent volcanoes from the Lombok-Sumbawa sector of the Sunda arc.

1.3 Field Work and Method of Study

This project is mainly laboratory-orientated and the principal objective of the field-work was to collect a representative suite of fresh volcanic rocks, and where they occurred, intrusive xenoliths, from each of the five young volcanoes being studied.

Most of the work was carried out at the Geology Department at the University of Tasmania, between March 1975 and March 1978. The study is mainly based on the results of: 1. microscopic examination of thin sections, 2. whole-rock, major- and trace-element analysis largely performed using XRF techniques, 3. microprobe analysis of mineral phases, 4. near-liquidus, high pressure experiments on a natural high-Al basalt-water system,

5. Sr-isotope determinations[1], and 6. some rare earth element (REE determinations).[2]

Most of the field work for this project was carried out in the first half of 1976 by myself and Dr. R. Varne, with some assistance from Ir. Soetoto from the University of Gadja Marda in Jogyakarta. Dr. Varne also made an earlier trip to Lombok in 1975.

In the field, attempts were made to sample fully the entire compositional range of lavas represented in each volcano. No mapping was undertaken. On Sumbawa, all the volcanoes occurred some distance from the only road and most field-work entailed the use of local boats and prolonged trips on foot. For instance, the scaling of Tambora volcano entailed a boat trip of several hours duration to reach a village at its foot, followed by an expedition lasting about 10 days from this village to the summit and return.

A more extensive network of roads exists on Lombok island, though again, the steep terrain and jungle-clad lower slopes of Rindjani volcano restricted access except by foot.

1.4 Acknowledgements

The number of people and organisations who have substantially contributed to bringing this thesis to fruition is large and though the following list attempts to cite and thank all these, I also extend a general acknowledgement to any others I may have overlooked.

First I would like to thank my supervisor, Dr. R. Varne of the Geology Department, University of Tasmania, who conceived the project and through whose efforts it was successfully started. He also contributed immeasurably to the development of the ideas and the assessment of the data presented in this thesis, both through his critical discussion through

Notes: 1. Sr-isotope determinations were performed by Dr. D.J. Whitford at the Department of Terrestrial Magnetism, Carnegie Institution of Washington. 2. REE determinations were made by Dr. S.R. Taylor and staff at the Research School of Earth Sciences, ANU, Canberra.

the course of the project and by his constructive comments on the draft manuscript during all stages of its development.

I would also like to thank the Indonesian Government for allowing us to do this work in its territory and for the assistance it provided in the field through the efforts of many of its employees and agencies. Of these I would like to single out the Indonesian Institute of Science (LIPI) who supported the project and organised the necessary formalities, including those associated with obtaining visas and the required Indonesian participation. The Geological Survey of Indonesia (GSI) in Bandung also provided valuable assistance particularly in the form of maps and aerial photographs. I also wish to thank the staff of the University of Gadja Marda in Jogyakarta, our counterpart institution in this project, and particularly Dr. Judy Bean for her help and Ir. Soetoto, who accompanied me to Sumbawa for two weeks. In Lombok and Sumbawa the assistance of the local government authorities is gratefully acknowledged, as is the hospitality and help rendered by the local villagers. P.T. Veneers is also thanked for its provision of transport and accommodation.

At the University of Tasmania I would like to thank the staff and graduate students in the Geology Department and in particular Mr. P. Robinson for his assistance in the XRF analysis work, Mr. B. Griffin for his assistance in the electron microprobe analysis work and with some computing and Mr. W. Doran for his preparation of many thin sections, polished sections and probe mounts. Professor D.H. Green is thanked for providing access to his experimental laboratory in Hobart, for his assistance in formulating the experimental program, for his useful discussion of the results and for reviewing the sections of the manuscript of this thesis which are related to the experimental work. Mr. W. Hibberson is also thanked for his assistance in making up and running the experimental charges.

Thanks also go to fellow graduate students at the University of Tasmania, in particular to Mr. D. Ellis, Mr. A.L. Jaques, Mr. G. Jenner, Dr. J.L. Walsh, Mr. A. Bush, Dr. C.J. Eastoe, Mr. R. Richardson and Mr. K. Spence, all of whom made useful individual contributions.

Dr. S.R. Taylor and his staff in the MS7 lab at R.S.E.S., ANU are thanked for REE analyses and Mr. N. Ware also at R.S.E.S. is thanked for allowing me access to the TPD probe. Dr. K.S.W. Campbell and the staff of the Geology Department at ANU are thanked for allowing me use of their department and in particular Dr. B. Chappell for his assistance and the use of his plotting equipment.

Dr. D.J. Whitford of the Carnegie Institution, Washington is thanked for doing Sr-isotope analyses and providing useful discussion and Drs. A. Ewart and A.S. Bagley of the University of Queensland are thanked for providing a copy of a least-squares mixing program. I would also like to thank my associates at the University of Adelaide for their indulgence and help during the final stages of preparation of this thesis. Mrs. Sue Brockhouse is thanked for her efficient and accurate typing of the thesis.

The major part of this work was completed while I was the recipient of a Commonwealth Postgraduate Research Grant, for which I am very grateful. The project was funded by research grants of the University of Tasmania, and the Australian Research Grants Committee.

1.5 Thesis Structure and Layout

The titles of each chapter are given in the table of contents. The thesis falls into two main sections; chapters 2 to 7 inclusive are mainly concerned with the presentation of the data, while chapters 8 to 12 are mainly concerned with the discussion of this data and the formulation of the conclusions. Chapter 13 briefly summarises the main conclusions.

Within the first section, chapter 2 provides the geological and tectonic background to the Indonesian region in general and to the Lombok-Sumbawa sector of the Sunda arc in particular. Following this, chapters 3, 4, 5 and 6 are largely a descriptive presentation of the petrological data for each volcano, including general petrography, mineralogy, mineral chemistry and whole-rock major- and trace-element geochemistry. The main details of the information contained in these four chapters are summarised in chapter 7.

FIG. 2·1

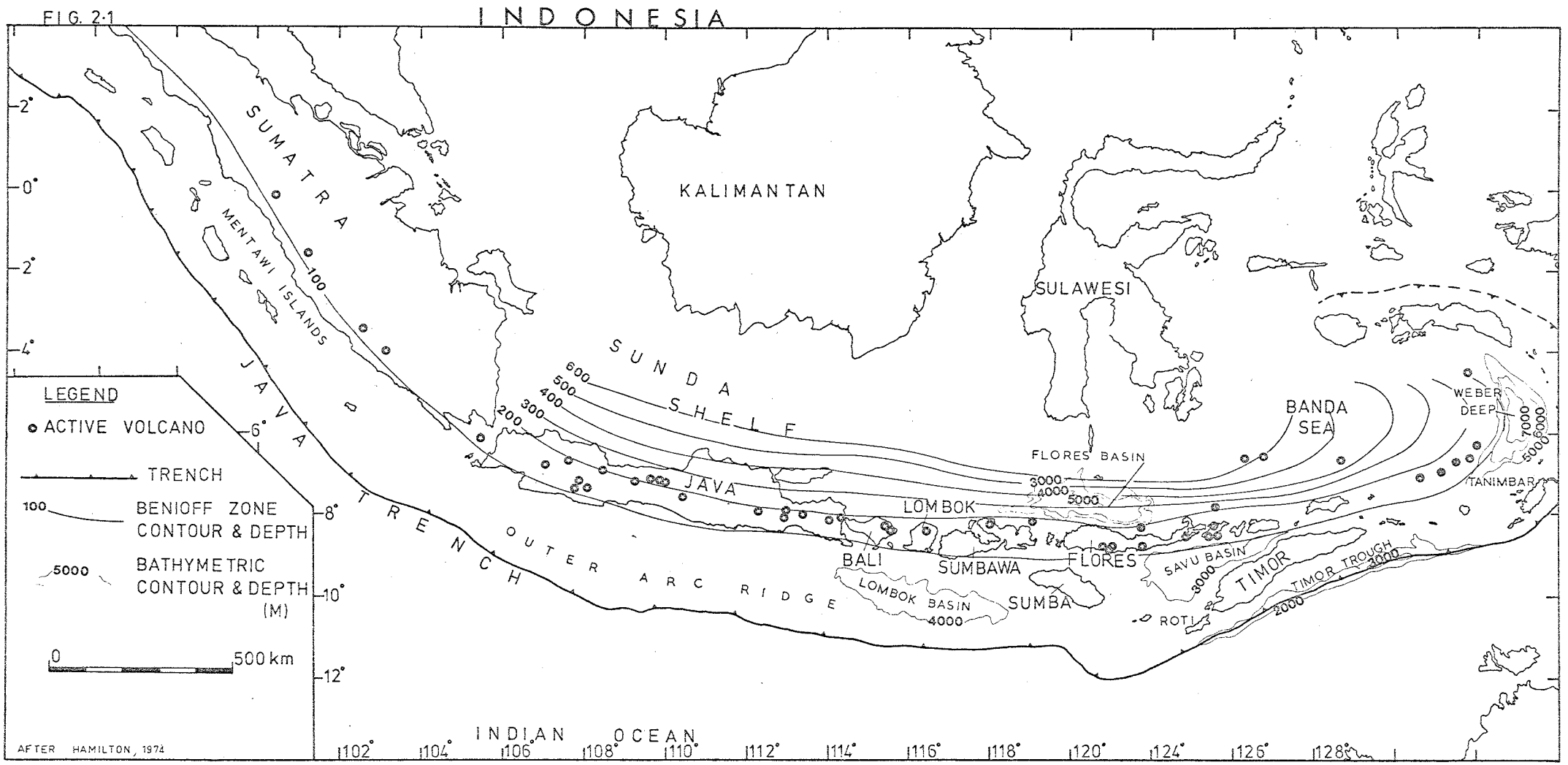
INDONESIA
KALIMANTAN
SUMATRA
MENTAWI ISLANDS
SULAWESI
SUNDA SHELF
JAVA TRENCH
OUTER ARC RIDGE
FLORES BASIN
BANDA SEA
WEBER DEEP
TANIMBAR
JAVA
LOMBOK
BALI
SUMBAWA
FLORES
SAVU BASIN
TIMOR
TIMOR TROUGH
LOMBOK BASIN
SUMBA
ROTI
INDIAN OCEAN
LEGEND
ACTIVE VOLCANO
TRENCH
BENIOFF ZONE CONTOUR & DEPTH
BATHYMETRIC CONTOUR & DEPTH (M)
0
500 km
AFTER HAMILTON, 1974
2°
0°
2°
4°
6°
8°
10°
12°
102°
104°
106°
108°
110°
112°
114°
116°
118°
120°
124°
126°
128°

Chapter 2

REGIONAL GEOLOGY AND TECTONIC SETTING OF THE SUNDA ARC.

2.1 *Introduction*

The main theme of this thesis relates to the petrology, geochemistry and petrogenesis of the volcanic rocks from the islands of Lombok and Sumbawa in the western end of the eastern Sunda Arc. Such being the case, the main emphasis within the thesis is on information and data yielded by the rocks themselves. However, any discussion of the petrology of these active, or recently inactivated centres which fails to take account of their regional, geological and tectonic settings will have neglected factors possibly highly significant to their genesis. Conversely, conclusions reached on petrological grounds may provide significant insight into regional geological or tectonic factors. This chapter therefore provides a summary of the regional geological and tectonic features of the area. However as the main emphasis on the thesis is in another direction this summary is brief and further detail can be obtained from the references cited.

2.2 *The Regional Tectonic Setting of the Indonesian Region.*

The Indonesian region, of which, the Sunda-Banda arc systems represent the southern margin, is tectonically, extremely complex. The Cenozoic history of the region reflects the interaction of three plates; 1. the Eurasian plate to the west; 2. the Pacific plate to the north-east; and 3. the Indian-Australian plate to the south. The Indian-Australian plate has a relative northward movement while the Pacific plate has a westward motion (Hamilton, 1977). Van Bemmelen (1949) provides a wealth of information on the geology of the region, while Hamilton's (1978) tectonic map summarises the main tectonic elements. Papers of Hamilton (1979, 1977 and 1973) and those of Katili (1975, 1973) and Katili and Soetadi (1971), provide discussion of the region in the light of plate tectonic theory.

2.3 *Regional Setting of the Volcanic Centres of Lombok and Sumbawa.*

The major tectonic features of the Sunda arc have been summarised by Foden and Varne (1979). The following summary is largely based on their assessment of the features of this arc. The Sunda arc of Indonesia, together with its easterly continuation, the Banda arc, is a spectacular feature, over 6000km in length. Over seventy volcanic centres occur along its length, which extends from the north-western tip of Sumatra to the Moluccas (fig. 2.1).

In plate tectonic theory the Sunda arc is a subduction system, marking the zone where the Indian-Australian plate is sliding obliquely beneath the Asian plate. From cursory observation the whole arc appears as a continuous, coherent, single tectonic feature, the volcanism, like the seismicity representing by-products of the subduction process. However, more detailed examination of the evidence reveals this arc system to be very complex. For instance there are marked differences in the histories of its western and eastern ends. In particular, the western end, represented by the islands of Java and Sumatra, is much older than the eastern end. Also the far eastern end of the arc, due to its close proximity to the Australian continental plate, is experiencing quite different influences at the present time to those in the central and western portions of the arc.

1. The Outer-Arc and Trench System

The Sunda arc is a double arc-trench system. The inner volcanic arc lies to the north, the outer non-volcanic arc to the south. Between the arcs lies the outer arc basin, a chain of elongate deeply filled troughs. South of the outer arc lies the Java Trench. This is a continuous, well defined feature as far east as Sumba. Along this segment it is up to 7km deep. South-east of Sumba (south of the eastern end of Sumbawa) the situation is less clear cut.

There is some suggestion that the trench is continued eastwards as the Timor Trough-Aru Basin-Ceram Trough system. Such a continuation involves a marked south-easterly offset in the trench system to the south of Sumba island. The Timor Trough system is of markedly different character to the Java trench. It is shallow, extending only to 3km and is bounded to the south by the Australian continent (Hamilton, 1974). The Savu Basin to the north of Roti and western Timor is in fact deeper than the Timor Trough (Hamilton, 1977) and may represent an inter-arc basin, forming a continuation with the Weber Basin, to the north-east, between the inner- and outer-Banda arcs. This feature was interpreted as the easterly extension of the Java Trench (Fitch, 1970), but the inter-arc interpretation has gained more recent support (Fitch, 1972; Fitch and Hamilton, 1974).

To the west of Sumba, the outer (non-volcanic) arc ridge is mainly submarine, but south of Sumatra is partly emergent to form outer arc islands such as Mentawi. South of Java the crest of the ridge is wholly submarine but relatively shallow in places. Eastwards, to the south of Lombok and Sumbawa, the crest of the ridge is deeply submerged, and does not continue smoothly into the Sumba-Roti-Timor outer arc sector. Rather it is displaced north and almost appears to coelesce with the inner arc in the vicinity of east Sumbawa-west Flores.

These discontinuities in the outer arc and trench, near Sumba, to the south of Sumbawa coincide with a hiatus in the regional linear belt of negative gravity anomalies associated with the Java trench. There is also a marked abse of shallow and intermediate earthquake activity south of Lombok (Hedervari, 1978; Ritsema, 1954). Audley-Charles (1975) considered this to be evidence of a major break between eastern and western sectors of the Sunda arc system. This hypothetical feature has been termed the Sumba Fracture (Audley-Charles, 1975; Katili, 1973) and interpreted as a substantial transcurrent or transform fault.

Hamilton (1979) also noted that the regularity of the Sunda arc system, with its subparallel elements of inner volcanic arc, outer arc basin, outer arc (melange) ridge and trench, is broken in this sector where the broad Sumba-Roti-Timor ridge trends southeastward across the strike belt elsewhere occupied by the outer arc basin. At the same time there is some evidence that Sumba island is geologically unlike Timor and may be allochthonous (Hamilton, 1977).

2. The Volcanic Arc.

In contrast to the outer arc, the inner arc is mainly subaerial and is marked by a line of active volcanoes that overlies 125-200 km depths to Benioff zone. The compositional relation between volcanism and seismicity is considered in chapter 12.

The islands of the volcanic inner arc diminish in size and decrease in age going eastwards. Sumatra is composed of well established continental crust, in part of Mesozoic and Palaeozoic age (Hamilton, 1978; Katili, 1974; Van Bemmelen, 1949). Java is smaller and although it is composed almost entirely of continental crust, this crust is mainly Cainozoic in age, and relatively thin and mafic (Van Bemmelen, 1949).

By contrast, the oldest exposed rocks in the arc to the east of Java are Miocene. Also, on these islands, a much larger proportion of aerially exposed sequences are of Quaternary - Recent age, composed largely of the products of presently active or recently inactivated volcanoes (Hamilton, 1978) The active volcanoes on Bali, Lombok and Sumbawa occur in the northern parts of the islands (fig. 2.1). Older rocks, including some as old as early Miocene, form the southern parts of the islands. On Bali and Lombok these are separated from the active volcanic zone by lowland plains underlain by Quaternary sediments and tuffs (Van Bemmelen, 1949; Matrais et al., 1972; Sudrajat, 1975). In south Bali these older rocks are mainly limestones, but in Lombok are associated with andesitic and dacitic volcanic rocks (Matrais et al., 1972) that also probably form the present sub-volcanic basement.

Similar Miocene sequences are also widespread in Sumbawa and west Flores (Van Bemmelen, 1949; Cardwell and Isacks, 1978) and may occur in Bali. Van Bemmelen suggested that Miocene deposits may correlate with the Southern Mountain sequences of east Java. He speculated that "breaking down of the Southern Mountains continues eastwards in Bali and Lombok, where the parts are separated by sea straits instead of alluvial plains".

Physiographic contrasts between Java and the islands of the central and eastern part of the Sunda arc (Sumbawa for instance) emphasise the more primitive character of the latter group. In Sumbawa the complexly indented, lobate coastline is a product of coalescence of young volcanoes which must have originated as submarine cones, growing to subaerial individuals separated by sea straits, later to be filled by redeposition of older volcanic material as well as new eruptions. Sangeang Api, a substantial, active offshore volcano near the northeast coast of Sumbawa (fig.4.1) will in all probability be similarly incorporated into the Sumbawa mainland in a geologically short time.

On the other hand the post-Quaternary volcanoes of Java, particularly those of central and western Java, are fed through older continental crust and in all probability were subaerial during most of their evolution. In east Java the Southern Mountains are flanked to the north by the great Quaternary volcanoes of the Solo zone. These are separated by an axial depression filled with Quaternary sediments and tuffs to form intermontane plains (the Blitar sub-zone), in a zonal distribution reminiscent of that in Bali and Lombok (Fig. 3.1).

In Sumbawa, as in Bali and Lombok, the active volcanoes in the north of the island seem to form a continuation along strike of the Solo zone. On Flores this line of active volcanoes continues in the northern part of the island, but there are also volcanoes in south Flores, leading Audley-Charles (1975) to postulate some southward displacement of the volcanic zone of the

inner arc along a continuation of a possible dextral transcurrent fault in southwest Sulawesi that is roughly parallel to his proposed Sumba fracture. However, there is little evidence that such a fault has been recently active (Cardwell and Isacks, 1978).

3. Crustal Thickness and Structure.

The relationship between seismicity and subduction have been the subject of numerous studies in this region (e.g. Fitch and Molnar, 1970; Fitch, 1970; Cardwell and Isacks, 1978), as has the relationship between the depth of seismicity and the composition of erupted volcanics (e.g. Hatherton and Dickinson, 1969; Whitford and Nicholls, 1976; Hutchison, 1975; Hutchison, 1976). These relationships, discussed with respect to the lavas of Quaternary to Recent volcanoes from the Lombok and Sumbawa sector of the Sunda arc, are considered in chapter 12.

Crustal velocity structure and thickness have also been investigated by seismic reflection and refraction studies (e.g. Curray et al., 1977; Hamilton, 1977).

The maximum depth of seismic activity increases from 200 km beneath Sumatra to about 600 km north of Lesser Sunda Islands to the east (Fitch, 1970). Crustal thicknesses also diminish markedly towards the east in the Javanese sector of the arc. The Sunda Shelf has continental thickness and velocity in the vicinity of west Java, while in the region of east Java-Bali it thins markedly and has a seismic velocity structure transitional between typical oceanic and continental profiles (Curray et al., 1977, Ben-Avraham and Emery, 1973).

East of Java, the Bali-Lombok-Sumbawa sector of the volcanic arc is flanked north and south by oceanic crust (Curray et al., 1977, Ben-Avraham and Emery, 1973) and lies at the "transitional edge of cratonisation" of the Sunda Shelf (Curray et al., 1977).

In the Bali-Lombok-Sumbawa-Flores sector of the arc, the Benioff seismic zone dips at a shallow angle from the axis of the trench to the axis of present volcanism. The active volcanoes are approximately 300 km from the trench, yet the seismic zone is less than 200 km below these. The seismic zone then plunges to 600 km depth only a further 200 kms from the trench (Cardwell and Isacks, 1978).

South of the Bali-Lombok-Sumbawa sector of the arc, linear magnetic anomalies of the Indian Ocean crust near the Java trench trend generally east-west, tangential to the curve of the arc (Ben-Avraham and Emery, 1973). DSDP 261 south of Sumbawa "bottomed" in late Jurassic sediments overlying basalt. Farther to the southeast the linear magnetic anomalies may strike ENE with the oceanic crust becoming older towards the Australian margin (Larson, 1975). The velocity structure of the oceanic crust south of the Java trench seems fairly typical of oceanic crust elsewhere in the Indian and Pacific Oceans and is generally about 5-7 km in thickness, although locally it is thickened to about 8 km, a feature that may be in some way related to its great age (Curray et al., 1977).

Beneath the Java trench the oceanic crust is about 11-13 km thick, significantly more than is usual. The mantle is also depressed beneath the trench south of Bali and Lombok. The Moho is about 24 km deep and may dip north. Seismic reflection records indicate that a strongly reflecting surface, presumably the top of the oceanic crust, dips north at only 7^{o} from the trench to a depth of 15 km beneath the outer arc ridge which appears to be a wedge of imbricated low-velocity material (Hamilton, 1977).

Refraction studies show that the crust beneath the outer arc basin in this arc sector between outer arc ridge and inner volcanic arc is apparently oceanic in character although depth to the Moho is greater than is normal for oceanic crust, about 18-25 km. Most of the additional crustal thickness is in the oceanic layer where thicknesses exceed 14 km. The Moho was detected at about 20 km beneath the southern slope of the Bali-Lombok sector of the

arc (Curray et al., 1977). As shown earlier, subvolcanic basement of the inner volcanic arc is probably Miocene in age. If the crust between the outer arc ridge and the inner volcanic arc is trapped oceanic crust of Cretaceous or Jurassic age (Curray et al., 1977), there is no obvious explanation of its abnormal thickness, nor indication of the nature of the transition to the younger rocks of the inner arc. There is also no indication of the nature of an apparently abrupt upward jump in the oceanic layer and Moho beneath or immediately north of the outer arc ridge.

Oceanic crust has also been detected north of Sumbawa but mantle arrivals were not detected, suggesting Moho depths of at least 15 km (Curray et al., 1977, Ben-Avraham and Emery, 1973).

East of Sumbawa the Flores Sea north of the inner volcanic arc is floored by oceanic crust, but to the south of the arc the Timor Sea is underlain by continental crust (Curray et al., 1977, Hamilton, 1977). In the sector of the arc east from Sumbawa to Alor island, north of Timor, relatively deep water troughs occur on the north side of the volcanic arc. Hamilton (1977) has suggested that due to the collision of this part of the arc with the Australian continental plate, northward subduction has ceased and southward subduction is being initiated in this region. However the earthquake activity pattern has as yet to demonstrate this.

West of Bali the oceanic layer is absent beneath the Sunda shelf north of east Java, where crustal thicknesses and velocities seem intermediate in character between oceanic and continental (Ben-Avraham and Emery, 1973), but here the crust south of the arc is oceanic (Curray et al., 1977).

2.4 Conclusions.

From the seismic reflection and refraction surveys it therefore appears that the Bali-Lombok-Sumbawa sector of the Sunda arc may be closely flanked both to the north and south by oceanic crust, perhaps the only sector of the arc where this is the case. South of the arc the oceanic crust is probably

of early Cretaceous or late Jurassic age, considerably older than any rocks known on the Lesser Sunda Islands.

The complexity of the Sunda arc and the manner in which it appears to diminish eastwards both in size and age have stimulated many tectonic reconstructions to explain its evolution (e.g. Katili, 1973; Hamilton, 1979; Van Bemmelen, 1949; Katili, 1975; Hutchison, 1973). The Bali-Lombok-Sumbawa sector of the arc may have reached its present position by migrating southward and eastwards from Sulawesi, either with rifting and opening of the Banda Sea behind it, or by jumping into its present position, breaking through and trapping older oceanic crust within and behind it. It may have developed as a link between two previously separate orogenic systems. The complexities of tectonic interpretation and reconstruction aside, it is noted that there is general agreement that the Bali-Lombok-Sumbawa sector of the Sunda arc has developed only since mid-Tertiary, possibly Miocene time, and that at present the oceanic crust of the Indian plate may be underthrusting this arc sector in a general northerly direction (Foden and Varne, 1979; Cardwell and Isacks, 1978; Le Pichon, 1968; Minster et al., 1974).

LOMBOK & EAST BALI

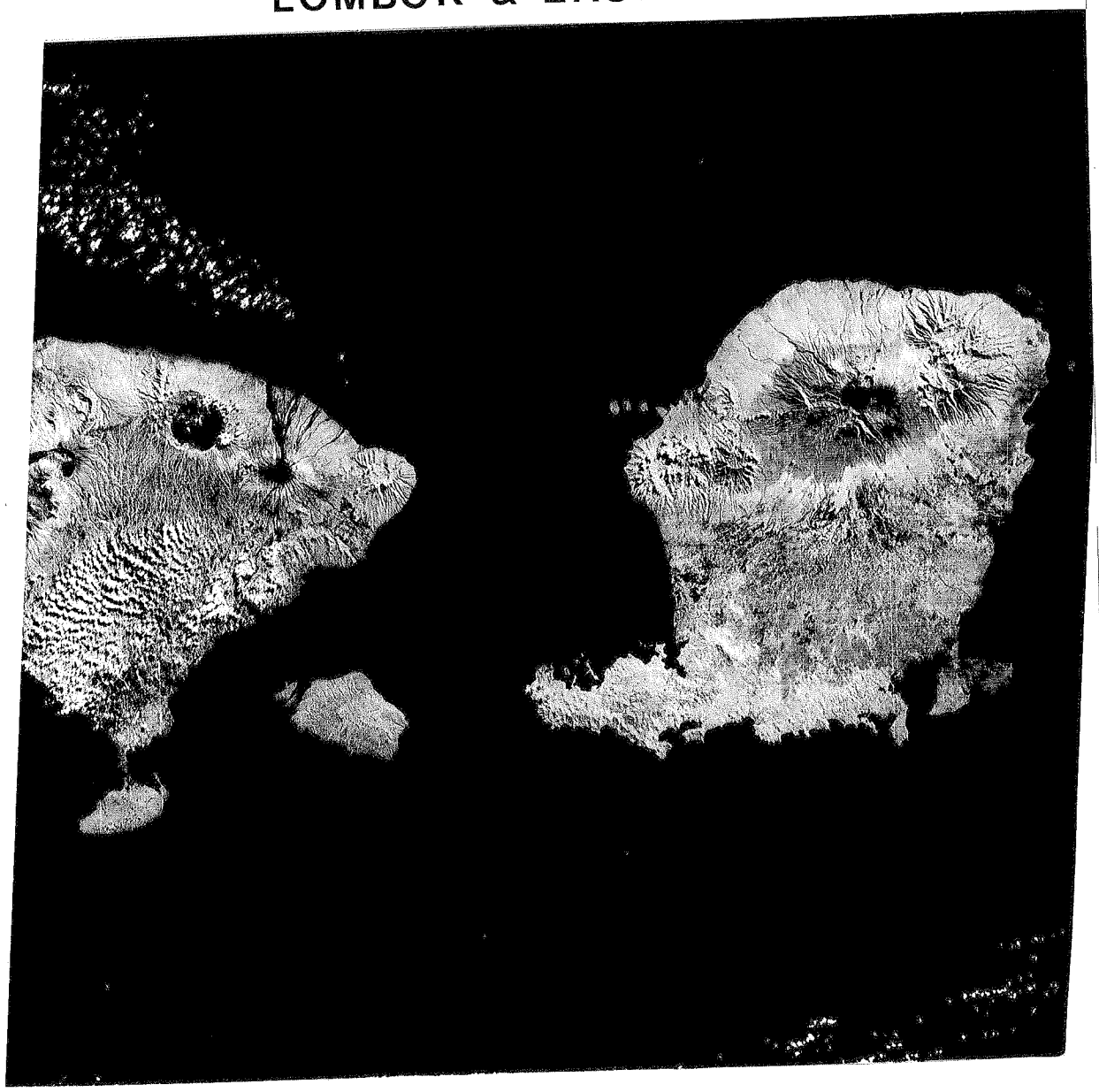

0 50 km

FIG. 3·1

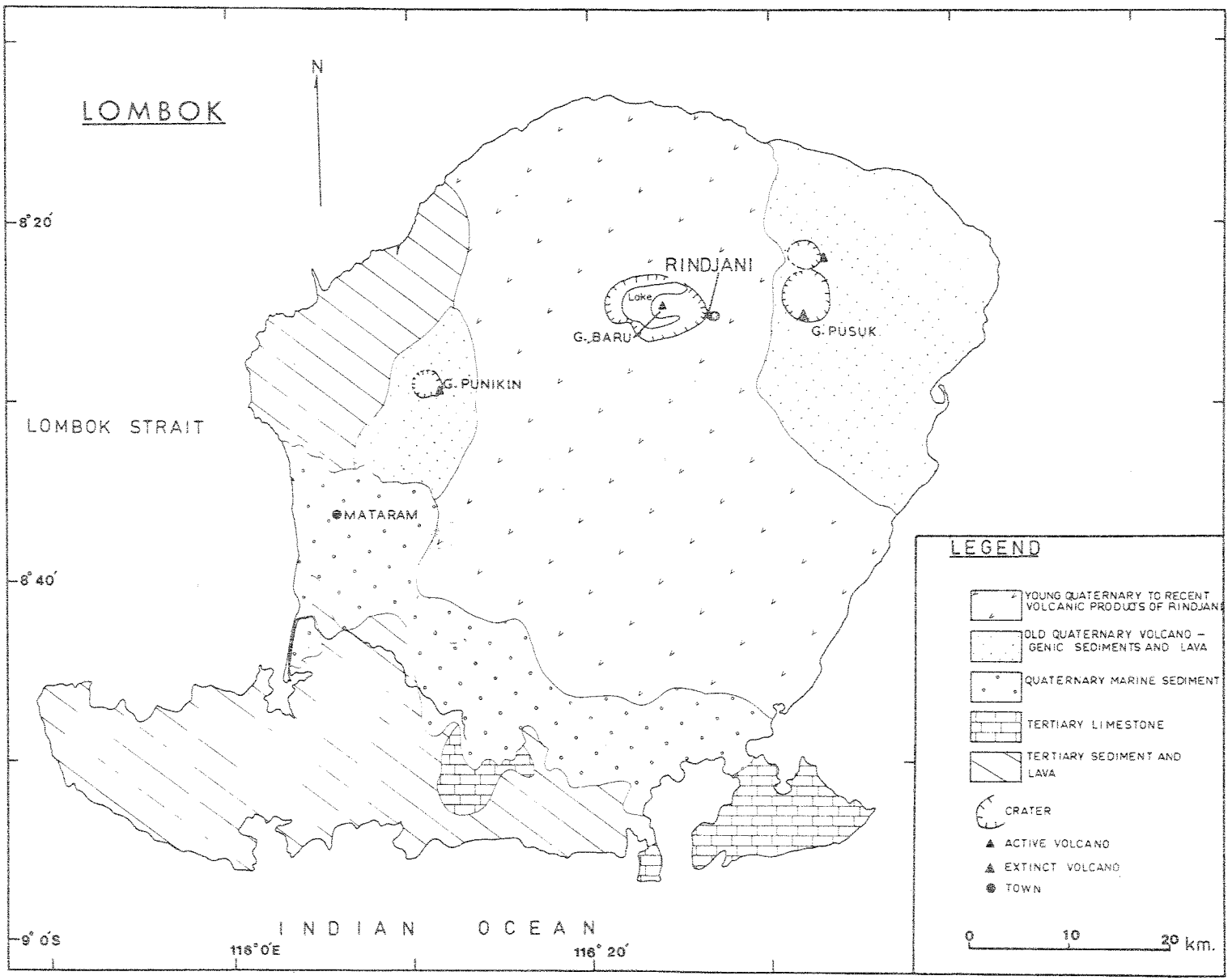
LOMBOK
N
8° 20′
8° 40′
9° 0′S
116° 0′E
116° 20′
RINDJANI
Lake
G. BARU
G. PUSUK
G. PUNIKIN
LOMBOK STRAIT
MATARAM
INDIAN OCEAN
LEGEND
YOUNG QUATERNARY TO RECENT VOLCANIC PRODUCTS OF RINDJANI
OLD QUATERNARY VOLCANO – GENIC SEDIMENTS AND LAVA
QUATERNARY MARINE SEDIMENT
TERTIARY LIMESTONE
TERTIARY SEDIMENT AND LAVA
CRATER
ACTIVE VOLCANO
EXTINCT VOLCANO
TOWN
0
10
20 km.

Chapter 3

PETROLOGY OF LAVAS FROM RINDJANI VOLCANO, LOMBOK ISLAND.

3.1 Introduction

Rindjani is a large, active, compound strato-volcano on the island of Lombok, in the western part of the east Sunda arc (figure 2.1). The volcano lies approximately 300 km north of the Java Trench and is situated about 170 km above the active north-dipping Benioff seismic zone (e.g. Hamilton, 1974; Hutchison, 1976) (figure 2.1). Summaries of the geology of Lombok are given by Matrais et al. (1972) and van Bemmelen (1949) (figure 3.1).

The oldest rocks outcropping on the island are exposed in its southern part and are Early Miocene andesitic and dacitic flows and breccias with associated volcanically-derived sediments. These Early Miocene deposits are overlain by Late Miocene limestones. More than three-fifths of the island is covered by Pleistocene to Recent products of Rindjani and its associated cones. These deposits range from basalts and andesites to dacites and also include blankets of pumice and tuff. This chapter presents the basic petrological data from these young lavas.

The lavas from Rindjani volcano are a petrologically diverse calcalkaline group ranging from ankaramites and high-Al "basalts" to andesites, high-K andesites and dacites. They show numerous petrographic, mineralogical and geochemical similarities to many members of this suite described from numerous circum-Pacific arcs (e.g. Ewart, 1976).

In this thesis the term "calcalkaline" is used to describe those suites from island- and continental marginal arcs which include aluminous basalts, andesites and in some cases dacites and rhyolites, which show little or no iron-enrichment and which have moderate alkali and in particular K_2O concentrations (basalts 0.6-2.0% K_2O, andesites 1.0-2.5% K_2O). Members of

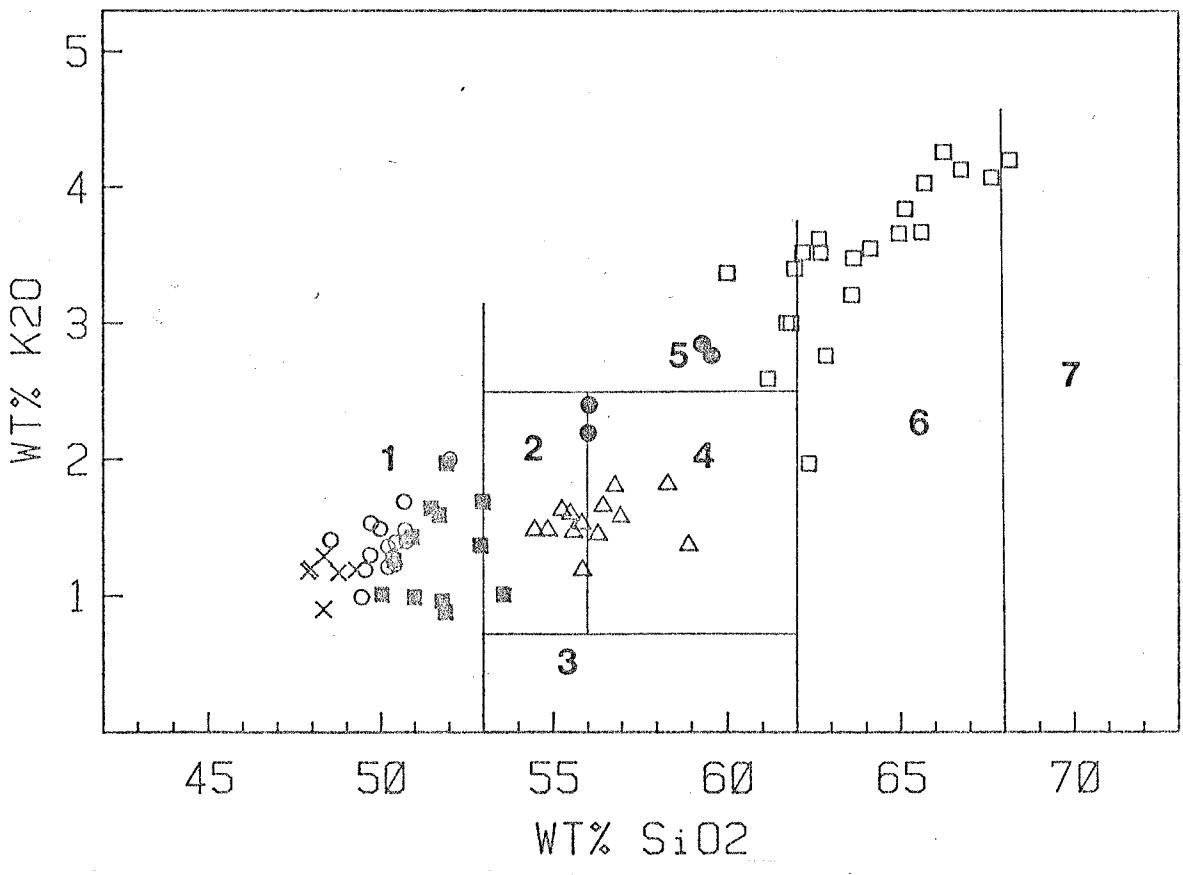

Figure 3.2

K_2O-SiO_2 variation of the Rindjani lavas. Individual symbols represent the following rock groups: crosses-ankaramites, open circles-ne-normative high-Al basalts, filled squares-ol-hy-normative high-Al basalts, triangles-andesites, filled circles-high-K, high-Sr andesites, open squares-dicites and high-K andesites. The numbered fields are those of Taylor (1969). 1. high-Al basalt 2. low-silica andesite 3. low-K andesite 4. andesite 5. high-K andesite 6. dacite 7. rhyolite.

this suite are equivalent to those of Kuno's (1959) Japanese "hypersthenic series" and in fact also conform to Peacock's (1931) original definition based on his alkali-lime index. In this thesis the term "calcalkaline" also connotes a degree of alkalinity between that of the arc tholeiite series (e.g. Jakeš and Gill, 1970; Jakeš and White, 1972, 1971) which was not recognised in this segment of the Sunda arc and the much more alkaline, undersaturated, K_2O-enriched suites from a number of the Sumbawan centres described in chapters 4, 5 and 6 of this thesis.

Members of the calcalkaline suite are commonly named arbitrarily according to their position on the K_2O-SiO_2 variation diagram (e.g. Taylor, 1969; also see figure 3.2). Although this scheme adequately characterises oversaturated lavas of the andesite-dacite- rhyolite group, its labelling of lavas with <53% SiO_2 as high-Al basalts is inadequate particularly because these "basalts" would not be termed as such using other widely accepted criteria (e.g. Coombs and Wilkinson, 1969). For instance, many Rindjani lavas with <53% SiO_2 are much less magnesian than basaltic rocks from other petrographic provinces, have lower Mg/Mg+ ΣFe values and have higher normative Ab/Ab+An+Or.

3.2 Petrographic Features of the Rindjani lavas

1. Ankaramites

This group of lavas appear to have been erupted relatively early in the history of the Rindjani complex and occur in west Lombok, possibly the products of the Punikin centre. They are the most mafic of the lavas of the Rindjani suite (MgO 8-14%) and are relatively Al_2O_3-poor (<16%). They are all *ne*-normative.

Modal analyses of two examples of this group (LB8 and LB11) are given in table 3.1. The ankaramites range from very phenocryst-rich porphyritic varieties (such as LB8, tables 3.1, 3.12) to relatively phenocryst-poor types (such as LB11, table 3.12), though the phenocryst-rich examples appear more common. Typically they are composed of phenocrysts of clinopyroxene, olivine,

Table 3.1

Rindjani Lavas: Modal Composition

Sample No.	Cpx	Opx	Ol	Amph	Biot	Ti-Mag	Plag	Apatite	G-Mass	Glass
LB8	36.5		12			0.2	4.5		47	
41632	1		5.7			0.3	11		82	
41621			4.5				3.5		92	
41637	8.5		3.5			3	31		54	
41647	8	4				4	35.5	tr		48.5
41622	8	2	.1[1]			2	26	.1	62	
41644	2		2.3			1.7	39	tr		55
41636	6.3	3.2				1.5	56		33	
41641	tr	tr		2	tr		9			89

[1] reacted olivine relicts

Abbreviations: Cpx-clinopyroxene, Opx-orthopyroxene, Ol-olivine, Amph-amphibole, Biot-biotite, Ti-Mag-titanmagnatite, Plag-plagioclase, G-Mass-groundmass.

Rock types: LB8 - ankaramite, 41632, 41621 - ne-normative, alkali olivine basalt, 41637 - basaltic andesite, 41647, 41622, 41644, 41636 - andesites, 41641 - dacite.

plagioclase and magnetite, set in very fine-grained groundmasses of clinopyroxene, olivine, plagioclase, magnetite and possibly nepheline and/or sanidine.

Clinopyroxene and olivine are by far the biggest (0.5 to 2 cm) and most abundant phenocryst phases and clinopyroxene is markedly more abundant than olivine. Plagioclase is much less abundant than either olivine or clinopyroxene and in some examples does not occur as a phenocryst phase at all. In their paucity or absence of plagioclase phenocrysts the ankaramites are quite distinct from most lavas comprising the other petrographic groups of the Rindjani suite.

Clinopyroxene phenocrysts are markedly zoned, the cores are pale green or almost colourless, Cr-rich diopside (ca 46.6 Mg 48.7 Fe 4.7, Mg/Mg+Fe = 0.91, table 3.2) and the rims are darker green, Al- Ti-rich augite (table 3.2), markedly more Fe-rich than the cores. The transition from core to rim is sharp. Many individual cpx[1] crystals are fragments of larger crystals, broken across both diopside core and augite rim without subsequent growth.

Olivine phenocrysts are rounded and embayed and range in composition from Fo 82.5 to Fo 88 (table 3.6). They lack the Cr-spinel inclusions found in some olivine megacrysts of similar composition from some high-Al basalts described in the next section.

Plagioclase phenocrysts, when they do occur, like those from many other basaltic and andesitic lavas of Rindjani, are very calcium-rich. They are often relatively unzoned with compositions ranging from calcic bytownite to anorthite (average ca. An 88) and are corroded with numerous glass and occasional cpx inclusions. Some do have finely zoned, more sodic rims around corroded cores (table 3.7).

Titanmagnetite is a scarce microphenocryst phase. A typical analysis is given in table 3.8. Compared with magnetites from the andesites these are more TiO_2-poor (27.5 mol.% U.sp.) and are relatively Al_2O_3 and MgO-rich.

[1] The words clinopyroxene and orthopyroxene are frequently abbreviated to cpx and opx respectively throughout the rest of this thesis.

The ankaramites resemble, both geochemically and petrographically, some basaltic lavas from the New Hebrides (Aoba and Epi islands, e.g. Warden, 1970; Gorton, 1977) and from the New Guinea Highlands (e.g. the olivine-augite absarokite from Mt. Giluwe, Jakes and White, 1969).

2. High-Al Basalts.

These lavas, together with basaltic andesites and andesites, make up the most voluminous portion of Rindjani's recent eruptives. They are aluminous (>17% Al_2O_3), have silica contents in the range 48-53% and have low to moderate MgO contents (ca. 3-6%).

The term, "basalt" has been used in a rather loose sense to characterise those lavas with <53% SiO_2. In fact, these lavas (with >17% Al_2O_3 and <53% SiO_2) are a diverse group. They straddle the plane of critical undersaturatio (fig. 3.11) and both *ne*- and *ol-hy*-normative groups show variation from relatively magnesian members (5-6% MgO), through to differentiated varieties with ca. 3.0% MgO and normative plagioclase compositions of An40 or less.

The more magnesian, *ne*-normative basalts (e.g. 41621, 41632, LB67 analyses given in table 3.13) are here termed alkali olivine basalts. These range through to relatively low MgO *ne*-normative lavas with normative plagioclase composition <An40, here termed hawaiites (e.g. 41678, analysis given in table 3.14). The *ne*-normative group shows continuous gradation to the *ol-hy*-normative group which spans a similar MgO range, generally with slightly lower total alkali content. These range from basalts with MgO >5% (e.g. 41676, analysis given in table 3.12) (olivine basalt) to more differentiated lavas with low MgO (basaltic andesite) e.g. 41637, 41634, analyses given in table 3.16).

For the most part the high-Al basalts are porphyritic lavas, though the more mafic members of the group (e.g. 41621, 41632, LB67 and 41676; tables 3.1 and 3.12, 3.13) are phenocryst-poor (<15%). The main phenocrysts are plagioclase, clinopyroxene and olivine, with some minor magnetite.

The relative proportion of olivine increases relative to that of plagioclase and clinopyroxene as the total proportion of phenocrysts decreases (compare modal analyses of lavas 41637, 41632 and 41621 in table 3.1), so that alkali olivine basalt 41621 has only 8% phenocrysts, comprising 4.5% olivine and 3.5% plagioclase with no cpx phenocrysts. On the other hand, basaltic andesite 41637 has 56% phenocrysts (3.5% olivine, 8.5% cpx, 31% plagioclase and 3% magnetite) and the proportion of olivine relative to cpx, and plagioclase is very much lower. Some of the relatively mafic alkali olivine basalts (e.g. 41632), while being relatively cpx-poor, do have occasional reacted, Cr-rich augite megacrysts. In addition to small, euhedral olivine phenocrysts (Fo75 - Fo82) some members of this group also contain large (up to 1cm), reacted, strained olivine megacrysts with inclusions of Cr-spinel. These olivine megacrysts (table 3.6) are magnesian and have compositions ranging from Fo83 to Fo92. The occurrence of similar magnesian olivine xenocrysts has been noted in a number of calcalkaline suites, for example, from; the Aleutians (Marsh, 1976), Tonga (Ewart et al., 1973), the Lesser Antilles (Sigurdsson et al., 1973; Arculus and Curran, 1972), Mt. Shasta, California (Anderson, 1974).

Clinopyroxene phenocrysts are relatively Al-, Ti-rich augites (table 3.3). Plagioclase, the main phenocryst in many of the less mafic members of this group, is very calcic, ranging from bytownite to anorthite in composition. Many individuals are zoned, zonation being normal, or with only minor reverse oscillations. However some of the most An-rich individuals (An84 - An94) are apparently unzoned and are commonly corroded and sieved. Plagioclase of this composition also occasionally forms corroded cores to other phenocrysts with more sodic outer margins. The very calcic plagioclase phenocrysts may occur in the same rock as individuals with much less An-rich cores (ca. An75) that show no sign of corrosion.

Magnetite phenocrysts are absent from many of the more mafic alkali olivine basalts, but occur as microphenocrysts in the more differentiated and more phenocryst-rich lavas.

Phenocrysts are set in a fine, plagioclase-rich groundmass. Plagioclase (about An50) occurs as elongate laths, often showing fluxion texture. Clinopyroxene is the most abundant groundmass phase after plagioclase, also occurring as tabular grains. Olivine (Fo54-64) occurs as small granules in the groundmasses of the more mafic and undersaturated rocks, but is rare in the *ol-hy*-normative basaltic andesites. Ti-rich magnetite occurs in the groundmasses of all lavas of the group, while sanidine and/or calcic anorthoclase is present in the groundmasses of some of the *ne*-normative lavas (e.g. 41632, 41678).

3. Low-silica Andesites and Andesites.

Modal analyses of typical representative members of this group are given in table 3.1. These lavas are *Q*-normative and are very phenocryst-rich (40-70%) and their phenocryst assemblages are dominated by plagioclase. Phenocrysts are characteristically strongly zoned and the most typical phenocryst assemblage is plagioclase-clinopyroxene-orthopyroxene-magnetite. This is set in an extremely fine-grained or commonly glassy matrix. Less commonly a few andesites contain phenocrysts of olivine, and orthopyroxene is absent from these. Partially reacted Ca-rich amphibole is also present in a few of the andesites investigated.

Where crystalline, the groundmasses of the andesites are composed of fine plagioclase laths, with small grains of clinopyroxene, orthopyroxene and magnetite. In other instances, finely crystalline groundmass is absent and phenocrysts and microphenocrysts are set directly in glass.

Plagioclase from the andesites often show marked variation in core composition. Some individuals have centres in the range An65-75, rhythmically zoned to outermost rim compositions in the range An58-40. Others may have

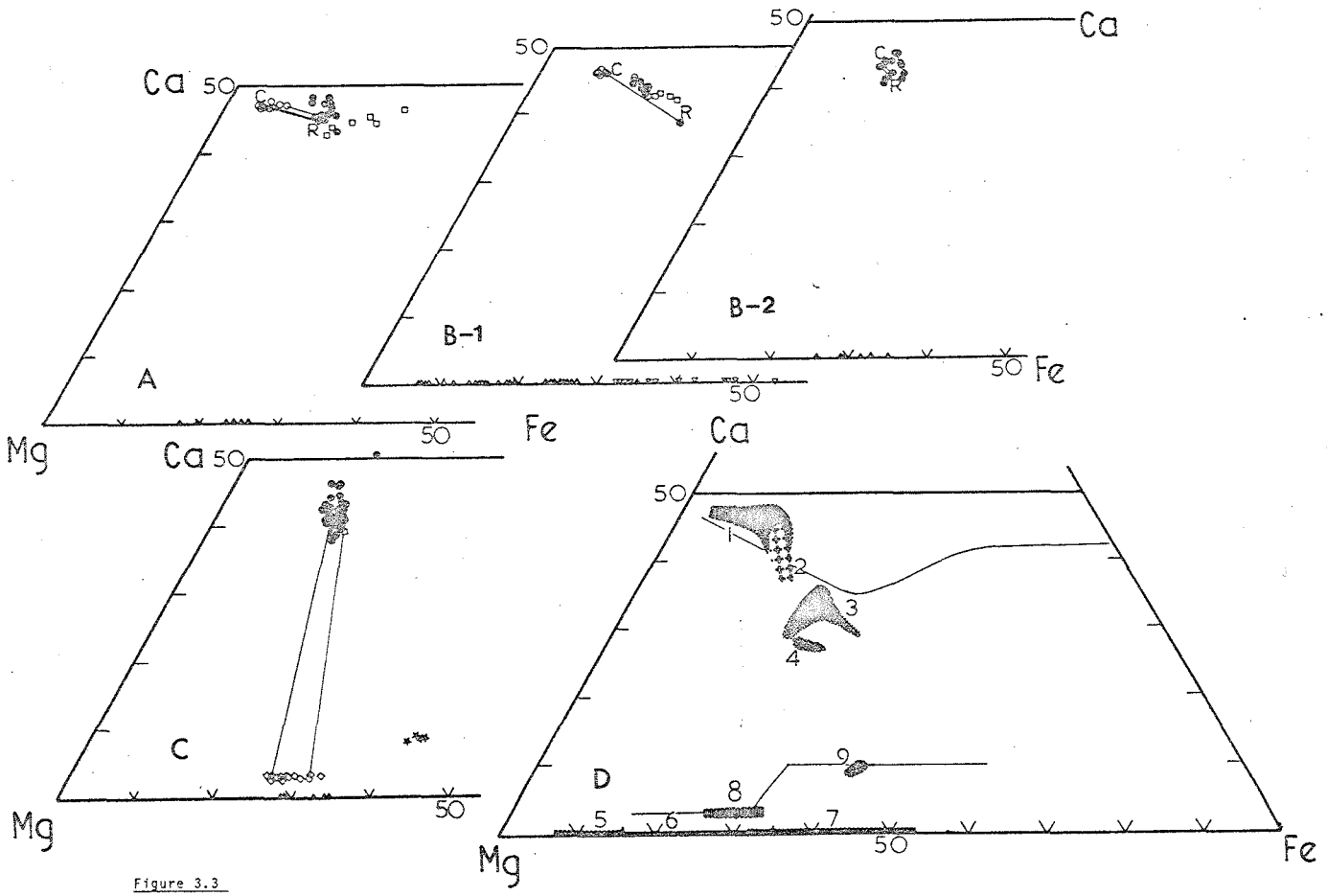

Figure 3.3

Compositional variation of Rindjani ferromagnesian minerals.Relative atomic proportions of Mg-,Ca- and Fe-end members.Diagrams A to C represent.: A - compositions of clinopyroxenes and olivine from ankaramite lavas.Open circles are compositions of diopsidic cores,filled circles are more Al- and Ti-rich augite phenocrysts and rims to diopside cores.Open squares are groundmass cpx.In diagrams A,B-1,B-2 and C filled triangles are olivine phenocrysts. B-1 - compositions of cpx and olivine from ne-normative high-Al basalts.Open circles are megacrysts and diopsidic cores,closed circles are phenocrysts and squares are groundmass cpx.Open triangles are olivine megacrysts,inverted open triangles are groundmass olivine. B-2 cpx and olivine compositions from ol-hy-normative high-Al basalts,symbols as in B-1.C- compositions of cpx,opx and olivine from andesites and dacites. Filled circles cpx phneocrysts,open squares groundmass cpx,open diamonds opx phenocrysts,stars opx groundmass.

Diagram D is a summary of the compositional fields of Rindjani ferromagnesian minerals.The fields are as follows: 1. cpx phenocrysts from basalts,2. cpx phenocrysts from andesites and dacites,3. composition of amphibole from basalts and andesites (often reacted),4. amphibole from dacites,5. olivine megacrysts or xenocrysts,6. olivine phenocrysts,7.groundmass olivine,8. opx phenocrysts from andesites and dacites and 9. groundmass opx from andesite and dacite.

extremely calcic cores (An85-90) of relatively homogeneous composition which may be corroded or contain bands or zones of inclusions filled with glass, gas, and more rarely cpx or magnetite. Outward from these cores there is a marked hiatus in the An85-70 range and the outer zone is normally and rhythmically zoned from An70 in the inner part of the margin around the calcic core, to about An50-40 at the rim. These outer margins are clear and inclusion-free.

The occurrence of extremely anorthite-rich plagioclase has been reported from a number of island- and continental marginal-arc, calcalkaline andesite suites (e.g. Whitford, 1976, from the western Sunda arc, Marsh, 1976, from the Aleutians, Rose et al., 1978 from Fuego volcano, Guatamala; Ewart, 1976).

Clino- and orthopyroxene also show marked zonation, though the actual compositional range encompassed from core to rim (figure 3.4) is relatively minor and mainly involves a decrease in the Ca-content of the cpx, the Mg/Mg+Fe ratios of both opx and cpx remaining relatively constant.

In contrast to the lavas with <53% SiO_2, magnetite occurs as a relatively abundant phenocryst phase and is generally more Ti-rich than that of the basalts.

Many andesites contain rare apatite as small microphenocrysts. These appear to be an early formed phase, often occurring as inclusions in plagioclase and magnetite. They have an unusual brown-mauve colour with numerous fine striations and appear to be identical to some described by Mertzman (1977) from the Medicine Lake andesite.

The andesites from Rindjani volcano are petrographically typical of the numerous examples of this calcalkaline rock-type erupted from many circum-Pacific arc volcanoes (see Ewart, 1976; for instance, for a general summary).

4. High-K Andesites and Dacites.

Based on Taylor's (1969) classification scheme (fig. 3.2), the division between these two groups is arbitrarily set at 62% SiO_2, and as members of

Figure 3.4

Plagioclase compositional variation from Rindjani lavas.. A Basalts,B- andesites, C dacites. Open circles - phenocrysts,closed circles- phenocryst rims, open squares- groundmass feldspar.In figure A tie-lines connect coexisting ground mass plagioclase and alkali feldspar.In figure B the line connecting C-1-2-3-R illustrates typical core-rim variation of a single phenocryst. In figure D phenocryst core variation is illustrated ; open circles-basalts,stars - andesites, open squares- dacites.Approximate groundmass trends are represented by the dashed curves.B-basalt,A-andesite,D-dacite. The shaded field B A is the field of normative feldspar composition of basalts and andesites, field D is that of the dacites.The two filled circles in field D are normative compositions of glasses in andesite groundmasses.

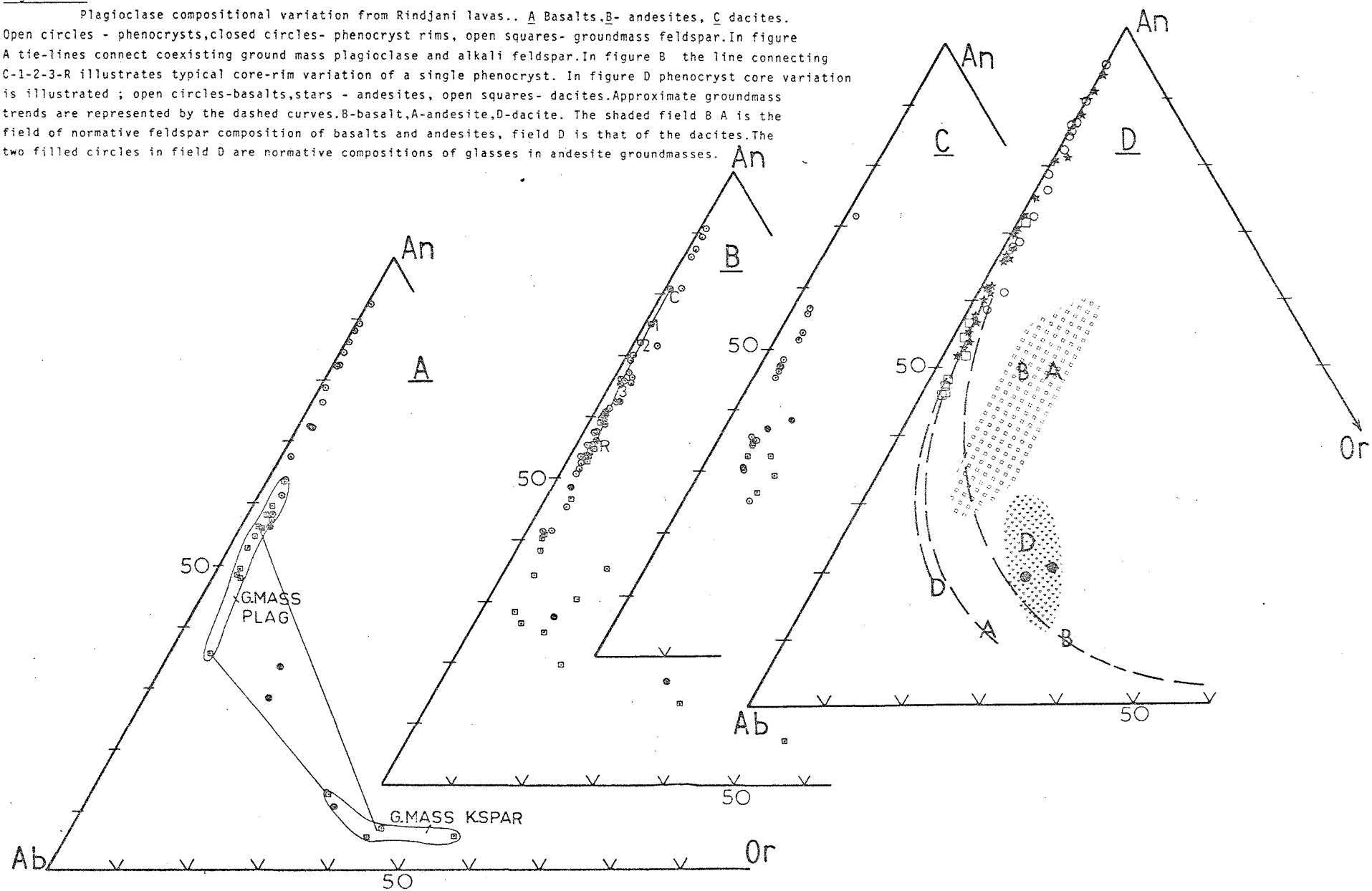

the two groups are otherwise petrographically similar, they are considered together.

In contrast to the andesite, the dacites and to a lesser extent, the high-K andesites are relatively phenocryst-poor (for instance see modal analysis of dacite 41641 in table 3.1), averaging 5-15% phenocrysts. The groundmass is often glass-rich (table 3.19), this glass having a siliceous composition very close to that of the most evolved dacites. Phenocrysts are plagioclase, opx, titan magnetite, minor cpx and hornblende and/or biotite in some samples.

Plagioclase is less markedly zoned than that of the andesites and is more often clear and free of inclusions or resorbtion features. Cores are about An70, while rims range from An50 to An40. Groundmass plagioclase occurs as fine tabular laths, of composition about An35-An40. Orthopyroxene (En70-68) is compositionally very like that of the andesites, whereas magnetite is generally more Ti-rich (Ulvospinel= 43 mol.%).(1)

Hornblende is a phenocryst phase in those dacite which are less phenocryst-rich and in general less plagioclase-rich. Compared with the reacted hornblende of the andesites, those of the dacites are generally fresh. In a few lavas fine groundmass laths of amphibole appear oxidised to magnetite. The fresh hornblende is slightly more Fe-rich than that of the andesite (Mg/Mg+Fe = 63), and is markedly less aluminous and less calcic. Occasional small flakes of biotite occur, often in those dacites with hornblende and in some high-K andesites (e.g. 41672) without hornblende.

5. Foreign Inclusions.

Although there are no ultramafic nodules or lithic inclusions of any kind in the lavas, there are a number of reacted phenocryst phases which could be interpreted as relicts of pre-eruption near-liquidus assemblages.

(1) Ulvospinel is sometimes abbreviated to Usp throughout the rest of this thesis.

Table 3.2 Representative Electron Microprobe Analyses of Clinopyroxenes from the low-Al Ankaramites from Rindjani

Analysis No.	1	2	3	4	5	6	7	8	9
Sample No.	LB8	LB8	LB8	LB8	LB8	LB8	LB10	LB10	LB10
Type	M		M	M	P		M	M	P
	core	- rim	core	core	core	- rim	core		
SiO_2	53.4	50.4	53.1	53.6	50.5	49.4	53.2	52.0	50.3
Al_2O_3	1.4	3.1	1.4	0.9	3.9	4.4	1.9	2.8	4.3
FeO	3.1	12.4	3.1	2.7	7.7	8.5	3.7	4.8	8.8
MgO	17.6	11.9	17.6	17.9	14.4	13.9	17.0	16.1	13.5
CaO	23.4	21.2	23.8	23.9	22.3	22.6	23.4	23.2	21.7
Na_2O	-	-	-	-	-	-	-	-	-
TiO_2	0.2	0.8	0.3	0.2	0.8	0.9	0.3	0.6	1.1
MnO	-	-	-	-	-	-	-	-	-
Cr_2O_3	0.8	0.1	0.7	0.9	0.2	0.1	0.5	0.4	0.1
Total	99.9	99.9	100.0	100.1	99.8	99.8	100.0	99.9	99.8
100 Mg/Mg+Fe (mol.)	91.11	63.10	91.00	92.28	76.92	74.45	89.11	85.57	73.16
	Number of Ions on the Basis of 6 Oxygens								
Si Z	1.945	1.909	1.939	1.955	1.880	1.851	1.943	1.910	1.874
Al Z	0.055	0.091	0.061	0.038	0.120	0.149	0.057	0.090	0.126
Al	0.006	0.047	-	-	0.051	0.045	0.025	0.032	0.064
Fe	0.093	0.393	0.095	0.081	0.239	0.266	0.113	0.149	0.276
Mg	0.958	0.672	0.958	0.971	0.799	0.776	0.925	0.882	0.751
Ca X + Y	0.916	0.860	0.931	0.934	0.890	0.908	0.916	0.914	0.868
Na	-	-	-	-	-	-	-	-	-
Ti	0.006	0.023	0.008	0.005	0.022	0.025	0.008	0.016	0.032
Mn	-	-	-	-	-	-	-	-	-
Cr	0.024	0.002	0.020	0.026	0.006	0.002	0.014	0.010	0.002
Z	2.000	2.000	2.000	1.993	2.000	2.000	2.000	2.000	2.000
X + Y	2.003	1.997	2.012	2.017	2.007	2.022	2.001	2.003	1.993
Total	4.003	3.997	4.012	4.010	4.007	4.022	4.001	4.003	3.993
	Molecular Proportions								
Ca	46.6	44.6	47.0	47.1	46.1	46.5	48.8	47.0	45.8
Mg	48.7	35.0	48.3	48.8	41.5	39.8	47.5	45.4	39.6
Fe	4.7	20.4	4.7	4.1	12.4	13.7	5.7	7.6	14.6
Ca/Ca+Mg (mol.)	0.490	0.561	0.493	0.490	0.527	0.539	0.497	0.509	0.504
$Al^{vi}Al^{iv}$	0.117	0.521	-	-	0.426	0.304	0.435	0.354	0.509

Notes: Lavas LB8 and LB10-low-Al ankaramites.

Abbreviations: M = megacryst, P = phenocryst.

Table 3.3 Representative Electron Microprobe Analyses of Clinopyroxenes from Rindjani Basaltic Lavas

Analysis No.	10	11	12	13	14	15	16	17	18	19	20	21	22
Sample No.	41632	41632	41632	41631	41631	41651	41624	41624	41624	41623	41632	41631	41651
Type	M	P	P	M	M	M	P	P	P	P	G	G	G
	core	core	core	core	- rim	core	core	- M.P.	- rim	core			
SiO_2	51.4	49.9	48.7	50.2	49.7	52.1	51.6	51.3	50.2	51.4	49.7	49.9	49.7
Al_2O_3	3.4	5.7	6.2	5.7	5.7	3.0	3.0	3.0	4.1	3.8	6.7	3.9	4.0
FeO	7.9	8.6	8.4	7.3	7.5	4.7	8.1	9.0	9.2	9.3	9.4	11.1	9.9
MgO	15.0	14.2	13.9	14.0	14.3	16.4	15.6	15.7	14.9	14.3	12.8	13.1	14.2
CaO	21.4	20.5	20.1	21.2	21.0	23.0	21.1	19.9	20.4	21.1	19.0	19.9	20.6
Na_2O	0.3	0.4	0.4	-	-	-	0.2	0.4	0.3	0.4	1.0	0.2	0.4
TiO_2	0.4	1.0	1.0	1.0	1.0	0.3	0.3	0.4	0.6	0.6	1.1	1.7	1.2
MnO	-	0.2	0.2	-	-	-	-	-	0.2	0.3	-	-	-
Cr_2O_3	0.2	0.2	0.2	0.6	0.6	0.5	0.1	0.2	0.1	-	0.1	-	-
Total	100.0	100.7	99.1	100.0	99.8	100.0	100.0	99.9	100.0	101.2	99.8	99.8	100.0
100 Mg/Mg+Fe (mol.)	77.2	74.8	74.6	77.45	77.30	86.20	77.3	75.7	74.3	73.5	70.81	67.77	71.88
						Number of Ions on the Basis of 6 Oxygens							
Si	1.906	1.842	1.827	1.855	1.839	1.910	1.913	1.906	1.872	1.887	1.849	1.976	1.862
Z Al^{VI}	0.094	0.158	0.173	0.145	0.161	0.090	0.087	0.094	0.128	0.113	0.151	0.124	0.138
Al^{IV}	0.057	0.089	0.100	0.104	0.088	0.039	0.045	0.039	0.054	0.052	0.143	0.049	0.039
Fe	0.244	0.264	0.264	0.224	0.233	0.143	0.252	0.280	0.286	0.286	0.292	0.349	0.310
Mg	0.827	0.783	0.777	0.770	0.793	0.895	0.859	0.872	0.826	0.794	0.710	0.734	0.793
Ca X + Y	0.851	0.810	0.807	0.838	0.833	0.906	0.837	0.794	0.813	0.840	0.757	0.802	0.827
Na	0.023	0.028	0.031	-	-	-	0.013	0.029	0.025	0.025	0.072	0.015	0.029
Ti	0.010	0.028	0.029	0.028	0.028	0.009	0.008	0.011	0.017	0.017	0.031	0.048	0.034
Mn	-	0.007	0.005	-	-	-	-	-	0.006	0.011	-	-	-
Cr	0.005	0.008	0.006	0.018	0.020	0.014	0.003	0.005	0.003	0.000	0.003	-	-
Z	2.000	2.000	2.000	2.000	2.000	2.000	2.000	2.000	2.000	2.000	2.000	2.000	2.000
X + Y	2.017	2.017	2.019	1.982	1.995	2.006	2.017	2.029	2.030	2.025	2.008	1.997	2.032
Total	4.017	4.017	4.019	3.982	3.995	4.006	4.017	4.029	4.030	4.025	4.008	3.997	4.032
						Molecular Proportions							
Ca	44.3	43.6	43.6	45.7	44.8	46.6	43.0	40.8	42.2	43.7	43.0	42.5	42.8
Mg	43.0	42.1	42.1	42.0	42.7	46.0	44.1	44.8	42.9	41.3	40.4	39.0	41.1
Fe	12.7	14.3	14.3	12.3	12.5	7.4	12.9	14.4	14.9	14.9	16.6	18.5	16.1
Ca/Ca+Mg (mol.)	0.507	0.508	0.509	0.521	0.512	0.503	0.494	0.476	0.496	0.514	0.516	0.522	0.511
Al^{vi}/Al^{iv}	0.605	0.563	0.578	0.719	0.547	0.443	0.522	0.417	0.422	0.460	0.946	0.394	0.279

Notes: 41632, 41631, 41651, 41624, 41623 - high-Al, ne-normative alkali olivine basalts/"hawaiites".

Abbreviations: M = megacryst, P = phenocryst, G = groundmass, M.P. = mid-point.

Table 3.4 Representative Clinopyroxene Analyses: Rindjani: Basaltic Andesites, Andesites and Dacites

Analysis No.	1	2	3	4	5	6	7	8	9	10	11	12	13	14	15	16	17	18	19	20
Sample No.	41637	41637	41637	41637	41625	41625	41625	41647	41647	41647	41644	41644	41644	41636	41636	41636	41636	41672	41645	41650
Rock Type	BA	BA	BA	BA	A	A	A	A	A	A	A	A	A	A	A	A	A	HKA	D	D
	core - rim		core - rim		[1]	[1]	[2]	P	P	P	core - rim		MP	core - rim		[3]	GM	P	P	P
SiO_2	51.4	52.3	49.6	50.7	51.5	51.4	52.1	52.4	52.4	51.8	52.6	53.1	51.4	51.8	52.4	51.6	51.6	52.4	52.2	52.2
Al_2O_3	2.7	1.9	4.8	3.2	2.5	2.2	2.0	1.4	1.4	2.0	1.2	2.4	2.0	2.0	2.6	2.8	2.1	1.8	1.5	1.9
FeO	8.1	9.1	8.5	10.0	9.7	9.9	9.1	9.4	9.4	9.4	10.2	9.7	10.2	10.5	10.2	10.0	10.7	8.5	10.0	8.2
MgO	15.5	15.4	14.2	14.6	15.6	16.0	15.9	14.8	14.8	15.4	15.7	15.3	14.8	15.2	15.1	15.4	15.2	15.8	14.4	14.9
CaO	21.2	20.4	21.8	20.5	19.6	19.1	20.0	20.6	20.7	20.0	18.9	17.8	19.6	19.5	18.4	18.9	19.5	20.0	21.5	21.5
Na_2O	0.3	0.3	0.3	0.2	-	-	-	0.6	0.5	0.7	0.5	0.8	0.7	0.3	0.5	0.4	0.3	0.3	0.4	0.4
TiO_2	0.4	0.3	0.7	0.6	0.6	0.6	0.5	0.3	0.3	0.4	0.3	0.4	0.5	0.5	0.3	0.4	0.4	0.6	0.5	0.5
MnO	0.1	0.3	0.1	0.2	0.4	0.5	0.4	0.4	0.4	0.3	0.5	0.3	0.5	0.2	0.3	0.3	0.2	0.3	0.5	0.6
Cr_2O_3	0.2	-	-	-	-	-	-	-	-	-	-	-	-	-	-	-	-	-	-	-
Total	99.9	100.0	100.0	100.0	99.9	99.7	100.0	99.9	99.9	100.0	99.9	99.8	99.7	100.0	99.8	99.4	100.0	99.7	101.0	100.2
100Mg/Mg+Fe (mol.)	77.4	75.1	74.8	72.2	74.1	74.3	75.7	73.9	73.8	74.5	73.2	73.9	72.2	72.1	72.6	73.2	71.68	76.8	72.1	76.5
Number of Ions on the Basis of 6 (O)																				
Si	1.910	1.942	1.850	1.895	1.919	1.916	1.934	1.954	1.955	1.931	1.961	1.963	1.926	1.934	1.946	1.920	1.929	1.946	1.940	1.940
Al^{iv}	0.090	0.058	0.150	0.105	0.081	0.084	0.066	0.046	0.045	0.069	0.039	0.037	0.074	0.066	0.054	0.080	0.071	0.054	0.060	0.060
Al^{vi}	0.030	0.028	0.061	0.038	0.029	0.014	0.021	0.016	0.017	0.018	0.014	0.069	0.016	0.022	0.058	0.044	0.025	0.024	0.004	0.022
Fe	0.250	0.282	0.266	0.312	0.301	0.309	0.282	0.292	0.292	0.293	0.319	0.298	0.319	0.328	0.316	0.312	0.335	0.264	0.310	0.254
Mg	0.859	0.854	0.791	0.812	0.863	0.891	0.879	0.825	0.824	0.855	0.872	0.843	0.828	0.846	0.838	0.854	0.847	0.873	0.799	0.825
Ca	0.842	0.813	0.872	0.822	0.784	0.762	0.793	0.826	0.826	0.799	0.757	0.704	0.785	0.780	0.732	0.755	0.781	0.794	0.858	0.857
Na	0.021	0.023	0.023	0.016	-	-	-	0.043	0.043	0.049	0.038	0.058	0.054	0.022	0.033	0.032	0.022	0.024	0.025	0.027
Ti	0.011	0.009	0.020	0.017	0.015	0.017	0.013	0.007	0.007	0.009	0.007	0.011	0.014	0.014	0.009	0.010	0.011	0.016	0.013	0.013
Mn	0.005	0.008	0.004	0.007	0.014	0.016	0.011	0.013	0.013	0.009	0.017	0.009	0.016	0.006	0.012	0.009	0.006	0.002	0.017	0.018
Cr	0.006	-	-	-	-	-	-	-	-	-	-	-	-	-	-	-	-	-	-	-
Z	2.000	2.000	2.000	2.000	2.000	2.000	2.000	2.000	2.000	2.000	2.000	2.000	2.000	2.000	2.000	2.000	2.000	2.000	2.000	2.000
X + Y	2.024	2.017	2.036	2.024	2.006	2.009	1.999	2.022	2.022	2.032	2.024	1.992	2.032	2.018	1.998	2.016	2.027	1.997	2.026	2.016
Molecular Proportions																				
Ca	43.2	41.7	45.2	42.3	40.2	38.9	40.6	42.5	42.5	42.1	38.9	38.2	40.6	40.0	38.8	39.3	39.8	41.1	43.6	44.2
Mg	44.0	43.8	41.0	41.2	44.3	45.4	45.8	42.5	42.4	43.9	44.8	45.7	42.8	43.3	44.4	44.4	43.1	45.2	40.6	42.6
Fe	12.8	14.5	13.8	16.0	15.5	15.7	14.4	15.0	15.1	15.0	16.3	16.1	16.6	16.7	16.8	16.3	17.1	13.7	15.8	13.1
Ca/Ca+Mg (mol.)	0.496	0.487	0.524	0.503	0.476	0.461	0.474	0.500	0.500	0.483	0.464	0.455	0.487	0.479	0.466	0.469	0.480	0.476	0.518	0.509
Al^{vi}/Al^{iv}	0.334	0.480	0.409	0.366	0.360	0.165	0.312	0.360	0.380	0.261	0.359	1.878	0.215	0.333	1.068	0.545	0.352	0.444	0.067	0.367

Notes: [1] Cpx rim to Opx 1 (Table 3.5).
[2] Cpx in glomerocryst of Cpx, Opx, Pl and Mag.
[3] Cpx rim to Opx (Table 3.5).

Abbreviations: BA - basaltic andesite; A - andesite; HKA - high-K andesite; D - dacite; P - phenocryst; MP - microphenocryst; GM - groundmass

Table 3.5 Representative Orthopyroxene Analyses: Rindjani Lavas

Analysis No.	1	2	3	4	5	6	7	8	9	10	11	12	13	14	15
Sample No.	41625	41625	41625	41625	41625	41647	41647	41647	41636	41636	41636	41636	11641	41641	41650
Rock Type	A	A	A	A	A	A	A	A	A	A	A	A	D	D	D
	core [1]	[2]	GM	GM	GM	P	P	P	GM	core [3]	rim [3]	PR	P	P	P
SiO_2	51.8	52.2	51.4	50.7	51.1	52.7	53.3	53.1	53.2	52.3	52.7	53.0	52.6	52.3	53.2
Al_2O_3	1.6	1.3	-	0.7	-	0.8	0.8	0.9	0.6	1.7	1.0	0.6	0.8	0.7	0.7
FeO	17.5	18.5	25.2	25.4	26.0	19.5	17.7	19.4	16.8	17.4	18.2	18.7	18.2	19.2	18.0
MgO	26.0	25.0	17.6	16.9	16.8	24.2	25.3	25.3	26.2	25.3	24.7	24.9	25.6	24.7	25.3
CaO	1.6	1.7	3.8	4.2	4.2	1.3	1.2	1.4	1.7	1.8	1.6	1.7	1.4	1.3	1.3
Na_2O	-	-	-	-	-	0.1	0.1	0.3	0.4	0.2	0.3	-	-	-	-
TiO_2	0.4	0.3	0.4	0.5	0.4	0.1	0.3	-	0.2	0.3	0.3	0.2	0.3	0.3	0.2
MnO	1.0	0.9	1.5	1.4	1.5	0.6	0.8	0.6	0.8	0.5	0.7	0.8	1.2	1.4	0.9
Cr_2O_3	-	-	-	-	-	-	-	-	-	-	-	-	-	-	-
Total	99.9	99.9	99.9	99.8	100.0	99.2	99.5	101.0	99.9	99.5	99.5	99.9	100.1	99.9	99.6
100Mg/Mg+Fe (mol.)	72.6	70.7	55.5	54.3	53.6	68.86	71.8	69.0	73.5	72.2	70.74	70.31	71.5	69.6	71.5
							Number of Ions on the Basis od 6 (O)								
Si	1.906	1.925	1.975	1.955	1.973	1.960	1.962	1.961	1.949	1.927	1.949	1.954	1.937	1.940	1.960
Al^{iv}	.070	0.057	-	0.031	-	0.035	0.034	0.038	0.026	0.073	0.044	0.025	0.033	0.031	0.030
Al^{vi}	-	-	-	-	-	-	-	-	-	0.001	-	-	-	-	-
Fe	0.538	0.572	0.809	0.818	0.840	0.606	0.546	0.599	0.515	0.536	0.563	0.578	0.559	0.596	0.554
Mg	1.426	1.378	1.010	0.971	0.968	1.341	1.388	1.335	1.432	1.389	1.361	1.368	1.404	1.366	1.388
Ca	0.063	0.065	0.157	0.174	0.174	0.052	0.048	0.057	0.067	0.071	0.063	0.068	0.054	0.052	0.050
Na	-	-	-	-	-	0.007	0.002	0.022	0.028	0.014	0.022	-	-	-	-
Ti	0.010	0.009	0.013	0.015	0.011	0.003	0.008	-	0.004	0.008	0.008	0.005	0.009	0.008	0.006
Mn	0.030	0.027	0.049	0.047	0.050	0.019	0.024	0.018	0.023	0.016	0.022	0.023	0.036	0.044	0.030
Cr	-	-	-	-	-	-	-	-	-	-	-	-	-	-	-
Z	1.976	1.982	1.975	1.986	1.973	1.995	1.996	1.999	1.975	7.000	1.993	1.979	1.970	1.971	1.990
X + Y	2.067	2.051	2.038	2.025	2.043	2.028	2.016	2.031	2.069	2.035	2.039	2.042	2.062	2.066	2.028
Ca	3.1	3.2	8.0	8.9	8.7	2.7	3.5	2.9	3.3	3.5	3.2	3.3	2.7	2.5	2.5
Mg	70.4	68.4	51.1	49.5	48.9	67.0	64.5	67.0	71.1	69.7	68.5	68.0	69.6	67.8	69.7
Fe	26.5	28.4	40.9	41.6	42.4	30.3	32.0	30.1	25.6	26.8	28.3	28.7	27.7	29.7	27.8
Al^{vi}/Al^{iv}	-	-	-	-	-	-	-	-	-	0.014	-	-	-	-	-

Notes: [1] Opx core with Cpx rim (analyses 5 and 6 Table 3.4).

[2] Opx in glomerocryst of Cpx, Opx, Pl, Mag (as for Cpx, analysis 7, Table 3.4).

[3] Analyses 10 and 11 are core and rim analyses of Opx rimmed by Cpx (analysis 16, Table 3.4).

Abbreviations:

A - andesite, D - dacite, GM - Groundmass, PR - phenocryst-rim, P - phenocryst.

Table 3.6

Representative Analyses of Olivine from Rindjani Lavas

Analysis No.	1	2	3	4	5	6	7	8	9	10	11	12	13	14	15	16	17	18	19	20
Sample No.	LB10	41631	41631	41631	41626	41621	LB8	LB8	41632	41632	41632	41632	41632	41631	41624	41626	41626	41637	41644	41644
Rock Type	AK	HAB	HAB	HAB	HAB	AK	AK	AK	HAB	HAB	HAB	HAB	HAB	HAB	HAB	HAB	HAB	BA	A	A
	M	M	M	M	M	M	P	P	P	P	G	G	G	P	P	P-C	P-R	P	P	MP
SiO_2	39.5	40.6	39.5	39.7	38.7	39.4	37.3	37.1	38.0	39.1	34.4	35.3	33.9	39.1	36.2	39.4	36.0	36.7	37.0	36.6
FeO	11.2	7.4	10.4	8.1	13.5	8.7	18.9	22.6	21.9	16.6	38.8	31.7	42.6	14.5	29.3	11.7	30.0	26.4	26.5	30.0
MgO	47.6	51.7	49.5	51.6	47.1	50.4	42.7	39.3	39.7	44.0	25.1	31.3	21.5	44.8	33.5	48.6	32.6	35.8	35.7	32.4
CaO	0.4	0.2	0.1	0.2	0.3	0.2	0.4	0.3	0.2	0.2	0.4	0.2	0.4	0.3	0.5	0.2	0.5	0.2	0.1	0.2
TiO_2	0.1	-	0.2	0.1	0.2	0.2	0.1	-	-	-	0.1	-	0.2	0.2	-	-	0.1	-	-	0
MnO	0.2	-	-	-	0.2	-	0.3	0.4	0.3	0.1	0.9	0.7	1.1	0.3	0.6	-	0.5	0.7	0.7	0.8
Total	99.0	99.9	99.7	99.7	100.0	98.9	99.7	99.7	100.1	100.0	99.7	99.2	99.7	99.2	100.1	99.9	99.7	99.6	100.0	100.0
100Mg/Mg+Fe	88.3	92.6	89.4	91.9	86.1	91.2	80.1	75.6	76.4	82.5	53.6	63.8	47.3	84.6	67.1	88.1	65.9	70.7	70.6	65.8
Number of Ions on the Basis of 4 oxygens																				
Si	0.987	0.986	0.975	0.971	0.969	0.974	0.963	0.974	0.987	0.989	0.981	0.972	0.986	0.985	0.979	0.976	0.979	0.984	0.987	0.997
Fe	0.234	0.150	0.215	0.166	0.283	0.180	0.408	0.496	0.476	0.352	0.925	0.729	1.037	0.306	0.663	0.243	0.683	0.589	0.591	0.680
Mg	1.773	1.872	1.825	1.882	1.758	1.858	1.643	1.538	1.538	1.662	1.067	0.283	0.934	1.682	1.353	1.795	1.319	1.422	1.419	1.310
Ca	0.011	0.005	0.004	0.005	0.008	0.005	0.011	0.009	0.005	0.004	0.012	0.007	0.013	0.008	0.014	0.005	0.015	0.006	0.002	0.007
Ti	0.002	-	0.003	0.002	0.003	0.004	0.002	-	-	-	0.003	-	0.004	0.003	-	-	0.002	-	-	-
Mn	0.004	-	-	-	0.004	-	0.006	0.009	0.006	0.003	0.021	0.015	0.027	0.007	0.013	-	0.012	0.015	0.015	0.018
Total	3.011	3.014	3.021	3.027	3.026	3.021	0.034	0.026	3.012	3.010	3.013	3.006	3.002	2.991	3.021	3.019	3.010	3.016	3.014	3.007

Abbreviations: AK - ankaramite, HAB - high-Al basalt,
BA - basaltic andesite, A - andesite,
M - megacryst/xenocryst, P - phenocryst,
G - groundmass, C - core, R - rim,
MP - microphenocryst.

Table 3.7

Representative Analyses of Feldspars from Rindjani Lavas

Analysis No.	1	2	3	4	5	6	7	8	9	10	11	12	13	14	15	16
Sample No.	LB8	41632	41651	41651	41651	41632	41632	41678	41678	41625	41625	41625	41625	41641	41641	41641
Rock type.	AK	HAB	HAB	HAB	HAB	HAB	HAB	HAB	HAB	A	A	A	A	D	D	D
	P(C)	P(C)	P-C	P-R	P	G	G-AF	P-C	P-R	P-C	P-R	P(C)	G	P-C	P-R	G
SiO_2	45.6	45.2	47.5	48.4	50.4	52.9	64.7	51.6	52.5	51.3	53.4	46.6	59.4	54.4	57.5	60.5
Al_2O_3	34.9	34.9	33.1	32.9	31.5	28.7	19.7	30.0	29.2	30.7	29.8	34.7	25.4	28.5	26.2	24.1
FeO	0.6	0.5	0.5	0.5	0.6	1.1	0.5	0.7	0.7	0.9	0.5	0.6	0.7	0.3	0.4	0.4
CaO	18.5	17.8	16.6	15.6	13.7	11.4	1.2	12.6	11.7	13.9	11.5	16.9	6.8	10.1	7.5	5.3
Na_2O	0.9	1.1	1.9	2.2	3.4	4.9	6.0	4.1	4.5	2.6	4.2	1.0	5.3	5.7	6.9	7.6
K_2O	0.1	0.1	0.1	0.1	0.2	0.5	7.6	0.5	0.7	0.7	0.4	0.1	2.3	0.5	0.9	1.7
Total	100.6	99.6	99.7	99.7	99.8	99.5	99.7	99.5	99.3	99.8	99.8	99.9	99.9	99.5	99.4	99.6
						Number of Ions on the basis of 8 oxygens										
Si	2.095	2.093	2.188	2.221	2.303	2.421	2.931	2.352	2.392	2.339	2.416	2.140	2.667	2.471	2.600	2.718
Al	1.889	1.905	1.797	1.780	1.696	1.549	1.052	1.615	1.567	1.652	1.587	1.878	1.344	1.526	1.396	1.276
Fe	0.023	0.019	0.019	0.019	0.023	0.042	0.019	0.027	0.028	0.032	0.018	0.023	0.026	0.011	0.015	0.015
Ca	0.909	0.883	0.819	0.767	0.671	0.559	0.058	0.614	0.571	0.678	0.557	0.832	0.327	0.492	0.363	0.255
Na	0.080	0.099	0.170	0.196	0.301	0.435	0.527	0.358	0.400	0.225	0.371	0.089	0.461	0.502	0.605	0.662
K	0.008	0.006	0.006	0.006	0.011	0.029	0.439	0.031	0.041	0.042	0.022	0.006	0.132	0.029	0.052	0.097
Total	5.003	5.006	5.000	4.989	5.005	5.035	5.026	5.035	5.042	4.968	4.981	4.968	4.958	5.031	5.030	5.023
An	91.2	89.4	82.3	79.2	68.2	54.6	5.7	61.2	56.3	71.7	58.6	89.7	35.5	48.1	35.6	25.1
mol.% Ab	8.0	10.0	17.0	20.2	30.6	42.5	51.4	35.7	39.5	23.8	39.1	9.6	50.1	49.1	59.3	65.2
Or	0.8	0.6	0.9	0.6	1.2	2.9	42.9	3.1	4.0	4.5	2.3	0.7	14.4	2.8	5.1	9.7

Abbreviations: Rock Types: AK - ankaramite, HAB - high-Al basalt, A - andesite, D - dacite, P - phenocryst, P(C) - corroded or reacted phenocryst, C - core, R - rim, G - groundmass, AF - alkali feldspar.

Table 3.8 Magnetite Electron Microprobe Analyses from Rindjani Lavas

Analysis No.	1	2	3	4	5	6	7	8	9	10	11	12	13
Sample No.	LB10	41631	41631	41631	41624	41651	41623	41625	41625	41647	41647	41639	41639
Rock Type	AK	AOB	AOB	AOB	AOB	AOB	AOB	A	A	A	A	D	D
	IC	GM	GM	MP	P	MP	IO	ICX	P	MP	MP	P	MP
SiO_2	-	-	-	-	0.09	-	-	-	-	0.21	1.22	0.23	0.33
TiO_2	9.72	8.60	25.85	6.96	9.25	19.48	8.54	10.92	11.18	14.73	13.73	14.78	14.49
Al_2O_3	4.85	2.38	-	1.99	5.33	0.72	9.99	4.29	3.52	1.96	2.53	2.41	2.74
Cr_2O_3	0.92	-	-	0.14	0.24	-	1.93	-	-	-	-	0.18	-
Fe_2O_3	45.41	49.46	19.96	52.94	45.92	30.90	41.09	43.47	43.82	38.45	37.03	37.47	37.42
FeO	35.08	39.55	54.68	37.55	35.66	48.18	33.97	40.02	39.95	42.86	43.97	43.01	43.46
MnO	0.40	-	-	0.40	0.38	-	-	-	0.31	0.29	0.40	0.58	0.57
MgO	3.60	-	-	-	3.02	0.71	4.46	1.30	1.22	1.47	0.81	1.31	0.99
CaO	-	-	-	-	0.07	-	-	-	-	-	0.29	-	-
Total	99.98	99.99	100.49	99.98	99.96	99.99	99.98	100.0	100.0	99.97	99.98	99.97	100.0
	Number of Ions on the Basis of 32 (O)												
Si	-	-	-	-	0.029	-	-	-	-	0.062	0.364	0.071	0.099
Al	1.652	0.845	-	0.712	1.820	0.255	3.296	1.488	1.227	0.686	0.882	0.844	0.958
Cr	0.211	-	-	0.034	0.054	-	0.427	-	-	-	-	0.042	-
Fe^{3+}	9.878	11.219	4.514	12.053	10.007	6.960	8.652	9.640	9.761	8.585	8.247	8.353	8.346
Ti	2.116	1.953	5.735	1.584	2.017	4.390	1.800	2.422	2.492	3.290	3.060	3.297	3.234
Mg	1.552	-	-	-	1.305	0.319	1.862	0.573	0.538	0.654	0.358	0.578	0.437
Fe^{2+}	8.487	9.980	13.753	9.510	8.644	12.071	7.958	9.873	9.901	10.646	10.893	10.667	10.784
Mn	0.099	-	-	0.102	0.095	-	-	-	0.077	0.075	0.102	0.145	0.143
Ca	-	-	-	-	0.025	-	-	-	-	-	0.293	-	-
$Mg/Mg + Fe^{2+}$	0.154	0.000	0.000	0.000	0.131	0.026	0.189	0.055	0.052	0.058	0.032	0.051	0.039
Cr/Cr + Al	0.113	0.000	0.000	0.046	0.029	0.000	0.115	0.000	0.000	0.000	0.000	0.048	0.000
$Fe^{3+}/Cr + Al + Fe^{3+}$	0.841	0.929	1.000	0.941	0.842	0.964	0.699	0.866	0.888	0.926	0.903	0.904	0.897
Mol % U.Sp.	27.50	24.83	71.68	20.10	26.59	54.85	24.37	31.22	31.95	42.48	43.57	42.87	42.50

Abbreviations: IC - inclusion in clinopyroxene, GM - groundmass, MP - microphenocryst, P - phenocryst, IO - inclusion in olivine, ICX - inclusion in cognate xenolith.

Rock Types: AK - ankaramite, AOB - alkali olivine basalt, A - andesite, D - dacite.

Table 3.9 Recalculated [1] Electron Microprobe Analyses of Cr-spinels from Rindjani Lavas

Analysis No.	1	2	3	4	5	6	7	8	9
Sample No.	41631	41631	41631	41631	41626	41626	41621	41631	41626
SiO_2	-	-	-	-	-	-	-	-	-
TiO_2	0.82	0.92	0.47	1.00	1.07	2.03	0.63	7.30	18.13
Al_2O_3	13.28	16.47	14.64	14.57	16.02	16.42	14.34	11.11	5.50
Cr_2O_3	51.87	48.92	55.41	44.46	45.59	37.86	52.94	31.56	22.10
Fe_2O_3	4.60	4.21	2.08	6.83	7.04	10.86	2.31	12.87	6.81
FeO	19.17	18.17	13.40	29.14	20.44	26.10	20.10	31.33	44.11
MnO	-	-	-	-	-	-	-	-	-
MgO	10.25	11.30	13.98	3.98	9.83	6.71	9.67	5.80	3.33
CaO	-	-	-	-	-	-	-	-	-
	Number of Ions on the Basis of 32 (O)								
Si	-	-	-	-	-	-	-	-	-
Al	4.078	4.954	4.356	4.654	4.882	5.111	4.397	3.565	1.838
Cr	10.680	9.866	11.050	9.520	9.314	7.903	10.885	6.792	4.954
Fe^{3+}	0.902	0.809	0.396	1.393	1.369	2.159	0.452	2.636	1.453
Ti	0.161	0.176	0.090	0.206	0.207	0.404	0.123	1.497	3.869
Mg	3.985	4.301	5.263	1.609	3.791	2.641	3.752	2.358	1.411
Fe^{2+}	4.181	3.880	2.830	6.607	4.423	5.770	4.376	7.139	10.470
Mn	-	-	-	-	-	-	-	-	-
Ca	-	-	-	-	-	-	-	-	-
Total	23.987	23.986	23.985	23.989	23.986	23.988	23.985	23.987	23.995
$Mg/Mg+Fe^{2+}$	0.488	0.526	0.650	0.196	0.461	0.314	0.462	0.248	0.119
Cr/Cr+Al	0.723	0.666	0.717	0.671	0.656	0.607	0.712	0.655	0.729
$Fe^{3+}/Cr+Al+Fe^{3+}$	0.058	0.052	0.025	0.089	0.087	0.142	0.029	0.202	0.176
Mol. % U.sp.	2.90	3.18	1.66	3.64	3.68	6.94	2.26	18.71	56.34

Notes: Cr-spinels 1, 2, 3, 7 and 8 inclusions in olivine megacrysts ≈ Fo 90-92.

Cr-spinel 4 - microphenocryst.

Cr-spinels 5, 6 and 9 inclusions in olivine megacryst ≈ Fo 86.

[1] Σ Fe determined as FeO by microprobe and recalculated to FeO and Fe_2O_3 by the method of Carmichael (1967).

Table 3.10

Representative Amphibole Analyses from Rindjani Lavas

	Fresh Amphiboles from Dacite Lavas			Fresh Cores from Reacted Amphibole from Andesites	
Analysis No.	1	2	3	4	5
Sample No.	41641	41641	41639	41645	LB41
SiO_2	41.47	42.52	43.04	40.59	39.10
Al_2O_3	10.76	10.32	10.08	13.18	15.21
FeO*	12.64	13.15	13.15	12.99	13.68
MgO	13.20	13.43	12.91	14.83	12.04
CaO	11.02	10.75	10.78	12.44	12.69
Na_2O	3.04	2.85	2.05	2.51	2.47
K_2O	0.94	0.86	0.93	0.49	0.86
TiO_2	3.34	3.11	3.86	2.09	2.34
MnO	0.27	0.33	0.17	0.13	0.00
Total	96.68	97.32	96.97	99.25	98.39
FeO	12.64	13.15	13.15	6.185	10.069
Fe_2O_3	0.00	0.00	0.00	7.563	4.013
	TETRAHEDRAL CATIONS (23 O)				
Si	6.2414	6.3467	6.4187	5.8434	5.7628
Al^{IV}	1.7586	1.6533	1.5813	2.1516	2.2372
Total	8.0000	8.0000	8.0000	8.0000	8.0000
	OCTAHEDRAL CATIONS (23 O)				
Al^{VI}	0.1506	0.1627	0.1909	0.0873	0.4057
Fe^{2+}	1.5910	1.6415	1.6401	0.7453	1.2411
Fe^{3+}	0.000	0.0000	0.000	0.8200	0.4452
Mg	2.9608	2.9875	2.8693	3.1845	2.6446
Mn	0.0344	0.0417	0.0215	0.0159	0.0000
Ti	0.3781	0.3491	0.4329	0.2265	0.2594
Total	5.1149	5.1826	5.1548	5.0795	4.9960
	M4 Site (23 O)				
Excess Oct.	0.1149	0.1826	0.1548	0.0795	0.000
Ca	1.7772	1.7193	1.7226	1.9206	2.0041
Na	0.1079	0.0981	0.1226	0.0000	0.0000
Total	2.0000	2.0000	2.0000	2.0000	2.0041
	A site (23 O)				
Na	0.7792	0.7267	0.4702	0.7012	0.7059
K	0.1805	0.1638	0.1769	0.0901	0.1017
Total	0.9597	0.8905	0.6471	0.7913	0.8676
Total Cations	15.9597	15.8905	15.6471	15.7913	15.8076
Quadrilaterals	4.03	10.95	20.93	0.00	0.00
Others	95.97	89.05	79.07	100.00	100.00
Ca	28.08	27.08	27.64	32.83	34.03
Mg	46.78	47.06	46.04	54.43	44.90
Fe	25.14	25.86	26.32	12.74	21.07
A	33.96	33.71	27.53	26.89	27.94
Al^{IV}	62.22	62.58	67.26	73.11	72.06
Na M4	3.82	3.71	5.21	0.00	0.00
BEST NAME	Mg Kaer.	Mg Kaer.	Mg Kaer.	Mg Hast.	Mg Hast.

These megacrysts include: (a) reacted, high-Al,-Ti cpx from some aluminous basalts (e.g. 41632), (b) mafic Cr-diopside in some ankaramites (e.g. LB8), (c) the remains of Ca-rich, subsilicic, aluminous amphibole in several basalts and andesites, (d) reacted olivine relicts in some andesites, (e) magnesian olivine xenocrysts with Cr-spinel inclusions from a number of *ne*-normative lavas. In addition, many andesites contain crystal-clots of essentially the same mineralogy as the phenocryst assemblage, very similar to those described by Stewart (1976). They appear to represent loosely interlocking aggregates of phenocryst minerals.

3.3 Mineral Chemistry

1. Feldspar.

Plagioclase is the modally dominant mineral of the suite and is the most abundant phenocryst and groundmass phase in most basalts and all andesites and dacites. The ankaramites are exceptional in that plagioclase phenocrysts are absent, but this phase is abundant as groundmass microlites. A few of the relatively mafic, phenocryst-poor, high-Al basalts (e.g. 41621, tables 3.1 and 3.12) have a higher proportion of olivine phenocrysts than plagioclase but again plagioclase is abundant in their groundmasses. Compositional variations of the plagioclase phenocrysts and groundmass microlites are summarised in figure 3.4 and in table 3.7.

Plagioclase exhibits the most extensive compositional variation of any mineral phase represented in the entire Rindjani suite (figure 3.4). There is a very general trend of decreasing anorthite content in plagioclases from basalt to andesite to dacite, individual phenocrysts show considerable variation from core to rim, and there are marked differences between phenocrystic and groundmass plagioclase. Furthermore there is considerable variation in composition of individual plagioclase cores from single samples of basaltic and in particular, andesitic composition.

Many andesites and basalts have plagioclase phenocrysts with very calcic cores (An85-An95), often as highly corroded, or sieved grains. These may coexist with other plagioclase phenocrysts with more sodic cores (An60-An75) (figure 3.4).

High-Al basalts have plagioclase phenocrysts with cores in the range An80-An95. These may be zoned with rims in the range An65-An75. Groundmass microlites have compositions in the range An35-An60. Occasional alkali feldspar also occurs in the groundmass of the more undersaturated high-Al basalts, generally exhibiting considerable tenary solid solution, ranging from potassic oligoclase to calcic anorthoclase (e.g. An13 Ab53.5 Or 33.5 - An 5.5 Ab 51.8 Or 42.7).

The andesites are characterised by plagioclase with highly developed zonation. However, in some cases the very calcic (An85-An90) individuals may occur as corroded unzoned isolated grains. In other instances these form corroded cores mantled by plagioclase of similar composition to that of the cores of uncorroded phenocrysts (An60-An70). These then show rhythmic, normal zonation to rims with compositions about An45. Andesites have groundmass plagioclase with compositions in the range An35-An55. The plagioclase phenocryst of the andesites may have bands which are rich in inclusions of glass (and in some cases possibly vapour) apparently representin short periods of corrosion. They may also have oscillatory zones where zonation is reversed, though overall, core-rim variations are normal.

Dacites have less complexly zoned plagioclase phenocrysts and generally encompass less compositional range. Phenocryst cores range from An45 to An60, while rim and groundmass composition are in the range An25-An38, with between 5 and 10 mol.% Or molecule. By comparison with the groundmass plagioclase of the andesites and basalts, those of the dacites show less extensive tenary solid solution, containing less Or molecule.

The compositional variations and relationships exhibited by plagioclase in the various rock types from the Rindjani Suite suggest a number of conclusions:

1. The greater extent of tenary solid solution in feldspars of the basalts and andesites (particularly those of the groundmass), compared with that shown by those of the dacites, suggests higher eruptive temperatures in the former groups, in view of the widening alkali feldspar-plagioclase solvus at lower temperatures (Carmichael et al., 1974, p.223).

2. The variability in composition of co-existing plagioclase cores from single samples of andesite or high-Al basalt (e.g. figure 3.4), together with the complex zonation of any plagioclase phenocrysts, suggests that physical conditions and/or liquid compositions were changing rapidly. Furthermore the rather abrupt change from plagioclase core compositions in the range An85-An90 to compositions in the range An60-An70 suggests an abrupt change in conditions of crystallisation. Experimental studies by Yoder (1969) and others show that the liquidus temperature of plagioclase is markedly depressed under conditions of increasing water pressure. This evidence suggests that the very anorthite-rich plagioclase may have crystallised from H_2O-bearing liquids at comparatively high pressures and that subsequent movement of this magma to lower pressures, possibly with at least partial degassing of the system, may then have resulted in the change in liquidus plagioclase composition to that of the more sodic cores (An60-An70). This would also result in partial resorption or corrosio of earlier anorthitic plagioclase as observed. This process is also suggested by the implausibly high temperatures calculated using the plagioclase geothermometer of Mathez (1976) on the basis of a "dry" system and anorthite-rich plagioclase core-bulk rock equilibrium (table 3.11). This feature has also been noted in other island arc suites (e.g. Rabaul Caldera, New Britain; Heming, 1977).

Table 3.11

Some Temperatures Yielded by Plagioclase and Cpx-Opx Geothermometry From Rindjani Andesites and Dacites (^{o}C)

ROCK TYPE	SAMPLE NUMBER	1	2	3	4
ANDESITE	41647		1185-1149	986-889	1018-974
	41644	1105	1104	825-758	
	41636	1052	988	772	1005-1027
	41672	1048			
DACITE	41650	1019	1051	758	
	41645				896
	41641	964	1184-1152	942-910	

Notes: Column 1 gives temperatures approximating those of the liquidus using the formulation of Mathez (1976, for plagioclase phenocryst core - bulk rock equilibria at PH_2O = 1.0 kbar.

Column 2 gives temperatures approximating the dry quench temperature again using the Mathez (1976) plagioclase geothermometer and coexisting groundmass or microphenocryst plagioclase compositions and glass analyses.

Column 3 is as for column 2 except that Mathez (1976) PH_2O = 1.0 kbar expression is used.

Column 4 uses coexisting cpx and opx microphenocryst compositions and the geothermometer of Wood and Banno (1973).

2. Pyroxene.

Pyroxene compositional variations are summarised in figure 3.3 and representative analyses are given in tables 3.2 and 3.5.

Ca-rich clinopyroxene is an important phenocryst phase in most basalts and occurs in all andesites and dacites. Some more mafic high-Al, alkali olivine basalts (e.g. 41621) which have only a few phenocrysts, are exceptional in that cpx is rare or absent as a phenocryst phase. In these, olivine is the principalphenocryst, while olivine and cpx co-exist in the groundmass. The low alumina, magnesian, ankaramites contain abundant cpx as the major phenocryst phase.

Clinopyroxenes represented in the Rindjani lavas fall into three groups:

1. Low-Al, low-Ti, magnesian, Cr-diopside occurring as megacrysts in the ankaramite lavas (table 3.2, figure 3.3A).
2. Aluminous, Ti-rich salite or Ca-rich augite with variable Cr, occurring as phenocrysts and megacrysts in the high-Al alkali olivine basalts and as rims to Cr-diopside megacrysts in ankaramite lavas (table 3.3, figure 3.3B).
3. Low-Al, low-Ti, Cr-free augite from the quartz-normative andesites and dacites (table 3.4, figure 3.3C).

The compositional range of cpx from the andesites and dacites is very limited, particularly in terms of Mg/Mg+Fe variation (0.70-0.75). This feature has been described from a number of other andesite suites; for instance from lavas of the Rabaul Caldera (Heming, 1977) and those of the Medicine Lake volcano (Mertzmann, 1977). The cpx of the andesites and dacites show most variation in Ca-content, rims becoming more Ca-poor with only slight decrease in Mg/Mg+Fe value (fig. 3.3C).

By comparison with the cpx of high-Al lavas with <53% SiO_2, those of the andesites and dacites are markedly less Al-rich (generally between 1.5 and 3.0 wt.% Al_2O_3, tables 3.3, 3.4) and are slightly less Ti-rich. They show no consistent core-rim variation with respect to these elements.

In contrast to clinopyroxene of the andesites and dacites (Q-normative lavas), the cpx of the alkali- and sub-alkali olivine basalts and associated lavas with <53% SiO_2, are markedly more aluminous (3-6 wt% Al_2O_3) and Ti-rich (>0.4 wt% TiO_2). They show considerable variation in Mg/Mg+Fe ratio, showing a decrease in this value from core to rim to groundmass and marked variation between different rocks in the general group (fig. 3.3B). They show a general trend of increasing Al and Ti and decreasing Si from core to rim.

Al and Ti substitution in the clinopyroxene lattice is a function of both silica activity of the liquid and pressure. Le Bas (1962) suggested that increasing Al in Ca-rich clinopyroxene was favoured by decreasing silica concentration in the host magma. Such a substitution is illustrated by the following reaction (e.g. Carmichael et al., 1974):

$$Ca\ Al_2\ SiO_6 + SiO_2 = Ca\ Al_2\ Si_2\ O_8$$

Ca-Tschermak anorthite

Pyroxene component

Furthermore, Yagi and Onuma (1967) postulate a pyroxene component - $Ca\ Ti\ Al_2O_6$, suggesting that Ti substitution into the Y-site is favoured by, and coupled to, Al substitution in the Z suite.

Le Bas (1962) and Kushiro (1960) suggest that increasing pressure will favour the increasing incorporation of Al into the Y site as Al^{VI} and will result in an increase in the Al^{VI}/Al^{IV} ratio.

Thus there are two interdependent effects which determine the Al and Ti content of cpx. Low silica activity favours the coupled substitution of Ti in the Y site and Al^{IV} in the Z site, as a Ca Ti Al_2 Si O_6 molecule, with a theoretical atomic Ti/Al ratio of 0.5. Increasing pressure favours the substitution of Al^{VI} in the Y site forming a Ca Al Al SiO_6 molecule.

The lower Al and Ti content of the cpx of the quartz-normative andesites and dacites compared with that of the cpx from the high-Al basaltic lavas (<53% SiO_2), and in particular those which are *ne*-normative appears to illustrate the effect of silica activity mentioned above. However Ti/Al ratios are considerably lower than 0.5 in both groups of pyroxenes, suggesting that the substitution diverges considerably from that predicted by Yagi & Onumas' (ibid) Ca Ti Al_2 O_6 molecule.

The other significant contrast between the cpx of the basaltic lavas and that of the andesites and dacites is the tendency for the basaltic pyroxenes to show considerable variation in Mg/Mg+Fe ratio, whereas that of the andesitic and dacitic pyroxenes remains constant while at the same time, the andesitic and dacitic pyroxenes become markedly less calcium-rich. These features suggest that the clinopyroxenes of the andesite-dacite group are reflecting the rather limited range in Mg/Mg+Fe ratios of these liquids and at the same time reflecting the trend of calcium depletion with advancing differentiation towards the most silicic dacite compositions. On the other hand the cpx of the basaltic lavas appear to reflect the rapidly changing Mg/Mg+Fe ratios in this group of lavas.

The alkali olivine basalt group also contain some slightly reacted clinopyroxene megacrysts, with relatively high Cr, Al and Ti contents (e.g. anal. 10, 13, table 3.3). These are quite similar to megacrysts

reported from a number of alkali basalt suites (e.g. Binns, 1969) and to some Al-rich augites occurring in wehrlite and pyroxenite nodules associated with these lavas (e.g. Becker, 1977). They differ from the associated phenocrystic and groundmass clinopyroxene mainly in their high Cr, high Al and slightly higher Al^{VI}/Al^{IV} ratio (>0.5 compared with 0.4 or less in the phenocryst and groundmass group). Some also have markedly higher Mg/Mg+Fe values (e.g. anal. 15 table 3.3). As previously discussed, Le Bas (1962) suggested that increasing pressure will favour the incorporation of Al into the Y site as Al^{VI} and will result in an increased Al^{VI}/Al^{IV} ratio. Aoki and Kushiro (1968) distinguished fields of phenocrystic igneous clinopyroxene and of clinopyroxene from inclusions in basaltic rocks (higher pressure) on this basis. Clinopyroxene similar to these megacrysts has been described from other island arc suites, for instance by Lewis (1973) in xenoliths erupted from St. Vincent volcano in the Lesser Antilles and by Arculus and Curran (1972) as xenocrysts in the lava of the same volcano.

The clinopyroxenes of the ankaramites are zoned grains up to 1cm long. They comprise a pale green core which is essentially unzoned, mantled by a wide, darker green rim. The cores of these clinopyroxenes are remarkably mafic, Cr-diopside (anal. 1, 4 table 3.2 and fig. 3.3A). They have very low Al (sometimes <1.0% Al_2O_3), Ti and Fe and high Cr and Mg, with Mg/Mg+Fe values as high as .92. These cores are rimmed by more Al-, Ti-rich augite, with Mg/Mg+Fe values of about .76 (table 3.2), essentially the same as those phenocrysts from the alkali olivine basalts. Compared with cpx phenocrysts and megacrysts from basaltic lavas these Cr-diopsides are far less aluminous, have negligible Na content, much lower Ti, higher Ca and higher Mg/Mg+Fe values. Compared with clinopyroxene from lherzolite xenoliths (e.g. Varne, 1977; Frey and Green, 1974) they are also depleted in Al and Na and are more Ca-rich. They

are not unlike the Cr-diopside of refractory harzburgite and dunite from high temperature, alpine-type peridotite bodies (e.g. Lizard, Green, 1964; Burro Mt., California, Loney et al., 1971, p. 291, table 7). They also resemble cpx synthesised during large degrees of melting of pyrolite at relatively low pressures (e.g. Green, 1973, table 3). Under these conditions (10 kbars., 1100°C, water saturated), Green (1973) found 28% partial melting of pyrolite, with olivine (Fo89) and Cr-diopside (Mg/Mg+Fe = .904) as residual phases. The ankaramites from Lombok also contain megacrysts of olivine, as magnesian as Fo 88.3. These relationships may suggest that these lavas sampled a refractory mantle zone at quite shallow depths (35 kms.?), the Cr-diopside representing a residual phase of a prior melting event.

Orthopyroxene (table 3.5) occurs in andesites and dacites with SiO_2 > 53%, both as phenocrysts and in the groundmass, again showing relatively restricted compositional variation (En 72-65) reflecting the limited iron enrichment of the andesite and dacite group (fig. 3.3C). Occasionally orthopyroxene phenocrysts are rimmed by clinopyroxene, suggesting that orthopyroxene crystallised first, in accordance with experimentally determined phase relationships determined for the Paracutin and Mt. Hood andesites, at low pressures (Eggler and Burnham, 1973).

3. Olivine.

Olivine occurs as fresh phenocrysts in most lavas with <53% SiO_2 and also in the groundmass of most *ne*-normative lavas. A few andesites lack orthopyroxene but contain fresh olivine phenocrysts. These may have embayed texture (e.g. 41644, tables 3.1, 3.6). Olivine compositional variation is summarised in figure 3.3 and representative analyses given in table 3.6.

The basalts with <53% SiO_2, excluding the ankaramites, contain abundant olivine and relatively scarce clinopyroxene. The proportion of olivine increases as the lavas become less phenocryst-rich (compare 41621 with 41632 in table 3.1), suggesting that olivine is the liquidus phase in this group. Many of the alkali olivine basalts contain olivines of a wide range of compositions, suggesting that fractional crystallisation of olivine may have been an important process. Olivine phenocrysts in these lavas range from Fo70 to Fo82, while they also contain xenocrysts which are often strained and partly resorbed, ranging in composition from Fo85 to Fo93. Such magnesian olivines have been described from basic members of a number of calcalkaline suites, for example, from Mt. Shasta (Anderson, 1974). On the basis of these very magnesian olivine compositions and the chemistry of associated trapped glasses, Anderson (1974) inferred that the basalts and andesites were derived from a hydrous picritic magma.

The Fe^{2+}-Mg distribution between olivine and liquid has been determined as K_D^* = 0.3 (Roeder and Emslie, 1970). On this basis, the range of olivine xenocryst compositions (Fo85-93) suggests $Mg/Mg+Fe^{2+}$ values of the co-existing liquids in the range 0.64-0.80, while the phenocrysts (Fo70-82) suggest a range of $Mg/Mg+Fe^{2+}$ values of between 0.41 and 0.8. These values are generally in accord with the observed whole-rock (≃ liquid?) $Mg/Mg+Fe^{2+}$ values assuming Fe^{2+} to be 0.85 of total Fe, suggesting this adopted Fe^{2+}/Fe^{3+} ratio to be appropriate and also suggesting that xenocrysts even as magnesian as Fo93, need not be the result of crystallisation from highly oxidised liquids, a conclusion which is also corroborated by the relatively low calculated Fe^{3+} content of

* $K_D = (Fe^{2+}/Mg)ol(Fe^{2+}/Mg)\ liq.$

included Cr-spinels (table 9.9). The olivine xenocrysts are as magnesian, (or in some instances more magnesian), as olivines from peridotite inclusions in basaltic rocks (e.g. Varne, 1977 table 3; Frey and Green, 1974, table 3), however they are invariably more Ca-rich than these (>0.1% CaO). Simkin and Smith (1970) showed that olivine from volcanic rocks has >0.1% CaO, while those of intrusive rocks and xenoliths have <0.1% CaO, which suggests that these olivine xenocrysts must have crystallised from a mafic lava, rather than representing accidental inclusions from a source peridotite.

4. Amphibole.

Microprobe analyses have been recalculated using the routines of Papike et al. (1974), to estimate the Fe^{3+} content and to classify the amphiboles on the basis of "other than quadrilateral" components (table 3.10). Amphibole compositional variation is summarised in figures 3.5 and 3.3D, and representative analyses given in table 3.10.

Amphiboles fall into two distinct groups: reacted and fresh.

1. Reacted amphiboles occur in andesites and very rarely, in basalts (e.g. LB65) and in some samples (e.g. basalt 41683) are completely reduced to magnetite-plagioclase-clinopyroxene pseudomorphs.

2. Fresh amphiboles in the dacites are late microphenocrysts. They occasionally include earlier plagioclase and pyroxene. Amphibole occurs as needle-like groundmass microlites.

The amphiboles are all members of the general hornblende group; kaersutite, Mg-hastingsite, pargasite. The amphiboles from the basalts and andesites are markedly more Ca- and Al-rich than those of the dacites (table 3.10). They also have slightly lower Na_2O, K_2O, and TiO_2 and slightly higher Mg/Mg+Fe values. They have particularly low silica

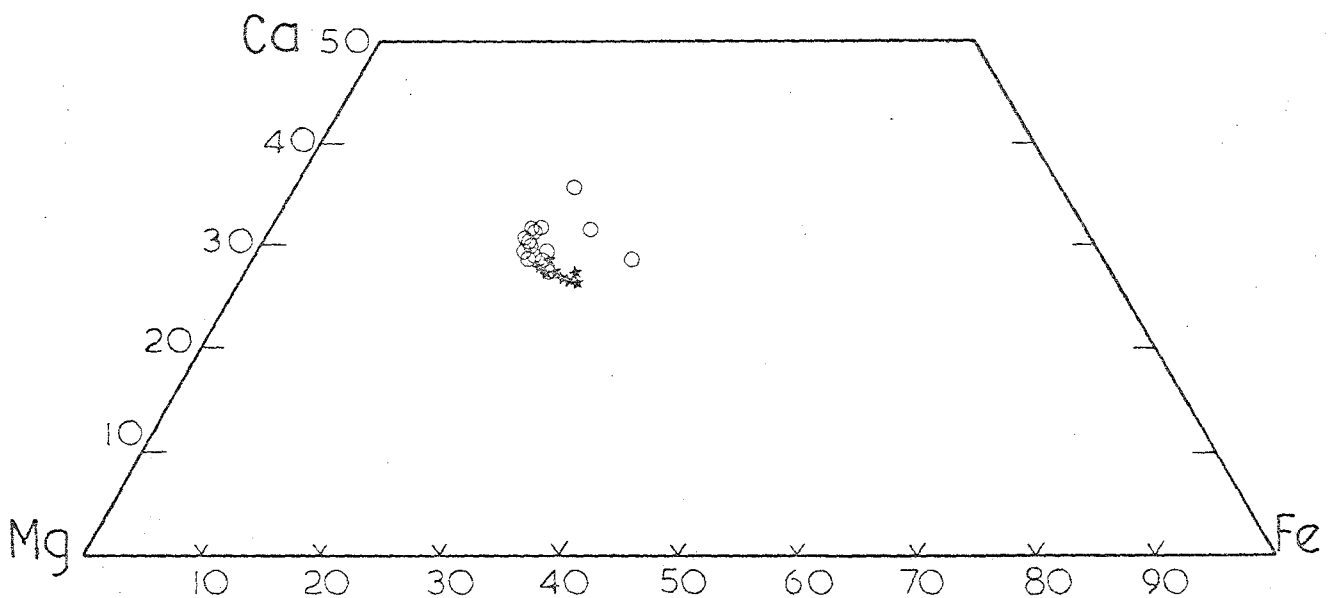

Figure 3.5

Compositions of amphiboles in Rindjani lavas. Open circles - amphibole from andesite and basalt lavas (generally partially reacted), stars - fresh amhibole from dacites.

contents (ca. 40 wt%). K_2O/Na_2O ratios of the amphiboles from the andesites are generally in the range 0.2-0.25 and are similar or slightly lower than the ratios of these lavas. K_2O/Na_2O ratios of amphiboles from the dacites are about 0.30 and are very markedly lower than those of the liquid.

5. Spinel.

Spinels in the Rindjani suite fall into two groups:

1. Al-rich, Cr-spinels occurring as inclusions in magnesian olivine xenocrysts in some of the aluminous basalts (table 3.9).
2. Ti-rich magnetite occurring as phenocryst and groundmass grains in basaltic andesite, andesite and dacite, and in the groundmass of mo basalts, but less commonly as phenocrysts (table 3.8).

Analyses of representative examples of both groups of spinel are presented in tables 3.8 and 3.9, and compositional trends are summarised in figure 3.6. Cr-spinel occurs only as small brown euhedral inclusions in olivine megacrysts.

In terms of their Cr/Cr+Al, Fe^{3+}/Fe^{3+}+Al+Cr and Mg/Mg+Fe^{2+} values (fig. 3.6) they plot in the field of spinels from stratiform intrusions, are like chromites of some high temperature peridotites and are also quite like the liquidus spinel from the Kilauea pumice, Hawaii (Evans and Wright, 1972). They show a trend of decreasing Cr/Cr+Al with decreasing Mg/Mg+Fe^{2+} values, like that of the Stillwater chromites (Jackson, 1969). (Marked variation in $\ln K_D$ ($K_D = \frac{(X\ Mg^{ol})\ (X\ Fe^{2+Sp})}{(X\ Fe^{2+ol})\ (X\ Mg^{Sp})}$) for the Fe^{2+}-Mg distribution between Cr-spinel and enclosing olivine is possibly suggestive of a significant decrease in temperature accompanying Cr and Mg depletion, a situation suggestive of fractional crystallisation.)

FIGURE 3. 6

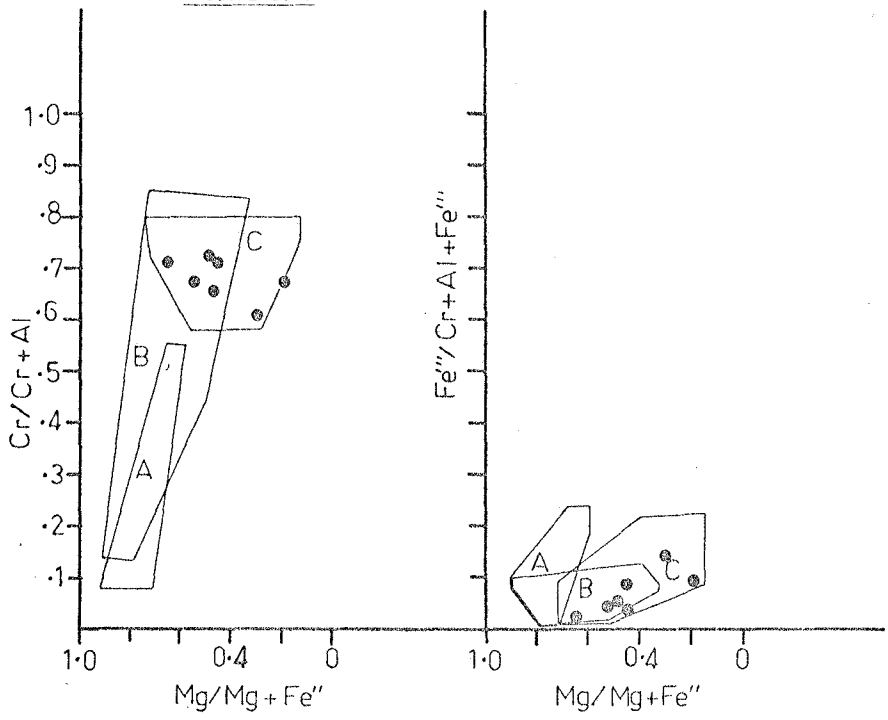

COMPOSITION OF Cr-SPINELS OCCURING AS INCLUSIONS IN MAGNESIAN OLIVINE XENOCRYSTS FROM RINDJANI NE-NORMATIVE HIGH-Al BASALTS. Fe^{3+} VALUES ARE RECALCULATED FROM MICROPROBE ANALYSES (FeO) BY THE METHOD OF CARMICHAEL (1967). FIELDS INDICATED ARE FROM IRVINE (1967) AND IRVINE AND FINDLAY (1972).

A- SPINEL FROM ULTRAMAFIC NODULES
B- SPINEL FROM ALPINE PERIDOTITES
C- SPINEL FROM LAYERED INTRUSIONS

Titan magnetite ranges in composition from about 25-50 mol.% ulvospinel, groundmass magnetites tending to have higher contents of Usp. component than co-existing phenocrysts from the same lava. Ewart (1976) also noted this feature from a suite of Tongan andesites. There is also a general trend of decreasing Mg and Al content of magnetites through the series; basalt-andesite dacite.

3.4 Geochemistry of the Rindjani Calcalkaline Suite.

Analyses of the Rindjani lavas are given in tables 3.12 - 3.18 C.I.P.W. norms, calculated according to the method of Kelsey (1963) are listed in appendix 2.

Major oxide and trace element characteristics of the Rindjani lavas are presented in figures 3.7 - 3.10, as MgO- and SiO_2- variation diagrams. A most striking feature is the extreme compositional diversity of the suite. Lavas range from *ne*-normative, mafic ankaramite, such as LB8 (table 3.12) with 48.3% SiO_2 and 14% MgO, through to silica-rich, *Q*-normativ dacites such as 41639 (table 3.18), which has 68% SiO_2 and 0.7% MgO.

The normative compositional variation is illustrated on the plot of normative *ne-ol-di-hy-Q* (figure 3.11). Lavas range from critically undersaturated to *ol-hy*-normative to *Q*-normative, passing right across the low pressure thermal divide (Yoder and Tilley, 1962). This type of compositional variation has been noted from the Lesser Antilles (e.g. Arculus, 1976) and other island arc suites and places some constraint on likely fractional crystallisation models (i.e. requires the bulk fractionate to be *ne*-normative).

On the A-M-F diagram (figure 3.12), the Rindjani suite shows an Fe-enrichment trend, between the tholeiitic Tongan- (Ewart et al., 1973) and the calcalkaline, Cascade-trends (Carmichael, 1964) and is very like that of the Aleutians (Marsh, 1976).

The geochemical variation of the Rindjani suite is considered in terms of six general groups of rocks, largely corresponding with those already outlined on petrographic grounds.

1. The ankaramites which are *ne*-normative, have low Al_2O_3 (<16%), low SiO_2 (<50%) and high MgO (>7%).
2. High-Al basalts - characterised by high Al_2O_3 (>17%), low to moderate MgO (3-6%) and which encompass both *ne*-and *ol-hy*-normative types.
3. Andesites (type 1) - characterised by relatively low K_2O (<2%), are quartz-normative, have SiO_2 concentrations in the range 53-60%, relatively low K_2O/Na_2O ratios (generally <0.4), are aluminous (>18% Al_2O_3) and have Sr concentrations <500ppm.
4. High-K_2O, high-Sr andesites (type 2). These are distinguished from the type 1 (low K_2O) andesites by their relatively high K_2O (>2%) and high Sr concentrations (500-750 ppm).
5. High-K_2O andesites (type 3) - characterised by high K_2O (generally >3%), low Sr (<400ppm) and high K_2O/Na_2O ratios (generally >0.5). They are petrographically and geochemically similar to the dacites.
6. Dacites - characterised by their silica content (>62%) and generally have low Al_2O_3, Sr, CaO, higher K_2O and higher K_2O/Na_2O ratios than the andesites.

Considering the general overall compositional variation exhibited by the complete range of rock types represented in the Rindjani suite, as illustrated by the MgO- and SiO_2-variation diagrams (figures 3.7 - 3.10), a number of factors come to light. In particular, many elements show two distinct trends, the high-Al basalt group representing the intersection of these.

Thus the ankaramite-high-Al basalt variation involves marked depletion of MgO, Ni and Cr and to a lesser extent CaO and Sc, while total Fe content remains constant and K_2O, SiO_2, Na_2O, Rb, Sr, Zr, Nb and Y show only slight

FIGURE 3.7

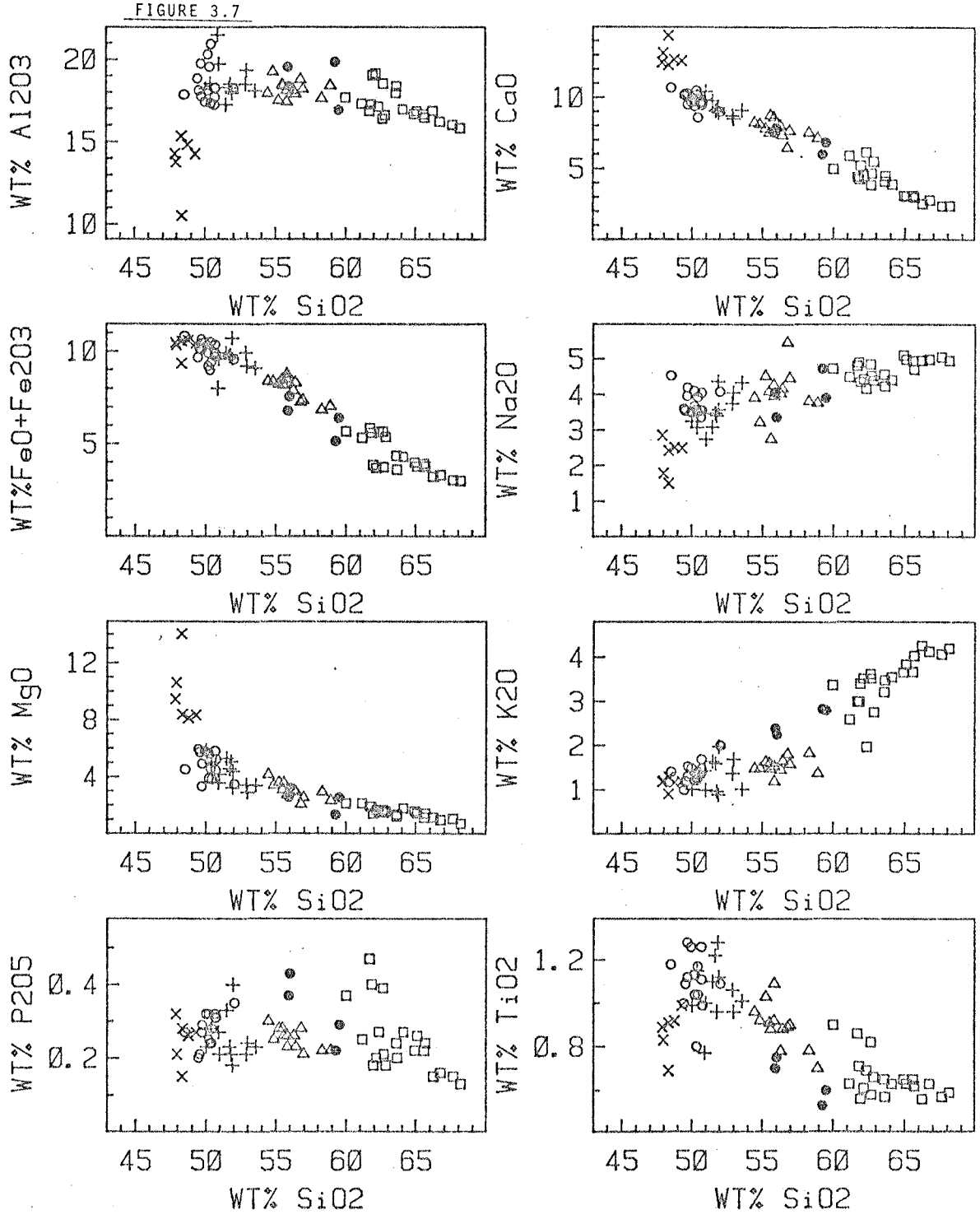

Figure 3.7

SiO_2 v. major element variation of Rindjani lavas. x - ankaramite, ○- ne-normative high-Al basalt, + - ol-hy-normative high-Al basalt, △- andesites, ◍- high-K,high-Sr andesite , □ - high-K andesite and dacite.

FIGURE 3.8

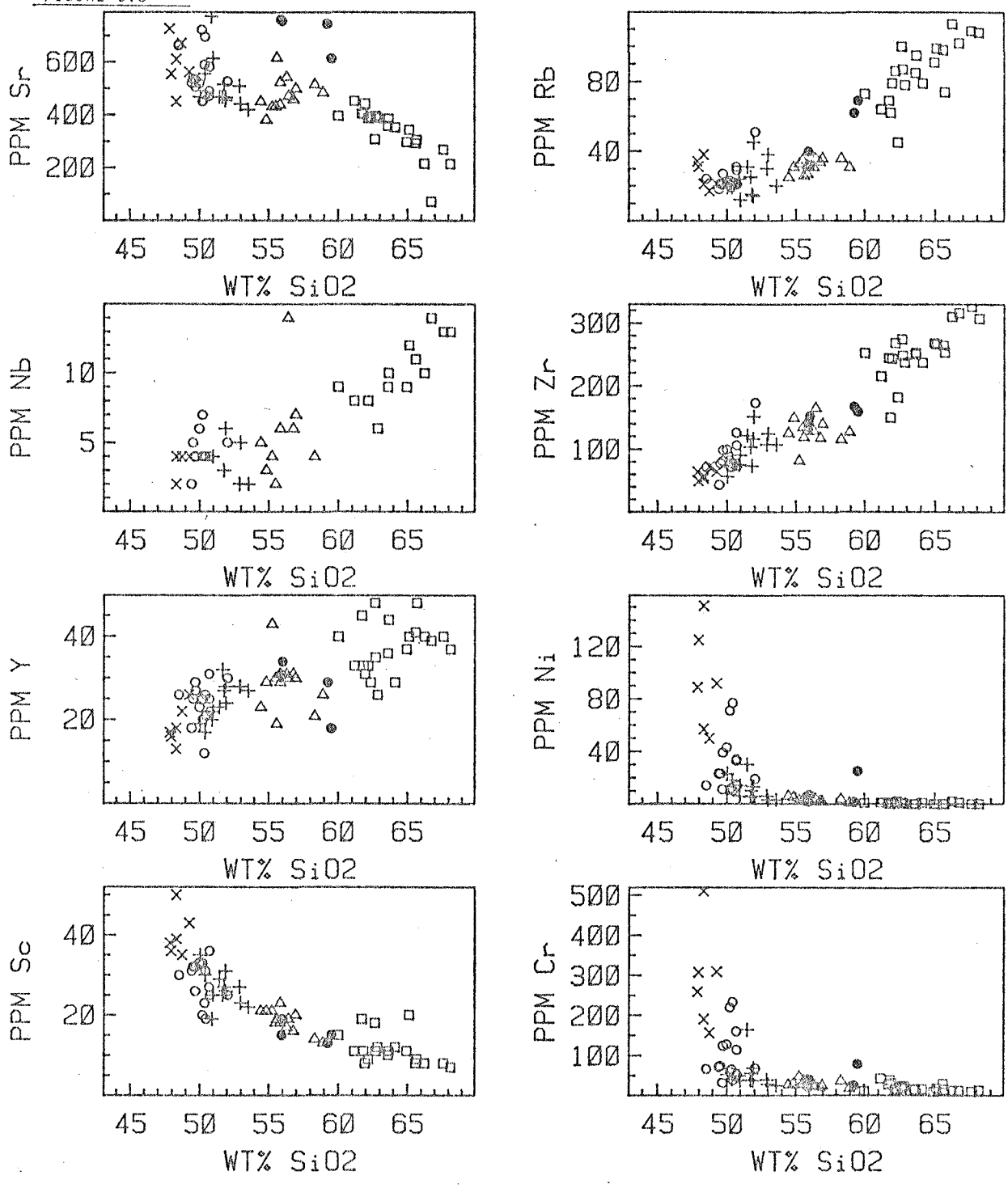

Figure 3.8

SiO_2 v. trace element variation of Rindjani lavas. Symbols are the same as those in figure 3.7.

FIGURE 3.9

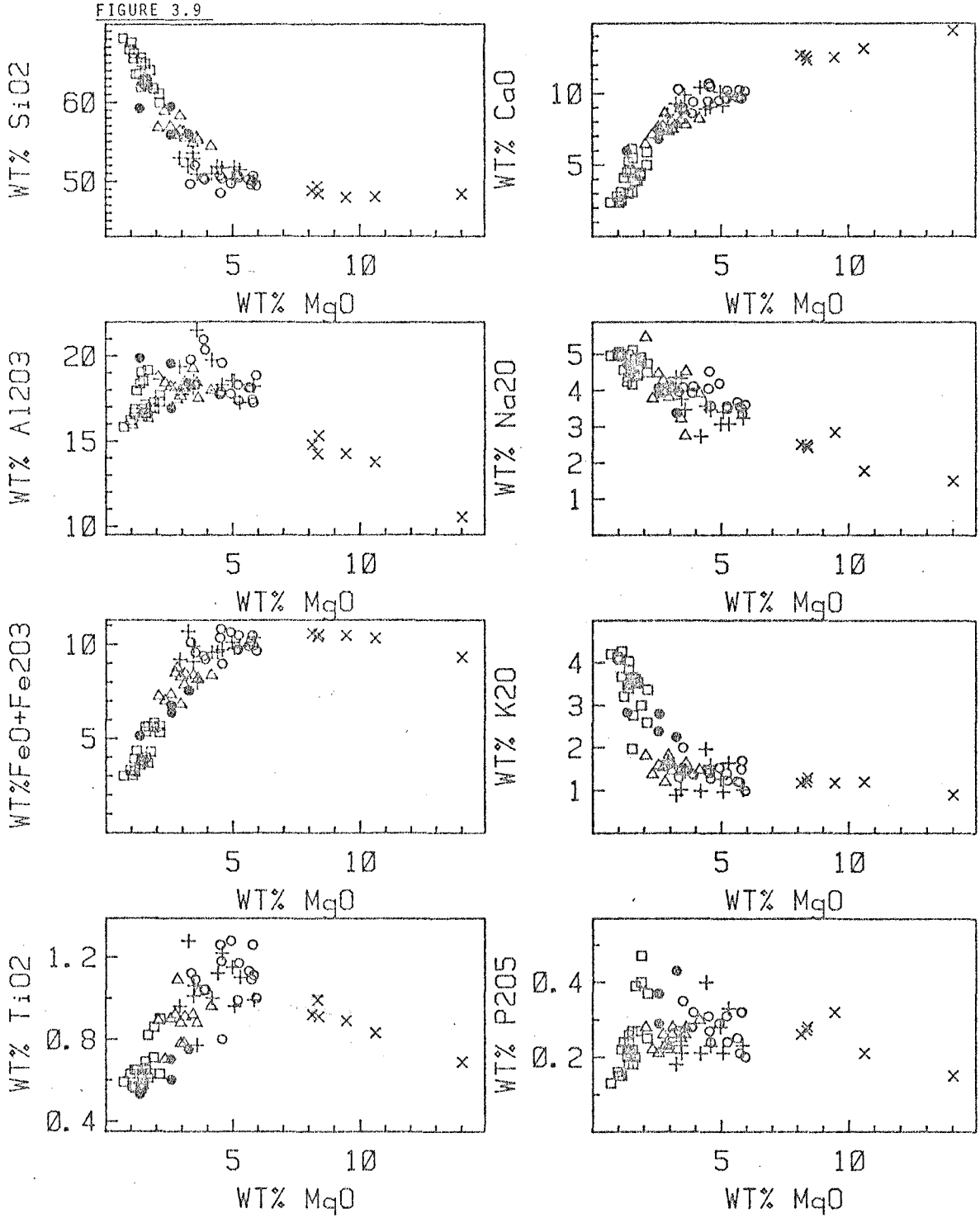

Figure 3.9

MgO v. major element variation of Rindjani lavas. Symbols are the same as those in figure 3.7.

FIGURE 3.10

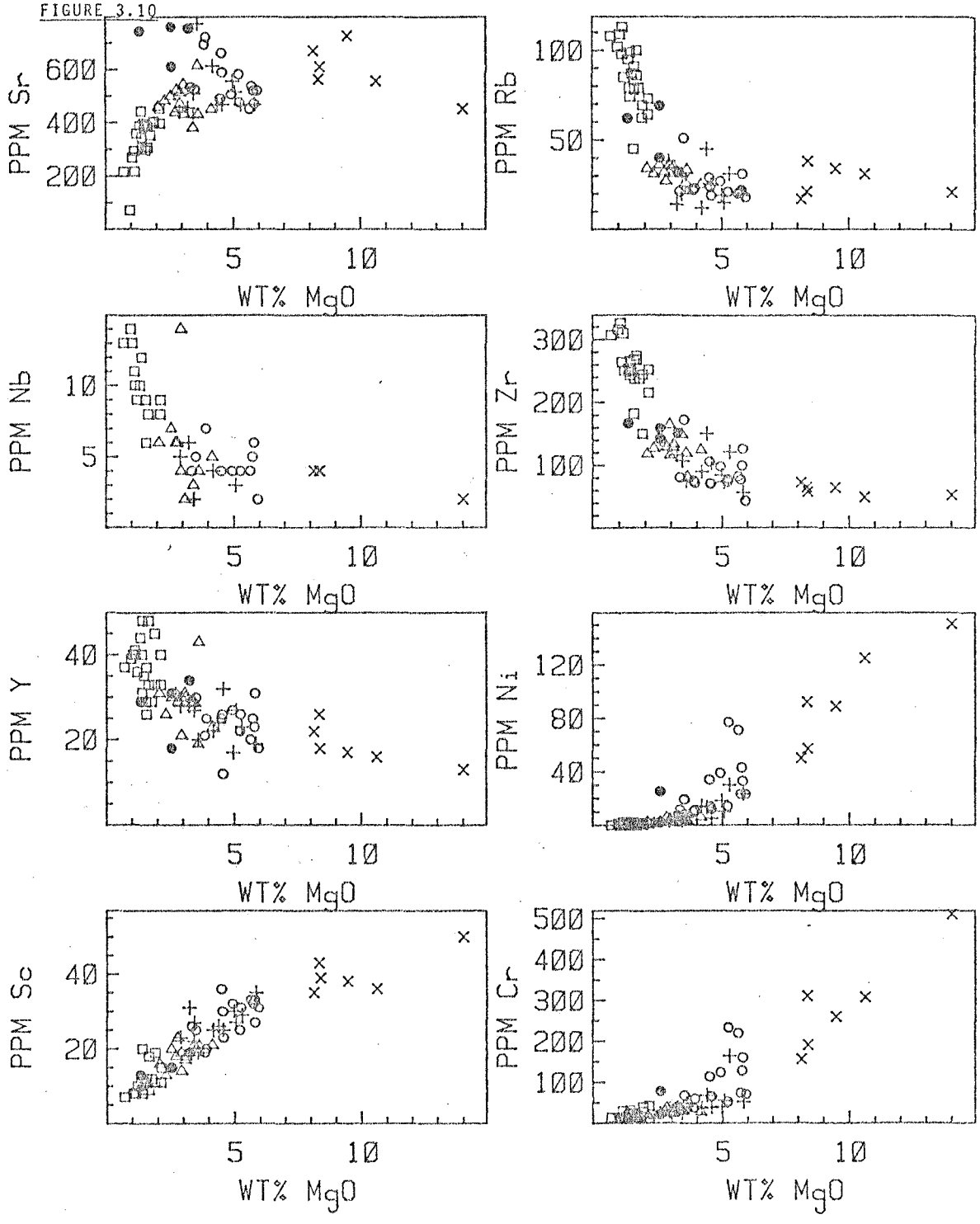

Figure 3.10

MgO v. trace element variation of Rindjani lavas. Symbols are the same as those in figure 3.7.

enrichment. This segment of the total compositional variation of the whole suite involes 80%of the MgO-variation and only 25% of the SiO_2 variation. On the other hand, the high-Al basalt-andesite-dacite trend involves much larger scale variation (enrichment) of SiO_2, K_2O, Rb, Zr, Nb and Na_2O and only 20% of the variation of MgO, which like CaO, total Fe, TiO_2, Ni, Cr and Sc is continuously depleted.

These same contrasts in geochemical variation are also illustrated in the A-M-F diagram (figure 3.12), where again the high-Al basalt group form the intersection of the two distinct trends. Here the ankaramite-high-Al basalt trend is one of relative Fe-enrichment, while the high-Al basalt-dacite trend is the familiar calcalkaline one, with marked total alkali-enrichment at almost constant Fe/Mg ratio.

1. Ankaramites.

These are ne-normative lavas characterised by low SiO_2, Al_2O_3, Na_2O, TiO_2 and Zr and high MgO, Ni, Cr, CaO and Sc. $Mg/Mg+Fe^{2+}$ values (0.62-0.75) are markedly higher than those of the other basaltic volcanics from Rindjani. They are very rich in normative diopside (26-40%). LB8 (table 3.12) in particular has very abundant cpx megacrysts which may have been accumulated at least in part, accounting for its very high CaO (14.38%) content and low Al_2O_3 (10.53%). Other lavas of this group are nearly aphyric (e.g. LB11) yet still have the high-CaO, MgO, Ca, Sc and Ni and low Al_2O_3 contents characteristic of the group as a whole, suggesting some members of the group are liquids.

Compared with the more aluminous basalts, the ankaramites have relatively high Sr concentrations (452-726ppm). They also have higher K_2O/Na_2O ratios (figure 3.12) and lower K/Rb ratios (figure 3.14). The ankaramites have phenocryst assemblages dominated by cpx with less abundant olivine and very minor plagioclase. Their compositional

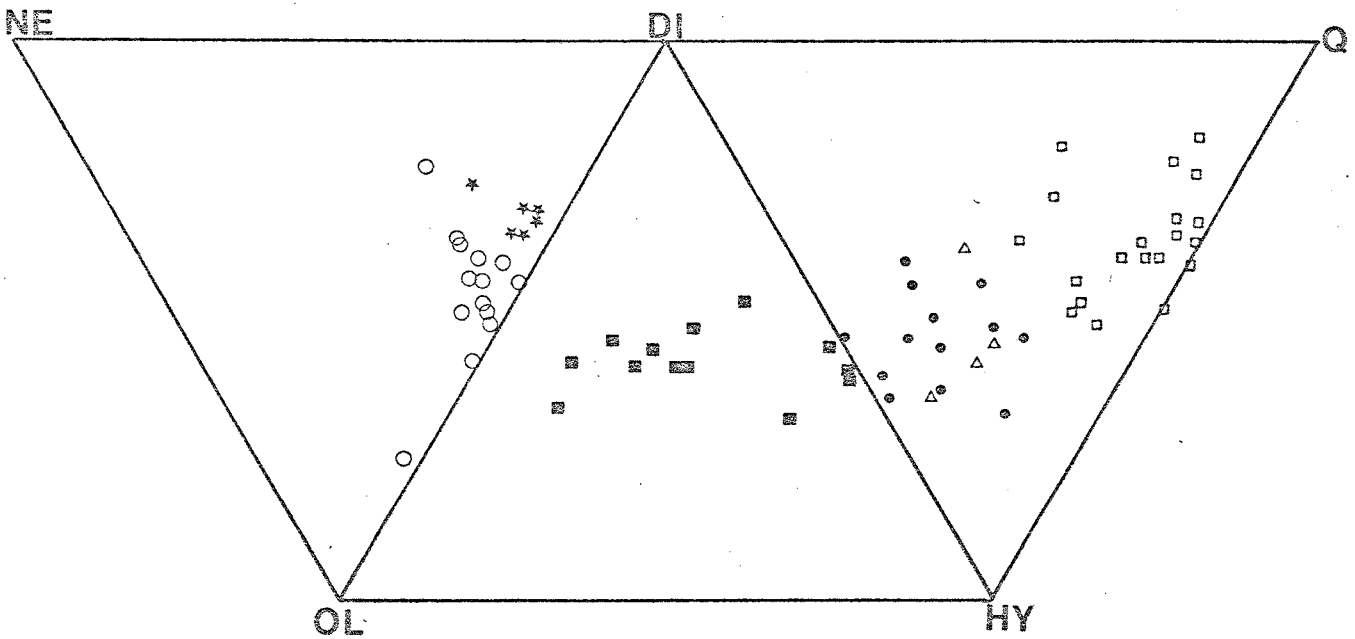

Figure 3.11

Normative ne - di - ol - hy - Q variation of the Rindjani suite. Stars- ankaramites, open circles - ne-normative high-Al basalts,filled squares - ol- hy -normative high-Al basalts, filled spots- andesites, open triangles - high-K,high-Sr andesites,open triangles - dacites and high-K andesites.

variations are consistent with fractionation (and perhaps in part, accumulation) of this cpx dominated assemblage. In particular they show trends of increasing Al_2O_3 with decreasing CaO (figure 3.15), increasing Sr with decreasing CaO (figure 3.16), decreasing CaO and MgO (figure 3.9) and relatively invariant SiO_2 suggesting cpx removal with little, if any, plagioclase involvement. Marked depletion of Ni with decreasing MgO suggests some olivine may also have been removed.

2. High-Al Basalts.

The high-Al basalt group (Al_2O_3 = 17-21 wt.%) (table 3.12-3.15) is characterised by Mg/Mg+Fe values that are markedly lower than those of the ankaramites but range from markedly higher values than those of the more silica-rich andesites, to values lower than those of some andesites (0.55-0.37).

High-Al basalts include groups both of *ne*- and of *ol-hy*-normative lavas (figure 3.11). The compositional distinction between these two groups is gradational, and the relatively MgO-rich (>5% MgO) high-Al basalts include both *ne*- and *ol-hy*-normative types. Members of both groups range from these more mafic lavas with between 48 and 50% SiO_2, up to 77ppm Ni, 230ppm Cr and 36ppm Sc and Mg/Mg+Fe values of about 0.57, to differentiated lavas with 52-53% SiO_2, 3% MgO, 50ppm Cr, about 10ppm Ni and Mg/Mg+Fe values of about 0.41.

The main distinction between the *ne*- and *ol-hy*-normative series is in their K_2O and Na_2O contents. Thus as illustrated by plots of K_2O v SiO_2 and K_2O+Na_2O v SiO_2 (figures 3.2 and 3.17), the *ne*-normative group tend to have higher K_2O and K_2O+Na_2O values at given SiO_2 concentrations than the *ol-hy*-normative group. In fact the more differentiated members of the former group tend to have higher K_2O concentrations than more siliceous and possibly more differentiated andesites. Thus at least with respect to these parameters, there is a marked divergence of trends originating

FIGURE 3.12

A-M-F variation Rindjani lavas.

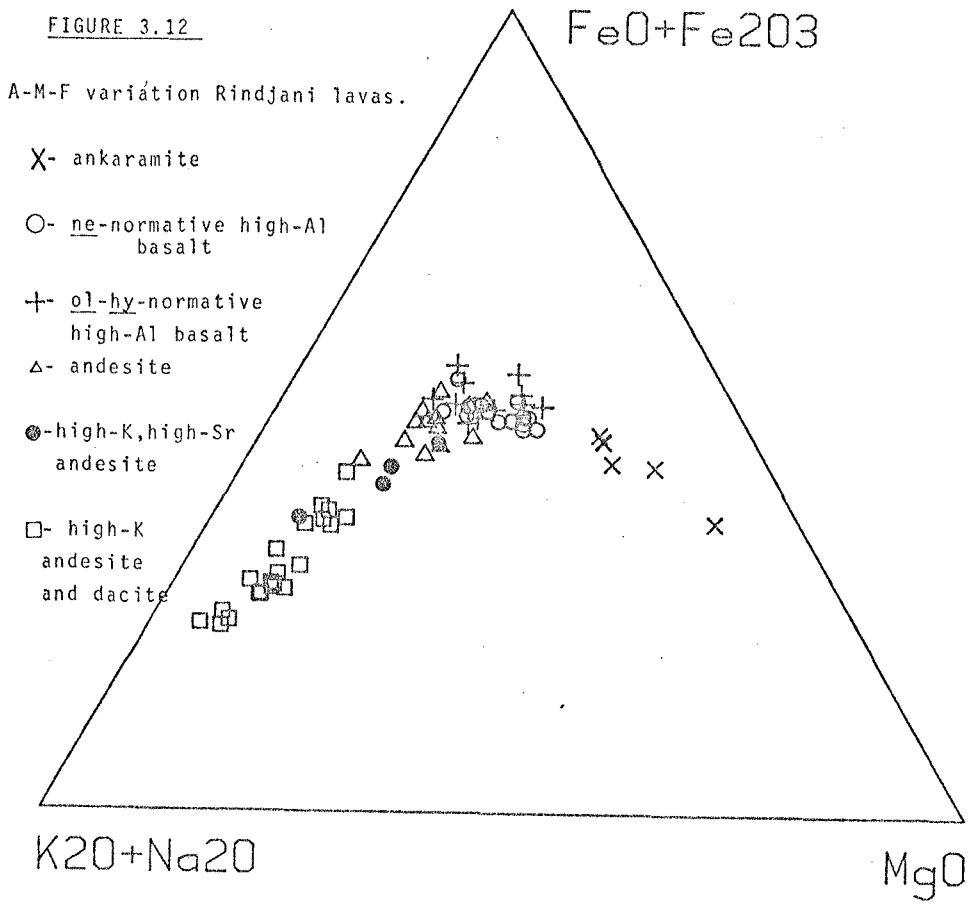

from the more mafic high-Al basalt field, the *ne*-normative group tending to show more marked alkali-enrichment and possibly less tendancy towards silica enrichment. The *ol-hy*-normative group on the other hand, have variable but generally lower K_2O and K_2O+Na_2O concentrations at given silica values, and some members of this group define a flat trend of limited enrichment of these with increasing SiO_2, colinear with the andesite trend.

On the grounds of the above observations it appears that there is some possibility that the more mafic high-Al basalts are fractionating to yield differentiates of two distinctly different types: 1. *ne*-normative, low MgO, K_2O- and total alkali-enriched, "hawaiite"-like lavas, such as 41678 (table 3.14) and 2. *ol-hy*-normative, more silica- and less K_2O- and total alkali-enriched basaltic andesites, such as 41634 (table 3.15). The first trend seems unlikely to yield andesite and is possibly like the trend shown by the Tambora trachybasalts (chapter 4) which may be differentiating to yield the associated *ne*-normative trachyandesites. The second trend may possibly yield the Rindjani andesites, which themselves show marked silica enrichment with relatively slight alkali enrichment.

Compared to the ankaramites, the high-Al basalts have slightly lower CaO contents (in the range 10.5-8.5%) and have similar total Fe contents. Like the ankaramites they show a general trend of CaO depletion with decreasing MgO (fig. 3.9). However, total Fe also shows a trend of depletion with decreasing MgO, whereas the ankaramites show constant or even slight enrichment of total Fe with MgO depletion. As a general group the high-Al basalts also show marked depletion of Ni and Cr with decreasing MgO and slightly less rapid depletion of Sc.

The high-Al basalts are the most TiO_2-rich of all the Rindjani lavas, concentrations mostly falling in the range 1.0-1.2%. Considering the TiO_2-MgO variation (figure 3.9), there is some suggestion

FIGURE 3.13

K_2O/Na_2O variation in Rindjani lavas.

X- ankaramite

○- ne-normative high-Al basalt

■- ol-hy-normative high-Al basalt

△- andesite

●- high-K,high-Sr andesite

□- high-K andesite and dacite.

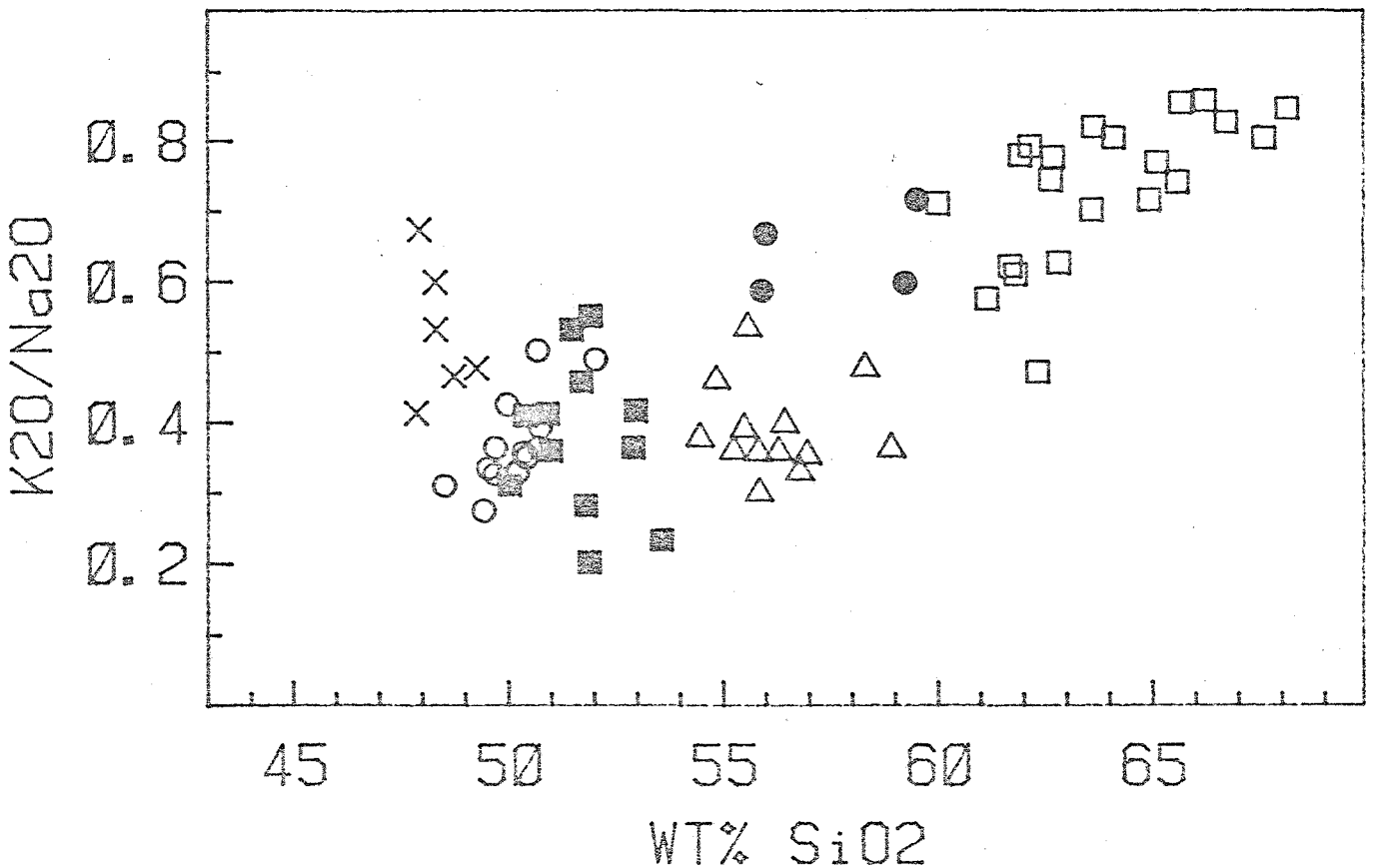

that TiO_2 variation changes from initial enrichment to depletion within the high-Al basalt field and the high-Al basalt-andesite-dacite trend is one of continuous depletion. P_2O_5, Al_2O_3 and Sr variations are less clear-cut and there is some suggestion that the *ne*-lavas are falling on trends of enrichment of these elements with decreasing MgO or increasing SiO_2, while the *ol-hy*-normative group show little variation and tend to merge with the andesite field.

In general, like K_2O, Rb, Zr and Nb tend to show positive correlation with SiO_2, though also like K_2O, these elements show considerable variation at any particular SiO_2 concentration. Thus rocks with about 52% SiO_2 may contain between 15 and 50ppm Rb.

The high-Al basalts have K/Rb ratios in the range 450 to 550 (fig. 3.14) and Rb/Sr ratios between 0.03 and 0.05.

3. Andesites.

The andesites are characteristically quartz-normative and have very high normative feldspar contents (>50%). They have relatively high Al_2O_3 contents (18-19.5%) and very low Ni (generally <5ppm). They are notable in that they show relatively slight K_2O-enrichment over a wide range of SiO_2 concentration (figure 3.2) and in some instances have lower K_2O concentrations than some basaltic lavas. K/Rb ratios (figure 3.14) are lower than those of the basalts, generally in the range 350-400 and Rb/Sr ratios are somewhat higher (0.04-0.08). $Mg/Mg+Fe^{2+}$ values are relatively constant over a wide SiO_2 range ($\simeq$0.44) and in fact, some of the more differentiated lavas with <53% SiO_2 have lower $Mg/Mg+\Sigma Fe$ values than the andesites (for instance "hawaiite" 41643 has $Mg/Mg+\Sigma Fe$ = 0.39 at 49.6% SiO_2, while andesite 41644 has $Mg/Mg+\Sigma Fe$ = 0.44 at 54.8% SiO_2).

FIGURE 3.14

K v. Rb variation of Rindjani lavas. K/Rb ratio contours are marked. .Symbols are the same as those in figure 3.12.

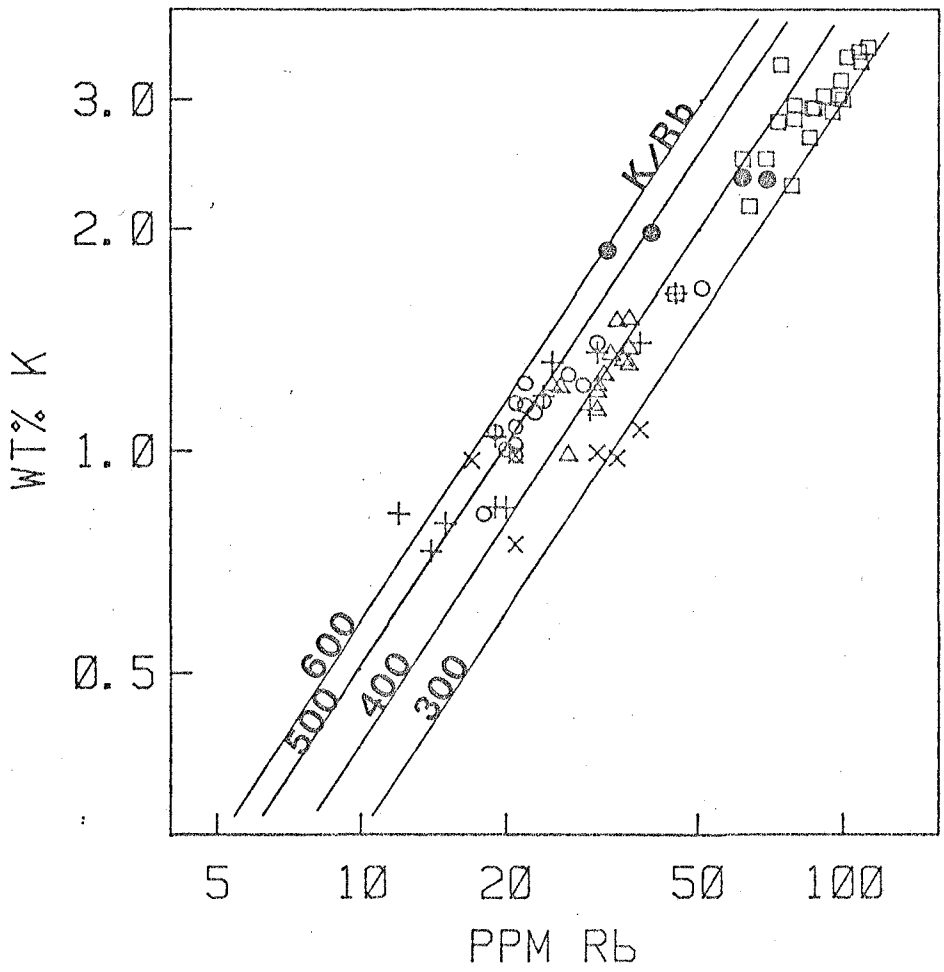

Andesites have slightly lower CaO and ΣFe than basalts and these components show a negative correlation with SiO_2. TiO_2 is also slightly lower and Ni and Cr markedly so. On the other hand, MgO, Sc, Al_2O_3, P_2O_5, K_2O, Na_2O, Y, Nb, Sr, Rb and Zr all show some overlap with the ranges of these elements shown by lavas with <53% SiO_2. Thus in terms of the MgO variation diagrams (figures 3.9-3.10), the discrimination of basaltic and andesite fields is often poorly defined. These factors suggest that some degree of divergent evolution exists. Thus if a basaltic parent magma is assumed, then evolved derivatives of this may or may not show SiO_2 enrichment. This problem is dealt with more rigorously in chapter 9.

4. High K_2O, high-Sr Andesites.

These are a small group of lavas (e.g. LB28, table 3.16), associated with the ankaramites from West Lombok, possibly eruptives of the Punikin centre. They are mineralogically like the "normal" andesites and although their general geochemical characteristics are similar they are distinguished from the other andesites by their high Sr and K_2O contents (figures 3.2, 3.8). Their Sr concentrations are in the range 500-750ppm and K_2O and Rb concentrations are about 50% higher than those of the normal andesite. They have slightly higher K_2O/Na_2O ratios (0.5-0.6) (figure 3.13) and similar Rb/Sr ratios, but markedly lower TiO_2 contents. They are distinguished from the other high-K_2O andesites (e.g. 41672) by the latter groups' low Sr (generally lower than that of the low-K_2O andesites), higher Rb/Sr, K_2O/Na_2O and occasionally low Al_2O_3.

5. High-K_2O Andesites and Dacites.

These rock-types are grouped together as their geochemical characteristics are continuous and the andesite-dacite division (Taylor, 1969) is an arbitrary one based on SiO_2 content. Petrographically this group is distinct from the type 1, andesites in being less phenocryst-rich (table 3.1

FIGURE 3.15

Al_2O_3 v. CaO variation of Rindjani lavas. Symbols as in figure 3.12.

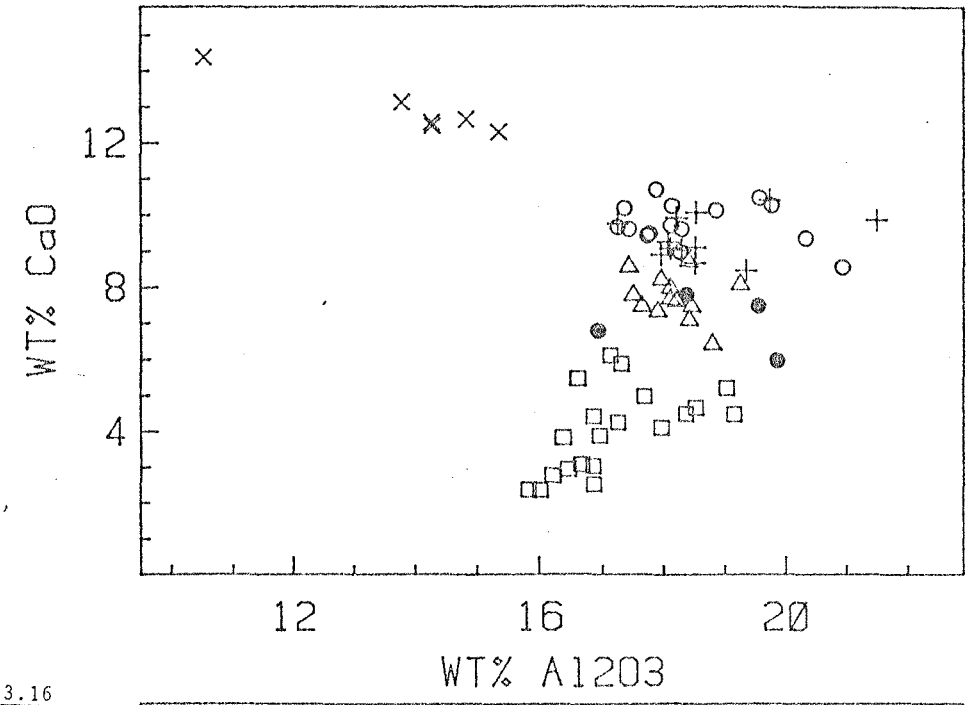

FIGURE 3.16

CaO v. Sr variation Rindjani lavas.

Symbols as in figure 3.12.

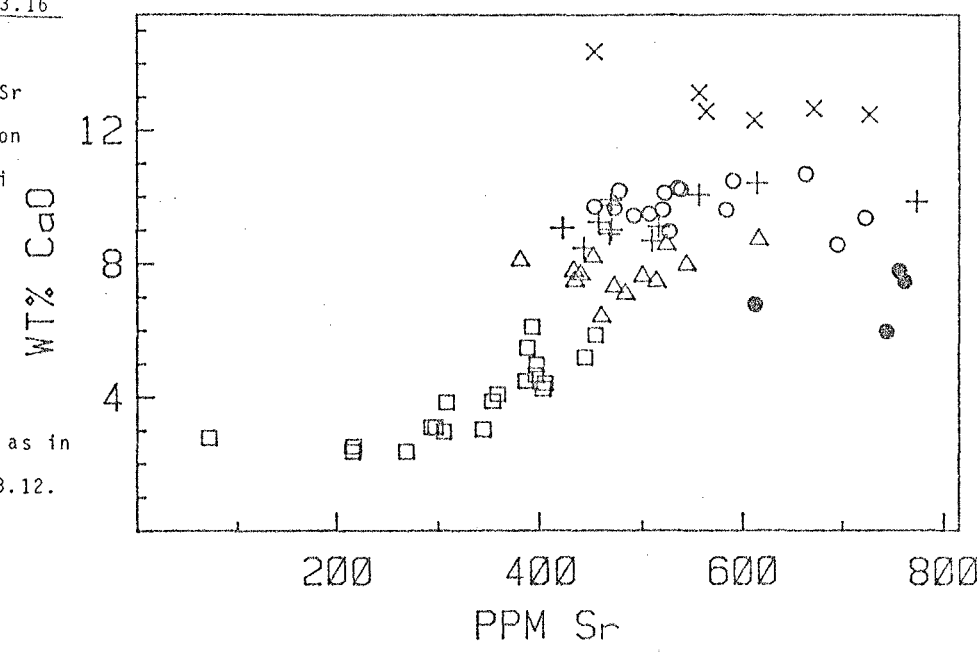

and in the common occurrence of amphibole and occasionally biotite. They are often glass-rich. Geochemically they are distinct from the andesites in having markedly lower CaO, ΣFe, TiO_2 and Sc. Ni concentration is very low, generally <2ppm and often below the detection-limit. Al_2O_3 is lower ar shows a depletion trend with increasing SiO_2. MgO concentration is also lower and shows a negative correlation with SiO_2. The dacites have a markedly lower normative feldspar content and a more Ab-rich composition (figure 3.4D). Compared with the andesites the high K_2O andesites and dacites have 2-3 times the concentration of K_2O, Rb, Nb and Zr. K_2O/Na_2O ratios are markedly higher (figure 3.13), while Sr is generally lower and decreases with increasing SiO_2. Rb/Sr ratios are much higher than those of the andesites and in one case are great than 1. K/Rb (3.20) (figure 3.14) are only slightly lower than those of the andesites and show relatively slight variation, in contrast to the basalts which show marked variation in this parameter.

These features, particularly the Sr, Al_2O_3, Rb/Sr and K_2O/Na_2O variations suggest very much that the high K_2O andesites and dacites have undergone considerable plagioclase separation relative to the low K_2O andesites.

6. Electron-microprobe analyses of Interstitial glasses.

Some andesites have an interstitial glassy mesostasis (e.g. 41644, 41647). Average analyses of a number of areas of this glass are given in table 3.19, together with their C.I.P.W. norms. These glasses bear a strong resemblance to the dacites in composition. They are quartz normative, with high SiO_2, K_2O, Na_2O and K_2O/Na_2O values and have low MgO, CaO, FeO and TiO_2. The similarity of this interstitial glass from the andesites to the dacite whole-rock composition, provides quite strong evidence that the dacites may be derived from andesites by fractional crystallisation processes.

FIGURE 3.17

K_2O+Na_2O v. SiO_2 variation Rindjani lavas.

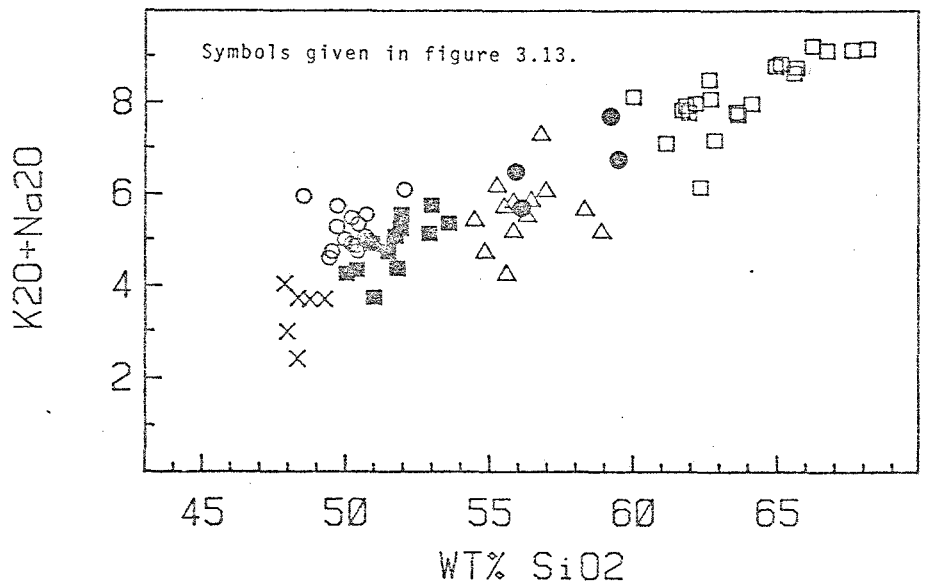

3.5 Summary.

This is a very brief resume of the main characteristics of the Rindjani suite, as described in this chapter.

Sampled lavas belong to four main groups: 1. ankaramite, 2. high-Al "basalt", 3. andesite, 4. high-K andesite and dacite. The ankaramites are all *ne*-normative, the high-Al basalts include both *ne*- and *ol-hy*-normative lavas, while the andesites and dacites are *Q*-normative. Geochemically the series from group 1 through to 4 is one of decreasing MgO, CaO, Ni, Cr and Sc and increasing SiO_2, though some of these elements show some overlap between different series, for instance the high-K- and "normal"-andesites. Mg/Mg+Fe ratio decreases markedly through the ankaramite series to the high-Al basalts, but shows little variation amongst the andesites and dacites.

The ankaramites are Al_2O_3-poor, and have phenocrysts of cpx and olivine, with little or no plagioclase. Some cpx phenocrysts have very magnesian Cr-diopside cores. High-Al basalts range from more mafic, relatively phenocryst-poor lavas which are olivine-rich and contain very magnesian olivine xenocrysts which include Cr-spinel, to less mafic, more phenocryst-rich types in which plagioclase and cpx are the main phases. The andesites are very phenocryst-rich rocks and like the high-Al basalts are very aluminous. Their phenocryst assemblages are plagioclase-dominated, with opx, cpx and magnetite and occasional reacted Ca-rich amphibole. They have siliceous glassy groundmass, which is of similar composition to the dacites. Like the high-Al basalts, the andesites contain extremely calcic plagioclase.

The dacites are often less aluminous than the andesites and are glass rich and phenocryst-poor. Compared to the andesites, the dacites and high-K andesites have 2-3 times the K_2O, Rb and Zr concentrations, higher K_2O/Na_2O and Rb/Sr ratios and very similar K/Rb ratios. The high-Al basalts have higher K/Rb ratios than the andesites.

Table 3.12

EAST SUNDA ARC VOLCANIC ROCKS

G.RINDJANI - LOMBOK ISLAND, BASALTIC LAVAS

Sample#	LB8	LB7	LB9	LB1	LB11	LB10	LB67	41676	LB47	41621
SiO_2	48.32	47.95	47.87	48.33	49.27	48.75	49.43	50.02	50.68	49.97
TiO_2	0.69	0.83	0.89	0.91	0.99	0.92	1.00	0.99	1.11	1.26
Al_2O_3	10.53	13.78	14.27	15.34	14.26	14.82	18.85	18.20	17.24	17.42
Fe_2O_3	1.53	1.69	1.72	1.73	1.71	1.74	1.58	1.70	1.63	1.72
FeO	7.81	8.64	8.75	8.81	8.70	8.85	8.08	8.65	8.31	8.75
MnO	0.17	0.17	0.20	0.20	0.18	0.19	0.18	0.20	0.19	0.19
MgO	14.02	10.61	9.47	8.39	8.35	8.13	5.93	5.84	5.81	5.78
CaO	14.38	13.14	12.48	12.30	12.58	12.66	10.14	9.92	9.67	9.62
Na_2O	1.50	1.78	2.85	2.42	2.49	2.51	3.60	3.24	3.36	3.50
K_2O	0.90	1.20	1.18	1.29	1.19	1.17	0.99	1.01	1.69	1.49
P_2O_5	0.15	0.21	0.32	0.28	0.27	0.26	0.20	0.23	0.32	0.32
H_2O+	2.33	3.08	2.09	2.27	1.59	2.86	0.58	1.33	0.71	0.73
Mg/Mg+Fe (t)	0.73	0.65	0.62	0.59	0.59	0.58	0.53	0.51	0.51	0.50
Mg/Mg+.85Fe	0.76	0.69	0.66	0.63	0.63	0.62	0.57	0.55	0.55	0.54
K_2O/Na_2O	0.60	0.67	0.41	0.53	0.48	0.47	0.28	0.31	0.50	0.43
Trace elements (ppm)										
Rb	21	31	34	38	21	17	18	19	31	22
Sr	452	556	726	611	563	671	522	469	472	520
Zr	53	49	64	57	64	72	43	56	126	99
Nb	2			4	4	4	2			6
Y	13	16	17	18	26	22	18	19	31	23
La	11									
Sc	50	36	38	39	43	35	31	35	27	33
Cr	510	307	259	190	309	156	71	52	160	128
Ni	151	125	89	57	92	50	23	23	33	43
Rb/Sr	0.046	0.056	0.047	0.062	0.037	0.025	0.034	0.041	0.066	0.042
K/Rb	356	321	288	282	470	571	457	441	453	562
K/Sr	16.53	17.92	13.49	17.53	17.55	14.48	15.75	17.88	29.73	23.79

FeO arbitrarily calculated from Fe^{++}= 0.85 total Fe

Notes: LB8,LB7,LB9,LB1,LB11,LB10 - ankaramites, LB67,LB47,41621 - ne-normative high-Al basalts,41676- ol-hy-normative high-Al basalt.Analyses normalised anhydrous, H_2O^+= pre-normalisation figure.Rock localities and mineralogy see appendix 1. CIPW norms are given in appendix 2.

Table 3.13

EAST SUNDA ARC VOLCANIC ROCKS

G.RINDJANI - LOMBOK ISLAND, BASALTIC LAVAS

Sample#	LB68	41632	LB51	LB65	41631	41624	LB71	41623	LB25	LB64
SiO_2	49.53	50.20	51.47	50.74	50.41	51.79	50.38	49.70	50.34	51.70
TiO_2	1.09	1.13	1.10	0.99	1.17	0.96	1.15	1.28	0.80	1.22
Al_2O_3	18.13	18.11	17.24	18.28	17.35	18.51	18.52	17.76	19.56	18.28
Fe_2O_3	1.67	1.62	1.62	1.59	1.72	1.61	1.66	1.75	1.47	1.59
FeO	8.49	8.28	8.29	8.12	8.77	8.19	8.45	8.90	7.50	8.13
MnO	0.19	0.18	0.18	0.20	0.17	0.19	0.19	0.18	0.19	0.19
MgO	5.72	5.63	5.29	5.21	5.24	5.07	4.97	4.92	4.57	4.57
CaO	10.24	9.71	9.76	9.62	10.19	9.11	10.08	9.49	10.48	9.02
Na_2O	3.54	3.67	3.08	3.56	3.50	3.40	3.07	4.19	3.57	3.47
K_2O	1.19	1.21	1.64	1.40	1.23	0.96	1.26	1.53	1.28	1.59
P_2O_5	0.21	0.25	0.33	0.31	0.24	0.21	0.28	0.29	0.24	0.23
H_2O+	0.53	0.83	0.98	0.61	1.91	0.81	0.68	0.82	1.51	0.70
Mg/Mg+Fe	0.51	0.51	0.49	0.49	0.48	0.48	0.47	0.46	0.48	0.46
Mg/Mg+.85Fe	0.55	0.55	0.53	0.53	0.52	0.52	0.51	0.50	0.52	0.50
K_2O/Na_2O	0.34	0.33	0.53	0.39	0.35	0.28	0.41	0.37	0.36	0.46
Trace elements (ppm)										
Rb	21	20	31	21	21	15	19	27	19	25
Sr	538	452	468	583	477	516	556	507	590	469
Zr	77	82	121	73	77	73	84	98	71	103
Nb	5	4			4	3		4		
Y	25	20	23	22	26	27	17	27	12	32
La		22.8								
Sc	32	33	29	25	31	27	30	32	23	25
Cr	74	219	164	53	233	55	40	124	66	39
Ni	23	71	30	14	77	10	18	39	12	5
Rb/Sr	0.039	0.044	0.066	0.036	0.044	0.029	0.034	0.053	0.032	0.053
K/Rb	470	502	439	553	486	531	551	470	559	528
K/Sr	18.36	22.22	29.09	19.94	21.41	15.45	18.81	25.05	18.01	28.15

Notes: FeO arbitrarily calculated as 0.85 total Fe. Analyses normalised anhydrous, H_2O^+=pre-normalisation figure. Rock localities and mineralogy given in appendix 1, CIPW norms given in appendix 2. All samples are ne-normative high-Al basalts except LB51, LB71 and LB64 which are ol-hy-normative high-Al basalt

Table 3.14

EAST SUNDA ARC VOLCANIC ROCKS

G.RINDJANI - LOMBOK ISLAND, BASALTIC LAVAS

Sample#	LB 19	41626	41692	41635	41651	41658	LB 26	41643	41678
SiO_2	48.52	50.71	51.92	50.98	50.20	50.43	50.91	49.68	52.03
TiO_2	1.18	1.26	1.12	1.00	1.04	1.04	0.77	1.12	1.09
Al_2O_3	17.87	17.72	17.95	19.73	20.32	20.94	21.49	19.76	18.26
Fe_2O_3	1.78	1.70	1.57	1.57	1.51	1.53	1.31	1.66	1.57
FeO	9.05	8.65	8.03	8.01	7.69	7.87	6.68	8.45	7.99
MnO	0.18	0.19	0.19	0.16	0.19	0.20	0.22	0.19	0.16
MgO	4.53	4.49	4.39	4.19	3.91	3.85	3.58	3.33	3.50
CaO	10.69	9.44	8.89	10.42	9.37	8.57	9.88	10.28	8.97
Na_2O	4.53	4.05	3.57	2.74	4.10	3.93	3.46	3.96	4.08
K_2O	1.41	1.48	1.97	0.99	1.36	1.39	1.43	1.30	2.00
P_2O_5	0.27	0.31	0.40	0.21	0.32	0.28	0.27	0.27	0.35
H_2O+	1.57	0.80	0.66	3.73	1.06	1.86	1.52	1.08	1.09
Mg/Mg+Fe	0.43	0.44	0.45	0.44	0.44	0.43	0.45	0.37	0.40
Mg/Mg+.85Fe	0.47	0.48	0.49	0.48	0.48	0.47	0.49	0.41	0.44
K_2O/Na_2O	0.31	0.37	0.55	0.36	0.33	0.35	0.41	0.33	0.49
Trace elements (ppm)									
Rb	24	29	45	12	23	22	24	21	51
Sr	663	491	467	614	722	695	773	535	527
Zr	71	106	151	90	72	76	75	81	173
Nb		4		4	7			4	5
Y	26	25	24	22	25	21	20	29	30
La									17.4
Sc	30	36	26	25	20	19	19	26	25
Cr	66	114	68	37	60	38	49	32	68
Ni	14	34	13	14	11	10	6	11	19
Rb/Sr	0.036	0.059	0.096	0.020	0.032	0.032	0.031	0.039	0.097
K/Rb	488	424	363	685	491	525	495	514	326
K/Sr	17.66	25.02	35.02	13.39	15.64	16.60	15.36	20.17	31.51

Notes: FeO arbitrarily calculated as 0.85 total Fe. Analyses normalised anhydrous, H_2O^+=pre-normalisation figure. Rock localities and mineralogy given in appendix 1, CIPW norms given in appendix 2. Rocks LB19, 41626, 41651, 41658, 41643 and 41678 are ne-normative high-Al basalts. 41692, 41635 and LB26 are ol-hy-normative high-Al basalts.

Table 3.15 EAST SUNDA ARC VOLCANIC ROCKS

G.RINDJANI - LOMBOK ISLAND, BASALTIC ANDESITES & ANDESITES

Sample#	41683	41634	41684	41637	LB 61	41647	41622	41627	41625	41687
SiO_2	51.89	52.90	53.57	52.97	54.46	54.84	55.49	55.84	55.82	55.24
TiO_2	1.28	1.06	1.01	0.96	0.96	0.92	0.91	1.09	0.92	1.03
Al_2O_3	18.06	18.50	18.10	19.35	17.96	19.25	18.45	17.42	18.11	17.50
Fe_2O_3	1.75	1.62	1.49	1.51	1.37	1.37	1.39	1.44	1.39	1.35
FeO	8.95	8.28	7.59	7.68	7.00	6.98	7.07	7.32	7.10	6.86
MnO	0.16	0.18	0.18	0.18	0.21	0.19	0.16	0.14	0.18	0.19
MgO	3.23	3.44	3.42	2.91	4.15	3.42	3.10	2.80	2.73	3.62
CaO	9.25	8.68	9.07	8.47	8.20	8.09	7.47	8.57	7.67	7.78
Na_2O	4.36	3.75	4.33	4.05	3.91	3.22	4.09	3.96	4.27	4.52
K_2O	0.88	1.37	1.01	1.69	1.48	1.48	1.60	1.19	1.53	1.63
P_2O_5	0.18	0.21	0.23	0.24	0.30	0.25	0.28	0.23	0.26	0.28
H_2O+	1.92	1.72	1.44	1.67	2.19	2.07	2.13	2.31	1.65	0.77
Mg/Mg+Fe	0.35	0.39	0.41	0.36	0.47	0.43	0.40	0.37	0.37	0.44
Mg/Mg+.85Fe	0.39	0.43	0.45	0.40	0.51	0.47	0.44	0.41	0.41	0.48
K_2O/Na_2O	0.20	0.37	0.23	0.42	0.38	0.46	0.39	0.30	0.36	0.36
Trace elements (ppm)										
Pb	14	30	20	38	25	31	35	27	32	33
Sr	456	510	421	442	451	381	433	524	439	432
Zr	116	107	107	124	125	149	134	129	136	82
Nb	6	2	2	5	5	3	2	6	6	4
Y	28	28	27	28	23	29	30	29	31	43
La		12					12.8			
Sc	31	27	22	23	21	21	18	23	18	21
Cr	38	39	25	28	27	30	27	37	29	48
Ni	6	6	3	3	6	5	2	5	3	3
Rb/Sr	0.031	0.059	0.048	0.086	0.055	0.081	0.081	0.052	0.073	0.076
K/Rb	522	379	419	369	491	396	380	366	397	410
K/Sr	16.02	22.30	19.92	31.74	27.24	32.25	30.68	18.85	28.93	31.32

Notes:FeO arbitrarily calculated as 0.85 total Fe.Analyses normalised anhydrous,H_2O^+=prenormalisation figure. Rock localities and mineralogy given in appendix 1,CIPW norms given in appendix 2.41683 is an ol-hy-normative high-Al basalt.41634,41684,41637,LB61 ,41647,41622,41627,41625 and 41687 low silica andesites .

Table 3.16

EAST SUNDA ARC VOLCANIC ROCKS

G.RINDJANI - LOMBOK ISLAND, ANDESITES

Sample#	LB 6	LB29	LB 28	41646	41644	41688	41636	LB 42	LB 41	41675
SiO_2	55.58	56.00	55.91	56.43	56.78	56.95	58.91	56.29	58.30	62.33
TiO_2	0.88	0.75	0.70	0.88	0.89	0.90	0.70	0.78	0.78	0.69
Al_2O_3	18.39	18.37	19.54	17.90	18.79	18.20	18.41	18.11	17.64	17.12
Fe_2O_3	1.34	1.24	1.11	1.36	1.19	1.21	1.15	1.29	1.12	0.92
FeO	6.83	6.32	5.68	6.93	6.08	6.15	5.88	6.58	5.73	4.71
MnO	0.19	0.24	0.20	0.18	0.19	0.18	0.17	0.17	0.17	0.16
MgO	3.58	3.24	2.55	2.94	2.07	2.55	2.32	3.07	2.94	1.55
CaO	8.73	7.80	7.49	7.31	6.42	7.62	7.09	7.97	7.47	6.11
Na_2O	2.75	3.37	4.07	4.17	5.47	4.46	3.77	4.04	3.81	4.17
K_2O	1.47	2.25	2.39	1.66	1.81	1.58	1.37	1.45	1.82	1.97
P_2O_5	0.26	0.43	0.37	0.23	0.28	0.21	0.22	0.26	0.22	0.27
H_2O+	0.67	2.63	2.65	2.26	0.95	0.82	1.61	0.99	0.88	1.07
Mg/Mg+Fe	0.44	0.44	0.41	0.39	0.34	0.39	0.37	0.41	0.44	0.33
Mg/Mg+.85Fe	0.48	0.48	0.44	0.43	0.38	0.42	0.41	0.45	0.48	0.37
K_2O/Na_2O	0.53	0.67	0.59	0.40	0.33	0.35	0.36	0.36	0.48	0.47
Trace elements (ppm)										
Rb	26	32	40	36	34	36	31	31	36	45
Sr	616	756	761	472	459	500	483	544	514	392
Zr	119	152	143	165	118	140	127	129	116	182
Nb				14	6	7			4	
Y	19	34	31	30	31	30	26	31	21	29
La										
Sc	19	19	15	19	16	20	13	17	14	
Cr	38	41	21	25	19	25	18	24	37	16
Ni	4	7	2	4	2	2	1	2	4	2
Rb/Sr	0.042	0.042	0.053	0.076	0.074	0.072	0.064	0.057	0.070	0.115
K/Rb	469	584	496	383	442	364	367	388	420	363
K/Sr	19.81	24.71	26.07	29.20	32.74	26.23	23.55	22.13	29.40	41.72

Notes:FeO arbitrarily calculated as 0.85 total Fe.Analyses normalised anhydrous,H_2O^+=pre-normalisation figure. Rock localities and mineralogy given in appendix 1.CIPW norms given in appendix 2. All rocks are andesites except LB29 and LB28 which are high-K,high-Sr andesites and 41675 which is a dacite.

Table 3.17

EAST SUNDA ARC VOLCANIC ROCKS

G.RINDJANI - LOMBOK ISLAND, HIGH K2O ANDESITES & DACITES

Sample#	LB 12	LB22	41672	LB 55	LB 69	LB 4	LB 3	41668	LB 2	41645
SiO_2	59.50	59.24	59.99	61.15	61.82	61.92	61.69	62.15	62.63	62.83
TiO_2	0.60	0.53	0.90	0.63	0.71	0.56	0.86	0.61	0.82	0.66
Al_2O_3	16.92	19.85	17.68	17.30	17.25	19.03	16.85	19.15	16.37	16.60
Fe_2O_3	1.05	0.84	0.93	0.87	0.92	0.63	0.96	0.60	0.93	0.88
FeO	5.35	4.30	4.74	4.45	4.67	3.21	4.88	3.08	4.73	4.49
MnO	0.24	0.17	0.18	0.26	0.19	0.09	0.17	0.10	0.16	0.14
MgO	2.56	1.33	2.13	2.12	1.88	1.40	1.90	1.66	1.66	1.57
CaO	6.79	5.97	4.98	5.88	4.25	5.21	4.42	4.48	3.83	5.48
Na_2O	3.91	4.73	4.74	4.50	4.91	4.36	4.82	4.44	4.86	4.40
K_2O	2.80	2.83	3.37	2.59	3.00	3.40	3.00	3.52	3.62	2.76
P_2O_5	0.29	0.22	0.37	0.25	0.40	0.18	0.47	0.20	0.39	0.18
H_2O+	2.95	1.00	1.30	0.77	0.35	0.47	0.46	1.13	0.37	0.77
Mg/Mg+Fe	0.42	0.32	0.41	0.42	0.38	0.40	0.37	0.45	0.35	0.35
Mg/Mg+.85 Fe	0.46	0.36	0.44	0.46	0.42	0.44	0.41	0.49	0.38	0.38
K_2O/Na_2O	0.72	0.60	0.71	0.58	0.61	0.78	0.62	0.79	0.74	0.63
Trace elements (ppm)										
Rb	69	62	73	64	62	79	69	86	100	78
Sr	612	743	397	453	403	443	405	386	308	388
Zr	159	167	252	215	150	243	244	268	274	237
Nb			9	8				8		6
Y	18	29	40	33	33	31	45	33	48	26
La										
Sc	15	13	15	11	11	8	19	9	18	12
Cr	78	25	11	42	38	31	27	13	18	24
Ni	25	2	1	1	<1	1	1	<1	1	<1
Rb/Sr	0.113	0.083	0.184	0.141	0.154	0.178	0.170	0.223	0.325	0.201
K/Rb	337	379	383	336	402	357	361	340	301	294
K/Sr	37.98	31.62	70.47	47.47	61.80	63.72	61.50	75.71	97.58	59.06

Notes: FeO arbitrarily calculated as 0.85 total Fe. Analyses normalised anhydrous, H_2O^+ =pre-normalisation figure. Rock localities and mineralogy given in appendix1. CIPW norms given in appendix 2. LB12 and LB22 are high-K, high-Sr andesites, 41672, LB55, LB69, LB4, LB3 are high-K andesites and LB2 and 41645 are dacites.

Table 3.18

EAST SUNDA ARC VOLCANIC ROCKS

G.RINDJANI - LOMBOK ISLAND, DACITES

Sample#	41691	41650	LB 60	LB 48	LB 43	LB 49	41677	41671	41638	41641	41664	41639
SiO_2	62.68	63.58	64.10	63.63	65.67	65.11	64.93	65.58	66.72	66.22	67.60	68.13
TiO_2	0.58	0.65	0.63	0.57	0.62	0.63	0.65	0.65	0.63	0.56	0.57	0.59
Al_2O_3	18.52	17.96	16.95	18.36	16.45	16.84	16.66	16.65	16.21	16.86	16.01	15.82
Fe_2O_3	0.61	0.71	0.70	0.59	0.62	0.62	0.65	0.64	0.54	0.53	0.50	0.49
FeO	3.12	3.63	3.59	3.00	3.15	3.15	3.33	3.28	2.77	2.69	2.53	2.51
MnO	0.10	0.14	0.14	0.10	0.13	0.12	0.11	0.13	0.11	0.10	0.11	0.10
MgO	1.47	1.21	1.77	1.34	1.42	1.41	1.57	1.12	0.96	1.14	1.04	0.70
CaO	4.66	4.09	3.88	4.49	2.96	3.03	3.09	3.09	2.78	2.52	2.36	2.37
Na_2O	4.53	4.57	4.41	4.24	4.71	4.99	5.11	4.95	4.99	4.96	5.06	4.96
K_2O	3.52	3.21	3.55	3.48	4.03	3.84	3.66	3.67	4.13	4.26	4.07	4.20
P_2O_5	0.21	0.24	0.27	0.20	0.24	0.26	0.22	0.22	0.16	0.15	0.15	0.13
H_2O+	0.56	0.87	1.35	0.55	1.06	0.36	1.05	1.04	1.37	1.07	0.69	0.57
Mg/Mg+Fe	0.42	0.34	0.43	0.40	0.41	0.40	0.42	0.34	0.34	0.39	0.38	0.30
Mg/Mg+.85Fe	0.46	0.37	0.47	0.44	0.45	0.44	0.46	0.38	0.38	0.43	0.42	0.33
K_2O/Na_2O	0.78	0.70	0.80	0.82	0.86	0.77	0.72	0.74	0.83	0.86	0.80	0.85
Trace elements (ppm)												
Rb	87	85	79	95	74	99	91	98	102	113	109	108
Sr	396	358	353	386	305	344	297	293	71	216	269	215
Zr	248	250	237	253	253	266	268	264	316	310	326	307
Nb		9		10		12	9	11	14	10	13	13
Y	35	36	29	44	48	40	37	41	39	40	40	37
La								25.9				
Sc	11	10	12	11	9	20	11	8		8	8	7
Cr	23	15	16	15	15	18	10	29	12	12	10	13
Ni	1	<1	1	<1	<1	<1	<1	<1	1	2	<1	<1
Rb/Sr	0.220	0.237	0.224	0.246	0.243	0.288	0.306	0.334	1.437	0.523	0.405	0.502
K/Rb	336	314	373	304	452	322	334	311	336	313	310	323
K/Sr	73.80	74.44	83.49	74.85	109.70	92.67	102.31	103.99	482.92	163.73	125.61	162.18

Notes: FeO arbitrarily calculated as 0.85 total Fe.Analyses normalised anhydrous, H_2O^+= pre-normalisation figure.Rock localities and mineralogy given in appendix 1.CIPW norms given in appendix 2. All rocks are dacites.

Table 3.19 Electron Microprobe Analyses of Interstitial Glasses from Rindjani Andesites and Dacites

Sample No.	41641	41650	41644	41647	41647 [1]
Lava [2]	D	D	A	A	A
SiO_2	70.85	68.29	68.28	70.25	69.14
Al_2O_3	15.62	18.39	14.78	15.22	13.82
Fe_2O_3	0.21	0.35	0.73	0.58	0.73
FeO	1.08	1.78	3.71	2.94	3.70
MgO	0.52	0.49	0.97	0.34	0.83
CaO	1.01	3.48	1.44	2.82	1.33
Na_2O	4.49	3.73	5.80	3.99	4.67
K_2O	5.89	3.17	3.43	3.26	5.14
TiO_2	0.31	0.26	0.93	0.55	0.70
P_2O_5	nd	nd	nd	nd	nd
MnO	-	0.08	-	0.09	-
Total	99.98	100.02	100.07	100.04	100.06
$Mg/Mg+\Sigma Fe$	0.422	0.294	0.283	0.149	0.254
K_2O/Na_2O	1.31	0.85	0.59	0.82	1.10
Q	18.66	25.04	15.39	26.11	17.00
C	0.02	2.50	-	-	-
or	34.81	18.73	20.27	19.26	30.32
ab	37.99	31.56	49.07	33.76	39.52
an	5.01	17.26	4.17	13.99	1.57
ne	-	-	-	-	-
di	-	-	2.51	-	4.28
hy	2.59	3.92	5.82	5.03	4.92
ol	-	-	-	-	-
mt	0.30	0.51	1.06	0.84	1.06
il	0.59	0.49	1.77	1.04	1.33
ap	-	-	-	-	-

Notes: 41641 average of five analyses
41644 average of five analyses

[1] Glass inclusion in clinopyroxene phenocryst in lava 41647.

[2] Abbreviations: D - dacite, nd - not determined, A - andesite, $Fe^{2+} = 0.85\ \Sigma Fe$.

fig. 4-1

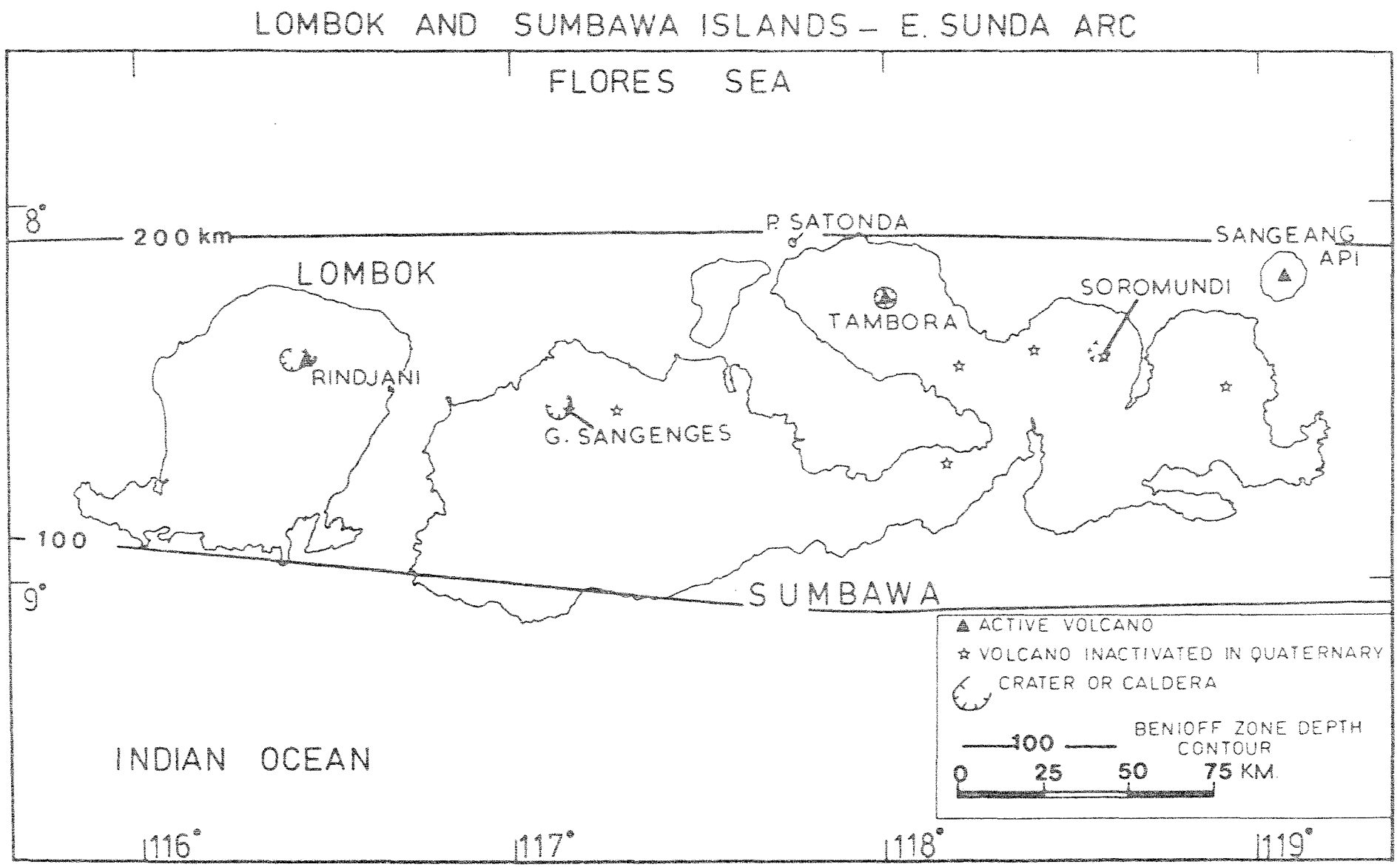
LOMBOK AND SUMBAWA ISLANDS – E. SUNDA ARC
FLORES SEA
8°
200 km
P. SATONDA
SANGEANG API
LOMBOK
SOROMUNDI
TAMBORA
RINDJANI
G. SANGENGES
100
9°
SUMBAWA
INDIAN OCEAN
ACTIVE VOLCANO
VOLCANO INACTIVATED IN QUATERNARY
CRATER OR CALDERA
100
BENIOFF ZONE DEPTH CONTOUR
0 25 50 75 KM.
116°
117°
118°
119°

Chapter 4.

PETROLOGY OF VOLCANIC ROCKS AND INTRUSIVES FROM G. TAMBORA/P.[1] *SATONDA*

4.1 *Introduction.*

Tambora is an active volcano on Sumbawa island (see figure 4.1). It is a very large stratovolcano that forms most of the Sanggar peninsula of north central Sumbawa. The volcano erupted with extreme violence in 1815, possibly following a long dormant period (perhaps of the order of several hundred years), forming a caldera 6 km in diameter and nearly 1 km in depth. Petroeschevsky (1949) gave brief petrographic descriptions of a number of lavas collected during his ascent of Tambora in 1947. In these he refers to olivine basalts, leucite tephrites and leucite basanites, as well as glassy lava bombs.

All rocks of the Tambora suite are *ne*-normative and are relatively potassium-rich, with K_2O/Na_2O ratios in the range 0.6-1.0. Using the nomenclature of Johnson et al. (1976), the Tambora lavas are potassic *ne*-trachybasalts and potassic *ne*-trachyandesites. They fall within the general field of volcanic rocks of the shoshonite-banakite association as defined by Joplin (1968).

In general, the Tambora lavas are intermediate in character between the high-Al basalt-andesite suite from Rindjani volcano and the highly undersaturated, very potassium-rich, leucite-rich lavas from G. Soromundi and G. Sangenges. They are distinguished from the G. Soromundi and G. Sangenges lavas by having less normative *ne* and no normative *lc* and by the occurrence of modal leucite only rarely in the groundmass. They are distinguished from the Rindjani calcalkaline lavas by the *ne*-normative character of the lavas with intermediate silica content (up to 57% SiO_2). Petrographically this is manifested in the absence of orthopyroxene from the Tambora trachyandesites and in the occurrence of olivine as both phenocrysts and groundmass grains.

1. P. = Pulau, Indonesian for island.

Modal analyses of representative rocks from the Tambora suite are given in table 4.5 andwhole-rock, major- and trace-element analyses are presented in tables 4.1-4.4.

There is a tendency for lavas with otherwise similar chemical compositions to have different textural and mineralogical characteristics. For instance amongst the *ne*-trachyandesite group (≈banakites), lavas T20 and T25 are holocrystalline, porphyritic lavas, with medium-grained groundmass, while T43, T41, T32 and a number of others, although near-identical in chemical composition (tables 4.3-4.4), are largely glassy with only 5-10% phenocrysts. Similarly, the lavas with <53% SiO_2 encompass varieties such as T9 (modal analysis, table 4.5, chemical analysis , table 4.2) with rare phenocrysts and very finely grained groundmass and range through more porphyritic types to highly porphyritic lavas with quite coarsely crystalline groundmass such as T30 (tables 4.2 & 4.5).

Leucite has crystallised in the relatively coarse groundmass of lavas such as T30 and T20. These features tend to suggest that the mineralogy of the erupted volcanic rocks is at least in part a function only of their high-level cooling history.

This study indicates that although some of the lavas contain abundant groundmass leucite they are unlike the leucite-bearing lavas from Soromundi and G. Sangenges (discussed elsewhere in this thesis), or those of Bata Tara (an isolated volcano in the Banda Sea, discussed by Brouwer (1939)) or Muriah in Java (Nicholls and Whitford, 1976). The latter group is more undersaturatec has leucite in the norm, may have leucite phenocrysts and is often more mafic.

4.2 Petrography of potassic ne-trachybasalts (<53% SiO_2)

Perhaps the most notable petrographic distinction, within the Tambora lava group, is the occurrence of olivine, both as a phenocryst and groundmass phase in those lavas with <53% SiO_2 and its general absence in those with >53% SiO_2, where phenocrysts of biotite occur.

Table 4.1

EAST SUNDA ARC VOLCANIC ROCKS

SATONDA ISLAND - SUMBAWA, TRACHYBASALTS

Sample#	PS8	PS2	PS4	PS7	PS3
SiO_2	49.21	49.31	49.39	49.44	49.48
TiO_2	0.98	0.98	1.00	1.01	0.99
Al_2O_3	17.07	17.58	17.89	17.94	17.56
Fe_2O_3	1.58	1.62	1.62	1.64	1.65
FeO	8.06	8.28	8.24	8.34	8.43
MnO	0.18	0.20	0.19	0.19	0.20
MgO	6.88	5.82	5.58	5.57	5.13
CaO	10.65	9.84	9.81	9.69	9.82
Na_2O	3.25	3.67	3.40	3.11	3.90
K_2O	1.78	2.22	2.42	2.57	2.35
P_2O_5	0.35	0.47	0.46	0.50	0.49
H_2O+	1.20	0.75	0.56	1.07	0.66
Mg/Mg+Fe	0.56	0.52	0.51	0.50	0.48
Mg/Mg+.85Fe	0.60	0.56	0.55	0.54	0.52
K_2O/Na_2O	0.55	0.60	0.71	0.83	0.60
Trace elements (ppm)					
Rb	39	63	59	64	58
Sr	842	948	981	1000	918
Zr	32	94	81	75	102
Nb	3	3	1	3	
Y	22	19	24	24	26
La					
Sc	33	23	26	29	20
Cr	84	56	54	77	54
Ni	27	16	26	28	19
Rb/Sr	0.046	0.066	0.060	0.064	0.063
K/Rb	379	293	341	333	336
K/Sr	17.55	19.44	20.48	21.34	21.25

Notes: FeO arbitrarily calculated as 0.85 total Fe. Analyses normalised anhydrous, H_2O^+ =pre-normalisation figure. Rock localities are given in appendix 1, together with mineralogy. CIPW norms are given in appendix 2. All samples are ne-trachybasalts.

Table 4.2

EAST SUNDA ARC VOLCANIC ROCKS

TAMBORA - SUMBAWA ISLAND

Sample#	T12	T17	T9	T8	T21	T2	T18	T3	T30	T13
SiO_2	48.26	48.78	48.85	49.21	49.22	49.83	49.87	50.74	51.39	51.49
TiO_2	0.97	0.96	0.99	0.91	0.93	0.92	0.90	0.92	0.68	0.87
Al_2O_3	17.95	17.93	18.44	17.27	17.65	18.03	18.21	17.59	20.56	17.15
Fe_2O_3	1.69	1.66	1.67	1.62	1.62	1.54	1.51	1.60	1.09	1.50
FeO	8.60	8.47	8.49	8.27	8.25	7.83	7.71	8.16	5.54	7.67
MnO	0.21	0.21	0.24	0.20	0.20	0.20	0.21	0.18	0.15	0.18
MgO	5.27	5.56	4.47	5.71	5.40	4.96	4.62	4.79	3.25	4.65
CaO	10.46	10.44	10.06	10.50	9.67	9.26	9.26	9.15	8.89	9.04
Na_2O	3.50	3.14	3.44	4.10	3.72	3.94	4.25	3.55	4.42	4.16
K_2O	2.67	2.47	2.89	1.71	2.92	3.10	3.06	2.94	3.56	2.89
P_2O_5	0.42	0.38	0.46	0.49	0.42	0.39	0.40	0.37	0.49	0.40
H_2O+	1.02	1.07	1.05	1.37	1.20	0.97	0.61	1.20	0.66	0.59
Mg/Mg+Fe	0.48	0.50	0.44	0.51	0.50	0.49	0.48	0.47	0.47	0.48
Mg/Mg+.85Fe	0.52	0.54	0.48	0.55	0.54	0.53	0.52	0.51	0.51	0.52
K_2O/Na_2O	0.76	0.79	0.84	0.42	0.78	0.79	0.72	0.83	0.81	0.69
Trace elements (ppm)										
Rb	77	189	93	35	75	73	79	69	97	86
Sr	1192	1113	1323	1228	1018	1020	1048	949	1352	981
Zr	120	94	92	91	115	96	84	93	89	100
Nb		3		4	3	2			3	
Y	18	24	30	23	28	26	24	35	12	25
La	23	23								
Sc	33	30	22	25	22	21	21	24	13	23
Cr	55	49	31	56	57	55	53	45	66	40
Ni	11	20	7	22	14	11	9	16	12	15
Rb/Sr	0.065	0.170	0.070	0.029	0.074	0.072	0.075	0.073	0.072	0.088
K/Rb	288	108	258	406	323	353	322	354	305	279
K/Sr	18.60	18.42	18.14	11.56	23.81	25.23	24.24	25.72	21.86	24.46

Notes: FeO arbitrarily calculated as 0.85 total Fe. Analyses are normalised anhydrous, H_2O^+=pre-normalised value. Rock localities and mineralogy are given in appendix 1. CIPW norms given in appendix 2.

All samples are ne-trachybasalts.

Table 4.3

EAST SUNDA ARC VOLCANIC ROCKS

TAMBORA - SUMBAWA ISLAND

Sample#	T5	T26	T10	T27	T36	T32	T31
SiO_2	51.48	52.19	53.33	54.72	54.85	55.09	54.92
TiO_2	0.66	0.67	0.64	0.57	0.66	0.69	0.68
Al_2O_3	21.10	20.09	20.26	19.68	19.99	19.66	19.74
Fe_2O_3	1.05	1.16	1.01	1.03	0.99	0.99	1.00
FeO	5.35	5.90	5.15	5.27	5.05	5.07	5.09
MnO	0.14	0.16	0.15	0.18	0.19	0.18	0.18
MgO	3.27	3.00	2.76	2.48	2.25	2.71	2.65
CaO	8.47	8.22	6.72	5.71	5.37	5.47	5.30
Na_2O	4.32	4.20	5.00	4.87	5.04	4.56	4.79
K_2O	3.68	3.96	4.47	4.91	5.04	5.03	5.12
P_2O_5	0.47	0.44	0.52	0.57	0.57	0.54	0.53
H_2O+	0.89	0.55	0.69	0.74	0.70	0.80	1.05
Mg/Mg+Fe	0.48	0.44	0.45	0.42	0.40	0.45	0.44
Mg/Mg+.85Fe	0.52	0.48	0.49	0.46	0.44	0.49	0.48
K_2O/Na_2O	0.85	0.94	0.89	1.01	1.00	1.10	1.07
Trace elements (ppm)							
Rb	90	107	121	129	137	132	153
Sr	1335	1170	1166	1029	1012	1036	980
Zr	83	113	167	152	137	145	146
Nb	4	4	6	5	6	8	8
Y	13	28	27	20	28	26	29
La						34	
Sc	13	16	10	10	10	10	9
Cr	46	32	26	45	40	34	20
Ni	9	9	3	1	<1	3	<1
Rb/Sr	0.067	0.091	0.104	0.125	0.135	0.127	0.156
K/Rb	339	307	307	316	305	316	278
K/Sr	22.88	28.10	31.83	39.61	41.35	40.31	43.37

Notes: FeO arbitrarily calculated as 0.85 total Fe.Analyses normalised anhydrous ,H_2O^+ = pre-normalisation figure.Rock localities are given in appendix 1 together with mineralogy.CIPW norms are given in appendix2.

Samples T10 to T31 are ne-trachyandesites,T5 and T26 are ne-trachybasalts.

Table 4.4

EAST SUNDA ARC VOLCANIC AND INTRUSIVE ROCKS

TAMBORA TRACHYANDESITES AND INTRUSIVE XENOLITHS

Sample#	T11	T25	T23	T43	T29	T41	T20	T28	T33	T4
SiO_2	54.41	55.34	55.17	56.11	56.40	56.04	56.10	48.51	49.17	50.03
TiO_2	0.59	0.65	0.67	0.61	0.60	0.61	0.61	1.04	1.16	0.88
Al_2O_3	20.40	19.98	19.78	19.90	19.88	19.71	19.49	17.57	14.63	18.93
Fe_2O_3	0.95	0.98	0.98	0.89	0.89	0.91	0.88	1.70	2.08	1.43
FeO	4.83	4.98	5.01	4.55	4.52	4.63	4.47	8.63	10.61	7.28
MnO	0.16	0.19	0.18	0.18	0.19	0.19	0.18	0.21	0.23	0.19
MgO	2.01	2.16	2.50	2.20	1.97	2.05	1.85	5.82	6.55	4.52
CaO	6.15	5.15	5.42	4.62	4.48	4.57	4.50	10.33	11.35	9.50
Na_2O	5.09	4.73	4.66	5.05	5.54	5.25	5.79	3.33	2.32	3.51
K_2O	4.91	5.30	5.08	5.39	5.09	5.54	5.69	2.58	1.55	3.27
P_2O_5	0.50	0.52	0.55	0.49	0.46	0.49	0.45	0.33	0.35	0.48
H_2O+	0.59	0.76	0.79	0.76	0.71	0.60	0.54	1.73	2.00	0.74
Mg/Mg+Fe	0.39	0.40	0.43	0.42	0.40	0.40	0.39	0.51	0.48	0.48
Mg/Mg+.85Fe	0.43	0.44	0.47	0.46	0.44	0.44	0.42	0.55	0.52	0.53
K_2O/Na_2O	0.96	1.12	1.09	1.07	0.92	1.06	0.98	0.77	0.67	0.93
Trace elements (ppm)										
Rb	132	139	117	130	137	140	142	59	33	89
Sr	1112	982	1012	930	916	945	923	991	1023	1204
Zr	144	139	137	143	197	150	194	94	57	89
Nb	8	6	8	9		8	8	4	1	4
Y	14	29	17	18	28	25	25	26	18	17
La							38.7			
Sc	11	11	10	16	19	8	8	22	32	41
Cr	25	22	43	22	19	42	21	43	55	67
Ni	3	<1	1	<1	<1	1	1	14	19	7
Rb/Sr	0.119	0.142	0.116	0.140	0.150	0.148	0.154	0.060	0.032	0.074
K/Rb	309	317	360	344	308	329	333	363	390	305
K/Sr	36.66	44.81	41.67	48.12	46.13	48.67	51.18	21.61	12.58	22.55

Notes: FeO arbitrarily calculated as 0.85 total Fe. Analyses quoted normalised anhydrous. H_2O^+= pre-normalisation figure. Rock localities and mineralogy given in appendix 1. CIPW norms given in appendix 2. Samples T11, T25, T23, T43, T29, T41 and T20 are ne-trachyandesites ("banakites"). T28, T33 and T4 are intrusive rocks erupted as fragments in tephra. They are alkali gabbros ("shonkinites").

Table 4.5 Tambora, Lavas and Intrusives: Modal Compositions

A. LAVAS

Sample No.	Cpx	Ol	Biot	Ti-Mag	Plag	Apat	Groundmass	Glass
PS8	11	4.3	0.2	3	24.5		57	
T17	7.3	2.0		1.7	14.5		74.5	
T2	10.5	2		2	20	tr	65.5	
T13	10.2	3.5	0.5	4.2	44	0.4	37.5	
T9	0.8	0.6		0.7	4.8		93.0	
T5	2.5	0.8		0.2	38.5		58	
T30	6	1.2	0.15	0.5	38	0.15	54	
T32	3		2	1.6	12	0.4		81
T20	2			0.9	7	0.1	90	

notes: Groundmass = plagioclase + sanidine ± Leucite + clinopyroxene ± olivine + magnatite + apatite ± biotite

B. INTRUSIVE XENOLITHS

Sample No.	Cpx	Ol	Biot	Ti-Mag	Plag	K-spar	Apat	Neph
T28	20.1	6.4	1.3	4	43	24	1	tr
T4	10.6	6.5	5.7	3.6	52	20.4	1	tr
T6	5.5		6.6	7.2	39	40.5	1	tr

Rock types: PS8, T17, T2, T13, T9, T5, T30 = potassic ne-trachybasalts ("shoshonites")

T32, T20 = potassic ne-trachyandesites ("banakites")

T28, T4, T6 = shonkinites (alkali gabbros)

Lavas with <53% SiO_2 are holocrystalline, (7-70% phenocrysts, table 4.5). Texturally they are very like the basaltic andesites from Rindjani (chapter 3) Similarly, the composition and relative proportions of phenocryst phases of Rindjani basaltic andesites and Tambora trachybasalts/-trachyandesites with <53% SiO_2, resemble each other (compare Tambora trachybasalt T2 in tables 4.2 and 4.5 with Rindjani basaltic andesite 41637, tables 3.4 and 3.8).

The Tambora series of lavas in general is distinguished from the Rindjani calcalkaline group particularly by the ubiquitous occurrence of groundmass K-feldspar, rimming of plagioclase by K-feldspar and by the occasional appearance of leucite.

Tambora lavas with <53% SiO_2 are composed of phenocrysts of plagioclase, cpx, olivine and titan magnetite, with occasional microphenocrysts of apatite and biotite. Typically, the groundmasses are composed of laths of plagioclase and sanidine and granules of cpx, olivine and magnetite. Apatite is a common groundmass phase and also occurs as small phenocrysts. Leucite is an occasion groundmass phase.

Like the Rindjani basalts and andesites, the Tambora trachybasalts common contain very anorthite-rich plagioclase (≈An 90) (figure 4.2, table 4.6). Similarly, individual plagioclase phenocrysts from the same lava may show large variations in core composition (from An85-An50). Very calcic plagioclase is often corroded or sieved and may contain inclusions of glass or clinopyroxene.

Plagioclase phenocrysts may show oscilliatory zoning and are frequently rimmed with a clear zone ranging in composition from andesine to potassic oligoclase composition. Sieved, or inclusion-rich areas of a grain are commonly restricted to specific zones so that plagioclase phenocrysts may have a clear, relatively unzoned calcic core, a band rich in corrosion channels, with inclusions of glass and pyroxene and then a finely zoned, relatively sodic, clear, rim. Such plagioclase textures are of course very characteristic of many convergent-plate volcanic suites (e.g. Ewart, 1976).

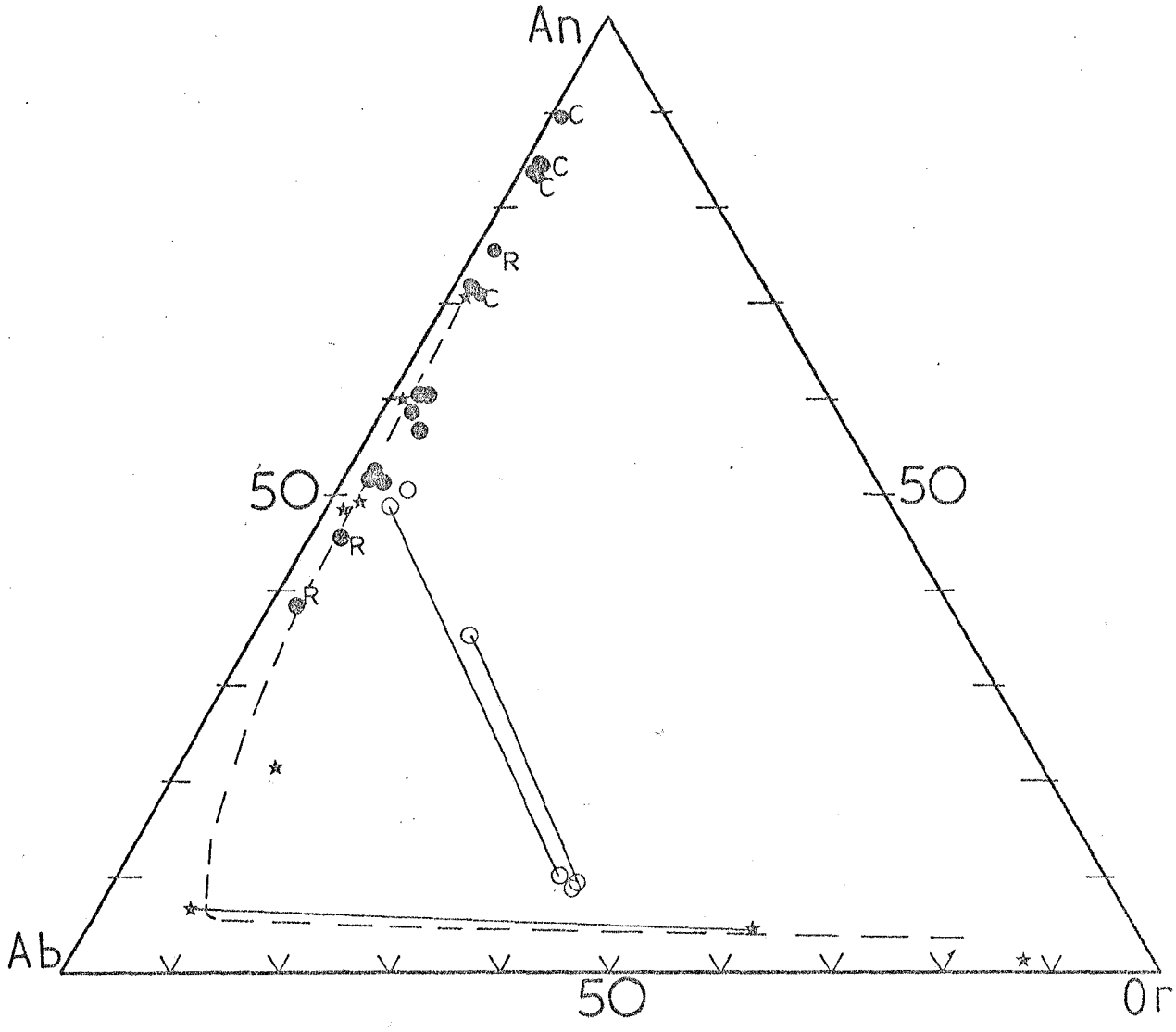

Figure 4.2

Plagioclase-alkali feldspar variation in Tambora lavas and intrusive rocks. Filled circles are phenocrysts from the lavas - cores-C,rims-R,open circles are groundmass plagioclase and alkali feldspar.Coexisting groundmass plag. and alkali feldspar are connected by tie-lines.Stars denote feldspar from alkali gabbro T28 Tie-line connects plagioclase rim composition with interstitial K-feldspar.The dashed line represents the approximate compositional variation of the feldspars of the intrusive rock,these showing markedly less ternary solid solution than those of the lavas.

Table 4.6

Representative Analyses of Feldspars from Tambora Lavas and Intrusives

Analysis No.	1	2	3	4	5	6	7	8	9	10	11	12	13
Sample No.	T13	T13	T13	T17	T17	T30	T32	T30	T30	T28*	T28*	T28*	T28*
	MP	P	P-C	P-C	P-R	P	P	G-AF	G-AF	P-C	P-R	G-AF	G-AF
SiO_2	51.4	50.7	51.8	47.4	47.7	47.5	48.7	63.0	61.8	50.1	62.9	63.5	63.5
Al_2O_3	30.1	30.6	29.7	33.1	32.8	34.1	32.4	21.7	20.2	31.1	21.1	20.1	19.1
FeO	0.4	0.5	0.7	0.6	0.6	0.5	0.6	0.2	0.4	0.5	0.33	-	-
MgO	-	-	-	-	-	-	-	-	-	0.2	-	-	-
CaO	12.3	12.9	11.7	16.8	16.8	16.5	14.6	2.1	1.9	14.2	4.9	0.9	0.3
Na_2O	4.6	4.3	5.7	1.5	1.7	1.0	3.1	5.7	5.1	3.1	8.9	3.8	1.4
K_2O	0.8	0.7	0.4	0.2	0.2	0.14	0.4	7.0	7.0	0.25	1.7	10.0	14.8
TiO_2	0.15	0.13	-	0.1	-	0.13	0.13	0.2	0.4	-	-	0.3	-
Total	99.75	99.83	100.0	99.7	99.8	99.8	99.93	99.9	96.8	99.5	99.8	98.6	
	Number of Ions on the basis of 8 oxygens:												
Si	2.351	2.320	2.369	2.180	2.195	2.172	2.234	2.845	2.878	2.300	2.821	2.920	2.957
Al	1.621	1.651	1.597	1.794	1.780	1.838	1.751	1.154	1.109	1.684	1.116	1.091	1.041
Fe	0.016	0.019	0.027	0.024	0.024	0.020	0.023	0.009	0.014	0.021	0.012	-	-
Mg	-	-	-	-	-	-	-	-	-	0.014	-	-	-
Ca	0.603	0.635	0.574	0.829	0.826	0.811	0.716	0.102	0.096	0.696	0.236	0.046	0.011
Na	0.411	0.382	0.503	0.139	0.153	0.086	0.272	0.503	0.461	0.272	0.773	0.334	0.124
K	0.049	0.039	0.024	0.013	0.009	0.008	0.023	0.403	0.414	0.015	0.097	0.586	0.879
Ti	0.005	0.004	-	0.004	-	0.005	0.005	0.007	0.013	-	-	0.009	-
Total	5.056	5.050	5.094	4.983	4.987	4.940	5.024	5.023	4.990	5.002	5.056	4.986	5.021
An	56.72	60.16	52.15	84.42	83.62	89.55	70.79	10.14	9.91	70.80	21.3	4.8	1.3
mol.% Ab	38.66	36.17	45.68	14.21	15.45	9.52	26.91	49.87	47.46	27.6	69.9	34.6	12.2
Or	4.63	3.67	2.17	1.37	0.93	0.93	2.3	39.99	42.63	1.5	8.8	60.6	86.5

Notes: Abbreviations: MP - microphenocryst, P - phenocryst, C - core, R - rim, G - groundmass, AF - alkali feldspar

Analyses 1-0 from Tambora lavas.

*Denotes feldspar from intrusive (T28).

Groundmass feldspars are plagioclase of labradorite to andesine compositions (ca. An40-An59) and sanidine (An10 Ab50 Or40 - An10 Ab47 Or43) (figure 4.2).

Clinopyroxene is the most abundant ferromagnesian mineral and though it exhibits some optical zonation actual compositional variations are relatively small (figure 4.3). Analysed examples range from Ca-rich augite to salite (Ca46 Mg41 Fe13, Mg/Mg+Fe = 0.76 - Ca46 Mg39 Fe15, Mg/Mg+Fe = 0.72), with between 3 and 4 wt.% Al_2O_3 and 0.7 and 1.0 wt.% TiO_2 (table 4.7). They are quite similar to the clinopyroxenes from the *ne*-normative, high-Al basalts from Rindjani and have markedly higher Ti and Al than cpx from Rindjani andesites.

In the most mafic lavas cpx is the most abundant mafic mineral, accompani by slightly less abundant olivine (e.g. PS8, T2, T17, tables 4.1 and 4.2 and 4.5), though they differ from the Rindjani ankaramites, for instance, in that they contain relatively abundant plagioclase.

In some of these lavas, particularly those of P. Satonda, the most mafic of the Tambora series, cpx occurs as tightly interlocking polycrystalline clots, occasionally including minor olivine and magnetite. Cpx also occurs in the groundmasses as fine granules.

Olivine occurs as subhedral phenocrysts in all lavas with <53% SiO_2 and also in the groundmasses. Phenocryst compositions (figure 4.3 and table 4.8) range from Fo71 to Fo62, while groundmass olivine is more iron-rich (Fo40). Small olivine inclusions may occur in plagioclase or cpx phenocrysts. In a few instances olivine is replaced by carbonate (e.g. T8) or is iddingsitized (T3) or embayed and corroded (T3).

Titanmagnetite is a minor phenocryst phase in most lavas and may occur as euhedral or as embayed anhedral-grains. Compositional variation is limited (20-35 mol.% Usp table 4.9).

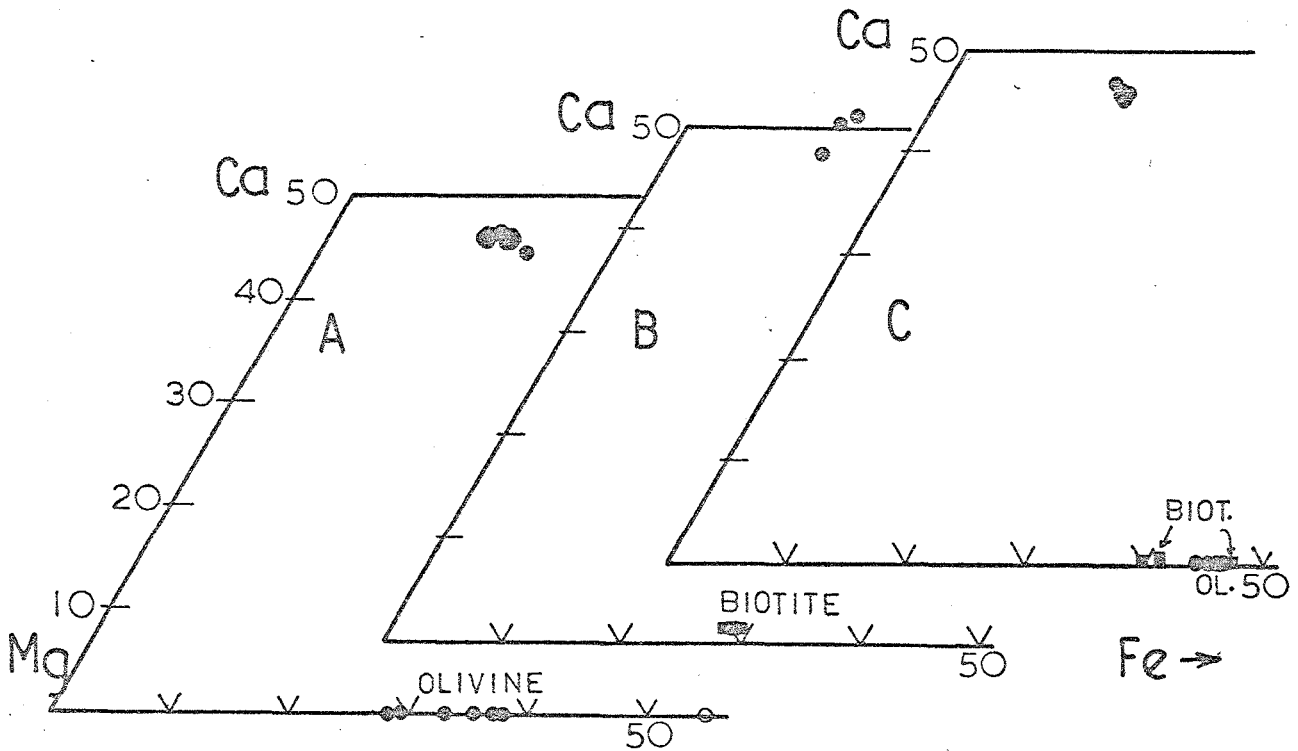

Figure 4.3

Compositions of Tambora ferromagnesian minerals in terms of relative atomic proportions of Ca-,Mg- and Fe-end-members..A = clinopyroxene and olivine of ne-trachybasalt lavas,B=clinopyroxene and biotite of ne-trachyandesite T32,C= clinopyroxene,biotite (squares) and olivine from alkali gabbro T28.In A the open circle denotes a groundmass olivine.

Table 4.7

Representative Analyses of

Clinopyroxenes from Tambora Lavas and Intrusives

Analysis No.	1	2	3	4	5	6	7
	T13	T13	T13	T30	T30	T28	T28
	P-C	P-R	P	P	G	P-I	P-I
SiO_2	51.4	50.6	50.4	49.7	51.5	49.8	50.4
Al_2O_3	3.3	4.1	3.9	5.0	2.5	4.1	3.7
FeO	8.1	8.4	8.9	9.5	9.3	8.6	9.3
MgO	14.0	13.8	13.2	12.9	13.3	13.2	13.6
CaO	21.9	22.0	22.0	21.5	22.1	22.3	22.0
Na_2O	-	-	-	-	-	0.4	-
K_2O	-	-	-	-	-	-	-
TiO_2	0.8	0.9	1.0	1.0	0.8	0.7	0.8
MnO	0.25	-	0.5	0.2	0.2	-	-
Total	99.75	99.80	99.90	99.80	99.7	99.10	99.8
100Mg/Mg+Fe	75.62	74.64	72.66	70.89	71.84	73.3	72.2
	Number of Ions on the basis of 6 oxygens.						
Si	1.909	1.884	1.884	1.858	1.925	1.879	1.885
Al	0.091	0.116	0.116	0.142	0.075	0.121	0.115
Al	0.054	0.063	0.054	0.080	0.036	0.060	0.046
Fe	0.259	0.260	0.277	0.296	0.292	0.270	0.292
Mg	0.776	0.766	0.737	0.722	0.744	0.744	0.759
Ca	0.874	0.878	0.882	0.863	0.885	0.902	0.883
Na	-	-	-	-	-	0.028	-
K	-	-	-	-	-	-	-
Ti	0.021	0.025	0.028	0.027	0.023	0.020	0.023
Mn	0.008	-	0.014	0.006	0.007	-	-
Z	2.000	2.000	2.000	2.000	2.000	2.000	2.000
X+Y	1.985	1.992	1.992	1.994	1.987	2.024	2.003
Ca/Ca+Mg(mol.)	0.530	0.534	0.545	0.544	0.543	0.548	0.538
Ca	45.98	46.10	46.50	45.90	46.06	47.0	45.6
mol.% Mg	40.85	40.23	38.87	38.35	38.75	39.0	39.3
Fe	13.17	13.67	14.63	15.75	15.19	14.0	15.1

Abbreviations: P - phenocryst, R - rim, C - core

G - groundmass, I - intrusive.

Notes: Analyses 1-5 from Tambora lavas,

6-7 from intrusive xenolith T28.

The groundmass has an intersertal to trachytic texture, with occasional small glassy areas between laths of plagioclase and sanidine and granules of cpx, olivine, titan magnetite and needles of apatite. Leucite occurs as a groundmass phase in those lavas with more coarsely crystalline groundmass (e.g. T3, tables 4.2 and 4.5). In these it occurs as large (up to 1mm), isotropic blobs containing numerous inclusions of microlites (plagioclase, cpx, sanidine, apatite). It lacks the characteristic twinning seen in the larger leucite phenocrysts and microphenocrysts in the leucite-normative lavas from Soromundi and G. Sangenges.

In a number of lavas, clear intersertal leucite was the last phase to crystallize. In this situation it occurs as near-spherical, faceless grains with a glass-like appearance, occupying large areas of the groundmass (e.g. T2

These leucites appear to be stoichiometric, with very little substitution of Fe^{3+}, unlike leucite described by Carmichael (1967) from the Leucite Hills locality in Wyoming. They are relatively CaO-rich, but are well within the range of leucite compositions of Deer et al. (1963, p.280).

4.3 Petrography of potassic ne-trachyandesites (>53% SiO_2)

Lavas with >53% SiO_2 (banakites or potassic *ne*-trachyandesites), closely resemble Joplin's (1969) banakite definition. In particular they are commonly rich in biotite phenocrysts (e.g. T32 modal analysis table 4.5 whole-rock analysis table 4.3). They differ petrographically from the lavas with <53% SiO_2 in that olivine is generally absent and many (e.g. T32, T43, T29, T41 table 4.3, 4.4) are glass-rich, with <15% phenocrysts. This group was described by Petroeschevsky (1949) as glassy lava-bombs. Many are scoriaceous and appear to represent the products of the last eruption of Tambora (1815). The modal analysis of trachyandesite T32 given in table 4.2 is typical of this group of lavas. T32 is composed of phenocrysts of cpx, plagioclase, sanidine, titan magnetite, biotite and occasional micro-phenocrysts of apatite set in a matrix largely composed of brown glass (analysis given in table 4.10)

Table 4.8

Representative Analyses of Olivine from Tambora Lavas and Intrusive Rocks

Analysis No.	1	2	3	4	5	6	7	8
Sample No.	T13	T13	T17	T30	T30	T28	T28	T28
	P	P	P	P	G	P-I	P-I	P-I
SiO_2	35.6	36.6	36.5	36.3	32.9	35.2	35.0	35.1
FeO	32.0	29.0	25.6	26.2	43.8	38.4	39.6	39.2
MgO	30.2	32.7	36.0	35.7	20.1	25.7	25.1	24.9
CaO	0.5	0.35	0.4	0.3	0.6	0.3	0.4	0.4
TiO_2	-	0.1	0.1	0.1	0.2	-	-	-
MnO	1.4	1.1	1.2	1.1	2.4	1.20	1.2	1.4
Total	99.7	99.85	99.8	99.7	100.0	100.8	101.3	101.0
	Number of Ions on the Basis of 4 oxygens.							
Si	0.983	0.991	0.975	0.971	0.972	0.989	0.986	0.989
FeO	0.738	0.655	0.571	0.587	1.083	0.905	0.933	0.925
Mg	1.243	1.319	1.431	1.425	0.883	1.078	1.055	1.045
Ca	0.014	0.010	0.012	0.009	0.017	0.010	0.011	0.012
Ti	-	0.002	0.002	0.003	0.004	-	-	-
Mn	0.033	0.026	0.026	0.026	0.060	0.029	0.028	0.034
Total	3.011	3.003	3.017	3.021	3.019	3.010	3.014	3.005
$100Mg/Mg+Fe$	62.77	66.81	71.47	70.83	44.93	54.4	53.1	53.0

Abbreviations: P - phenocryst; G - groundmass; I - intrusive

Clinopyroxene phenocrysts (table 4.7 and figure 4.3) are salites or Ca-rich augites identical to those of the less silica-rich lavas, showing rather limited compositional variety (Ca47 Mg40 Fe13, Mg/Mg+Fe = 0.75 - Ca51 Mg35 Fe14, Mg/Mg+Fe = 0.72). Plagioclase phenocrysts range from labradorite to bytownite (An70-An84) and are also similar to those of the more mafic lavas of this suite. They may be zoned and/or corroded or sieved, often with clear outer zones and with K-feldspar rims. Sanidine occurs as clear, untwinned, tabular grains with a composition An9 Ab50 Or41 (table 4.6, figure 4.2). Biotite analyses are given in table 4.11. They show very limited variation and their Mg/Mg+ΣFe values range from 0.70 to 0.72. They contain quite substantial amounts of TiO_2 (ca. 6.50 wt.%). Titan magnetite has a composition of about 22 mol.% Usp., again rather similar to that of the lavas with <53% SiO_2.

Holocrystalline lavas, compositionally identical to the glassy-trachy-andesites also occur (for example T20; see modal analysis in table 4.5 and whole rock analysis in table 4.4). These are porphyritic lavas with phenocrysts of augite, plagioclase (labradorite-bytownite) and titan magnetite, with occasional microphenocrysts of apatite and flakes of biotite. Their groundmass is composed of euhedral, coarsely crystalline, andesine and sanidine, with minor augite, magnetite, apatite needles and abundant leucite as clear, glassy interstial material and round ocelli, rich in inclusions of other groundmass minerals.

4.4 Intrusive Rocks.

Unlike the xenoliths from Sangeang Api, Soromundi and G. Sangenges, which appear at least in part to be of cumulate origin, and do not resemble their associated lavas in bulk composition, these from Tambora (samples T28, T33, T4 and T6 see table 4.5 for representative modal analyses and table 4.4 for whole-rock geochemical data) have compositions not unlike those of the

Table 4.9

Representative Analyses of

Magnetite from Tambora Lavas and Intrusive Rocks

Analysis No.	1	2	3	4	5
Sample No.	T13	T13	T17	T30	T28
	P	P	P	P	I
SiO_2	-	-	-	-	-
Al_2O_3	5.3	3.1	6.6	4.4	5.6
FeO	37.1	40.8	31.2	41.7	40.2
Fe_2O_3	44.1	42.2	49.9	40.6	41.6
MgO	1.6	0.9	4.9	0.5	0.7
CaO	-	-	-	-	-
Cr_2O_3	0.2	-	-	0.5	-
MnO	0.5	0.6	-	0.4	0.6
TiO_2	9.2	12.0	7.0	11.8	10.7
Total	98.0	99.6	99.6	99.4	99.4
	Number of cations based 32 oxygens				
Si	-	-	-	-	0
Al	1.867	1.091	2.224	1.538	1.953
Fe^{2+}	9.274	10.192	7.460	10.3	9.949
Fe^{3+}	9.909	9.475	10.725	9.051	9.256
Mg	0.713	0.401	2.088	0.221	0.309
Ca	-	-	-	-	-
Cr	0.047	-	-	0.117	-
Mn	0.126	0.152	-	0.100	0.150
Ti	2.068	2.700	1.505	2.632	2.382
Total	24.00	24.00	24.00	24.00	24.00
Mol.% U.spinel	26.98	34.33	19.66	34.08	31.00

Abbreviations: P - phenocryst; I - intrusive.

Table 4.10

Representative Microprobe Analysis

of Glass from Tambora - Trachyandesite T32

Analysis		C.I.P.W. Norm.	
SiO_2	56.2	*An*	4.0
Al_2O_3	19.4	*Ab*	17.3
Fe_2O_3*	1.8	*Or*	41.4
FeO	3.0	*Di*	14.5
MgO	0.8	*Wo*	0.4
CaO	4.8	*Ne*	19.4
Na_2O	6.3	*Mt*	1.1
K_2O	7.0	*Il*	1.5
TiO_2	0.8		
Total	100.1	Qt_3	33.0
		Ne	36.9
100Mg/Mg+Fe	23.2	Ks	30.1
K_2O/Na_2O	1.11		

Notes: Analysis by electron microprobe, Fe determined as FeO and arbitrarily recast to FeO .65 ΣFe, Fe_2O_3 .35 ΣFe for purposes of norm calculation.

Table 4.11

Representative Analyses of Biotite from Tambora Lavas and Intrusive Rocks

Analysis No.	1	2	3	4	5
Sample No.	T32	T32	T28	T28	T28
	P	P	I	I	I
SiO_2	35.6	36.2	35.6	35.5	36.1
Al_2O_3	15.7	15.4	14.4	15.0	14.5
FeO	11.2	11.7	21.0	18.1	17.5
MgO	15.9	15.9	13.0	14.5	14.8
CaO	0.5	0.4	-	0.2	-
Na_2O	-	-	0.1	0.3	-
K_2O	10.5	10.7	9.8	9.5	9.3
MnO	-	-	0.2	0.3	-
TiO_2	6.5	6.4	0.3	0.4	0.5
Total	95.9	96.7	94.4	93.8	92.7
	Number of Ions on the Basis of 22 oxygens.				
Si	5.260	5.310	5.566	5.521	5.622
Al	2.737	2.666	2.663	2.746	2.655
Fe	1.379	1.433	2.741	2.351	2.282
Mg	3.504	3.482	3.033	3.355	3.449
Ca	0.073	0.057	-	0.037	-
Na	-	-	0.029	0.075	-
K	1.984	2.011	1.955	1.880	1.849
Mn	-	-	0.029	0.033	-
Ti	0.717	0.702	0.031	0.043	0.059
Total	15.654		16.108	16.041	15.916
$100Mg/Mg+Fe$	71.76	70.84	52.50	58.80	60.20

Abbreviations: P - phenocryst; I - intrusive xenolith

lavas, and may represent actual liquid compositions. Substantiating this, on MgO-variation diagrams (figures 4.4 and 4.5), they plot on, or close to, the volcanic rock trends, within the general field of the lavas. They appear to represent shallow-level intrusive equivalents of the magmas erupted to yield the Tambora volcanic rocks.

They are composed of phenocrysts of cpx, olivine, plagioclase, magnetite, apatite and biotite, with sanidine which poikilitically encloses these phenocrysts. Interstitial areas are composed of finely intergrown potassium feldspar and nepheline. Coronas or rosettes of biotite rim, and appear to be partly replacing olivine and in particular, magnetite, and to a lesser extent cpx. Olivine is also partly replaced by magnetite.

They bear a striking resemblance in chemical composition, mineralogy and texture to alkali gabbros or shonkinites, from the Shonkin Sag laccolith in Montana (Hurlbut, 1939; Nash and Wilkinson, 1970, 1971).

Plagioclase (table 4.6, figure 4.2) is zoned and has core compositions in the range An60-An72, while rims range from An48 to An21 (with 8.8 mol.% Or molecule). Interstial oikocrystic and groundmass feldspar (table 4.6, figure 4.2) range from Or 60.6 (An 4.8) to Or 95.7 (An 4.2).

Olivine (table 4.8) is very iron-rich with Mg/Mg+Fe values that range from 0.53 to 0.55 and high concentrations of MnO (1-2%). The olivine of the intrusive rocks is considerably more Fa-rich than that of the phenocrysts of the lavas and also has markedly lower Mg/Mg+Fe values than the clinopyroxene (Mg/Mg+Fe = 0.72 - 0.73) coexisting in the xenoliths. Clinopyroxene has a restricted compositional range and is virtually the same composition as the phenocrysts in the lavas (table 4.7, figure 4.3). Cpx is of salite or Ca-augite composition (Ca47 Mg49 Fe14, Mg/Mg+Fe = 0.73 to Ca 46.1 Mg 38.4 Fe 15.5, Mg/Mg+Fe = 0.72), with about 0.7-0.9% TiO_2 4% Al_2O_3 and <3% Na_2O. Biotite (table 4.11, figure 4.3) is of somewhat variable composition and has Mg/Mg+ΣFe values ranging from 0.525 to 0.602. It is notably TiO_2-poor,

FIGURE 4.4

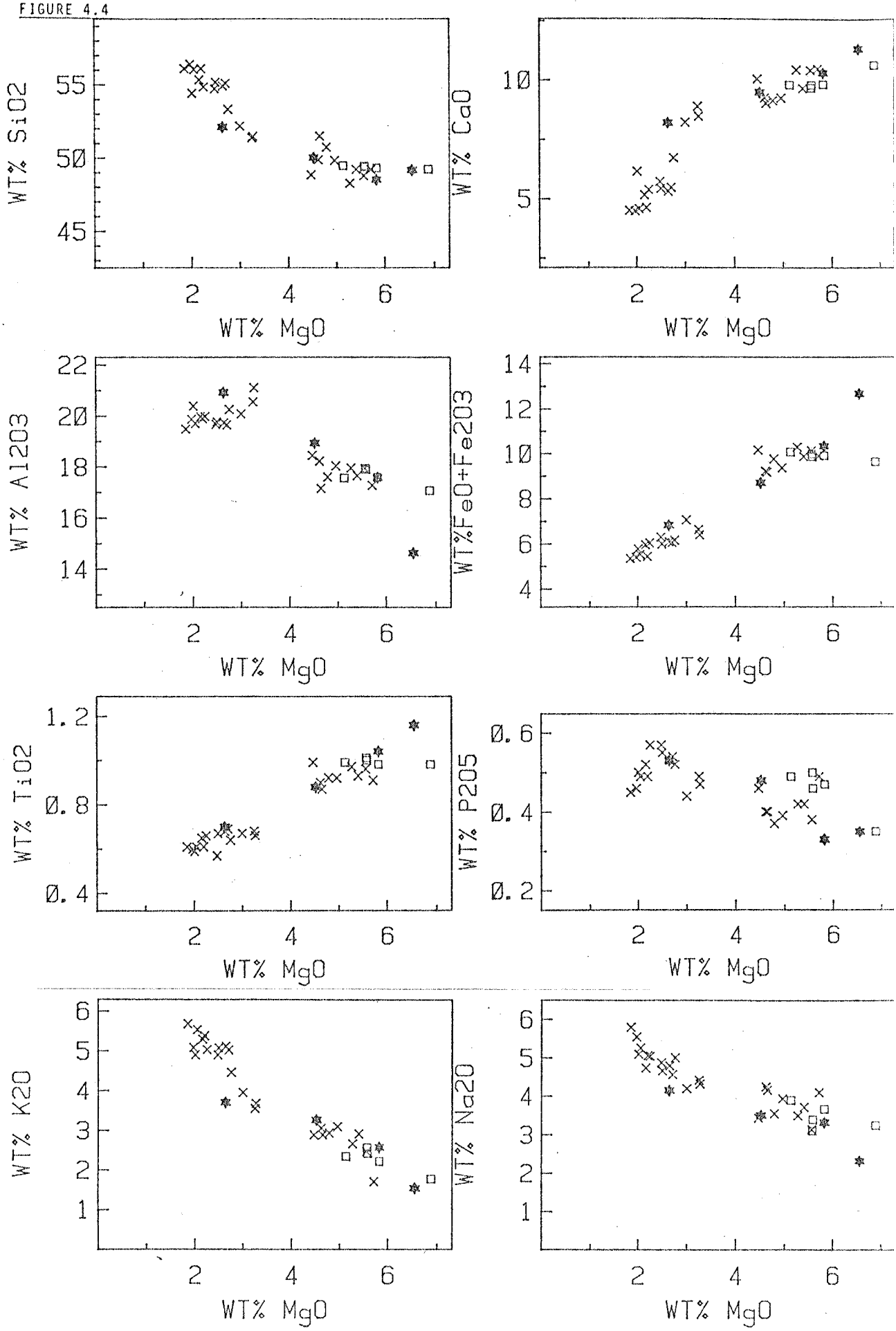

Figure 4.4

MgO v. Major Element variation of the lavas and intrusive rocks from Tambora volcano and of the lavas from its offshore parasitic cone P.Satonda.Tambora lavas are denoted by crosses (X) and intrusive nodules by stars (*) .Open squares denote lavas from P.Satonda.

FIGURE 4.5

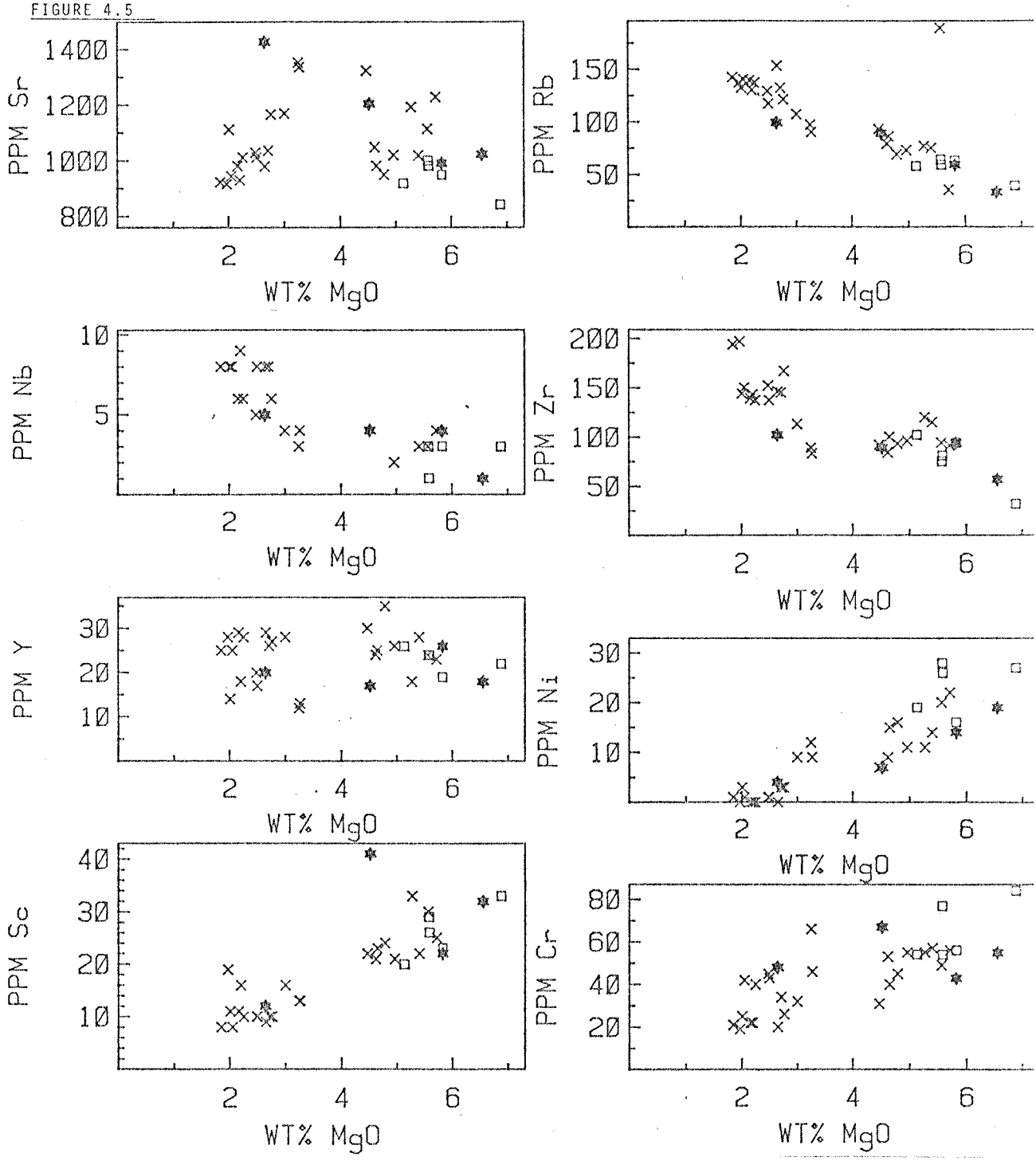

Figure 4.5

MgO v. Trace Element variation of lavas and intrusive rocks from Tambora volcano and of its offshore parasitic cone P.Satonda.Tambora lavas are denoted by denoted by crosses (X) and intrusive nodules by stars (*).Open squares denote lavas from P.Satonda .

having only 0.5-0.3%. By comparison the biotites of the trachybasalts (table 4.11, figure 4.3) have Mg/Mg+Fe values of about 0.71 - 0.72 and 5.0 - 6.0 wt.% TiO_2. Magnetite is similar to that of the lavas having ca. 30 mol.% Usp.

4.5 Geochemistry of the Tambora Lavas and Intrusive Rocks.

The lavas of the Tambora volcano (including those of its parasitic cone, P. Satonda) are entirely *ne*-normative, including the trachyandesites with as much as 57% SiO_2. In fact, the most undersaturated lava (T20, table 4.4), with 11.49% normative nepheline is also the most silica-rich. This is quite unlike the Rindjani suite where differentiation appears to lead to increasing quartz-normative, silica-enriched, derivatives.

The lavas of the Tambora suite are K_2O-, Sr and Rb-rich and have quite high P_2O_5 concentrations. These elements are markedly more concentrated in the Tambora lavas than in those of Rindjani volcano.

Features the suite has in common with the Rindjani suite as well as with volcanic rocks of convergent-plate volcanic arcs in general include: high Al_2O_3, relatively low MgO, TiO_2, Zr and Nb and limited variation in Mg/Mg+ΣFe in rocks with intermediate silica content (i.e. limited iron enrichment on the AMF diagrams (figure 4.6)). Both trachybasalts and trachyandesites have low Ni concentrations and show marked enrichment of LIL elements with increasing SiO_2.

Rocks similar to this group of lavas are uncommon in most other island arc environments. They are perhaps equivalent to the shoshonites as described by Joplin (1969), but the absarokite-shoshonite-banakite series from Wyoming (Nicholls and Carmichael, 1969) is oversaturated, and more silica-rich members contain orthopyroxene, in marked distinction to those lavas from Tambora. The most similar rocks are the potassium-rich lavas of the Roman Province, Italy (Appleton, 1972). Appleton (1972) describes two series: A K_2O-rich one and a relatively K_2O-poor one, that is similar to the Tambora suite.

FIGURE 4.6

A-M-F variation of Tambora Lavas (+), P.Satonda lavas (○) Tambora intrusives (✱), Sangeang Api olivine-bearing (●) and amphibole bearing (□) lavas and coarse-grained intrusive xenoliths (▲).

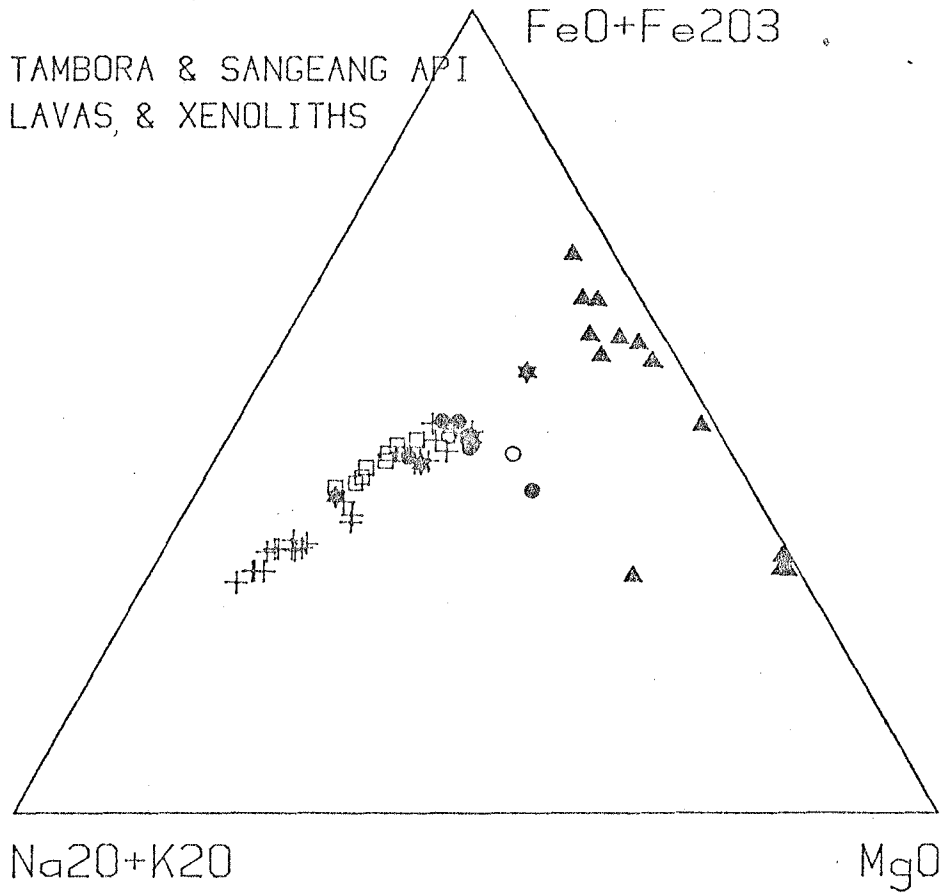

1. Geochemical variation trends.

Data are presented both in tabular form (tables 4.1-4.4) and as MgO variation diagrams (figures 4.4 and 4.5). The lavas of Sangeang Api volcano are somewhat similar to those of Tambora, (but with important distinctions) and the data from both these volcanoes areplotted on figures 4.7 and 4.8.

Compared with the Rindjani calcalkaline suite, the Tambora volcanic rock: shows less compositional diversity and generally show more coherent variation trends. In very general terms, SiO_2, Al_2O_3, K_2O, Na_2O, Rb, Zr and Nb all show negative correlation with MgO (figures 4.4 and 4.5). K_2O/Na_2O and Rb/Sr ratios also increase with decreasing MgO, while the K/Rb ratio, though showin some variation, generally remains constant throughout the series (figure 4.9). Sr and P_2O_5 and to a less marked extent, Al_2O_3, show trends of initial enrich ment with decreasing MgO followed by depletion.

Considering the variation trends in more detail, there are a number of significant features.

A. There is a marked gap in the MgO variation trends between 3.5 and 4.5% MgO. Although this may be a sampling deficiency, this zone appears to represent a definite discontinuity in the range of a number of other elements and a marked inflection in the variation curves of most major- and trace-elements. This discontinuity appears to reflect a transition from relatively cpx-olivine-rich lavas to types relatively more plagioclase- and/or glass-rich. Olivine is always present as a phenocryst phase in the more MgO-rich lavas (to the right of the gap in figures 4.4 and 4.5), whereas it is scarce or absent from those on the MgO-poor side. This discontinuity may be akin to that already noted from the Rindjani series, between the andesites and high-K_2O andesites and dacites.

FIGURE 4.7

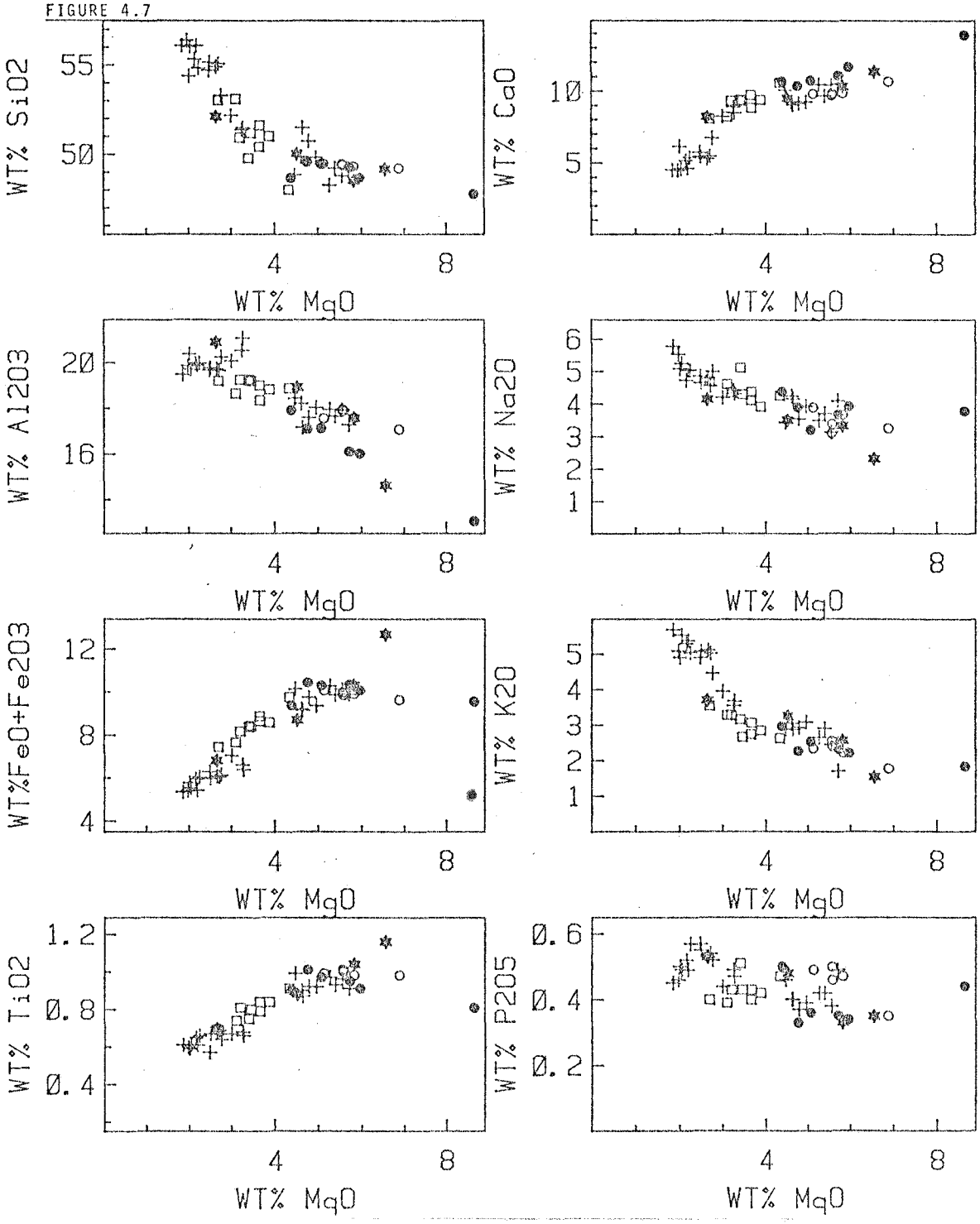

Figure 4.7

MgO v. Major Element variation of Tambora lavas (+),P.Satonda lavas (○) Tambora intrusives (✱),Sangeang Api olivine megacryst bearing (◉) and amphibole bearing (□) lavas.

FIGURE 4.8

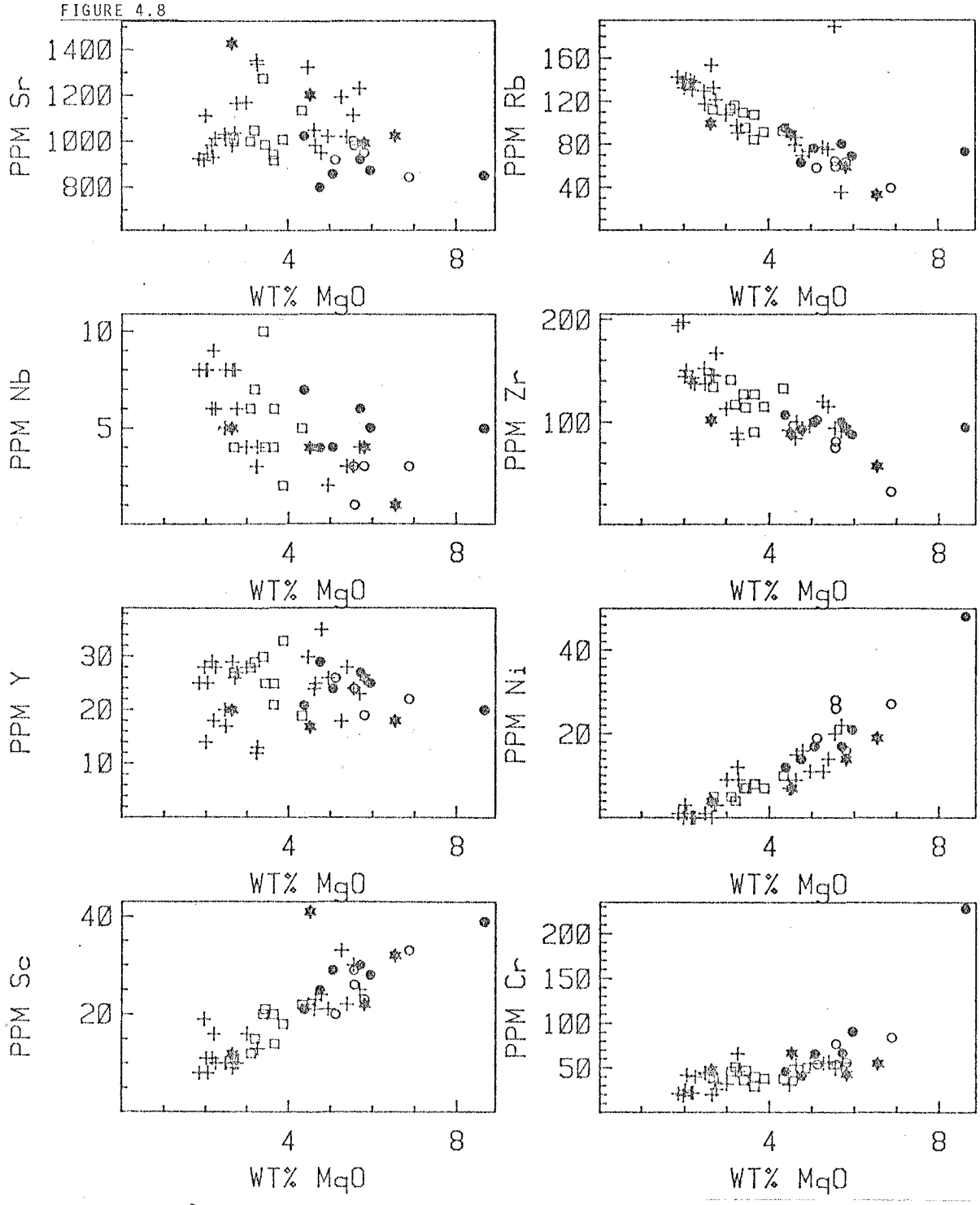

Figure 4.8

MgO v. Trace Element variation of Tambora (P.Satonda) lavas and intrusives and Sangeang Api lavas .Symbols denote the same samples as in figure 4.7.

With respect to decreasing MgO and the trends on the high MgO side of the gap; CaO shows an increased rate of depletion, total Fe, TiO_2 and Sc show a decreased rate of depletion, Al_2O_3 and Sr show a change from enrichment to marked depletion trends, SiO_2, K_2O, Na_2O, Zr and Nb show decreased rates of enrichment. The Rb/Sr ratio also increases very rapidly. There is a marked decrease in the proportion of normative *di* and *ol* and an increase in the proportion of normative feldspar, which also becomes relatively less An-rich.

B. P_2O_5 also shows a very marked inflection, but at lower MgO contents than that of Sr and Al_2O_3. It shows a steady trend of enrichment with decreasing MgO right through to about 2.3% MgO and then decreases rapidly with further MgO depletion.

C. K_2O and K_2O/Na_2O show trends of enrichment with increasing SiO_2 (figures 4.10 and 4.11). However, at about 56% SiO_2 there is marked inflection in the trends and these components show negative correlation with SiO_2 between 56 and 57% silica. This inflection correlates with the appearance of biotite in these rocks.

2. P. Satonda Lavas.

These are relatively richer in clinopyroxene and olivine than the other basaltic lavas collected from the main Tambora cone. Their phenocryst assemblages are also relatively clinopyroxene enriched by comparison with the Rindjani alkali olivine basalts. In this respect they are more like the basaltic andesites from Rindjani. The P. Satonda lavas are amongst the most mafic of the general Tambora group and generally fall on linear extensions of the Tambora trend towards the high MgO end of the area (figures 4.4 and 4.5). There is some suggestion of a slight inflection of MgO variation trends for a number of elements at about 5% MgO. In

FIGURE 4.9

K v. Rb (log-log) variation of Tambora lavas and intrusives and Sangeang Api lavas.

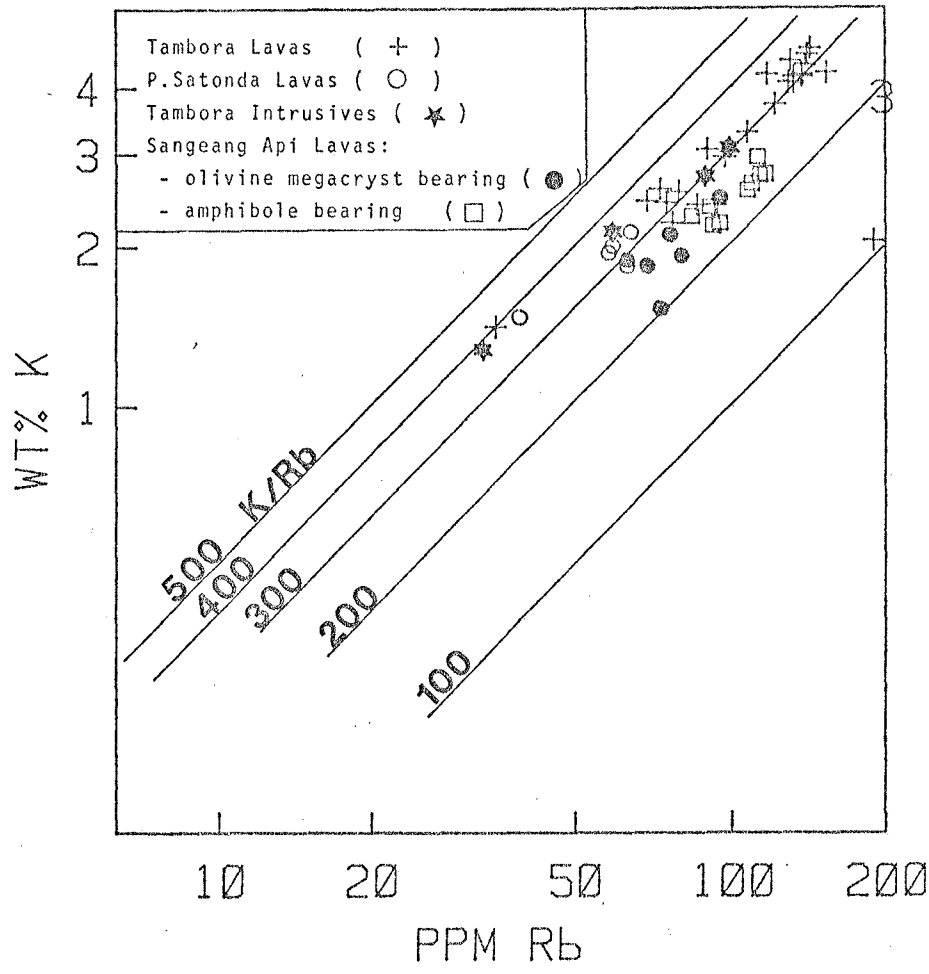

particular ΣFe and TiO_2 show horizontal or even slight enrichment trends with decreasing MgO, changing to marked depletion trends at ca. 5% MgO. This probably reflects the appearance of magnetite as an important phase at this point in the differentiation of the suite.

3. Intrusive Rocks.

In contrast to the presumed cumulate xenoliths from Sangeang Api (chapter 5) the intrusive rocks from Tambora (T28, T33, T4, T6, tables 4.4 and 4.5, figures 4.4 and 4.5) are of very similar composition to the associated lavas. They have similar MgO contents, similar Mg/Mg+Fe values and comparable, high K_2O, Rb and Sr contents. They generally plot within the field of the Tambora lavas, or in one case (that of T33) on a slightly high-MgO extension of this general group (figures 4.4 and 4.5). This one rock may be of partly accumulative origin as it has markedly higher ΣFe, TiO_2 and Sc compared with the lavas of similar MgO content. The other xenoliths appear to represent direct crystallisation products of the liquids similar to lavas erupted by the Tambora volcano. As discussed previously, they are both petrographically and compositionally quite similar to the shonkinites of the Shonkin Sag laccolith.

4.6 Comparison of the Tambora lavas with those of Rindjani.

Comparison of the geochemistry and geochemical variation of the Tambora and Rindjani suites shows that although the Rindjani alkali olivine basalts resemble the more magnesian Tambora lavas, there are important differences in K_2O, Rb, Sr and P_2O_5 concentrations.

The differentiation paths of the two suites also show important differences: the Tambora lavas retain their *ne*-normative character, whereas the more evolved Rindjani lavas (with >53% SiO_2) are *Q*-normative.

Table 4.12 shows the compositions of two typical high-Al, *ne*-normative, alkali olivine basalts from Rindjani and two Tambora trachybasalts. It is

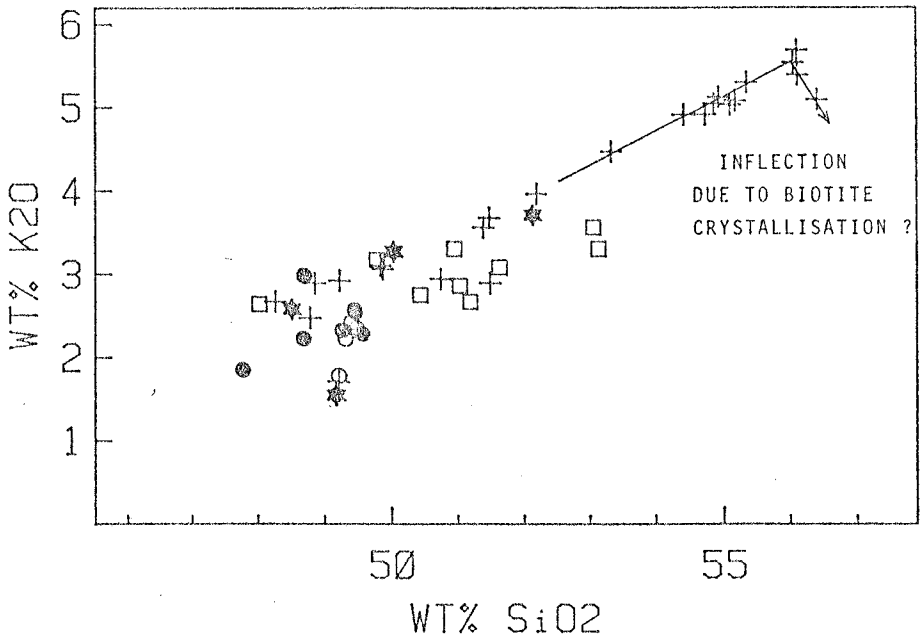

FIGURE 4.10 K_2O v. SiO_2 variation ; Tambora Lavas and Intrusives (+ P.Satonda) and Sangeang Api Lavas.Symbols as in figure 4.9.

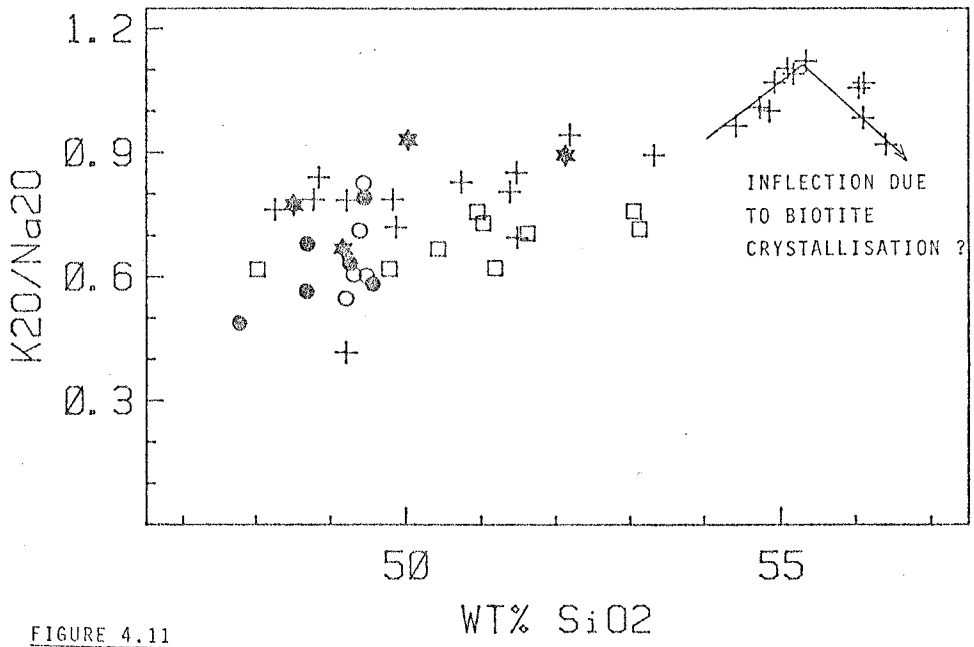

FIGURE 4.11 K_2O/Na_2O v. SiO_2 variation of Tambora lavas and intrusives (+P.Satonda) and Sangeang Api lavas .Symbols as in figure 4.9.

apparent that the two sets of analyses are very similar with respect to concentrations of SiO_2, Al_2O_3, ΣFe, MgO, Na_2O, CaO, MnO, Sc, Nb, Y, Cr, Mg/Mg+Fe, Rb/Sr and Zr/Nb values, but possess significantly different K_2O, P_2O_5, Rb and Sr values.

The Tambora trachybasalts have 2-3 times the concentration of K_2O, Rb, Sr and P_2O_5 than do the otherwise compositionally similar basalts from Rindjani. Yet TiO_2 concentrations are slightly higher in the Rindjani basalts and though Zr may be very slightly enriched in the Tambora trachybasalts, its enrichment is significantly less than that of Rb and Sr. Thus the Tambora lavas have markedly higher Sr/Zr and lower Zr/Rb ratios. The Rb/Sr ratios of both sets of basalts are very similar, while the Tambora trachybasalts have markedly lower K/Rb and higher K_2O/Na_2O ratios.

The similarity of the Rb/Sr ratios of the two groups may be significant in the light of their identical $^{87}Sr/^{86}Sr$ ratios (chapter 8).

The geochemical distinctions between the Rindjani and Tambora suites are further manifested in their mineralogy. In particular the Tambora lavas contain no orthopyroxene, even in representatives with intermediate silica content, whereas the Rindjani lavas with >53% SiO_2 do contain this phase. This is apparently a product of the more undersaturated character of the Tambora suite. The Tambora lavas contain groundmass sanidine and occasionally leucite, whereas these phases are absent from the Rindjani lavas due to the less alkaline character of the latter group.

Chapter 5

PETROLOGY OF LAVAS AND XENOLITHS FROM SANGEANG API

5.1 *Introduction*

Sangeang Api is an island-volcano off the north-east corner of Sumbawa (fig. 4.1), which apart from an entry in Neumann van Padang's (1951) catalogue of active volcanoes (Cat. 6, 4-4) has been the subject of only one publication (Ehrat, 1928). It has had a recent history of activity, having erupted violently in 1911 and 1953.

The Sangeang Api lavas are all undersaturated and show some geochemical similarities to the lavas of Tambora. In terms of Johnson et al.'s (1976) nomenclature, they range from relatively mafic potassic phonolitic tephrites and potassic *ne*-trachybasalts to potassic *ne*-trachyandesites. Sangeang Api is of particular interest however, in that it has erupted a diverse suite of mafic and ultramafic, coarse-grained intrusive rocks, which occur both as xenoliths in some lavas and as isolated blocks in tephra deposits.

This chapter discusses the petrography, mineralogy and geochemistry of both the lavas and intrusive rocks from Sangeang Api and also considers the affinities of the xenoliths to suites of mafic and ultramafic nodules erupted by volcanoes elsewhere.

5.2 *Petrographic Features of the Xenoliths and Erupted Intrusive Blocks*

The Sangeang Api coarse-grained blocks and xenoliths occur as isolated boulders and cobbles in fragmental volcanic deposits, as well as xenolithic inclusions within lava flows. In the lavas they range in size from small disaggregated fragments a few millimeters across, up to larger individuals 15-20 cm in diameter. Boulders and cobbles range up to 30 cm in diameter.

Some xenoliths appear to be in a reaction relationship with the enclosing lavas (plate 1), though many show no sign of reaction.

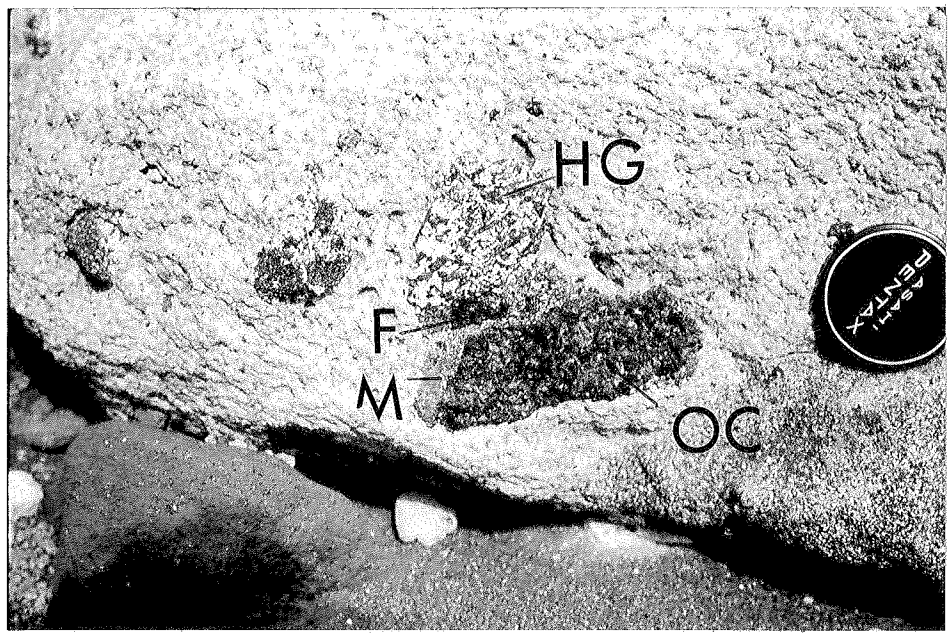

Plate 1

Composite xenolith in a ne-trachybasalt boulder in the 1953 lahar, Sangeang Api.

OC - olivine clinopyroxenite

HG - hornblende-anorthite-magnetite gabbro

f - fragment of olivine clinopyroxenite

M - fine gabbroic matrix.

The xenolith was incorporated in the trachybasalt magma after the fragmentation of the olivine clinopyroxenite and hornblende gabbro bodies and after subsequent re-incorporation of these fragments in a later fine gabbroic matrix.

The intrusive blocks and xenoliths range from clinopyroxene-rich varieties, lacking plagioclase, with variable amounts of olivine, magnetite, amphibole, phlogopite and apatite, through to plagioclase-rich (gabbroic) varieties with cpx and/or amphibole, magnetite, biotite/phlogopite and apatite.

Textures appear to be mainly of igneous origin, though some have undergone textural modification and deformation. Many individual nodules are composite and contain fragments of one coarse-grained rock-type included in another. Others are veined or partially disaggregated and suspended in a new coarse matrix, with which early fragments may show reaction.

Modal analyses of the Sangeang Api intrusive rocks are presented in tables 5.1 and 5.2 and the following distinct mineral assemblages and/or rock-types have been recognised.

1. olivine-clinopyroxenite (± phlogopite)
2. magnetite-clinopyroxenite
3. hornblende-magnetite-clinopyroxenite
4. alkali (phlogopite ± hornblende)-clinopyroxenite
5. plagioclase (anorthite)-bearing varieties (ranging from anorthite-hornblendite to cpx-gabbro).

The modal variation of the main component minerals in each of the above groups are summarised in figures 5.1 and 5.2, while whole-rock, major and trace element analyses of representative members of each of these groups are given in table 5.4.

5.2.1 Olivine Clinopyroxenites

These are the only xenoliths which contain more than a small amount of olivine, invariably lack plagioclase and contain little or no magnetite.

Modal analyses of typical members of this group (samples B23, B5, B4 and B9) are given in table 5.1. They are generally coarse-grained (cpx-2-4 cm) and are also often quite inhomogeneous. In handspecimens, some are

Table 5.1

Sangeang Api, Xenoliths - Modal Composition

Sample No.	Cpx	Ol	Amph	Phl.	Ti-Mag	Plag	Apat.	Reacted Amph.
Group 1								
B23	79	19		1	1			
B5	83.5	10	5	1	0.5			
B9	87	8	0.8	4	0.2			
B4	90	0.5	8	0.5	1			
Group 2								
B29	90			0.5	9	0.5		
B2D	83			0.1	15.5	1.0	0.1	
B1A	81.5				15	3		0.5
B2E	80.5	0.5	0.1		15.5	3.5	tr.	
B28	74				21	5		
B25x	75		3		16	6		
B2A	69	0.2	1.5	0.8	21	7.5		
B2H	69	tr.			11	20		
Group 3								
B20	47.5		39		13	0.5		
Group 4								
B21	79.5	0.2	16.5	0.2	1.7	1.7	0.1	
B16	75		12.5	3.5	8	1		
B22	72		11		12	5		
B13	60		9	30	1			
B6B	65		10	1	13	4.5	0.5	6
B15	48	4.5	5.5	11.5	7.5	22.5	0.5	
B14	68		5.3	1	8	17	0.7	
Group 5								
B1B	8		37		5	12	1	37
B24	15		49	1	8	24	3	
B7	19		20		11	30	tr	20
B14f	24		20	7	13	35	1	
B8	26		21		11	42		
B17	29		17	0.3	10	42	1.7	
B6A	31.5		10	0.3	7	48	0.1	3
B11	30		9		12	49		
B10	37		4	1	8	50		
B27x	21.5		4.5	0.3	3.7	56.5		13.5

Notes: Group 1 = olivine clinopyroxenites, Group 2 = magnetite clinopyroxenites Group 3 = hornblende-magnetite-clinopyroxenite, Group 4 = alkali clinopyroxenite, Group 5 = cumulate clinopyroxene, amphibole, plagioclase, magnetite, apatite gabbro.

Abbreviations: Cpx-clinopyroxene, Ol-olivine, Amph-amphibole, Phl-phlogopite, Ti-Mag-titan-magnetite, Plag-plagioclase, Apat-apatite.

Table 5.2 Least Squares Estimates of Modal Composition of Some Sangeang Api Xenoliths

Sample No.	B5	B5	B22	B22	B7	B7	B11	B11
Xenolith Type [2]	1	1	4	4	5	5	5	5
	obs.	est.	obs.	est.	obs.	est.	obs.	est.
SiO_2	48.42	48.41	41.90	42.10	39.47	39.57	38.96	39.33
Al_2O_3	4.24	4.22	7.72	7.61	17.64	17.58	19.58	19.41
FeO_T [1]	8.16	8.15	16.12	16.12	12.85	12.84	13.56	13.59
MgO	17.50	17.51	11.97	11.73	8.48	8.34	6.06	5.78
CaO	20.55	20.56	19.69	19.43	15.27	15.15	16.70	16.08
Na_2O	0.22	0.23	0.64	0.27	1.39	0.95	0.83	0.39
K_2O	0.04	0.18	0.15	0.23	0.60	0.81	0.22	0.13
TiO_2	0.59	0.68	1.41	1.71	1.55	1.85	1.26	1.12
P_2O_5	0.01	-	0.02	-	0.05	-	0.02	-
MnO	0.14	0.04	0.12	-	0.18	0.03	0.15	0.05
ΣR^2		0.0384		0.4203		0.4014		0.8570
Component (Wt%)								
Olivine		10.19		-		-		-
Cr-diopside		45.97		15.64		-		-
Augite		33.08		56.97		19.25		29.94
Amphibole		11.10		10.93		40.33		8.77
Plagioclase		-		4.25		30.55		45.53
Magnetite		0.18		12.43		10.85		12.52

Notes: See Table for reference to composition of minerals used in these calculations.

Abbreviations: obs - observed composition.

est - estimated composition.

[1] FeO_T = total iron as FeO.

[2] Xenolith Types: 1. olivine clinopyroxenite

4. alkali clinopyroxenite.

5. gabbroic cumulate.

Table 5.3

EAST SUNDA ARC VOLCANIC ROCKS

SANGEANG API - SUMBAWA, LAVAS

Sample#	B43	B44	B39	B38	B31	B29	B25	B34	B36	B35	B28	B27	B18	B42	B32
SiO_2	47.77	48.68	49.26	49.45	49.56	48.69	48.02	51.03	51.63	50.43	51.19	49.78	50.95	53.13	53.05
TiO_2	0.81	0.91	0.95	0.97	1.01	0.90	0.91	0.84	0.79	0.84	0.80	0.75	0.81	0.74	0.69
Al_2O_3	13.05	16.01	16.10	17.12	17.10	17.91	18.88	18.83	18.35	19.00	19.19	19.25	19.25	18.65	19.21
Fe_2O_3	1.57	1.65	1.70	1.69	1.71	1.54	1.60	1.41	1.42	1.46	1.38	1.37	1.34	1.26	1.22
FeO	8.00	8.44	8.65	8.62	8.74	7.84	8.16	7.20	7.24	7.43	7.06	7.02	6.85	6.41	6.23
MnO	0.17	0.20	0.21	0.21	0.22	0.21	0.12	0.22	0.21	0.22	0.23	0.21	0.21	0.22	0.22
MgO	8.65	5.96	5.72	5.07	4.76	4.38	4.33	3.88	3.66	3.65	3.45	3.40	3.20	3.10	2.69
CaO	13.90	11.67	11.06	10.74	10.36	10.68	10.59	9.38	8.82	9.71	9.30	9.37	9.31	8.19	8.05
Na_2O	3.79	3.93	3.67	3.21	3.91	4.38	4.27	3.92	4.37	4.12	4.30	5.12	4.36	4.61	4.69
K_2O	1.85	2.22	2.32	2.54	2.28	2.98	2.64	2.86	3.08	2.75	2.67	3.17	3.30	3.30	3.56
P_2O_5	0.44	0.34	0.35	0.36	0.33	0.50	0.47	0.42	0.43	0.40	0.43	0.51	0.43	0.39	0.40
H_2O+	1.14	1.07	1.08	0.95	0.87	1.22	1.09	1.21	1.35	0.87	0.96	1.00	1.57	0.87	1.05
Mg/Mg+Fe	0.62	0.52	0.50	0.47	0.45	0.46	0.45	0.45	0.43	0.43	0.43	0.42	0.41	0.42	0.40
Mg/Mg+.85Fe	0.66	0.56	0.54	0.51	0.49	0.50	0.49	0.49	0.47	0.47	0.47	0.46	0.45	0.46	0.43
K_2O/Na_2O	0.49	0.56	0.63	0.79	0.58	0.68	0.62	0.73	0.70	0.67	0.62	0.62	0.76	0.72	0.76
Trace elements (ppm)															
Rb	73	69	80	76	63	95	92	91	107	84	95	109	116	113	112
Sr	850	872	919	856	799	1023	1135	1007	916	943	984	1273	1047	999	1010
Zr	95	88	100	100	93	107	133	115	127	90	114	127	117	141	134
Nb	5	5	6	4	4	7	5	2	6	4	4	10	7	6	4
Y	20	25	27	24	29	21	19	33	25	21	25	30	29	28	27
La	38.8						37.5								40.8
Sc	39	28	30	29	25	21	22	18	14	20	21	20	15	12	11
Cr	228	91	67	66	41	46	38	38	40	29	47	36	51	46	38
Ni	48	21	17	17	14	12	10	7	8	8	7	7	4	5	5
Rb/Sr	0.086	0.079	0.087	0.089	0.079	0.093	0.081	0.090	0.117	0.089	0.097	0.086	0.111	0.113	0.111
K/Rb	210	267	241	277	300	260	238	261	239	272	233	241	236	242	264
K/Sr	18.07	21.14	20.96	24.63	23.69	24.18	19.31	23.58	27.92	24.21	22.53	20.67	26.17	27.42	29.26

Notes: FeO arbitrarily calculated as 0.85 total Fe. Analyses normalised anhydrous, H_2O^+ = pre-normalisation figure

Rock localities and mineralogy given in appendix 1. Modal analyses of B43,44,38,35 and 27 are also given in table 5.7. CIPW norms are given in appendix 2. According to the nomenclature of Johnson et al. (1976) lavas B43,25,44,29 and27 are phonolitic tephrites and all other lavas are potassic ne-trachybasalts.

Table 5.4

EAST SUNDA ARC XENOLITHS

SANGEANG API - SUMBAWA,XENOLITHS

Sample#	B23	B5	B4	B2G	B13	B22	B25	B2H	B24	B7	B11	B10	B8
SiO_2	45.41	48.42	50.19	45.24	42.47	41.90	40.48	41.39	37.60	39.47	38.96	42.24	38.31
TiO_2	0.40	0.59	0.60	1.14	1.37	1.41	1.54	1.31	1.56	1.55	1.26	0.90	1.31
Al_2O_3	3.12	4.24	4.52	5.20	11.88	7.72	7.80	10.72	17.09	17.64	19.58	19.17	19.55
Fe_2O_3	1.76	1.36	1.09	2.20	1.63	2.69	3.12	2.63	2.29	2.52	2.66	2.06	2.36
FeO	8.97	6.94	5.58	11.20	8.32	13.70	15.93	13.43	11.70	12.85	13.56	10.48	12.07
MnO	0.19	0.14	0.11	0.19	0.09	0.12	0.21	0.22	0.16	0.18	0.15	0.13	0.16
MgO	24.44	17.50	14.97	13.95	17.76	11.97	11.64	10.61	8.66	8.48	6.06	6.18	6.72
CaO	15.27	20.55	22.49	20.42	10.32	19.69	17.74	18.66	16.91	15.27	16.70	17.87	17.15
Na_2O	0.33	0.22	0.39	0.37	0.82	0.64	1.22	0.75	1.08	1.39	0.83	0.78	0.98
K_2O	0.10	0.04	0.05	0.07	5.32	0.15	0.28	0.07	0.85	0.60	0.22	0.16	0.42
P_2O_5	0.01	0.01	0.01	0.02	0.01	0.02	0.04	0.19	2.09	0.05	0.02	0.02	0.93
H_2O+	0.61	0.73	0.74	1.04	1.39	1.19	1.54	1.32	1.28	1.15	1.26	0.94	1.21
Mg/Mg+Fe	0.81	0.79	0.80	0.65	0.76	0.57	0.53	0.54	0.53	0.50	0.40	0.47	0.46
Mg/Mg+.85Fe	0.83	0.82	0.83	0.69	0.79	0.61	0.57	0.58	0.57	0.54	0.44	0.51	0.50
K_2O/Na_2O	0.30	0.18	0.13	0.19	6.49	0.23	0.23	0.09	0.79	0.43	0.27	0.21	0.43
Trace elements (ppm)													
Rb	5	<1	5	<1	262	<1	6	1	6	2	2	1	3
Sr	68	119	121	107	148	200	221	656	1293	1071	1006	960	1125
Zr	18	15	27	49	76	55	54	44	41	32	5	<1	7
Nb	<0	<0	0	0	2	1	1				<0	1	2
Y	5	12	10	15	7	17	12	25	24	12	12	12	7
La	1		2				7						10
Sc	81	115	134	103	56	80	99	71	47	42	39	41	35
Cr	260	330	293	386	126	107	63	52	62	45	47	44	49
Ni	196	89	60	45	105	44	38	24	9	15	14	21	4
Rb/Sr	0.074	<0	0.041	<0	1.770	<0	0.027		0.005	0.002	0.002	0.001	0.003
K/Rb	166		83		169		387	1162	1176	2491	913	1328	1162
K/Sr	12.21	2.79	3.43	5.43	298.42	6.23	10.52	0.89	5.46	4.65	1.82	1.38	3.10

Notes: FeO arbitrarily calculated as 0.85 total Fe.Analyses normalised anhydrous, H_2O^+=pre-normalisation figure.
Rock localities and mineralogy given in appendix 1.CIPW norms given in appendix 2.Modal analyses are given in table 5.1.
B23,5 and 4 are olivine clinopyroxenites.B2H and B25 are magnetite clinopyroxenites.B22 and B13 are alkali clinopyroxenites and B2G,B24,7,11,10 and B8 are hornblende-magnetite-anorthite-cpx gabbros.

very olivine-rich and tend towards dunites, while others are entirely composed of clinopyroxene. Most appear to have between 75 and 95 vol.% cpx and 0 to 20 vol.% olivine.

Texturally they are idiomorphic to hypidiomorphic (plate 2A) and tend towards more granoblastic-polygonal textures with decreasing grain siz Clinopyroxene grains are subhedral, or occasionally, euhedral. Olivine is anhedral, often with "wormy", embayed texture and is occasionally included in large cpx grains (plate 2A). Olivine may have been partially resorbed before it was incorporated in these rocks.

Magnetite is a rare phase, occurring interstitially and as rare inclusions in olivine. Phlogopite and more rarely, pargasitic amphibole occur interstitially as post-cpx,-olivine (intercumulate ?) grains (plate 2A). These phases occupy triple grain intersections and form thin fims along cpx or olivine grain-boundaries. Rarely, amphibole mimetically replaces small areas of some cpx grains.

The olivine-clinopyroxenites have undergone some textural re-equilibration since they originally crystallised. Olivine shows kink band development, while cpx may also show multiple twinning, undulose and mosaic extinction and a tendency towards new-grain formation and polygonitization around the margins of large grains. Islands of large, original remnant igneous cpx may be preserved surrounded by equigranular polygons of cpx and olivine with 120^{0} triple-point grain boundary intersections (plate 3D and 4C). Interstitial phlogopite develops wavy cleavage and extinction, kink-bands and dislocations.

5.2.2 Magnetite Clinopyroxenite

These are composed of cpx and magnetite, with little or no amphibole or phlogopite. Olivine only occurs rarely and then generally as inclusions in cpx. Plagioclase occurs as an interstitial (or intercumulate ?) phase in proportions varying from 0.5 to 20 vol.%.

PLATE 2. Olivine clinopyroxenite and magnetite-clinopyroxenite

A. Olivine clinopyroxenite B23. Showing hypidiomorphic granular texture, subhedral-euhedral clinopyroxene (CPX), subhedral-anhedral olivine (OL) and interstitial phlogopite (Ph) and very minor magnetite (MG).

B. Magnetite clinopyroxenite B29. Showing subhedral clinopyroxene (CPX), interstitial magnetite (MG) and very minor interstitial plagioclase (Pl). Some replacement of clinopyroxene replacement my amphibole (a). The apparent order of crystallisation is: 1. CPX 2. Magnetite 3. Plag.

C. Magnetite clinopyroxenite B2H. This rock is similar to B29 in Plate B, but with much more abundant plagioclase (Pl). The texture suggests an original magnetite clinopyroxenite such as that in Plate B, which has undergone some dissaggregation with later precipitation of plagioclase. Clinopyroxene shows hour-glass zoning (e.g. at point -a).

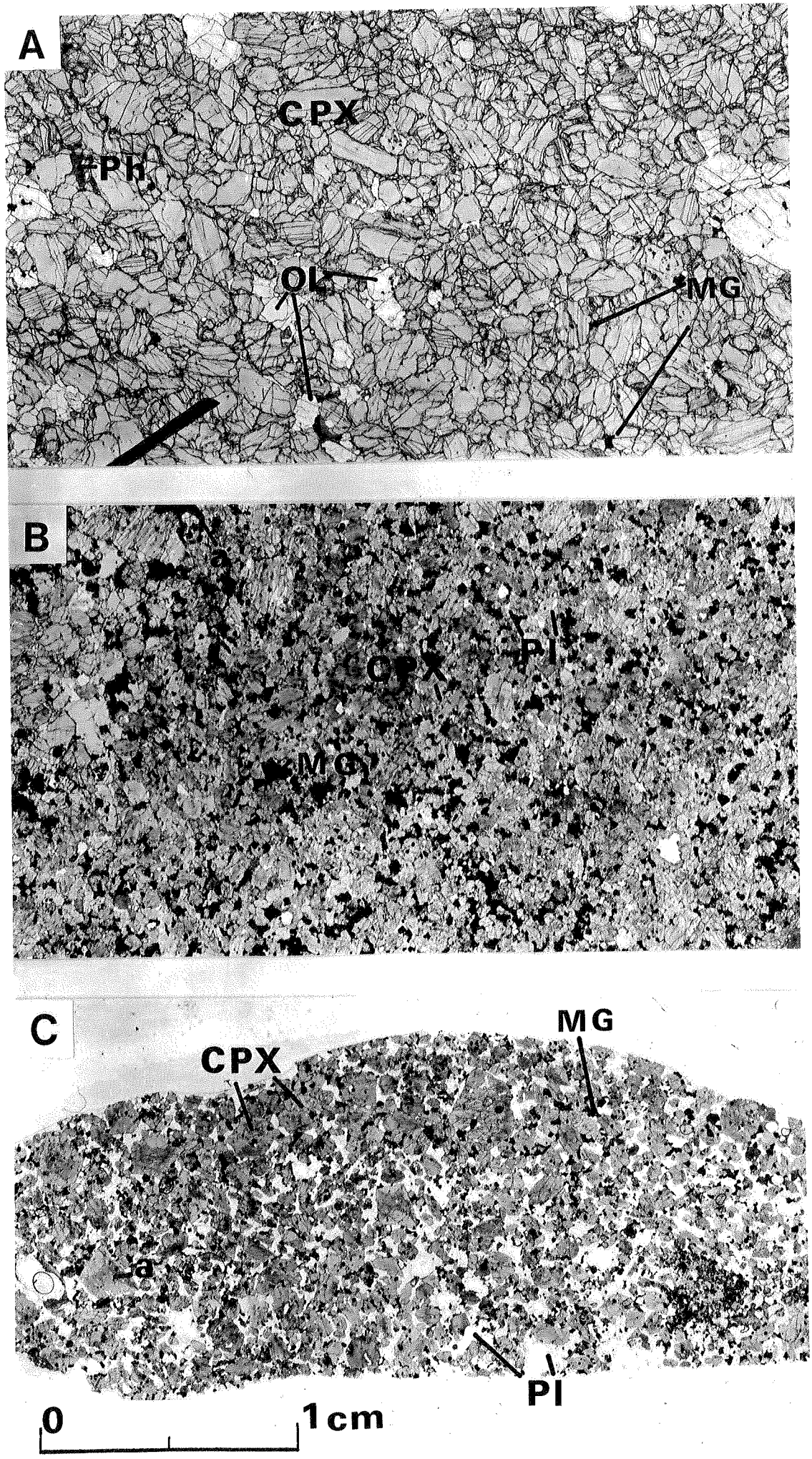
A
CPX
PH
OL
MG
B
CPX
PI
MG
C
MG
CPX
PI
0
1cm

The modal variation of the main mineral components of members of this group are presented in figures 5.1 and 5.2 and modal analyses are given in table 5.1 (samples B29, B2D, B1A, B2E, B28, B25x, B2A, B2H).

The proportion of magnetite is relatively constant (10-15%). Texturally the group is rather like the olivine-clinopyroxenites, with hypidiomorphic textures, tending in some cases, towards more polygonal textures. Typical examples of magnetite clinopyroxenites are illustrated in plates 2B and C.

Magnetite generally occurs as an interstitial/intercumulate phase, as scalloped grains between cpx grain boundaries and at grain intersections (see plate 2B). In some instances extensive interstitial areas are filled with magnetite which poikilitically includes cpx grains. Clinopyroxene is often zoned, with diopsidic cores and more Al- and Ti-rich rims. Some show hour-glass zoning (plate 2C).

Magnetite appears to be more abundant in fine-grained areas of these rocks and its precipitation, at least in part, appears to post-date some deformation of original cpx. Plagioclase is a still later phase and its precipitation often appears to have accompanied partial disaggregation of the original cpx-magnetite rock (see plate 2C). This suggested by; 1. the inclusion in interstitial plagioclase of cuspate magnetite grains which apparently acquired their original shape by interstitial growth around cpx and 2. by the occasional occurrence of "clumps" of tightly interlocking magnetite-clinopyroxenite, preserving the original plagioclase-free texture of the rock.

While in some instances the introduction of plagioclase during partial disaggregation of the intrusive appears to have been a very late-stage event, possibly as the xenolith was carried up by the erupting lava, more often this must have occurred earlier. This is demonstrated by the fact that the intercumulate plagioclase is often deformed or strained, suggesting that the plagioclase-infiltrated magnetite-clinopyroxenite must have been

PLATE 3. Alkali Clinopyroxenite

A. Alkali clinopyroxenite B13. Originally a clinopyroxenite with later partial replacement of cpx by phlogopite (Ph) which was partially deformed (plate B) and then partially disaggregated with interstitial precipitation of amphibole (A).

B. A more magnified detail of part of Plate A. Showing the strained phlogopite with curving cleavage (Ph) and partial resorbtion of clinopyroxene (same scale as Plate D).

C. Alkali clinopyroxenite B22, showing cataclasis of clinopyroxene and interstitial amphibole (A). Plagioclase is an unstrained infilling mineral after cpx cataclasis (Pl) (scale as in Plate D).

D. Marginal polygonitisation of clinopyroxene in alkali clinopyroxenite B21.

E. Olivine with reaction corona of clinopyroxene (CPX) and phlogopite (Ph) (scale as in F).

F. Patchy replacement of clinopyroxene by amphibole.

G. Alkali clinopyroxenite B21. Disaggregated clinopyroxene (CPX) with later amphibole (A) and phlogopite (Ph).

H. Zone of cataclasis in alkali clinopyroxenite B22 showing increasing granulation of clinopyroxene from A towards the centre of the zone of cataclasis B (scale as in Plate D).

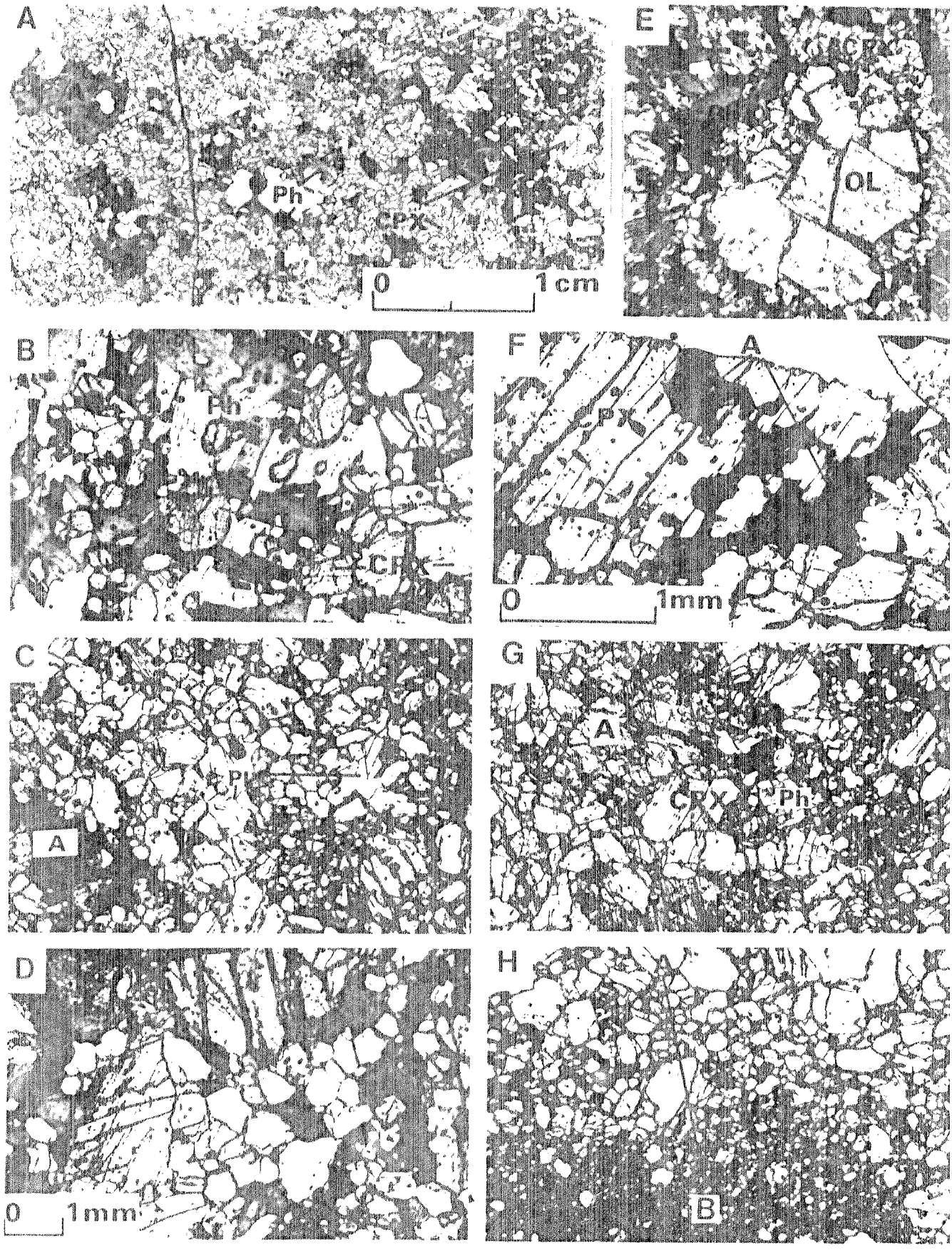
A
Ph
CPX
0
1 cm
E
OL
B
Ph
CPX
A
F
A
PX
0
1mm
C
PL
A
G
A
CPX
Ph
D
0
1mm
H
B

constituted as a solid mass prior to its inclusion in the magma which brought it to the surface.

The plagioclase (anorthite) exhibits fine twin lamellae, which taper and pinch-out and which may be bent or deformed (plate 5C). In some cases plagioclase has also been broken. These features are in contrast to the plagioclase which occurs in the lavas as phenocrysts or as obviously late-stage infiltrations or veins in some xenoliths. These have broader, straight, parallel-sided albite twin lamellae of equal width.

5.2.3 Hornblende-Magnetite-Clinopyroxenite

Only one example of this xenolith-group was collected (B20, table 5.1). However this example was very friable and it is possible that they may not survive eruption very readily without becoming disaggregated.

This group of nodules is composed of loosely interlocking aggregates of euhedral to subhedral cpx, amphibole and magnetite, with occasional euhedra of apatite and very rarely, small interstitial patches of clear, unstrained plagioclase.

The example examined was undeformed and clearly of cumulate origin, with very little post-cumulate growth or interstitial infilling. In contrast to the olivine-clinopyroxenites and magnetite-clinopyroxenites, olivine is absent and clinopyroxene, amphibole and magnetite all appear to have crystallised at the same stage. The presence of apatite is also in contrast to the two previously described groups.

5.2.4 Alkali-Clinopyroxenites

This is a complex group of xenoliths and most members appear to represent modified olivine- and magnetite-clinopyroxenites. They were originally cpx-rich cumulates which have become enriched in phlogopite and amphibole by a variety of mechanisms. These include; direct precipitation, mimetic replacement, reaction and disaggregation and veining.

Many appear to have undergone a number of stages of deformation and some show cataclastic or flaser textures (plate 3H). Some record traces of several deformation events punctuated by precipitation of different post-cumulate mineral phases.

Modal analyses of members of this group are given in table 5.1 and variations are portrayed in figures 5.1 and 5.2.

In detail, the important features of this group of nodules are well illustrated by xenolith B13 (tables 5.1 and 5.4) and are illustrated in plate 3.

This is a phlogopite-rich clinopyroxenite and is essentially magnetite-free. It appears to represent a modification of a clinopyroxene-rich cumulate like the olivine-poor members of the olivine-clinopyroxenite group (e.g. B4) and has developed by five distinct stages.

1. Formation of a hypidiomorphic clinopyroxene cumulate, with adcumulate growth. Larger pyroxene grains show recognisable zoning, with pale, diopsidic cores and darker Ca-rich augite rims.
2. The original clinopyroxenite then underwent some deformation. Clinopyroxene is strained, with mosaic extinction and marginal granulation and development of finer-grained, granular-polygonal textured areas with 120^{o} triple grain intersections.
3. The modified clinopyroxenite was then partly disaggregated followed by large-scale interstitial phlogopite crystallisation. This is coarse-grained and envelopes the primary cpx including the texturally modified polygons and deformed grains.

   There is some suggestion that the cpx and liquid may have been in a reaction-relationship as cpx is embayed and resorbed where included in poikilitic phlogopite (plate 3B).

4. This cpx-phlogopite rock was then further deformed and the phlogopite itself developed wavy extinction, kink bands and dislocation features (plate 3B).

5. Finally the deformed cpx-phlogopite rock was again partly disaggregated followed by the interstitial crystallisation of amphibole which poikilitically envelopes pre-existing phlogopite and cpx, forming large oikocrysts (plate 3A, G). Amphibole is undeformed.

Nodule B16 (table 5.1) is another alkali clinopyroxenite showing a similar sequence of events to that illustrated by B13 (above). However this xenolith is more magnetite-rich and may represent a modified magnetite-clinopyroxenite (plate 2B). In addition some cpx grains include small embayed, resorbed olivine grains, suggesting that olivine crystallisation may have preceded the appearance of cpx and that furthermore it may have been in a reaction relationship with the liquid once major cpx crystallisation began.

This nodule appears to have developed by a similar sequence to B13, with phlogopite and the amphibole following cpx (plate 3A, B), however unlike the previous example small interstitial areas of anorthitic plagioclase postdate amphibole (plate 3C).

Other alkali-clinopyroxenites (B22, B21, B14 and B15; tables 5.1 and 5.4) again have similar histories to those just described, representing modified olivine- or magnetite-clinopyroxenites. Some of these have zones of severe cataclasis (plate 3H) and the extent to which primary phases are deformed and/or replaced by phlogopite and amphibole can be seen to decrease out from these. In some, olivine is surrounded by reaction coronas of cpx, phlogopite and amphibole or in some cases can be seen to have been completely replaced by mosaics of these minerals (plate 3E).

PLATE 4.

A. Large, euhedral amphibole grain from hornblende-anorthite-magnetite gabbro B27 with fresh core (A) and reacted rim of clinopyroxene, plagioclase, magnetite and olivine.

B. and D. Amphibole-rich hornblende gabbro B7. Plate D shows the marked foliation largely resulting from the alignment of elongate amphibole grains. Amphibole-rich layers (e.g. centered about point A) are interspersed with more plagioclase-, clinopyroxene-rich zones (center about P1). Amphibole (A) shows reaction rim development as in Plate (e.g. point RA) and zones of partial melting (encircled area G). Plate B is an enlarged detail of the encircled area G in Plate D. Adjacent to the melt zone is an area of amphibole reaction (RA). Melt zones are characterised by brown glass (G) from which have crystallised clinopyroxene, plagioclase and olivine and in some cases a secondary amphibole (rhonite) (see table 5.5) for analyses of glass and crystals).

C. Magnetite clinopyroxenite B29 showing clinopyroxene with pale, Cr-rich diopside core (C) and darker green, more Al- and Ti-rich augite rim (R). The margin of the core is rimmed by small magnetite crystals.

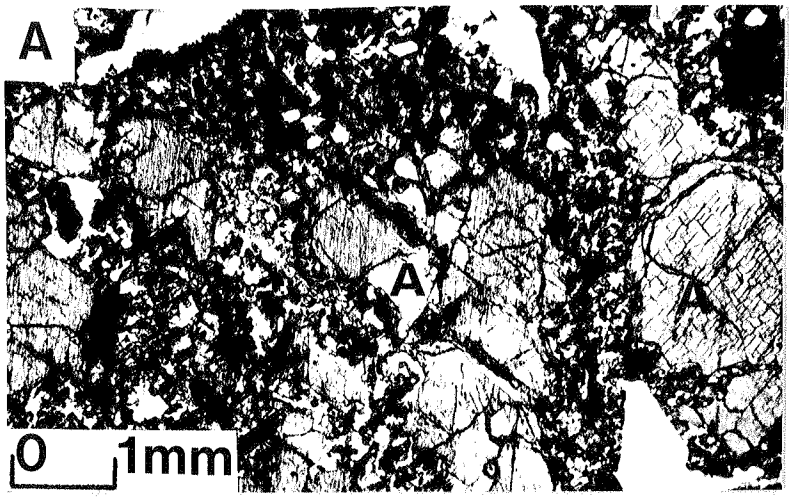
A
A
A
0
1mm

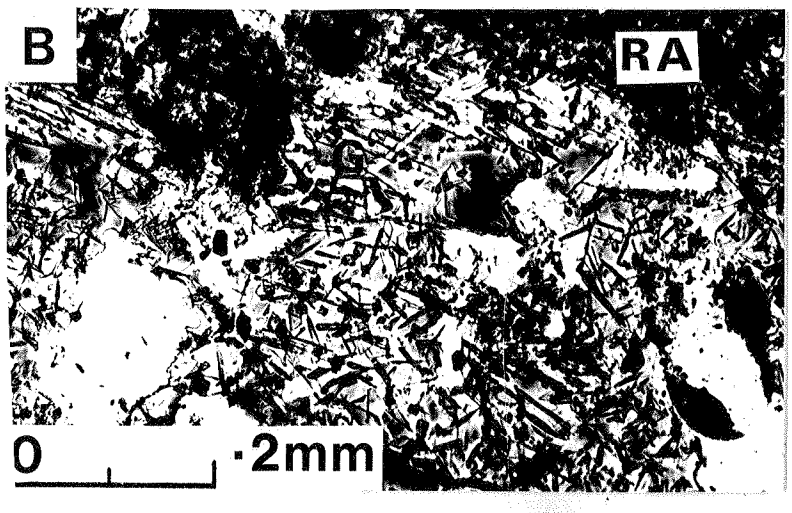
B
RA
0
·2mm

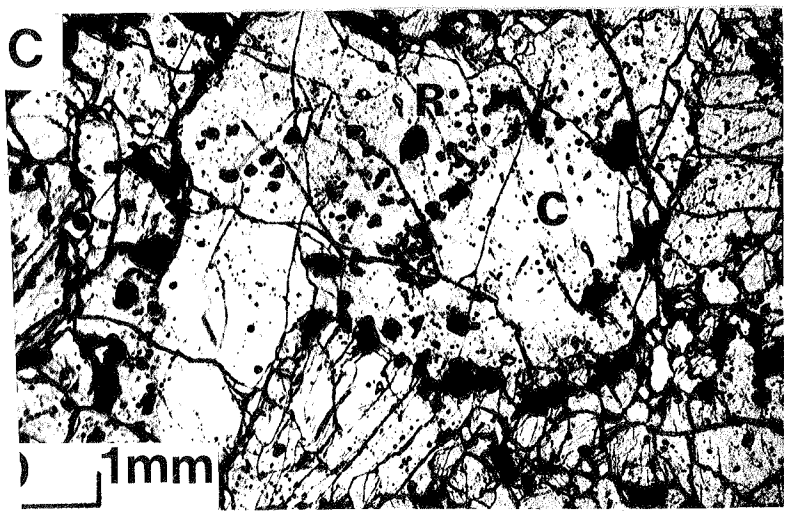
C
R
C
1mm


D
Pl
RA
A
0
1cm

Table 5.5 A Analyses [2] of Primary Amphibole and its Breakdown Products in Xenolith B7

Analysis No.	1		2	3		4		5 [1]		6	
Phase	Amph	Struct. 23(O)	Glass	Cpx	Struct. 6(O)	Ol	Struct. 4(O)	Amph	Struct. 23(O)	Pl	Struct. 8(O)
SiO_2	40.58	5.492	50.89	51.83	1.922	36.84	0.977	29.61	4.947	53.14	2.434
Al_2O_3	14.19	2.449	21.93	3.12	0.136	-	-	13.38	2.635	28.29	1.527
Fe_2O_3	-	-	-	-	-	-	-				-
FeO	10.96	1.342	2.49	8.83	0.274	24.20	0.536	27.47	3.838	0.26	0.010
MgO	13.89	3.031	-	15.04	0.831	37.21	1.470	5.90	1.470	-	-
CaO	12.54	1.967	1.94	19.39	0.771	0.62	0.017	9.11	1.631	11.11	0.545
Na_2O	2.12	0.602	11.35	0.1	0.007	-	-	1.98	0.642	5.67	0.504
K_2O	1.91	0.357	10.65	0.2	0.009	-	-	1.67	0.357	1.12	0.065
TiO_2	2.83	0.312	0.72	1.05	0.029	0.17	0.003	6.66	0.836	-	-
MnO	-	-	-	0.26	0.008	0.67	0.015	0.26	0.037	-	-
Total	99.02	16.00	99.97	99.82	3.989	99.71	3.019	96.04	16.393	99.59	5.086
100Mg/Mg+ΣFe	69.31			75.22		73.26		27.70			
					C.I.P.W. Norm						
or	-		13.71					-			
ab	-		-					-			
an	23.57		-					22.69			
ns	-		9.89					-			
mt	-		-					22.11			
di	12.60		6.36					16.18			
hy	-		-					-			
wo	-		1.04					-			
ol	31.77		-					6.41			
ne	9.72		28.99					9.08			
lc	8.85		38.60					7.74			
cs	7.13		-					0.61			
il	5.37		1.37					12.65			
					Molecular Proportions						
Ca	31.0		49.95	41.1			0.8	23.5			
Mg	47.8		0.0	44.3			72.70	21.2			
Fe	21.2		50.05	14.6			26.50	55.3			
Mol. % An										45.2	

Notes: (a) Amphibole column 1 is the primary amphibole (average of 3 analyses) of xenolith B7.

(b) Glass column 3 (average of 4 analyses) formed by the breakdown of primary amphibole 1 (see plate 3, A,B, and D).

(c) Cpx (3), olivine (4), amphibole (rhonite) (5) and plagioclase (6) are crystallisation products of glass (2) (see plate 3B).

[1] All iron quoted as FeO (electron microprobe analysis), norm calculated with Fe^{2+}/Fe^{3+} ratio of 0.5 (13.66% FeO, 15.25% Fe_2O_3).

[2] Electron microprobe analyses.

Table 5.5B Analyses [1] of Primary Amphibole and its Breakdown Products from Xenolith BIB

Analysis No.	1		2		3		4		5		6
Phase	Amph.	Struct. 23(O)	Cpx	Struct. 6(O)	Amph.	Struct. 23(O)	Ol	Struct. 4(O)	Plag.	Struct. 8(O)	Mag.
SiO_2	40.21	5.949	42.38	1.598	40.75	5.877	37.54	0.973	52.47	2.397	-
Al_2O_3	13.96	2.435	11.53	0.513	27.12	4.611	-	-	28.94	1.558	9.52
Fe_2O_3	-	-	-	-	-	-	-	-	0.45	0.015	35.68 [2]
FeO	10.35	1.281	7.42	0.234	3.11	0.375	19.88	0.431	-	-	35.76
MgO	13.96	3.078	11.06	0.622	5.24	1.126	41.46	1.601	-	-	5.26
CaO	11.88	1.883	22.89	0.925	11.94	1.845	0.31	0.008	11.08	0.542	0.17
Na_2O	2.71	0.777	0.75	0.055	2.82	0.788	-	-	5.94	0.526	-
K_2O	1.83	0.345	-	-	3.24	0.596	-	-	0.69	0.040	-
TiO_2	2.90	0.322	3.97	0.113	1.33	0.144	-	-	0.30	0.010	12.66
MnO	-	-	-	-	-		0.68	0.015	-	-	0.27
Total	97.80	16.072	100.0	4.060	95.55	15.364	99.87	3.027	99.87	5.089	99.32
100Mg/Mg+1.Fe	70.62		72.64		75.01		78.80				12.14
					C.I.P.W. Norm						
an	20.53				51.78						
di	13.53				-						
ol	30.64				11.86						
ne	12.42				12.93						
lc	8.48				11.87						
cs	6.68				2.30						
kp	-				2.28						
il	5.51				2.53						
					Molecular Proportions						
Ca	30.2		51.9		55.1		0.4				
Mg	49.3		34.9		33.7		78.5				
Fe	20.5		13.2		11.2		21.1				
Mol. % An									48.92		
Mol. % U.Sp.											35.62

Notes: (a) Amphibole 1 - primary amphibole (average of 5 analyses).

(b) Cpx 2, Amph 3, Ol4, Plagioclase 5 and magnetite 6 are breakdown products of amphibole 1 (see plate 3A).

[1] Analyses by electron microprobe.

[2] Fe_2O_3 calculated by the method of Carmichael (1967).

Table 5.6 Least Squares, Mass-balance of Sangeang Api Xenolith Amphiboles in Terms of their Breakdown Products

A. Amphibole B7

	obs	est
SiO_2	39.44	40.13
Al_2O_3	13.80	12.74
FeO_T	11.21	11.48
MgO	13.28	12.50
CaO	12.79	12.33
Na_2O	2.04	2.01
K_2O	1.99	0.96
TiO_2	2.86	2.53
P_2O_5	-	-
MnO	-	0.14

Component	Wt. Fraction
Olivine	0.1788
Cpx	0.4324
Plag.	0.1958
Mag.	0.0651
Glass	0.0806

= amphibole B7 (est.)

ΣR^2 = 3.6855

B. Amphibole BIB

	obs	est
SiO_2	40.21	40.87
Al_2O_3	13.77	12.81
FeO_T	10.35	10.68
MgO	13.96	13.17
CaO	11.88	11.47
Na_2O	2.71	2.27
K_2O	1.83	1.15
TiO_2	2.90	2.17
P_2O_5	-	-
MnO	-	0.16

Component	Wt. Fraction
Olivine	0.2010
Cpx	0.3877
Plag.	0.2073
Mag.	0.0478
Glass	0.0982

= amphibole BIB (est.)

ΣR^2 = 3.4649

Notes: Modal analyses of xenoliths B7 and BIB are given in Table 5.1

Compositions of breakdown minerals used in these calculations are given in Table 5.5 A,B.

In some instances zones of cataclasis have late-stage, interstitial plagioclase infillings or veins, these being undeformed.

The petrographic features of the Sangeang Api alkali-clinopyroxenites suggest a number of crystallisation sequences:

1. clinopyroxene-phlogopite-amphibole.
2. olivine-clinopyroxene-magnetite-phlogopite-amphibole-plagioclase.

In both these sequences there is some evidence that cpx may be in reaction relationship with the liquid during phlogopite crystallisation. Amphibole also appears to be the product of cpx-liquid reaction in some instances. In sequence 2 there is also some suggestion that olivine was the earliest phase to precipitate and was also in a reaction relationship with the liquid once cpx appeared. Reaction of olivine also takes place when phlogopite appears, yielding cpx and phlogopite. The implications of the phase relations implied by these crystallisation sequences are discussed later in this thesis (chapters 10 and 11).

It appears that the apparent on-going deformation of the alkali-clinopyroxenite xenoliths may be punctuated by the sequential precipitation of minerals whose stability fields are likely to be partly dependant on P or P_{H_2O}. If this is the correct interpretation then it may be the result of a diapiric intrusive mechanism.

5.2.5 Group 5: Plagioclase-rich intrusive rocks.

Members of this group of nodules differ from those of the four groups described previously. Plagioclase is an abundant phase and amphibole and magnetite assume different crystallisation roles. Whereas in the previous groups, plagioclase and amphibole in particular, almost invariably crystallised after olivine, clinopyroxene, magnetite and phlogopite, in this group, any one or more of the group cpx, amphibole,

PLATE 5. Gabbroic Xenoliths

A. Gabbro B8, showing the undeformed assemblage of euhedral amphibole (A and subhedral clinopyroxene (C) and plagioclase (P1) and magnetite (black grains).

B. Gabbro B11, similar to B8 in plate A, with elongate amphibole (A), subhedral clinopyroxene (C) and plagioclase (P1) and magnetite. Crossed nicols. Anorthitic plagioclase shows typical tapering twin lamellae.

C. Strained anorthitic plagioclase from gabbro B27 (crossed nicols).

D. Typical hornblende-anorthite-magnetite gabbro B24 (cumulate) B24. Amphibole as dark grey, more granular crystals, plagioclase (white) and black magnetite.

E. Cumulate clinopyroxene (grey) and plagioclase (white) and an intercumulate amphibole oikocryst (dark grey) in gabbro B10.

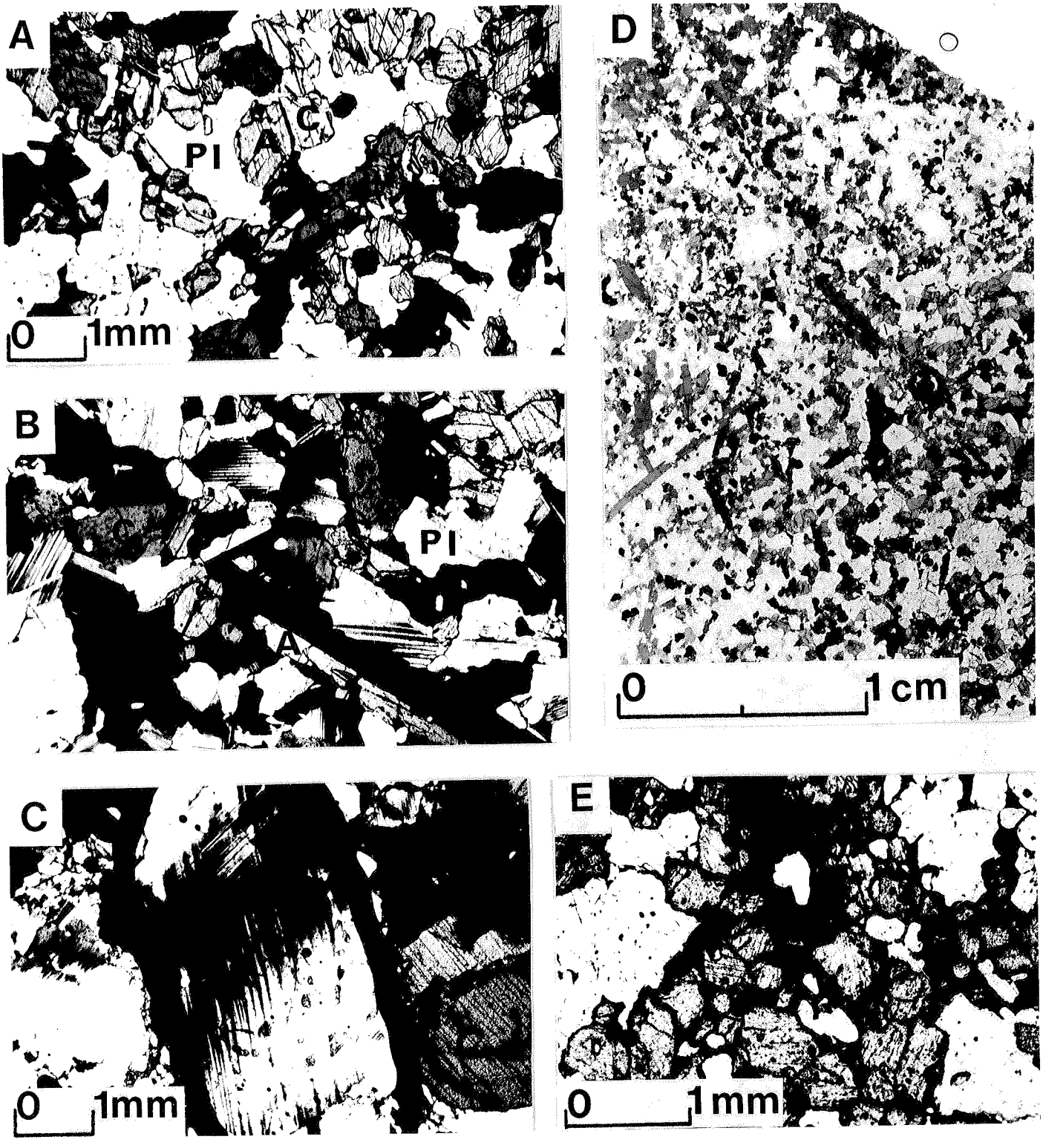
A
Pl
A
C
0
1mm
B
C
Pl
A
D
0
1 cm
C
0
1mm
E
0
1mm

plagioclase and magnetite may be amongst the earliest phases to precipitate. These rocks contain no olivine.

In general textures are suggestive of a cumulate origin (see plates 5A - 5E) though this cannot be established unequivocally. Plates 5A-E and 4D illustrate some of the main textural features of this group of xenoliths. Amphibole, cpx, plagioclase, magnetite and apatite may each occur as euhedral to subhedral grains, possibly of cumulate origin (plates 5A, B, D and 4D), while amphibole, magnesian biotite and magnetite also sometimes occur as interstitial oikocrysts, possibly of postcumulate origin (plate 5E). Plagioclase and cpx also occasionally show growth around their rims suggestive of adcumulate growth.

The rocks of this group are medium to fairly coarse-grained, grain size ranging from 1 to 20 mm. Amphibole sometimes occurs as elongate laths in harrisite-like texture (plate 5D).

Some xenoliths show layered or foliated textures either due to variations in grain size, or the relative enrichment of one mineral compared with the others. For instance B7 (plate 4D) has layers enriched in aligned, elongate amphibole and others in which more equant plagioclase and cpx are more abundant. These features are also possibly suggestive of cumulate origin.

Figures 5.2 and 5.1 illustrate the variation in the proportions of the main minerals in these xenoliths. Figure 5.1, showing the variation in the proportions of plagioclase, cpx and amphibole is particularly interesting as the members of this group fall on a linear trend which projects through the amphibole apex with an almost constant plagioclase/cpx ratio of about 1.6. Thus the main variation in the group is in the relative abundance of amphibole and plagioclase+cpx. Furthermore through this series there is a distinct change in the role of amphibole. In the most

FIGURE 5.1

VARIATION IN THE MODAL PROPORTIONS OF MAGNETITE-PLAGIOCLASE - AMHPIBOLE+PHLOGOPITE IN SANGEANG API XENOLITHS. SYMBOLS DENOTE THE FOLLOWING INTRUSIVE ROCK-TYPES:

X-OLIVINE CLINOPYROXENITE

∇-MAGNETITE-CLINOPYROXENITE

⊙-ALKALI CLINOPYROXENITE

●-GABBRO

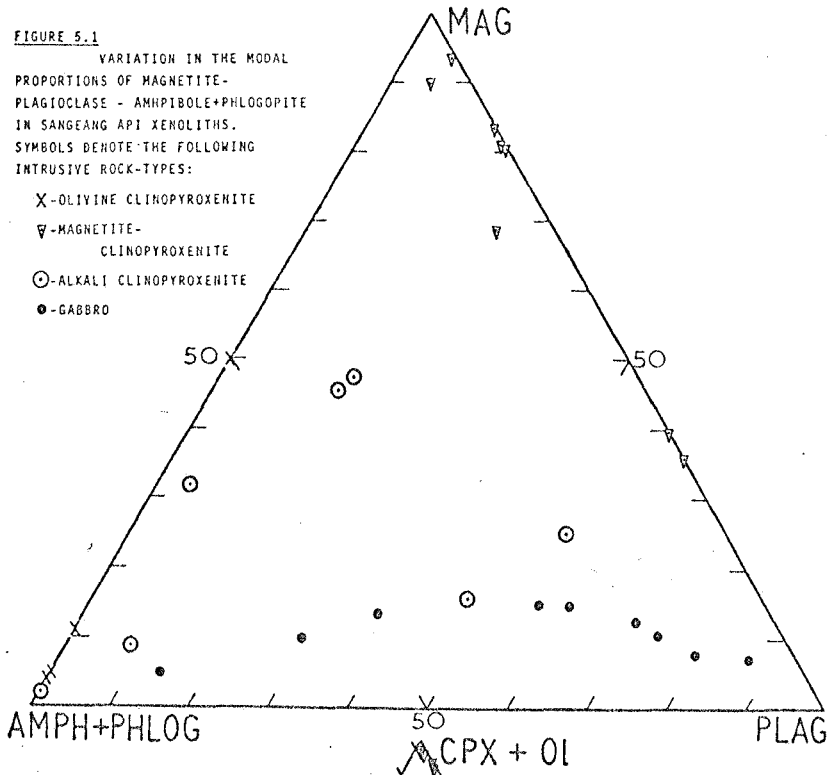

FIGURE 5.2

VARIATION IN THE MODAL PROPORTIONS OF CLINOPYROXENE+OLIVINE-PLAGIOCLASE - AMPHIBOLE+PHLOGOPITE.

SYMBOLS DENOTE THE SAME SAMPLES AS IN FIG. 5.1

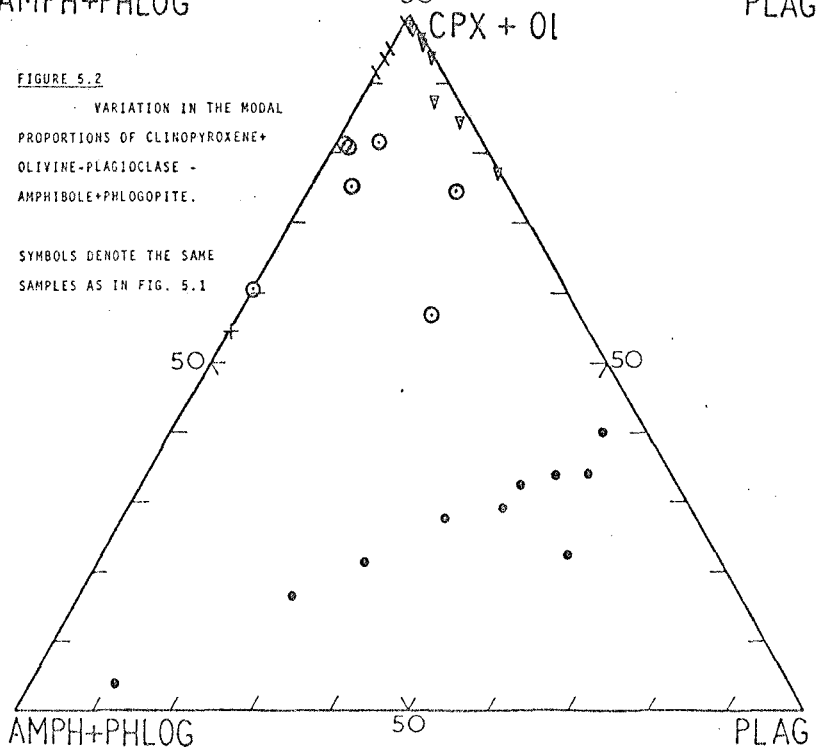

amphibole-rich members of the group (e.g. B24 and B7, tables 5.1 and 5.4, plates 4D, 5D), amphibole appears to have crystallised earliest and is in some cases included in later plagioclase or cpx grains. In the most amphibole-poor members however (e.g. B10, tables 5.1 and 5.4, plate 5E) plagioclase and cpx are the first-formed phases followed by magnetite and amphibole is a late interstitial (intercumulate ?) phase (plate 5E).

Unlike the previous groups of xenoliths, members of this group do not show complex histories and generally appear to have resulted from a single-stage event; either sequential or simultaneous precipitation of the major mineral phases, sometimes followed by interstitial or intercumulate mineral precipitation.

Members of this group are often undeformed, though some have apparently undergone some shearing or cataclasis. This has resulted in strained plagioclase with wavy extinction and irregular twin lamellae (, plate 5C).

A particular feature of a number of members of this xenolith-group is the reaction of amphibole. This is displayed by the amphiboles of a number of xenoliths (e.g. B1B, B7, B27 and B6, plate 4 A,B and D) while that of others (e.g. B8, B24 and B11) show no signs of breakdown.

In general amphiboles are tending to breakdown around their margins and along cleavage traces (plate 4A) to assemblages of magnetite, cpx and plagioclase (tables 5.5 and 5.5), though in some cases olivine is recognised and more rarely nepheline and a secondary amphibole (tables 5.5 and 5.6). In some instances the amphibole is partially melting to yield an assemblage of olivine-cpx-magnetite-plagioclase and liquid (brown glass) (e.g. B7 plates 4B and D). This is apparently an incongruent melting reaction and the breakdown assemblage is similar to that determined experimentally by Holloway (1973) in the system pargasite-H_2O-CO_2 in the low pressure region where the amphibole liquidus retreats rapidly to low temperatures.

Table 5.7

Sangeang Api, Lavas: Modal Composition

Sample No.	Cpx	Ol	Amph	Biot	Ti-Mag	Plag	Apat	Reacted Amph	Reacted Biot	G-Mass
B43	13.2	6.5			0.5	0.3				79.5
B44	20.5	3			3	17.5				56
B38	15	2.6			3	18				61
B35	10.5		2.4		2.6	17	0.5			67
B27	15		0.2	0.2	3.5	25	0.3	0.9	0.9	54

5.3 *Petrography of the Sangeang Api Lavas*

The lavas associated with the mafic and ultramafic intrusives described in the previous section are critically undersaturated, moderately potassic ($K_2O/Na_2O \simeq 1$) lavas with low to low-intermediate silica content (table 5.3). They are geochemically and petrographically quite like the Tambora lavas, though in both respects there are small but significant differences between the two suites. They may be classified as shoshonites (Joplin, 1968), though they are more undersaturated than many so-termed associations. Alternatively, using the nomenclature of Johnson et al. (1976), they are potassic phonolitic tephrites, potassic *ne*-trachybasalts and potassic *ne*-trachyandesites.

Like the Tambora lavas, the most consistent distinction between this suite and the Rindjani calcalkaline lavas is in the ubiquitous occurrence of groundmass alkali feldspar.

Two distinct petrographic groups are recognised; those with amphibole, and those without. This distinction also corresponds with that made on the basis of some geochemical parameters, in particular the amphibole-bearing group generally have <4.5% MgO, while the other group have >4.5% MgO. Furthermore the amphibole-free group is characterised by the occurrence of olivine megacrysts and quite abundant olivine phenocrysts, while the amphibole-bearing group has no olivine megacrysts and only relatively scarce olivine phenocrysts. Members of both groups contain groundmass olivine.

The amphibole-free, olivine megacryst-bearing lavas (e.g. B38, B39, B41 and B31, tables 5.7 and 5.3) are meso- to melanocratic, often vesicular lavas, while the amphibole-bearing group (B28, B35, B34, B36, B42, B32, B25 and B27, tables 5.7 and 5.3) tend to be more leucocratic. Both groups are generally porphyritic, plagioclase phenocryst-rich lavas with abundant

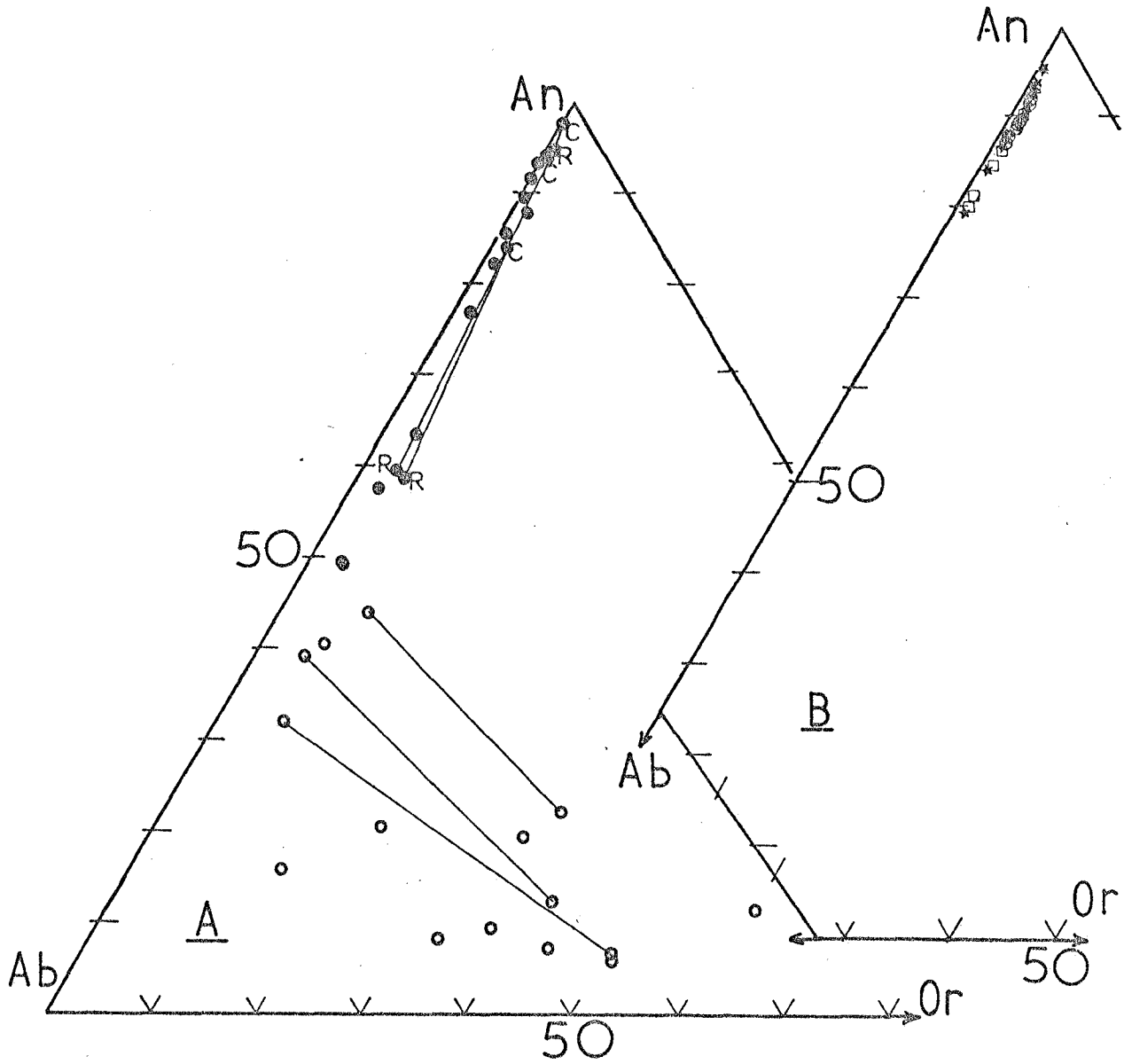

FIGURE 5.3

PLAGIOCLASE AND ALKALI FELDSPAR VARIATION IN SANGEANG API LAVAS AND XENOLITHS. A -LAVAS, B -XENOLITHS. IN DIAGRAM A FILLED CIRCLES DENOTE PHENOCRYSTS ,R=RIM,C=CORE. OPEN CIRCLES ARE GROUNDMASS FELDSPARS.COEXISTING GROUNDMASS PLAGIOCLASE AND ALKALI FELDSPAR ARE CONNECTED BY TIE-LINES. IN DIAGRAM B ,OPEN CIRCLES DENOTE PLAGIOCLASE OF MAGNETITE CLINOPYROXENITE,STARS- PLAGIOCLASE OF GABBROIC INTRUSIVES AND OPEN SQUARES-ALKALI CLINOPYROXENITES.

Table 5.8

Representative Analyses of Feldspars from Sangeang Api Intrusives and Lavas

Analysis No.	1	2	3	4	5	6	7	8	9	10	11	12	13	14	15	16	17
Sample No.	B2H	B1B	B11	B10	B15	B27	B38	B27	B39	B38	B27	B38	B38	B39	B39	B39	B38
Rock Type	X	X	X	X	X	L	L	L	L	L	L	L	L	L	L	L	L
						M	M	P	P	P	MP	PR[1]	MP	GK	GP	GK	GK
SiO_2	45.3	46.4	46.2	44.7	47.3	45.7	46.8	49.4	48.8	47.7	55.7	52.0	51.8	63.7	56.7	62.6	60.1
Al_2O_3	35.1	34.3	34.5	34.2	33.7	35.1	34.2	30.9	32.4	33.5	28.2	29.6	29.9	20.1	26.4	20.9	22.1
FeO	0.4	0.4	0.4	0.6	0.5	0.4	0.6	1.0	0.6	0.5	0.4	0.9	0.9	0.4	0.6	0.4	1.0
CaO	18.6	17.0	18.2	18.4	17.2	17.9	17.1	15.1	16.0	16.4	8.9	12.3	12.7	2.7	8.3	1.8	4.7
Na_2O	0.8	1.6	0.6	1.0	1.3	1.0	0.9	2.3	1.8	1.6	5.8	4.2	3.7	5.5	6.5	5.8	4.7
K_2O	0.4	0.2	0.2	0.2	0.15	0.2	0.2	0.3	0.2	0.3	0.5	0.7	0.6	7.7	0.9	8.2	6.8
Total	100.6	99.9	100.1	99.1	100.2	100.3	99.8	99.0	99.8	100.0	99.5	99.7	99.6	100.1	99.4	99.7	99.4
Number of Ions on the Basis of 8 Oxygens																	
Si	2.083	2.138	2.125	2.089	2.170	2.099	2.153	2.287	2.239	2.188	2.516	2.380	2.371	2.892	2.572	2.857	2.752
Al	1.901	1.863	1.870	1.884	1.822	1.903	1.857	1.685	1.753	1.812	1.502	1.597	1.613	1.073	1.412	1.124	1.197
Fe	0.017	0.015	0.015	0.023	0.019	0.018	0.023	0.039	0.022	0.019	0.015	0.034	0.034	0.014	0.023	0.015	0.038
Ca	0.918	0.839	0.897	0.921	0.845	0.880	0.842	0.747	0.786	0.806	0.431	0.603	0.623	0.131	0.403	0.088	0.231
Na	0.071	0.139	0.054	0.091	0.116	0.089	0.076	0.207	0.160	0.142	0.508	0.373	0.328	0.479	0.572	0.513	0.419
K	0.025	0.011	0.012	0.012	0.009	0.011	0.009	0.018	0.011	0.017	0.029	0.041	0.035	0.445	0.052	0.477	0.399
Total	5.014	5.005	4.972	5.020	4.981	4.999	4.965	4.983	4.970	4.986	5.000	5.028	5.004	5.034	5.033	5.076	5.047
Mol.% An	90.5	84.8	93.2	90.0	87.2	89.8	90.8	76.9	82.1	83.4	44.5	59.3	63.2	12.4	39.3	8.2	22.1
Ab	7.0	14.1	5.6	8.8	11.9	9.1	8.2	21.3	16.7	14.7	52.5	36.7	33.3	45.4	55.7	47.6	39.9
Or	2.5	1.1	1.2	1.2	0.9	1.1	1.0	1.8	1.2	1.8	3.0	4.0	3.5	42.2	5.0	44.3	38.0

Abbreviations: X - xenolith, L - lava, M - megacryst, P - phenocryst, MP - microphenocryst, PR - phenocryst rim, GK - groundmass K-feldspar, GP - groundmass plagioclase.

Notes: (1) Analysis 12 forms rim around megacryst core (analysis 7).

clinopyroxene. In both groups clinopyroxene occurs both as large megacrysts and smaller phenocrysts.

While plagioclase is generally the most abundant phenocryst phase it often occurs as relatively small grains, particularly in the more mafic lavas, and particularly in the amphibole-free group, appears to have crystallised after some of the larger olivine and cpx grains.

Plagioclase compositions are discussed in sections 5.4 and compositional variation is summarised in figure 5.3 while representative analyses are given in table 5.8. Plagioclase phenocrysts are zoned, with cores in the range An 80 to 85 and outer rims of andesine or labradorite composition. Some are corroded and inclusion-rich, while the amphibole-bearing lavas in particular often contain xenocrysts of very calcic plagioclase (An 90), which have thin, tapering twin lamellae and are apparently derived from the gabbroic xenoliths.

All the lavas contain large (up to 1 cm) cpx megacrysts as well as abundant smaller phenocrysts. Megacrysts are generally more mafic and more calcic than the phenocrysts (see section 5.4, 5 and table 5.8).

The amphibole-free lavas contain large (up to 1 cm), often partially resorbed olivine megacrysts with compositions like those of the olivine-clinopyroxenite xenoliths (about Fo 80). These coexist with olivine phenocrysts which are smaller and more Fe-rich and are often zoned (Fo 70 - Fo 60). Both groups of lavas have groundmass olivine, which is of very variable composition (Fo 70 - Fo 45) and may be Mn-rich (up to 4% MnO) (table 5.9).

The lavas which do not contain olivine megacrysts contain reacted megacrysts of pargasitic amphibole (table 5.10, also see section 5.4, 2), which have very similar compositions to some amphiboles from the gabbroic xenoliths.

Table 5.9

Representative Analyses of Olivines from Sangeang Api Lavas

Analysis No.	1	2	3	4	5	6	7	8
Sample No.	B43	B43	B39	B39	B39	B39	B27	B27
	M	M	M	P	P	MP	G	G
SiO_2	39.8	39.7	39.0	36.4	36.6	33.5	35.1	34.7
FeO	11.7	11.6	17.4	27.8	26.2	42.0	33.1	35.8
MgO	47.3	47.4	42.2	34.1	35.6	21.1	28.0	25.7
CaO	0.3	0.4	0.2	0.4	0.3	0.6	0.4	0.5
TiO_2	0.1	0.1	-	-	0.1	0.1	-	0.1
MnO	-	-	0.3	1.0	0.9	2.4	2.6	3.2
Cr_2O_3	0.1	0.1	0.1	-	-	-	-	-
Total	99.3	99.3	99.2	99.7	99.7	99.7	99.2	100.0
			Number of Ions on the Basis of 4 Oxygens.					
Si	0.992	0.990	0.999	0.983	0.979	0.982	0.987	0.984
Fe	0.244	0.242	0.373	0.628	0.587	1.030	0.778	0.849
Mg	1.757	1.761	1.612	1.372	1.420	0.922	1.173	1.086
Ca	0.008	0.011	0.005	0.011	0.009	0.019	0.012	0.015
Ti	0.001	0.001	-	-	0.002	0.002	-	0.002
Mn	-	-	0.007	0.023	0.020	0.059	0.062	0.077
Cr	0.002	0.002	0.002	-	-	-	-	-
Total	3.005	3.007	2.999	3.017	3.018	3.015	3.012	3.014
100Mg/Mg+Fe	87.8	87.9	81.2	68.6	70.8	47.2	60.1	56.1

Abbreviations: M - megacryst, P - phenocryst, MP - microphenocryst, G - groundmass.

Table 5.10

Representative Analyses of Amphiboles from Sangeang Api Xenoliths and Lavas

Analysis No.	1	2	3	4	5	6	7	8	9	10	11	12	13	14	15
Sample No.	B5	B5	B13	B13	B21	B16	B18	B7	B24	B11	B10	B35	B35	B27	B27
Rock Type	X1	X1	X2	X2	X2	X2	X3	X3	X3	X3	X3	L	L	L	L
SiO_2	40.7	41.3	39.5	39.9	40.0	39.6	40.7	39.6	38.9	40.9	40.7	40.2	39.2	38.9	38.8
Al_2O_3	13.4	13.5	14.4	14.5	14.2	14.0	13.6	13.7	14.9	14.2	13.7	13.8	14.3	15.2	15.0
FeO	10.6	10.5	11.6	12.0	10.9	13.7	10.5	11.0	12.4	11.8	12.0	12.3	12.4	10.7	11.2
MgO	15.3	15.6	13.9	13.9	13.9	12.5	13.7	13.5	13.2	14.1	13.8	13.5	14.3	14.3	13.8
CaO	12.2	11.8	11.9	12.2	12.1	12.0	11.9	12.4	12.6	12.1	12.4	11.7	12.0	12.2	11.6
Na_2O	1.9	2.1	2.1	2.0	2.3	2.2	2.4	2.0	2.1	1.8	2.3	2.1	2.0	2.0	2.2
K_2O	1.7	1.6	1.8	1.8	1.7	2.0	1.8	2.0	2.0	1.5	1.7	1.5	1.7	1.9	1.8
TiO_2	1.7	1.7	2.1	2.2	2.2	2.2	2.8	2.9	2.5	2.2	2.3	2.2	2.3	2.3	2.5
MnO	-	-	-	-	-	-	-	-	-	-	-	-	-	-	-
Total	97.5	97.9	97.3	98.5	97.3	98.2	97.4	97.1	98.6	98.6	98.9	97.3	98.2	97.5	96.9
K_2O/Na_2O	0.89	0.76	0.86	0.9	0.74	0.91	0.75	1.00	0.95	0.83	0.74	0.71	0.85	0.95	0.82
Number of Ions on the Basis of 23 Oxygens.															
Si	6.024	6.063	5.895	5.884	5.943	5.922	6.031	5.934	5.772	6.002	5.990	5.995	5.874	5.786	5.812
Al	2.330	2.343	2.527	2.522	2.492	2.472	2.379	2.424	2.610	2.463	2.379	2.431	2.523	2.665	2.649
Fe	1.313	1.283	1.445	1.479	1.352	1.712	1.299	1.377	1.537	1.445	1.477	1.531	1.555	1.331	1.403
Mg	3.374	3.408	3.090	3.058	3.088	2.795	3.023	3.001	2.923	3.092	3.035	2.993	2.972	3.170	3.081
Ca	1.935	1.860	1.905	1.932	1.928	1.926	1.884	1.991	2.004	1.895	1.952	1.871	1.925	1.944	1.862
Na	0.541	0.582	0.617	0.559	0.655	0.645	0.701	0.575	0.600	0.506	0.645	0.609	0.589	0.577	0.639
K	0.313	0.302	0.336	0.329	0.331	0.375	0.341	0.387	0.383	0.279	0.310	0.289	0.320	0.361	0.344
Ti	0.193	0.183	0.234	0.250	0.245	0.246	0.309	0.321	0.275	0.239	0.255	0.249	0.263	0.257	0.282
Mn	-	-	-	-	-	-	-	-	-	-	-	-	-	-	-
Total	16.037	16.025	16.068	16.013	16.03	16.091	15.967	16.009	16.100	15.921	16.043	15.968	16.021	16.092	16.072
100Mg/Mg+Fe	72.0	72.75	68.1	67.4	69.5	62.0	69.9	68.6	65.5	68.1	67.3	66.2	65.7	70.4	68.7
Ca/Ca+Mg	0.364	0.353	0.381	0.387	0.384	0.408	0.384	0.399	0.407	0.380	0.391	0.385	0.393	0.380	0.377

Notes: X - xenoliths, L - lavas, X1 - olivine clinopyroxenites, X2 - alkali pyroxenites, X3 - gabbroic xenoliths. The amphibole in the olivine clinopyroxenite nodules is interstitial to early crystallised ol and cpx. In the alkali pyroxenites it is also interstitial to early cpx, and is also partially replacing the cpx. In the gabbroic xenoliths amphibole is an early crystallised primary phase except in B10 where it is a late phase occurring as intercumulate (?) oikocrysts. In the lavas, the amphibole occurs as partially reacted megacrysts.

The groundmasses of the lavas are generally composed of fine interlocking laths of plagioclase (An 32 - An 50), small tabular clinopyroxene, small granular olivine and magnetite, needles of apatite and generally relatively Ca-rich alkali feldspar (An 15 Ab 70 Or 15 - An 11 Ab 27 Or 62). Som have a glassy mesostasis and a few contained very fine grains of a cancrinite-vishnevite group mineral (microsommite).

One member of the olivine megacryst-bearing group of lavas phonolitic tephrite B43 (tables 5.7 and 5.3), differs significantly from most other lavas of the suite, in that it contains no plagioclase phenocrysts and abundant, very large megacrysts of olivine and clinopyroxene. These megacrysts are particularly mafic and in fact are generally more magnesian than representatives of the same phases in the olivine-clinopyroxenite xenoliths. The compositions of these megacrysts are essentially identical to those of the ankaramites from Rindjani (e.g. LB8, chapter 3).

Clinopyroxenes are zoned with Cr-diopside cores (Ca 48 Mg 48 Fe 4, Mg/Mg+Fe = 0.92, 1% Cr_2O_3) and augite rims (Ca 49 Mg 42 Fe 9, Mg/Mg+Fe = 0.83). Associated olivine has a composition in the range Fo 87 - Fo 88 (table 5.11).

5.4 *Mineral Chemistry of the Sangeang Api Lavas and Intrusive Rocks*

1. Clinopyroxene

This is ubiquitous to all xenoliths and lavas. Representative analyses of clinopyroxenes from each of the main intrusive rock-types as well as megacryst, phenocryst and groundmass minerals from the lavas are given in tables 5.11-5.13. Compositional variations are summarised in standard pyroxene-quadrilateral diagrams in figures 5.5 and 5.12.

The main compositional variations of the clinopyroxenes of these rocks involve Mg, Fe, Ca, Al and Ti. A characteristic of all clinopyroxenes, (though there are significant differences between pyroxenes of the individual xenolith-types and phenocrysts and groundmass) is their very Ca-rich, Na-poor

Table 5.11

Representative Analyses of Clinopyroxene from Sangeang Api Lavas

Analysis No.	1	2	3	4	5	6	7	8	9	10	11
Sample No.	B43	B43	B43	B35	B35	B27	B27	B39	B39	B39	B38
	M	M	M	P	G	P	P	M	R(1)	G	G
SiO_2	53.6	53.6	51.5	51.3	43.8	48.7	48.2	51.0	50.9	49.9	49.5
Al_2O_3	1.4	1.4	3.4	3.9	8.7	6.7	6.2	3.8	4.0	4.1	5.5
FeO	2.7	2.7	5.5	7.0	11.1	8.1	9.0	6.6	7.7	11.3	10.5
MgO	17.3	16.8	15.0	14.5	10.6	12.9	12.7	15.2	14.6	12.0	12.4
CaO	23.8	24.3	23.8	22.5	23.6	22.7	21.7	22.2	21.9	20.5	19.5
Na_2O	-	-	-	-	-	-	-	0.3	-	0.5	-
TiO_2	0.3	0.3	0.5	0.6	1.9	1.0	1.8	0.6	0.7	1.2	1.6
MnO	-	-	-	-	-	-	0.3	-	-	0.3	0.3
Cr_2O_3	1.0	1.0	0.2	-	-	-	-	-	-	-	-
Total	100.1	100.1	99.9	99.8	99.7	100.1	99.9	99.7	99.8	99.8	99.3
				Number of Ions on the Basis of 6 Oxygens.							
Si	1.953	1.954	1.902	1.900	1.682	1.815	1.807	1.890	1.890	1.882	1.863
Al^{IV}	0.047	0.0457	0.098	0.099	0.318	0.185	0.193	0.110	0.110	0.118	0.137
Al^{VI}	0.013	0.014	0.050	0.071	0.076	0.108	0.081	0.056	0.065	0.063	0.106
Fe	0.081	0.081	0.170	0.217	0.356	0.252	0.282	0.205	0.239	0.355	0.329
Mg	0.937	0.911	0.826	0.800	0.607	0.714	0.709	0.839	0.808	0.674	0.695
Ca	0.928	0.950	0.942	0.893	0.971	0.907	0.872	0.882	0.871	0.829	0.786
Na	-	-	-	-	-	-	-	0.022	-	0.037	-
Ti	0.008	0.008	0.014	0.017	0.055	0.028	0.051	0.017	0.019	0.035	0.045
Mn	-	-	-	-	-	-	0.009	-	-	0.010	0.009
Cr	0.028	0.029	0.006	-	-	-	-	-	-	-	-
Total	3.995	3.993	4.007	3.998	4.065	4.010	4.005	4.020	4.003	4.003	3.970
100Mg/Mg+Fe	92.0	91.8	82.9	78.7	62.9	73.9	71.5	80.4	77.2	65.5	67.9
Ca/Ca+Mg	0.497	0.511	0.533	0.527	0.615	0.559	0.551	0.512	0.519	0.552	0.530
Mol.% Ca	47.7	48.9	48.6	46.7	50.2	48.4	46.7	45.8	45.3	44.6	43.4
Mg	48.1	46.9	42.6	41.9	31.4	38.1	38.2	43.5	42.2	36.3	38.4
Fe	4.2	4.2	8.8	11.4	18.4	13.5	15.1	10.7	12.5	19.1	18.2

Abbreviations: M - megacryst, P - phenocryst, R - rim, G - groundmass.

Notes: The detection-limit for Na_2O on the electron-probe was about 0.25% and on this basis most of the above pyroxenes must have <0.25% Na_2O.

(1) Analysis 9 is of an outer rim to megacryst, analysis 8 and is compositionally equivalent to the phenocrysts.

Table 5.12 Representative Electron Microprobe Analyses of Clinopyroxenes from Sangeang Api Xenoliths

Analysis No.	1	2	3	4	5	6	7	8	9	10	11	12	13	14
Sample No.	B23	B23	B5	B5	B5	B5	B4	B9	B9	B25	B25	B25	B2H	B2H
Xenolith type:	1	1	1	1	1	1	1	1	1	2	2	2	2	2
	core - rim		core - rim		core - rim					core - rim				
SiO_2	50.5	49.7	53.2	52.0	51.6	48.6	52.1	49.5	49.8	51.1	50.5	50.6	50.2	49.8
Al_2O_3	4.2	5.1	2.4	3.7	2.7	4.4	3.6	5.1	5.2	3.7	4.6	4.0	4.5	4.9
FeO	6.2	6.3	5.1	6.1	5.6	7.2	5.6	6.3	6.9	5.8	6.5	7.0	7.3	7.6
MgO	14.3	14.0	14.8	14.1	15.8	13.3	14.4	14.7	13.6	14.7	13.7	13.8	13.8	13.6
CaO	23.8	23.7	23.8	23.4	23.6	25.2	23.5	23.5	23.4	23.7	23.6	23.2	23.1	23.1
Na_2O	-	-	-	-	-	-	-	-	-	-	-	-	-	-
TiO_2	0.7	0.9	0.5	0.5	0.5	0.8	0.5	0.7	0.8	1.0	1.0	0.9	0.9	0.8
MnO	-	-	-	-	-	-	-	-	-	-	-	0.2	-	-
Cr_2O_3	0.20	0.10	0.2	0.1	0.2	0.1	0.2	0.3	0.1	0.1	0.1	0.1	0.1	0.1
Total	99.9	99.8	100.0	99.9	100.0	99.6	99.9	100.1	99.8	100.1	100.0	99.8	99.9	99.9
100 Mg/Mg+Fe (mol.)	80.43	79.84	83.88	80.46	83.41	76.70	82.10	80.69	77.84	81.86	78.87	77.84	77.11	76.06
	Number of Ions on the Basis of 6 Oxygens													
Si	1.874	1.848	1.953	1.919	1.905	1.832	1.919	1.837	1.853	1.887	1.872	1.883	1.868	1.855
Al^{IV}	0.126	0.152	0.047	0.081	0.095	0.168	0.081	0.163	0.174	0.113	0.128	0.116	0.132	0.145
Al^{VI}	0.058	0.072	0.057	0.080	0.023	0.027	0.075	0.057	0.081	0.049	0.073	0.059	0.065	0.069
Fe	0.192	0.196	0.155	0.188	0.173	0.227	0.173	0.194	0.215	0.180	0.201	0.218	0.227	0.238
Mg	0.791	0.776	0.810	0.775	0.869	0.747	0.790	0.812	0.754	0.807	0.757	0.766	0.765	0.755
Ca	0.946	0.944	0.937	0.925	0.934	1.018	0.928	0.933	0.933	0.937	0.937	0.925	0.921	0.922
Na	-	-	-	-	-	-	-	-	-	-	-	-	-	-
Ti	0.020	0.025	0.013	0.014	0.014	0.022	0.014	0.019	0.022	0.026	0.028	0.025	0.025	0.023
Mn	-	-	-	-	-	-	-	-	-	-	-	0.006	-	-
Cr	0.005	0.001	0.007	0.003	0.006	0.003	0.006	0.008	0.003	0.004	0.003	0.003	0.003	0.004
Z	2.000	2.000	2.000	2.000	2.000	2.000	2.000	2.000	2.000	2.000	2.000	2.000	2.000	2.000
X + Y	2.012	2.010	1.979	1.985	2.019	2.044	1.986	2.023	2.008	2.003	1.999	2.002	2.006	2.011
Total	4.012	4.010	3.979	3.985	4.019	4.044	3.986	4.023	4.008	4.003	3.999	4.002	4.006	4.011
	Molecular Proportions													
Ca	49.0	49.3	49.2	49.0	47.3	51.1	49.0	48.1	49.1	48.7	49.5	48.4	48.1	48.2
Mg	41.0	40.5	42.6	41.0	44.0	37.6	41.9	41.9	39.6	42.0	40.0	40.1	40.1	39.4
Fe	10.0	10.2	8.2	10.0	8.7	11.3	9.1	10.0	11.3	9.3	10.5	11.5	11.8	12.4
Ca/Ca+Mg (mol.)	.545	.549	.536	.544	.518	.577	.540	.535	.553	.537	.553	.547	.546	.550
Al^{VI}/Al^{IV}	0.460	0.474	1.212	0.987	0.237	0.164	0.930	0.350	0.552	0.434	0.570	0.513	0.495	0.476

Notes: Type 1 xenoliths - olivine clinopyroxenites

Type 2 xenoliths - magnetite clinopyroxenites

Table 5.13

Representative Analyses of Clinopyroxenes

from Sangeang Api-Alkali Pyroxenite and Gabbroic Xenoliths.

Analysis No.	1	2	3	4	5	6	7	8	9	10
Sample No.	B13	B13	B22	B22	B16	B15	B10	B24	B8	B8
Xenolith Type	A	A	A	A	A	A	G	G	G	G
	C	R	C	R		(1)				
SiO_2	53.0	47.2	51.6	48.8	48.9	51.5	45.8	47.3	49.4	45.7
Al_2O_3	1.6	7.5	3.0	5.7	5.4	2.9	5.8	6.7	4.9	8.5
FeO	5.1	8.2	4.2	7.4	8.9	6.2	7.4	8.6	7.9	9.4
MgO	16.2	12.9	15.8	13.0	12.5	14.9	12.4	12.7	12.7	10.9
CaO	23.4	22.9	23.9	23.8	23.1	23.8	22.7	24.4	23.9	23.8
Na_2O	-	-	-	-	0.4	-	0.2	-	-	0
TiO_2	0.4	1.1	0.5	1.0	0.7	0.6	0.8	1.1	0.9	1.6
MnO	-	-	-	-	-	-	-	-	-	-
Cr_2O_3	0.2	-	0.8	-	-	-	-	-	-	-
Total	99.9	99.8	99.8	99.7	99.9	99.9	95.1	99.7	99.7	99.9
Si	1.949	1.771	1.899	1.827	1.838	1.908	1.807	1.783	1.853	1.731
Al^{IV}	0.051	0.229	0.101	0.173	0.162	0.092	0.193	0.217	0.147	0.269
Al^{VI}	0.018	0.102	0.031	0.079	0.077	0.035	0.078	0.080	0.069	0.110
Fe	0.157	0.257	0.128	0.232	0.279	0.192	0.243	0.271	0.248	0.298
Mg	0.888	0.721	0.868	0.725	0.700	0.823	0.728	0.713	0.710	0.615
Ca	0.922	0.921	0.943	0.955	0.930	0.945	0.958	0.941	0.961	0.965
Na	-	-	-	-	0.029	-	0.014	-	-	-
Ti	0.011	0.031	0.014	0.028	0.020	0.017	0.023	0.031	0.025	0.046
Mn	-	-	-	-	-	-	-	-	-	-
Cr	0.005	-	0.128	-	-	-	-	-	-	-
Total	4.002	4.032	4.008	4.018	4.037	4.011	4.042	4.037	4.013	4.034
100Mg/Mg+Fe	85.0	73.7	87.2	75.8	71.5	81.1	75.0	72.4	74.1	67.4
Ca/Ca+Mg	0.509	0.561	0.520	0.568	0.571	0.535	0.568	0.570	0.575	0.611
Mol.% Ca	47.0	48.6	48.6	49.9	48.7	48.2	49.7	48.9	50.1	51.5
Mg	45.1	37.9	44.8	38.0	36.7	42.0	37.7	37.0	37.1	32.7
Fe	7.9	13.5	6.6	12.1	14.6	9.8	12.6	14.1	12.8	15.8

Notes: 1. Analysis 6, from B15, is of cpx-reaction rim around olivine of Fo81 (see plate 3E).

Abbreviations: A - alkali clinopyroxenite, G - gabbroic xenolith, C - core, R - rim

Analyses 1 and 2 and 3 and 4 are coexisting core-rim pairs.

*The detection limit for Na_2O is about 0.25%.

composition (in almost all examples Na is below the detection limit for this element on the electron microprobe used ca. 0.2 - 0.3% Na_2O).

Compositional variations of these clinopyroxenes are somewhat akin to those of shallow-level intrusions of differentiating alkali basalt magma (e.g. the Shiant Sill; Gibb, 1973).

The main variations in clinopyroxene composition are considered in terms of seven distinct petrographic groupings; 1. olivine clinopyroxenites; 2. magnetite clinopyroxenites; 3. gabbroic intrusives; 4. alkali clinopyroxenites; 5. lava megacrysts; 6. lava phenocrysts; 7. lava groundmass clinopyroxenes.

In general it is found that with the exception of the cpx from the alkali clinopyroxenite and occurring as megacrysts, the cpx of all the other groups fall into distinct, recognisable, compositionally unique fields. Overall, clinopyroxenes range from Cr-diopside to salite to Ca-augite in composition.

(a) Mg/Mg+Fe and Ca/Ca+Mg variations

Variation in Mg/Mg+Fe and Ca/Ca+Mg provides the main discriminant between pyroxenes of the above petrographic groupings. In particular variations of these parameters define four distinct fields; 1. olivine clinopyroxenites; 2. magnetite clinopyroxenites and gabbros; 3. phenocrysts; 4. groundmass pyroxenes. Each grouping shows a general trend of increasing Ca/Ca+Mg with decreasing Mg/Mg+Fe (figure 5.4). At the same time the pyroxenes of the four groups just mentioned show a general trend of decreasing Mg/Mg+Fe from group 1 (olivine clinopyroxenites) to group 4 (groundmass pyroxenes). This trend is also accompanied by a general trend of decreasing Ca/Ca+Mg at any particular Mg/Mg+Fe value. Thus pyroxenes of the olivine clinopyroxenites are relatively more Ca-rich than those of the magnetite clinopyroxenite and gabbroic xenoliths which in turn are more Ca-rich than the phenocrysts which are generally more calcic than the groundmass clinopyroxenes (figure 5.4).

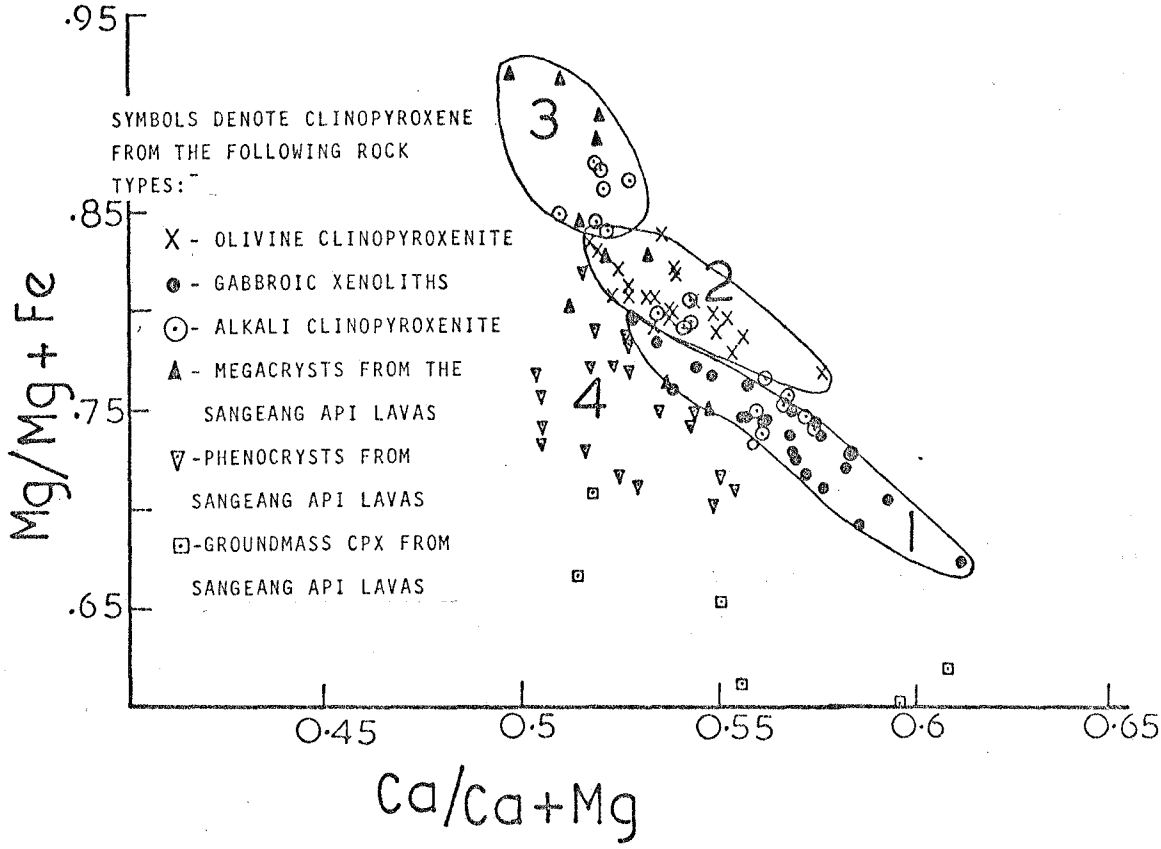

FIGURE 5.4

VARIATION IN Mg/Mg+Fe AND Ca/Ca+Mg RATIOS (ATOMIC) IN CLINOPYROXENES FROM SANGEANG API LAVAS AND XENOLITHS. FIELD 1.-CPX OF GABBROIC XENOLITHS,2.-CPX OF OLIVINE CLINOPYROXENITE,3.-Cr-DIOPSIDE MEGACRYSTS FROM LAVA B43 AND CORES IN ALKALI CLINOPYROXENITE CPX,4-CPX PHENOCRYSTS FROM LAVAS.

Within any given group, core-rim variations and slight differences between clinopyroxene compositions of different rocks of the same group, describe trends of decreasing Mg/Mg+Fe with increasing Ca/Ca+Mg. Thus a series of subparallel trends are shown on figure 5.4. There is almost no overlap between the pyroxenes of the olivine clinopyroxenite and those of the plagioclase-bearing gabbroic xenoliths and there is only slight overlap between this latter group and phenocryst compositions.

Some clinopyroxenes from the alkali clinopyroxenites are zoned with rather pale cores (compared to their more greenish rims), with higher relief, poor cleavage and larger 2V. These are markedly more magnesian than the rim compositions, (figures 5.4, 5.5) and are relatively Ca-rich. They are slightly more mafic than the most magnesian analysed cpx from the olivine clinopyroxenites. Furthermore, the megacrysts from the mafic ankaramite or phonolitic tephrite B43 (table 5.11) are even more mafic than the diopsidic cores from the alkali clinopyroxenites. Both these groups of mafic, Cr-diopsides have similar Ca/Ca+Mg values (ca. 0.5) to those of the slightly less mafic clinopyroxenes of the olivine clinopyroxenites. Thus in view of the "normal" trend of decreasing Ca/Ca+Mg with increasing Mg/Mg+Fe shown by the other clinopyroxenes, these diopsides are even more relatively Ca-rich than the olivine clinopyroxenite pyroxenes.

Other megacrysts plot on a general trend of decreasing Mg/Mg+Fe at constant or only slightly increasing Ca/Ca+Mg, from the field of these most mafic compositions to compositions the same as those of the phenocrysts (figure 5.4). Intermediate compositions fall in both the olivine-clinopyroxenite and gabbroic fields (figure 5.4). This same trend is also exhibited by the core-rim variation of a single cpx megacryst of very similar type from ankaramite LB8, from Rindjani, on Lombok Island (figure 5.6). Thus the megacrysts appear to represent a sampling of a

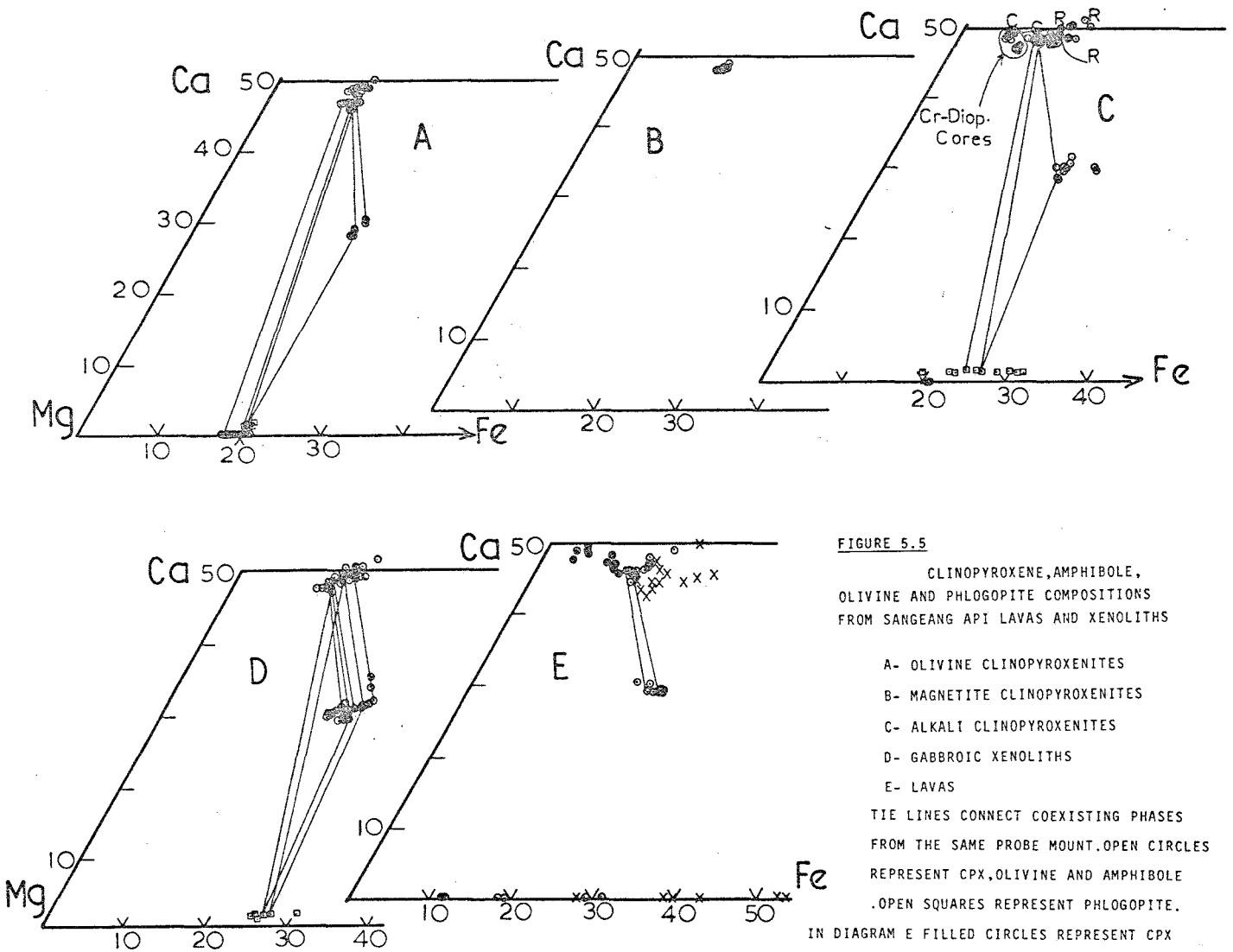

FIGURE 5.5

CLINOPYROXENE, AMPHIBOLE, OLIVINE AND PHLOGOPITE COMPOSITIONS FROM SANGEANG API LAVAS AND XENOLITHS

A- OLIVINE CLINOPYROXENITES

B- MAGNETITE CLINOPYROXENITES

C- ALKALI CLINOPYROXENITES

D- GABBROIC XENOLITHS

E- LAVAS

TIE LINES CONNECT COEXISTING PHASES FROM THE SAME PROBE MOUNT. OPEN CIRCLES REPRESENT CPX, OLIVINE AND AMPHIBOLE. OPEN SQUARES REPRESENT PHLOGOPITE. IN DIAGRAM E FILLED CIRCLES REPRESENT CPX AND OLIVINE MEGACRYSTS, OPEN CICLES- ARE CPX AND AMPHIBOLE PHENOCRYSTS AND CROSSES ARE GROUNDMASS CPX AND OLIVINE. MAFIC Cr-DIOPSIDE CORES FROM ALKALI PYROXENITES ARE CIRCLED IN DIAGRAM C.

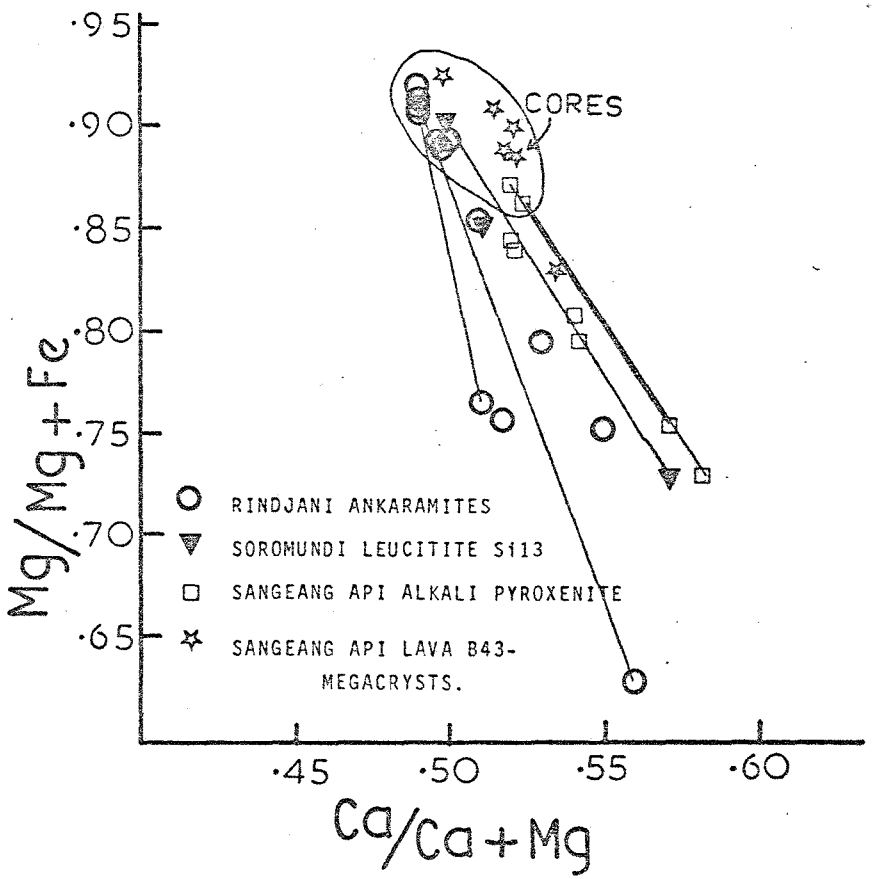

FIGURE 5.6

Mg/Mg+Fe (atomic) v.Ca/Ca+Mg (atomic) VARIATION IN MAFIC CLINOPYROXENE (Cr-DIOPSIDE) CORES OCCURING AS MEGACRYSTS IN LAVAS FROM SANGEANG API,RINDJANI AND SOROMUNDI VOLCANOES AND IN ALKALI PYROXENITE XENOLITHS FROM SANGEANG API,TOGETHER WITH THE COMPOSITIONS OF MORE Al- AND Ti-RICH AUGITE RIMS.CORES ARE IN THE AREA ENCIRCLED.

representative selection of the clinopyroxene of all xenolith types and in the case of those of lava B43, appear to have sampled some which are even more mafic than those represented in the available xenolith samples.

The pyroxene variation of the alkali clinopyroxenites is similar. Clinopyroxenes from these rocks tend to show wide core-rim variations, which cut-across the "normal" variation trends shown by pyroxenes from one xenolith type. The mafic early cores are mantled by successively less mafic outer zones. These outer zones also appear to correspond with the later stage precipitation of phlogopite and/or amphibole. In terms of variation in Mg/Mg+Fe and Ca/Ca+Mg (figure 5.4) for core to rim, the clinopyroxenes of this xenolith group record a variation from their mafic, Cr-diopside-cores to cpx like that of the olivine clinopyroxenites, to rims which fall in the field of gabbroic xenolith clinopyroxenes.

(b) Al-Ti variation

Low silica activity in the liquid is likely to favour Al^{IV} substitution into the Z-site (e.g. Le Bas, 1962), coupled with Ti substitution in the Y-site (Yagi and Onuma, 1967). Increased pressure is likely to favour Al-substitution into the Y-site (e.g. Kushiro, 1960), yielding high Al^{VI}/Al^{IV} ratios (e.g. Aoki and Kushiro, 1968).

The cpx of the Sangeang Api lavas and xenoliths show a general overall trend of increasing Al and Ti with decreasing Mg/Mg+Fe (figures 5.7 and 5.8). The most mafic clinopyroxenes, for instance, the Cr-diopside megacrysts from lava B43 and the mafic cores of cpx from the alkali clinopyroxenites all have very low Al and Ti concentrations (tables 5.11 and 5.13). This is also true of the very magnesian Cr-diopside occurring in cores in megacrysts from the Rindjani ankaramites described in chapter 3 and is also true of virtually identical megacrysts in some of the leucitic lavas from G. Sangenges and Soromundi (chapter 6, table 6.8).

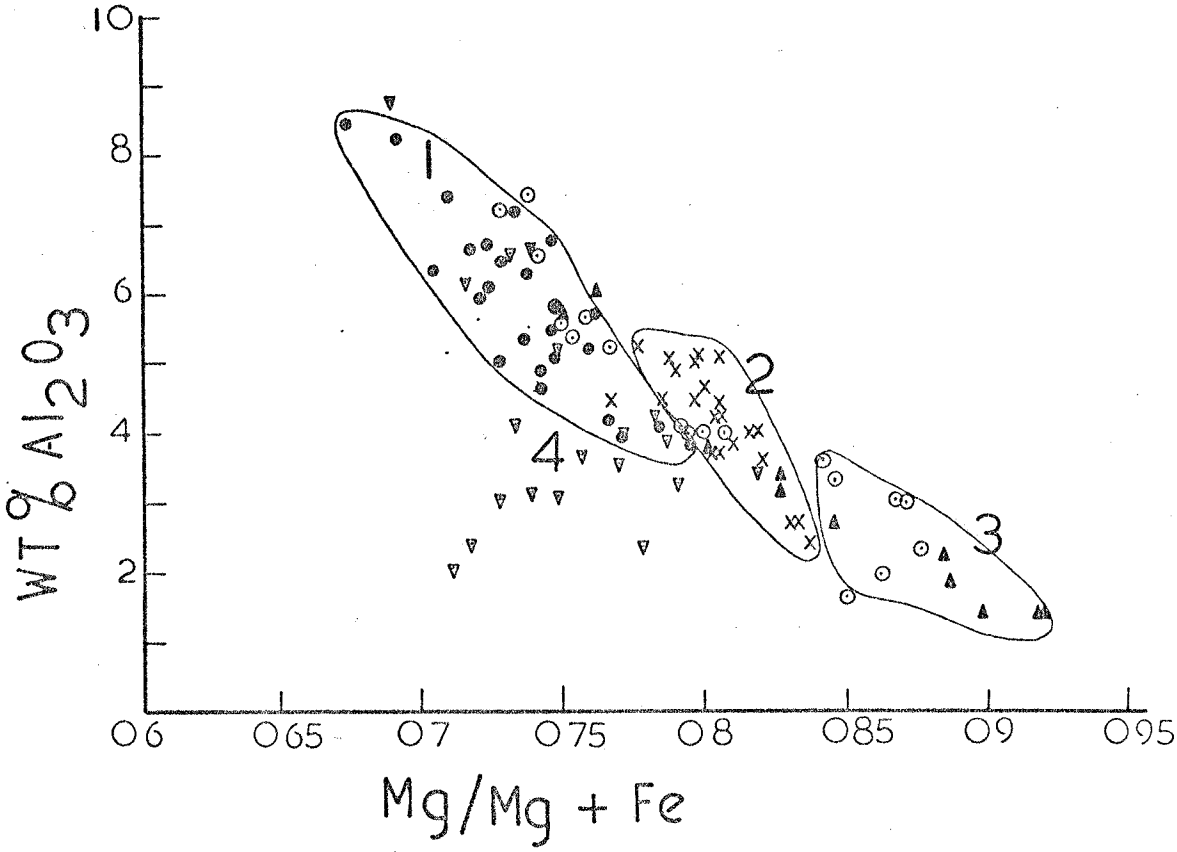

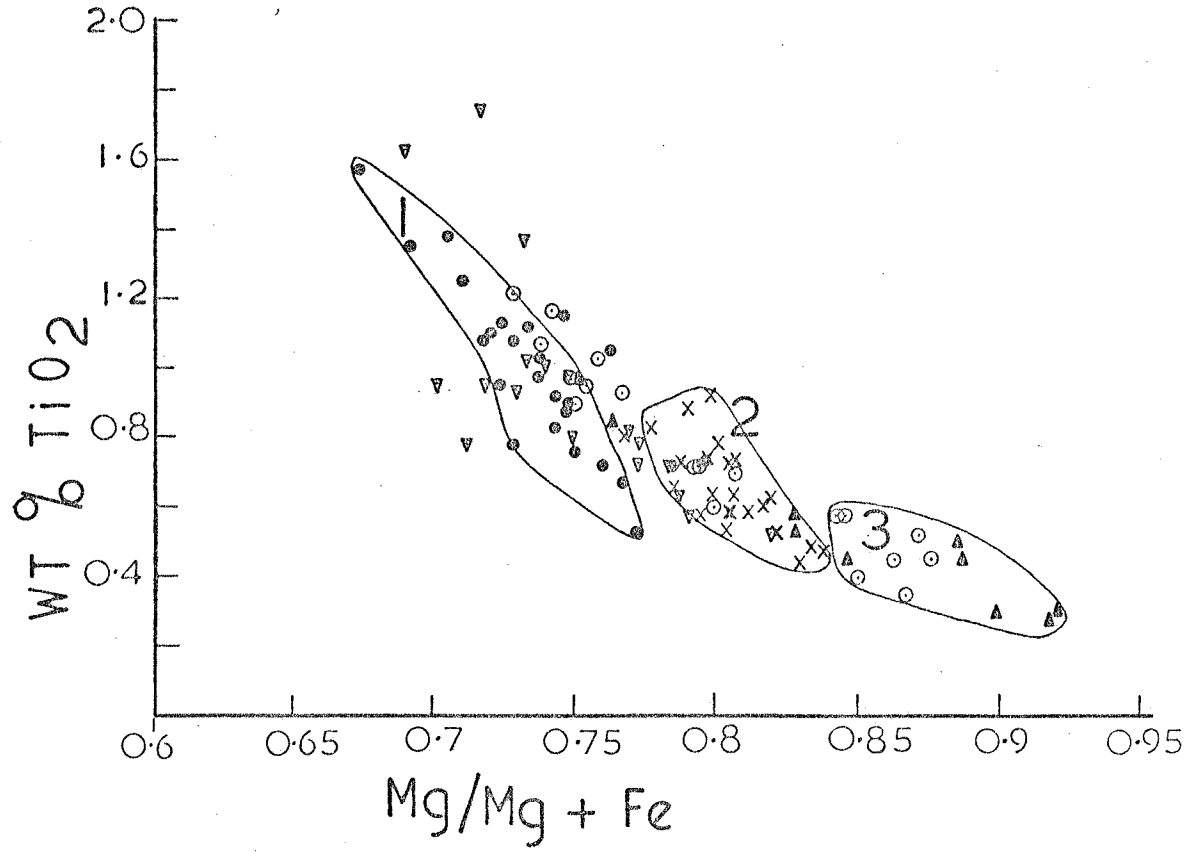

FIGURE 5.7

VARIATION IN Al_2O_3 (WT.%) AND Mg/Mg+Fe (atomic) IN CPX FROM SANGEANG API LAVAS AND COARSE-GRAINED XENOLITHS.FIELDS ARE: 1.CPX FROM GABBROIC XENOLITHS,2.CPX FROM OLIVINE CLINOPYROXENITES,3.CPX FROM ALKALI CLINOPYROXENITES OCCURING AS CORES AND MEGACRYSTS FROM LAVA B43 (SEE FIG. 5.6),4. CPX PHENOCRYSTS FROM SANGEANG API LAVAS. SYMBOLS DENOTE CPX FROM THE FOLLOWING ROCK-TYPES: X -OLIVINE CLINOPYROXENITE, ⊛ -GABBROIC XENOLITHS, ⊙-ALKALI CLINOPYROXENITE, ▲ -MEGACRYSTS FROM LAVAS, ▽ -PHENOCRYSTS FROM LAVAS.

FIGURE 5.8

VARIATION IN TiO_2(WT.%) V. Mg/Mg+Fe (atomic) IN CPX FROM SANGEANG API LAVAS AND XENOLITHS.LABELLED FIELDS AND SYMBOLS HAVE THE SAME CONNOTATION AS IN FIG. 5.7.

Comparing the pyroxenes from the lavas and the xenoliths (figure 5.7), there is a tendency for the phenocrystic clinopyroxenes to fall away from the xenolithic clinopyroxene trend having lower Al_2O_3 than clinopyroxenes from the xenoliths with similar Mg/Mg+Fe values. This trend is emphasised by the groundmass cpx compositions, where several analyses give Mg/Mg+Fe values <0.7 and Al_2O_3 <6%. This tendency applies less to the TiO_2 variation.

This feature is also illustrated by the TiO_2 v Al_2O_3 variation (figure 5.9). A number of the phenocryst and groundmass clinopyroxenes plot at markedly lower Al_2O_3 values than cpx of the xenoliths and megacrysts with similar TiO_2 concentrations (i.e. they are relatively more Ti-rich than the pyroxenes of the intrusive rocks.

The most mafic, diopsidic clinopyroxenes from the olivine-clinopyroxenites, alkali clinopyroxenites and occurring as megacrysts in lava B43, as discussed previously are remarkably Al- and Ti-poor. The less magnesian clinopyroxenes from these xenoliths and those of the gabbroic xenoliths, are more Al- and Ti-rich (figure 5.9). Furthermore, the Al-Ti variation trend (figure 5.9), appears to comprise two distinct linear arrays. The most mafic, Al-poor clinopyroxenes (cores) from the olivine clinopyroxenites, alkali clinopyroxenites and the megacrysts from B43, lie on a trend with a markedly flatter slope than do the less mafic and more Al-rich members of these groups (outer zones and rims) and all clinopyroxene of the gabbro group.

This is illustrated well if the alkali clinopyroxenite data is plotted alone (figure 5.10). This transition must represent a change in the nature of the Al- and Ti-substitution, predominantly in Ca Tschermak's molecule ($Ca\ Al_2\ SiO_6$) to a coupled Al-Ti substitution as the $Ca\ Ti\ Al_2\ O_6$ molecule as postulated by Yagi and Onuma (1967). This would then also correspond to a decrease in the Al^{VI}/Al^{IV} ratio of the clinopyroxenes and may represent a response to decreasing pressure (Al^{VI}/Al^{IV} ratios of these most mafic

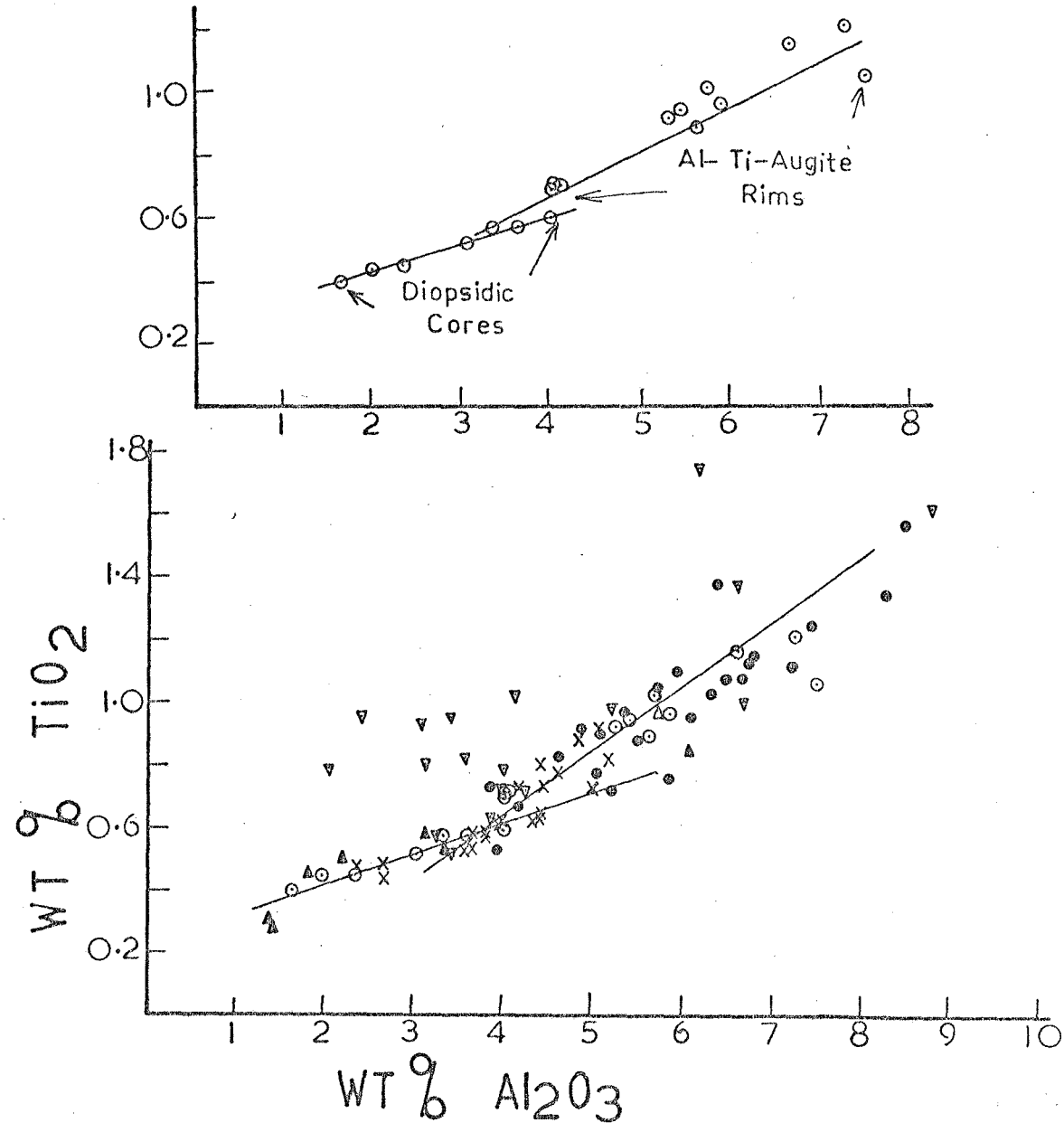

FIGURE 5.9 (lower diagram)

VARIATION IN TiO_2 v. Al_2O_3 (WT.%) IN CLINOPYROXENE FROM SANGEANG API LAVAS AND XENOLITHS. SYMBOLS REPRESENT CPX OF THE SAME ROCK-TYPE AS IN FIG. 5.7. LINES INDICATE THE CHANGE Ti-Al VARIATION FROM THE MAFIC DIOPSIDIC CPX (LOW Ti & Al) TO THE LESS MAFIC AUGITES.

FIGURE 5.10 (upper diagram)

THIS SHOWS THE SAME TiO_2 v. Al_2O_3 VARIATION AS FIG. 5.9 , SHOWING ONLY THE VARIATION IN COMPOSITION OF CPX FROM THE ALKALI CLINOPYROXENITES.

pyroxenes do indeed tend to be quite high, some in fact as high as 0.9. However, as the calculation of the Al^{IV}/Al^{VI} partition is largely dependant on the quality of the silica analysis, in view of the low Al concentrations, small variations in the silica determinations within the limits of precision of the electron probe are likely to produce considerable apparent variation in Al^{IV}/Al^{IV} ratios).

This tendency towards Al substitution in the Ca Ti Al_2 O_6 molecule in favour of Ca-Tschermak's molecule may be even further extended in the case of the phenocryst and groundmass pyroxenes. In this case Ti is even more markedly enriched relative to Al, compared with the pyroxenes of the xenoliths

The low-Al, -Ti, mafic, diopsidic clinopyroxenes from the olivine clinopyroxenites, alkali clinopyroxenites and also occurring as megacrysts in lava B43, have high Cr-concentrations, and in fact are the only pyroxenes with significant Cr. Cr concentration shows rapid depletion with decreasing Mg/Mg+Fe. Those with Mg/Mg+Fe values about 0.9 have about 1.0% Cr_2O_3, while those more Fe-rich than Mg/Mg+Fe = 0.77, have very low Cr concentrations (<0.1% Cr_2O_3). The gabbroic xenoliths, which have pyroxenes mostly more iron-rich than Mg/Mg+Fe = 0.77, have whole-rock Cr concentrations of about 60ppm or less and their clinopyroxenes are likely to have at most 120ppm Cr. This factor tends to suggest a fractional crystallisation mechanism, where the Cr-content of the liquid is rapidly depleted by the crystallisation of early, high temperature, mafic diopside.

All pyroxenes, including the most mafic diopsides, have very low Na_2O contents (almost all less than the detection limit of about 0.25%). Thus the Cr-diopside have a very refractory character which is somewhat at odds with their presence in association with markedly alkali lavas. This problem is even more marked in the case of some leucitic lavas from Soromundi, (chapter 6), for instance, where identical megacrysts occur in highly undersaturated lavas.

2. Amphibole

Amphibole occurs in five distinct roles in the suites of lavas and intrusive rocks from Sangeang Api volcano.

1. As late-stage interstitial or intercumulate, somewhat poikilitic grains in the olivine clinopyroxenite nodules (plate 2A).
2. As a second stage phase in the alkali clinopyroxenites, replacing earlier cpx and occupying interstial areas between primary cpx grains, often in association with phlogopite (plates 3A, C and G).
3. As primary, early-formed grains in hornblende-magnetite-clinopyroxenite (e.g. B20) and in the most mafic, amphibole-rich members of the gabbroic xenolith suite (e.g. B1B, B7 and B24 (plates 5A, B and D).
4. As late-stage intercumulate, poikilitic oikocrysts in some of the least mafic, least amphibole-rich members of the gabbroic xenolith group (e.g. B10 plate 5E).
5. As somewhat corroded or reacted phenocrysts/megacrysts in some of the lavas (e.g. B27, B35).

Analyses of typical examples of amphibole from each of these roles are given in table 5.10, while overall variations are summarised in the Fe-Mg-Ca quadrilateral diagram (figure 5.11).

All the amphiboles are members of the Ca-rich hornblende group and according to the criteria of Papike et al. (1974), they are all either pargasites or magnesian hastingsites. Compared with the clinopyroxenes, the compositional variation of the amphiboles is more restricted and this might indicate that crystallisation of amphibole was confined to a more limited episode in the evolution of the liquids from which the xenolith minerals precipitated (either limited by liquid composition and/or by PH_2O, fO_2, P and T). Though there is certainly some correlation between the Mg/Mg+Fe ratio of coexisting cpx and amphibole (figure 5.12).

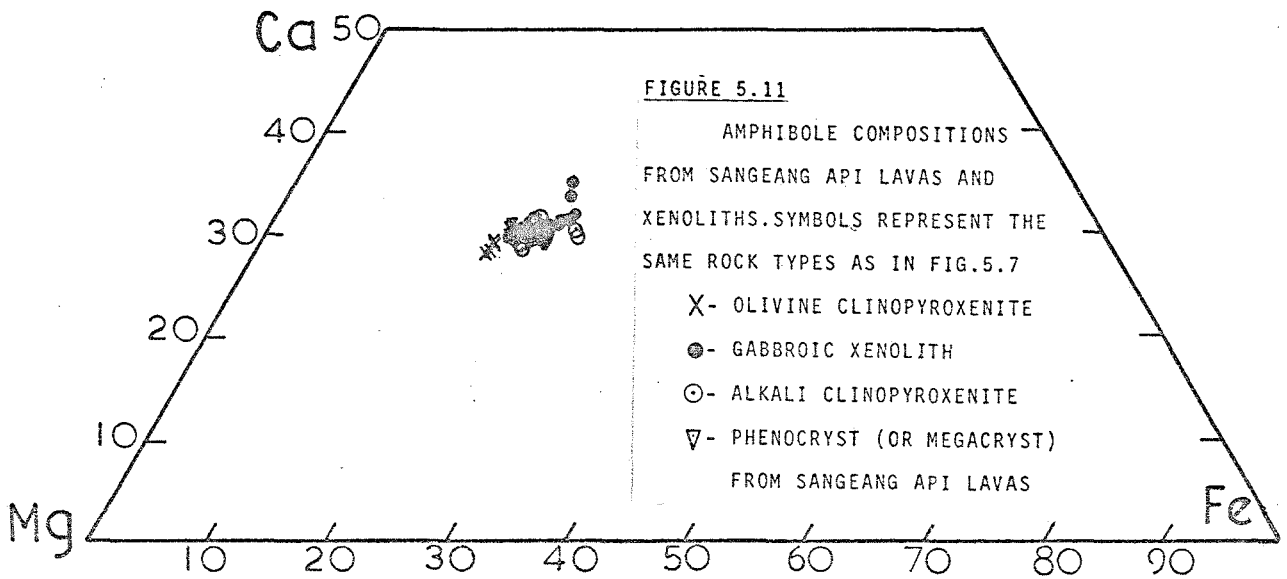

FIGURE 5.11

AMPHIBOLE COMPOSITIONS FROM SANGEANG API LAVAS AND XENOLITHS. SYMBOLS REPRESENT THE SAME ROCK TYPES AS IN FIG. 5.7

X- OLIVINE CLINOPYROXENITE

●- GABBROIC XENOLITH

⊙- ALKALI CLINOPYROXENITE

▽- PHENOCRYST (OR MEGACRYST) FROM SANGEANG API LAVAS

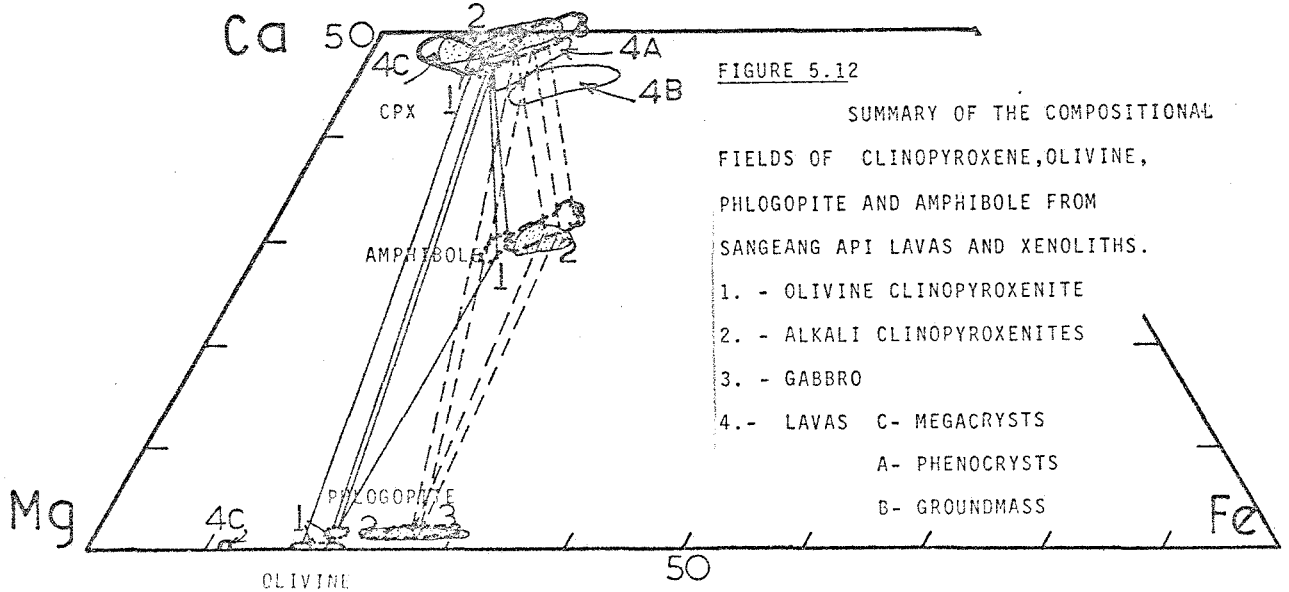

FIGURE 5.12

SUMMARY OF THE COMPOSITIONAL FIELDS OF CLINOPYROXENE, OLIVINE, PHLOGOPITE AND AMPHIBOLE FROM SANGEANG API LAVAS AND XENOLITHS.

1. - OLIVINE CLINOPYROXENITE
2. - ALKALI CLINOPYROXENITES
3. - GABBRO
4. - LAVAS C- MEGACRYSTS
   A- PHENOCRYSTS
   B- GROUNDMASS

The general impression, considering the paragenetic sequence implied by the xenolith assemblage, is that cpx started to crystallise earlier than amphibole (olivine clinopyroxenite) and continued to crystallise later (the most plagioclase - cpx-rich gabbros such as B10). There may however have been one phase on the sequence where amphibole was precipitating either earlier and/or simultaneously with cpx, as the modally dominant phase. This segment represented by the hornblende clinopyroxenites (e.g. B20) and the most amphibole-rich gabbros (e.g. B7, B1B, B24).

The most important compositional variation amongst the analysed amphiboles, is that of Mg-Fe substitution. Mg/Mg+ΣFe values range from 0.62 to 0.75. The amphiboles are Ca- and Al-rich and Si-poor.

Like the clinopyroxenes, the amphiboles show some systematic variation of Ca/Ca+Mg with Mg/Mg+Fe, these two ratios showing a negative correlation (figure 5.13). As in the case of the clinopyroxenes, there are distinct groupings of amphiboles from different xenolith types. The pargasite from the olivine clinopyroxenites are slightly more mafic and more Ca-rich than most of those from the gabbroic xenoliths and from the lavas. The amphiboles from the most amphibole-rich members of the gabbroic suite (B7, B1B, where amphibole is the earliest phase, plot on the same Ca/Ca+Mg v Mg/Mg+Fe trend as the pargasite from the olivine clinopyroxenites and are relatively more calcic than the other (later?) amphiboles.

The phenocrysts from the lavas fall in this field of the relatively Ca-poor group of amphiboles from the gabbroic xenoliths. As in the case of the clinopyroxenes, the alkali clinopyroxenites again show a tendency to straddle these two groups (figure 5.13).

The amphiboles are all relatively K_2O-rich with between 1.5 and 2.5% K_2O and in this respect are quite distinct from those of the Rindjani suite (chapter 3). The pargasite amphibole occurring as reacted xenocrysts in

FIGURE 5.13

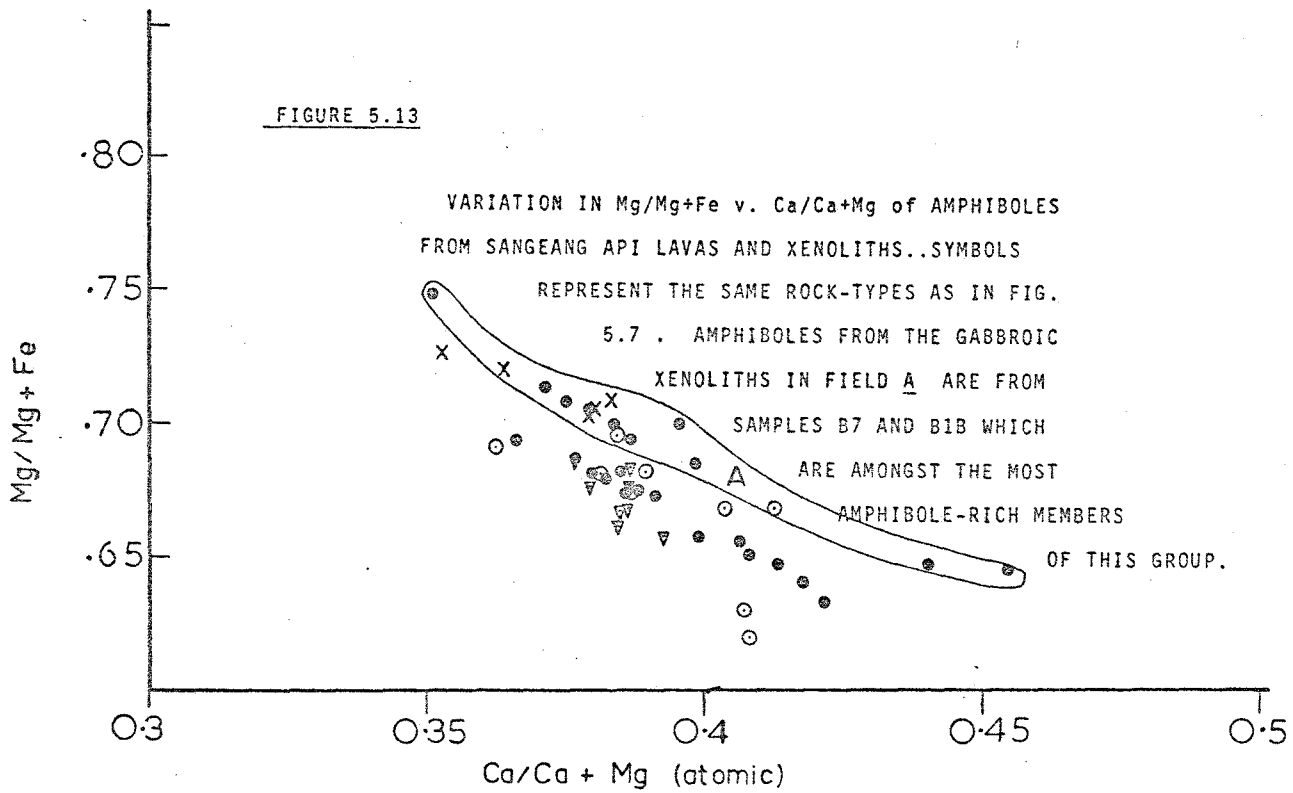

VARIATION IN Mg/Mg+Fe v. Ca/Ca+Mg of AMPHIBOLES FROM SANGEANG API LAVAS AND XENOLITHS..SYMBOLS REPRESENT THE SAME ROCK-TYPES AS IN FIG. 5.7 . AMPHIBOLES FROM THE GABBROIC XENOLITHS IN FIELD A ARE FROM SAMPLES B7 AND B1B WHICH ARE AMONGST THE MOST AMPHIBOLE-RICH MEMBERS OF THIS GROUP.

some of the Rindjani basalts and andesites generally have considerably less than 1% K_2O, while the less Ca-rich, less aluminous hornblendes from the Rindjani dacites have about 1% K_2O.

These Sangeang Api amphiboles show a slight trend of K_2O-enrichment with decreasing Mg/Mg+Fe. The Na_2O-content of the Sangeang Api amphiboles all show rather limited variation and average about 2% Na_2O and in this respect are rather similar to all the Rindjani amphiboles. Thus the Sangeang Api amphiboles have markedly higher K_2O/Na_2O ratios (0.7 - 0.8) compared to those of the Rindjani amphiboles (0.2 - 0.3). It appears that in this respect the amphibole composition probably reflects the relatively more K_2O-rich nature of the Sangeang Api liquids. Helz (1973) for instance suggests that K_2O-levels in hornblendes are a function of the K_2O concentratio of the magma, and are insensitive to variations in T, fO_2 etc. In this respect the slight increase in K_2O content of the amphibole with decreasing Mg/Mg+Fe values is thus possibly indicative of rising K_2O-levels in the differentiating liquid, possibly as a function of falling temperature and fractional crystallisation.

Ti and Al are the other most significantly variable components of the amphiboles, both showing enrichment with declining Mg/Mg+Fe (figures 5.14 and 5.15). The Ti content of the amphiboles from the most amphibole-rich gabbroic xenoliths (i.e. those where amphibole appears to be the earliest phase, e.g. B7 and B1B) are markedly higher than those of all other amphibole groups. This may be a function of the Ti-content of the liquid. As discussed in section 5.5, the compositional variation of the Sangeang Api lavas show a marked early TiO_2-enrichment trend with differentiation, followed by a later TiO_2-depletion trend. Furthermore, if the intrusives are considered as potential cumulates from these evolving liquids, then as discussed in section 5.6 and in chapter 9, there is a case to be made for considering the early TiO_2-enrichment stage to be due to crystallisation of

FIGURE 5.14

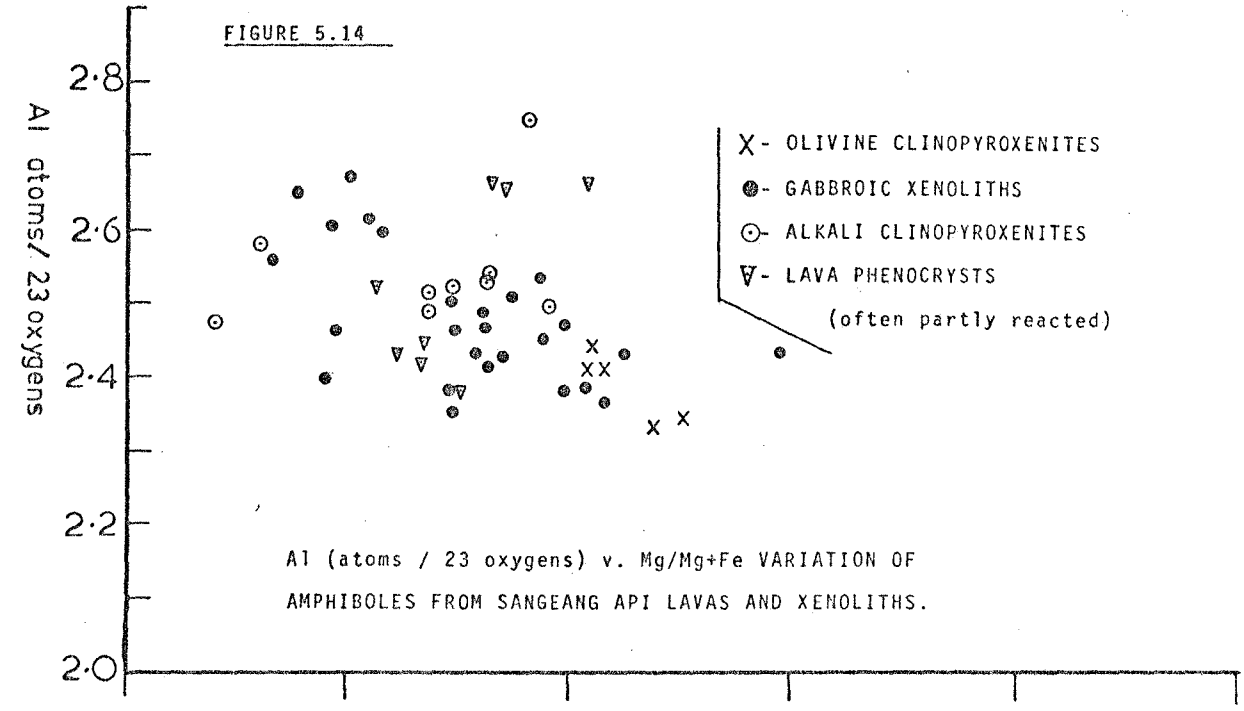

Al (atoms / 23 oxygens) v. Mg/Mg+Fe VARIATION OF AMPHIBOLES FROM SANGEANG API LAVAS AND XENOLITHS.

FIGURE 5.15

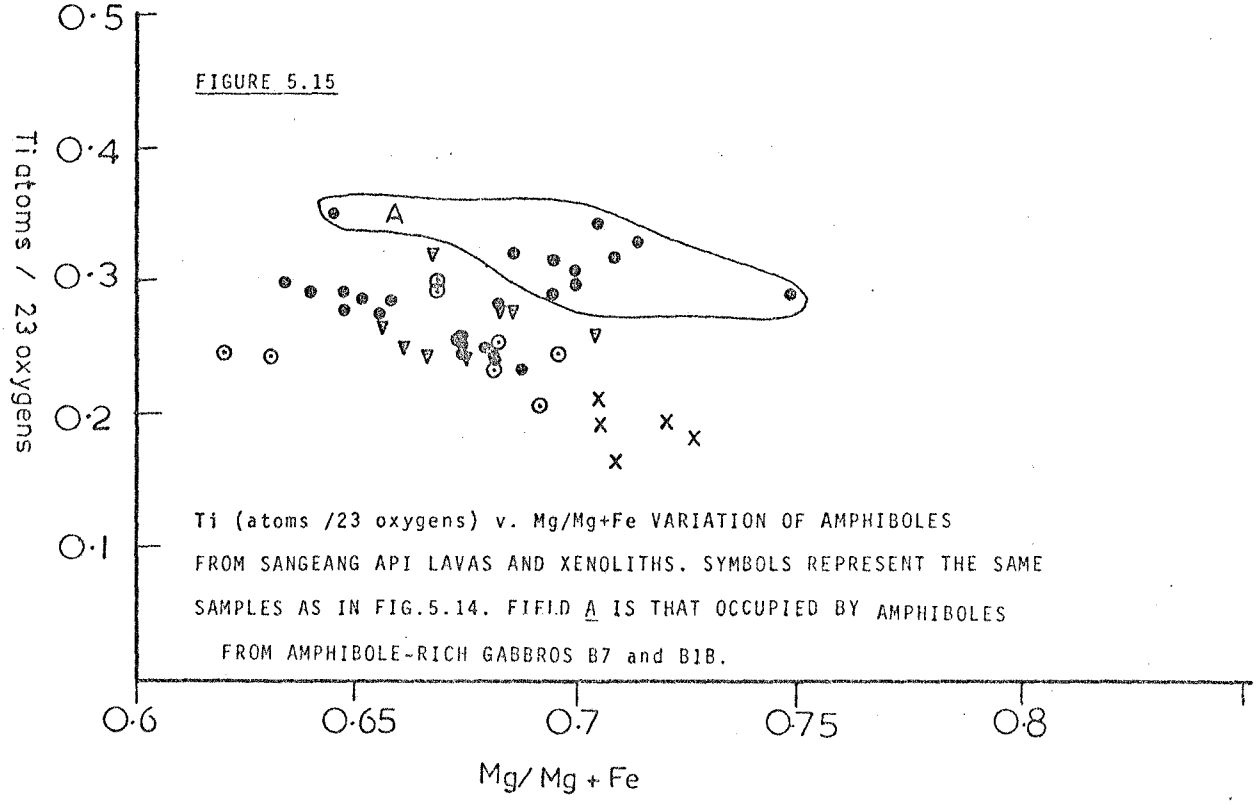

Ti (atoms /23 oxygens) v. Mg/Mg+Fe VARIATION OF AMPHIBOLES FROM SANGEANG API LAVAS AND XENOLITHS. SYMBOLS REPRESENT THE SAME SAMPLES AS IN FIG.5.14. FIELD A IS THAT OCCUPIED BY AMPHIBOLES FROM AMPHIBOLE-RICH GABBROS B7 and B1B.

a Ti-poor, cpx-olivine assemblage (like that of the olivine clinopyroxenites) and the transition to the Ti-depletion trend to be due to the onset of crystallisation of amphibole- and magnetite-rich assemblages. Thus if these most amphibole-rich xenoliths (B7, B1B, B24), represent the earliest assemblages in this new crystallisation phase, then they are potentially likely to have access to the most Ti-rich liquids (i.e. at the inflection point in the Ti-MgO variation diagrams in figure 5.25).

Similarly the Al-variation of the amphiboles (figure 5.14) may also be a function of variation in the Al-content of the liquids.

The amphiboles occurring as reacting phenocrysts in some of the Sangeang Api lavas are of very similar composition to those of the more plagioclase-rich gabbros (e.g. B24).

The general compositional variation of the amphiboles probably reflects the compositional variation of the liquids from which they crystallised, particularly variations in Al, Ti, K and Mg/Mg+Fe. The Ca/Ca+Mg v Mg/Mg+Fe groupings may reflect the same type of variations reflected in the cpx groupings based on these ratios. As will be discussed later, this may represent an effect due to variations in H_2O and P, possibly the same process which apparently results in the crystallisation of very Ca-rich, anorthitic plagioclase.

3. Olivine

The occurrence of olivine in the Sangeang Api intrusive rocks is restricted to the olivine clinopyroxenites and some alkali clinopyroxenites and rarely, as occasional grains, often included in clinopyroxene, in the magnetite clinopyroxenites. In the lavas it occurs as megacrysts and phenocrysts in those lavas from which amphibole is absent and as groundmass grains in most lavas.

In the intrusive rocks the olivine is generally euhedral and in a number of the alkali clinopyroxenites it is surrounded by reaction rims of

Table 5.15 Representative Olivine Analyses: Sangeang Api Xenoliths

Analysis No.	1	2	3	4	5	6	7	8	9	10	11	12 [1]
Sample No.	B5	B5	B5	B5	B5	B23	B23	B9	B9	B9	B21	B15
Xenolith Type	1	1	1	1	1	1	1	1	1	1	4	4
SiO_2	39.7	39.8	36.1	38.7	38.5	38.4	39.6	38.7	39.3	39.3	38.3	38.6
FeO	19.2	19.1	23.1	17.9	17.7	18.0	19.5	18.4	18.3	18.5	19.3	17.5
MgO	40.5	40.4	39.9	42.8	43.2	42.8	39.6	42.0	42.0	41.9	41.7	42.9
CaO	0.2	0.28	0.35	0.25	0.24	0.27	0.24	-	0.17	0.20	0.13	0.18
TiO_2	-	-	0.13	-	-	-	-	-	-	-	0.12	0.13
MnO	0.3	0.39	0.39	0.19	0.17	0.34	0.20	0.4	0.18	-	0.54	0.61
Cr_2O_3	-	-	-	0.1	0.1	0.1	0.1	-	-	-	-	-
Total	99.9	99.97	99.97	99.94	99.91	99.91	99.24	99.50	99.95	99.90	100.09	99.92
100Mg/Mg+Fe(mol.)	78.99	79.03	73.48	81.00	81.30	80.90	78.70	80.30	80.35	80.14	79.38	81.37
					Number of Ions on the Basis of 4 (O)							
Si	1.016	1.018	0.951	0.988	0.983	0.983	1.014	0.988	1.002	1.003	0.984	0.985
Fe	0.411	0.409	0.508	0.382	0.378	0.385	0.417	0.392	0.390	0.395	0.415	0.374
Mg	1.545	1.540	1.566	1.628	1.643	1.632	1.542	1.600	1.596	1.594	1.597	1.632
Ca	0.005	0.007	0.009	0.007	0.007	0.007	0.007	-	0.005	0.005	0.004	0.005
Ti	-	-	0.003	-	-	-	-	-	-	-	0.002	0.002
Mn	0.006	0.008	0.009	0.004	0.004	0.007	0.004	0.008	0.004	-	0.012	0.013
Cr	-	-	-	0.002	0.002	0.002	0.002	-	-	-	-	-
Total	2.984	2.982	3.046	3.011	3.016	3.016	2.985	3.005	2.998	2.997	3.013	3.012

Notes: Type 1 xenoliths: olivine clinopyroxenites

Type 2 xenoliths: alkali clinopyroxenites

[1] Rimmed by reaction corona of Cpx and phlogopite (see plate 2E).

clinopyroxene and phlogopite (e.g. B15, plate 3E). Typical analyses of representative examples of each group of olivines are given in table 5.15.

The olivine in the intrusive rocks (mainly the olivine clinopyroxenites) is of very restricted composition and almost all analysed examples have Mg/Mg+Fe values falling between 0.785 and 0.810. The Mg/Mg+Fe values of these olivines are very close to those of the coexisting cpx.

The amphibole-free lavas have olivine phenocrysts and megacrysts, as well as phenocrysts of plagioclase. A few, B43, for instance, appear only to contain megacrysts of cpx and olivine and contain no plagioclase phenocrysts. The olivine in this rock, like the cpx, is markedly more magnesian than that analysed from the olivine clinopyroxenites and have a composition of Mg/Mg+Fe = 0.878. In other lavas (B39, for instance), where olivine megacrysts coexist with phenocrysts, the olivine megacrysts have the same composition as that of the olivine clinopyroxenite (Mg/Mg+Fe = 0.8), while the phenocrysts are more iron-rich, are zoned, and have a more variable composition. Cores are about Fo70, while rims may be Fo60 or more Fe-rich. The groundmass olivine is often quite iron-rich, but is very variable and Mg/Mg+Fe values ranged from 0.7 to 0.45.

Besides the Mg-Fe variation, the olivines show significant variation in their Mn- and Ca-contents. The concentrations of both these elements increase with decreasing Mg/Mg+Fe ratio, the groundmass olivine being the most Mn and Ca-rich. The xenolith and megacryst olivine have very low Mn-content, while the most Fa-rich groundmass olivine have up to 4% MnO. While there is a marked trend of increasing Ca with increasing Fa-content of the olivines, the intrusive olivine, though relatively less calcic than the olivine of the lavas, is nevertheless relatively Ca-enriched compared with the olivines of most intrusive rocks (Simkin and Smith, 1970).

Table 5.16

Representative Analyses of Phlogopite from Sangeang Api Xenoliths

Analysis No.	1	2	3	4	5	6	7(1)	8	9	10	11
Sample No.	B5	B9	B9	B13	B13	B21	B15	B15	B24	B10	B10
Xenolith Type	1	1	1	2	2	2	2	2	3	3	3
SiO_2	35.2	35.2	36.7	35.1	35.0	35.3	35.7	34.3	34.7	35.3	36.6
Al_2O_3	16.4	15.9	16.7	16.7	16.6	16.0	15.9	15.4	15.3	16.2	16.6
FeO	9.0	9.1	9.3	9.8	10.2	8.7	10.6	12.7	12.5	11.2	11.4
MgO	19.6	19.4	20.3	18.7	18.6	20.0	18.1	15.8	16.1	17.3	17.5
CaO	0.6	0.5	0.6	0.5	0.4	0.5	0.6	0.5	0.6	-	0.5
Na_2O	-	-	-	-	-	-	-	-	0.5	0.5	-
K_2O	9.4	9.4	9.5	9.6	9.7	10.5	9.6	9.6	9.5	8.9	10.8
TiO_2	2.5	2.4	2.4	2.1	2.2	2.2	3.9	4.3	3.9	3.5	4.1
MnO	-	-	-	-	-	-	-	-	-	-	-
Cr_2O_3	0.2	0.1	0.2	0.1	0.1	-	-	0.1	-	-	-
Total	92.9	91.9	95.6	92.6	92.8	93.2	94.4	92.6	93.1	92.9	97.4
Number of Ions on the Basis of 22 Oxygens											
Si	5.280	5.325	5.330	5.304	5.279	5.301	5.306	5.274	5.307	5.325	5.299
Al	2.892	2.841	2.854	2.970	2.953	2.836	2.785	2.787	2.748	2.879	2.841
Fe	1.128	1.153	1.127	1.236	1.284	1.095	1.315	1.634	1.598	1.410	1.377
Mg	4.389	4.374	4.403	4.199	4.193	4.466	4.010	3.610	3.662	3.901	3.791
Ca	0.090	0.084	0.089	0.082	0.069	0.081	0.100	0.074	0.098	-	0.078
Na	-	-	-	-	-	-	-	-	0.163	0.156	-
K	1.807	1.809	1.762	1.840	1.861	2.010	1.828	1.876	1.847	1.710	1.987
Ti	0.280	0.274	0.263	0.239	0.254	0.251	0.437	0.503	0.451	0.394	0.449
Mn	-	-	-	-	-	-	-	-	-	-	-
Cr	0.024	0.016	0.020	0.020	0.016	-	-	0.008	-	-	-
Total	15.890	15.875	15.848	15.886	15.910	16.040	15.781	15.766	15.873	15.774	15.821
100Mg/Mg+Fe	79.6	79.1	79.6	77.3	76.6	80.3	75.3	68.8	69.6	73.5	73.4

Notes: (1) Analysis 7 of phlogopite in reaction-rim around olivine Fo81 (see plate 3E).

Xenolith types: 1 - olivine clinopyroxenite, 2 - alkali clinopyroxenite, 3 - gabbroic. In the olivine clinopyroxenites, phlogopite is a late interstitial phase, in the alkali pyroxenites it is a late phase and occurs interstitially or as a replacement of earlier olivine or clinopyroxene. In the gabbros, phlogopite is also late as a reaction product (as in B24) or as postcumulate (?) oikocrysts (B10).

4. Phlogopite

Phlogopite occurs both as a reaction product, partially or totally replacing primary minerals in some xenoliths, or in some cases as primary, late-stage interstitial crystallisation products. The olivine clinopyroxenites (e.g. B9, B5), contain thin interstitial growth of primary phlogopite where it assumes the latter role, while in a number of alkali clinopyroxenites it is apparently a later product, replacing primary clinopyroxene (e.g. B13, plates 3A, B, B16, B21) and in some cases replacing olivine (e.g. B15, plate 3E).

Phlogopite also occurs in some gabbroic xenoliths in some cases (for instance, B24) apparently as a product of reaction of small amounts of interstitial liquid with primary amphibole and magnetite and in other cases (for instance, B10) occurring as late stage, poikilitic interstitial oikocrysts.

Typical analyses of phlogopite are given in table 5.16. The main compositional variation is in Mg, Fe and Ti with minor variation in K. All other components (Al, Si, Ca) are invariant. K only shows very slight variation, increasing marginally with decreasing Mg/Mg+Fe ratio (figure 5.16). The Mg/Mg+Fe values range from 0.8 to 0.67 and as in the case of the clinopyroxenes and amphibole, the phlogopite of the olivine clinopyroxenite is most mafic, while that of the gabbroic xenoliths is more Fe-rich.

The phlogopite of the alkali clinopyroxenites again spans the widest range and includes both the most Fe-rich and the most magnesian compositions analysed (figure 5.16).

Ti shows the biggest variation of all elements in the phlogopites (figure 5.17). While there is a general trend of increasing Ti with decreasing Mg/Mg+Fe, there are two distinct fields of phlogopites on the basis of Ti-content. The phlogopite of the olivine clinopyroxenite is

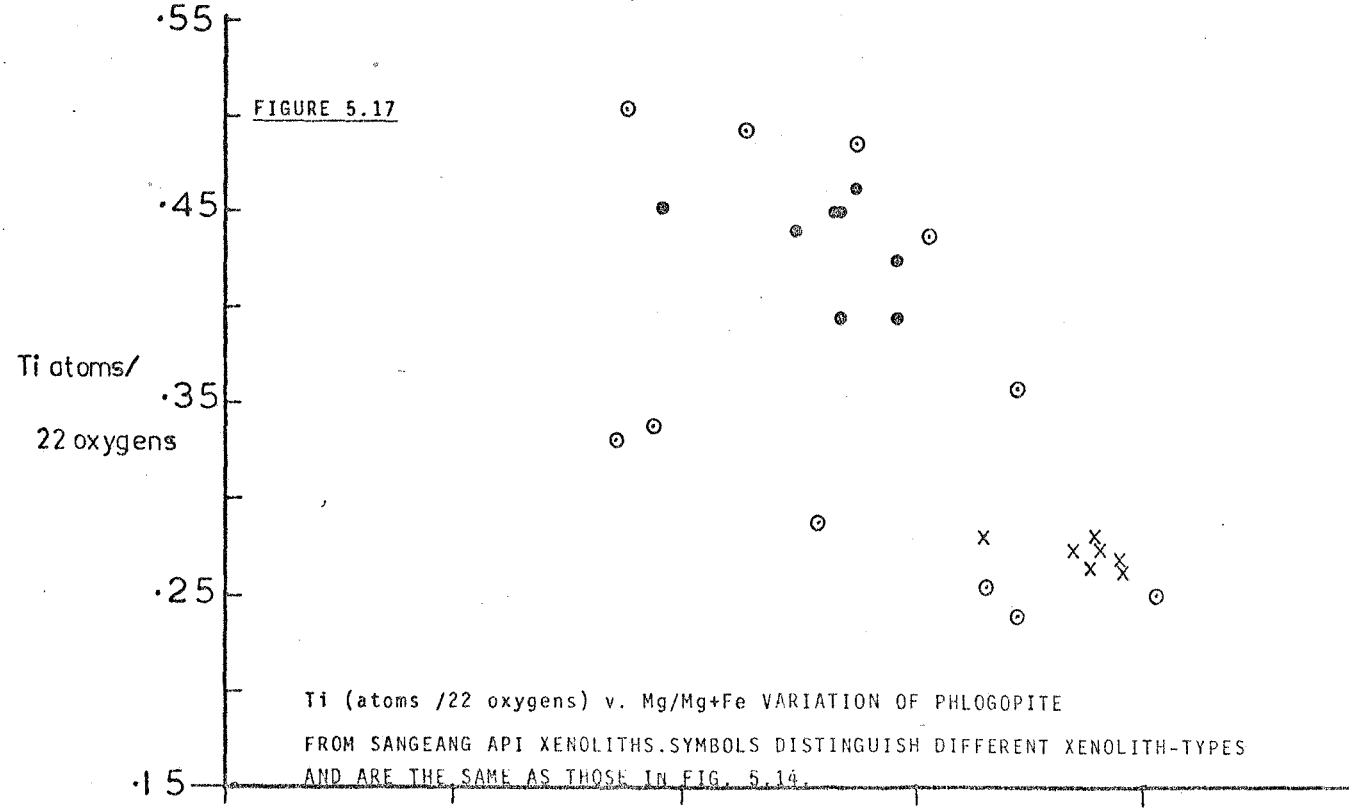

FIGURE 5.17

Ti (atoms /22 oxygens) v. Mg/Mg+Fe VARIATION OF PHLOGOPITE FROM SANGEANG API XENOLITHS. SYMBOLS DISTINGUISH DIFFERENT XENOLITH-TYPES AND ARE THE SAME AS THOSE IN FIG. 5.14.

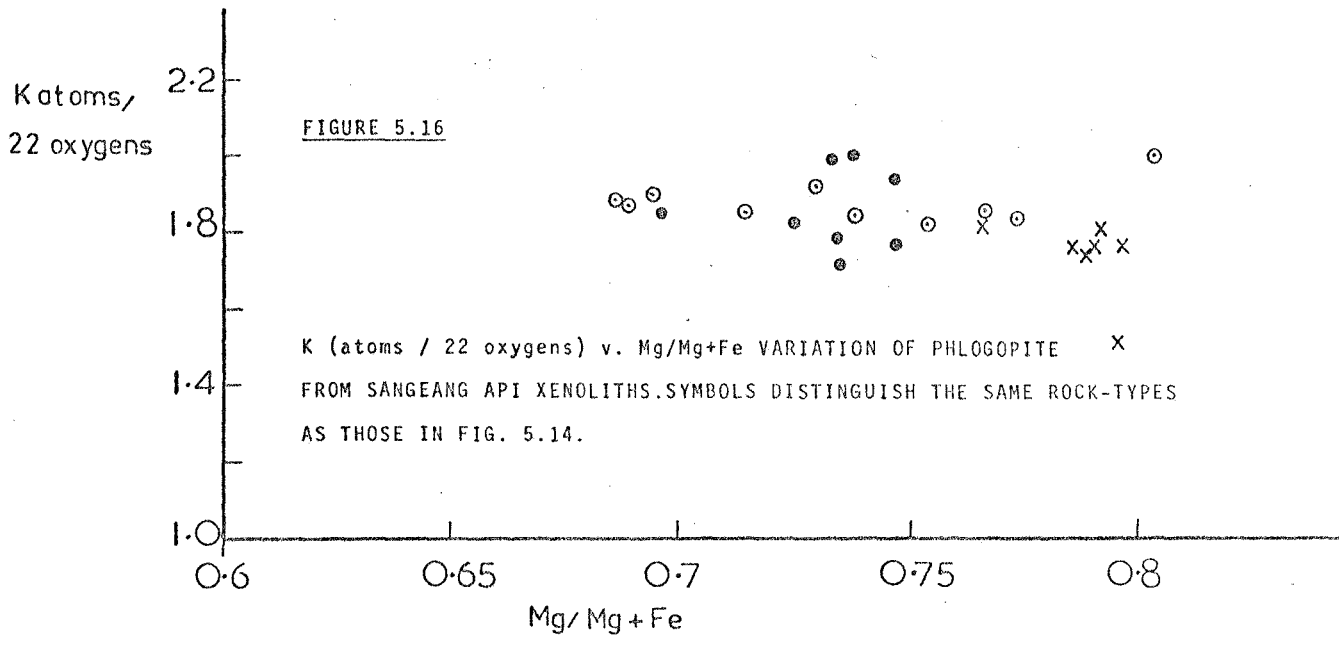

FIGURE 5.16

K (atoms / 22 oxygens) v. Mg/Mg+Fe VARIATION OF PHLOGOPITE FROM SANGEANG API XENOLITHS. SYMBOLS DISTINGUISH THE SAME ROCK-TYPES AS THOSE IN FIG. 5.14.

markedly less Ti-rich than that of the gabbroic xenoliths (figure 5.17). Phlogopite of the essentially plagioclase-free alkali clinopyroxenites (B21, B13 and B16) fall into this same group. Phlogopite of alkali clinopyroxenite B15, which appears to have originally been an olivine clinopyroxenite, but has reacted with a later liquid which has precipitated plagioclase, falls in the field of the gabbroic phlogopites. In this sample phlogopites forming a reaction rim around olivine are slightly more mafic and slightly less Ti-rich than other phlogopites in the same sample.

The Ti-variation of the phlogopites essentially reflects that of the cpx and amphibole, in that in each case, the plagioclase (and magnetite)-bearing xenoliths contain the more Ti-rich examples of each phase.

5. Feldspar

Feldspar compositions from the intrusive rocks and lavas are summarised in the An-Ab-Or diagram in figure 5.3. Representative analyses are given in table 5.8. Most lavas (with the exception of B43) contain plagioclase phenocrysts and all contain groundmass-plagioclase and alkali feldspars. The gabbroic xenoliths are plagioclase-bearing and the appearance of plagioclase in these is earliest with respect to the other minerals in those which are most amphibole-poor (e.g. B10). The olivine clinopyroxenites contain no plagioclase, while in some magnetite-clinopyroxenites and alkali clinopyroxenites occurs interstitially, later than the ferromagnesian minerals.

The plagioclase of all the intrusive rocks, display very little compositional variation (table 5.8, figure 5.3). They are all remarkably calcic and all fall within the range An85 to An95. Most average about An90 with about 8-9 mol.% Ab molecule and 1 mol.% Or. As described in the petrography section the plagioclase of the intrusive rocks are quite distinct from those of the lavas, in that they are generally not zoned and

by their twin lamellae, which in contrast to those of the extrusive rocks, are of unequal thickness and often taper and pinch-out. These plagioclases are recognised as xenocrysts in a number of lavas, particularly those in which amphibole is present and are markedly more Ca-rich than the most calcic phenocryst cores (figure 5.3).

The phenocryst cores are quite Ca-rich (An85) and are zoned to rim compositions of about An50-65. Microphenocrysts have cores in this labradorite-field, while groundmass plagioclase is of andesine composition (An32-An50), with between 4 and 8 mol.% Or molecule. Coexisting with these groundmass plagioclases are alkali feldspars of quite variable composition, showing considerable ternary solid solution (figure 5.3, table 5.8). Compositions range from anorthoclase (An15 Ab70 Or15) to calcic sanidine (An11 Ab27 Or62).

6. Magnetite

A titanmagnetite is the sole oxide-phase in all the members of the Sangeang Api suite. It occurs both as phenocrysts and in the groundmass of the lavas and in all the intrusive rocks, with exception of some olivine clinopyroxenites and alkali clinopyroxenites. In the latter two xenolith groups it is a very minor accessory. In the other xenoliths it is quite abundant, maintaining a relatively constant modal abundance (ca. 15 vol.%).

The main compositional variation is in terms of Ti, Al, Mg, Ca and Mn. Representative analyses of magnetite from the various xenolith groups and from the lavas (phenocrysts and groundmass grains) are given in table 5.18).

In general, the magnetites are all relatively Ti-poor, ranging from 15 to 28 mol.% Ulvospinel. There is a general trend of increasing Ulvospinel component from the magnetite of the xenolith to the phenocrystic magnetite to the groundmass magnetite. The magnetite of the xenoliths has a rather restricted range of Ti content, ranging from 15 to 18 mol.% Usp.

Table 5.18

Representative Analyses of Magnetite from Sahgeang Api Lavas and Xenoliths

Analysis No.	1	2	3	4	5	6	7	8	9	10
Sample No.	B23	B23	B2H	B2H	B8	B24	B11	B39	B39	B27
Rock Type	OC	OC	MC	MC	G	G	G	L	L	L
								MP	M	MP
Al_2O_3	8.3	7.9	6.8	7.9	5.7	5.4	6.3	7.8	7.9	3.9
FeO	29.3	29.0	31.3	33.3	33.6	32.2	32.8	34.1	33.7	40.2
Fe_2O_3	50.0	49.7	50.2	43.6	50.9	54.9	52.7	46.9	46.9	46.0
MgO	5.8	5.0	4.2	4.6	2.2	3.2	3.2	3.5	3.8	-
CaO	-	-	-	-	-	-	-	-	-	-
MnO	-	-	0.6	0.6	0.5	0.5	-	-	-	1.3
TiO_2	5.9	5.4	6.6	9.3	6.1	5.4	5.7	7.6	7.7	10.0
Cr_2O_3	1.1	0.7	0.2	0.2	0.1	0.1	-	-	0.4	-
Total	100.4	97.7	99.9	99.5	99.1	101.7	100.7	99.9	100.4	101.4
Al	2.736	2.680	2.294	2.646	1.979	1.827	2.133	2.624	2.642	1.355
Fe^{2+}	6.852	7.026	7.492	7.913	8.277	7.706	7.879	8.168	7.994	9.908
Fe^{3+}	10.510	10.806	10.802	9.313	11.272	11.797	11.380	10.091	10.001	10.191
Mg	2.417	2.164	1.792	1.948	0.966	1.372	1.370	1.484	1.606	-
Ca	-	-	-	-	-	-	-	-	-	-
Mn	-	-	0.145	0.144	0.125	0.111	-	-	-	0.324
Ti	1.240	1.168	1.421	1.987	1.351	1.161	1.231	1.629	1.643	2.216
Cr	0.243	0.151	0.045	0.045	0.023	0.023	-	-	0.090	-
Total	23.998	23.996	23.992	23.996	23.994	23.997	23.994	23.997	23.976	23.995
mol.% U.spinel	16.4	15.5	18.6	26.3	17.5	15.1	16.0	21.5	21.7	28.5

Abbreviations: OC - olivine clinopyroxenite, MC - magnetite clinopyroxenite, G - gabbroic xenolith, L - lava, MP - microphenocryst, M - megacryst.

Note: Analyses recalculated from electron microprobe analyses. FeO and Fe_2O_3 values recalculated from FeO by the method of Carmichael (1967).

The magnetite of olivine clinopyroxenites (table 5.18), is the most Al_2O_3 and MgO-rich of all those of the various xenolith groups. This also contains significant Cr_2O_3 (>1%) and no detectable MnO. Mgo ranges from >5% i the magnetite of the olivine clinopyroxenites down to about 3-4% in that of th gabbroic xenoliths. Similarly Al_2O_3 decreases from >8% to between 5 and 6%. Cr_2O_3 decreases from >1% to <0.3%, while MnO increases from ∿0% to about 0.3-0.4%. By comparison, the phenocryst and groundmass magnetite of the lavas generally have >20 mol.% Usp , have no detectable Mg, relatively low Al_2O_3 (<4%), little or no Cr and high Mn (>1% MnO) (table 5.18). At the same time in some lavas, xenocrystic magnetite, identical to that of the gabbroic intrusives is recognised, with higher MgO, Cr_2O_3, Al_2O_3 and lower MnO and TiO_2.

5.5 *Geochemistry of the Sangeang Api Lavas*

The major- and trace-element, whole-rock analyses of the Sangeang Api lavas are given in table 5.3. Compositional variations are summarised as MgO-variation diagrams in figures 5.18 and 5.19, 4.7 and 4.8.

All lavas are *ne*-normative and in terms of Johnson et al.'s (1976) terminology, they are mostly potassic *ne*-trachybasalts (figure 5.20). Some of the least mafic rocks (e.g. B32, B42) show transition towards the potassic *ne*-trachyandesite field. Lava B43, while being considerably more magnesian than most other analysed lavas, is also the most *ne*-normative (15.94%) and falls in Johnson et al.'s (ibid) phonolitic tephrite field.

The suite is moderately potassic, with K_2O/Na_2O ratios ranging from 0.49 to 0.76. The suite is also moderately alkaline in character, with high concentrations of Rb (63-113ppm), Sr (799-1273ppm) and K_2O (1.85%-3.56%). K/Rb ratios are low, almost all <300. Yet, Zr (88-141ppm), TiO_2 (<1.0%) and Nb (4-10ppm) concentrations are low by comparison with those from alkaline lavas from non-arc environments.

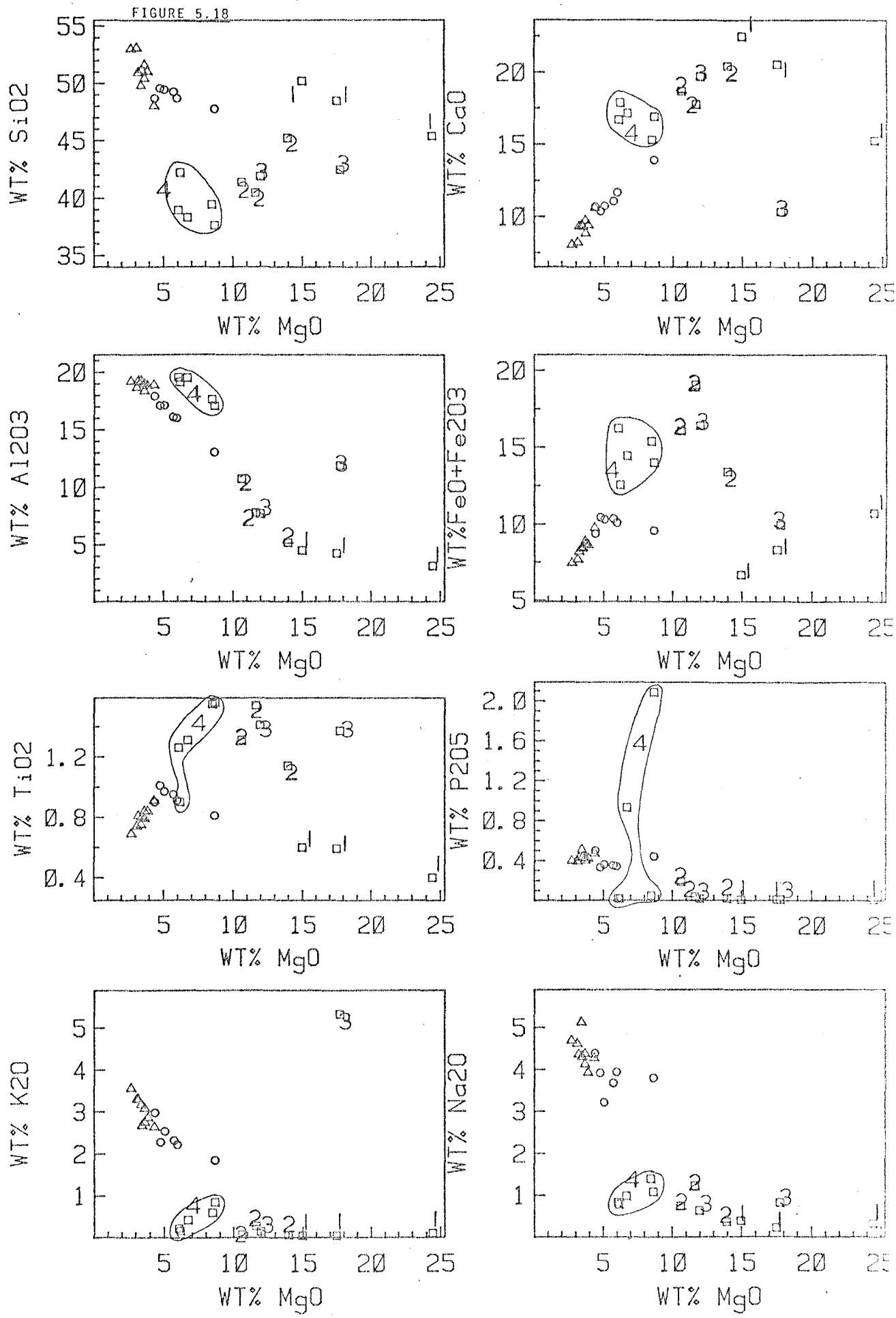

FIGURE 5.18

MgO v. MAJOR ELEMENT VARIATION OF SANGEANG API LAVAS AND XENOLITHS.

○- OLIVINE MEGACRYST-BEARING LAVAS (AMPH.-FREE), △-AMPHIBOLE-BEARING LAVAS, □-XENOLITHS.

1.- OLIVINE CLINOPYROXENITES,2.- MAGNETITE CLINOPYROXENITES,3.-ALKALI CLINOPYROXENITES,4.GABBROS

FIGURE 5.19

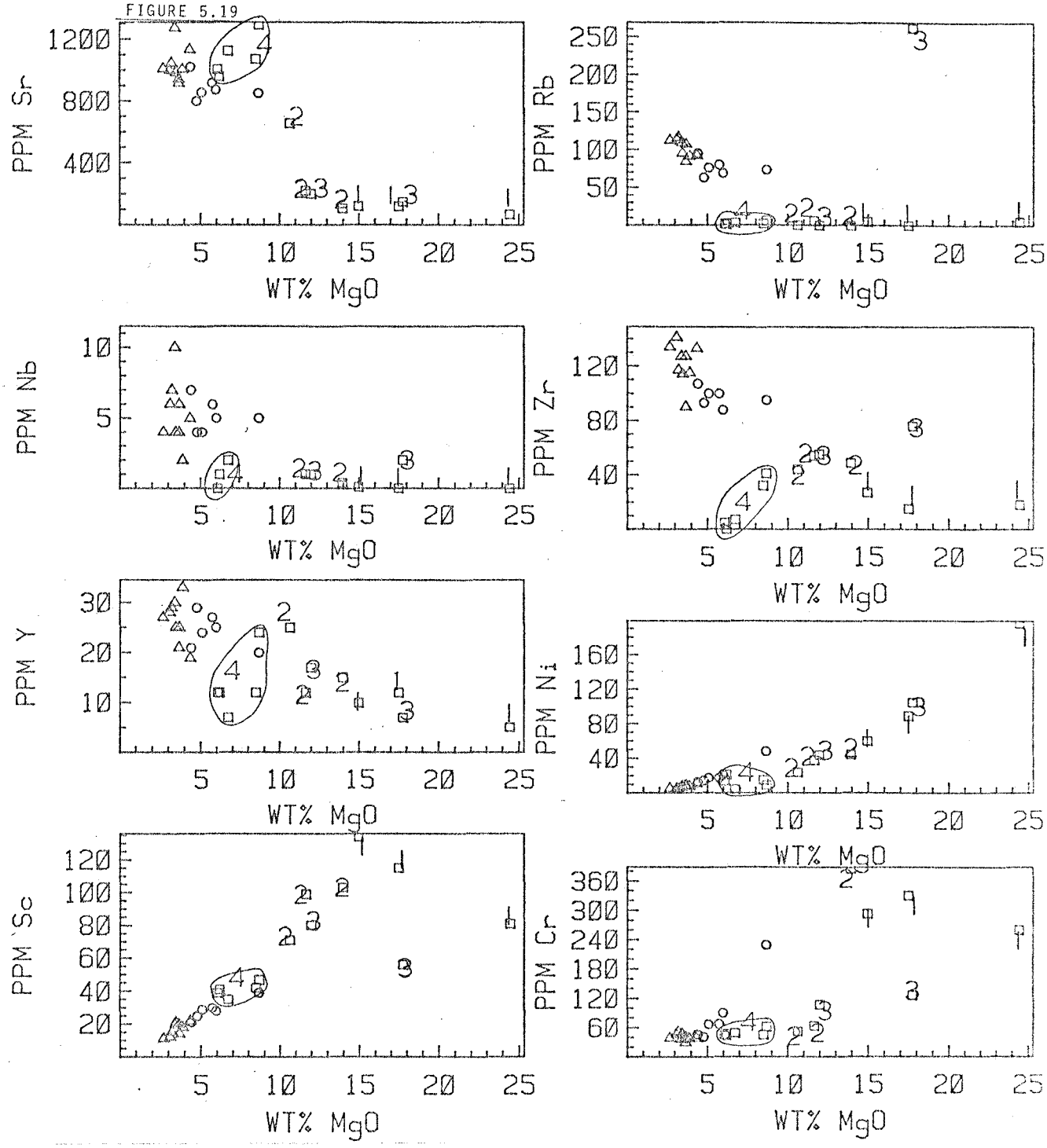

FIGURE 5.19

MgO v. TRACE ELEMENT VARIATION OF SANGEANG API LAVAS AND XENOLITHS. SYMBOLS AND NUMBERS ARE THE SAME AS IN FIG. 5.18.

SiO_2 shows a limited range, from 47.77% to 53.13%. On the other hand MgO shows quite large variation, decreasing through this silica range from 8.65% to 2.69%. This trend of increasing SiO_2 and decreasing MgO is also accompanied by one of decreasing CaO, Ni, Cr and Sc.

The most mafic lava (B43) has low Al_2O_3 (13.9%) and this shows a trend of enrichment with decreasing MgO. Lavas with <4% MgO are aluminous, with between 18 and 19% Al_2O_3. The more mafic lavas (with MgO $\geq$5%) plot on the same trend of CaO depletion - Al_2O_3 enrichment (figure 5.18, 4.7) as the ankaramites from Rindjani and most of the feldspathoid-bearing lavas from Soromundi and G. Sangenges.

There is a general trend of increasing K_2O/Na_2O, Rb, Zr and Nb with decreasing MgO, though the relationship of these elements is in fact more complex. For instance, while B43 is by far the most mafic lava (with 8.65% MgO), it contains higher concentrations of Rb, Zr and P_2O_5 than B44 with 5.96% MgO, or B31 with 4.76% MgO. These factors tend to suggest that some of the compositional diversity of the Sangeang Api suite is not entirely attributable to fractional crystallisation of a single primary magma. This conclusion is also indicated by the variation in $^{87}Sr/^{86}Sr$ ratios of the lavas and xenoliths from this suite, discussed in chapter 8, and by the REE geochemistry discussed in chapter 9.

As discussed previously, the Sangeang Api lavas show a rough sub-division into olivine-bearing, amphibole-free and amphibole-bearing, olivine-free varieties. These are distinguished on the variation diagrams presented in figures 5.18 and 5.19 and show some marked geochemical distinctions. The olivine-bearing lavas (olivine as phenocrysts) have higher MgO contents (>4.5%) and the compositional variations with respect to MgO show marked inflections at this MgO value. In particular, those lavas with >4.5% MgO show trends of TiO_2- and ΣFe-enrichment, while lavas with <4.5% MgO plot on a marked TiO_2- and ΣFe-depletion trend.

FIGURE 5.20

DIFFERENTIATION INDEX (DI) V. NORMATIVE ne

VARIATION OF TAMBORA AND SANGEANG API LAVAS .FIELDS MARKED AFTER JOHNSON ET. AL. (1976)

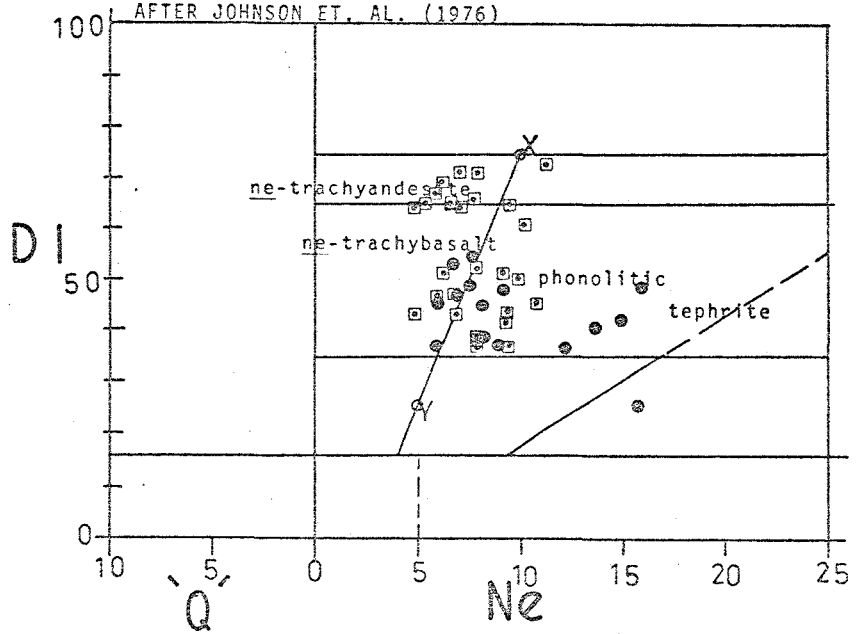

□- TAMBORA ●- SANGEANG API

LINE X-Y IS THAT OF COOMBS AND WILKINSON (1969)
DIVIDING MILDLY AND HIGHLY UNDERSATURATED LAVAS.

This MgO value also represents an increase in the range of enrichment of SiO_2, K_2O, Na_2O, Rb and Zr with decreasing MgO (figures 5.18, 5.19 and 4.7, 4.8). At the same MgO value, the rate of CaO depletion increases and the rate of Al_2O_3 enrichment decreases with decreasing MgO.

These factors suggest that if the suite is differentiating by some fractional crystallisation mechanism, then the bulk assemblage extracted changed when the liquid had 4.5% MgO. Liquids with >4.5% MgO crystallised a bulk assemblage which was relatively more MgO-rich and TiO_2- and Fe-poor than liquids with <4.5% MgO. These inflections in the MgO-variation diagrams then result from the fact that at >4.5% any given percentage variation in MgO represents a smaller percentage of crystallisation and extraction than does an equivalent MgO variation in liquids with <4.5% MgO.

There is also some suggestion that P_2O_5 may be depleted with decreasing MgO at MgO values of <4.5% MgO. This suggests the appearance of apatite at this stage. Mafic lava B43 however is exceptional in that it has anomalously high P_2O_5 compared with the other more magnesian members of the trachybasalt group.

The olivine bearing lavas (i.e. those with >4.5% MgO), show relatively little variation in Rb/Sr ratio with variations in MgO (figure 5.21), values averaging about 0.085. This is a markedly higher Rb/Sr ratio than that of the basaltic lavas from either Rindjani or Tambora. The amphibole-bearing lavas from Sangeang Api have more variable Rb/Sr ratios, which generally increase with decreasing MgO.

The Sangeang Api lavas, particularly the more aluminous, less mafic examples are similar to those of Tambora volcano. However marked distinctions do occur. First, petrographic distinctions exist, in that many of the Sangeang Api lavas are amphibole-bearing, while this mineral does not appear at all in the Tambora lavas. Secondly, the Sangeang Api lavas have

FIGURE 5.21

MgO V. Rb/Sr VARIATION OF SANGEANG API AND TAMBORA LAVAS.

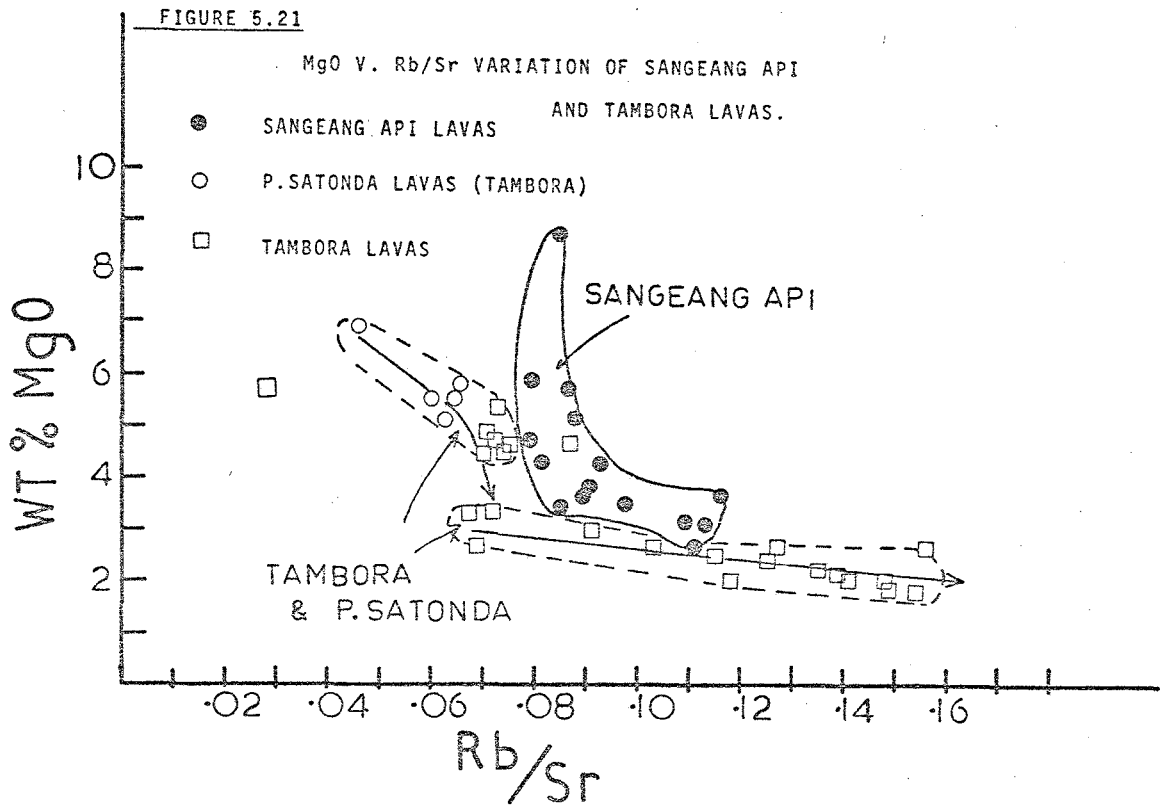

markedly higher Rb/Sr ratios. This distinction is most marked in the more mafic lavas, where trachybasalts of the Tambora suite, with between 5 and 6% MgO have Rb/Sr ratios mostly in the range 0.06-0.075. Lavas in this MgO range from Sangeang Api have Rb/Sr ratios between 0.075 and 0.09 (figure 5.21). The distinction between the two suites is also exhibited in their K/Rb ratios. Those of Sangeang Api are considerably lower (<300) than those of the Tambora lavas (>300) (figure 4.9). The Sangeang Api lavas have slightly lower K_2O contents than those of the Tambora suite, and on the K_2O-SiO_2 plot (figure 4.10), the Sangeang Api suite has a slightly flatter slope.

Some of the Sangeang Api lavas are markedly more undersaturated than those from Tambora, having a higher proportion of normative nepheline. In fact there may be two distinct groups of Sangeang Api lavas on the basis of their proportions of normative nepheline. One group with >12% (B43, B44, B29, B25, B27) and the rest with <10%. Most Tambora lavas have <10% normative-*ne* and the lava with the highest proportion (T20) is the most differentiated, least mafic, trachyandesite. By contrast, the most undersaturated Sangeang Api lavas (e.g. B43, B44) are amongst the most mafic members of the suite and in fact the lavas with the lowest MgO concentrations (B42, B32) are amongst the least undersaturated (ca. 6% normative-*ne*).

It appears that because of the association of the Sangeang Api lavas with amphibole-rich intrusive rocks of possible cumulate origin and the presence of amphibole phenocrysts in some lavas, the Sangeang Api suite may have partly evolved by amphibole fractionation. This may account for some of the differences between this, and the Tambora suite. In particular, the slightly less marked K_2O enrichment.

FIGURE 5.22

K v. Rb (log-log) variation of Tambora lavas and intrusives and Sangeang Api lavas.

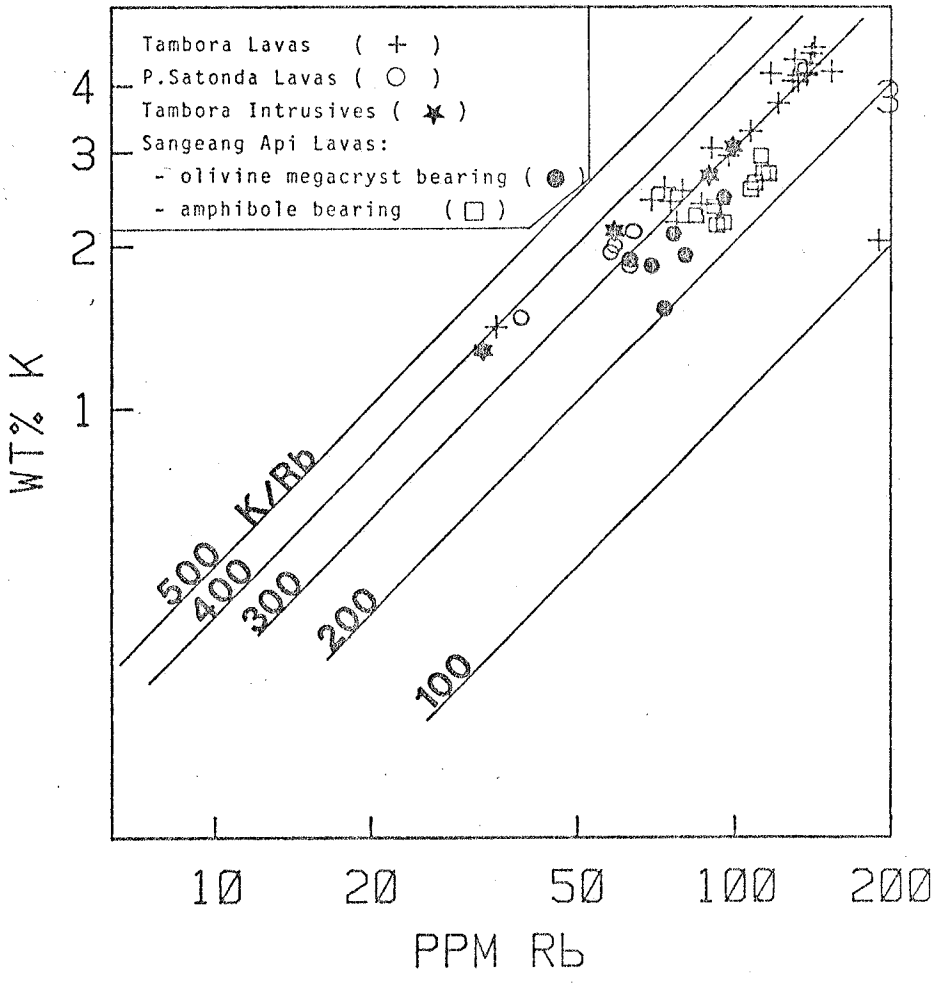

However, the higher Rb/Sr, $^{87}Sr/^{86}Sr$ and K/Rb ratios of the most mafic members of the Sangeang Api suite tends to suggest that at least some of the contrast between the two suites must be embodied in the compositions of their primary magmas.

5.6 Geochemistry of the Sangeang Api Intrusive Rocks

The analysed xenoliths and nodules represent members of the following previously established groups:

1. Olivine-clinopyroxenites (B23, B5, B4).
2. Magnetite-clinopyroxenite (B2H (+B25x?)).
3. Hornblende gabbros (B24, B7, B8, B11, B10).
4. Alkali clinopyroxenite (B22, B13 (+B2G?)).

The compositional variation of the intrusive nodules and xenoliths from Sangeang Api, are summarised in figures 5.18 and 5.19. Analyses are given in table 5.4.

The compositional variations of the intrusive rocks are relatively scattered as might be expected if they are largely of accumulative origin. Furthermore their compositions largely reflect the modal variation of their component minerals. Thus the plagioclase-bearing xenoliths (many of the hornblende-gabbros group) are Al_2O_3 and Sr-rich by comparison with members of the other groups. The magnetite-clinopyroxenites and hornblende-gabbros are relatively more Fe- and TiO_2-rich than the olivine-clinopyroxenite, mainly by virtue of their magnetite and amphibole contents. The olivine-clinopyroxenite groups are more MgO-, CaO-, Ni- and Cr-rich than the other xenoliths, reflecting the composition of their component olivine and clinopyroxene.

There is a general trend of decreasing MgO through the sequence from olivine clinopyroxenite to magnetite clinopyroxenite to plagioclase-rich gabbroic xenoliths (figures 5.18 and 5.19). This reflects the decrease in

proportion of ferromagnesian silicate minerals, the relative increase in the proportion of magnetite and the decreasing MgO content of the ferromagnesian minerals.

The olivine clinopyroxenites (B23, B5, B4) are essentially composed of olivine and clinopyroxene. The modal proportion of olivine decreasing from about 19 vol.% in B23 to <1 vol.% in B4. This variation is reflected in the MgO and ΣFe contents of this group of xenoliths, B23 having higher MgO and ΣFe than B4, which is essentially clinopyroxene. The Mg/Mg+ΣFe ratio of the group are very constant at 0.81, irrespective of their olivine to clinopyroxene ratios.

The olivine-clinopyroxenite B4 is largely composed of cpx (with minor amphibole) and its bulk analysis is very like that of an electron microprobe analysis of individual cpx from this rock (table 5.12). Hence the trace element content of this rock is likely to approximate those of the clinopyroxene of this xenolith group. Thus the concentrations of these trace elements, in particular Ni, Cr, Sc and Sr, can be viewed in terms of clinopyroxene-liquid distribution coefficients. Therefore if these concentrations are compatible with equilibrium with concentrations of these elements in the assorted lavas, a postulated cumulate origin for this group of xenoliths is reinforced.

Thus, the Sr concentrations of B4 (121ppm) and the average concentration of Sr in the Sangeang Api basaltic lavas (about 1000ppm) suggest a clinopyroxene-liquid distribution coefficient of about 0.12. This is a value reasonably close to those determined on natural phenocryst-groundmass pairs, for instance by Ewart and Taylor (1969) or Philpotts and Schnetzler (1970) or experimentally by Sun et al. (1974). In the same way, Cr values suggest distribution coefficients of about 10, Sc values about 4 and Ni values about 3. These values are again generally close to those accepted as appropriate for cpx-liquid distribution coefficients for these elements (table 9.1).

Because most other xenoliths have significant proportions of more than one mineral, this approach is of limited applicability to other groups. The most olivine-rich of the olivine-clinopyroxenite xenolith group, B23, has about 20% olivine. The xenolith has 196ppm Ni compared with B4, which has <1% olivine and 60ppm Ni. This implies that the olivine has about 750ppm Ni, a markedly lower value than that expected from mantle derived olivine (e.g. Sato, 1977). The basaltic lavas from Sangeang Api have low Ni values (50-20ppm) and this implies olivine-liquid distribution coefficients in the range 20-30. These are high values, though within the upper range (relatively low temperature, and or low MgO liquids?) of those values determined experimentally (e.g. Leeman and Scheidegger, 1977).

The plagioclase-bearing xenoliths, B11 and B10 have about 50% plagioclase and about 1000ppm Sr. If the Sr content of cpx, amphibole and magnetite in these rocks is assumed to be very small compared with that of plagioclase, then the Sr content of the plagioclase must be of the order of 2000ppm. This is about twice the concentration of Sr in the lavas implying a plagioclase-liquid distribution coefficient of about 2. This is again compatible with experimentally determined values (e.g. Sun et al. 1974).

Thus in a general way, the trace element concentrations of the intrusive rocks are consistent with precipitation from magmas similar to the Sangeang Api extrusives. This factor tends to suggest that the intrusive rocks could represent accumulations of minerals crystallised in equilibrium with liquids like those of the Sangeang Api lavas.

The gabbroic intrusive rocks show considerable variation in the relative modal proportion of amphibole and clinopyroxene and plagioclase. The ratio of plagioclase to clinopyroxene remaining approximately constant, while the proportion of amphibole varies from about 50% in B24 to about 4% in B10. This trend also marks a transition in the role of amphibole from the dominant, earliest-formed phase to a late interstitial (intercumulate?) role.

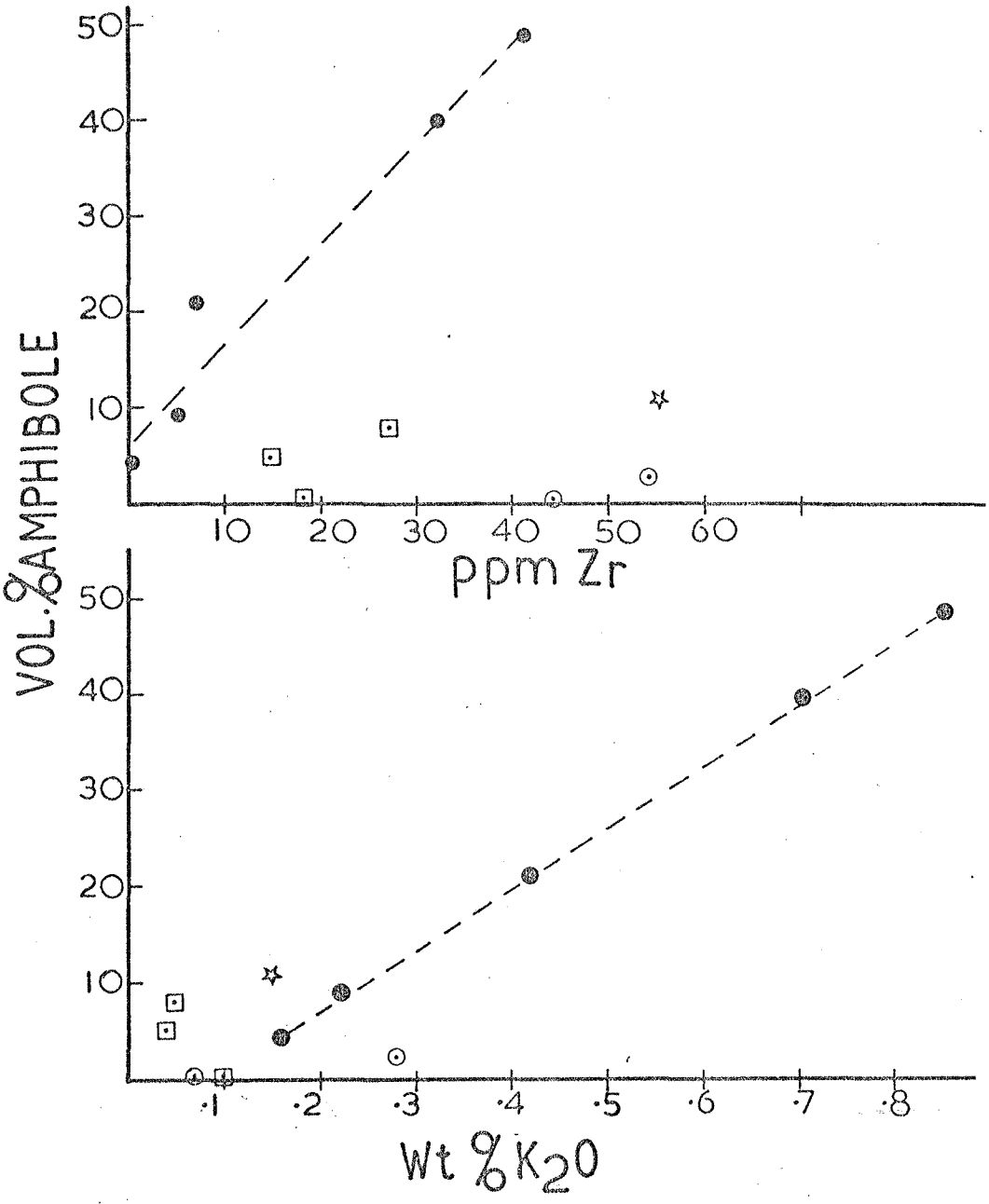

Figure 5.23

The variation of modal % amphibole v. concentration of Zr and K_2O for Sangeang Api xenoliths.

filled spots - gabbroic xenoliths

open circles - olivine clinopyroxenites

star - alkali clinopyroxenite

open squares - magnetite clinopyroxenite.

Illustrating that particularly in the gabbros that concentrations of Zr and K_2O are a direct function of the amount of amphibole and suggest that these elements in this group of nodules are largely resident in the amphibole.

This variation is also marked by a systematic variation in a number of geochemical parameters as a function of modal proportion of amphibole. For instance there is a more or less linear decrease in the concentration of K_2O, TiO_2, Zr and to a lesser extent Rb (figure 5.23) as a function of decreasing amphibole content in these xenoliths. This is consistent with the thesis that the geochemistry of the intrusive rocks being a function of their modal mineralogy, in turn consistent with an accumulative origin. It also demonstrates that amphibole is a potential "sink" for incompatible or moderately incompatible trace- and minor elements.

It is informative to consider the relationship of the mineralogy and compositional variation trends of the intrusive rocks and the compositional variation of the associated lavas (figures 5.18 and 5.19). Though the intrusive do display rather scattered compositional variations, they do show some recognisable trends. Consider first, the mineralogical variation with MgO variation (figure 5.24). Xenoliths with >ca. 17% MgO are clinopyroxene (+ olivine) dominated, with relatively minor magnetite. With decreasing MgO, magnetite appears (and remains relatively constant at about 10-11 vol.%) and amphibole appears and increases in modal abundance to about 8% MgO. Plagioclase first appears at about 10% MgO and increases with decreasing MgO and is most abundant in the rocks with lowest MgO content (a dilution effect). SiO_2, CaO, Cr, Ni, Sc all decrease with decreasing MgO, while Sr and Al_2O_3 increase. All other analysed major, minor and trace elements show rough trends of enrichment with MgO depletion until MgO has decreased to about 8.00%, followed by a trend of depletion. This maximum corresponds to the group of xenoliths with the largest proportion of amphibole. This behaviour is particularly marked with respect to K_2O, Na_2O, TiO_2, P_2O_5, ΣFe, Zr and Y (figures 5.18 and 5.19).

This behaviour is interesting in the light of the previously described inflection of the compositional variation trends of the Sangeang Api lavas at about 4.5% MgO. This inflection also marks the transition from the

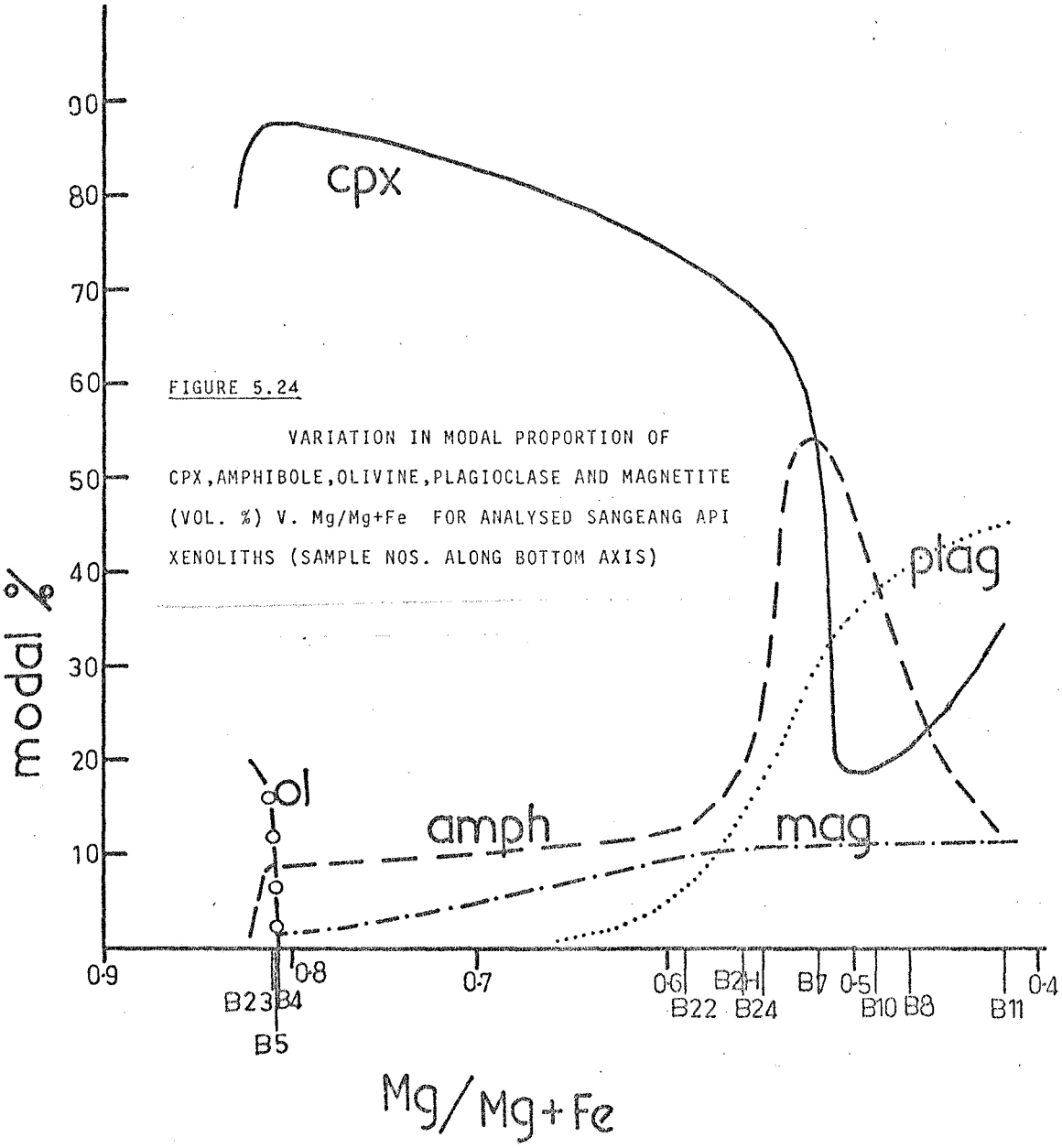

FIGURE 5.24

VARIATION IN MODAL PROPORTION OF CPX, AMPHIBOLE, OLIVINE, PLAGIOCLASE AND MAGNETITE (VOL. %) V. Mg/Mg+Fe FOR ANALYSED SANGEANG API XENOLITHS (SAMPLE NOS. ALONG BOTTOM AXIS)

more MgO-rich, olivine-bearing lavas to the less MgO-rich amphibole-bearing lavas. In particular the transition from trends of TiO_2- and ΣFeO + Fe_2O_3-enrichment with decreasing MgO amongst the lavas with >4.5% MgO to depletion trends at <4.5% MgO appears to complement the variation of these elements in the xenoliths. Thus the high MgO, low ΣFe and low TiO_2 olivine-clinopyroxenite lie on a high-MgO extension of the olivine-bearing lava-trend. The more TiO_2- and ΣFe-rich, MgO-poor, amphibole-rich xenoliths fall on an extension of the TiO_2- and ΣFe-depletion trends of the amphibole-bearing xenoliths. Thus, at least qualitatively, the Sangeang Api intrusive rocks appear to embody ranges of compositions both in terms in their modal and mineralogy and bulk chemistry, which fulfil the potential role of fractionally crystallized accumulates from the Sangeang Api lava suite. A series of idealized variation diagrams are shown in figure 5.25, illustrating the possible relationship between the compositional trends of the Sangeang Api lavas and xenoliths and showing possible instantaneous fractionation trends at tie lines.

It is rather tempting to conclude from these possible relationships that the crystallisation history of the lavas has been encapsulated in the erupted xenolith-suite. The xenoliths may indicate a crystallisation course initiated by the precipitation of olivine and clinopyroxene, passing then into a field occupied by amphibole, cpx, magnetite (+ minor apatite), from which olivine is absent, presumably as a result of a reaction relationship with the liquid yielding cpx and/or amphibole. The course of this path then leads the liquid into the stability field of plagioclase and gradually out of that of amphibole.

The possible role of the xenoliths and their component minerals as accumulates whose fractionation may account for the differentiation of the Sangeang Api lavas is tested more quantitatively in chapter 9. The phase

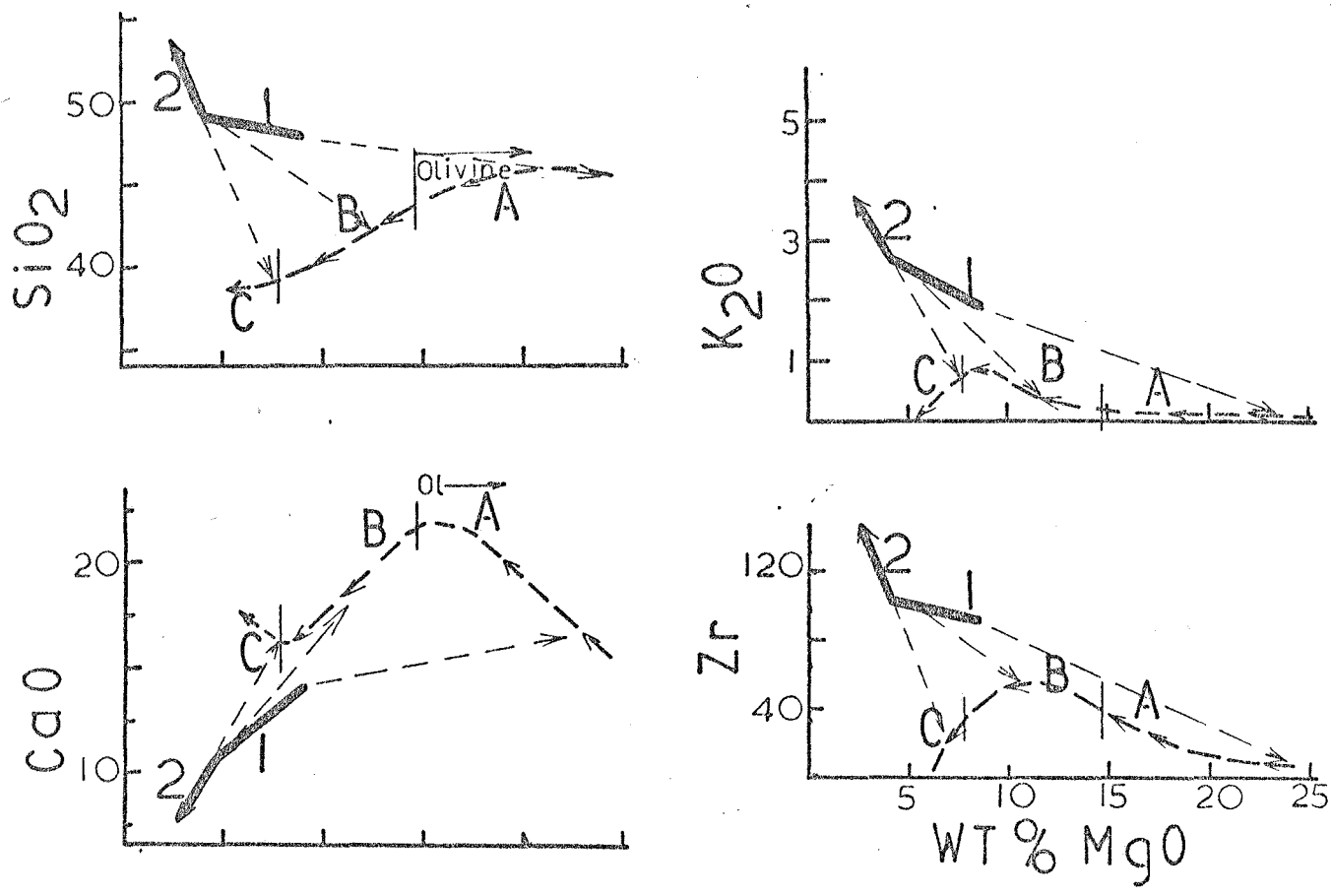

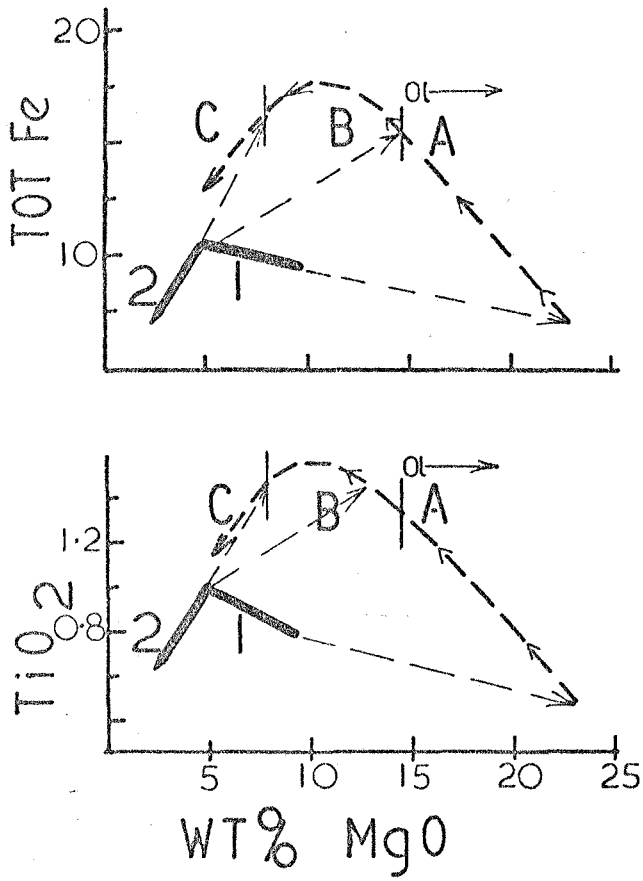

FIGURE 5.25

IDEALIZED COMPOSITIONAL VARIATION TRENDS FOR SANGEANG API LAVAS AND XENOLITHS FOR SOME MAJOR- AND TRACE-ELEMENTS v. MgO. SOLID LINE REPRESENTS THE LAVA TREND AND THE THICK DASHED LINE THAT OF THE INTRUSIVES.THE OLIVINE MEGACRYST BEARING LAVAS OCCUPY SEGMENT 1 OF THE TREND AND THE AMPHIBOLE -BEARING LAVAS SEGMENT 2.THREE SEGMENTS OF THE XENOLITH TREND AR DISTINGUISHED: A-OLIVINE-CPX ASSEMBLAGES (OLIVINE IS ABSENT TO THE LEFT OF THE DASH MARKED OLIVINE OL, B-AMPHIBOLE-MAGNETITE-RICH ASSEMBLAGES WITH INCREASING PLAGIOCLASE TOWARDS C , AND ,C-PLAGIOCLASE-RICH ASSEMBLAGES (+CPX,AMPH,MAG). POSSIBLE CUMULATE-LIQUID RELATIONSHIPS (IF THE XENOLITHS ARE CUMULATES) ARE INDICATED BY THE DASHED ARROWS, THE LIQUID MOV ING FROM 1 to 2 AS THE CUMULATE ASSEMBLAGES MOVE FROM A TO B TO C.

relationships implied by the crystallisation sequences preserved in the mineralogy of the xenoliths are examined more closely in chapters 10 and 11.

Finally, considering the alkali pyroxenites (for instance B13 and B22, tables 5.1 and 5.4); here petrographic evidence presented previously suggested that these represented modified clinopyroxenite or olivine-clinopyroxenite (type 1) This apparently resulted from secondary introduction of amphibole (in the case of B22) and/or phlogopite (in the case of B13). Similar nodules have erupted from a number of alkaline (and often relatively potassic) volcanoes in a diversity of tectonic settings (e.g. Uganda; Lloyd and Bailey, 1975, Holmes and Harwood, 1937, Roman Province, Italy; Appleton, 1972, Hopi Buttes, Utah; Lewis, 1973, Eifel, Rhine Rift; Lloyd and Bailey, 1975).

These have been attributed to a number of origins, though Lloyd and Bailey (1975) suggest mantle metasomatism. The alkali pyroxenites from the Sangeang Api intrusive suite, are geochemically similar to members of the olivine-clinopyroxenite group (table 5.4), thus if this group are accumulative in origin, it is possible that the alkaline pyroxenites represent modifications of earlier formed clinopyroxene-olivine dominated accumulative assemblages. In the case of B13 the addition of phlogopite has resulted in very high K_2O (5.32%) and Rb (262ppm) concentrations and only slightly higher Sr. B22 is amphibole-rich on the other hand and has very low Rb and relative to the "normal" clinopyroxenites is slightly enriched in Na_2O, K_2O, TiO_2, ΣFe, Al_2O_3, Sr and Y. It is possible that the amphibole and phlogopite result from either reaction of early formed (higher temperature?) cumulate assemblages with small amounts of trapped residual liquid "percolating" through this clinopyroxene-rich crystal pile or by the reaction with newly introduced liquids of a later "spasm" of eruption.

Why the relative importance of secondary amphibole and phlogopite varies is uncertain. It may be a function of pressure, as suggested by Lloyd and Bailey (1975) or differing compositions of reacting "fluids" or liquids.

5.7 *Summary of the Main Petrological Features of the Sangeang Api Intrusive Rocks (Xenoliths) and Lavas and Discussion of some Aspects of their Petrogenesis.*

5.7.1 Intrusive Rocks (xenoliths and erupted blocks).

Five distinctive groups of intrusive rocks were distinguished on the basis of petrographic features, in particular modal mineralogy and textures:

1. Olivine Clinopyroxenites: Characterised by clinopyroxene and less important olivine, with interstitial or intercumulate (?) phlogopite and/or amphibole. Magnetite is rare or absent from this group and plagioclase is completely absent.
2. Magnetite Clinopyroxenites: These are largely composed of clinopyroxene and magnetite with variable amounts of interstitial (intercumulate?) plagioclase. Amphibole is a rare constituent replacing clinopyroxene. Olivine is an occasional rare inclusion in some clinopyroxene grains.
3. Hornblende - magnetite - clinopyroxenites: This group is only represented by a few examples (e.g. B20, table 5.1). Hornblende appears as early-formed euhedral grains together with clinopyroxene and magnetite. Apatite is a minor accessory and plagioclase is a rare interstitial phase. These appear to be hornblende-magnetite - clinopyroxene cumulates.
4. Hornblende-gabbros: These form a series with considerable modal variation in their amphibole content relative to that of plagioclase and clinopyroxene. In general this series appears to be amphibole-anorthite-clinopyroxene-magnetite$\pm$ apatite cumulates. The progression

from amphibole-rich members of this group (e.g. B7, B1B, B24) to amphibole-poor types (e.g. B10) marks the progressively changing role of amphibole, from the earliest crystallised cumulate phase to a late-stage intercumulate. Magnesian biotite or phlogopite occurs as an interstitial phase in some of these rocks apparently the result of reaction between the intercumulate liquid and amphibole and magnetite or in some cases as intercumulate poikilitic oikocrysts.

5. Alkali clinopyroxenites: These are characterised by primary clinopyroxene and sometimes olivine and/or magnetite with secondary amphibole and phlogopite and occasionally plagioclase.

Order of Crystallisation

The xenoliths appear to encapsulate a number of crystallisation sequences.

1. Olivine clinopyroxenites: These suggest the sequence: 1. Olivine 2. Clinopyroxene 3. phlogopite $\pm$ amphibole.
2. Magnetite Clinopyroxenites: These suggest a sequence: 1. clinopyroxene 2. magnetite 3. plagioclase. The occurrence of olivine inclusions in some clinopyroxene grains also suggests an olivine crystallisation phase may predate the clinopyroxenes.
3. Hornblende-magnetite-clinopyroxenite: These suggest a sequence of: 1. Almost simultaneous crystallisation of amphibole and clinopyroxene 2. magnetite 3. apatite and plagioclase.
4. Gabbroic xenoliths: These suggest a gradual change in sequence from: A. 1. Amphibole 2. clinopyroxene + plagioclase
   3. magnetite + apatite
   to B. 1. Clinopyroxene + plagioclase + magnetite
   2. amphibole + biotite.

5. Alkali clinopyroxenites: These represent modification of early olivine clinopyroxenite or magnetite clinopyroxenite by the progressive addition of: 1. phlogopite 2. amphibole and 3. plagioclase.

Reaction Relationships

A number of reaction relationships are inferred from the petrographic variation shown by the xenoliths:

1. There is a possibility that olivine is being eliminated by reaction with a liquid to yield clinopyroxene in some olivine clinopyroxenites and magnetite clinopyroxenites.
2. Clinopyroxene is reacting to yield amphibole and/or phlogopite in some clinopyroxenites, to yield the alkali clinopyroxenites.
3. Olivine is also reacting to yield phlogopite and/or clinopyroxene in some alkali clinopyroxenites (e.g. B15, plate 3E).
4. In some amphibole-rich xenoliths (e.g. B7, B1B, the amphibole is being partially melted to yield an assemblage: olivine + clinopyroxene + feldspar + very alkali-rich liquid (plate 4A,B,D).

A number of observed mineral associations are also possibly important. In particular:

1. Primary, cumulate olivine and amphibole do not coexist in any single intrusive assemblage.
2. Olivine and plagioclase do not coexist in any intrusive assemblage, except as breakdown-products of partially fused amphibole.
3. Olivine-bearing intrusive rocks are generally magnetite-free.

5.7.2 General features of the Lavas

The phenocryst assemblages of the lavas show quite specific correlation with certain assemblages in the intrusive xenoliths. As described previously, there are two distinct groups.

1. Olivine-bearing lavas: These have olivine phenocrysts and/or megacrysts and clinopyroxene phenocrysts and/or megacrysts. This phenocryst or megacryst assemblages are equivalent to the assemblages in the olivine-clinopyroxenite and magnetite-clinopyroxenite intrusive xenoliths. In most instances, megacrysts of olivine and clinopyroxene are compositionally similar to counterparts in the above xenoliths. In some instances these are associated with later stage phenocrysts of olivine, clinopyroxene and plagioclase which are compositionally distinct from the megacrysts and their counterparts in the xenoliths.

If all the megacrysts and phenocrysts crystallised from the same liquid, then a sequence:

$$\underset{\text{(megacrysts)}}{ol + cpx \pm \text{magnetite}} \rightarrow \underset{\text{(phenocrysts)}}{ol + cpx + \text{plagioclase} + \text{magnetite}}$$

is inferred.

2. Amphibole-bearing lavas: These contain megacrysts of amphibole (partly reacted), clinopyroxene and anorthite. Olivine is absent as a phenocryst phase. Phenocrysts are; clinopyroxene, more Al-rich plagioclase (An and magnetite. The groundmass comprises; olivine + plagioclase + k-spar + cpx + magnetite + apatite ± feldspathoid. Thus the inferred sequence of crystallisation is as follows:

1. Amphibole + clinopyroxene + anorthite plagioclase + magnetite (megacryst assemblage).
2. Clinopyroxene + plagioclase (more Ab-rich) + magnetite (phenocryst assemblage).
3. Olivine + clinopyroxene + plagioclase + sanidine + magnetite ± feldspathoid (groundmass assemblage).

Considering the xenolith mineralogy, the first assemblage corresponds to that of the more amphibole-rich gabbros such as B24 (tables 5.1 and 5.4), the second assemblage corresponds to the assemblage of the amphibole-poor

or -absent gabbros (for instance B10) and the groundmass assemblage is like that of the partially melted glass after amphibole (for instance in B7 or B1B).

5.7.3 Summary of the Mineral Compositions of the Sangeang Api Lavas and Intrusives

There are a number of important features related to the mineral chemistry of this suite:

1. The phenocrysts from the Sangeang Api lavas generally show similar compositional characteristics to those of the equivalent minerals from the associated intrusive rocks. However, in most cases the composition of these phenocrysts are not identical to those of any of the xenolith groups. For instance, while all the clinopyroxenes of the Sangeang Api lavas and xenoliths are very Ca-rich, those occurring as phenocrysts in the lavas are slightly (but significantly) less calcic than any represented in the intrusive rocks. At the same time, all the lavas do contain megacrysts or xenocrysts which have direct analogues in the xenolith suites. Furthermore, the olivine phenocrystic lavas generally contain megacrysts of minerals from the plagioclase-free, olivine-bearing xenoliths (olivine clinopyroxenites and alkali clinopyroxenites) while the lavas without olivine phenocrysts contain megacrysts (or xenocrysts?) of the amphibole-bearing gabbroic xenolithic minerals.

2. The sequence; olivine-clinopyroxenite, amphibole gabbro, phenocryst assemblage, groundmass assemblage, generally represents one of decreasing Ca-content of calcium-bearing phases, increasing Ti content of titaniferous phases and decreasing Mg and Mg/Mg+Fe content of ferromagnesian phases.

However, some of these parameters show overlapping relationships. Thus some clinopyroxene phenocrysts are more magnesian and have higher Mg/Mg+Fe ratios than clinopyroxene of the gabbroic xenoliths. These phenocrysts are at the same time less calcic, less aluminous and more titanian than the gabbroic clinopyroxene with same Mg/Mg+Fe value.

These features suggest that the composition of the liquid is not the sole factor controlling the composition of the precipitated minerals Thus, while Mg/Mg+Fe ratio may reflect that of the liquid, the Ca, Al an Ti content may well be a function of P_{H_2O}, P and possibly fO_2.

3. When considering the compositional variation of the minerals of the alkali-clinopyroxenites and those represented as megacrysts and phenocrysts in the lavas, some interesting features emerge. In particular if the range of compositions of cpx and amphibole are considered, both these appear to have sampled the mineral compositions from a number of xenolith types.

The alkali clinopyroxenites have clinopyroxenes with mafic cores which are both relatively more magnesian, more calcic and less titanian than those of the most mafic examples from the olivine clinopyroxenites (fig. 5.8). The composition of outer rim and secondary clinopyroxene and amphibole forms a transgressive trend, successively falling in the compositional fields of these minerals from the olivine clinopyroxenites and then gabbros. Thus the alkali pyroxenites encapsulate the entire range of the compositions embodied in the primary xenoliths. The trend from core to rim and from first- to late-stage minerals in the alkali pyroxenites cuts across the core-rim variation trends of single-origin, primary xenoliths.

If the systematic variation of the minerals within the olivine clinopyroxenite and gabbroic xenoliths suggests gradual changes in possible variables (i.e. T, P_{H_2O}, liquid composition), in situ and hence at constant pressure, then the transgressive compositional variation of the alkali pyroxenite minerals suggests more abrupt or catastrophic variation of possible variables. This then suggests that the minerals of the alkali pyroxenites have either precipitated from several liquids of different compositions and/or at different temperatures, pressures or water contents.

If pressure is a variable parameter, then it must follow that any individual alkali pyroxenite must have its origin at various depths. This is borne out to some extent by field- and hand-specimen evidence. For instance B15 is an alkali pyroxenite which was included in a gabbroic xenolith. Thus in this case an original olivine clinopyroxenite cumulate may have been fragmented and carried up by a later magma pulse. This later magma then precipitated an amphibole-cpx-anorthite-magnetite assemblage, minerals equivalent to which form the second-stage phases in the original olivine clinopyroxenite, partly as vein material. Reaction between the original assemblage (ol + cpx) and the new liquid has also yielded phlogopite.

Another possible mechanism is that of diapiric intrusion. Deformation of some alkali pyroxenites may support this. Here an original olivine clinopyroxenite cumulate body may be intruded to a higher level in the crust and then interact with a new intrusion of magma at this lower pressure.

The megacrysts in the erupted lavas show a similar transgressive relationship. However, whereas the mineral compositions of the alkali pyroxenites converge on the field of those of the gabbroic inclusions, the megacrysts converge on that of the phenocrysts minerals.

5.7.4 Crystallisation Conditions

The likely P/T fields in which the xenolith assemblages may crystallise, together with the likely effects of a H_2O- and fO_2-variation are discussed more fully in chapters 9 and 10, however some general considerations are made here.

1. The presence of hydrous minerals indicates that the liquids from which the xenoliths precipitated contained appreciable amounts of water.
2. The generalised crystallisation sequence indicated by the xenoliths; 1. olivine 2. cpx 3. amphibole ± magnetite ± phlogopite ± apatite 4. plagioclase, with olivine and cpx tending to disappear in favour of amphibole and/or phlogopite, is generally that shown by many experimental studies in basaltic systems (e.g. Holloway and Burnham, 1972; Yoder, 1969) with water present during isobaric cooling at pressures in the range 3-10 kbars.
3. The effects of water are particularly important with respect to the upper stability temperature of plagioclase (e.g. Yoder, 1969), so that in water saturated systems the plagioclase liquidus retreats rapidly to lower temperature with increasing pressure. Plagioclase may be on the liquidus at one atmosphere but rapidly retreats to well below at slightly higher pressures. Thus the plagioclase-rich assemblages amongst these xenoliths may also represent lower pressure precipitates from relatively water-rich liquids. Further, the relative reversal of crystallisation order in the gabbroic group from early appearance of amphibole, before plagioclase to late appearance of amphibole after plagioclase, cpx and magnetite, is suggestive of crystallisation with decreasing pressure and/or water pressure in the relatively low pressure region where the amphibole liquidus retreats rapidly to lower temperatures (≈1-3 kbars).

4. The calcic composition of the plagioclase is likely to be due to the effects of elevated water pressure (e.g. Yoder, 1969). This factor may also be important in the development of very Na-poor pyroxenes.

5. The generally high Ca-content of the cpx and amphibole are interesting as is the trend of decreasing Ca/Ca+Mg described in the transition from one xenolith group to another towards the phenocryst field. It is possible that this effect is partly due to the increased competition for Ca when plagioclase starts to crystallise. This explanation does have some problem however in that the phenocrysts have a less Ca-rich cpx than the gabbros while in both cases cpx coexists with plagioclase. It is possible that the gabbroic xenoliths have crystallised at slightly elevated pressure (as well as higher pH_2O as evidenced by their calcic plagioclase) and this may then have the effect of promoting the coupled substitution of Ca and Al^{VI} as the Ca-Tschermak's molecule:

$$Ca\ Al_2\ SiO_6$$

This may then suggest that the even more calcic cpx and amphibole of the more mafic xenoliths represent higher pressures still, though at the same time the absence of plagioclase and the possible higher temperatures of these assemblages may be important.

6. The ability of the liquids to precipitate large volumes of magnetite tends to suggest that they are relatively oxidised and hence indicates rather high fO_2 values.

In summary it is suggested that the Sangeang Api xenoliths have precipitated from hydrous, alkaline basaltic magmas, probably at relatively low pressures (<10 kbars) under conditions of relatively high fO_2. There

is some suggestion of polybaric crystallisation (the gabbroic xenoliths representing lower pressure products than the plagioclase-free modules) and in the case of the alkali pyroxenites, these apparently have a multiple origin and hence sampled both fields. The close coherence of the megacryst assemblages of the lavas to assemblages represented in the xenoliths, suggests that the lavas may have crystallised the xenolith assemblages at depth and as such the xenoliths are probably cumulates from the fractional crystallisatio of the liquids erupted as the volcanic rocks of the Sangeang Api.

5.8 Comparison of Sangeang Api intrusive rocks with xenolith suites and mafic to ultramafic igneous bodies elsewhere.

Nodule assemblages of the type erupted by Sangeang Api volcano have been reported from a few other island arc volcanoes. Suites from Oshima-Oshima volcano, S.W. Hokkaido, Japan (Katsui et al., 1978), from Iki island, Japan (Aoki, 1970) and the Aleutian Bogoslof (Arculus et al., 1977) and Kanaga islands (Delong et al., 1975) all closely resemble the Sangeang Api xenolithic lithogies. Inclusion from some Lesser Antilles lavas (e.g. Lewis, 1973) also show some similarities.

Clearly the Sangeang Api xenoliths are not members of either of the two broadly defined meantle derived nodule groups which are erupted by intra-plate alkaline to sub-alkaline volcanoes.

These two suites have been referred to by Kuno (1969) as the "lherzolite" and the "wehrlite-dunite-pyroxenite" series and have been subsequently described by numerous authors (e.g. Best, 1970; Irvine, 1974; Wiltshire and Shervais, 1975). These nodules differ from the Sangeang Api xenoliths in their textures ("lherzolite" series nodules have metamorphic textures), their mineral assemblages (orthopyroxene, aluminous spinel and garnet are not found in the Sangeang Api nodules) and their mineral compositions (in the mantle derived group pyroxenes are more aluminous, clinopyroxenes are less calcium rich and more sodic and phlogopite and amphibole (tables 5.19 and 5.21) are more magnesian and Cr-rich).

The Sangeang Api xenoliths have mineral assemblages which are more like those of the cognate xenoliths that are commonly recorded from continental (e.g. S.E. Australia; Ellis, 1976) and oceanic (e.g. Comores island; Frisch and Schminke, 1969; Canary Island; Upton and Wadsworth, 1972) interplate volcanoes. Rock types included in this group include dunite, wehrlite, olivine-clinopyroxenite, hornblendite and gabbro.

Even though the mineral assemblages of these xenoliths resemble those of the Sangeang Api group, some compositional differences are observed. In particular, the Indonesian nodules have more calcic plagioclase, less TiO_2-rich amphibole and phlogopite (tables 5.19 and 5.21) and generally less sodic and more calcic clinopyroxene.

Amongst mafic and ultramafic intrusive bodies, the Alaskan-type, concentric-zoned complexes (e.g. Irvine, 1973; Taylor et al., 1963) show stron affinities with the Sangeang Api xenolith suite.

These complexes are composed of: olivine-clinopyroxenite, hornblende-magnetite-clinopyroxenite, magnetite clinopyroxenite and hornblende-anorthite pegmatite. All these rock-types have close analogies amongst the Sangeang Api nodules. In particular, the very magnetite-rich character of a number of the Sangeang Api clinopyroxenites is also a characteristic feature of Alaskan-type ultramafic complexes, as is the absence of magnetite from the olivine-clinopyroxenite. A number of the Alaskan bodies are mica-bearing and Irvine (1974) and Findlay (1969) suggested that their parent magma may be alkaline, as is the case in this example from the Sunda Arc.

The similarity between the Alaskan zoned ultramafic complexes and the Sangeang Api nodules is also carried to their mineral compositions and as shown in tables 5.19 and 5.20 amphiboles and clinopyroxenes from both localities exhibit very similar compositional features.

Table 5.19

Analyses of Hornblendes from Various Mafic and Ultramafic Xenoliths

Analysis No.	1	2	3	4	5	6	7	8	9
SiO_2	42.48	41.0	40.1	41.05	40.06	38.76	40.39	42.8	45.19
Al_2O_3	14.56	14.6	15.0	12.69	14.41	15.42	12.35	13.8	15.43
Fe_2O_3	3.92	4.1	4.5	n.d.	n.d.	10.00	n.d.	n.d.	1.27
FeO	9.51	10.5	6.6	11.06	10.73	2.16	11.86	4.5	2.04
MgO	11.63	13.2	15.1	12.64	14.17	12.52	12.45	17.9	17.98
CaO	12.26	11.6	12.4	13.71	12.26	11.49	11.45	9.7	10.11
Na_2O	2.53	2.7	1.5	2.14	2.47	2.32	2.60	3.7	3.47
K_2O	0.41	0.4	0.8	1.37	0.25	1.22	0.83	1.13	0.04
TiO_2	1.38	2.7	1.7	2.11	2.22	5.08	5.80	1.2	1.28
MnO	0.33	-	0.1	0.17	0.16	0.16	0.16	0.06	-
Cr_2O_3	-	-	-	-	-	-	-	1.7	0.97

A. Hornblendes from Alaskan-Type Ultramafic Complexes

1. Hornblende from hornblende-anorthite pegmatite, Duke Island. Irvine, 1973, table 12, anal. 2.
2. Hornblende from Knight Inlet, Hornblendite, British Columbia. Taylor et al. 1969, table 1, anal. 4.
3. Hornblende from hornblende-pyroxenite Urals, U.S.S.R. Taylor et al. 1969, table 1, anal. 6.

B. Amphibole from Inclusions in Island Arc Lavas

4. Amphibole from hornblende gabbro inclusion in 1927 basalt, Bogoslof Island, Alaska. Arculus et al. 1977, table 3.
5. Amphibole from hornblende gabbro nodule, calcalkaline lava, St. Lucia, L. Antilles. Wills, 1974.

C. Amphibole from Cognate Xenoliths in Alkaline Basalts

6. Kaersutite from clinopyroxenite Iki-Island, Japan, Aoki, 1970, table 5, anal. 2.
7. Kaersutite from gabbro xenolith in basalt, Mauritius. Baxter, 1978, table 2, anal. 1.

D. Amphibole from Lherzolite Nodules

8. Pargasite from spinel lherzolite, San-Carlos, Arizona. Frey and Prinz, 1978, table 4B, anal. 2.
9. Amphibole, in spinel lherzolite, Victorian basanite. Frey and Green, 1974, table 4, anal. 1.

Note: Analyses of Sangeang Api amphiboles given in table 5.10

Table 5.20

Analyses of Clinopyroxene from Alaskan-Type Ultramafic Complexes and Nodule from Island Arc Basalt

Analysis No.	1	2	3	4	5
SiO_2	51.94	51.74	51.50	48.42	53.79
Al_2O_3	1.52	1.42	4.31	6.38	1.41
FeO	3.54	6.14	5.45	5.95	3.10
MgO	18.56	15.85	15.20	14.53	17.15
CaO	22.82	23.44	23.42	22.86	23.77
Na_2O	0.09	0.14	0.47	0.66	0.23
TiO_2	0.13	0.28	0.32	0.68	0.10
Cr_2O_3	0.32	0.04	0.38	-	0.31

1. Cpx from dunite, Union Bay, Alaska. Ruckmick and Noble, 1959, table 1.
2. Cpx from olivine clinopyroxenite, Tulameen. Findlay, 1969, table 6.
3. Cpx from olivine clinopyroxenite, Halls Cove Complex, Alaska. Irvine, 1974, table 10 anal. 2.
4. Cpx from hornblende-magnetite-clinopyroxenite, Halls Cove, Alaska. Irvine, 1974, table 10 anal. 4.
5. Cpx from dunite nodule, Kanaga Island basalt. Delong et al. 1975, table 3, anal. 1.

Note: Analyses of cpx from Sangeang Api nodules presented in tables 5.12 and 5.13.

Table 5.21

Analyses of Phlogopites from Ultramafic Nodules

Analysis No.	1	2	3	4	5
SiO_2	36.25	40.1	39.7	40.7	39.98
Al_2O_3	16.91	12.02	13.9	12.8	13.45
FeO	7.89	9.35	3.12	2.63	3.57
MgO	19.15	17.4	24.8	26.5	18.73
CaO	-	0.0	0.03	0.02	-
Na_2O	0.93	1.00	0.92	0.75	0.03
K_2O	9.12	8.36	9.06	9.31	9.64
TiO_2	4.19	6.15	1.45	0.28	9.13
MnO	0.06	-	0.10	0.01	-
Cr_2O_3	0.10	-	1.60	0.86	0.71

1. Phlogopite from alkali clinopyroxenites (amphibole-rich) from West Eifel, Germany. Becker, 1977 table 3, anal. 1.
2. Phlogopite megacryst. Jan Mayen Island, Flower, 1969.
3. Secondary phlogopite from garnet lherzolite, Kimberley Mines, South Africa, Carswell, 1975, table 2, anal. 1.
4. Primary phlogopite from garnet lherzolite, Kimberley Mines, South Africa, Carswell, 1975, table 2, anal. 1.
5. Phlogopite from garnet lherzolite, Lashaine Volcano, Tanzania. Dawson et al. 1970, table 7, anal. 1.

Note: Analyses of phlogopite from Sangeang Api nodules are given in table 5.16.

Chapter 6

PETROLOGY OF LAVAS FROM G. SOROMUNDI AND G. SANGENGES

6.1 Introduction

These two volcanoes are situated on the island of Sumbawa. G. Sangenges lies in the centre of the western end of the island (figure 4.1), while Soromundi is at the eastern end of Sumbawa, on the north coast, on the western side of the entrance to Bima Bay (figure 4.1).

The petrography of the lavas from these two volcanoes are discussed together for a number of reasons:

1. The erupted suites of both these volcanoes include extremely undersaturated, potassium-rich, leucite-bearing lavas (analyses given in tables 6.1 - 6.4), of an unusual type not commonly encountered in island arcs.

2. There is relatively limited chemical data available on the mineralogy of these lavas at this stage and such as is available is best discussed in the context of both groups of these lavas, simultaneously.

3. They are both eroded volcanic cones which became inactive in the Quaternary (Sudradjat, 1975), unlike the other, active volcanoes discussed in this thesis. This factor then introduces some uncertainties about the spatial relationship of these volcanoes to the trench and Benioff Zone when they were active.

Sampled lavas from G. Sangenges fall into three mineralogically and geochemically distinctive groups:

A. A highly undersaturated, feldspathoid-rich series, which contain both normative *ne* and *lc*. Chemical analyses of this group (samples S22, S21, S17 S19, S9A, S9B, S23) are given in table 6.1

B. A moderately alkaline, slightly undersaturated, plagioclase-phyric group of lavas with small amounts of normative *ne*, but no normative *lc*. These contain abundant groundmass potassium feldspar, but little or no modal feldspathoid. These lavas are mineralogically and geochemically similar to

TABLE 6.1

EAST SUNDA ARC VOLCANIC ROCKS

G.SANGENGES - SUMBAWA ISLAND,LEUCITE-BEARING LAVAS

Sample#	S3	S23	S21	S27	S22	S17	S19	S9
SiO_2	47.06	45.88	43.86	45.38	43.65	44.77	44.71	44.52
TiO_2	0.89	0.91	1.09	1.05	1.07	1.12	1.09	1.14
Al_2O_3	9.16	11.13	11.09	12.79	12.54	12.64	13.20	13.31
Fe_2O_3	1.76	1.76	2.04	1.92	1.96	2.11	1.96	2.15
FeO	8.98	8.98	10.38	9.78	10.01	10.74	9.99	10.95
MnO	0.16	0.17	0.20	0.18	0.21	0.18	0.18	0.20
MgO	11.84	10.78	9.00	8.29	8.25	8.00	7.77	7.25
CaO	16.51	15.20	15.16	14.38	14.41	14.55	13.88	14.19
Na_2O	2.68	1.85	2.03	1.73	2.40	2.20	2.07	2.55
K_2O	0.36	3.03	4.34	3.81	4.61	3.09	4.42	3.14
P_2O_5	0.58	0.31	0.81	0.69	0.88	0.59	0.74	0.61
H_2O+	2.68	1.13	1.40	1.75	1.35	1.94	1.34	1.61
Mg/Mg+Fe	0.67	0.65	0.57	0.56	0.56	0.53	0.54	0.50
Mg/Mg+.85Fe	0.70	0.68	0.61	0.60	0.59	0.57	0.58	0.54
K_2O/Na_2O	0.13	1.64	2.14	2.20	1.92	1.40	2.14	1.23
Trace elements (ppm)								
Rb	95	125	191	246	192	117	319	201
Sr	667	691	753	849	902	750	836	865
Zr	93	81	187	122	194	80	139	138
Nb	5	6	7	4	6	5	6	5
Y	25	29	38	20	34	19	25	32
La							37	
Sc	51	58	51	53	44	53	49	48
Cr	407	281	200	129	168	101	70	66
Ni	91	54	42	35	37	27	30	22
Rb/Sr	0.142	0.181	0.254	0.290	0.213	0.156	0.382	0.232
K/Rb	31	201	189	129	199	219	115	130
K/Sr	4.48	36.40	47.85	37.26	42.43	34.20	43.89	30.14

Notes: FeO arbitrarily calculated as 0.85 total Fe.Analyses normalised anhydrous,H_2O^+= pre-normalisation figure.Rock localities and mineralogy given in appendix 1 (see also table 6.7) .CIPW norms given in appendix 2. Rocks S3,23,21,27,22,19 are olivine leucitites, S17 - leucitite/olivine leucitite,S9 - leucite tephrite.

TABLE 6.2

EAST SUNDA ARC VOLCANIC ROCKS

G.SANGENGES - SUMBAWA ISLAND, NE-NORMATIVE LAVAS

Sample#	S8	S28	S5	S16	S1
SiO_2	48.58	50.55	50.90	50.24	52.65
TiO_2	1.04	0.98	0.89	0.97	0.87
Al_2O_3	16.92	18.51	17.93	18.74	18.38
Fe_2O_3	1.80	1.51	1.52	1.51	1.31
FeO	9.20	7.71	7.77	7.72	6.69
MnO	0.22	0.18	0.20	0.20	0.19
MgO	5.77	4.45	4.27	4.24	3.51
CaO	11.12	9.67	10.10	10.08	9.16
Na_2O	2.82	3.77	3.25	3.34	3.43
K_2O	2.04	2.21	2.71	2.37	3.25
P_2O_5	0.50	0.46	0.46	0.58	0.56
H_2O+	2.50	0.90	2.17	1.61	2.81
Mg/Mg+Fe	0.49	0.47	0.45	0.45	0.44
Mg/Mg+.85Fe	0.53	0.51	0.49	0.49	0.48
K_2O/Na_2O	0.72	0.59	0.83	0.71	0.95
Trace elements (ppm)					
Rb	64	61	61	41	85
Sr	860	724	820	893	1138
Zr	104	138	121	135	136
Nb	5	3	5	5	4
Y	28	32	24	33	35
La		29			
Sc	28	26	23	18	16
Cr	33	48	52	45	34
Ni	12	8	11	15	4
Rb/Sr	0.074	0.084	0.074	0.046	0.075
K/Rb	265	301	369	480	317
K/Sr	19.69	25.34	27.44	22.03	23.71

Notes: FeO arbitrarily calculated as 0.85 Fe .Analyses normalised anhydrous. H_2O^+ is the prenormalisation value .Rock localities and mineralogies are given in appendix 1.CIPW norms are given in appendix 2. All lavas are ne-normative trachybasalts .

TABLE 6.3

EAST SUNDA ARC LAVAS AND XENOLITH

G.SANGENGES - SUMBAWA ISLAND, O-NORMATIVE ANDESITES AND XENOLITH

Sample#	S10	S11	S26	S15	S7	S12
SiO_2	52.14	52.85	56.12	59.69	60.51	39.89
TiO_2	0.98	1.01	0.60	0.50	0.46	1.51
Al_2O_3	19.13	18.38	18.77	18.35	17.79	19.30
Fe_2O_3	1.58	1.61	1.12	0.88	0.83	2.36
FeO	8.03	8.19	5.69	4.46	4.26	12.01
MnO	0.26	0.19	0.17	0.19	0.18	0.20
MgO	4.59	4.45	3.26	2.51	1.93	7.38
CaO	8.61	8.67	7.71	6.66	6.20	15.07
Na_2O	2.75	2.91	3.88	3.97	4.33	1.15
K_2O	1.60	1.45	2.37	2.48	2.65	0.49
P_2O_5	0.32	0.28	0.31	0.30	0.30	0.64
H_2O+	3.52	1.85	0.96	2.01	0.61	1.89
Mg/Mg+Fe	0.46	0.45	0.46	0.46	0.41	0.48
Mg/Mg+.85 Fe	0.50	0.49	0.51	0.50	0.45	0.52
K_2O/Na_2O	0.58	0.50	0.61	0.62	0.61	0.43
Trace elements (ppm)						
Rb	30	22	83	80	85	7
Sr	525	480	773	835	837	855
Zr	74	63	152	198	191	30
Nb	5	3	5	9	10	<0
Y	27	24	20	20	20	32
La						
Sc	23	23	14	9	9	43
Cr	44	28	33	36	42	33
Ni	4	4	7	2	4	17
Rb/Sr	0.057	0.046	0.107	0.096	0.102	0.008
K/Rb	443	547	237	257	259	581
K/Sr	25.30	25.08	25.45	24.66	26.28	4.76

Notes: FeO arbitrarily calculated as 0.85 total Fe.Analyses quoted normalised anhydrous , H_2O^+ value is the pre-normalisation ignition loss.Rock localities and mineralogies are given in appendix 1.CIPW norms are given in appendix 2.Samples S10 and S11 a e basaltic andesites, S26,15 and S7 are hornblende andesites and S12 is a hornblende gabbro (cumulate ?) xenolith-.

TABLE 6.4

EAST SUNDA ARC VOLCANIC ROCKS

G.SOROMUNDI - SUMBAWA ISLAND,LEUCITE-BEARING LAVAS

Sample#	Si17	Si16	Si6	Si13	Si11	Si14	Si10	Si12	Si15	Si3	Si1	Si9	Si18
SiO_2	45.48	44.89	46.94	47.31	47.55	45.05	47.01	47.49	49.52	50.04	49.22	49.24	39.25
TiO_2	0.97	0.98	0.93	0.94	0.90	1.02	0.91	0.93	0.83	0.92	0.81	0.84	1.40
Al_2O_3	11.84	11.82	13.47	13.94	15.82	14.81	15.61	16.03	16.64	17.38	17.55	17.68	8.31
Fe_2O_3	1.82	1.87	1.72	1.72	1.73	1.87	1.74	1.80	1.50	1.58	1.55	1.52	3.06
FeO	9.26	9.54	8.75	8.77	8.82	9.53	8.86	9.17	7.67	8.08	7.89	7.76	15.57
MnO	0.18	0.19	0.20	0.10	0.21	0.23	0.21	0.22	0.21	0.20	0.20	0.22	0.33
MgO	10.49	10.47	8.46	7.25	6.20	6.06	6.58	5.66	4.17	4.00	3.93	3.38	10.04
CaO	14.10	14.28	13.11	13.13	11.17	13.18	12.01	12.07	10.14	9.80	9.76	10.05	18.70
Na_2O	2.21	2.33	2.70	3.20	3.75	2.98	3.37	2.86	4.33	4.00	4.83	4.68	0.84
K_2O	3.16	3.07	3.29	3.20	3.41	4.48	3.28	3.32	4.47	3.52	3.80	4.00	0.66
P_2O_5	0.50	0.56	0.42	0.43	0.44	0.79	0.43	0.46	0.52	0.49	0.46	0.62	1.82
H_2O+	1.95	1.67	1.16	1.32	1.27	1.84	1.59	2.15	2.06	1.81	1.32	1.33	2.18
Mg/Mg+Fe	0.63	0.62	0.59	0.56	0.52	0.49	0.53	0.48	0.45	0.43	0.43	0.40	0.49
Mg/Mg+.85Fe	0.67	0.66	0.63	0.60	0.56	0.53	0.57	0.52	0.49	0.47	0.47	0.44	0.53
K_2O/Na_2O	1.43	1.32	1.22	1.00	0.91	1.50	0.97	1.16	1.03	0.88	0.79	0.85	0.79
Trace elements (ppm)													
Rb	168	194	102	133	104	297	99	114	142	166	102	144	5
Sr	959	1027	1150	1154	1587	1490	1479	1511	1707	1466	1579	2401	504
Zr	97	111	117	97	107	177	128	127	137	122	121	119	120
Nb	5	8	9	9	11	13	9	10	12	8	13	15	5
Y	17	15	22	20	20	27	22	27	32	20		23	50
La								79				99	
Sc	45	44	36	35	28	30	29	31	22	18	18	16	58
Cr	277	221	239	213	89	69	119	123	61	53	55	39	122
Ni	54	47	28	24	16	14	18	18	10	8	8	4	24
Rb/Sr	0.175	0.189	0.089	0.115	0.066	0.199	0.067	0.075	0.083	0.113	0.065	0.060	0.010
K/Rb	156	131	268	200	272	125	275	242	261	176	309	231	1096
K/Sr	27.36	24.82	23.75	23.02	17.84	24.96	18.41	18.24	21.74	19.93	19.98	13.83	10.87

Notes: FeO arbitrarily calculated as 0.85 total Fe.Analyses quoted as normalised anhydrous.The H_2O^+ value is the pre-normalisation ignition loss.Rock localities and mineralogies are given in appendix 1 and CIPW norms in appendix 2. Petrographic descriptions are also given in table 6.7.Samples represent the following rock-types: Si17 and Si16 - madupite,Si6,13,11 and Si12 - leucite lamproite/leucite tephrite,Si14 - leucitite, Si15,3,1 and Si9 - leucite tephrite. Si18 is an hornblende-apatite clinopyroxenite (cumulate ?) xenolith .

TABLE 6.5

G. Sangenges, Lavas & Xenoliths: Modal Composition

A. LAVAS

Sample No.	Cpx	Ol	Amph	Biot	Ti-Mag	Leucite	Plag	Apat	G-Mass
S23	25.5	5.2			0.3				69
S21	39.5	2[2]			3.5	12[3]		0.1	43
S17	31.2	1[1]			4	8.5[3]	0.2		55
S3	51	3			2				44
S5	17	1.4[1]			2.5		30	0.1	49
S7	3.5		6		1.5		33.5		55.5

B. XENOLITH

S12	22		18.5		9		50	0.5	

[1] olivine partly carbonated

[2] olivine partly iddingsitized

[3] leucite microphenocrysts

Rock types: Group A: S23, S21, S17 - Olivine leucitite
S3 ankaramitic leucitite

Group B: S5 potassic ne-trachybasalt (shoshonite)

Group C: S7 hornblende andesite (calcalkaline suite).

the potassium *ne*-trachybasalts and trachyandesites from Tambora and Sangeang Api volcano (≈ "shoshonites") and chemical analyses of representative examples are given in table 6.2 (samples S8, S16, S5, S28, S1).

C. A group of *Q*-normative lavas with large phenocrysts set in very fine-grained or glassy, silica-rich groundmasses. They are often hornblende-, or hypersthene-bearing. These lavas represent members of a calcalkaline series and are similar to some andesites or dacites from Rindjani volcano. Chemical analyses of representative members of this group are given in table 6.3 (samples S10, S11, S15, S7).

The lavas from G. Soromundi all contain modal feldspathoid (leucite ± nepheline) and in this respect are related to the group A lavas from G. Sangenges. They are further related by their geochemical similarities (section 6.4), in particular, their low SiO_2, high K_2O and high K_2O/Na_2O ratios, but differ in more detailed characteristics. The Soromundi lavas contain phenocrysts of phlogopite and amphibole, absent from the G. Sangenges' series A lavas. Some Soromundi lavas contain abundant normative *ne*, but no normative *lc* (Sil1, 12, 15, 5, 1 and 9; table 6.4, norms, appendix 2).

6.2 Petrology of Highly Undersaturated Lavas from G. Sangenges (Group A Lavas) and G. Soromundi.

Previous work on these two volcanoes is very restricted. Hunderwadel (1921) gave very brief descriptions of some lavas from G. Sangenges, referring to olivine-bearing basalts and pyroxene and hornblende andesites and dacites of the calcalkaline series, as well as briefly alluding to the existence of more alkaline varieties.

Leucite-bearing lavas from Soromundi were described by Brouwer (1943), who compared these with similar leucitic lavas from the island of Batoe Tara in the Banda Sea, north of the Flores (Brouwer, 1938).

TABLE 6.6

Soromundi Lavas and Xenolith: Modal Compositions

A. LAVAS

Sample No.	Cpx	Ol	Amph	Phl/Biot	Reac Phl/Biot	Mag	Leucite	Plag	Apat	G-Mass
Si17	40				9	1	1			49
Si13	38	4		1		3.5	1			52.5
Si14	35					4	15			46
Si12	21.5		2.1	5		3.8			0.2	67.4
Si15	27					4.5	21	7.5		40
Si9	25			tr		3.4	4.5	15.6	tr	51.5

B. XENOLITH

Sample No.	Cpx	Amph	Biot	Mag	Plag	Apat
Si18	55	31	0.2	6.6	0.2	7

Rock types: Si17 - madupite, Si13, Si12 - leucite lamproite, Si14 - leucitite, Si15, Si9 - leucite tephrite
Si18 - alkali pyroxenite

These highly undersaturated lavas are all characterised by the presence of leucite either as phenocrysts, microphenocrysts or groundmass grains. They all contain abundant very Ca-rich clinopyroxene, both as phenocrysts and in the groundmass. However they show considerable variation in their other phenocryst and groundmass minerals. They may variously contain phenocrystic olivine, phlogopite, amphibole and plagioclase, and groundmass plagioclase, nepheline and olivine.

These highly undersaturated lavas are named according to the definitions listed in the glossary of Sorensen (1974, p. 559). The less differentiated lavas are olivine leucitites (olivine + leucite + augite with feldspar lacking), leucitites (as for olivine leucitite, but without olivine), leucite lamproites (leucitites with amphibole and/or phlogopite) or madupites (Cross, 1897; Carmichael, 1967) (phenocrysts of diopside and phlogopite). The more differentiated lavas show transition towards leucite tephrite or leucite basanite with the appearance of plagioclase.

1. The *lc*-normative lavas of G. Sangenges (group A).

Chemical analyses of members of this group (S23, S22, S21, S17, S9A, S9B and S19) are given in table 6.1. Petrological summaries are given in table 6.7, while modal analyses of representative examples are given in table 6.5.

Lavas within this general group differ from one another largely in their relative proportion of phenocrysts or megacrysts of olivine and clinopyroxene and in the presence or absence of groundmass feldspar. S23 and S22, for example, are porphyritic, with abundant (>30%) large olivine and clinopyroxene phenocrysts. On the other hand, S9A, S9B and S19 are nearly aphyric with <5% olivine and clinopyroxene phenocrysts. Rocks S21, S17, S9A and S9B have significant proportions of feldspar in their groundmasses, but S19 is entirely feldspar-free.

Table 6.7 Summary of the Petrology of Highly Undersaturated Lavas from G. Sangenges and G. Soromundi

Sample No.	Phenocrysts	Microphenocrysts	Groundmass	Mg/Mg + Σ Fe	Comments	Rock Type
A. Gunung Sangenges group A lavas						
S3	cpx, ol	mag.	cpx, le, ne, mag, ol, ap.	0.68	very abundant ol and cpx phenocrysts/megacrysts, rare g.mass f.spar	olivine leucitite
S23	cpx, ol	cpx, ol	cpx, le, ne, mag, ol, ap, f.spar	0.66	g.mass f.spar (oligoclase, andesine and sanidine) rare	olivine leucitite
S21	cpx, mag	ol, le	le, cpx, ol, mag, ap, ne ?	0.59	olivine microphenocrysts iddingsitized	olivine leucitite
S22	cpx, ol	mag, le	le, cpx, ol, mag, ap, ne ?	0.57		olivine leucitite
S19	cpx, ol		cpx, le, ne, mag, ol, ap	0.56	nearly aphyric, ol resorbed, no mag phenocryst, no f.spar	leucitite - olivine leucitite
S17	cpx, mag	cpx, ol	cpx, le, mag, f.spar, ap	0.55	v. rare ol (carbonated), g.mass plag and san., reacted plag. xenocrysts	leucitite - leucite tephrite
S9	cpx, (ol)		cpx, le, ol, ne, plag, san, ap, mag	0.52		
B. Gunung Soromundi lavas						
Si17	cpx, phl		cpx, mag, le, ne, ap	0.65	large megacrysts of cpx, phl. oxide-rich g.mass	madupite
Si16	cpx, phl		cpx, mag, le, ne, ap	0.64	large megacrysts of cpx, phl. oxide-rich g.mass	madupite
Si6	cpx, phl, ol	ol	cpx, le, mag, f.spar, ap	0.61	ol partly iddingsitized, rare g.mass f.spar	leucite lamproite - leucite tephrite
Si13	cpx, (ol), phl	le, mag	cpx, le, ol, mag, f.spar, ap, ne ?	0.57	ol megacryst reacting to cpx, g.mass san and andesine	leucite lamproite - leucite tephrite
Si11	cpx, amph, phl, mag	ap, mag	cpx, le, ne, plag, san, ap, mag	0.54	significant plag and san. in g.mass, microphenocrysts of ap	leucite lamproite - leucite tephrite
Si14	cpx, le	le, ne	cpx, le, ne, mag, plag, san, ap	0.51	very abundant le, ne microphenocrysts, very rare g.mass f.spar	leucitite
Si12	cpx, amph, phl, mag	plag	cpx, le, ne, mag, plag, san, ap	0.05	microphenocrysts of plag (andesine-labradorite)	leucite lamproite - leucite tephrite
Si15	cpx, le	le	cpx, le, ne, plag, san, mag, ap	0.47	relatively abundant groundmass f.spar	leucite tephrite
Si3	cpx, le	le	cpx, le, ne, plag, san, mag, ap	0.45	relatively abundant groundmass f.spar	leucite tephrite
Si1	cpx, le	le	cpx, le, ne, plag, san, mag, ap	0.45	relatively abundant groundmass f.spar	leucite tephrite
Si9	cpx, plag, phl		cpx, le, mag, f,spar, ap	0.41	phenocrysts of plag (labradorite), g.mass v. le-rich	leucite tephrite

Abbreviations: cpx - clinopyroxene; ol - olivine; mag - magnetite; le - leucite; ne - nepheline; plag- plagioclase; f.spar - feldspar; san - sanidine; phl - phlogopite; amph - amphibole; ap - apatite; g.mass - groundmass

The lavas are characterised by phenocrysts of clinopyroxene (table 6.8) and less abundant olivine (table 6.9), set in a fine-grained groundmass of leucite, clinopyroxene, magnetite, generally olivine, sometimes nepheline and sometimes plagioclase (oligoclase-andesine) and sanidine.

Leucite (table 6.10) often occurs as microphenocrysts (e.g. S22, S21), but is always smaller and later than the clinopyroxene and olivine phenocrysts. Magnetite also appears as microphenocrysts, though is generally rare in this role and often is completely absent (e.g. S23, S19).

Large olivine phenocrysts (0.5-1.5cm) are often highly embayed and may have prominent iddingsite rims. Core compositions (table 6.9) are fairly magnesian (Fo 87 - Fo 89). Some are deuterically replaced by carbonate, apparently during the ascent and eruption of the magma, as the rocks are otherwise fresh. Smaller microphenocrysts of olivine are often euhedral and may also be iddingsitized. Small groundmass olivine grains are generally fresh and relatively iron-rich (Fo 55 - Fo 60).

In some instances olivine is rimmed by clinopyroxene apparently the result of a reaction relationship between the liquid and olivine (cf. Schairer and Yoder, 1960). Olivine may also occur as inclusions within large clinopyroxene megacrysts.

The general impression is that olivine has been stable at some early stage in the evolution of these lavas, but has undergone degradation and reaction as they approached the surface, during eruption.

Clinopyroxene is the most prominent phenocryst phase and is also abundant in the groundmasses. Some phenocrysts (megacrysts) are very large (up to 2.5 cm long) and these are often prominently zoned. Cores (table 6.8) are pale coloured, diopsidic (ca 47.5 Mg 47.5 Fe 5, 100 Mg/Mg+Fe = 90), with high Cr concentrations and low Ti and Al. These are mantled by darker green rims (table 6.8) of more Al-, Ti-rich, Cr-poor augite/salite composition (Ca 48.2, Mg 38.2, Fe 13.6, 100 Mg/Mg+Fe = 74).

Table 6.8

Representative Analyses of Clinopyroxenes

from Sumbawan Leucititic Lavas

Analysis No.	1	2	3	4	5	6
	M	M	P-C	P-R	G	
SiO_2	52.6	52.7	46.4	47.8	48.2	50.5
Al_2O_3	1.5	1.8	8.3	6.8	6.2	3.9
FeO	3.3	5.0	8.6	9.2	8.3	5.9
MgO	17.4	16.2	11.8	11.4	13.1	14.7
CaO	24.1	23.4	23.3	23.6	22.9	23.7
Na_2O	-	-	-	-	-	-
TiO_2	0.4	0.4	1.4	1.0	1.1	0.8
Cr_2O_3	0.7	0.5	-	-	-	0.3
MnO	-	-	-	-	-	-
Total	100.0	100.0	99.8	99.8	99.8	99.8
	Number of Ions on the Basis of 6 oxygens					
Si	1.927	1.938	1.747	1.803	1.807	1.874
Al^{IV}	0.065	0.062	0.253	0.197	0.193	0.126
Al^{VI}	-	0.016	0.116	0.105	0.081	0.045
Fe	0.101	0.154	0.271	0.290	0.260	0.183
Mg	0.950	0.888	0.662	0.641	0.732	0.813
Ca	0.946	0.922	0.940	0.954	0.920	0.942
Na	-	-	-	-	-	-
Ti	0.011	0.011	0.040	0.028	0.031	0.022
Cr	0.020	0.014	-	-	-	0.009
Mn	-	-	-	-	-	-
Total	4.019	4.005	4.029	4.018	4.025	4.014
100Mg/Mg+Fe	90.3	85.2	70.9	68.8	73.8	81.6
Ca/Ca+Mg	0.499	0.509	0.587	0.598	0.557	0.537
Ca	47.4	46.9	50.2	50.6	48.1	48.6
Mg	47.6	45.2	35.4	34.0	38.3	41.9
Fe	5.0	8.9	14.4	15.4	13.6	9.5

Notes: Analyses 1 and 2 are typical of those of large megacrysts occurring in Soromundi and G. Sangenges leucite-bearing lavas. Analyses 3 and 4 are typical of phenocryst compositions from these same lavas and cpx ol. This same composition may rim the megacrysts. Analysis 6 is of a cpx-reaction rim around olivine (anal. 1, table 6.9) from Soromundi lava Si13.

Abbreviations: M - megacryst, P - phenocryst, C - core, R - rim, G - groundmass

This type of clinopyroxene zonation has been observed in a number of lavas from the suites described in this thesis. These include the ankaramites from Lombok (LB8) and the Sangeang Api potassic *ne*-trachybasalts and phonolitic tephrites (e.g. B43) and in the pyroxene of some clinopyroxenite xenoliths (e.g. B5, B22) from Sangeang Api.

Central cores are sometimes resorbed or corroded, with corrosion pits filled by glass or finely crystalline groundmass material. Smaller, euhedral phenocrysts and microphenocrysts have salite compositions similar to those of the outer zones of the larger megacrysts. They sometimes show hour-glass structure. Groundmass clinopyroxene has very low silica and high Al and Ti content (table 6.8) and is of Ca-rich salite composition (Ca 50 Mg 35.5 Fe 14.5 100 Mg/Mg+Fe = 71).

Leucite (table 6.10) occurs as small euhedral, icositetrahedral phenocrysts in a number of lavas (e.g. S22, S21). These show characteristic twinning on {110} and very weak, low 1st order birefringence. All other lavas contain abundant, isotropic, anhedral, often sphericle, groundmass leucite.

Compositionally, leucite is stoichiometric, with no substitution of Na (table 6.10), contains small amounts of Ca and little or no iron (cf. iron-rich leucites described by Carmichael, (1967) from a number of potassium-rich lavas, including those of Leucite Hills).

Feldspar (table 6.10) occurs (with clinopyroxene and olivine) in the groundmasses of some of the more differentiated lavas (e.g. S9A), generally as fine laths, needles or small tabular grains, interstitial to the leucite and comprise plagioclase (oligoclase-andesine) and sanidine. This suggests a transition from olivine leucitite towards leucite tephrite or leucite basanite.

Nepheline occurs as fine interstitial grains in the groundmass of many lavas of this group. Apatite also occurs in the groundmass as a ubiquitous accessory.

One lava (S17) contains large, subhedral phenocrysts (xenocrysts?) of bytownite plagioclase which is undergoing reaction to yield a uniaxial mineral of moderately high relief, tentatively identified as a member of the gehlenite-melilite-akermanite series.(?)

In summary, the highly undersaturated lavas of G. Sangenges are olivine leucitites and leucitites with phenocrysts of clinopyroxene and olivine. Leucite is a ubiquitous microphenocryst/groundmass phase. The lavas show transition towards leucite tephrite or leucite basanite with appearance of plagioclase and sanidine in the groundmass.

Lava S3 (tables 6.1 and 6.5), does not contain normative leucite. However it may be a variant of the *lc*-normative lavas S23 and S22, with extremely abundant olivine and clinopyroxene, probably of accumulative origin.

2. Highly Undersaturated potassium-rich lavas from G. Soromundi.

The petrographic characteristics of this group (samples Si17, Si16, Si13, Si14, Si10, Si11, Si12, Si15, Si3, Si1 and Si9) are summarised in table 6.7. Their chemical analyses are given in table 6.4 and model analyses of representative examples in table 6.6.

These lavas show geochemical similarities to the group discussed in the previous section, from G. Sangenges. At the same time they differ in some important geochemical and petrographic characteristics. In contrast to the undersaturated lavas from G. Sangenges olivine is a rare or absent phenocryst phase, while amphibole and/or phlogopite occur frequently.

The Soromundi lavas are porphyritic with clinopyroxene as their major phenocryst phase and with abundant groundmass clinopyroxene and leucite.

Phenocryst assemblages include: cpx + phlogopite, cpx + phlogopite + olivine, cpx + amphibole + phlogopite + magnetite, cpx + leucite, cpx + plagioclase + phlogopite.

The leucite-bearing lavas from Soromundi include more differentiated examples than those sampled from the G. Sangenges suite (with some lavas having Mg/Mg+Fe values <0.50). These contain significant groundmass feldspar (oligoclase-andesine and sanidine) and some (e.g. Si12, Si9) also contain phenocrysts or microphenocrysts of bytownite (table 6.10).

The most mafic lavas (e.g. Si17, Si16) are spectacular, with a phenocryst assemblage of clinopyroxene and phlogopite, set in a fine groundmass of leucite, nepheline, magnetite, olivine, apatite and clinopyroxene. These bear a marked resemblance to the madupites described by Cross (1897) and Carmichael (1967) from Leucite Hills, Wyoming.

The phenocrysts of clinopyroxene and phlogopite are very large (up to 3cm). The clinopyroxene is zoned in the same way as that from the G. Sangenges lavas, with a pale green diopsidic cone (Ca 47.5, Mg 47.5, Fe 5, 100 Mg/Mg+Fe = 90 to Ca 47, Mg 45, Fe 8, 100 Mg/Mg+Fe = 85; table 6.8) and a darker green outer zone of a Ca-rich augite-salite composition (Ca 48.6, Mg 42, Fe 9.4, 100 Mg/Mg+Fe = 81.6; table 6.8). Smaller phenocrysts are more Al- and Ti-rich (Cr-diopside cores have very low Al and Ti contents, averaging about 1.4% Al_2O_3 and 0.3 - 0.4% TiO_2. The outer rims of phenocrysts and groundmass clinopyroxene may have up to 8.0% Al_2O_3 and 1.4% TiO_2; see table 6.8) and groundmass clinopyroxene even more so (table 6.8).

In many rocks (e.g. Si16, Si17), very large phlogopite megacrysts are often almost entirely pseudomorphed, and replaced by fine mosaics of magnetite leucite and clinopyroxene. However, a few lavas do contain fresh phlogopite (e.g. Si13). In this example, phlogopite occurs both as individual phenocryst and as inclusions in olivine and clinopyroxene. Typical analyses are given in table 6.12. The phlogopite included in olivine is slightly more magnesian

Table 6.9

Representative Analyses of Olivine

from Sumbawan Leucititic Lavas

	1	2	3
	M	M	G
SiO_2	38.7	39.6	34.6
FeO	10.6	11.1	36.0
MgO	49.3	48.0	26.3
CaO	0.3	0.6	0.7
TiO_2	0.1	0.1	0.2
MnO	-	-	2.0
Total'			
	Number of Ions on the Basis of 4 oxygens		
Si	0.966	0.985	0.980
Fe	0.221	0.231	0.853
Mg	1.834	1.779	1.110
Ca	0.008	0.016	0.021
Ti	0.002	0.002	0.004
Mn	-	-	0.048
Total	3.031	3.013	3.016
100Mg/Mg+Fe	89.2	88.5	56.6

Abbreviations: M - megacryst, G - groundmass.

Notes: Olivine No. 1 from Soromundi lava Si13 is rimmed by cpx, (anal. 6, table 6.8).

(100Mg/Mg+Fe = 79.45) than the phlogopite phenocrysts (100Mg/Mg+Fe = 77.72) and is markedly more Ti-rich (4.6% TiO_2 compared with 3.8 - 2.9% TiO_2 in the phenocrysts).

Only two lavas contain olivine in their phenocryst/megacryst assemblages (Si6, Si13). In both these cases, the olivine is resorbed or embayed and often partly iddingsitized. They are magnesian and range from Fo 88.5 to Fo 89.2 (table 6.9). That of Si13 is mantled by a reaction rim of clinopyroxene (100Mg/Mg+Fe = 81.68, Ca 48.6, Mg 42, Fe 9.4; table 6.8). Many of the lavas however do contain groundmass olivine with a composition of Fo 55 - Fo 60 (table 6.9).

Amphibole is an important phenocryst phase in a number of these lavas and like phlogopite, is often surrounded by a magnetite-rich reaction-rim. No microprobe analyses of this phase are available, but it is optically very similar to pargasitic hornblende analysed from the Sangeang Api xenoliths (optically +ve, large $2V \simeq 80^{o}$, extinction angle $\gamma:Z \simeq 25^{o}$, with pleochroic scheme: α pale brown, β straw coloured, and γ more greenish or darker brown. Some examples are apparently partly oxidised and in this case, the pleochroic scheme takes on a more reddish hue.

All lavas contain leucite, either as subhedral or euhedral icositetrahedra with characteristic multiple twin lamellae, showing slight, low 1st order birefringence, or as anhedral, isotropic groundmass grains. Analyses are given in table 6.10. They are stoichiometric, with no detectable Na-substitution small amounts of Ca and very minor Fe substitution. Nepheline is a significant groundmass phase and in a few lavas (Si14), also occurs as small euhedral, hexagonal microphenocrysts.

Magnetite is a common microphenocrystic constituent and is very abundant in the groundmass of all lavas, containing 20-30 mol.% ulvospinel.

Apatite is a ubiquitous groundmass mineral and also occurs as a minor microphenocryst phase in some lavas (e.g. Si11).

Table 6.10

Representative Analyses of Groundmass Leucite and Alkali Feldspar from Sumbawan Leucitite Lavas

	1	2		3
	G	G		G
SiO_2	53.9	52.43	SiO_2	61.5
Al_2O_3	22.6	21.7	Al_2O_3	23.9
FeO	-	0.2	FeO	0.5
CaO	1.3	1.2	CaO	2.7
K_2O	22.2	24.4	Na_2O	7.0
Total			K_2O	4.0
			Total	
	Number of Ions on the basis of 6 oxygens			Ions on 8 oxygen basis
Si	1.980	1.963	Si	2.765
Al	0.979	0.958	Al	1.267
Fe	-	0.006	Fe	0.019
Ca	0.051	0.048	Ca	0.130
K	1.041	1.166	Na	0.610
Total	4.050	4.140	K	0.229
			Total	5.020
			An	13.4
		mol%.	Ab	62.9
			Or	23.7

Notes: Analyses 1 and 2 are typical groundmass leucite, Analysis 3 is of typical groundmass alkali feldspar. Some Soromundi and G. Sangenges leucitites also contain phenocrysts of plagioclase (An90-An70) and groundmass plagioclase (An60-An40).

Abbreviation: G - groundmass.

Table 6.12

Analyses of Phlogopite from Soromundi Lavas

	1	2	3
	I	P	P
SiO_2	35.0	36.3	35.2
Al_2O_3	16.7	15.9	16.9
FeO	8.7	10.1	11.8
MgO	18.9	19.3	17.2
CaO	0.4	0.5	0.5
Na_2O	-	-	-
K_2O	10.8	10.4	10.0
TiO_2	4.6	2.9	3.8
Total	95.1	95.4	95.4
	Number of Ions on the basis of 22 oxygens		
Si	5.160	5.343	5.217
Al	2.902	2.759	2.953
Fe	1.073	1.243	1.463
Mg	4.153	4.234	3.799
Ca	0.063	0.079	0.079
Na	-	-	-
K	2.032	1.953	1.891
Ti	0.510	0.321	0.424
Total	15.893	15.932	15.827
100Mg/Mg+Fe	79.5	77.3	72.2

Abbreviations: I - inclusion in olivine,
P - phenocryst

6.3 Petrology of the less Alkaline Suites from G. Sangenges.

As already discussed, G. Sangenges is a volcano that became inactive in the Quaternary and its cone has become heavily dissected. Samples taken largely from boulder streams and young, actively eroding rivulets, high on the slopes of the remnant volcanic cone (now heavily vegetated), included not only members of the *lc*-normative suite (Group A) already described, but also less alkaline *ne*-trachybasalts (Group B) like those already described from Tambora and Sangeang Api and *Q*-normative calcalkaline andesites (Group C) like those from Rindjani. While it is not possible to determine the actual temporal eruptive sequence of these three very different suites, the fact that they are all being shed from high on the eroding cone of G. Sangenges, does suggest that this volcano must have erupted each of these three suites sometime during its period of activity.

1. Petrology of potassic *ne*-trachybasalts (Group B)

The *ne*-normative trachybasalts from G. Sangenges (samples S8, S16, S5, S28, modal analysis of S5 given in table 6.5 and geochemical analyses given in table 6.2), like members of this group from Sangeang Api and Tambora, are porphyritic lavas with large phenocrysts of cpx (augite), less abundant olivine and microphenocrysts of magnetite. Plagioclase is the most abundant phenocryst, though is generally smaller and possibly later than cpx and olivine (some cpx and olivine is included in plagioclase). It occurs as zoned tabular grains, some with the familiar, inclusion-rich, corroded, calcic-bytownite-anorthite cores and zoned out to rims of labradorite-andesine composition. Outermost rims are mantled by sanidine. The phenocrysts are set in groundmasses which may be relatively coarse-grained, comprising mainly plagioclase, with cpx, magnetite and olivine, set in a K-feldspar matrix.

Apatite is a relatively common accessory, both as microphenocrysts and in the groundmass.

2. Petrology of the Andesites (Group C).

The *Q*-normative (Group C) suite from G. Sangenges has geochemical and petrographic affinities with the Rindjani calcalkaline suite. Samples representing this suite are S10, S11, S15 and S7 (see table 6.3, which presents whole-rock analyses, and table 6.5, that gives a representative modal analysis).

They are porphyritic, plagioclase-rich lavas, which do not contain olivine. Plagioclase is the largest and most abundant phenocryst phase. It is complexly zoned, with cores of labradorite-bytownite, zoning out to rims of andesine.

These andesites contain clinopyroxene phenocrysts and commonly amphibole and/or orthopyroxene (hypersthene). Microphenocrysts of magnetite are also common.

The phenocrysts are set in a very fine-grained groundmass, largely composed of plagioclase laths (oligoclase-andesine), which are themselves set in a matrix of brown glass.

6.4 Geochemistry of the Lavas from Soromundi and G. Sangenges.

Both these suites, as described in the preceding sections, are characterised by the presence of highly distinctive, feldspathoid-rich lavas, quite unlike the lavas typical of most island arcs. These are not only petrographically unusual, but are also geochemically extreme. Lavas sampled from the eroded cone of G. Sangenges also contain members of two other recognisably distinct series, one characterised by the presence of olivine and plagioclase phenocrysts and groundmass alkali feldspar and the other, still more plagiophyric, without olivine and commonly with hornblende phenocrysts.

Although the feldspathoid-bearing lavas from both Soromundi and G. Sangenges are related in their leucite-bearing character, the two series are otherwise petrographically distinct and some differences are also apparent in their geochemical characteristics.

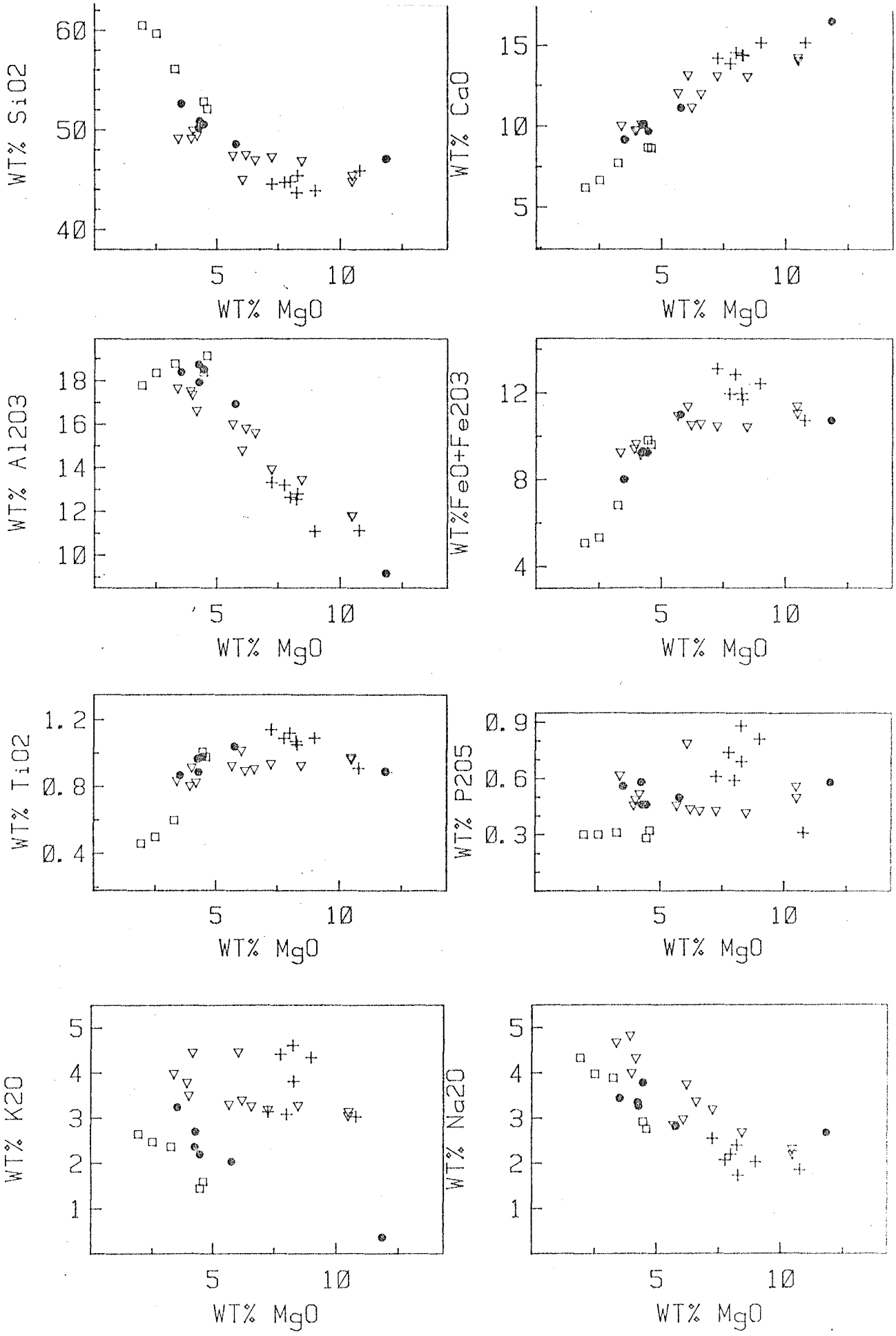

Figure 6.1

MgO v. Major Element variation amongst lavas from G.Sangenges and Soromundi Volcanoes Sumbawa. The symbols represent the following groups of lavas: ▽-Soromundi Lavas, + - G.Sangenges,leucite-bearing series, ● - G.Sangenges, ne-trachybasalt series, □ -G.Sangenges,Q-normative,calcalkaline series.

FIGURE 6.2

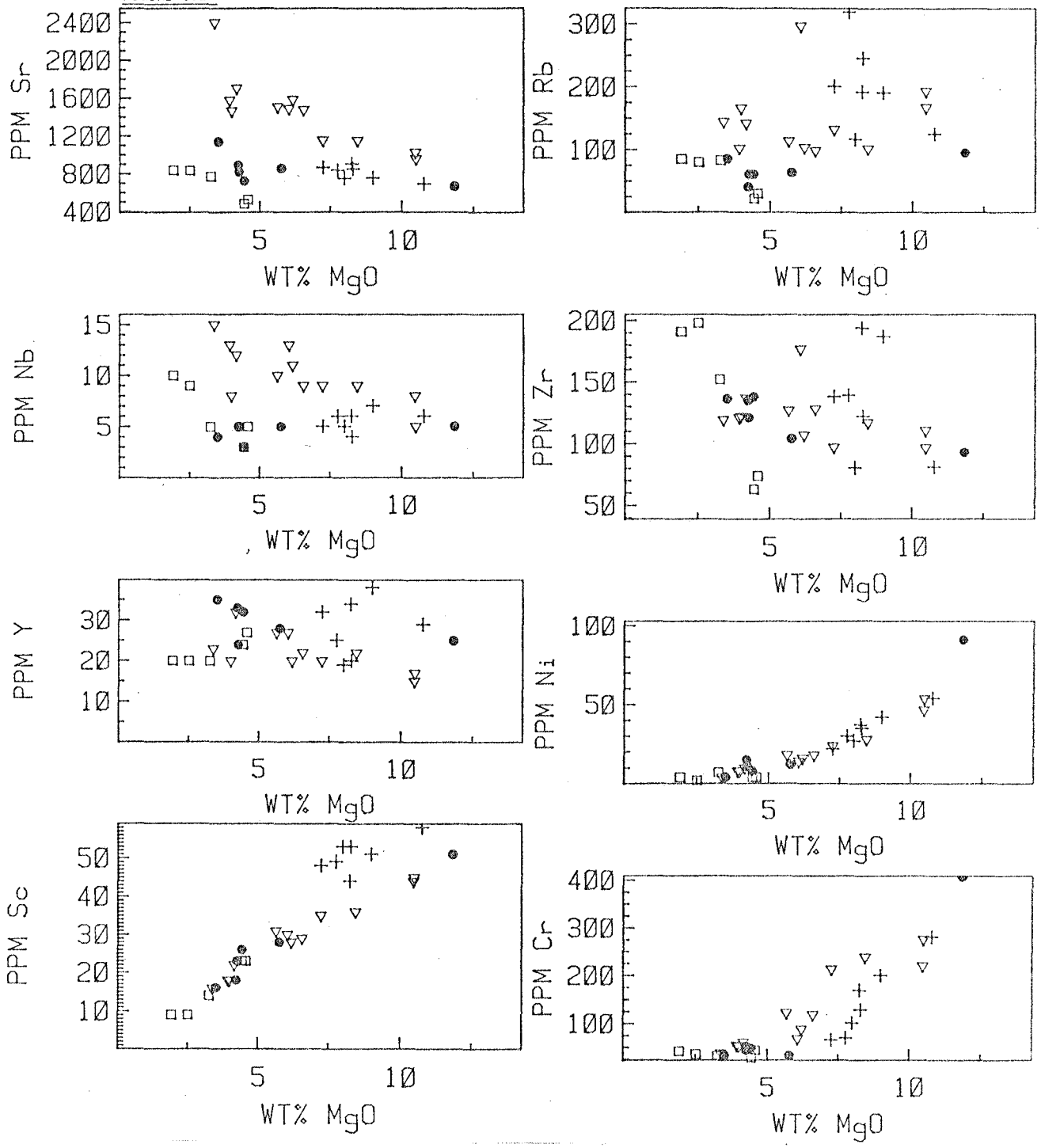

Figure 6.2

MgO v. Trace Element variation of Soromudi and G.Sangenges lavas. The sample-groups represented by the different symbols are the same as figure 6.1.

1. Soromundi Lavas.

Major- and trace-element whole-rock analyses of this group of lavas are given in table 6.4, while their compositional variations are displayed as MgO-variation diagrams in figures 6.1 and 6.2.

All lavas are highly undersaturated with 10-18% normative *ne* and most also contain normative *lc* (up to 20%).

All lavas are silica-poor (45-51% SiO_2) and many are relatively mafic with up to 10.5% MgO and Mg/Mg+ΣFe values of up to 0.65. They range with increasing silica to relatively low MgO varieties (down to 3.38% MgO) with a Mg/Mg+ΣFe value of 0.41. Lavas with lower MgO concentration (e.g. Si3, Si1, Si9; tables 6.4 and 6.6) are relatively aluminous and contain phenocrysts of plagioclase. Normative *lc* is absent from lavas with <6.0% MgO, though they still contain leucite as microphenocrysts or in their groundmasses.

High MgO lavas have low Al_2O_3 (those with >10% MgO have <12% Al_2O_3) and Al_2O_3 increases with decreasing MgO to ca. 17.6% in the least magnesian members of the suite.

The most mafic lavas are very calcium-rich (14% CaO) and there is a positive correlation between CaO and MgO (figure 6.1). Sc, Cr and Ni also show positive correlation with MgO. CaO shows a good positive correlation with Sc, the most mafic lavas having very high Sc concentrations (45ppm) (figure 6.3). Al_2O_3 also shows a marked negative correlation with CaO (figure 6.4B) and these lavas plot on the same CaO-Al_2O_3 variation trend as the ankaramites from Lombok (figure 6.5). These variations suggest clinopyroxene-control, particularly in view of the positive correlation of CaO, Sc and Cr and the abundance of clinopyroxene phenocrysts.

While the lavas have quite high MgO concentrations, their Ni concentrations are not exceptionally high (<50ppm). In this they seem to contrast with the much less magnesian high-Al basalts from Rindjani (for instance 41632, with 5.63% MgO) which may nevertheless have higher Ni concentrations (e.g. 41632 - 71ppm Ni, 41631 - 77ppm Ni).

FIGURE 6.3

CaO v. Sc variation of Soromundi and G.Sangenges lavas (symbols as in figure 6.1).Illustrating the simultaneous depletion of Ca and Sc sugestive of the effects of CPX crystallisation.

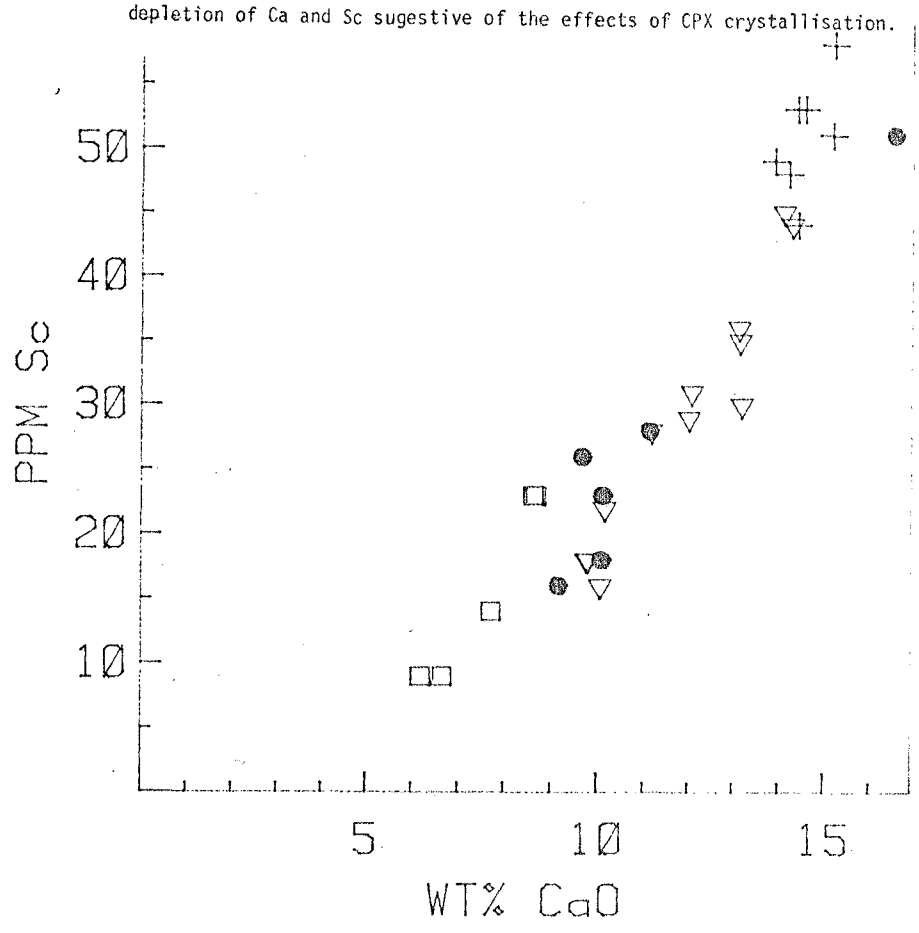

The most mafic lavas from Soromundi (e.g. Si17, Si16) have low Na_2O contents (ca. 2.3%) and Na_2O increases with decreasing MgO to about 4.8%. In contrast the lavas have very high K_2O concentrations (3.07 - 4.48%), which correlate very poorly with MgO. For instance Si3 with 4.0% MgO has 3.52% K_2O, while Si17 with 10.49% MgO has 3.16% K_2O (figure 6.1). The most mafic lavas (e.g. Si17, Si16) have very high K_2O/Na_2O ratios (1.43) and there is a general decrease in this value with decreasing MgO or increasing SiO_2 to about 0.8 (figure 6.6).

The suite is characterised by extremely high Rb concentrations (102-297 ppm). These are 5-15 times higher than concentrations in Rindjani basaltic rocks and 2-4 times higher than in the Tambora or Sangeang Api trachybasalts. Like K_2O, Rb shows rather poor correlation with MgO (figure 6.2) and many of the most mafic lavas are amongst the most Rb-rich. Sr concentrations are also very high (959 - 2401ppm) and this shows quite good negative correlation with MgO, the least mafic lavas having the highest Sr concentrations.

The most mafic lavas have high Rb/Sr ratios (0.18) and there is general trend of decreasing Rb/Sr ratio with decreasing MgO (this trend is quite contrary to that shown by the Rindjani or Tambora Suites) and together with the Al_2O_3-enrichment trend suggest plagioclase-fractionation has not occurred. Similarly the negative correlation of Sr and CaO (figure 6.4A) shown by this suite in contrast to that of the plagiophyric Rindjani and Tambora suites.

The Soromundi lavas have low, but variable K/Rb ratios, ranging from 125 to 309 (figure 6.7). Again the most mafic lavas tend to have the lowest K/Rb ratios.

While the Soromundi lavas have much higher concentrations of Rb, Sr and K_2O than the basaltic lavas of the Rindjani suite, other incompatible trace elements are not similarly enriched. Nb and Zr concentrations in particular are only slightly enriched compared with concentrations in the

FIGURE 6.4 A

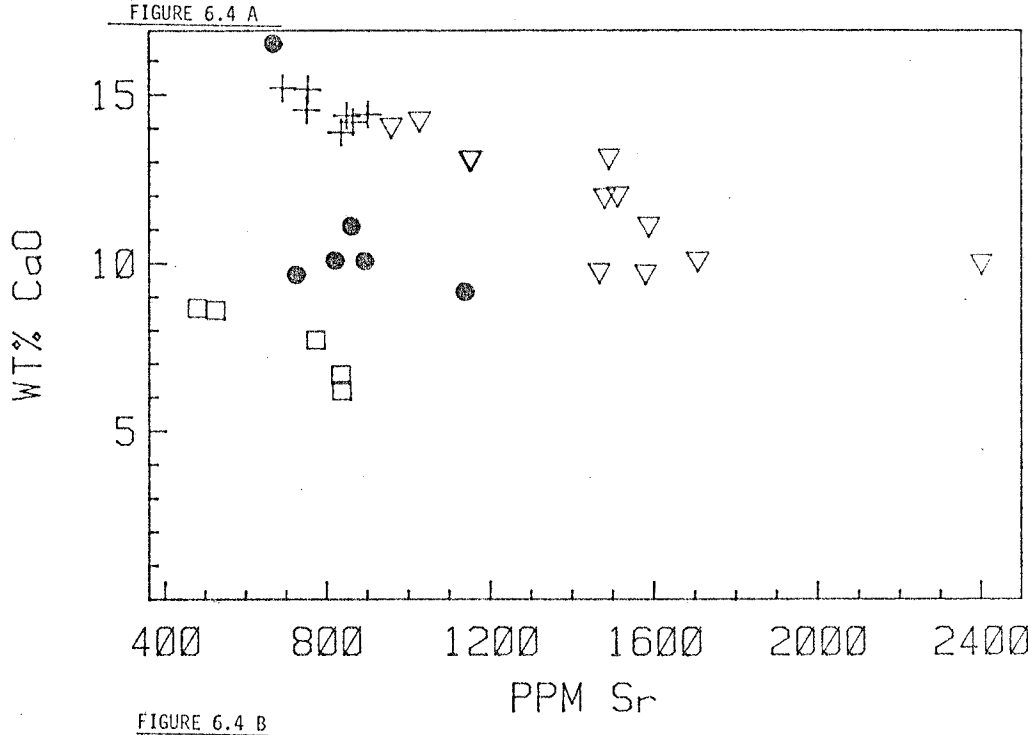

FIGURE 6.4 B

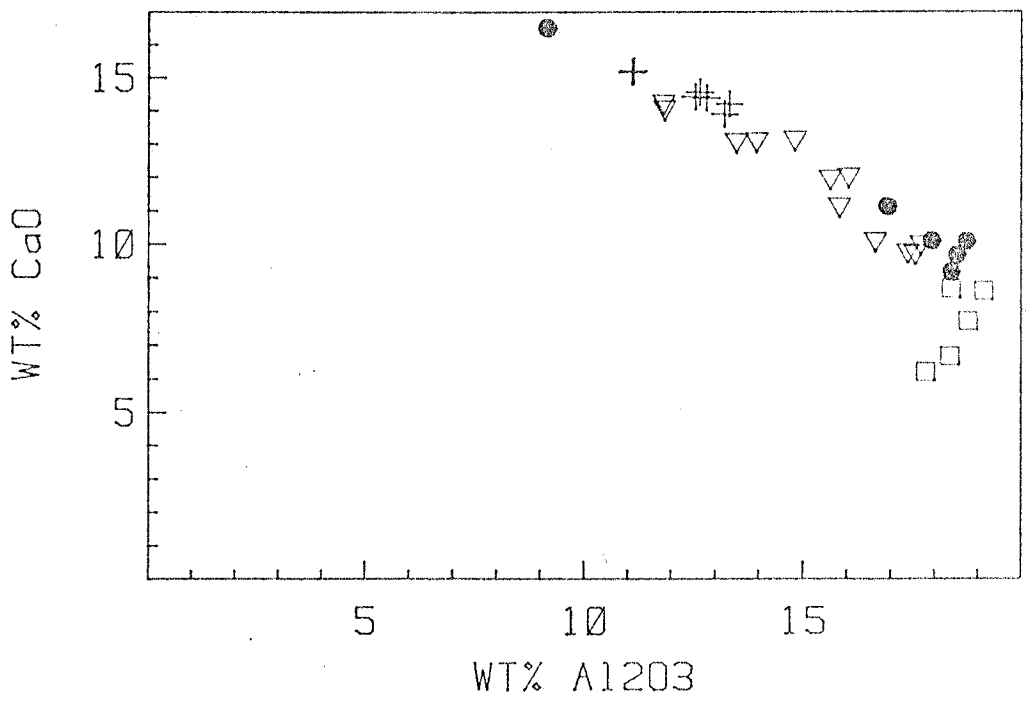

FIGURE 6.4 (upper) A.

Wt.% CaO v. ppm Sr variation of Soromundi and G.Sangenges lavas.Symbols as in figure 6.1.Illustrating the contrasting trends of Ca-depletion/Sr-enrichment shown by the plagioclase -free leucitites (cpx control) and Ca- and Sr-depletion of the plagioclase-bearing lavas.

FIGURE 6.4 (lower) B.

Wt.% CaO v. Wt.% Al_2O_3 variation of Soromundi and G.Sangenges lavas.Symbols as in figure 6.1. Showing a similar pattern to that in figure 6.4 A above.CaO-depletion - Al_2O_3 -enrichment in the Cpx-rich ,plagioclase -free leucitites ,Al_2O_3 variation changing to depletion in the plagioclase -rich lavas (see also figure 6.5)

Rindjani calcalkaline basalts. Both of these elements show reasonably well developed negative correlation with MgO and respectively range from 5 to 15ppm and 97 to 137ppm.

TiO_2 concentrations are similar or slightly lower than those of the Rindjani basalts, averaging about 1.0% and show no significant variation through the suite. Similarly P_2O_5 shows very little variation through the suite, generally falling in the range 0.45 - 0.6%, slightly enriched by comparison with the Rindjani lavas.

Y shows a reasonable negative correlation with MgO and a relatively low concentration in the most-mafic lavas (15ppm).

2. The geochemistry of the feldspathoid-bearing lavas from G. Sangenges.

These lavas are similar to those discussed above, from Soromundi, though as discussed in the preceding petrography section, there are significant contrasts. In particular the Soromundi series contain hydrous phases (phlogopite and amphibole), absent from the G. Sangenges series. Similarly, though the groups resemble one another geochemically, there are certain differences.

Major- and trace-element, whole-rock analyses of the G. Sangenges feldspathoidal series are given in table 6.1 (lavas S22, S21, S17, S19, S9A, S9B and S23) and compositional variations are summarised as MgO-variation diagrams in figures 6.1 and 6.2. All these lavas are highly undersaturated with both *ne* (7.95-11.69%) and *lc* (10.10-21.36%) in the norm (see appendix 1). All the lavas are silica-poor (43.65%-45.88%), Al_2O_3-poor (11.09-13.31%) and are rather mafic. MgO ranges from 10.78% to 7.25% and Mg/Mg+ΣFe values from 0.52 to 0.66. Al_2O_3, ΣFe, TiO_2, Na_2O and Sr show trends of enrichment with decreasing MgO Ifigures 6.1 and 6.2). CaO, Sc, Ni and Cr on the other hand show positive correlation with MgO. Like the Soromundi lavas this group show trends of Al_2O_3 and Sr-enrichment with CaO depletion (figures 6.4A and B), while Sc and CaO show positive correlation (figure 6.3).

FIGURE 6.5

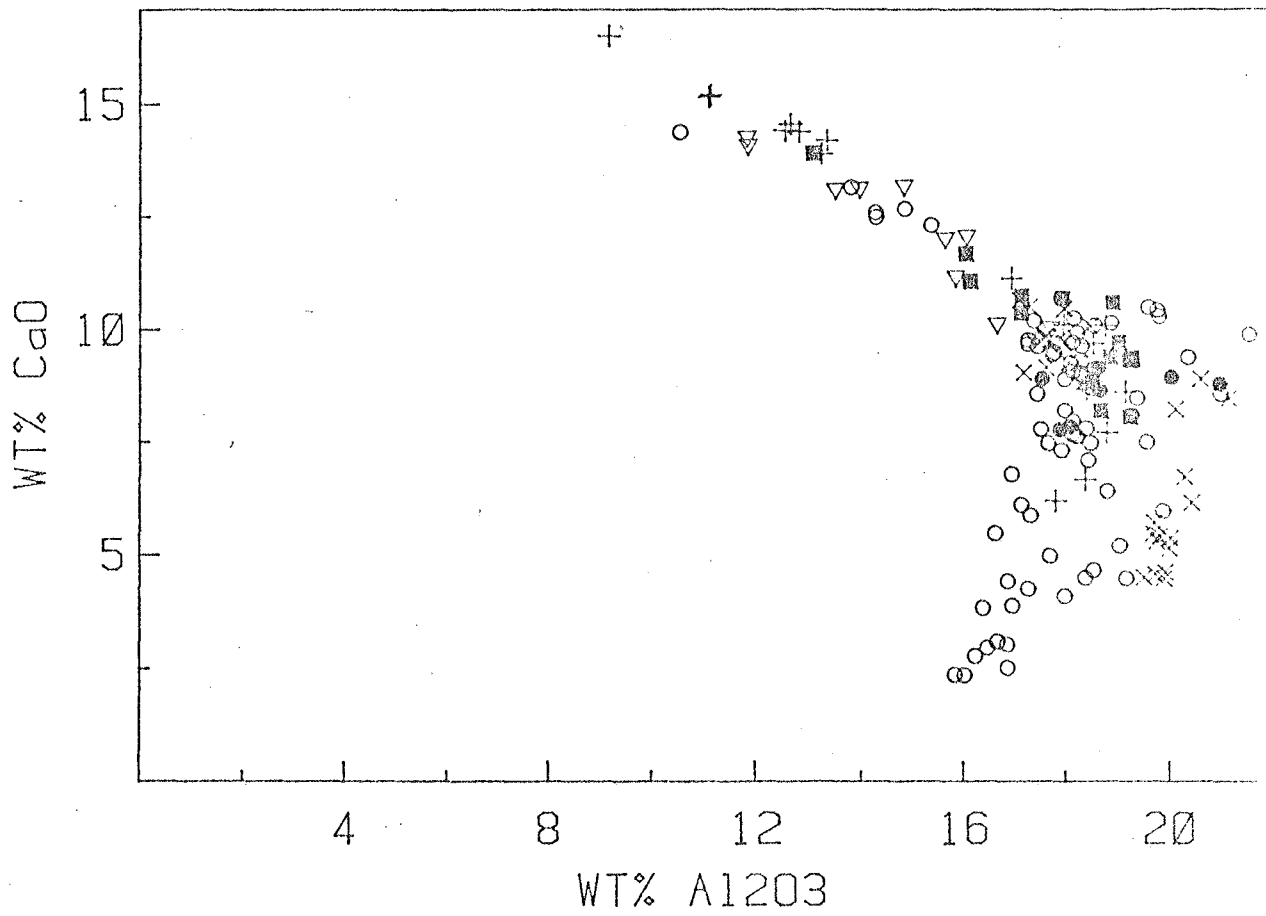

Figure 6.5

CaO v. Al_2O_3 variation of all analysed lavas from this sector of the Sunda Arc. Individual symbols represent lavas of the following volcanoes or suites: ○ - Rindjani calcalkaline suite, Lombok island, ◍ - Agung calcalkaline suite, Bali island, X - Tambora ne- trachybasalts and - trachyandesit Sumbawa island, □ -Sangeang Api, phonolitic tephrites and ne-trachybasalts, ▽ - Soromundi, leucite-bear lavas, Sumbawa, + - G.Sangenges, leucitic lavas, trachybasalts, calcalkaline basaltic andesites and hornblende andesites, Sumbawa. Illustrating the Ca-depletion-Al - enrichment trend common to CPX-rich members of the diverse range of the suites from the Lombok-Sumbawa sector of the Sunda Arc.

Again, these variations suggest cpx removal (or accumulation) together with some olivine. Significantly however, K_2O, Rb, Nb, Zr, Y and P_2O_5 show very poorly defined trends with respect to MgO (figures 6.1 and 6.2) and it seems unlikely that their variation can be attributed to simple fractional crystallisation of the clinopyroxene-olivine phenocryst assemblage. These elements would be expected to be incompatible with respect to this assemblage and would be expected to show a simple negative correlation. For instance, S21 is one of the most mafic lavas of the group with 9.00% MgO. Comparing this lava with S9A, which has 7.25% MgO, S21 has considerably higher P_2O_5, K_2O, Zr and Nb concentrations and very similar Rb. In view of this it would be unlikely that S21 yielded S9A by fractionation of its cpx and olivine phenocrysts.

These factors notwithstanding however, the group are certainly related and show certain common, and distinctive features. They are all K_2O-rich (3.03-4.61%), generally have low Na_2O (1.73-2.55%) and very high K_2O-Na_2O ratios (1.23-2.20). Some G. Sangenges lavas have higher K_2O/Na_2O ratios than members of the Soromundi suite (figure 6.6).

Unlike the suites from the other volcanoes considered in this thesis, the K_2O/Na_2O v SiO_2 plot (figure 6.8) actually shows a steep negative trend. Similarly K_2O also shows a negative correlation with SiO_2 (figure 6.9).

Like the Soromundi suite, this also has very high (and variable) Rb concentrations (117-319ppm) and quite high Sr concentrations (691-902ppm). Rb/Sr ratios are very high (0.156-0.381), slightly higher than those of the Soromundi lavas and 10 times those of the Rindjani basalts. Zr concentrations are relatively low (80-194ppm), generally slightly higher than those of Soromundi lavas of equivalent MgO content. Zr concentrations are only of the order of 1-2 times those in the Rindjani basalts even though Rb concentrations are between 9 and 18 times those of the Rindjani group basalts.

FIGURE 6.6

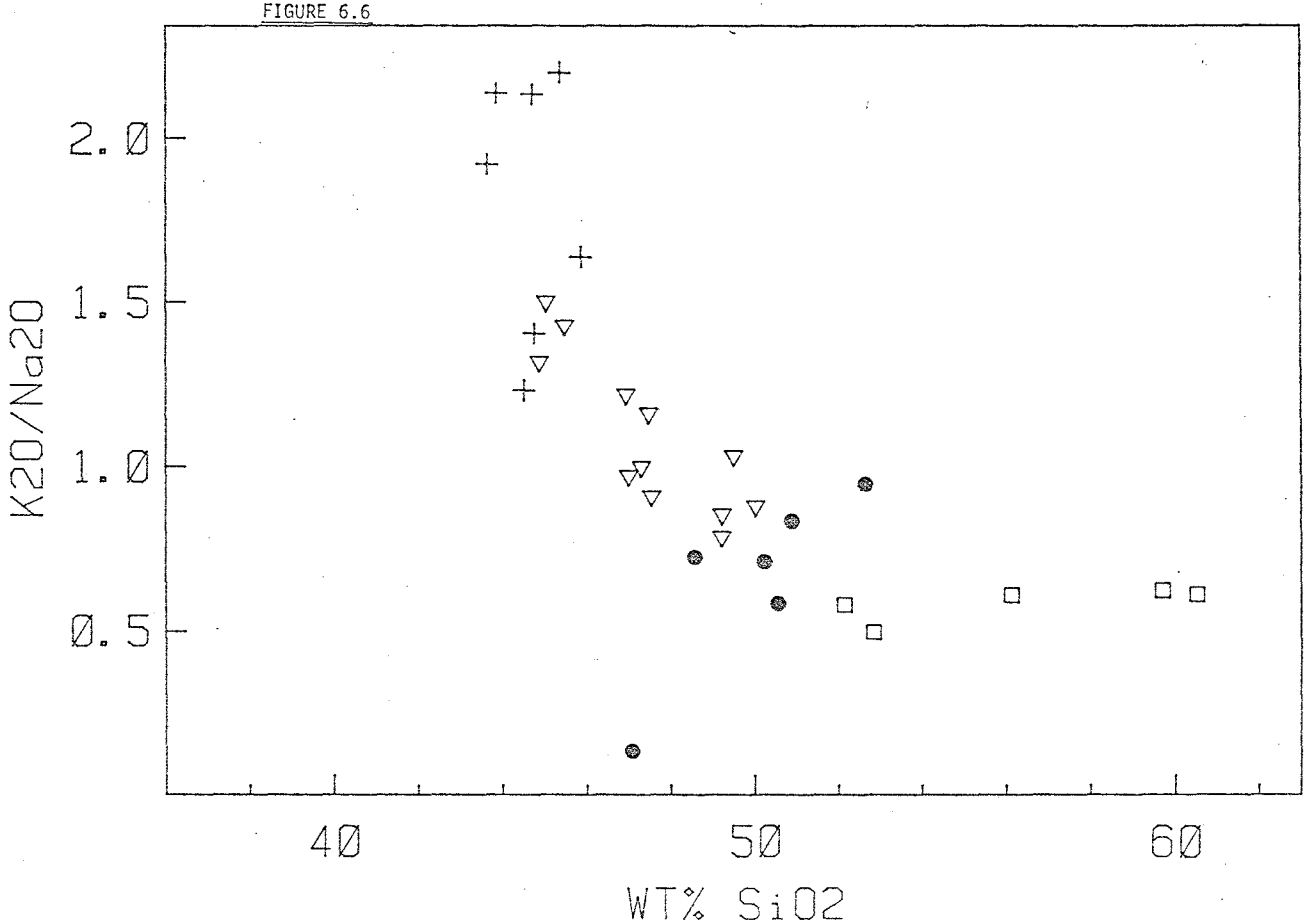

FIGURE 6.6

K_2O/Na_2O v. SiO_2 variation of lavas from Soromundi and G.Sangenges .Symbols are the same as those in figure 6.1. (see also figure 6.8).

P_2O_5 values are relatively high (0.31-0.88%), slightly higher than the Soromundi lavas, though again, relative to the Rindjani high-Al basalts, they are much less P_2O_5-enriched than they are Rb-enriched. TiO_2 concentrations are very similar to those of the Soromundi, Tambora and Sangeang Api suites (averaging 1.0%) and are marginally depleted in this moderately incompatible element by comparison with the Rindjani high-Al basalts.

Like the Soromundi lavas, in spite of their relatively high MgO concentrations, the G. Sangenges group have somewhat lower Ni and Cr concentrations than many of the less mafic Rindjani high-Al basalts. Again, like the Soromundi lavas, this group have very high Sc concetrations (up to 58ppm).

While MgO-variation trends are scattered, there are a few recognisable relationships which emphasise slight distinctions with the Soromundi suite. In particular, TiO_2 and $FeO+Fe_2O_3$ both show trends of slight enrichment with decreasing MgO, while the Soromundi lavas show rather constant values for these parameters at >5% with depletion at <5% MgO (figure 6.1). It is possible that these slight differences result from the crystallisation of amphibole and/or phlogopite in the Soromundi group, which are likely to be more TiO_2- and Fe-rich than the cpx-olivine assemblage of the G. Sangenges group.

In general, the similarities of the Soromundi and G. Sangenges leucite-bearing groups are marked and set them apart from all the other suites considered in this thesis. Briefly their most distinctive features are: very high K_2O, Rb, Sr concentrations, high Rb/Sr ratios, high K_2O/Na_2O ratios, low K/Rb ratios, highly undersaturated and low silica character and the relatively high MgO concentrations and Mg/Mg+Fe ratios.

FIGURE 6.7

K v Rb variation of Soromundi and G.Sangenges lavas.Contours show K/Rb ratios.

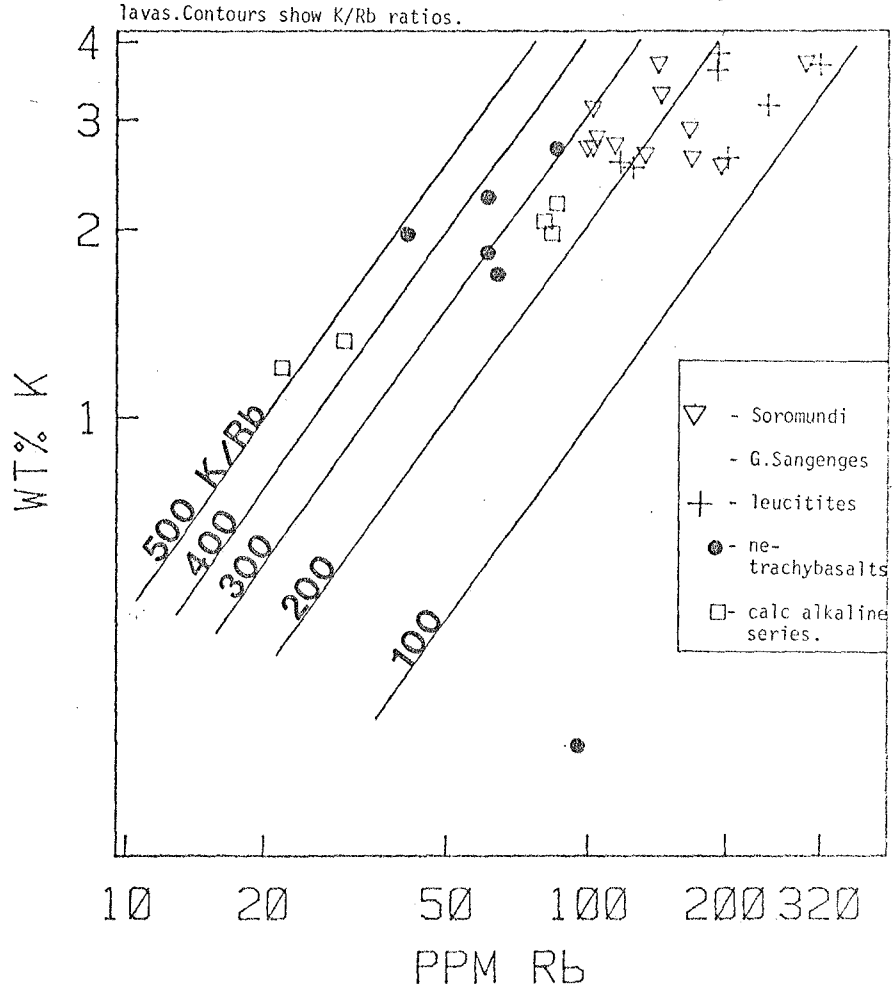

3. Geochemistry of the G. Sangenges trachybasalt group (S8, S16, S5, S28, S1).

Whole-rock, major- and trace-element analyses of these lavas are given in table 6.2 and their compositional variations presented as MgO-variation diagrams in figures 6.1 and 6.2. Both petrographically and geochemically these lavas are equivalent to the trachybasalts from Tambora and some of this same group, from Sangeang Api. They are markedly less extreme in their geochemical composition than the feldspathoid-bearing groups from both G. Sangenges and Soromundi.

They are characteristically only slightly undersaturated with <5% normative-ne. Compared with feldspathoidal groups, they are more silica-rich (48.5-52.6%), more aluminous (>17% Al_2O_3), less K_2O-, Rb-, P_2O_5-, CaO-, MgO-, Ni-, Cr- and Sc-rich. They have markedly higher K/Rb ratios (mostly >300), lower Rb/Sr ratios (<0.075)and lower K_2O/Na_2O ratios (0.59-0.90).

Rb concentrations are about half those of the leucitic lavas, TiO_2, Zr and Nb concentrations are the same, or only slightly lower, and Y concentrations are slightly higher.

Generally, both petrographically and mineralogically these lavas are like the trachybasalts from Tambora. For instance lava S28 from this group (table 6.2) is compositionally very like trachybasalt T9 (table 4.2) from Tambora. Both groups of trachybasalts form a suite generally intermediate between the high-Al basalts from Rindjani and the leucitic series from G. Sangenges and Soromundi.

4. The geochemistry of the G. Sangenges calcalkaline lavas (S10, S11, S26, S15, S7).

This group are petrographically distinguished from the trachybasalts by a general absence of olivine, by their relatively more plagioclase-rich character, and the lack of either K-feldspar or feldspathoid, and by the occurrence of hornblende phenocrysts.

Geochemically they are distinctive in their *Q*-normative character and in their more silica-rich (52-60% SiO_2) nature as well as by the much greater range of silica values. They range from basaltic andesites (S10, table 6.3) to relatively siliceous hornblende andesites (S7, table 6.3).

In common with the basaltic andesites and andesites of the Rindjani calcalkaline series, these lavas are MgO-poor (<5%), aluminous (19.8-17.1% Al_2O_3) and show trends of SiO_2-, K_2O-, Na_2O-, Rb-, Nb- and Zr-enrichment with decreasing MgO (figures 6.1 and 6.2).

In contrast to the leucitic and trachybasaltic series from G. Sangenges, Al_2O_3 shows a negative correlation with MgO (figure 6.1) and a positive correlation with CaO (figure 6.4B), in this calcalkaline group. This suggests plagioclase plays a more important role in the differentiation of this group.

By comparison with the more alkaline members of the G. Sangenges' suite, this group have markedly lower K_2O concentrations (1.45%-2.65%) and lower K_2O/Na_2O ratios (<0.6). Basaltic andesites have markedly lower Rb concentrations (20-30ppm) than the alkaline basaltic lavas from the same suite and Rb increases with decreasing MgO and increasing SiO_2, to about 85ppm in the most silica-rich andesites. The basaltic andesites (e.g. S10, S11) have relatively low Rb/Sr ratios (ca. 0.05), markedly lower than those of the leucitic lavas (often >0.2) and slightly higher than those of the trachybasalts. Rb/Sr ratios increase to about 0.1 in the more silica-rich andesites (e.g. S7).

In contrast to the other two series from G. Sangenges, this group shows marked TiO_2- and ΣFe-depletion trends. They also contain very markedly lower P_2O_5 concentrations (ca. 0.3%).

Like the Rindjani basaltic andesites and andesites, this group have very low Ni (<7ppm), Cr and Sc concentrations.

Figure 6.9.

Variation of K_2O v. SiO_2 for all lavas analysed in this thesis from this sector of the Sunda Arc.Three series are illustrated in this figure and figure 6.8.

1. The Calcalkaline Series
2. The Ne-Normative Trachybasalt and Trachyandesite Series
3. The Leucite-Bearing Series

The symbols represent the following rock types/suites in this figure and figure 6.8:

- ● - Calcalkaline basalts and andesites ,Agung Volcano, Bali
- ○ - Calcalkaline lavas from Rindjani Volcano,Lombok
- □ - Basalts and Andesites of the Calcalkaline Series from G.Sangenges,Sumbawa
- X - Tambora Lavas,Sumbawa.
- ■ - Sangeang Api lavas,Sumbawa.
- ▲ - Ne-trachybasalts and -trachyandesites,G.Sangenges Sumbawa.
- ┼ - Leucitite Series lavas,G.Sangenges
- ▽ - Leucitite lavas,Soromundi.

Figure 6.8

Variation of K_2O/Na_2O v. SiO_2 for all lavas analysed from this sector of the Sunda Arc,showing the same three series as in figure 6.9 .

FIGURE 6.9

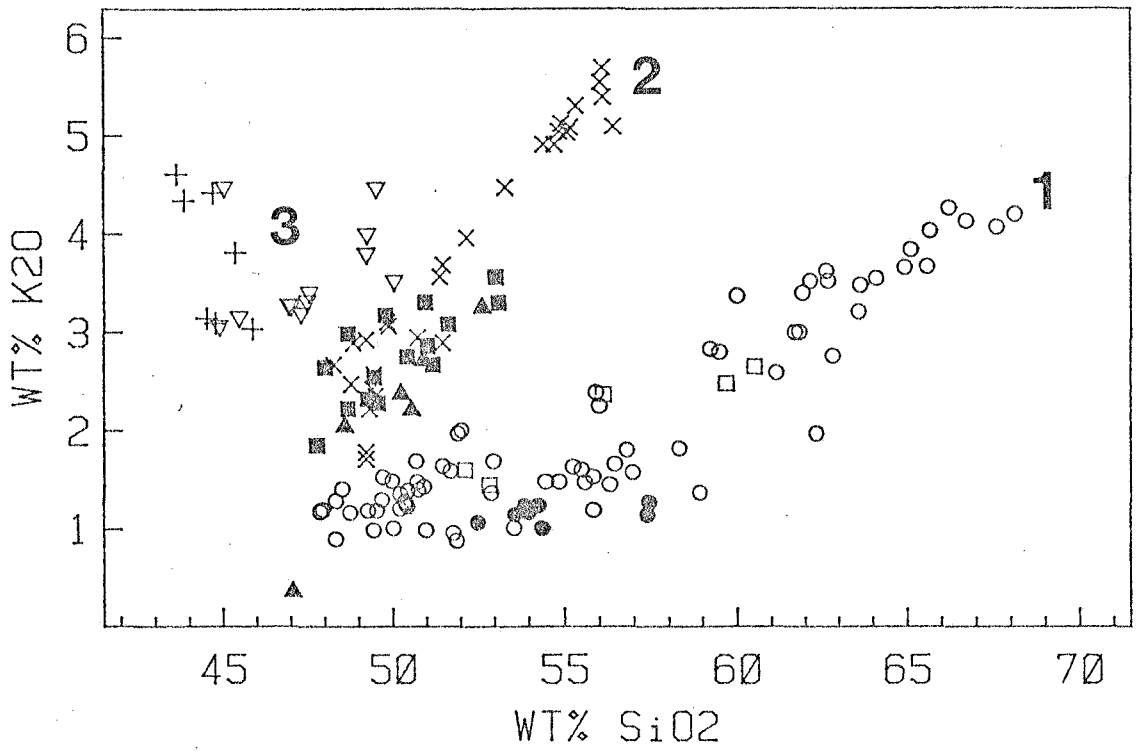

FIGURE 6.8

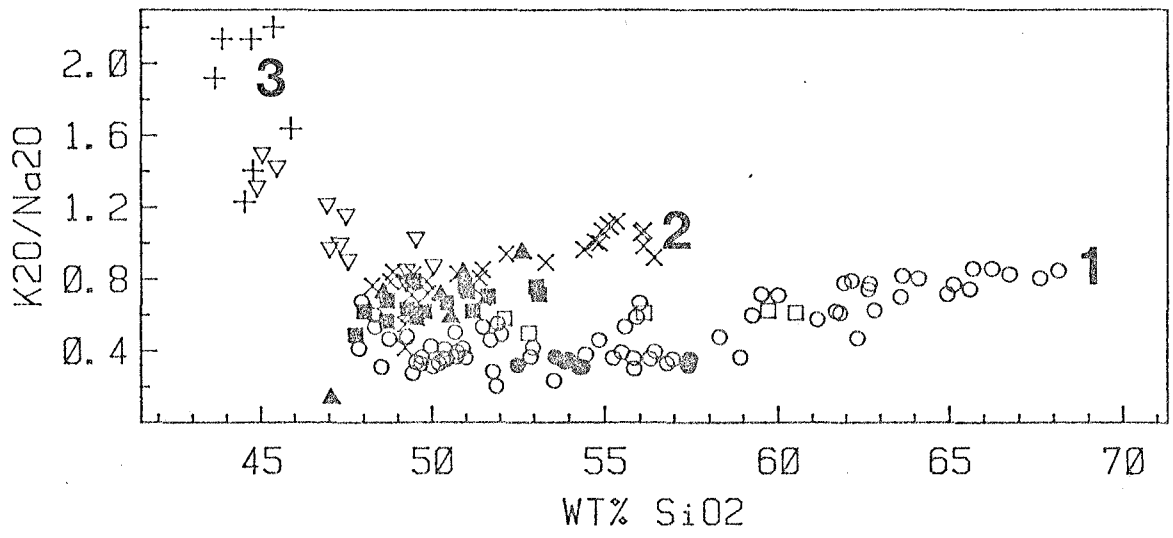

5. Intrusive Rocks (Coarse-grained Xenoliths)

Analyses of two xenoliths from the Soromundi and G. Sangenges suites are given in tables 6.3 and 6.4 (S12 from G. Sangenges and Si18 from Soromundi). Both these are of possible cumulate origin and bear considerable mineralogical and geochemical resemblance to members of the Sangeang Api intrusive suite. In particular S12 from G. Sangenges is rich in plagioclase and amphibole with clinopyroxene, apatite and magnetite and is very like the amphibole-rich members of the hornblende-gabbro group from Sangeang Api (e.g. B24 or B8, tables 5.1and 5.4). It has low silica, high Al_2O_3 (19.30%), is relatively ΣFe-, TiO_2-, and CaO-rich, has high Sr, low Rb, very low Rb/Sr ratio and moderately high K_2O, Na_2O and P_2O_5. Ca and Ni concentrations are quite low, while Sc is quite high.

Si18, from Soromundi, is plagioclase-free, comprising: cpx + amphibole · apatite + magnetite + minor biotite (tables 6.4 and 6.6). It is very like the hornblende-clinopyroxenite B20 (table 5.1) from Sangeang Api, and is texturally similar to the olivine-clinopyroxenites. This xenolith has low Al_2O_3 (8.3%) and is very ΣFe- and CaO-rich with quite high MgO (10.04%). It has relatively high K_2O and Na_2O and a fairly high K_2O/Na_2O ratio of about 0.7. The TiO_2 concentration is also relatively high (1.40%) and the P_2O_5-content is very high (1.82%). Compared with the Soromundi lavas, this xenolith has very low Rb (5ppm), somewhat lower Sr (504ppm), similar Cr and Ni concentrations and higher Sc and Y concentrations. Zr (120ppm) is present at about the same concentration as in the lavas. The K/Rb ratio (ca. 1000) is much higher than that of the lavas, while the Rb/Sr ratio is much lower (ca. 0.009).

Chapter 7

GENERAL RESUME AND COMPARISON OF THE PETROLOGICAL FEATURES OF ALL THE VOLCANIC SUITES FROM THE LOMBOK-SUMBAWA SECTOR OF THE SUNDA ARC

7.1 *Introduction.*

This chapter briefly reviews the petrological data presented in the preceding four chapters. The major mineralogical features of each group are summarised and the major differences and similarities between different suites are emphasised.

The remaining chapters of the thesis then attempt to answer such questions as: What is the origin of the considerable compositional diversity of the suites from this part of the Sunda Arc? What is the origin of the contrasting compositional variation trends shown by different suites? What is the origin of the contrasting mineralogy of various petrographic groups? What is the nature and possible compositional variations of the ultimate source of the lavas?

7.2 *Petrological Features.*

The suites of volcanic rocks described in the preceding four chapters from the five volcanoes on Lombok and Sumbawa islands (G. Rindjani, G. Sangenges, G. Tambora, G. Soromundi and Sangeang Api) display great compositional variety. They range from silica-rich *Q*-normative dacites of Rindjani volcano (such as 41639, table 3.18) to highly undersaturated, *Lc*-normative, very silica-poor, olivine leucitites (such as S21, table 6.1) of G. Sangenges. Between these extremes lies a variety of ankaramites, high-Al basalts, quartz-normative andesites, undersaturated trachybasalts and trachyandesites.

In summary, the lavas of all the volcanoes fall into three groups:

1. A Calcalkaline series: this includes the lavas from Rindjani volcano and the quartz-normative group (C) from G. Sangenges.
2. A series of potassic, *ne*-normative trachybasalts and trachyandesites (≈ "shoshonites"): this group includes the lavas of Tambora and Sangeang Api volcanoes and the feldspathoid-free, *ne*-normative series (B) from G. Sangenges.
3. A highly undersaturated, feldspathoid-bearing (leucite) series: this group including the lavas from Soromundi and the feldspathoidal group (A) from G. Sangenges.

In simplest terms the transition through these series from group 1, through 2, to 3, represents one of the increasing alkalinity and increasing under-saturation. Some of the most mafic lavas of the Rindjani suite are slightly *ne*-normative, but all of the more silica-rich lavas (>53% SiO_2) are *Q*-normative. Members of series 2 are all slightly *ne*-normative, whereas those of the third group are all normatively *ne*-rich (>10% in most cases) and in most cases also contain normative leucite.

Petrographically, these transitions are marked by variations in groundmass assemblages. The calcalkaline lavas have groundmass plagioclase, whereas the second (trachybasalt-trachyandesite) series is characterised by the presence of ubiquitous, groundmass K-feldspar (sanidine). In rare cases, a few of these lavas may also have occasional feldspathoid (either leucite in some Tambora trachyandesites or microsommite group minerals in a few members of the Sangeang Api group of lavas). Lavas of the third series are often entirely plagioclase-free, contain groundmass leucite ± nepheline and may also contain leucite microphenocrysts.

The individual petrographic groups represented in each volcano are summarised as follows:

1. Rindjani

A. Ankaramite: The most mafic lavas of the Rindjani series. Relatively Al_2O_3-poor, MgO- and CaO-rich. Phenocrysts dominated by cpx, with less important olivine. Plagioclase is rare or absent. Cpx is zoned with mafic, Cr-diopside cones and Al-augite rims.

B. High-Al basalt: Lavas with <53% SiO_2, *ne*- to *ol-hy*-normative, >17% Al_2O_3 and <6% MgO. The most mafic individuals are phenocryst-poor and in these olivine is the main phenocryst with very minor, very Ca-rich plagioclase. Cpx only appears as rare corroded grains. Olivine compositions are very variable with some megacrysts, which may contain Cr-spinel inclusions, as magnesian as Fo90. Less mafic high-Al basalts are relatively phenocryst-rich with abundant plagioclase and with cpx, olivine and magnetite.

C. Andesite: Aluminous, (>18% Al_2O_3), plagioclase-rich *Q*-normative lavas with low MgO and Ni. Olivine is rare or absent and phenocrysts comprise plagioclase + opx + cpx + magnetite, often set in glassy or very fine grained groundmass. Phenocrysts are zoned and comprise 60-70% of the rock.

D. Dacite and High-K andesite: These contain 2-3 times the K_2O, Rb, Nb and Zr concentrations of the andesites and are often less aluminous. They may be glassy and are often phenocryst-poor. Phenocrysts comprise plagioclase + opx + cpx ± hornblende + magnetite.

2. Tambora (and P. Satonda).

A. Trachybasalt: In some respects they are like the *ne*-normative high-Al basalts from Rindjani and are aluminous, relatively MgO-poor, phenocryst-rich, *ne*-normative lavas with assemblages dominated by plagioclase with abundant cpx and olivine. Groundmasses are composed of olivine, cpx, plagioclase, sanidine, magnetite and apatite.

B. Trachyandesite: These are relatively plagioclase-rich lavas but have decreasing phenocryst abundance towards the most silica-rich end members. The latter group are often glass-rich with biotite phenocrysts. Olivine is rare or absent as a phenocryst phase, but may occur in the groundmasses. Unlike the Rindjani andesites, lavas of this group are all *ne*-normative and opx does not appear. Groundmasses are plagioclase and sanidine-rich with cpx, olivine, magnetite and apatite, or glassy.

3. Sangeang Api.

A. Olivine megacryst-bearing trachybasalt: These from mafic, Al-poor B43 which is plagioclase-phenocryst-free with large megacrysts/phenocrysts of cpx and olivine and is very like the Rindjani ankaramites, to more aluminous, less mafic, plagioclase phenocryst-bearing varieties which are like the Tambora trachybasalts. These contain large megacrysts of cpx and olivine as well as less mafic phenocrysts of these phases and also contain plagioclase and magnetite phenocrysts. Groundmasses are composed of plagioclase, cpx, olivine, magnetite, sanidine and apatite.

B. Felsic trachybasalt: These are aluminous, MgO-poor (<4.5%), plagiophyric lavas with other phenocrysts or microphenocrysts of cpx, magnetite, occasionally olivine and apatite. They are distinguished from the previously described group in being less mafic, in the absence of olivine megacrysts and by the occurrence of reacting amphibole megacrysts. Cpx megacrysts compositionally similar to those in the gabbroic xenoliths are recognised and occasional large, anorthitic plagioclase also has the same composition as those in these xenoliths. Groundmasses are composed of plagioclase, cpx, olivine, magnetite, sanidine, apatite and rare feldspathoid.

4. Soromundi.

Madupite, lamproite, leucite tephrite: These are K_2O-rich, SiO_2-, Al_2O_3-poor, relatively mafic volcanic rocks. Leucite occurs in the groundmass and as microphenocrysts. Cpx is the main phenocryst phase, with phlogopite and/or amphibole. Plagioclase appears in some of the least mafic varieties. Olivine occurs only rarely as xenocrysts, generally reacted, with occasional cpx-rims.

5. G. Sangenges.

A. Olivine leucitite, leucitite, leucite tephrite: K_2O-rich, SiO_2-, Al_2O_3-poor, mostly without plagioclase phenocrysts. Leucite appears in the groundmass and as small phenocrysts. Cpx is the major phenocryst and olivine is also generally present.

B. Trachybasalt: These are aluminous, relatively MgO-poor (<7% MgO), plagiophyric rocks with cpx, olivine and magnetite phenocrysts and groundmasses of plagioclase, sanidine, cpx, olivine, magnetite and apatite. They are like the Tambora trachybasalts.

C. Andesite and basaltic andesite: These are *Q*-normative, aluminous, MgO-poor rocks, showing marked silica-enrichment. Phenocrysts are dominated by large zoned plagioclases with cpx, magnetites and hornblendes. Groundmass is very fine-grained, plagioclase-rich, with cpx and magnetite.

7.3 Mineralogical Features.

A number of features are of interest. In the first place, the occurrence of extremely Ca-rich plagioclase (An85-An95) often as corroded grains, is very widespread. These occur in the Rindjani basalts and andesites as well as in many of the more alkaline suites. Secondly, cpx-dominated assemblages often with relatively minor olivine and little or no plagioclase are common. Thus there is marked petrographic similarity between the Rindjani ankaramites and some of the Sangeang Api lavas (B43). In both these instances cpx is zoned with Cr-diopside cores (which are Al- and Ti-poor) with very mafic compositions ($Mg/Mg+\Sigma Fe = 0.90$) which are mantled by less mafic more Al- and Ti-rich augite. These "megacrysts" are commonly associated with olivine which is markedly less mafic than the most mafic cpx compositions. This assemblage is rather like that of the very alkaline lavas, in particular those from G. Sangenges, with the exception that leucite also occurs. In the case of Soromundi similar cpx occurs, though olivine is very rare and when it is present, is markedly reacted. Amphibole and/or phlogopite appear instead of olivine.

These assemblages are very like some represented in the Sangeang Api xenolith suite. The olivine clinopyroxenites have considerably more abundant cpx than olivine, and olivine disappears in those where amphibole becomes an important phase (hornblende-clinopyroxenites e.g. B20).

The phenocryst assemblage; plagioclase + olivine + cpx ± magnetite ± apatite is also a recurrent one, common to many of the Rindjani, high-Al basalts and the trachybasalts from Tambora, Sangeang Api and G. Sangenges. The opx-bearing assemblage of the Rindjani andesites is probably a silica-oversaturated analogue of this.

The olivine dominated assemblage of the more mafic Rindjani high-Al basalts is unique, both in the absence or scarcity of cpx and in the very magnesian character of some of these olivines (up to Fo 92).

7.4 Geochemical Features.

Considering now the general geochemical features which characterise the differences between the three main distinct petrographic groups previously defined (1. calcalkaline series, 2. *ne*-normative trachybasalt "shoshonite" series, 3. alkaline "leucititic" series). The transition through these series (from 1 to 3) are marked by increasing concentrations of K_2O, Rb, Sr, Ba and increasing K_2O/Na_2O and Rb/Sr ratios and decreasing K/Rb ratio. P_2O_5 and Nb increase slightly, while Zr, TiO_2 and Na_2O maintain rather similar values in all the more mafic members of each of these groups. The distinction between the three groups are well illustrated in the K_2O/Na_2O v SiO_2, K_2O v SiO_2 and Rb v MgO plots shown in figures 12.1 - 12.6. There is a marked decrease in the extent of silica variation from the Rindjani group through to the Soromundi or G. Sangenges feldspathoidal series. Differentiation in the Rindjani series largely proceeds with marked SiO_2-enrichment while at the other extreme, the G. Sangenges leucitites show virtually no SiO_2 variation with variation of other parameters.

It is interesting to analyse the differences in the differentiation paths of the different groups of lavas by looking in detail at the comparison between the two least dissimilar groups; those from Rindjani and Tambora.

The general impression grained, in chapter 4, from a comparison of the aluminous basaltic lavas from Rindjani and Tambora, was that while most geochemical parameters were very similar, the latter suite appeared to have gained K_2O, Rb and Sr. This conclusion is further reinforced when the more alkaline lavas from G. Sangenges and Soromundi are considered, and it is difficult to see how crystal-liquid fractionation can relate these suites. This opens the possibility of a separate supply of these, and related elements. These problems are further discussed in chapters 9 and 12.

Considering the differentiation of the more evolved lavas of the Rindjan and Tambora suites, a number of important contrasts arise. Both suites show trends of SiO_2-enrichment, though the most siliceous Tambora lavas contain only 57% SiO_2, while the Rindjani suite extends to 68% SiO_2. In the Rindjani suite, this represents an approximately five-fold enrichment of Rb and a three-to-four fold enrichment of K_2O, compared with concentrations of these elements in the basalts. The most differentiated Tambora lavas on the other hand, contain about three times the basaltic K_2O and Rb concentrations.

The most evolved trachyandesites from Tambora (with 56-57% SiO_2), have similar CaO, ΣFe, MgO, TiO_2, differentiation index[1] (ca. 70-73) and normative feldspar composition (ca. An15) to the Rindjani dacites with SiO_2 contents in the range 64-64%. However, compared with these same dacites, the Tambora lavas have higher Al_2O_3, higher K_2O/Na_2O ratios, higher P_2O_5, Rb and Sr concentrations but lower Zr concentrations.

1. Note: Differentiation Index (D.I.) is that of Thornton and Tuttle (1960).

These factors suggest that while the Rindjani suite is showing a characteristic calcalkaline differentiation trend, with extensive silica enrichment, accompanied by rather more gradual enrichment or depletion of other elements, the Tambora Suite is showing a tendency to approach the differentiation trends shown by the alkali basalt magma in differentiating towards a phonolitic or trachytic residual liquid (e.g. Coombs and Wilkinson, 1969).

This tendency is carried even further when the highly undersaturated lavas from Soromundi and G. Sangenges are considered. These might show quite considerable variations in ΣFe, MgO, CaO, Al_2O_3, Sr and Rb, yet SiO_2 shows relatively minor variation.

Chapter 8

SR-ISOTOPE GEOCHEMISTRY AND ITS IMPLICATIONS

8.1 *Introduction*

Sr-isotope data provide useful information to place constraints on various petrogenetic models for the Sunda Arc lavas. In particular the Sr-data are used to:

1. Evaluate postulated fractional crystallisation models, particularly those of the Rindjani suite (basalt-andesite-dacite) and the Tambora suite (trachybasalt-trachyandesite). If such models are valid then postulated basaltic parents and dacitic or trachyandesitic differentiates should have similar $^{87}Sr/^{86}Sr$ ratios. If such is the case, then it must be noted that this can only be regarded as contributing evidence in favour of the proposed model and not definite proof. On the other hand dissimilar ratios provide strong discrediting evidence for simple fractional crystallisation mechanisms.
2. To evaluate the Sr-isotope geochemistry of lavas of this segment of the Sunda Arc compared with regional trends described from the more westerly portions of the arc (Whitford, 1975) and from the Banda Arc to the east (Whitford et al., 1977; Magaritz et al., 1978).
3. To evaluate source characteristics.
4. To enable comparison with available world-wide Sr-isotope data from convergent-plate marginal volcanic suites as well as with that of volcanic rocks from other environments to be made.

8.2 *Analytical Techniques*

Sr-isotope determinations were carried out by Dr. D.J. Whitford at the Carnegie Institution of Washington, Department of Terrestrial Magnetism.

TABLE 8.1

Sr-isotope analyses of East Sunda Arc Volcanics and Xenoliths.

	SiO_2	K_2O	Mg.No.	Rb	Sr	Rb/Sr	K/Rb	$^{87}Sr/^{86}Sr$	$\pm 2\sigma_m$
Rindjani									
LB8	48.32	0.90	0.74	21	452	0.046	356	0.70388	±5*
41632	50.20	1.21	0.52	20	452	0.044	502	0.70386	±6
41678	52.03	2.00	0.42	51	527	0.096	325	0.70398	±5
41634	52.90	1.37	0.40	30	510	0.058	379	0.70398	±7
41622	55.49	1.60	0.42	35	433	0.080	379	0.70398	±6
LB69	61.82	3.00	0.39	62	403	0.154	401	0.70394	±6
41671	65.58	3.67	0.36	98	293	0.334	311	0.70402	±6
Tambora									
T17	48.78	2.47	0.52	189	1113	0.169	108	0.70385	±6
T13	51.49	2.89	0.50	86	981	0.087	279	0.70399	±6
T32	55.09	5.03	0.47	132	1036	0.127	316	0.70395	±6
T20	56.10	5,69	0.40	142	923	0.154	332	0.70389	±6
Sangeang Api									
B43	47.77	1.85	0.64	73	850	0.085	210	0.70500	±5
B25	48.02	2.64	0.46	92	1135	0.081	238	0.70486	±6
B35	50.43	2.75	0.44	84	943	0.089	272	0.70460	±6
B32	53.05	3.56	0.41	112	1010	0.111	264	0.70485	±6
Xenoliths									
B23	45.41	0.10	0.81	5	68	0.073	166	0.70496	±7
B4	50.19	0.05	0.81	5	121	0.041	83	0.70480	±7
B25x	40.48	0.28	0.54	6	221	0.027	387	0.70477	±6
B8	38.31	0.42	0.47	3	1125	0.002	1162	0.70466	±5
G. Sangenges									
S19	44.71	4.42	0.56	319	836	0.381	115	0.70529	±6
S28	50.55	2.21	0.49	61	724	0.084	301	0.70412	±8
Soromundi									
Si12	47.49	3.32	0.50	114	1511	0.075	242	0.70488	±7
Si9	49.24	4.00	0.41	144	2401	0.059	232	0.70527	±7

Notes: Mg. No. Atomic Mg/Mg + ΣFe *i.e. ±.00005

All $^{87}Sr/^{86}Sr$ ratios normalised to $^{86}Sr/^{88}Sr = 0.1194$ and repeated relative to E + A $SrCO_3$, $^{87}Sr/^{86}Sr = 0.70800$.

ANALYST: D.J. Whitford, Carnegie Institution of Washington. (Sr-isotope analyses)

Techniques used were those outlined by James et al. (1976) and Whitford and Jezek (1977). The analyses were normalized to $^{86}Sr/^{88}Sr = 0.1194$ and reported relative to Eimer and Amend $SrCO_3$ $^{87}Sr/^{86}Sr = 0.70800$.

8.3 Results of Sr-Isotope Analysis

The results and some of the implications of the Sr-isotope geochemistry of these lavas have been discussed by Whitford, Foden and Varne (1978). $^{87}Sr/^{86}Sr$ ratios were determined on a number of representative samples from each of the main volcanoes considered in this thesis (Rindjani, Tambora, Sangeang Api, Soromundi and G. Sangenges). Most analyses were performed on rocks from the three active volcanoes, which have more clearly defined suites (Rindjani, Tambora and Sangeang Api).

A representative group of xenoliths from Sangeang Api were also analysed (olivine clinopyroxenite B23, olivine-poor clinopyroxenite B4, magnetite-clinopyroxenite B25 and cumulate hornblende gabbro B8), including a coexisting lava-xenolith pair (B25-B25x).

Measured $^{87}Sr/^{86}Sr$ ratios are listed in table 8.1. Analyses of six lavas from the Rindjani calcalkaline suite, ranging from basalts through andesites to dacites, all show relatively low $^{87}Sr/^{86}$ ratios that are isotopically almost indistinguishable from each other and range from 0.70386 to 0.70402 (table 8.1, figures 8.1 and 8.6). Similarly, the four *ne*-normative trachybasalts and trachyandesites from Tambora volcano are also characterised by relatively constant and low ratios (0.70385-0.70399), indistinguishable from those of the Rindjani suite. On the other hand, geochemically similar, though not identical, lavas from Sangeang Api have both higher and more variable $^{87}Sr/^{86}Sr$ ratios, which also show some suggestion of a trend of decreasing ratios from the most mafic basalt (B43) to the more differentiated lavas (figure 8.2). Analysed ratios range from 0.70500 to 0.70469.

FIGURE 8.1

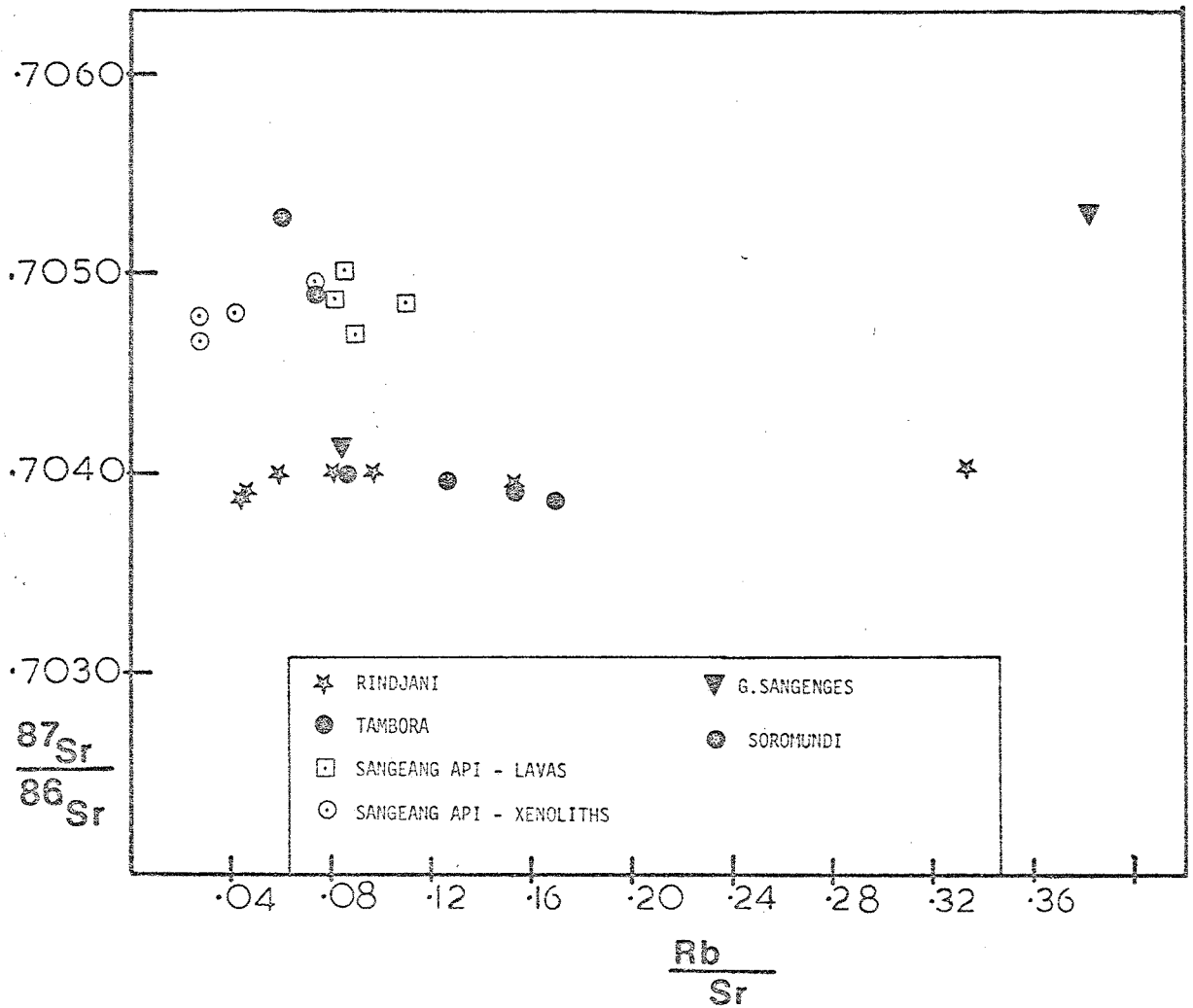

Figure 8.1 $^{87}Sr/^{86}Sr$ v. Rb/Sr variation of lavas and xenoliths (Sangeang Api) from volcanoes in the Lombok-Sumbawa sector of the Sunda Arc .Illustrating the relatively low and invariant Sr-isotopic ratios of the Tambora and Rindjani lavas and the higher and more variable values from the more alkaline volcanoes (Sangeang Api,Soromundi and G.Sangenges).

The leucite-bearing lavas from Soromundi and that from G. Sangenges (S19) are also characterised by high and variable $^{87}Sr/^{86}Sr$ ratios (0.70488-0.70529), including the highest ratios determined in this study. The less potassic, *ne*-normative trachybasalt S28, from G. Sangenges, (from the group B series discussed in chapter 6 as similar to the Tambora and Sangeang Api suites) has a lower ratio (0.70412), but still higher than those of the Rindjani and Tambora series. Lavas from Soromundi, G. Sangenges and Sangeang Api show an inverse correlation between $^{87}Sr/^{86}Sr$ and the ratio K/Rb (figure 8.6).

$^{87}Sr/^{86}Sr$ ratios of the four xenoliths from Sangeang Api range from 0.70466 to 0.70496. This range is almost identical to that shown by the associated lavas, and as in the case of the lavas, the most mafic xenoliths have the most radiogenic Sr (figure 8.2). Xenolith B25x and its host lava B25 have very similar $^{87}Sr/^{86}Sr$ ratios (figure 8.2).

$^{87}Sr/^{86}Sr$ ratios of the xenoliths show positive correlation with a number of geochemical variables, including MgO, 1/Sr and Rb/Sr (figures 8.2 - 8.4). The correlation between $^{87}Sr/^{86}Sr$ and Rb/Sr yields a pseudoisochron (Brooks et al., 1976) indicating an apparent "age" of about 102 m.y. ($\lambda^{87}Rb = 1.42 \times 10^{-11} yr^{-1}$) (Whitford, Foden and Varne, 1978). Because of the small number of samples, the limited dispersion in $^{87}Sr/^{86}Sr$ and uncertainties in Rb/Sr ratios, however, the 2σ error in this "age" is 41 m.y. Further the exact meaning of this "age" is uncertain and whether it represents the real age of the rocks or some sort of mixing event is open to conjecture. This problem is discussed more fully in the following sections.

8.4 *Discussion of the Sr-Isotopic Composition of Volcanic Rocks in General and its Implications*

The Sr-isotope geochemistry of volcanic rocks in general and its bearing on the source and petrogenesis of these has been the subject of protracted

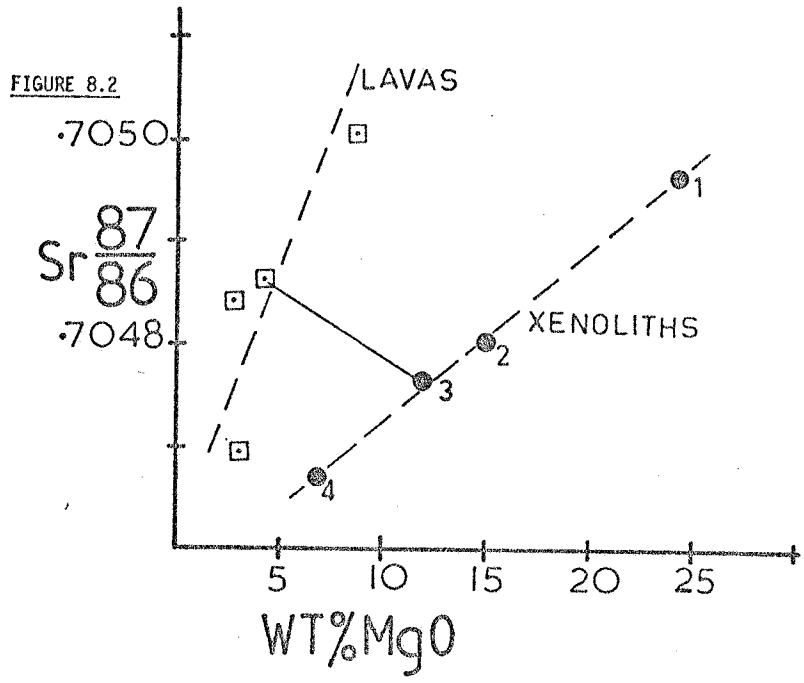

Figure 8.2

$^{87}Sr/^{86}Sr$ v. Wt.% MgO for the Sangeang Api lavas and xenoliths.. Open squares -lavas, Filled circles-xenoliths Xenoliths 1 and 2 are olivine clinopyroxenites,3 is a magnetite clinopyroxenite and 4 a gabbro.There is a good positive correlation between MgO and $^{87}Sr/^{86}Sr$ amongst the analysed xenoliths. The tie-line connects a xenolith and its host lava .

discussion. Hurley et al. (1967) and Faure and Hurley (1963) first applied Sr-isotopes to magma genesis. They suggested that as granitoid crustal rocks have high Rb/Sr ratios relative to likely upper mantle, they are likely to become enriched in ^{87}Sr and that magmas resulting from crustal anatexsis or which have assimilated crustal material, will have higher initial $^{87}Sr/^{86}Sr$ ratios than those of purely mantle origin. Thus $^{87}Sr/^{86}Sr$ ratios of young volcanic rocks from the islands and ridges of the ocean basins, where no silicic crust exists, should have relatively low values reflecting those of the source mantle.

While the above is generally true, it is found that a considerable range of initial $^{87}Sr/^{86}Sr$ ratios occurs in oceanic lavas. In particular those of the ocean islands range from 0.703 to 0.706 (e.g. Gast, 1967, Sun and Hanson, 1975). Mid ocean ridge basalts (MORB) show low values with a generally more restricted range (ca. 0.702-0.703, Sun and Hanson, 1975), while Hart and Brooks (1977) quote a total $^{87}Sr/^{86}Sr$ range for oceanic basalts of 0.7023-0.7065. This tends to suggest that the mantle source region is not be isotopically homogeneous.

The source and nature of these isotopic inhomogeneities have been discussed in a number of recent studies. In particular, Sun and Hanson (1975), on the basis of oceanic Pb- and Sr-isotopic data, proposed that ocean island and mid-ocean ridge volcanism tap different mantle sources isolate from each other by the convective cells. Apparent isochrons presented by Sr- and Pb-isotopic data then suggest that mantle heterogeneities are long-lived and possibly arose ca. 2,000 m.y. ago. A similar date for the origin of mantle heterogeneity was determined by Brooks et al. (1976) (1.6 b.y. $\pm$ 0.2 b.y. with an initial $^{87}Sr/^{86}Sr$ ratio of 0.7023) on the basis of Sr-data from ocean islands. Hart and Brooks (1977) then suggested that separate mantle reservoirs originated at this time with limiting Rb/Sr ratios of <0.005 (to account for the low present-day $^{87}Sr/^{86}Sr$ ratios of MORBS

≈0.702) and >0.05 (to account for the radiogenic Sr of some ocean islands with $^{87}Sr/^{86}Sr$ ratios up to 0.7065). Interestingly, however Hart and Brooks (1976) pre-1.7 b.y. mantle Sr-growth curve extrapolates to a present-day $^{87}Sr/^{86}Sr$ value of 0.7037 which is the average value of both ocean islands and island arcs.

These factors notwithstanding, the available data suggests that for whatever reason, the present-day mantle is likely to have $^{87}Sr/^{86}Sr$ ratios which range from 0.702 to 0.706. Furthermore, Sr-isotope compositions of kimberlite and K_2O-rich mafic, undersaturated lavas of probable mantle origin, from some continental areas are also very radiogenic (e.g. Bell and Powell, 196

These factors tend to suggest that Sr-isotope geochemistry may in fact place only fairly loose constraints on the source of island arc volcanic rocks. This is particularly true where arc volcanic rocks have moderately high initial ratios (say >0.7040) allowing a variety of hypothetical sources ranging from partial melting of oceanic crust with some admixture of alkaline oceanic island-, or oceanic sediment- or sea water-component, through to mantle derived melts which are either initially radiogenic or are contaminated by sialic crustal material (Gill and Compston, 1973).

8.5 *Comparison of the Sr-Isotopic Data from the Lombok-Sumbawa Sector of the Sunda Arc with that from Other Island Arcs*

The range and mean values of $^{87}Sr/^{86}Sr$ ratio data from convergent plate margin volcanic rocks, compiled from a number of sources, including the tabulations of Kay et al. (1978) and Whitford (1975) are presented in table 8.2. There is a marked recurrence of mean values in the range $^{87}Sr/^{86}Sr$ 0.7036-0.7041. The isotopic composition of Sr from Rindjani and Tambora volcanoes both average 0.7039 and fall very close to the quoted average ratio of both island arcs and ocean islands, of 0.7037 (e.g. Hart and Brooks, 1976).

In general $^{87}Sr/^{86}Sr$ values from oceanic island arcs are relatively low, but there is considerable overlap with values reported from continental marginal arcs. The Cascades province of western USA has produced some of the lowest values reported from any covergent plate volcanic suite (0.7026, Church and Tilton, 1973; Hedge et al., 1970). Lavas from the Aleutian islands (Kay et al., 1978) also have very low $^{87}Sr/^{86}Sr$ ratios (0.7028-0.7037).

Perhaps significantly, young, often tholeiite-dominated arcs, built entirely on oceanic crust, for instance, the South Sandwich islands (Gledhill and Baker, 1973) and the Marianas islands (Meijer, 1976), tend to show rather limited range of $^{87}Sr/^{86}Sr$ values and in both the cases cited above average values are almost exactly those of the 0.7037 average for all arc volcanics (South Sandwich mean = 0.7037, Marianas mean = 0.7038).

On the basis of both Pb and Sr isotopic evidence, Meijer (1976) argued that contamination of melts derived from the subduction zone by melting of an oceanic sediment component, was unlikely. He suggested that his data were consistent with melting of either altered subducted lithosphere or of sub-arc mantle. However the general similarity of the Marianan lavas, in terms of general petrographic features, geochemistry and Sr-isotopic composition, to those of many suites which have erupted through continental crust, suggests that the involvement of crustal material is not a necessary factor in the production of calcalkaline volcanic rocks. On the other hand, Kay et al. (1978) suggest on the basis of Pb and Sr isotopic data, that volcanic rocks of the Aleutian Arc may represent liquids derived from the sub-arc mantle or from subducted oceanic crust, which have been contaminated by melts derived from the fusion of small amounts of continent-derived sediment in the subduction zone.

While it appears that relatively low $^{87}Sr/^{86}Sr$ ratios occur in volcanic rocks of both continental marginal- and island-arcs, high $^{87}Sr/^{86}Sr$ ratios (>0.7045) are generally confined to continental marginal suites (e.g. Andes; Klerkx et al., 1977, James et al., 1976, Noble et al., 1975, Mediterranean; Pe and Gledhill, 1975) or from island arcs with older, thick, or continental-type crust (e.g. New Zealand; Ewart and Stipp, 1968, Papua-New Guinea; Page and Johnson 1974). These factors suggest that crustal contamination may be a factor in some of those provinces where lavas are erupting through thick, old, sialic crust.

It is also possible, as Brooks et al. (1976) suggest, that both isotopic variability and high initial ratios are inherited from heterogeneous mantle sources which have undergone long-term differentiation. In the case of older continental marginal arcs, such differentiation is suggested to have resulted by accretion of heterogeneous lithosphere, which may be of considerable age and whose melting will yield lavas with radiogenically enriched, but also variable, Sr-isotope ratios.

In general, as suggested in the preceding section, the range of isotopic composition of mantle Sr is likely to be large (0.702-0.706). This factor makes confident identification of the source of Sr in convergent plate volcanic arc magmas impossible. However the indirect evidence provided by the frequent occurrence of ratios in the range 0.7035-0.7040 (ave. 0.7037), from arcs with quite varied tectonic settings, tends to argue against the contamination-type models, which would presumably yield variable ratios. The similarity of the average isotopic composition of Sr from ocean islands and island arcs also tends to support a mantle origin for the bulk of the Sr in arc lavas.

Table 8.2

Comparison of Sr-Isotopic Data from Volcanic Rocks of Convergent Plate Margins

A. Arcs Outside the Indonesian Region

Location	$^{87}Sr/^{86}Sr$ Range	Average Value	No. of Samples	Source Reference
Japan - Hokkaido (b,a,d)	0.7027-0.7059	0.7038	46	Katsui et al. (1974) Hedge & Knight (1969)
- North Honshu	0.7026-0.7058	0.7057	8	Hedge & Knight (1969)
Saipan	0.7030-0.7043	0.7036	4	Pushkar (1968)
Izu Islands	0.7032-0.7049	0.7037	8	Pushkar (1968)
Mariana Arc (b,a)	0.7037-0.7038	0.7038	2	Meijer (1976)
Tonga	0.7038-0.7043	0.7040	8	Gill & Compston (1973)
Fiji	0.7030-0.7048	0.7038	58	Gill & Compston (1973) Gill (1972) in Whitford (1975)
New Hebrides	0.7034-0.7043	0.7038	8	Gorton (1974)
New Georgia (Solomon Islands) (b,a,d)	0.7030-0.7042	0.7037	13	Gill & Compston (1973)
South Sandwich Island (b,a,d)	0.7031-0.7041	0.7037	11	Gledhill & Baker (1973)
Bismarck Arc	0.7034-0.7040	0.7035	33	Peterman et al. (1970) Page & Johnson (1974)
Bougainville	0.7037-0.7039	0.7038	4	Page & Johnson (1974)
Eastern Papua	0.7042-0.7053	0.7047	3	Page & Johnson (1974)
New Guinea Highlands	0.7036-0.7044	0.7041	7	Page & Johnson (1974)
Aleutian Islands	0.7028-0.7037	0.7032	24	Kay et al. (1978)
Alaskan Peninsula (b,a)	0.7030-0.7034	0.7031	3	Arulus et al. (1977), Scholl et al. (1976) Hedge (1966)
New Zealand - Taupo Region (b)	0.7041-0.7043	0.7042	4	Ewart & Stipp (1968)
New Zealand - Taupo Region (a)	0.7045-0.7062	0.7055	12	Ewart & Stipp (1968)
Lesser Antilles -				
Monserrat St. Kitts	0.7029-0.7035	0.7032	2	Donnelly et al. (1971)
St. Lucia (b,a,d,r)	0.7035-0.7092	0.7063	10	Pushkar et al. (1973)
St. Vincent (b,a,d)	0.7037-0.7043	0.7040	14	Pushkar et al. (1973)
Cascades	0.7026-0.7047	0.7037	33	Hedge et al. (1970), Church & Tilton (1973)
Guatemala, El Salvador, Nicaragua	0.7029-0.7047	0.7039	13	Pushkar (1968)
Peru -				
central (a,d)	0.7042-0.7051	0.7046	4	Noble et al. (1975)
southern (Barroso)	0.7054-0.7068	0.7062	8	James et al. (1976)
southern (Areguipa)	0.7067-0.7079	0.7074	16	James et al. (1976)
Chile -				
central, southern (b,a)	0.7038-0.7042	0.7040	6	Klerkx et al. (1977
northern (a,d)	0.7050-0.7070	0.7060	12	Klerkx et al. (1977)
northern (r)	0.7052-0.7104	0.7080	8	Klerkx et al. (1977)
Western Italy (high-K lavas)	0.7068-0.7114	0.7092	22	Hurley et al. (1966)
Greece (Santorini) (b,a)	0.7045-0.7057	0.7050	6	Pe and Gledhill (1975)

B. Indonesia

Sumatra-Java (calcalkaline and tholeiitic suites)	0.70407-0.70594	0.70476	62	Whitford (1975)
Bali	0.70384-0.70407	0.70397	6	Whitford (1975)
Lombok (Rindjani) (b,a,d)	0.70386-0.70402	0.70395	7	This thesis
Sumbawa (alkaline lavas)	0.70385-0.70529	0.70455	12	This thesis
East Sunda & Banda Arcs	0.70544-0.70909	0.70651	20	Whitford et al. (1977)

Notes: All isotopic ratios normalized to 0.70800 for $^{87}Sr/^{86}Sr$ for E and A $SrCO_3$ except those of Kay et al. (1978) and Whitford (1975) (NBS 987 = 0.71022).

Abbreviations: b - basalt, a - andesite, d - dacite, r - rhyolite.

8.6 *Comparison of Sr-Isotope Data from Lombok and Sumbawa Islands with that from other parts of the Sunda and Banda Arcs.*

The ranges and mean values of the Sr-isotopic compositions of lavas from the western parts of the Sunda Arc, reported by Whitford (1975), from the far-eastern Sunda Arc and from the Banda Arc (Whitford et al., 1977) are given in the second part of table 8.2. Whitford (1975) recognised an eastward decrease in $^{87}Sr/^{86}Sr$ ratio from western Java towards Bali and Lombok islands. The data presented in this thesis from Lombok (Rindjani volcano) and from one Sumbawan volcano (Tambora), maintain this trend. Without exception, the $^{87}Sr/^{86}Sr$ ratios of the Rindjani and Tambora lavas (0.70385-0.70402) are lower than any reported by Whitford from Javanese or Sumatran volcanoes. Only values reported from Balinese volcanoes, immediately to the west of Lombok (G. Seraja, G. Agung and G. Batur) approach those of Rindjani and Tambora. While the Rindjani and Tambora Sr-isotope data extend Whitford's trend, that from the more alkaline Sumbawan volcanoes, Sangeang Api, G. Sangenges and Soromundi is markedly more radiogenic and the possible implications of this feature are discussed in the following subsections.

The easterly decrease in $^{87}Sr/^{86}Sr$ ratio is possibly significant in the light of the probable eastward change in crustal structure and age of the islands from Java to Lombok and Sumbawa. Java and Sumatra contain abundant volcanic and intrusive rocks of at least Mesozoic age (e.g. Van Bemmelen, 1949), while the islands of Lombok and Sumbawa have no rocks older than Miocene (see chapter 2 and Audley-Charles, 1975; Katili, 1975). Further, the islands are located on the eastern edge of the Sunda Shelf, in a zone where crustal thickness is apparently rapidly diminishing from near-continental thickness and velocity beneath Java to thinner, transitional oceanic/continental crust beneath Lombok and Sumbawa (Curray et al., 1977).

This transition in crustal type is akin to that described by Kay et al. (1978) from the Aleutians, where that arc lies partly on thin oceanic crust of the Bering Sea and partly on thicker continental-type crust of the Bering Shelf. In this case however, no significant variation in Sr-isotope composition was noted. Kay et al. (1978) interpreted their data to suggest that crustal type was not an important influence on Sr-isotope composition, whereas the data from the Sunda Arc does suggest that it may have some influence.

Whitford et al. (1977) and Whitford and Jezek (1978) report extremely high $^{87}Sr/^{86}Sr$ ratios (0.7054-0.7091) from islands at the extreme eastern end of the Sunda Arc and from the Banda Arc. The Indonesian arc appears to be in collision with the Australian continental plate in this region (Carter et al., 1976) and the very high $^{87}Sr/^{86}Sr$ ratios of erupted lavas may be due to melting of continentally derived sediments and/or continental crust in the subduction zone (Whitford et al., 1977).

The Sr-isotope ratios of these lavas are generally much higher than even those of the relatively $^{87}Sr/^{86}Sr$-enriched alkaline lavas from Sumbawa. In contrast to the undersaturated alkaline lavas from Sumbawa, these radiogenic Sr-enriched lavas are silica-rich, oversaturated volcanic rocks. Andesites and dacites from Ambon are cordierite-bearing and *co*-normative, which together with their high $^{87}Sr/^{86}Sr$ are characteristics believed to typify the S-type granitoids.

It is suggested that only in the Bali-Lombok-Sumbawa sector of the arc, flanked north and south by oceanic crust, are the Sr ratios likely to be mantle derived.

8.7 Discussion of the Sr-Isotope Data and its Implications

The $^{87}Sr/^{86}Sr$ ratios of the lavas of the Rindjani calcalkaline suite are all relatively low and show no significant variability (0.70386-0.70402)

in rocks which range from mafic ankaramite (LB8) through andesite to quite siliceous dacite (41671). Thus the similarity of these Sr-isotopes ratios tends to support a common source for all lavas of the Rindjani suite, unless coincidentally, different sources are involved which have the same Sr-isotopic composition.

These factors then allow two possible interpretations (and perhaps others): Either the suite has inherited its compositional diversity from varied extent or condition of equilibrium fusion of an isotopically homogeneous source, or the compositional range is due to some sort of differentiation of a basaltic parent (perhaps fractional crystallisation). The viability of these alternatives are examined using major- and trace-element data in chapter 9.

These data also throw some light on the general problem of andesite genesis. Magnesian ankaramite LB8 and typical andesite 41622 have very similar $^{87}Sr/^{86}Sr$ ratios implying a common source. As discussed in chapter 9, it is very unlikely that the mafic basaltic lava LB8 could have resulted from partial melting of subducted oceanic lithosphere and in general such a mafic basaltic composition would imply the product of fusion of peridotitic mantle. As the ankaramite and the andesite are associated in the same suite and have very similar Sr-isotope compositions, this then is indirect evidence that the andesitic source may also be the sub-arc mantle. Of course it is possible that the basalts of the Rindjani suite resulted from mantle fusion and that the andesites originated by fusion of the downgoing slab, but in this case it would seem coincidental that their Sr-isotope ratios are so similar.

The $^{87}Sr/^{86}Sr$ ratios of the Tambora *ne*-normative trachybasalts and trachyandesites also fall within a restricted range (0.70385-0.70399) and are virtually the same as those of the Rindjani suite. This then allows

the interpretation that all members of the suite are derived from the same isotopically homogeneous source, and/or that the trachyandesites may be differentiates of the associated trachybasalts.

Apparently both Rindjani and Tambora are tapping an isotopically similar source, in spite of the fact that, as discussed in chapters 4 and 12, the markedly higher K_2O, Rb and Sr concentrations of the Tambora lavas suggest that other geochemical differences might between the sources of the two volcanoes.

The fact that the $^{87}Sr/^{86}Sr$ ratios of the lavas of the other alkaline volcanoes from Sumbawa (Sangeang Api, G. Sangenges and Soromundi) are markedly higher (0.70412-0.70529) than those from Rindjani and Tambora suggests that these alkaline volcanoes must be tapping at least some component of their liquids from a source which is dissimilar to that yielding the other two suites. This is particularly so for the Sangeang Api suite where the lavas are very young and part of a well defined suite and where the same isotopic variation is displayed by associated intrusive nodules. In view of the somewhat similar geochemistries of the Tambora and Sangeang Api suites, this contrast in their Sr-isotope geochemistries is problematic and suggests that the rather subtle compositional differences between the two suites noted in chapter 5 (the Sangeang Api lavas have higher Rb/Sr ratios lower K/Rb ratios and slightly higher normative *ne*) may be significant.

The most K_2O-rich, leucite-bearing lavas from Soromundi and G. Sangenges (Si9, S19) have the most radiogenic Sr (0.70527-0.70529) and there is a rough trend of increasing $^{87}Sr/^{86}Sr$ ratio with increasing K_2O amongst the lavas of the Sangeang Api-Soromund-G. Sangenges (figure 8.5). As the lavas of each of these volcanoes show significant ranges of $^{87}Sr/^{86}Sr$ ratios, it appears that simple fractional crystallisation is unlikely to account for

the geochemical variation within each of these suites. The variability of Sr-isotope ratios suggests that there must be at least two distinct sources of Sr involved in these suites.

Several models for magma generation which involve the variable incorporation of more than one component with isotopically dissimilar Sr may be envisaged. Mantle-derived melts may be contaminated by the incorporation of variable amounts melt with more radiogenic Sr either from the subducted lithospheric slab or from the lower crust of the arc itself. The dehydration or partial fusion of the downgoing slab may yield water or small amounts of melt which could rise and react with the overlying peridotite resulting in the segregation of Rb/Sr-enriched heterogeneities either in the form of melt-rich zones or of mica peridotite. If these heterogeneities had relatively high Rb/Sr ratios and if they existed for a significant period of time, then they would become relatively enriched in radiogenic Sr. A subsequent melting event might incorporate variable proportions of melt derived from these heterogeneities and from unenriched mantle, thus yielding erupted liquids with a range of $^{87}Sr/^{86}Sr$ ratios.

Several other possibilities also exist. The source heterogeneities may be entirely of mantle origin. In this case liquids may be derived from different mantle regions, which have different Sr-isotope ratios. Alteration of the immediate mantle source by an alkaline, $^{87}Sr/^{86}Sr$-enriched component, with subsequent melting to yield eruptive lavas, or the alteration of the mantle source by a LIL-element enriched component which need not necessarily have a high $^{87}Sr/^{86}Sr$ ratio, but which yields regions with high Rb/Sr ratios which become relatively enriched in radiogenic Sr with time, are other possible explanations.

Apart from Rindjani, the amount of Sr-isotope data from the volcanoes of this sector of the Sunda Arc is limited and it is not possible to assess

the applicability of the above models precisely. However, as already discussed, the tectonics and geology of this sector of the arc suggest that contamination by old sialic, radiogenic Sr-enriched crust is unlikely. Furthermore, the Sr-isotopic variation of the Sangeang Api lavas, where the most mafic lava in the suite has also the most radiogenic Sr, also tends to discount crustal contamination, as the trend expected from this process would be opposite to that observed.

Contamination by melts generated in the subduction zone also appears unlikely. There is a general trend of increasing Sr^{87} with increasing concentration of K, Rb, Sr, normative *ne* and *lc*. The first formed melts of olivine tholeiite-pelagic sediment mixtures in the subduction zone are likely to be silica-rich and *Q*-normative (Stern and Wyllie, 1973; Green and Ringwood, 1972), and even for very small degrees of fusion are likely to be markedly less LIL-enriched than the Sumbawan leucitites. As a result it would seem unlikely that the supply of such a component to the mantle wedge (assuming that this melt is in fact $^{87}Sr/^{86}Sr$ rich, due either to the effects of seawater alteration or pelagic sediment incorporation) would result in the Sr-isotope-compositional variations seen in the Sumbawan alkaline lavas (i.e. one would expect a trend of decreasing undersaturation with increasing $^{87}Sr/^{86}Sr$ ratio).

It therefore seems likely that the $^{87}Sr/^{86}Sr$ variation seen within the suites from this sector of the Sunda Arc is of mantle origin. If this is the case then the variation may be due either to disequilibrium melting of a heterogeneous mantle, where these heterogeneities have existed for a significant period of time, or to mixing processes involving melts tapped from separate mantle domains.

Data from Sangeang Api, Soromundi and G. Sangenges tend to suggest that increasing $^{87}Sr/^{86}Sr$ ratio is associated with increasing concentrations of K, Rb, Sr and decreasing K/Rb ratio (see figures 8.5 and 8.6). This tends

to support a two end member model in which a LIL element-enriched component with a high $^{87}Sr/^{86}Sr$ ratio is mixed either with a melt with lower concentrations of these elements and with less radiogenic Sr, or enriches the source of this component prior to melting.

The main problem associated with these models is presented by the Tambora data. Here we have a suite which has some of the alkaline character of those mentioned above, but not the radiogenic Sr. This tends to suggest that the alkaline component is not initially enriched in radiogenic Sr, and hence the variation in Sr-isotopic composition within the group of more alkaline volcanoes, may not be simply due to mixing of two liquid components. If a separate liquid component is to be invoked, then it is required that this invade the upper mantle source region and yield Rb/Sr-enriched heterogeneities. The life-span of these then determines the $^{87}Sr/^{86}Sr$ ratio of melts produced when fusion finally takes place. In this model, Tambora lavas would be required to have resulted from melting of short-lived heterogeneities, while the leucitites may have been derived from older ones.

A simple mixing model is still a slight possibility. Figure 8.6 shows the variation of $^{87}Sr/^{86}Sr$ v K/Rb of lavas for which Sr isotope data is available. A curve is shown for the mixing of two hypothetical liquid components; A. an alkaline liquid with K_2O = 8.43%, Rb = 350 ppm, K/Rb = 200, Sr = 1400 ppm and $^{87}Sr/^{86}Sr$ = 0.7055 B. an alkali-poor liquid with K_2O = 0.87%, Rb = 12 ppm, K/Rb = 600, Sr = 500 ppm and $^{87}Sr/^{86}Sr$ = 0.7038. The mixing curve produced by these end members shows reasonable adherence to the data trend, particularly if it is noted that most of the lavas plotted are not primary liquids and fractional crystallisation may have modified their K/Rb ratios. In this model, because, relative to the low alkali component B, the postulated contaminant A is much more enriched in Rb and K relative to Sr, mixing produces an initial trend from B of rapidly

FIGURE 8.3

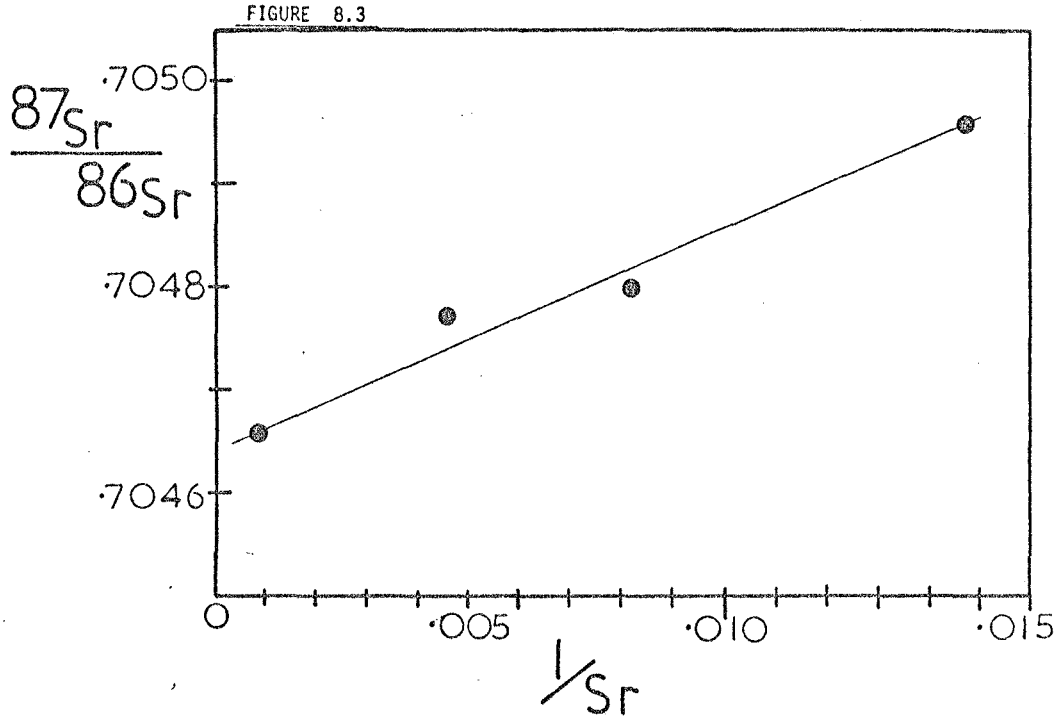

FIGURE 8.4

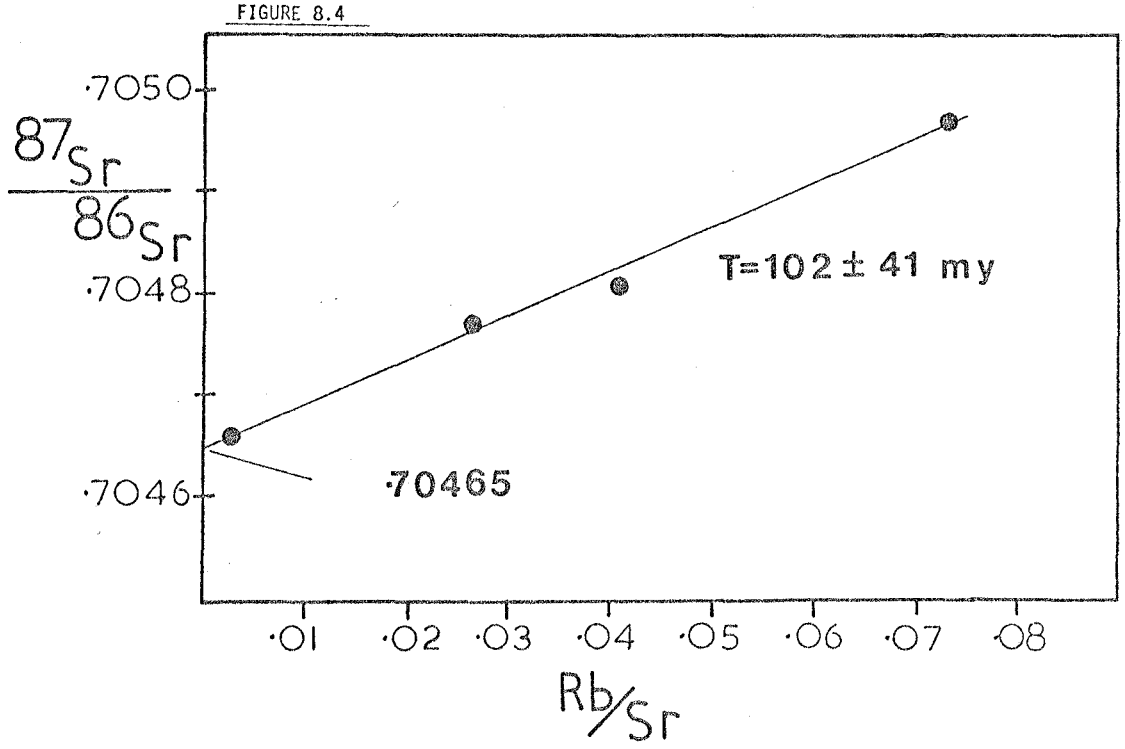

Figure 8.3

$^{87}Sr/^{86}Sr$ v. 1/Sr variation of Sangeang Api xenoliths.

Figure 8.4

$^{87}Sr/^{86}Sr$ v. Rb/Sr "pseudoisochron" plot of Sangeang Api xenoliths. Yielding an apparent "age" of 102 my + 41 my . and an initial ratio of 0.70465. ($\lambda\ ^{87}Rb = 1.42 \times 10^{-11}\ yr^{-1}$) .

increasing Rb and K and decreasing K/Rb with only slight increase in $^{87}Sr/^{86}Sr$ ratio. Thus if the Rindjani primary liquid was represented by component B, then the Tambora suite could be derived from a primary liquid with up to 10% of the hypothetical alkaline component A, while the other more alkaline suites would require between 20 and 60% of this component.

Of course this is a very simplistic model and added complications are introduced by considering liquids derived from variable proportions of fusion of the same source, or if the mixing process took place as an alteration of the source prior to fusion.

8.8 The Sr-Isotopic Composition of the Sangeang Api Lavas and Xenoliths: Implications

The association of lavas and coarse-grained intrusive rocks in the Sangeang Api suite are of particular interest. While the actual origin of the nodules is by no means clear, calculations and discussion presented in chapter 9 suggest that they are of appropriate mineralogy and geochemistry to represent cumulate precipitates from liquids like those of the Sangeang Api lavas and that the compositional variation of these lavas could result from fractionation of assemblages represented amongst the nodules.

However, because those lavas for which Sr-isotope data are available have different $^{87}Sr/^{86}Sr$ ratios, this simple model is untenable. Furthermore the nodules show the same range of $^{87}Sr/^{86}Sr$ values and yield a pseudoisochron (fig. 8.4) with an apparent "age" of 102 $\pm$ 41 my.

If the "age" of the xenoliths as indicated by the pseudoisochron is real, then why do the analysed lavas, some of which are <100 years old (B25 is from the 1911 flow) and none of which are older than Quaternary, also display an almost identical range of isotopic composition? As there is no possibility that the lavas are anything like 100 my old, then for reasons discussed in the previous section, it is likely that they are

FIGURE 8.5

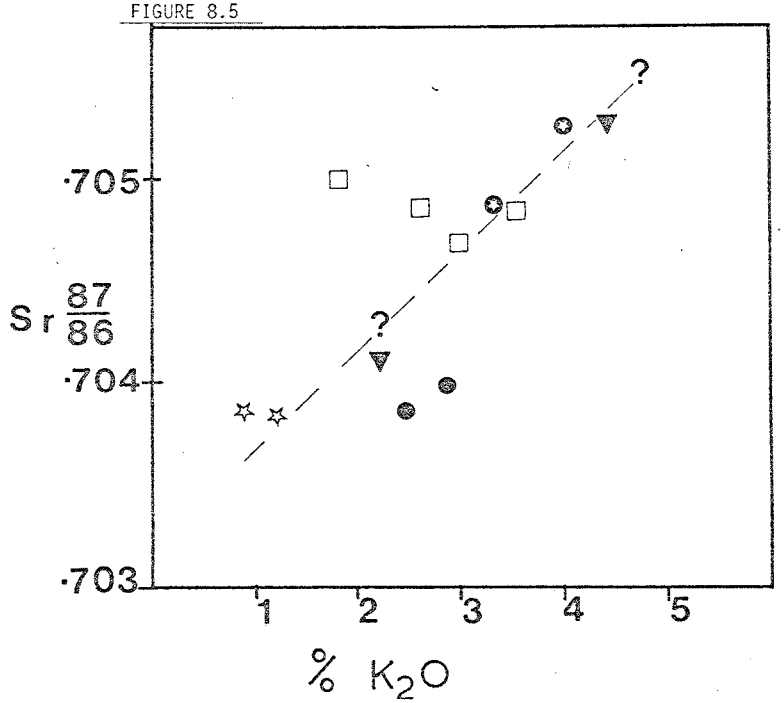

Figure 8.5

$^{87}Sr/^{86}Sr$ v. Wt.% K_2O variation of Soromundi and G.Sangenges K-rich suites, Sangeang Api lavas and Tambora and Rindjani basalts. Illustrating a slight suggestion of a positive correlation between K and $^{87}/$ 86 Sr isotope ratio. Symbols as in figure 8.1

reflecting isotopic variability in the mantle source. The four lavas for which data are available, must either represent samples of four different batches of liquid, or different mixtures of two or more isotopically dissimilar components.

If the nodules are really about 100 my. old, then they cannot possibly be cumulates of the Sangeang Api magmas represented by the lavas. On the other hand, if they are as young as the lavas, then they may represent precipitates from an isotopically varied suite of liquids, liquids which display the same isotopic range as the associated lavas. Or, they may be recording a mixing or contamination event.

The positive correlation of $^{87}Sr/^{86}Sr$ and 1/Sr (figure 8.3) in the nodules lends some support to the last suggestion. The olivine clinopyroxenites (B23 and B4) have the most radiogenic Sr and have low Sr concentrations (68 and 148 ppm respectively), while the hornblende anorthite gabbro B8 has the least radiogenic Sr and much higher Sr concentration (1125 ppm). Thus a much smaller amount of a radiogenic Sr-enriched contaminant would have to be added to the mafic, Sr-poor olivine clinopyroxenites to yield a significant increase in their $^{87}Sr/^{86}Sr$ ratio, than to the Sr-rich plagioclase-bearing rocks. In this case all the intrusive rocks may have precipitated from a liquid whose $^{87}Sr/^{86}Sr$ ratio may have been as low or lower than that of the xenolith with the lowest ratio (B8, 0.70466) and have then been modified by reaction with later, more radiogenic Sr-rich liquids. This contamination may have taken place by the introduction of the interstitial, and in some cases obviously secondary, phlogopite and amphibole found in some xenoliths. In this model, the liquids invoked, may or may not be represented in the young Sangeang Api lava suite.

FIGURE 8.6

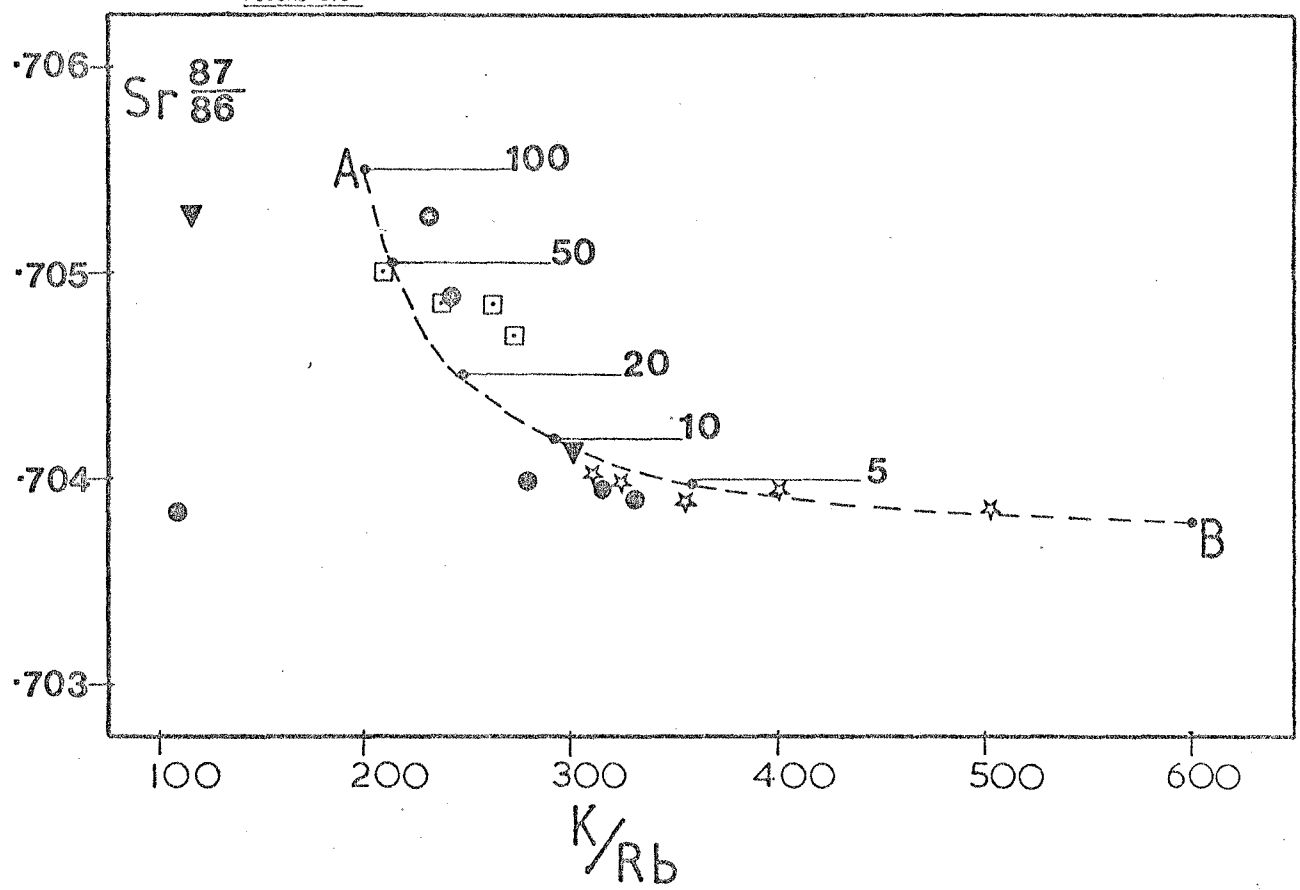

Figure 8.6

$^{87}Sr/^{86}Sr$ v. K/Rb variation for lavas from the Lombok-Sumbawa sector of the Sunda Arc .Symbols as in figure 8.1.The variation yields a suggestion of an asymptotic curve possibly interpretable as the result of end-member mixing.(note that any post-mixing magmatic differentiation process which changes the K/Rb ratio of the liquid will displace compositions away from the ideal original curve at constant $^{87}Sr/^{86}Sr$ values but variable K/Rb).A curve produced by the mixing of two hypothetical end members, which approximates the trend of the data from this sector of the Sunda Arc is plotted.A = alkaline component;8.4% K_2O,350 ppm Rb,1400 ppm Sr,K/Rb =200 $^{87}Sr/^{86}Sr$ = 0.7055.B= "normal liquid" ; 0.9% K_2O,12 ppm Rb,500 ppm Sr,K/Rb=600 $^{87}Sr/^{86}Sr$ = 0.7038 .Figures 5 to 100 indicate the percentage of A added to B.

8.9 *Conclusions*

With respect to many of the suites considered in this study, the available Sr isotope data create more problems than it solves. The main conclusions that can be drawn are as follows:

1. The bulk of the Sr in the lavas from this sector of the Sunda Arc is probably of mantle origin.
2. All the lavas of the Rindjani calcalkaline suite may have a common source and the more silica-rich lavas may be the products of fractional crystallisation of the associated basalts.
3. The lavas of more alkaline volcanoes (Sangeang Api, Soromundi and G. Sangenges) have a more complex origin, their petrogenesis probably requiring processes which may include: mixing, source hetrogeneity and disequilibrium melting and certainly require more than one source of Sr.
4. The Sangeang Api lavas do not represent a single series of liquids, related by fractional crystallisation, similarly the associated intrusive rocks do not represent simple cumulate precipitates of any one batch of evolving magma.
5. The Tambora lavas may all be derived from the same isotopically homogeneous source and isotopic data allows members of the suite to be related by fractional crystallisation.

Chapter 9

FRACTIONAL CRYSTALLISATION AND ITS ROLE IN THE ORIGIN AND DIFFERENTIATION OF THE LAVAS FROM THE LOMBOK-SUMBAWA SECTOR OF THE SUNDA ARC

9.1 *Introduction*

This, and chapters 10, 11 and 12 are mainly concerned with the examination of the origin of the lavas under investigation and the sources of their compositio diversity. This chapter concentrates on the role of fractional crystallisation and the ability of this mechanism to account for compositional variation within particular suites. The phase relationships implied by the conclusions drawn in this chapter are examined in the light of published experimental data in chapter 10 and are further tested by new experiments described in chapter 11. Chapter 12 examines those aspects of the compositional diversity, within and between separate suites, which are not explicable in terms of fractional crystallisation models.

9.2 *Modelling Procedures*

This chapter is mainly devoted to detailed examination of the geochemical variation of each suite and to attempts to model this variation. The general approach adopted has been used quite commonly in recent petrogenetic studies (e.g. Arculus, 1976 or Ewart, 1973). The process involves combination of the major element compositions of postulated parental compositions with the compositio of mineral phases which may have crystallised from (or accumulated in) the parent, to yield a differentiate. A least-squares mixing program similar to that described by Bryan et al. (1969) is used to match observed and estimated compositions. For instance rock A, containing phenocrysts x, y and z, may be thought to be parental to rock B, rock B being produced by crystallisation and removal of some proportion of rock A's phenocryst minerals, $xX + yY + zZ$. To test this idea, a least squares approximation of rock A as a mixture of the compositions of phenocrysts x, y and z and postulated fractionated rock B (thought to represent the residual liquid) is calculated. Solutions to these

Table 9.1 Distribution Coefficients Used in Modelling Calculations

Number	1	2	3	4	5	6	7	8	9	10	11	12	13	14	15
Phase	Cpx	Cpx	Cpx	Opx	Opx	Ol	Plag.	Amph	Garnet	Magnetite	Apatite	Apatite	Apatite	Phlogopite	Biotite
Source Reference *	1,2	2	5	1	6	1	1	1	1		10	11	12	13	14
La	0.1	0.35	0.35	0.03	0.05	0.01	0.1	0.2	0.005	0.05	18	34	52	0.034	0.32
Ce	0.15	0.50	0.45	0.031	0.082	0.01	0.1	0.25	0.007	0.05	18	34.7	52	0.034	0.32
Nd	0.35	1.11	0.65	0.034	0.120	0.01	0.1	0.45	0.03	0.05	27.4	57.1	81	0.032	0.29
Sm	0.55	1.67	1.10	0.047	0.16	0.01	0.1	0.60	0.25	0.05	29.3	62.8	90	0.031	0.26
Eu	0.60	1.56	1.15	0.06	0.093	0.01	0.25 [8]	0.70	0.35	0.05	20.5	30.4	50	0.030	0.24
Gd	0.70	1.85	1.15	0.10	0.23	0.01	0.1	0.75	0.97	0.05	27.2	56.3	60	0.030	0.28
Dy	0.75	1.93	1.10	0.15	0.33	0.01	0.1	0.80	3.17	0.05	25.6	50.7	69	0.030	0.29
Ho	0.70	1.80	1.20	0.20	0.53	0.01	0.1	0.65	5.00	0.05	19.0	37.0	45	0.034	0.35
Yb	0.62	1.58	0.95	0.45	0.73	0.01	0.1	0.40	9.00	0.050	13.1	24.0	37	0.042	0.44
Y [(a)]	0.70	1.80	1.2	0.20	0.53	0.01	0.1	0.65	1.4 [4]	0.02	19	37	45	0.034	0.35
Ba	0.03	0.03	0.13	0.01	0.003	0.001	.4 [8]/.2 [2]	0.50	0.04	0.001	0.5 (?)	0.5 (?)	0.5 (?)	1.09	9.7
Rb	0.02 [4]	0.02	0.03	0.015	0.002	0.001	0.07	0.25	0.03	0.0001	0.1	0.1	0.1	3.06	2.24
Sr	0.16[2]/0.4[3]	0.3	0.50	0.01	0.008	0.001	2.0 [3]	0.50	0.008	0.0001	0.5 (?)	0.5 (?)	0.5 (?)	0.081	
Cs	0.01	0.01	0.02	0.001	0.001	0.001	0.05 (?)	0.1 (?)	0.02	0.0001	0.1	0.1	0.1		
Pb	0.02	0.02	0.03	0.001	0.001	0.001	0.5 (?)	0.1 (?)	0.001	0.001	0.1	0.1	0.1		
Zr	0.02	0.02	0.02	0.001	0.001	0.001	0.001	0.25 [15]	0.001	0.01	0.1	0.1	0.1		
Hf	0.02	0.02	0.02	0.001	0.001	0.001	0.001	0.1	0.001	0.01	0.1	0.1	0.1		
U	0.001	0.001	0.001	0.001	0.001	0.001	0.001	0.1	0.001	0.0001	0.1	0.1	0.1		
Th	0.001	0.001	0.001	0.001	0.001	0.001	0.001	0.1	0.001	0.0001	0.2	0.2	0.2		
Ni	3	3	3	4 [7]	4 [7]	14 [8]	0.01	7 [10]	0.7	10 [8]	0.001	0.001	0.001	13 [9]	13 [9]
Cr	10 [8]	10	10	1	1	1	0.06	5 [1]	20	1-150 [8,10]	0.001	0.001	0.001	17 [9]	17 [9]
Sc	3	7	5	1	3	0.5	0.03	3	8	2 [8]	0.001	0.001	0.001		

Notes: *(a)* Y values taken as the same as those for Ho.

(?) estimated values.

* Source References:

1 Lopez-Escobar, L., Frey, F.A. and M. Vergara (1977).

2 Arth, J.G. (1976) (Cpx 2 has higher distribution coefficients, in equilibrium with dacitic-rhyolitic liquids).

3 Sun, C.O., Williams, R.J. and S.S. Sun (1974) (at 1120°C).

4 Frey, F.A., Green, D.H. and Roy, S.D. (in press, 1978).

5 Harris, K.L., Nicholls, I.A. (in press, 1978) (anderitic values).

6 Arth (*ibid.*) (average rhyolitic value).

7 Frey, F.A., Green, D.H. and Roy, S.D. (*ibid.*) (Opx average value).

8 Murali, A.V., Leeman, W.P., M.-S., Ma and R.A. Schmitt (in press, 1978).

9 Gill, J.B. (1978).

10 Arth, J.G. (*ibid.*) (low apatite value).

11 Arth. J.G. (*ibid.*) (average apatite value).

12 Zielinski, and Frey, F.A. (1970).

13 Arth, J.G., (*ibid.*) (basaltic value).

14 Arth, J.G., (*ibid.*) (rhyolitic rocks).

15 Kesson, S. and Price, R.C. (1972).

calculations supply estimates of the relative proportions of individual mineral phases crystallised, as well as the proportion of liquid remaining (representing the derivative rock B).

As an additional test, the trace element content of the postulated derivative lava (B) can then be calculated. Using the Rayleigh fractionation expression (e.g. Greenland 1970) and the relative proportion and total percentage of minerals crystallised, as calculated in the least-squares model, together with the appropriate mineral-liquid distribution - coefficients[1] (table 9.1) and the concentration of the trace element in question in the parent lava (A), the likely concentration of this element in the fractionated lava (B) can be calculated. This can then be compared with the observed value.

9.3 Source and Origin of the Rindjani Calcalkaline Suite

The source of the volcanic suites of island- and continental marginal-arcs is the subject of controversy. Some arcs, such as the Peruvian and Chilean Andes, are dominated by andesitic or basaltic-andesitic lavas (e.g. Noble et al., 1975; James et al., 1976; Klerkx et al., 1977) thus much of the controversy is about the origin of andesite. Because andesite is unlike the differentiates produced by fractional crystallisation of basalts, in provinces where those basalts are of undisputed mantle origin (e.g. ocean islands), many special theories for its origin have arisen.

Note: Distribution coefficients are in many cases poorly known and are in many cases a function of several variables (for instance, T, P, fO_2 or liquid composition). Irving (1978) presents a comprehensive review of much of the available data for a wide range of minerals and trace elements and several recent articles (e.g. Frey et al., 1978) present several alternative sets of partition coefficient data which are each believed to apply to particular aspects of the models they present. Data presented in table 9.1, and used in this thesis are culled from numerous sources and these sources are also quoted. In general values quoted are average or "accepted" numbers and generally chosen to apply to the specific rock-type in which they are used (e.g. basalt, andesite or dacite).

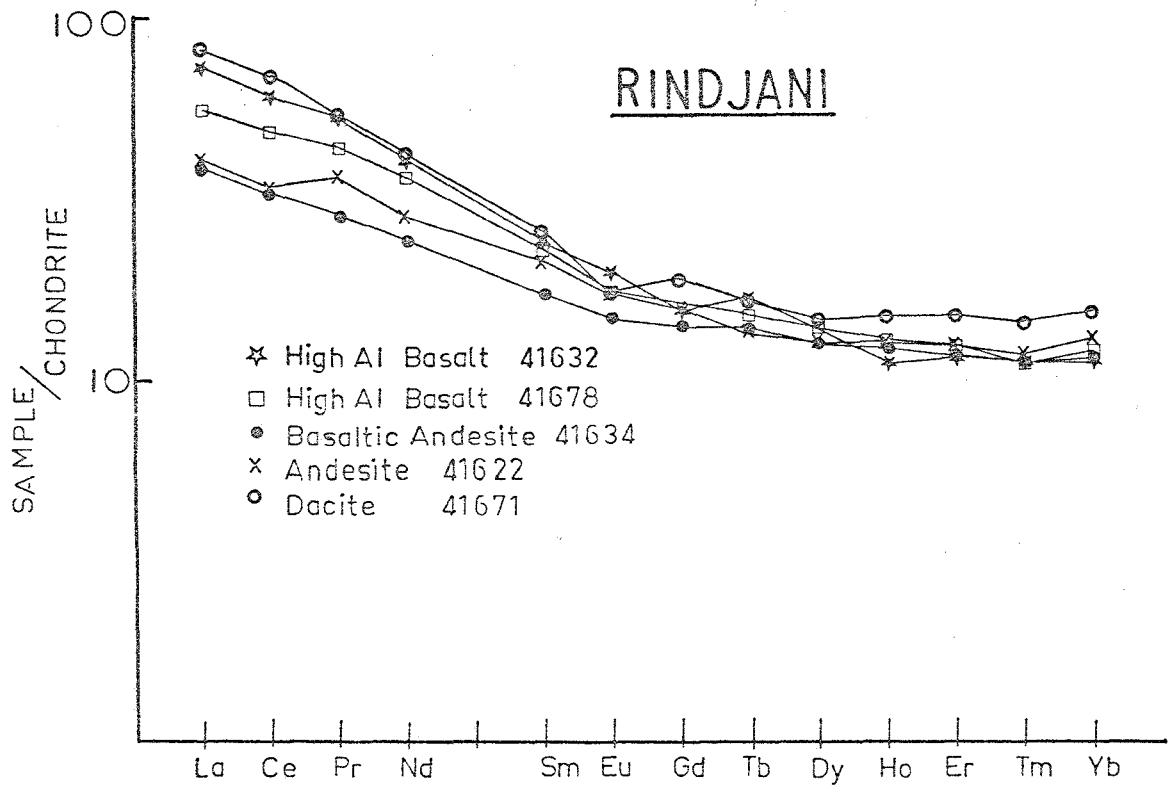

FIGURE 9.1

Chondrite -normalised REE patterns of Rindjani calcalkaline lavas .(Actual values given in table 9.3).

Reviews of possible mechanisms for the origin of andesites have been published by a number of authors (e.g. Ringwood, 1974; Boettcher, 1973; Gill, 1978). Proposed mechanisms fall into two broad groups. One group suggests that quartz-normative liquids are primary products of melting in the source region; which may be hydrous, upper mantle peridotite (e.g. Green, 1973; Nicholls, 1974; Mysen and Boettcher, 1975), or subducted ocean floor tholeiitic basalt (amphibolite or eclogite).

The other group of mechanisms call on various fractional crystallisation schemes to produce andesites, dacites and rhyolites from basalt parent magmas. These fractional crystallisation schemes variously emphasise the roles of: magnetite (e.g. Osborn, 1959, 1969), olivine (e.g. Nicholls and Ringwood, 1972, 1973; Nicholls, 1974) and amphibole (e.g. Bowen, 1928; Ringwood, 1974; Sigurdsson et al., 1973; Allen et al., 1975; Allen and Boettcher, 1971, Holloway, 1973; Cawthorn and O'Hara, 1976; Cawthorn et al., 1973; Eggler, 1972)

It is unlikely that the Rindjani calcalkaline suite has originated by partial melting of the basaltic portion of the downgoing slab. The Benioff zone is 170 km below Rindjani volcano and as the amphibolite-eclogite transition will occur between 80 and 100 km (e.g. Ringwood, 1974), the downgoing slab in this region is likely to be in the eclogite facies.

As demonstrated by Stern (1974) and Stern and Wyllie (1973), compositions of primary liquids formed by partial melting of olivine tholeiite at 30 kbs do not match the observed calcalkaline trends. Further, the REE patterns of melts formed in equilibrium with eclogitic residue are likely to be highly fractionated with high La/Yb ratios, unlike the patterns from any of the lavas of this (see Chapter 12), or many other calcalkaline suites (e.g. Gill, 1974). Further, the concentrations of LIL elements (e.g. K, Rb, Sr, Ba) in both basalts and andesites are such that they could only be achieved by very small degrees of partial melting of a source composed of depleted ocean floor tholeiite. This is then in conflict with the relatively mafic character of many of the basaltic lavas from Rindjani, whose MgO, CaO, Cr, Ni and Sc concentrations would require large degrees of fusion of olivine tholeiite source.

Table 9.3 Rare Earth Element * and U, Th, Pb, Hf, Ba, Cs *, Analyses of Representative Lavas from Rindjani Volcano

Sample No.	41632			41678			41634			41622			41671		
	ppm		ppm/cond.	ppm		ppm/cond.	ppm		ppm/cond.	ppm		ppm/cond.	ppm		ppm/cond.
La	22.87	± 1.87	72.59	17.42	± 1.94	55.31	12.08	± 0.47	38.35	12.84	± 1.07	40.77	25.98	± 1.24	82.48
Ce	48.88	± 4.74	60.12	39.10	± 5.05	48.09	26.62	± 0.34	32.73	27.46	± 1.99	33.78	56.52	± 2.62	69.52
Pr	6.14	± 0.50	52.94	5.06	± 0.66	43.66	3.29	± 0.08	28.39	4.24	± 0.12	36.51	6.32	± 0.26	54.52
Nd	24.00	± 1.78	40.20	21.48	± 1.68	35.98	14.42	± 0.67	24.16	16.90	± 1.73	28.32	25.09	± 1.01	42.03
Sm	4.59	± 0.26	23.91	4.34	± 0.34	22.63	3.28	± 0.14	17.10	4.09	± 0.23	21.30	4.98	± 0.13	25.95
Eu	1.41	± 0.14	19.52	1.26	± 0.08	17.56	1.05	± 0.03	14.62	1.24	± 0.07	17.19	1.26	± 0.04	17.37
Gd	4.01	± 0.39	15.47				3.60	± 0.05	13.90	4.12	± 0.30	15.92	4.96	± 0.27	19.16
Tb	0.82	± 0.07	16.75	0.73	± 0.03	14.82	0.67	± 0.02	13.60	0.66	± 0.03	13.54	0.81	± 0.03	16.63
Dy				4.57	± 0.31	14.07	4.05	± 0.20	12.47	4.13	± 0.30	12.69	4.75	± 0.20	14.63
Ho	0.80	± 0.04	10.96	0.93	± 0.04	12.73	0.89	± 0.05	12.20	0.90	± 0.05	12.62	1.10	± 0.03	15.10
Er	2.45	± 0.21	11.50	2.60	± 0.17	12.22	2.48	± 0.12	11.63	2.65	± 0.17	12.46	3.22	± 0.09	15.11
Tm	0.33	± 0.02	11.03	0.33	± 0.02	10.98	0.33	± 0.02	11.12	0.35	± 0.03	11.68	0.43	± 0.01	14.39
Yb	2.37	± 0.15	11.42	2.48	± 0.11	11.92	2.31	± 0.05	11.11	2.69	± 0.12	12.92	3.23	± 0.09	15.55
Lu (est.)	0.369			0.385			0.359			0.418			1.88	± 0.06	
ΣREE	123.5			104.9			75.4			82.7			140.5		
Y	20		10	30		15	28		14	30		15	41		20.5
ΣREE + Y	143.5			134.9			103.4			112.7			181.5		
La/Yb	9.64		6.35	7.02		4.64	5.22		3.45	4.77		3.16	8.04		5.30
Eu/Eu *	1.0			1.0			1.0			0.93			0.77		0.77
La/Sm	4.98		3.03	4.01		2.44	3.68		2.24	3.14		1.91	5.21		3.18
Sm/Eu	3.25		1.22	3.44		1.29	3.12		1.17	3.30		1.24	3.95		1.49
Gd/Yb	1.69		1.35				1.56		1.25	1.53		1.23	1.54		1.23
U	2.17	± 0.21	216.88	1.40	± 0.08	140.19	0.66	± 0.03	66.39	0.95	± 0.03	95.16	2.96	± 0.09	296.04
Th	6.83	± 0.76	184.54	6.19	± 0.20	167.27	2.54	± 0.08	68.69	3.17	± 0.22	85.59	10.89	± 0.41	294.36
Pb208				4.29	± 0.34	2.39	3.86	± 0.34	2.14	3.30	± 0.43	1.83	8.55	± 0.28	4.75
Pb207				2.02	± 0.15	3.37	1.99	± 0.13	3.32	1.68	± 0.13	2.80	4.32	± 0.18	7.19
Pb206				2.25	± 0.5	3.75	2.12	± 0.17	3.53	1.75	± 0.12	2.92	4.59	± 0.17	7.64
ΣPb				8.56			7.96			6.73			17.46		
Hf	4.00	± 0.12	21.06	3.48	± 0.16	18.35	2.62		13.79	3.07	± 0.22	16.20	5.85	± 0.21	30.80
Pb207/206				0.818	± 0.019		0.846	± 0.038		0.841	± 0.035		0.941		
Pb208/206				2.047	± 0.079		2.046	± 0.078		2.064	± 0.056		1.862		
Th/U	3.14		0.85	4.42		1.19	3.85		1.03	3.33		0.90	3.68		0.99
Ba	896	± 73	358.4	428	± 67	171.4	378	± 22	151.26	374	± 28	149.5	829	± 19	331.6
Cs	0.23		1.18	0.96		5.33	0.51		2.83	0.54		3	2.97	± 0.13	16.5
Zr/Hf	20.5			49.7			40.8			43.6			45.1		
La/Rb	1.14			0.34			0.40			0.37			0.27		
La/Zr	0.28			0.10			0.11			0.10			0.10		
K/Ba	11.2			38.8			30.1			35.5			36.7		

* Analysed by spark-source mass spectroscopy (MS7), at the Research School of Sciences, A.N.U.

If partial melting of the downgoing slab is eliminated then the mantle wedge and the crust remain as potential dominant sources. A crustal origin is unlikely both because of the thinness of the crust in this segment of the arc and because the Rindjani suite has abundant relatively mafic basaltic rocks and to produce these in the crust would require extremely high geothermal gradients. At the same time $^{87}Sr/^{86}Sr$ ratios for basalts, andesites and dacites are uniform and amongst the least radiogenic of any determined from the Sunda Arc (Whitford, Foden and Varne, 1979), which suggests a similar source for basalts and andesites and tends to discount contamination by sialic crustal material.

This then points to a mantle origin for the entire suite. Experimental studies of Nicholls (1974) and Green (1976) suggest that quartz normative liquids with >55% SiO_2 are not potential mantle peridotite melts, and while water saturated melting of peridotite can yield oversaturated melts with >55% SiO_2 at <10 kbs these are still constrained to have Ni contents and Mg/Mg+Fe values compatible with equilibrium with mantle olivine. The Rindjani andesites have very low Ni concentrations and low Mg/Mg+Fe values and are unlikely to be primary melts of mantle peridotite. These factors suggest that though the Rindjani suite is of mantle origin, all the andesites and dacites as well as many of the basalts have probably been modified by fractional crystallisation processes.

Two possible options then exist for the origin of the Rindjani andesites: 1. either the andesites are fractionated liquids derived from basaltic parents, perhaps some the high-Al basalts actually sampled, or 2. the andesites are fractionated liquids derived from more mafic "primary andesite" parents, not represented in the sampled Rindjani suite. However, the fact that the andesites have consistently lower concentrations of Ni, Cr, Sc and Mg than most of the fractionated basaltic lavas, suggests that they are more fractionated than these. This tends to support the fractionation of the andesites and low MgO, high-Al basalts from similar parents. If a hypothetical primary andesite did exist it would seem coincidental that this always reached the surface in a more fractionate state than basalts derived from the primary high-Al basalt parent.

In fact as demonstrated in the following section, simple crystallisation and removal of the phenocrysts of the sampled high-Al basalts failed to produce resultant differentiates like the sampled Rindjani andesites. This may indicate that the mechanism is wrong, or that the parent magmas used were inappropriate. If the former situation is true, then alternative explanations can be sought, and this is the course of action adopted in this thesis.

9.4 Fractional crystallisation and the differentiation of the Rindjani suite

1. Ankaramites:

Qualitatively, their geochemical variations are consistent with removal (or addition) of the clinopyroxene-dominated phenocryst assemblage, to produce sympathetic variation of Cr, Ni, Sc, MgO, CaO and Mg/Mg+Fe and antipathetic variation of these parameters with Al_2O_3, K_2O, Na_2O, Rb, Sr, Zr, Nb and Y (figures 3.7 - 3.10). They plot on a well defined trend of CaO depletion and Al_2O_3 enrichment, quite distinct from that shown by the other members of the Rindjani suite (figure 9.2). This trend is very like that shown by many of the clinopyroxene-rich alkaline lavas from Sumbawa (figure 6.5).

The combined least-squares mixing and trace-element modelling technique described earlier was used to reproduce the observed trend within the ankaramite group, by fractionating the cpx-olivine phenocryst assemblage. Thus one of the more mafic ankaramites (LB7, table 9.5) was modelled as a combination of one of the most differentiated examples (LB1, table 9.5) and analysed olivine and clinopyroxene phenocrysts. As described in chapter 3, the clinopyroxene phenocrysts of the ankaramites are zoned with Cr-diopside cores and Al-augite rims, so that the mixing calculation used both these compositions. The calculated approximation to LB7 (table 9.5), was a very close match to the observed composition of this lava and the calculation suggests that LB1 could result from removal from LB7 of 15% of an assemblage of 26.4% olivine, 15.4% Cr-diopside and 58.2% Al-augite. The calculated trace-element variations on the basis of these mineral proportions (table 9.6A) give a close approximation to the values found in LB1. In particular, the trace elements "incompatible" in terms of this mineral assemblage, Rb, Sr and Zr, very closely match the observed values.

Table 9.5 Least-squares Mixing Computations to Model Possible Fractional Crystallisation Processes in the Rindjani calcalkaline suite

A. Approximation of ankaramite LB7 in terms of its phenocryst and postulated derivative lava, LB1 (ankaramite).

Lava	AK	AK	AK
Sample No.	LB7	LB7	LB1
	obs.	est.	
SiO_2	47.95	48.08	48.33
Al_2O_3	13.78	13.48	15.34
FeO_T	10.10	10.22	10.30
MgO	10.61	10.45	8.39
CaO	13.14	12.96	12.30
Na_2O	1.78	2.06	2.42
K_2O	1.20	1.10	1.29
TiO_2	0.83	0.86	0.91
P_2O_5	0.21	0.24	0.28
MnO	0.17	0.18	0.20

Component	Wt. Fraction	Cumulate Mode (Wt. Fract.)
Olivine	0.0389	0.2630
Cpx A	0.0228	0.1542
Cpx B	0.0862	0.5828
Lava LB1	0.8513	

= ankaramite LB7 (est.)

ΣR^2 = 0.2717

	Cumulate Composition
SiO_2	46.93
Al_2O_3	2.82
FeO_T	9.85
MgO	22.38
CaO	16.56
Na_2O	0.00
K_2O	-
TiO_2	0.59
P_2O_5	-
MnO	0.06
100 Mg/ Mg + ΣFe	80.19

B. Approximation of ankaramite LB11 in terms of possible derivative lava, alkali olivine basalt 41621 and phenocrysts.

Lava	AK	AK	AOB
Sample No.	LB11	LB11	41621
	obs.	est.	
SiO_2	49.27	49.27	49.97
Al_2O_3	14.26	14.26	17.42
FeO_T	10.20	10.17	10.20
MgO	8.35	8.36	5.78
CaO	12.58	12.57	9.62
Na_2O	2.49	2.54	3.50
K_2O	1.19	1.06	1.49
TiO_2	0.99	1.23	1.26
P_2O_5	0.27	0.23	0.32
MnO	0.18	0.15	0.19

Component	Wt. Fraction	Cumulate Mode (Wt. Fract.)
Olivine	0.0201	0.0698
Cpx	0.2288	0.7944
Plag.	0.0262	0.0910
Mag.	0.0129	0.0448
Lava 41621	0.7132	

= ankaramite LB11 (est.)

ΣR^2 = 0.0775

	Cumulate Composition
SiO_2	47.31
Al_2O_3	6.38
FeO_T	10.04
MgO	14.72
CaO	19.82
Na_2O	0.14
K_2O	0.01
TiO_2	1.13
P_2O_5	-
MnO	0.04
100 Mg/ Mg + ΣFe	72.32

C. Approximation of ankaramite LB11 in forms of its phenocrysts (+ amphibole) and possible derivative lava LB28 (high K_2O, high Sr andesite).

Lava	AK	AK	HKSA
Sample No.	LB11	LB11	LB28
	obs.	est.	
SiO_2	49.27	49.28	55.91
Al_2O_3	14.26	14.26	19.54
FeO_T	10.20	10.21	6.28
MgO	8.35	8.35	2.55
CaO	12.58	12.56	7.49
Na_2O	2.49	2.39	4.07
K_2O	1.19	1.16	2.39
TiO_2	0.98	1.16	0.70
P_2O_5	0.27	0.16	0.37
MnO	0.18	0.24	0.20

Component	Wt. Fraction	Cumulate Mode (Wt. Fract.)
Olivine	0.0160	0.0281
Cpx	0.2718	0.4770
Amph.	0.1677	0.2943
Plag.	0.0842	0.1478
Mag.	0.0301	0.0528
Lava LB28	0.4342	

= ankaramite LB11 (est.)

ΣR^2 = 0.0596

	Cumulate Composition
SiO_2	43.89
Al_2O_3	10.14
FeO_T	12.84
MgO	12.70
CaO	16.33
Na_2O	1.10
K_2O	0.23
TiO_2	1.50
P_2O_5	-
MnO	0.26
100 Mg/ Mg + ΣFe	63.80

Abbreviations: AK = ankaramite, AOB = alkali olivine basalt, HKSA = high K_2O, high Sr andesite, obs. = observed composition, est. = calculated composition.

Notes: FeO_T = total Fe as FeO.

Refer to Table 9.17for the locality of mineral compositions used in these calculations.

Table 9.6

Calculated Trace Element Variation Trends for Rindjani Lavas

A. Ankaramite LB7 —— Ankaramite LB1

	C_o	C_1 (est)	C_1 (obs)	% Discrep.
Sample No.	LB7		LB1	
% crystallisation	14.87			
Ni	125	57	57	0
Sc	36	29	39	-25.6
Rb	31	36	38	- 5.2
Sr	556	632	611	- 3.4
Zr	49	57	57	0
Y	16	17	26	-34.6
Nb	-	-	-	-

Minerals crystallised: Olivine, augite, Cr-diopside

B. Ankaramite LB11 —— alkali olivine basalt 41621

	C_o	C_1 (est)	C_1 (obs)	% Discrep.
Sample No.	LB11		41621	
% crystallisation	28.68			
Ni	92	36	43	-16.3
Sc	43	26	33	-21.2
Rb	21	29	22	+31.8
Sr	563	711	520	+36.7
Zr	64	89	99	-10.1
Y	26	30	23	+30.4
Nb	4	6	6	0

Minerals crystallised: Olivine, cpx, plag, magnetite

C. Ankaramite LB11 to high Sr, high K_2O andesite LB28

	C_o	C_1 (est)	C_1 (obs)	% Discrep.
Sample No.	LB11		LB28	
% crystallisation	56.58			
Ni	92	5	2	+150.0
Sc	43	13	15	-13.3
Rb	21	44	40	+10.0
Sr	563	840	761	+10.4
Zr	64	136	143	- 4.9
Y	26	38	31	+22.6
Nb	4	9	-	-

Minerals crystallised: Olivine, cpx, amph, plag, magnetite

D. Alkali olivine basalt 41632 —— alkali olivine basalt 41626

	C_o	C_1 (est)	C_1 (obs)	% Discrep.
Sample No.	41632		41626	
% crystallisation	10.96			
Ni	71	46	34	+35.3
Sc	33	36	36	0
Rb	20	22	29	-24.1
Sr	452	438	491	-10.8
Zr	82	92	106	-13.2
Y	20	22	25	-11.2
Nb	4	4.4	4	+10.0

Minerals crystallised: Olivine, cpx, plag, amph, cpx, plag, mag, apatite

E. Olivine basalt 41676 —— andesite 41622

	C_o	C_1 (est)	C_1 obs)	% Discrep.
Sample No.	41676		41622	
% crystallisation	44.15			
Ni	23	2	2	0
Sc	35	19	18	+ 5.6
Rb	19	31	35	-11.4
Sr	469	491	433	+13.4
Zr	56	92	134	-31.3
Y	19	26	30	-13.3
Nb	-	-	2	-

F. Olivine basalt LB67 —— andesite 41687

	C_o	C_1 (est)	C_1 (obs)	% Discrep.
Sample No.	LB67		41687	
% crystallisation	41.12			
Ni	23	4	3	+33.3
Sc	31	26	21	+23.8
Rb	18	29	33	-12.1
Sr	522	492	432	+13.9
Zr	43	70	82	-14.6
Y	18	26	43	-39.5
Nb	2	3.4	4	-15.0

Minerals crystallised: Olivine, cpx, amph, plag, magnetite

G. Basaltic andesite 41637 —— high K_2O andesite 41672

	C_o	C_1 (est)	C_1 (obs)	% Discrep.
Sample No.	41637		41672	
% crystallisation	48.71			
Ni	3	1	1	0
Sc	23	27	15	+80.0
Rb	38	72	73	- 1.4
Sr	442	336	397	-15.4
Zr	124	233	252	- 7.5
Y	28	48	40	+20.0
Nb	5	9	9	0

Minerals crystallised: Olivine, cpx, plag, mag

H. Andesite 41622 —— dacite LB3

	C_o	C_1 (est)	C_1 (obs)	% Discrep.
	41622		LB3	
	62.06			
Ni	2	1	1	0
Sc	18	20	19	+ 5.2
Rb	35	69	69	0
Sr	433	323	405	-20.2
Zr	134	275	244	+12.7
Y	30	53	45	+17.8
Nb	2	4	-	-

Minerals crystallised: Opx, cpx, plag, mag

I. Andesite 41622 to dacite 41671

	C_o	C_1 (est)	C_1 (obs)	% Discrep.
	41622		41671	
	62.06			
Ni	2	1	0	-
Sc	18	23	8	+187.5
Rb	35	88	98	- 10.2
Sr	433	296	293	+ 10.2
Zr	134	352	264	+ 33.3
Y	30	57	41	+ 39.0
Nb	2	5.3	11	- 51.8

Minerals crystallised: Opx, cpx, plag, mag

Notes: Calculations assume Rayleigh Fractionation and use the mineral proportions and % crystallisation calculated in the least-squares mixing routine. (tables 9.5, 9.7 & 9.10)

Distribution coefficients are given in Table 9.1 in the following columns: cpx 1, cpx 2 & 3 (andesite-dacite), opx 4, plag 7, amph, 8, mag 10, apatite 11, biotite 15.

In many respects, the ankaramites would appear to represent logical parental compositions to the high-Al basalt group. However some inconsistencies exist; the mineralogies of the two groups are different: the ankaramites are clinopyroxene-rich and the high-Al basalts olivine-rich. Furthermore, the ankaramites appear to be slightly more alkaline than the high-Al basalts. Consider for instance, the least mafic ankaramites (e.g. LB2, LB10, table 3.12): These have MgO contents that are markedly higher (ca. 8% MgO) than even the most mafic high-Al basalts (e.g. 41632, 41621, LB67, 41676 tables 3.12 and 3.13) yet these ankaramites have slightly higher P_2O_5 concentrations, similar or slightly higher K_2O and Rb and quite markedly higher Sr concentrations (figures 3.7 and 3.8). Thus if an assemblage clinopyroxene + olivine $\pm$ some plagioclase, were removed from an ankaramite to yield a high-Al basalt-like differentiate, this differentiate would be likely to have quite markedly higher concentrations of the incompatible elements mentioned above. Sr variations in particular are not easily explained by this mechanism, because the least mafic ankaramite, has only ca. 15% Al_2O_3, but >600ppm Sr, whereas mafic high-Al basalts have >17% Al_2O_3 and ca. 500ppm Sr. Fractionation of the dominantly clinopyroxene-olivine mineral assemblage of the ankaramites would result in both Al_2O_3 and Sr-enrichment, in the fractionates. It seems unlikely that enough plagioclase could be incorporated in the fractionated cumulate to allow the necessary Al_2O_3-enrichment, while sufficiently depleting the Sr content of the liquid.

The above hypothesis was tested using the least-square mixing and trace element calculations previously outlined. Ankaramite LB11 (table 9.5B) was estimated as a combination of its phenocrysts; clinopyroxene, olivine, plagioclase and magnetite (clinopyroxene + olivine are dominant) and high-Al basalt 41621 (table 9.5B). The results of this model are given in table 9.5B and table 9.6B. The major element content of the estimate of ankaramite LB11 is quite close to the observed values, except that, as discussed above, the K_2O and P_2O_5 concentrations of the ankaramite are slightly too high to yield

Figure 9.2

CaO v Al_2O_3 variation of the Rindjani calcalkaline lavas. X- ankaramites, ○- *ne*-normative high-Al basalts, ■- *ol-hy*-normative high-Al basalts, △ - andesites, ●- high-K, high-Sr andesites, □- dacites and high-K andesites.

Line A-A illustrates the variation of the ankaramites and a few high-Al basalts, involving Ca-depletion and Al-enrichment. The ankaramites have mainly cpx phenocrysts and little if any phenocrystic plagioclase and trend A-A is probably cpx-dominated fractionation (at least within the ankaramite group). Trend B then illustrates the increasing importance of plagioclase removal in the transition from the high-Al basalts to the andesites and dacites as indicated by the change to a trend of both Al- and Ca-depletion.

Figure 9.2

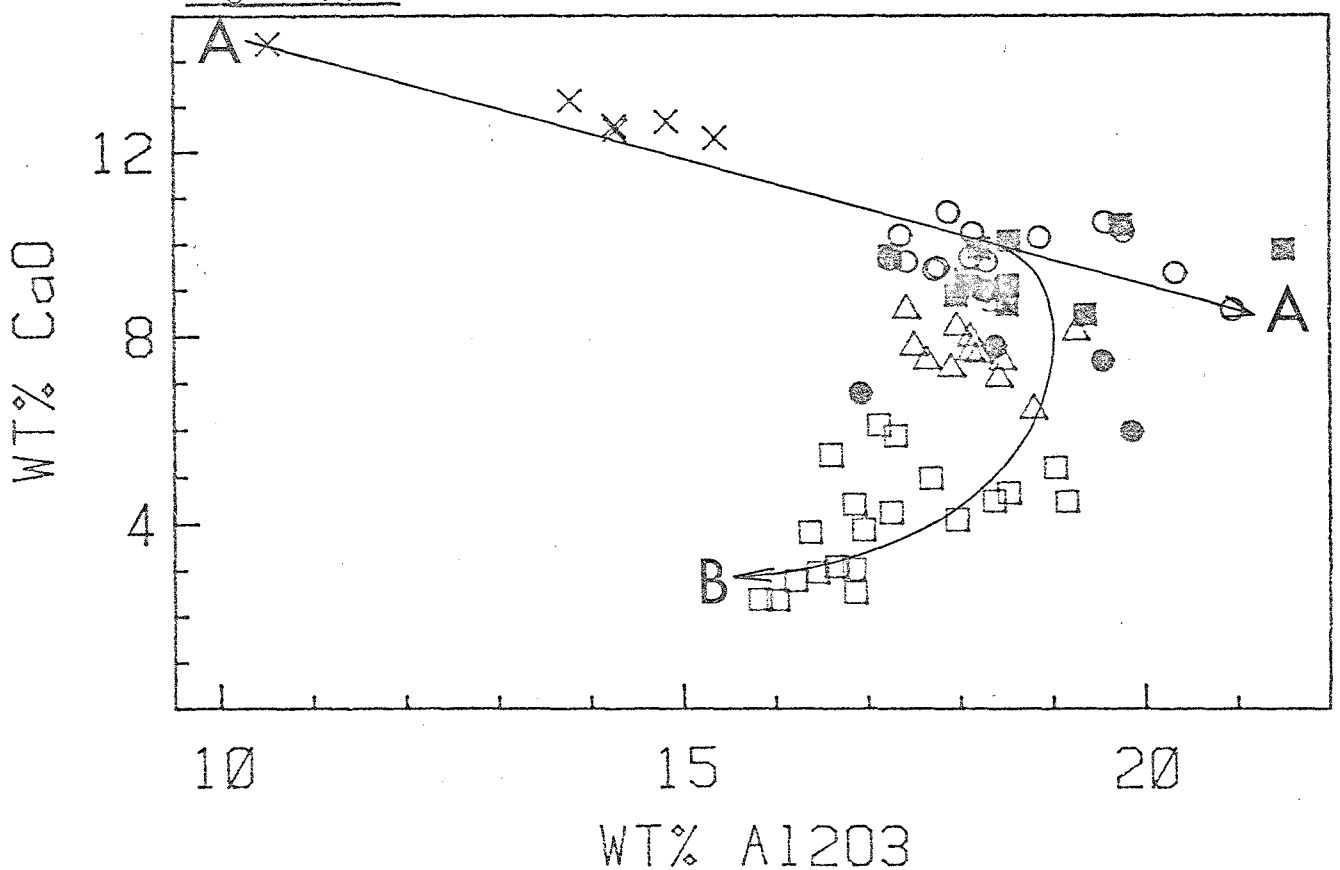

those of the high-Al basalt. The TiO_2 concentration would also appear to be slightly too low in the ankaramite. Considering the trace-element calculations, (table 9.6B) the calculations based on the Rb and Sr contents of the initial ankaramite yield calculated estimates of these in the high-Al basalt that are about 30% too high.

These calculations suggest that the ankaramites are not good parental candidates for the high-Al basalt group.

2. High-Al basalts and andesites:

If the andesites are products of fractional crystallisation of basaltic parents, then the high-Al basalt group represent candidates for this role. Compositional variations (figures 3.7-3.10), show that at least some of the members of the general high-Al basalt group lie on extensions of the andesite's trend. However several factors indicate that such a connection is not simply the result of fractionation of the observed phenocryst assemblages.

Even the most mafic members of the high-Al basalt group (e.g. 41632 or LB67, tables 3.12 and 3.13) have $Mg/Mg+Fe^{2+}$ values <0.6 and <80 ppm Ni and are therefore unlikely to represent primary mantle-derived melts capable of coexisting with olivine of about Fo90. The increasing importance of olivine and the presence of magnesian olivine xenocrysts in the more magnesian high-Al basalts, together with initial trends of rapid Ni depletion with decreasing MgO suggests that olivine fractionation may have played an important role prior to the precipitation of the common plagioclase-clinopyroxene-olivine phenocryst assemblage.

As olivine becomes the major near-liquidus phase in the more magnesian members of the *ne*-normative aluminous basalt group, with less important clinopyroxene, Foden and Varne (1980) calculated a possible primary liquid capable of coexisting with a possible mantle olivine (ca. Fo89) by the addition of olivine and clinopyroxene (see table 9.8).

Many of the high-Al basalts are *ne*-normative with $Fe^{2+} = 0.85\Sigma Fe$ and even with much lower Fe^{2+}/Fe^{3+} ratios still remain critically undersaturated.

Table 9.7 Least-squares Mixing Computations to Model Possible Fractional Crystallisation Processes in the Rindjani Calcalkaline Suite

D. Approximation of alkali olivine basalt 41632 in terms of postulated derivative basalt 41626 and its phenocrysts.

Lava	AOB	AOB	AOB
Sample No.	41632	41632	41626
	obs.	est.	
SiO_2	50.28	50.24	50.78
Al_2O_3	18.13	18.15	17.74
FeO_T	9.75	9.81	10.18
MgO	5.64	5.65	4.50
CaO	9.72	9.77	9.45
Na_2O	3.68	3.72	4.06
K_2O	1.21	1.32	1.48
TiO_2	1.13	1.13	1.26
P_2O_5	0.25	0.28	0.31
MnO	0.18	0.18	0.19

Component	Wt. Fraction	Cumulate Mode (Wt. Fract.)
Olivine	0.0365	0.3262
Cpx	0.0052	0.0465
Plag.	0.0702	0.6273
Lava 41626	0.8904	

= alkali olivine basalt 41632

ΣR^2 = 0.0234

	Cumulate Composition
SiO_2	44.91
Al_2O_3	21.05
FeO_T	6.65
MgO	14.65
CaO	12.11
Na_2O	0.97
K_2O	0.05
TiO_2	0.05
P_2O_5	-
MnO	0.10
100 Mg/ Mg + ΣFe	79.69

E. Approximation of olivine basalt 41676 in terms of andesite 41622 and possible mineral assemblage prior to eruption.

Lava	OB	OB	A
Sample No.	41676	41676	41622
	obs.	est.	
SiO_2	50.02	50.04	55.49
Al_2O_3	18.20	18.16	18.45
FeO_T	10.10	10.05	8.32
MgO	5.84	5.74	3.10
CaO	9.92	9.97	7.46
Na_2O	3.24	3.13	4.09
K_2O	1.01	1.10	1.59
TiO_2	0.99	1.44	0.91
P_2O_5	0.23	0.17	0.27
MnO	0.20	0.10	0.16

Component	Wt. Fraction	Cumulate Mode (Wt. Fract.)
Amph.	0.2601	0.5825
Cpx	0.0209	0.0468
Plag.	0.1383	0.3097
Mag.	0.0268	0.0600
Apat.	0.0004	0.0009
Lava 41622	0.5585	

= olivine basalt 41676

ΣR^2 = 0.2499

	Cumulate Composition
SiO_2	42.64
Al_2O_3	17.58
FeO_T	12.09
MgO	8.98
CaO	12.99
Na_2O	1.89
K_2O	0.47
TiO_2	2.08
P_2O_5	0.04
MnO	0.03
100 Mg/ Mg + ΣFe	56.96

F. Approximation of olivine basalt LB67 in terms of possible andesite derivative (41687) and a possible pre-eruptive mineral assemblage.

Lava	AOB	AOB	A
Sample No.	LB67	LB67	41687
	obs.	est.	
SiO_2	49.43	49.45	55.24
Al_2O_3	18.85	18.85	17.50
FeO_T	9.50	9.46	8.08
MgO	5.92	5.92	3.62
CaO	10.14	10.11	7.78
Na_2O	3.60	3.40	4.52
K_2O	0.99	1.06	1.63
TiO_2	1.00	1.25	1.03
P_2O_5	0.20	0.16	0.28
MnO	0.18	0.14	0.19

Component	Wt. Fraction	Cumulate Mode (Wt. Fract.)
Olivine	0.0306	0.0738
Cpx	0.0349	0.0841
Amph.	0.1235	0.2977
Plag.	0.1963	0.4731
Mag.	0.0296	0.0713
Lava 41687	0.5888	

= alkali olivine basalt LB67

ΣR^2 = 0.1146

	Cumulate Composition
SiO_2	40.86
Al_2O_3	20.61
FeO_T	11.37
MgO	9.12
CaO	13.34
Na_2O	1.78
K_2O	0.25
TiO_2	1.56
P_2O_5	-
MnO	0.06
100 Mg/ Mg + ΣFe	58.84

Abbreviations: AOB = alkali olivine basalt, OB = olivine basalt, A = andesite

Notes: FeO_T = total Fe as FeO, obs. = observed composition, est. = estimated composition.

Refer to Table 9.17 for locality of mineral compositions used in these computations.

Due to the existence of a low-pressure thermal divide (e.g. Yoder and Tilley, 1962), fractionation of a plagioclase-clinopyroxene-olivine assemblage will not yield *Q*-normative residual liquid. Some of the high-Al "basalts" (e.g. 41678, table 3.14) are differentiated, with low MgO and Ni contents and with higher K_2O contents than most andesites, yet have <53% SiO_2 and are still *ne*-normative. These are perhaps most properly termed "hawaiites". Many of the high-Al basalts, particularly those which are undersaturated, fall on a trend of marked K_2O-enrichment with limited silica-enrichment, which is divergent from that produced by the extrapolation of the andesite trend to low silica values (figure 9.3).

Tables 9.6 and 9.7 show the results of mixing and trace element model calculations which suggest that the low MgO, high-Al basalt 41626 (table 3.14) can be derived from 41632, (one of the more mafic members of the group) by removal of 11% of an assemblage comprising 62.8% plagioclase, 32.6% olivine and 4.6% clinopyroxene, an assemblage very like the actual phenocryst assemblage of 41632 and 41626. This trend is one of marked K_2O- and limited SiO_2-enrichmen and does not yield the andesites (see figure 9.3).

On the basis of this plagioclase-clinopyroxene-olivine phenocryst trend, it is possible to demonstrate that to produce the Rindjani andesites with about 55% SiO_2, would require a high-Al basaltic parent to have about 0.7% K_2O (with 50% SiO_2 and 5.8% MgO). In fact of those analysed, no high-Al basalts from Rindjani had less than 0.9% K_2O and those with <1.0% K_2O are very rare (2 out of 40) and are affected by clinopyroxene and plagioclase accumulation. Thus while it may be possible to produce andesites by low-pressure olivine/clinopyroxene/plagioclase/magnetite fractionation of high-Al basalt parents, no such potential parents were found from Rindjani, in spite of extensive sampling.

The andesites have lower K/Rb ratios than the high-Al basalts (figure 3.14) and as the phenocryst assemblage of the latter group is essentially K_2O-free, both K and Rb are nearly incompatible. Fractionation of the high-Al basalts'

Table 9.8

A possible Primary Liquid Calculated from Rindjani High-Al Basalt Compared with a Possible Primary Victorian Alkali Olivine Basalt

	A	xchond.	B	xchond.
SiO_2	48.47		48.00	
Al_2O_3	14.63		13.91	
FeO_T	10.75		10.92	
MgO	12.15		11.39	
CaO	8.65		8.35	
Na_2O	2.94		3.23	
K_2O	0.97	16.8	1.18	20.45
TiO_2	0.92	8.85	2.14	20.6
P_2O_5	0.20	1.11	0.51	2.85
MnO	0.16		0.16	
(1) $100Mg/Mg+Fe^{2+}$	70.32		68.62	
(2) $100Mg/Mg+Fe^{3+}$ olivine	88.76		87.94	
La	18.41	58.44	23	73.0
Ce	39.43	48.50	49	60.3
Nd	19.54	32.73	23	38.5
Sm	3.77	19.63	5.53	28.8
Eu	1.16	16.11	2.02	28.0
Gd	3.31	12.77		
Dy	3.09	9.51		
HO	0.66	9.04	0.98	13.42
Yb	1.95	9.37	1.77	8.51
Y	16.5	8.25	27	13.5
U	1.73		1.1	
Th	5.46		2.9	
Hf	3.31		3.9	
Ba	717.2		350	
Cs	0.18			
Rb	16		24	
Sr	365		543	
Zr	67		152	
Ni	553		364	
Cr	327		388	
Sc	33		23	

A. A possible primary liquid calculated from Rindjani alkali olivine basalt 41632 by the addition of 20% of an assemblage of olivine (80%) and clinopyroxene (20%).

B. A possible near-primary lherzolite-bearing alkali olivine basalt from Mt. Frazer, W. Victoria (69-1036) (Frey et al., 1978).

Notes: 1. calculated as $Fe^{2+} = 0.85\ \Sigma Fe$.

2. equilibrium olivine calculated on the basis of $K_D\ ^{(Fe/Mg)}_{(Ol/liq)} = 0.30$ (Roeder and Emslie, 1970).

Trace element concentrations in col. A calculated from the values for high-Al basalt 41632 given in tables 3.13 and 9.3 using the Rayleigh Fractionation model ($Cl/Ci = F^{(D-1)}$) K_{DS} used are given in table 9.1.

plagioclase-clinopyroxene-olivine assemblage will not produce appreciable changes in the K/Rb ratio of the liquid. It appears that while compositional variation within the high-Al basalt field is explicable in terms of fractionation of phenocryst assemblages, such a mechanism is unlikely to yield the andesites. Yet some of the less K_2O-rich, more mafic, *ol-hy*-normative high-Al basalts (e.g. 41676, table 3.12) do fall on extensions of the andesite trend (figure 9.3) and may represent parents to the andesites, a model discussed below.

Evaluating low-K_2O, high-Al basalt 41676 (table 9.9) as a possible andesite parent: if Rb was a "perfectly" incompatible element, then its enrichment from 19 ppm in the basalt to 35 ppm in typical andesite 41622 (table 9.9) would represent a minimum of 46% fractional crystallisation. On this basis the major and trace-element composition of the necessary cumulate can be calculated (table 9.9). Because of its high K_2O content (0.3%), this postulated fractionate cannot represent any combination of the phenocryst phases represented in the basalt or andesite (plagioclase, olivine, clinopyroxene, orthopyroxene, magnetite). The only phenocryst phase with any K_2O is plagioclase and this contains <0.3%.

This then suggests the possibility of amphibole fractionation, perhaps component supported by the occurrence of scarce, Ca-rich amphibole relicts in some Rindjani basalts and andesites.

Amphibole may have lower Mg/Mg+Fe value than coexisting olivine and clinopyroxene (e.g. Green et al., 1974, Heltz, 1973), if such is the case then its removal will produce less marked iron enrichment than the removal of olivine or clinopyroxene. However, amphibole is still likely to have a markedly higher Mg/Mg+Fe value than the coexisting liquid (see chapter 11). The low Mg/Mg+Fe value of the calculated cumulate (table 9.9) (0.56) is much lower than that of any olivine, clinopyroxene or amphibole phenocrysts or xenocrysts in the Rindjani basalts or andesites (total range 0.92 - 0.65) and suggests the additional presence of magnetite.

Table 9.9 The Derivation of Rindjani Andesite by Fractional Crystallisation of Basaltic Parent

	Basalt 41676	Andesite 41622	Cumulate [1]
SiO_2	50.02	55.49	43.53
Al_2O_3	18.2	18.4	17.90
FeO	10.1	8.3	12.4
MgO	5.8	3.1	9.1
CaO	9.9	7.5	12.8
Na_2O	3.2	4.1	2.2
K_2O	1.01	1.60	0.3
TiO_2	0.99	0.91	1.1
P_2O_5	0.23	0.28	0.17
MnO	0.20	0.16	0.25
Ni	23	2	48
Sc	35	18	55
Rb	19	35	0
Sr	469	433	512
Zr	56	134	-36
Y	19	30	6
Mg/Mg+Fe	0.52	0.42	0.56

[2] Apparent bulk distribution coefficients for trace elements

	A Surface equilibrium	B Total equilibrium
Ni	4.99	23.9
Sc	2.09	3.06
Rb	0	0
Sr	1.13	1.18
Zr	< 0	< 0
Y	0.25	0.20

Notes: [1] Cumulate calculated on the basis that Rb is assumed to be completely incompatible and its enrichment from 19 ppm in the basalt to 35 ppm in the andesite represents ca. 46% crystallisation.

[2] Crystal-liquid distribution coefficients calculated for true fractional crystallisation (Rayleigh fractionation) (A) and equilibrium crystallisation (B), assuming $D_{Rb} = 0$.

The calculated bulk Sr distribution coefficient of 1.13 (table 9.9) also suggests that plagioclase is probably involved, as most other minerals are likely to have Sr distribution coefficients considerably <1. Finally, the presence of small amounts of P_2O_5 (0.17%) in the cumulate suggests that accessory amounts of apatite may also be extracted. These arguments suggest that if the andesites are fractional crystallisation products of parent magmas represented by Rindjani high-Al basalts, then the cumulate may be dominated by amphibole and plagioclase, with significant magnetite and some apatite, perhaps with minor olivine or clinopyroxene.

This conclusion was tested using the least-squares mixing and trace element modelling techniques used previously and the results of this calculation are given in tables 9.6 and 9.10. Thus these calculations suggest that basalt 41676 may yield andesite 41622 by crystallisation of 44.15% of an assemblage with ca. 58% amphibole, 4.5% clinopyroxene, 31% plagioclase, 6% magnetite and minor apatite. This model allows reasonable matching of most major- and trace-element trends and in particular the moderate rate of enrichment of K_2O with increasing SiO_2, (figure 9.3), though there is some discrepancy in TiO_2 and Zr.

3. High-K andesite and dacite:

The dacites are phenocryst-poor and have much higher K_2O/Na_2O and Rb/Sr ratios, but only slightly lower K/Rb ratios than the andesites. They show trends of Sr- and Al_2O_3-depletion and have negative Eu-anomalies (figure 9.1, table 9.3). These features are consistent with plagioclase fractionation. Concentrations of incompatible elements including K, Rb, Nb and Zr are all 2-3 times greater than those of the andesites.

As already discussed, the andesites are very phenocryst-rich (50-70%) and their assemblages are plagioclase-dominated. It should be noted that, though very phenocryst-, and particularly plagioclase-rich, the andesites do not show evidence of crystal accumulation (plagioclase). They have higher Rb/Sr ratios than the basalts and show slight negative Eu-anomalies, both

Table 9.10 Least-squares Mixing Computations to Model Possible Fractional Crystallisation Processes in the Rindjani calcalkaline suite.

G. Approximation of basaltic andesite 41637 in terms of its phenocrysts and postulated derivative lava 41672 (high K_2O andesite).

Lava	AB	AB	HKA
Sample No.	41637	41637	41672
	obs.	est.	
SiO_2	52.97	52.97	59.99
Al_2O_3	19.35	19.38	17.68
FeO_T	9.01	8.98	5.58
MgO	2.90	2.92	2.13
CaO	8.47	8.47	4.98
Na_2O	4.05	3.87	4.74
K_2O	1.68	1.81	3.37
TiO_2	0.96	1.14	0.90
P_2O_5	0.24	0.18	0.37
MnO	0.18	0.12	0.18

Component	Wt. Fraction	Cumulate Mode (Wt. Fract.)
Olivine	0.0158	0.0321
Cpx	0.0775	0.1576
Plag.	0.3408	0.6930
Mag.	0.0577	0.1173
Lava 41672	0.5129	

= basaltic andesite 41637

ΣR^2 = 0.0878

	Cumulate Composition
SiO_2	45.46
Al_2O_3	21.06
FeO_T	11.97
MgO	3.73
CaO	12.05
Na_2O	2.95
K_2O	0.18
TiO_2	1.38
P_2O_5	-
MnO	0.06
100 Mg/ Mg + ΣFe	35.70

H. Approximation of andesite 41622 in terms of its phenocrysts and postulated derivative lava, dacite LB3.

Lava	A	A	D
Sample No.	41622	41622	LB3
	obs.	est.	
SiO_2	55.49	55.48	61.69
Al_2O_3	18.45	18.44	16.85
FeO_T	8.32	8.30	5.75
MgO	3.10	3.13	1.90
CaO	7.46	7.46	4.42
Na_2O	4.09	4.20	4.82
K_2O	1.59	1.59	3.00
TiO_2	0.91	1.03	0.86
P_2O_5	0.27	0.23	0.47
MnO	0.16	0.11	0.17

Component	Wt. Fraction	Cumulate Mode (Wt. Fract.)
Opx	0.0486	0.0944
Cpx	0.0599	0.1163
Plag.	0.3569	0.6930
Mag.	0.0496	0.0963
Lava LB3	0.4867	

= andesite 41622

ΣR^2 = 0.0332

	Cumulate Composition
SiO_2	47.01
Al_2O_3	15.88
FeO_T	10.70
MgO	4.27
CaO	10.31
Na_2O	3.60
K_2O	0.25
TiO_2	1.19
P_2O_5	-
MnO	0.44
100 Mg/ Mg + ΣFe	41.56

I. Approximation of andesite 41622 in terms of its phenocrysts and postulated derivative lava, dacite 41671.

Lava	A	A	D
Sample No.	41622	41622	41671
	obs.	est.	
SiO_2	54.26	54.26	65.14
Al_2O_3	18.04	18.04	16.54
FeO_T	8.17	8.15	4.00
MgO	3.03	3.04	1.11
CaO	7.30	7.30	3.07
Na_2O	4.00	4.01	4.92
K_2O	1.56	1.53	3.65
TiO_2	0.89	1.02	0.65
MnO	0.16	0.08	0.13

Component	Wt. Fraction	Cumulate Mode (Wt. Fract.)
Opx	0.0594	0.0991
Cpx	0.0690	0.1151
Plag.	0.4118	0.6870
Mag.	0.0592	0.0987
Lava 41671	0.3794	

= andesite 41622

ΣR^2 = 0.0262

	Cumulate Composition
SiO_2	49.30
Al_2O_3	19.62
FeO_T	11.06
MgO	4.37
CaO	10.22
Na_2O	3.57
K_2O	0.25
TiO_2	1.30
MnO	0.04
100 Mg/ Mg + ΣFe	41.32

Abbreviations: AB = basaltic andesite, HKA = high-K_2O andesite, A = andesite, D = dacite, obs. = observed composition, est. = estimated composition.

Notes: FeO_T = total Fe as FeO.

See Table 9.17 for locality of mineral compositions used in calculations.

features suggesting plagioclase removal rather than accumulation. It is very likely therefore, that the andesite's residual liquid, now groundmass or glass, will have precisely those geochemical features shown by the dacites and high-K andesites. In other words, the high-K andesites and dacites, which are glassy, crystal-poor rocks, whose bulk compositions are essentially the same as the liquid at eruption, may have formed in equilibrium with the plagioclase-dominated andesite phenocryst assemblage. This is also suggested by the similarity of the andesite's interstitial glass and the bulk dacite composition (table 3.19).

The results of least-squares mixing and trace element modelling calculations shown in table 8 further bear-out the same hypothesis. The mineral proportions yielded by this calculation are the same as those of the actual andesite and hence the composition of the cumulate (point 5, figure 9.3) is close to that of the bulk phenocryst assemblage.

These calculations suggest that the compositional variation within the basaltic andesite-andesite group (e.g. trend A, figure 9.3) cannot result from phenocryst fractionation as this produces much more marked K_2O enrichment. This is illustrated by the trends produced by the segregation of the cumulates 4 and 5 from the basaltic andesite 41637 and andesite 41622 respectively, in figu 9.3. The discontinuity between the andesite and dacite fields (trends A and D, figure 9.3) suggests a change in the differentiation process from that producing the andesite trend to that yielding the dacites.

As the high-K andesite-dacite group are liquid-dominated on eruption, and the basaltic andesite-andesite group 50-70% crystalline, so the connection between the subparallel andesite (A) and dacite (D) trends in figure 9.3 is essentially a liquid-crystal distribution coefficient relationship. The separation of the two fields in figure 9.3 is the result of segregation of small amounts of the liquid component of magmas of the andesite group from their phenocrysts. The dacite "trend" in figure 9.3 is essentially the locus of the compositions of residual liquids after 50-70% crystallisation of the andesite's phenocryst assemblage. Samples which fall between the two trends, A and D

Figure 9.3

Upper diagram shows the K_2O v. SiO_2 variation of the Rindjani suite. X- ankaramites, ○-*ne*-normative high-Al basalts, +- *ol-hy*-normative high-Al basalts △- andesites, ●- high-K, high-Sr andesites, □- high-K andesites and dacites. The approximate trends of the main groups of lavas are marked. HAB - high-Al basalt, A - andesite, D - high-K andesite and dacite. This illustrates the divergent nature of the basalt and andesite trends and the sub-parallel nature of the andesite and high-K andesite-dacite trends.

The lower diagram illustrates the differentiation models discussed in this chapter. Trends HAB, A and D are the same as those in the upper diagram. ▲- high-Al basalts, ●- andesites and basaltic andesites, □- high-K andesite and dacite. The points numbered 1 to 5 are the calculated cumulates.

Point PM is the calculated primary liquid which can yield basalt 41632 by removal of 20% of an olivine-cpx assemblage represented by point 1 (see table 9.8). The trend produced by this process is shown as a dotted line (PM .... 41632). Point 2 is the composition of basalt 41632's phenocryst assemblage, the subtraction of which yields basalt 41626 (see mixing model D, table 9.7) and illustrates that removal of the basalt's phenocrysts does not yield the andesite trend (A). Point 3 is the amphibole-bearing cumulate assemblage calculated to yield andesite 41622 from basalt 41676 (see model E, table 9.7). Points 4 and 5 are the compositions of the phenocryst assemblages of basaltic andesite 41637 and andesite 41622 respectively. The trends shown illustrate mixing models G and I (table 9.10) and show that the removal of the andesite's phenocryst assemblages produce trends markedly divergent from that shown by the andesite group itself (trend A).

FIG 9.3

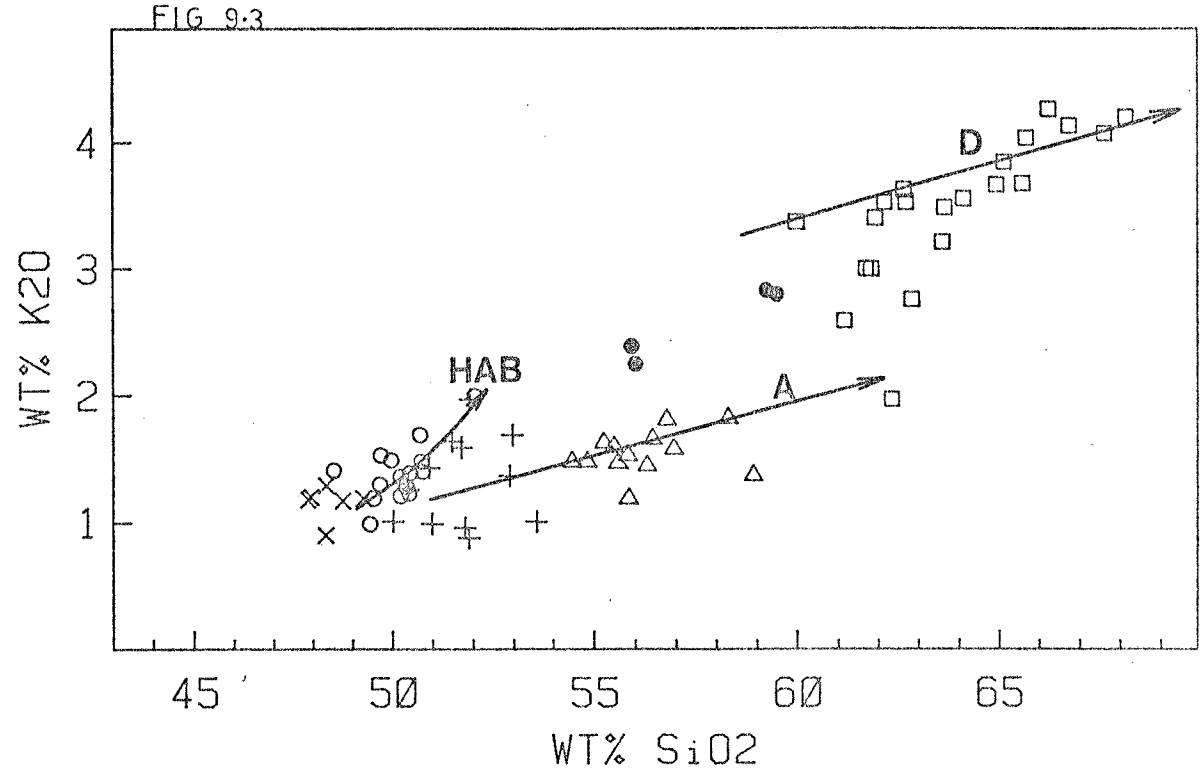
WT% K20
WT% SiO2
HAB
A
D
1
2
3
4
45
50
55
60
65

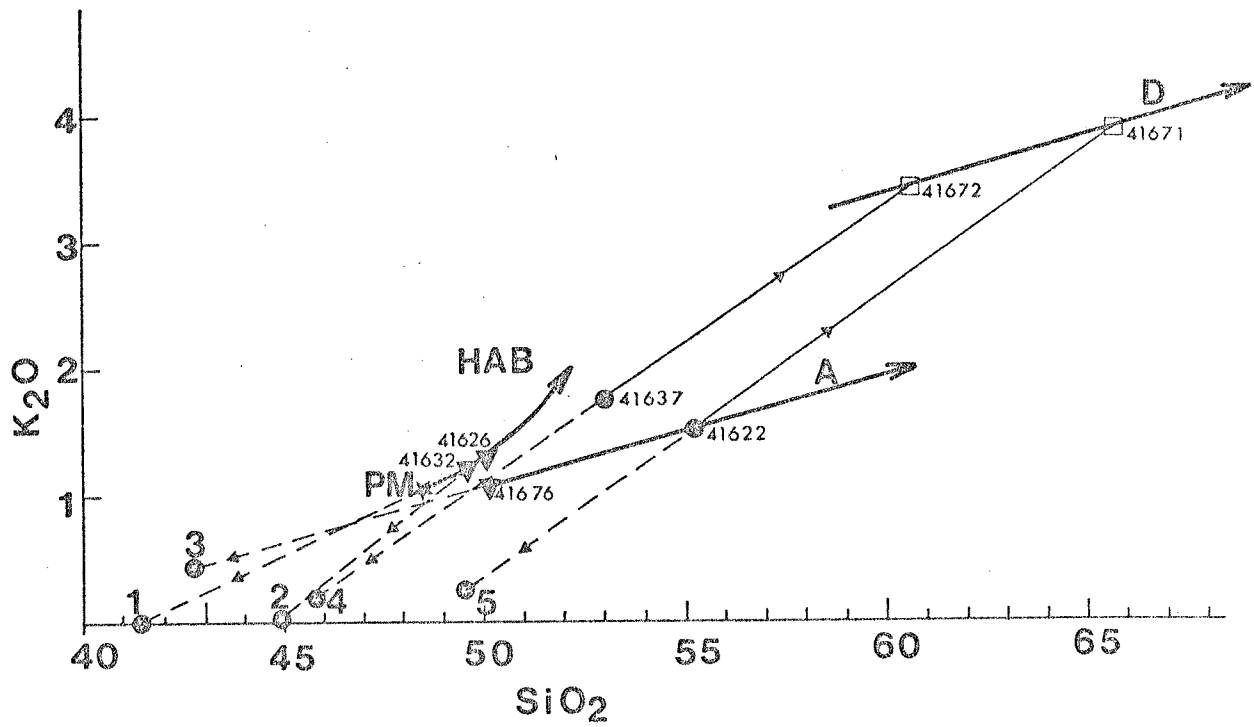
K2O
SiO2
HAB
A
D
PM
41626
41632
41637
41622
41676
41671
41672
1
2
3
4
5
40
45
50
55
60
65

in figure 9.3 represent the result of imperfect segregation, with varying proportions of phenocryst and liquid components.

9.5 Summary of Various Fractional Crystallisation Processes that may have occurred in the Rindjani Suite

The main conclusions drawn from the calculations and discussion in the preceding sections are:

1. Compositional variation within the ankaramite group is explicable in terms of fractional crystallisation or accumulation of the phenocryst assemblages. These assemblages are dominated by cpx and olivine and the calculations suggest that approximately 7.2 wt.% removal in the proportions: cpx, 74% and olivine, 26% assemblage yields a variation of 1% in the whole-rock MgO content.
2. It seems unlikely that the high-Al basalts are derived from the ankaramites by fractionation of phenocryst assemblages of either suite.
3. Some variation within the general high-Al basalt group can be accounted for by removal of the observed plagioclase + ol + cpx phenocryst assemblages. Their fractionation could yield low magnesian, relatively alkali-enriched "hawaiite"-like derivatives, but would not yield andesites.
4. For the most mafic high-Al basalts to have been derived from melts in equilibrium with mantle olivine, they must have undergone, before eruption, approximately 20% fractionation of an assemblage of about 80% olivine, 20% cpx $\pm$ minor Cr-spinel.
5. The andesites can represent derivatives of the high-Al basalts only if amphibole + plagioclase + magnetite ($\pm$ ol $\pm$ cpx) or some other undiscovered assemblage has crystallised and been fractionated.
6. Fractionation of the erupted phenocryst assemblages of the andesites may yield high-K andesite-dacite derivatives, but would not reproduce the trends within the low-K andesite group. It thus appears that the compositional diversity of the andesites may be primary or, if the andesites are derived from high-Al basalts my amphibole-dominated

fractionation as suggested in point 5, then by differing amounts of crystal fractionation.

9.6 Fractional Crystallisation and the Differentiation of the Tambora Suite

The petrographic features and compositional variation trends of the Tambora lava suite were described in chapter 4 (including the lavas from Tambora's parasitic cone, P. Satonda). In General compositional variation is consistent with differentiation by crystal fractionation, with MgO, Ni, Sc, Cr and CaO consistently decreasing and K_2O, Rb, SiO_2, Zr, Nb and Na_2O concentrations increasing through the suite. Furthermore, the compositional variation from the low-MgO trachybasalts (such as T5 or T30) to the most SiO_2-rich MgO-poor trachyandesites is characterised by depletion of CaO, Sr, Al_2O_3 and a steady increase in the Rb/Sr and K_2O/Na_2O ratios, features suggestive of fractionation of an assemblage dominated by plagioclase.

The changes in slope, in some cases very pronounced, of MgO-variation diagrams between 3 and 4% MgO, suggest that lavas with >4% MgO, if differentiati occurred as a result of crystal-liquid fractionation, were differentiated by fractionation of a slightly different assemblage than those with <3% MgO. The flatter slopes of trends of incompatible elements (K_2O, Rb, Zr and NbO (figures 4.4 and 4.5), with respect to MgO variation in lavas with >4% MgO, suggests that these lavas were crystallising a bulk assemblage with a higher MgO concentration than those lavas with <3% MgO (i.e. any given percentage MgO variation in those lavas with >4% MgO represents a smaller proportion of crystallisation than does that same proportion of MgO variation in those lavas with <3% MgO).

This observation then concurs with the observed phenocryst assemblages, where the trachybasalts with >4% MgO are relatively more cpx- and olivine-rich.

The K and Rb concentrations of the Tambora lavas lie on a well defined linear trend (figure 4.9), the K/Rb ratio remaining relatively constant, in

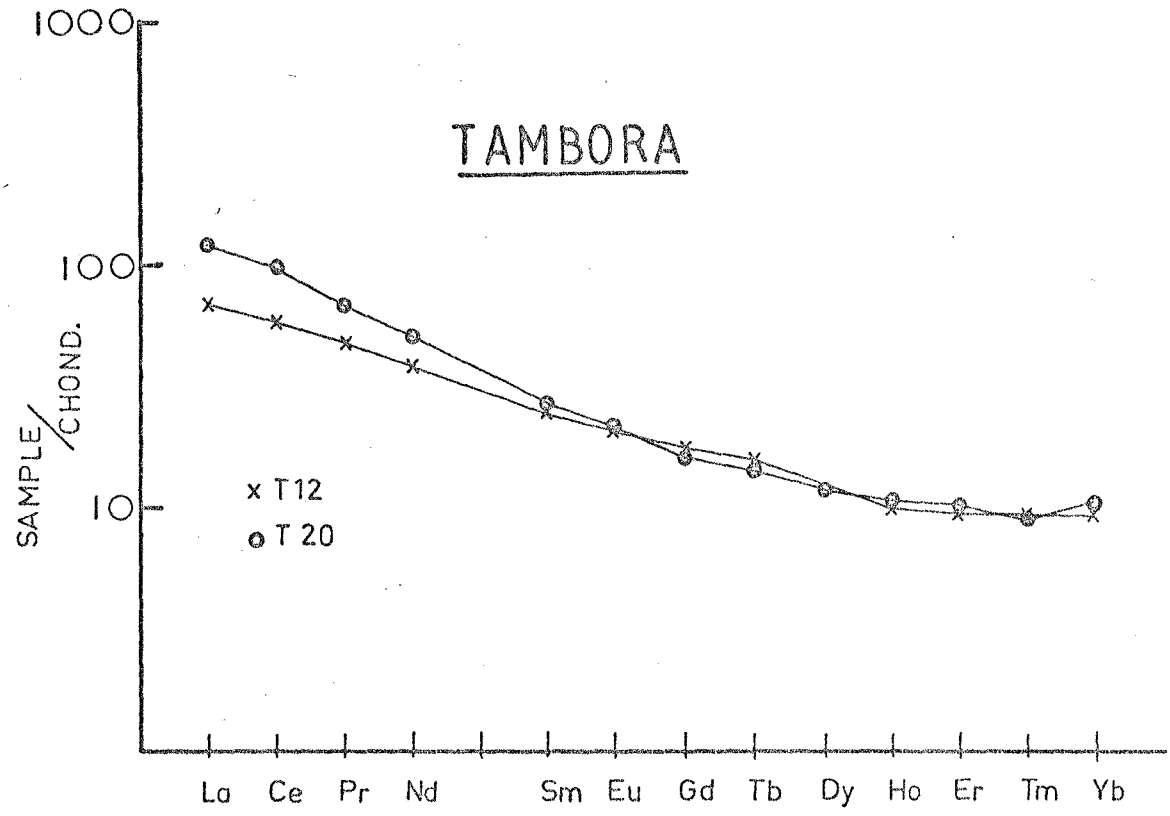

FIGURE 9.4

Chondrite-normalised REE patterns of Tambora lavas. (see also table 9.4).
T12 - ne-trachybasalt, T20 ne-trachyandesite.

contrast to their behaviour in the high-Al basalts and andesites of the Rindjani suite. This suggests that both these elements maintain similar (low) distribution coefficients with respect to the crystallising mineral assemblage through the sequence from trachybasalt to trachyandesite. This is consistent with the crystallisation of the plagioclase-, clinopyroxene-, olivine-dominated phenocryst assemblages observed in most of the Tambora trachybasalts and some trachyandesites (only the most silicic are biotite-bearing). In contrast, an explanation of the transition from the Rindjani high-Al basalts to the andesites requires that a K_2O-bearing phase (interpreted as amphibole) be fractionated, this absent from the eruptive phenocryst assemblage of these rocks.

The discontinuity in the MgO variation trend between 4 and 3% MgO is in some ways akin to that in the Rindjani suite between the andesites and dacites. In both cases, glass-rich, more phenocryst-poor lavas are common amongst the lavas on the more differentiated side of the gap, but are rare among the more magnesian lavas. However, unlike the relationship between the Rindjani dacites and andesites, the highly Al_2O_3- and Sr-enriched character of the Tambora lavas on the low-MgO side of this gap (e.g. T30, T5) suggests that the main plagioclase-crystallisation event occurred after the event which lead to the discontinuity.

If the discontinuity in the MgO-variation trend is interpreted in the same general way as that between the Rindjani andesites and dacites, then it could be due to the segregation of a liquid in equilibrium with the phenocryst assemblage of the trachybasalts. Once segregated, this liquid must then have crystallised its plagioclase-rich phenocryst assemblage.

At about 2% MgO, or 55% SiO_2, there are also marked inflections in the P_2O_5 v MgO (figure 4.4) and K_2O and K_2O/Na_2O v SiO_2 (figures 4.10 and 4.11) variation diagrams, P_2O_5, K_2O and K_2O/Na_2O variations all changing from increasing to decreasing trends. These inflections correspond with the appearance of abundant biotite and an increase in the relative abundance of apatite in these lavas.

Figure 9.5

CaO v Sr variation of Tambora (and P. Satonda) lavas and intrusives and Sangeang Api lavas1.

○- P. Satonda lavas, +- Tambora lavas (*ne*-trachybasalts and *ne*-trachyandesites) ☆- Tambora intrusives, ●- olivine megacryst bearing lavas from Sangeang Api, □- amphibole bearing lavas from Sangeang Api.

Two trends are illustrated. A-A is that of Ca-depletion, Sr-enrichment where plagioclase is thought to be a less important fractionating phase and trend B, involving the Tambora *ne*-trachyandesites where both Ca and Sr are showing depletion trends and plagioclase is assumed to be an important fractionating phase.

Figure 9.5

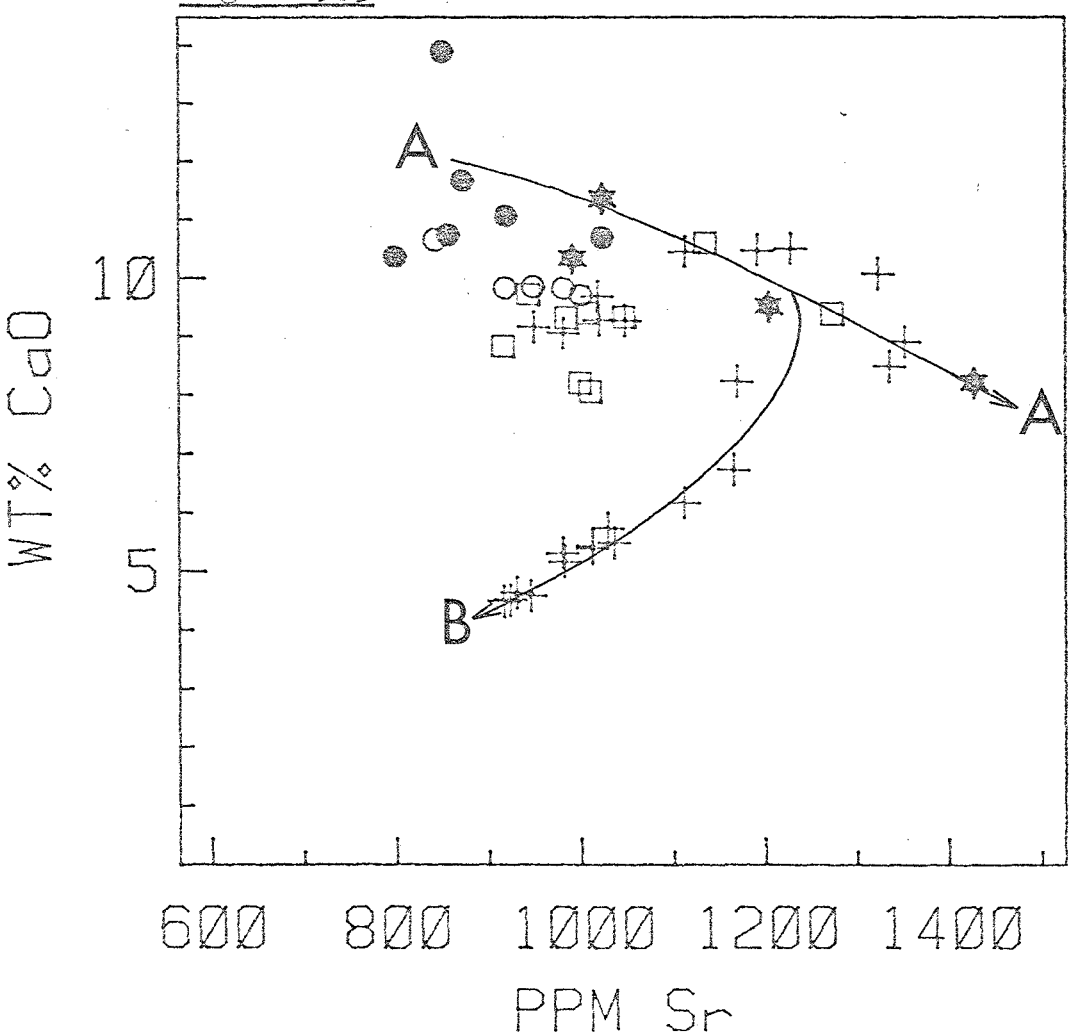

Thus, throughout the Tambora suite, there is a consistent correlation between the phenocryst assemnlages of the lavas and their compositional variation. Fractional crystallisation of the existing phenocryst assemblage could account for the differentiation of the Tambora lavas.

A least-squares mixing approach, the same as that used in developing the Rindjani models, was used to test the proposal that the derivation of various stages of the Tambora suite may have resulted from fractionation of observed phenocryst assemblages. This idea was tested in three stages.

1. The derivation of the low MgO, very Al_2O_3-rich trachybasalts (T30) from the more mafic trachybasalts (T12).
2. The derivation of the trachyandesites (T32) from the low-MgO, Al_2O_3-rich trachybasalts (T30).
3. The derivation of the most differentiated (siliceous) trachyandesites (T20) from the slightly less silica-rich trachyandesites (T32).

The results of these three models are given in table 9.11. They show some discrepancies between observed and estimated compositions, but are in general accord with the conclusions based on the geochemical variations already discussed. In particular, the changes in the relative proportions of the mineral phases (in wt.%) though the three stages are in accord with the observed variations in modal phenocryst abundances. The proportions of the crystal extract calculated to account for the transition from trachybasalt T12 to T30, for instance, is markedly more clinopyroxene + olivine-rich relative to plagioclase, compared with that calculated to effect the transition from trachybasalt T30 to trachyandesite T32.

Apatite was not included in the models, though the consistently, slightly low "estimated" values for P_2O_5 (about 0.1% low), in comparison with th "observed" values, suggests that a small amount of apatite could have been involved in each stage.

Trace element calculations were also performed in the same way as in the previous Rindjani example. Results are given in table 9.12. These model the

Table 9.11 Least-squares Mixing Computations to Model Possible Fractional Crystallisation Processes in the Tambora Alkaline Suite

A. Approximation of trachybasalt T12 in terms of its phenocrysts and postulated derivative - trachybasalt T30.

Lava	TB	TB	TB					
Sample No.	T12	T12	T30					
	obs.	est.						Cumulate Composition
SiO_2	48.26	48.31	51.39	Component	Wt. Fraction	Cumulate Mode (Wt. Fract.)	SiO_2	42.24
Al_2O_3	17.95	17.91	20.56	Cpx	0.1338	0.4151	Al_2O_3	12.49
FeO_T	10.12	10.12	6.52	Olivine	0.0335	0.1039	FeO_T	17.74
MgO	5.27	5.21	3.25	Plag.	0.1090	0.3382	MgO	9.37
CaO	10.46	10.38	8.89	Mag.	0.0460	0.1427	CaO	13.58
Na_2O	3.50	3.45	4.42	Lava T30	0.6751		Na_2O	1.45
K_2O	2.67	2.48	3.56	= potassic ne-trachybasalt T12			K_2O	0.22
TiO_2	0.97	1.00	0.68				TiO_2	1.69
P_2O_5	0.42	0.33	0.49	ΣR^2 = 0.0654			P_2O_5	-
MnO	0.21	0.16	0.15				MnO	0.19
							100Mg/ Mg + ΣFe	48.49

B. Approximation of trachybasalt T30 in terms of its phenocrysts and postulated derivative lava, -trachyandesite T32

Lava	TB	TB	TA					
Sample No.	T30	T30	T32					
	obs.	est.						Cumulate Composition
SiO_2	51.39	51.53	55.09	Component	Wt. Fraction	Cumulate Mode (Wt. Fract.)	SiO_2	45.07
Al_2O_3	20.56	20.51	19.66	Cpx	0.0798	0.2767	Al_2O_3	23.43
FeO_T	6.52	6.52	5.96	Olivine	0.0029	0.0100	FeO_T	8.16
MgO	3.25	3.11	2.71	Plag.	0.1872	0.6491	MgO	4.22
CaO	8.89	8.67	5.47	Mag.	0.0185	0.0641	CaO	16.62
Na_2O	4.42	3.37	4.56	Lava T32	0.6994		Na_2O	0.63
K_2O	3.56	3.54	5.03	= potassic ne-trachybasalt T30			K_2O	0.09
TiO_2	0.68	0.73	0.69				TiO_2	0.84
P_2O_5	0.49	0.38	0.54	ΣR^2 = 1.2052			P_2O_5	-
MnO	0.15	0.15	0.18				MnO	0.10
							100Mg/ Mg + ΣFe	47.96

C. Approximation of trachyandesite T32 in terms of its phenocrysts and postulated derivative lava T20.

Lava	TA	TA	TA					
Sample No.	T32	T32	T20					
	obs.	est.						Cumulate Composition
SiO_2	55.09	54.96	56.10	Component	Wt. Fraction	Cumulate Mode (Wt. Fract.)	SiO_2	41.96
Al_2O_3	19.66	19.68	19.49	Cpx	0.0390	0.2995	Al_2O_3	19.05
FeO_T	5.96	5.94	5.26	Biotite	0.0333	0.2557	FeO_T	10.00
MgO	2.71	2.68	1.85	Plag.	0.0503	0.3863	MgO	8.01
CaO	5.47	5.73	4.50	Mag.	0.0076	0.0584	CaO	13.55
Na_2O	4.56	5.19	5.79	Lava T20	0.8824		Na_2O	0.65
K_2O	5.03	5.38	5.69	= trachyandesite T32			K_2O	2.77
TiO_2	0.69	0.86	0.61				TiO_2	2.51
P_2O_5	0.54	0.40	0.45	ΣR^2 = 0.6644			P_2O_5	-
MnO	0.18	0.16	0.18				MnO	0.03
							100Mg/ Mg + ΣFe	58.80

Abbreviations: TB - potassic ne-trachybasalt, TA - potassic ne-trachyandesite, obs. = observed composition, est. = calculated composition.

Notes: FeO_T = total Fe as FeO.

Refer to Table 9.17 for locality of mineral compositions used in calculations.

Table 9.12 Calculated Trace Element Variation Trends for Tambora Lavas

T12 ——— T30

	A. C_o	C_1 (est)	C_1 (obs)	% Discrep.
Sample No.	T12		T30	
% crystallisation	32.49			
Ni	11	3.2	12	-73.3
Sc	33	26	13	+100.0
Rb	77	112	97	+ 15.5
Sr	1192	1318	1352	- 2.5
Zr	120	177	89	+ 98.9
Y	18	23	12	+91.7
Nb	-	-	-	-
Minerals crystallised	Cpx, olivine, plag, magnetite			

T30 ——— T32

	B. C_o	C_1 (est)	C_1 (obs)	% Discrep.
Sample No.	T30		T32	
% crystallisation	30.06			
Ni	12	9	3	+200.0
Sc	13	13	10	+ 30.0
Rb	97	136	132	+ 3.0
Sr	1352	1196	1036	+ 15.4
Zr	89	127	145	- 12.4
Y	12	16	26	- 38.5
Nb	3	4.3	-	-
Minerals crystallised	Cpx, olivine, plag, magnetite			

T32 ——— T20

	C. C_o	C_1 (est)	C_1 (obs)	% Discrep.
Sample No.	T32		T20	
% crystallisation	11.76			
Ni	3	1.8	1	+80.0
Sc	10	9	8	+12.5
Rb	132	135	142	- 4.9
Sr	1036	1047	923	+13.4
Zr	145	163	194	-15.9
Y	26	28	25	+12.0
Nb	-	-	-	-
Minerals crystallised	Cpx, biotite, plag, magnetite			

Notes: Calculations based on a Rayleigh Fractionation model

$$\left(\frac{C_1}{C_o} = F^{(D-1)}\right).$$

Distribution coefficients are given in Table 9.1 in the following columns: Cpx 1 (and 2 for T32 ——— T20), Ol 6, plag 7, magnetite 10, apatite 11, biotite 15.

Mineral proportions and % crystallisations are taken from previously tabulated least-squares mixing computations, table 9.11.

variation of Rb and Sr well throughout the series, but some of the other elements do not behave as might be expected (for instance, why does low MgO trachybasalt, T30, have a lower Zr concentration than the more mafic T12?).

9.7 The Differentiation of the Tambora Suite; Conclusion

The general conclusion is that the compositional variation of the Tambora suite can be accounted for by simple fractional crystallisation of plausible assemblages of observed phenocrysts. These phenocryst assemblages are plagioclase-bearing, with the role of plagioclase assuming greater importance with advancing differentiation, and may be attributable to a low-pressure regime.

The assemblage whose crystallisation is responsible for the compositional variation within the trachybasalt group (clinopyroxene + olivine + plagioclase + magnetite) resembles that previously calculated as responsible for the compositional variations in the high-Al basalt group from Rindjani, yielding low-MgO, high-Al basalts or "hawaiites" as differentiates, but is richer in clinopyroxene and poorer in olivine.

Two questions arise:

1. The inflection, representing the change from Al_2O_3- and Sr-enrichment trends to those of depletion, with respect to decreasing MgO, is apparently caused by the increase in the proportion of crystallisation of plagioclase relative to the ferromagnesian phases. Is this effect controlled by the composition of the liquid? Or does it result from some change in physical conditions, for instance a drop in temperature or pressur or a loss of water vapour, which might in turn affect the relative positions of the liquidus and liquidus of incoming of plagioclase?
2. What is the origin of the gap in the MgO variation between 3 and 4% MgO, where the transition to the more plagioclase-enriched assemblage occurs? McBirney (1969) describes such discontinuities in the compositional variation of lavas from a number of calcalkaline volcanoes.

Some aspects of the above problems are discussed further in chapter 9, though the general conclusion is that rapid onset of plagioclase crystallisation and compositional discontinuity may both be results of sudden pressure-release, possibly attendant on exsolution of water vapour.

9.8 Evolution of the Sangeang Api Lava/Intrusive Suite

Sangeang Api is unusual amongst the volcanoes of this sector of the arc in having erupted a diverse suite of coarse-grained mafic and ultramafic intrusive rocks both as inclusions in lavas and as loose blocks in tephra deposits. This association of lavas and intrusive rocks has the potential to provide additional insight into the petrogenetic processes involved in the Sangeang Api volcano and may have applicability to problems of arc petrogenesis in general.

The coarse-grained xenolith suite could have been formed by several different processes:

1. Accidental or cognate samples of the upper mantle and/or lower crust?
   or ...
2. Cumulates derived from the crystallisation of liquids of broadly basaltic composition, like the lavas with which they were erupted?
   or ...
3. Products of some other process or the products of multistage processes, combining two or more of the above mechanisms?

Consideration of the data presented in chapter 5 allows some of these options to be evaluated and places some constraints on likely processes.

Textures are clearly primarily igneous in origin, though the effects of at least some later deformation, such as polygonitisation, sub-grain formation and cataclasis are widespread.

Bulk chemical compositions of the intrusive rocks are very different to those of the lavas and hence it is clear they are not simply intrusive equivalents of the same magma(s).

The xenoliths bear a marked resemblance to rock-types represented in the Alaskan-type, zoned ultramafic complexes, a similarity which is further reinforced by the almost identical compositions of their component minerals. Further the Sangeang Api lavas are very like the Bridget Cove group which Irvine (1973) considered could potentially have precipitated the Alaskan-type assemblages, as cumulates.

Even the most mafic members of the Sangeang Api xenolith-suite are unlike upper mantle material from the peridotitic upper mantle generally believed to underlie oceanic and continental provinces. Thus if any of the xenoliths are of mantle origin the mantle beneath the arc must be relatively iron-rich, Ti-poor, essentially of little-deformed igneous character and lacking opx and garnet in contrast to the more commonly accepted spinel- or garnet-lherzolite mantle believed to exist beneath other igneous provinces.

Of course the upper mantle of some non-arc provinces has also been shown to have an igneous component (for instance Frey and Prinz, 1978; Wilshire and Shervais, 1975) which yields the so-called Al-augite type ultramafic nodules (e.g. Frey and Prinz, 1978; Irving, 1974). Though as already shown in chapter 5, the cpx from these are significantly different from those of the Sangeang Api nodules. However if a completely different mantle is proposed, then this compositional difference is not surprising.

Thus a mantle origin for at least some of the Sangeang Api nodules cannot be completely dismissed, though the large differences between such an upper mantle and the more traditional upper mantle concept would have far-reaching consequences for magma generation.

Attempts to model such a process are difficult. If the mantle source-region is not dominated by olivine with a composition of about Fo90, or Ni concentrations of the order of 2000 ppm, then any constraints which we may like to assume normally exist to allow the recognition of "primary liquids", no longer apply. If we have no way of selecting a "primary" magma, then we have no means of assessing the extent to which lavas may have changed in composition since the magmas first segregated from the source rocks.

2. The intrusive rocks are unlikely to have been derived by fractional crystallisation of a single intrusive, differentiated mafic or ultramafic magma. For instance, the range of bulk compositions is quite extreme; MgO ranges from 24.4% to 6.0%, Al_2O_3 from 3.12 to 19.55% although all are very Ca-rich, and with relatively constant CaO contents (22.5 - 15.3% CaO, with the exception of one alkali pyroxenite with only 10.3% CaO). It is difficult to envisage a differentiation mechanism which would yield a six-fold variation in Al_2O_3 concentration and yet maintain a consistently high CaO content when so many of the crystallising phases are themselves so Ca-rich.

The variation of some trace elements is even more extreme. Rb varies from <1 ppm to 260 ppm and Sr from 68 to 1290 ppm. Furthermore if depletion in MgO concentration or decreasing Mg/Mg+Fe value are taken as indicators of advancing differentiation then it might be expected that those rocks in which these parameters are low might have the highest Rb, Zr and other incompatible element concentrations, but this is not the case. The rocks with highest Rb concentrations are those with most phlogopite and in no case does phlogopite appear to be a primary phase, but seems to be either a replacement mineral or a late-stage interstitial phase. Similarly, rocks with the highest Sr concentrations are those with the largest proportion of plagioclase and those with the highest K_2O have the highest proportions

of amphibole and/or phlogopite. Thus as discussed in chapter 5 the compositional variation shown by the intrusive rocks is more likely to be a function of their mineralogy than the reverse. This conclusion is more consistent with a cumulate origin than one of differentiating magmatic intrusion.

Although on mineralogical and geochemical grounds, the xenoliths could represent accumulations of phases crystallised by liquids like the erupted lavas, the series of lavas and xenoliths probably do not represent the simultaneous crystallisation products and differentiating liquid of one parent magma. The Sr-isotope results for instance (chapter 8), clearly indicate this.

The deformation of some of the xenoliths also suggests they have had a more complex history and implies that they must have been part of a solid rock mass prior to their entrainment in the lava which transported them to the surface. Such being the case it is unlikely that they represent cumulates of the lava which enclosed them. Similarly, the occurrence of olivine clinopyroxenite fragments in possibly cumulate, gabbroic assemblages, the inclusion of reacted alkali pyroxenite in gabbroic xenoliths some with veins of gabbroic material and the apparent origin of the alkali pyroxenites themselves as reaction products of olivine clinopyroxenite, all indicate that many of the intrusive rocks have had a complex history.

On the other hand, some xenoliths are very friable and are undeformed and may represent the crystallisation products of lavas with which they erupted. Similarly megacrysts which are compositionally equivalent to phases in the intrusive rocks may also represent components of recently formed cumulate assemblages.

Thus while the intrusive rocks from Sangeang Api may have an origin as cumulates from lavas like those with which they were erupted, it is probable that they record the passage of many erupting magmas throughout the history of this volcano.

9.9 Fractional Crystallisation

This section attempts to use the same least-squares mixing and trace element modelling techniques described previously to demonstrate whether or not:

1. The major element compositional variation trend of the lavas can be reproduced by fractionation of the assemblages present in the xenoliths.
2. The relative proportions of minerals thus implied are similar to those in the xenoliths.
3. The trace element variations seen in the actual lavas are appropriate to the defined models?

In general, the xenoliths have mineral assemblages which are likely to crystallise relatively close to the liquidus in somewhat alkaline, broadly basaltic systems at pressures <10 kbars (see chapters 10 and 11). Furthermore, if the sequence of crystallisation of individual xenoliths, together with evidence provided by the alkali pyroxenites and also the megacryst and phenocryst assemblages of the lavas are all taken into account, then a paragenetic sequence is implied. This is illustrated in figure 9.6. The main features are: 1. an early olivine-clinopyroxene stage, 2. a later amphibole-clinopyroxene-magnetite ± plagioclase stage, and 3. a plagioclase-clinopyroxene-olivine-magnetite eruptive stage. As discussed in chapter 10, the transition from stage 1 to 2 can result from decreasing temperature in the <10 kbar region. Amphibole and/or phlogopite may appear at the expense of olivine, though it does seem more likely that the olivne-out curve lies at higher temperatures than the amphibole liquidus and in fact amphibole may be appearing at the expense of clinopyroxene. The transition from the olivine-absent, amphibole-bearing xenolith assemblages to the olivine-bearing

FIGURE 9.6

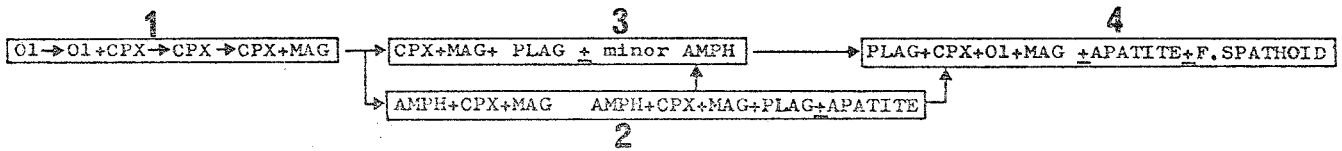

A POSSIBLE CRYSTALLISATION SEQUENCE FOR THE SANGEANG API MAGMAS AS IMPLIED BY THE MINERAL ASSEMBLAGES AND PETROGRAPHIC FEATURES OF THE XENOLITHS AND LAVAS. ASSEMBLAGE 1 IS THAT OF THE OLIVINE CLINOPYROXENITES, CLINOPYROXENITES AND MAGNETITE CLINOPYROXENITES AND MARKS THE DISAPPEARANCE OF OLIVINE AND THE APPEARANCE OF MAGNETITE AND PROVIDES MEGACRYSTS WHICH OCCUR IN THE MOST MAFIC LAVAS (eg B43). ASSEMBLAGES FORMED IN THIS FIELD MAY REACT IN FIELD 2 TO YIELD ALKALI CLINOPYROXENITES. THE SEQUENCE AFTER FIELD 1 MAY TAKE ONE OF TWO PATHS; FIELD 3 IS THAT OF INCREASINGLY IMPORTANT PLAGIOCLASE CRYSTALLISATION AND REPRESENTS ASSEMBLAGES SHOWN BY THE INCREASINGLY PLAGIOCLASE-RICH MAGNETITE CLINOPYROXENITES (eg B2H), FIELD 2 IS THE FIELD OF PRIMARY AMPHIBOLE CRYSTALLISATION AND SHOWS PROGRESSION FROM PLAGIOCLASE-FREE TO PLAGIOCLASE-BEARING ASSEMBLAGES. THIS IS THE FIELD OF CRYSTALLISATION OF THE GABBROIC XENOLITHS AND PROVIDES THE MEGACRYSTS OF THE LESS MAFIC LAVAS (THOSE SHOWING Ti-, Fe-DEPLETION) AND IS THE FIELD OF ALTERATION OF OLIVINE CLINOPYROXENITE TO ALKALI CLINOPYROXENITE. CRYSTALLISATION MAY PROGRESS OUT OF THE AMPHIBOLE FIELD SO THAT AMPHIBOLE BECOMES AN INTERCUMULATE PHASE MARKING A PROGRESSION TO FIELD 3 AND ASSEMBLAGES SUCH AS THOSE SHOWN BY GABBRO B10. FIELD 4 IS THAT OF THE CRYSTALLISATION OF THE PHENOCRYSTS AND GROUNDMASS MINERALS OF THE LAVAS AND MARKS THE REAPPEARANCE OF OLIVINE AND THE DISAPPEARANCE OF AMPHIBOLE AND THE FINAL CRYSTALLISATION OF FELDSPATHOIDAL MINERALS.

phenocryst assemblages may be due to decreasing pressure in the low-pressure region (<ca. 3 kbar), in view of the rapid retreat of the amphibole liquidus to low temperatures at low pressures (see chapter 10). This reaction is also apparently illustrated by the breakdown of amphibole in some xenoliths to glass + plagioclase + clinopyroxene + olivine.

A magma may therefore initially precipitate an olivine-clinopyroxene assemblage, followed by amphibole-bearing assemblages which contain increasing amounts of plagioclase through this interval. The magma may then erupt to the surface, during which stage any amphibole still carried will undergo reaction and resorbtion, plagioclase will crystallise abundantly and olivine will reappear. The composition of the liquid would constantly change as crystallisation proceeded and the geochemical variation trends would show inflections at points where transition from one assemblage to another took place.

This is an idealised scheme and as discussed in the previous section any single batch of liquid may not necessarily take this entire differentiation course, nor do the individual intrusive rocks representing the crystallisation products of the liquid at various points in its evolution, necessarily represent the products of the particular lava with which they were erupted.

Considering the compositional variation of the xenoliths and lavas shown as MgO-variation diagrams in figures 5.18 and 5.19, or in diagrammatic form in figure 5.25, the compositional relationship of the magma differentiation to the xenoliths, is consistent with the above model. In particular, the xenoliths either fall on extrapolations of the linear parts of the liquid trend, or where this trend is curved, on tangents. Further, the change from the relatively, Fe-, Ti-poor, MgO-rich olivine-clinopyroxenite to the markedly more Fe- and Ti-rich, amphibole-, magnetite-rich xenoliths correlates well

with the reversal of the trends involving these elements in the lavas. Other less marked inflections in trends involving other elements also occur at this point.

In order to test the hypotheses; 1. that the xenoliths are cumulates having crystallised from liquids like the Sangeang Api lavas, 2. that the compositional variation of the lavas actually results from the precipitation and segregation of these cumulate phases, and 3. that the inflections in the geochemical variation trends of the entire lava suite result from changes in the mineral assemblages crystallised by the liquids and that these changes are embodied in the changing mineralogies of the intrusive rocks, a least-squares mixing technique like that used in previous sections of this chapter was used.

For the sake of these calculations, the differentiation of the lavas have been considered in terms of the two distinct trends previously described i.e. the Fe-, Ti-enrichment and depletion trends. The more mafic lavas fall on the first of these and this trend extrapolates to the olivine-clinopyroxenite xenolith compositions (e.g. B5, B4 and B23; tables 5.4 and 5.1), while the second of these trends involves the less mafic lavas (<4.5% MgO) and extrapolates to the compositions of the more amphibole-rich gabbroic xenoliths (e.g. B24, tables 5.4 and 5.1) (see figure 5.25). Lavas comprising these two trends have megacryst assemblages equivalent to the mineralogy of the xenoliths to which they respectively extrapolate. The most mafic lavas in each of these two sequences are B43 (see table 5.3) and B25 (see table 5.3) respectively. Thus the mixing calculations whose results are presented in tables 9.13 and 9.14, attempt to match the compositions of these rocks by combining the compositions of more differentiated members of the trend in question, with mineral assemblages present as megacrysts in the lavas and present in the xenoliths which fall on the extrapolation of the trends, as

Table 9.13 Least-squares Mixing Computations to Model Sangeang Api Fractional Crystallisation Processes

A. Approximation of possible parental lava (B43) in terms of olivine clinopyroxenite B5 and possible derivative lava B44.

Lava	PT	PT	TB					
Sample No.	B43	B43	B44					Composition of Cumulate (xenolith B5 [1])
	obs.	est.						
SiO_2	47.77	47.94	48.68	Component	Wt. Fraction	Cumulate Mode [1]	SiO_2	48.42
Al_2O_3	13.05	13.03	16.01	Xenolith B5 [1]	0.2342	1.000	Al_2O_3	4.24
FeO_T	9.41	9.37	9.92	Lava B44	0.7519		FeO_T	8.16
MgO	8.65	8.58	5.96				MgO	17.50
CaO	13.90	13.59	11.67	= potassic ne-phonolitic tephrite B43			CaO	20.55
Na_2O	3.79	3.01	3.93				Na_2O	0.22
K_2O	1.85	1.68	2.22	ΣR^2 = 0.8110			K_2O	0.04
TiO_2	0.81	0.82	0.91				TiO_2	0.59
P_2O_5	0.44	0.26	0.34				P_2O_5	0.01
MnO	0.17	0.18	0.20				MnO	0.14
							100 Mg/ Mg + ΣFe	79.26

B. Approximation of possible parental lava B43 in terms of olivine clinopyroxenite xenolith B5 and possible derivative lava B38.

Lava	PT	PT	TB					
Sample No.	B43	B43	B38					Composition of Cumulate (xenolith B5 [1])
	obs.,	est.						
SiO_2	47.77	48.04	49.45	Component	Wt. Fraction	Cumulate Mode [1]	SiO_2	48.42
Al_2O_3	13.05	12.96	17.12	Xenolith B5 [1]	0.2928	1.000	Al_2O_3	4.24
FeO_T	9.41	9.33	10.14	Lava B38	0.6848		FeO_T	8.16
MgO	8.65	8.60	5.07				MgO	17.50
CaO	13.90	13.37	10.74	= potassic ne-phonolitic tephrite B43			CaO	20.55
Na_2O	3.79	2.26	3.21				Na_2O	0.22
K_2O	1.85	1.75	2.54	ΣR^2 = 2.7482			K_2O	0.04
TiO_2	0.81	0.84	0.97				TiO_2	0.59
P_2O_5	0.44	0.25	0.36				P_2O_5	0.01
MnO	0.17	0.18	0.21				MnO	0.14
							100 Mg/ Mg + ΣFe	79.26

C. Approximation of possible parental lava B43 in terms of its phenocrysts and megacrysts and possible derivative lava B38.

Lava	PT	PT	TB					
Sample No.	B43	B43	B38					
	obs.	est.						Cumulate Composition
SiO_2	47.77	48.02	49.45	Component	Wt. Fraction	Cumulate Mode (Wt. Fract.)	SiO_2	48.13
Al_2O_3	13.05	12.95	17.12	Olivine	0.0203	0.0666	Al_2O_3	4.59
FeO_T	9.41	9.42	10.14	Cpx	0.2452	0.8044	FeO_T	8.47
MgO	8.65	8.44	5.07	Plag.	0.0209	0.0685	MgO	16.46
CaO	13.90	13.49	10.74	Mag.	0.0184	0.0604	CaO	20.50
Na_2O	3.79	2.18	3.21	Lava B38	0.6745		Na_2O	0.06
K_2O	1.85	1.72	2.54				K_2O	0.01
TiO_2	0.81	0.91	0.97	= potassic phonolitic tephrite B43			TiO_2	0.83
P_2O_5	0.44	0.24	0.36	ΣR^2 = 2.9372			P_2O_5	-
MnO	0.17	0.14	0.21				MnO	-
							100 Mg/ Mg + ΣFe	77.59

Abbreviations: PT = potassic phonolitic tephrite, TB = potassic ne-trachybasalt, obs. = observed composition, est. = calculated composition.

Notes: FeO_T = total iron as FeO.

[1] See Table of modal analyses for the mineralogy of xenolith B5. (table 5.1)

See table 9.17 for locality of mineral compositions used in calculations.

Table 9.14 Calculated Trace Element Variation Trends for Sangeang Api Lavas

	Fractionation of ol. clinopyroxenite B5 from B43 to yield B44				Fractionation of mineral assembly of xenolith B5 (modal analysis) from B43 to yield B44			
	A.				A2.			
	C_o	C_1 (est)	C_1 (obs)	% Discrep.	C_o	C_1 (est)	C_1 (obs)	% Discrep.
Sample No.	B43		B44		B43		B44	
% crystallisation	24.81				24.81			
Ni	48	36	21	+71.4	48	18	21	-14.3
Sc	39	16	28	-42.8	39	24	28	-14.3
Rb	73	97	69	+40.6	73	95	69	+37.7
Sr	850	1093	872	+25.3	850	1080	872	+23.8
Zr	95	121	88	+37.5	95	125	88	+42.0
Y	20	23	25	- 8.0	20	22	25	-12.0
Nb	5	7	5	+40.0	5	-	5	-
Minerals crystallised	xenolith B5				Olivine, Cpx, amph, mag = xenolith B5			

	Fractionation of ol. clinopyroxenite B5 from B43 to yield B38				B43 ———— B38			
	B.				C.			
	C_o	C_1 (est)	C_1 (obs)	% Discrep.	C_o	C_1 (est)	C_1 (obs)	% Discrep.
Sample No.	B43		B38		B43		B38	
% crystallisation	31.52				32.55			
Ni	48	32	17	+88.2	48	15	17	-11.7
Sc	39	8	29	-72.4	39	21	29	-27.6
Rb	73	107	76	+40.8	73	107	76	+40.8
Sr	850	1190	856	+39.0	850	1135	856	+32.6
Zr	95	132	100	+32.0	95	139	100	+39.0
Y	20	24	24	0	20	24	24	0
Nb	5	7	4	+75.0	5	7	4	+75.0
Minerals crystallised	xenolith B5				Olivine, Cpx, plag., mag.			

Notes: Calculations based on a Rayleigh Fractionation model $\left(\frac{C_1}{C_o} = F^{(D-1)}\right)$.

Distribution coefficients are given in Table 9.1 in the following columns: Cpx 1, Ol 6, Plag. 7, Amph 8, magnetite 10, apatite 11.

Mineral proportions and % crystallisation are taken from previously tabulated least-squares mixing calculations (table 9.13).

Models A and C simply remove the analysed composition of xenolith B5 (olivine clinopyroxenite) from lava B43.

Model B uses the model analysis of the xenolith and theoretical distribution coefficients.

described above (also see figure 5.25). In addition to individual mineral compositions, whole-rock xenolith compositions were also used. Thus the less mafic trachybasalts, B44 and B38 which fall on the same Fe-, Ti-enrichment trend as the most mafic rock of the suite, B43, were used to approximate B43 using both the bulk composition of olivine-clinopyroxenite xenolith B5 (tables 5.4 and 5.1) and also the compositions of individual megacrysts. The results of these models are presented in table 9.13A-C. In general the models yield a satisfactory approximation to B43, the assumed parent magma, though this approximation is not perfect. The best models are those which utilize the bulk composition of the xenolith (in this case B5) rather than the megacryst/phenocryst assemblage, as in the case of model C (table 9.13). Significantly however, the bulk composition of the calculated cumulate where individual minerals are used is very similar to the composition of the xenolith B5. Furthermore, essentially the same cumulate composition allow B43 to be modelled as a combination of trachybasalt B44 or the slightly less mafic, B38 (table 9.13). This suggests that a similar cumulate assemblage was fractionating throughout the course of differentiation of this segment of the liquid trend.

The most persistent discrepancy in these calculations, between the observed composition of B43 and the one calculated is in the K_2O and P_2O_5 concentrations, which are markedly lower in the calculated version. This then suggests that the mafic lava, B43 is in fact too K_2O and P_2O_5 rich to yield the differentiated lavas here modelled.

Table 9.14 presents calculated trace element contents of trachybasalts B44 and B38 based on the mixing calculations in table 9.13 and using the trace element content of postulated parental lava B43 as the starting concentrations. In these calculations models A, B and C are based on the equivalently lettered models in table 9.13. Models A1 and B simply subtract the concentrations of trace elements as analysed in xenolith B5 (table 9.14)

Table 9.15 Least-squares Mixing Computations to Model Possible Fractional Crystallisation Processes in the Sangeang Api Suite

D. Approximation of possible parental lava B25 in terms of its phenocrysts and possible derivative lava B28.

Lava	TB	TB	TB
Sample No.	B25	B25	B28
	obs.	est.	
SiO_2	48.02	48.11	51.19
Al_2O_3	18.88	18.89	19.19
FeO_T	9.60	9.59	8.30
MgO	4.33	4.38	3.45
CaO	10.59	10.38	9.30
Na_2O	4.27	3.74	4.30
K_2O	2.64	2.40	2.67
TiO_2	0.91	1.02	0.80
P_2O_5	0.47	0.74	0.43
MgO	0.12	0.19	0.23

Component	Wt. Fraction	Cumulate Mode (Wt. Fract.)
Cpx	0.0055	0.0298
Amph	0.1091	0.5907
Plag.	0.0431	0.2333
Mag.	0.0174	0.0942
Apatite	0.0096	0.0519
Lava B28	0.8135	

= potassic ne-trachybasalt B25

ΣR^2 = 0.4869

	Cumulate Composition
SiO_2	35.01
Al_2O_3	17.74
FeO_T	15.39
MgO	8.51
CaO	15.22
Na_2O	1.31
K_2O	1.24
TiO_2	2.01
P_2O_5	2.13
MgO	0.04
100Mg/ Mg + ΣFe	49.63

E. Approximation of possible parental lava B25 in terms of its phenocrysts and possible derivative lava B32.

Lava	TB	TB	TA
Sample No.	B25	B25	B32
	obs.	est.	
SiO_2	48.02	48.10	53.05
Al_2O_3	18.88	18.88	19.21
FeO_T	9.60	9.59	7.33
MgO	4.33	4.35	2.69
CaO	10.59	10.42	8.05
Na_2O	4.27	3.57	4.69
K_2O	2.64	2.77	3.56
TiO_2	0.91	1.03	0.69
P_2O_5	0.47	0.69	0.40
MnO	0.12	0.16	0.22

Component	Wt. Fraction	Cumulate Mode (Wt. Fract.)
Cpx	0.0370	0.1200
Amph	0.1440	0.4672
Plag.	0.0878	0.2849
Mag.	0.0293	0.0957
Apatite	0.0101	0.0327
Lava B32	0.6916	

= potassic ne-trachybasalt B25

ΣR^2 = 0.6034

	Cumulate Composition
SiO_2	37.00
Al_2O_3	18.15
FeO_T	14.67
MgO	8.07
CaO	15.73
Na_2O	1.07
K_2O	0.99
TiO_2	1.78
P_2O_5	1.34
MnO	0.04
100Mg/ Mg + ΣFe	49.50

F. Approximation of possible parental lava B25 in terms of xenolith B24 [1] and possible derivative lava B32.

Lava	TB	TB	TA
Sample No.	B25	B25	B32
	obs.	est.	
SiO_2	48.02	48.23	53.05
Al_2O_3	18.88	18.51	19.21
FeO_T	9.60	9.24	7.33
MgO	4.33	4.48	2.69
CaO	10.59	10.69	8.05
Na_2O	4.27	3.59	4.69
K_2O	2.64	2.73	3.56
TiO_2	0.91	0.95	0.69
P_2O_5	0.47	0.91	0.40
MnO	0.12	0.20	0.22

Component	Wt. Fraction	Cumulate Mode (Wt. Fract.)
Xenolith B24 [1]	0.3010	1.000
Lava B32	0.6958	

= potassic ne-trachybasalt B25

ΣR^2 = 1.0138

	Cumulate Composition (xenolith B24 [1])
SiO_2	34.60
Al_2O_3	17.09
FeO_T	13.76
MgO	8.66
CaO	16.91
Na_2O	1.08
K_2O	0.85
TiO_2	1.56
P_2O_5	2.09
MnO	0.16
100Mg/ Mg + ΣFe	52.86

Abbreviations: TB = potassic ne-trachybasalt, TA = potassic ne-trachyandesite, obs. = observed composition, est. = calculated composition.

Notes: FeO_T = total Fe as FeO.

[1] See Table of modal analyses for the mineralogy of xenolith B24. (table 5.1)

See Table 9.17 for locality of mineral compositions used in calculations.

Table 9.16 Calculated Trace Element Variation Trends for Sangeang Api Lavas

	B25 ——— B28				B25 ——— B32			
	D.				E.			
	C_o	C_1 (est)	C_1 (obs)	% Discrep.	C_o	C_1 (est)	C_1 (obs)	% Discrep.
Sample No.	B25		B28		B25		B32	
% crystallisation	18.65				30.84			
Ni	10	4	7	-42.8	10	3	5	-40.0
Sc	22	18	21	-14.3	22	15	11	+36.0
Rb	92	109	95	+14.7	92	126	112	+12.5
Sr	1135	1184	984	+20.3	1135	1204	1010	+19.2
Zr	133	158	114	+38.6	133	184	134	+37.3
Y	19	17.4	25	-30.4	19	19	27	-29.6
Nb	5	6	4	+50.0	5	7	4	+75.0
Minerals crystallised	Cpx, amph, plag, mag, apatite				Cpx, amph, plag, mag, apatite			

Removal of xenolith B24 from lava B25 to yield B32

	F.			
	C_o	C_1 (est)	C_1 (obs)	% Discrep.
Sample No.	B25		B32	
% crystallisation	30.42			
Ni	10	10	5	+100.0
Sc	22	11	11	0
Rb	92	129	112	+15.2
Sr	1135	1072	1010	+ 6.1
Zr	133	173	134	+29.1
Y	19	17	27	-37.0
Nb	5	-	4	-
Minerals crystallised	xenolith B24			

Notes: Calculations based on Rayleigh Fractionation equation $(\frac{C_1}{C_o} = F^{(D-1)})$.

Distribution coefficients used are the same as previous Table. (9.14)

Mineral proportions and % crystallisation are taken from previously tabulated least-squares mixing calculations (table 9.15)

Model G is a simple removal of the analysed xenolith B24.

in the proportions calculated in the mixing model (table 9.13), from the B43 trace element concentrations. Model A2 uses the point counted modal proportion of minerals in B5 (table 5.1) and the appropriate distribution coefficients (table 9.1) and the Rayleigh fractionation expression. Model C uses the calculated mineral proportion, the published distribution coefficients and again the Rayleigh expression. In general the models using the mineral proportions and distribution coefficients yield better results, particularly in the case of those elements which have distribution coefficients >1 in terms of the dominantly clinopyroxene-olivine assemblage (Sc and Ni). The most important problem with these trace element calculations, as in t case of K_2O and P_2O_5 in the major element calculations already discussed, are the consistently high estimates of Rb, Sr and Zr concentrations yielded using the concentrations of these elements from B43 to model the less mafic differentiates. This again suggests that the mafic lava B43 has a higher concentration of incompatible elements than a hypothetical parent magma which might yield the trachybasalts B44 and B38, even though the major element concentration of such a parent were probably similar.

In a similar fashion to the cases described above, the Fe-, Ti-depletion trends were modelled. Thus the most mafic trachybasalt of this segment of the Sangeang Api variation trend, B25, was calculated as a combination of each of two of the more differentiated trachybasalts (B28 and B32) and the minerals from the more amphibole-rich gabbroic xenoliths. The results of these mixing calculations are given in table 9.15. The proposed models yield fairly satisfactory results and proportions of minerals so yielded are in fact very similar proportions in the xenolith B24 (table 5.1). The actual bulk composition of xenolith B24 was used in model F and this also yielded a reasonably good approximation of lava B25, as 69.6% differentiated trachybasalt B32 and 30.1% xenolith B24 (which is composed of 15% clinopyroxene, 49% amphibole, 8% magnetite, 24% plagioclase and 3% apatite). Trace element calculat

based on these models are presented in table 9.16, and are again reasonably consistent with the proposed model.

In general, these calculations do suggest that the Sangeang Api intrusive rocks can be cumulates of the Sangeang Api lavas and that the differentiation trends of which may result from initial precipitation of magnesian, clinopyroxene-rich, olivine-clinopyroxenite assemblages, while the later part of the trend might result from crystallisation of relatively more Fe-rich, amphibole-magnetite-cpx-plagioclase-apatite-assemblages. However, some inconsistencies occur, and the problem was further examined using REE data.

9.10 *Petrogenetic Implications of the Rare Earth Element Geochemistry of the Sangeang Api Lavas*

REE patterns for three representative lavas from the Sangeang Api suite are presented in figure 9.7. B43 is the most mafic lava analysed from the suite. B25 is a less mafic trachybasalt and B32 is the most silica-rich, MgO-poor trachybasalt/andesite. These REE patterns present some interesting features:

1. As discussed earlier in this chapter, B43 has large megacrysts of Cr-diopside (Mg/Mg+Fe = 0.90) and olivine (∿Fo85), which may represent accumulated debris. However, if this were the case then such an accumulation of megacrysts would be expected to dilute the incompatible trace element content of the lavas. Yet this lava has a higher LREE content than the more differentiated trachybasalt B25. This same problem was encountered with respect to K_2O, Rb and P_2O_5 levels earlier in this chapter and suggests that LIL- and incompatible element levels in B43 are too high to yield liquids like the more differentiated trachybasalts (e.g. B25), purely by the removal of the megacrysts. Furthermore, B43 has the highest $^{87}Sr/^{86}Sr$ ratio. (As discussed in chapter 8 the variability of the isotopic composition of Sr amongst the Sangeang Api

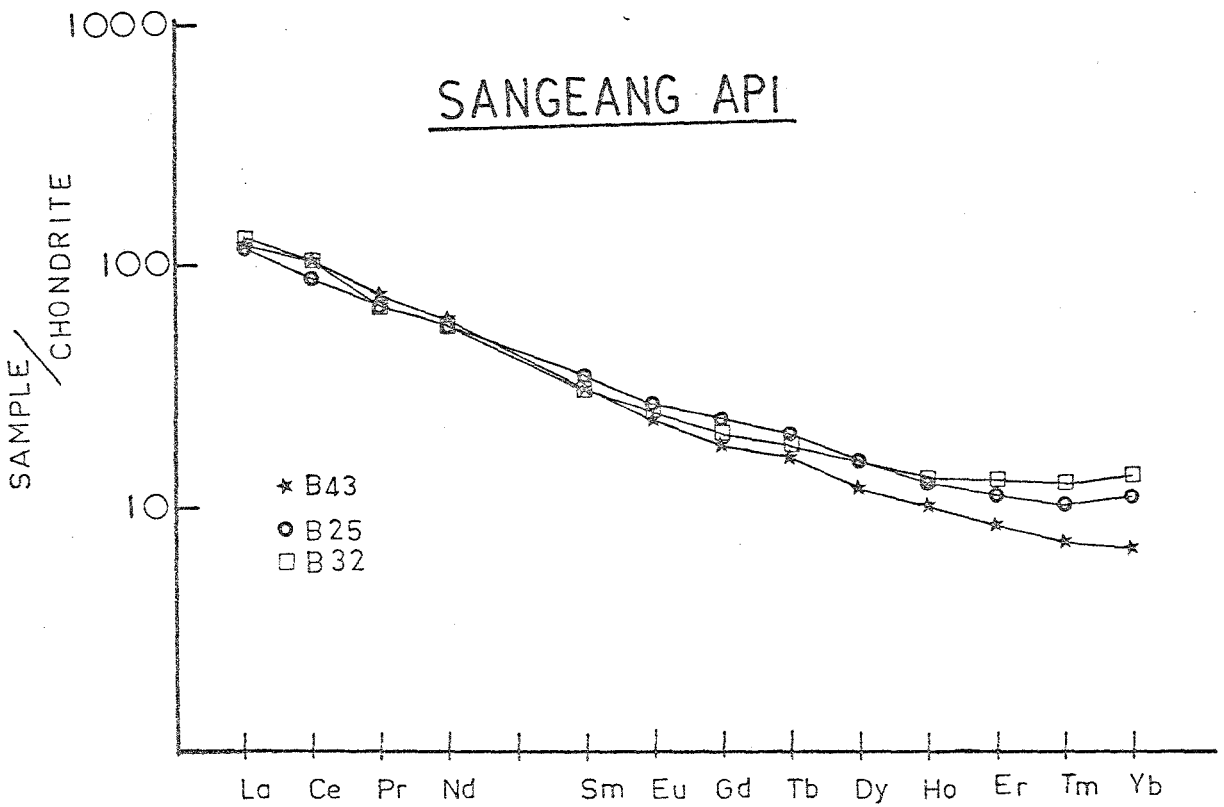

FIGURE 9.7

Chondrite-normalised REE patterns of Sangeang Api lavas .(see also table 9.4). B43 - most mafic lava of the Sangeang Api suite ,phonolitic tephrite,B25 and B32 ne-trachybasalts (B32 is the most silica-rich,MgO-poor lava of the Sangeang Api suite).

lavas indicates the possibility that a geochemically heterogeneous source is being tapped by this volcano.)

Although the LREE content of B43 is very similar to that of the two more MgO-poor Lavas (B25, B32), it has a significantly lower HREE content and is unique amongst all the Sunda Arc lavas analysed for REE in this study, in having a markedly fractionated pattern without the flat HREE character (figure 9.7). Consequently, B43 has a La/Yb ratio (27) higher than those of lavas from Rindjani and Tambora as well as the other lavas from Sangeang Api.

2. The trachybasalt (B25) and trachybasalt/andesite (B32) have almost identical REE patterns, though B32 has significantly higher Rb, K_2O and Rb/Sr ratio, lower Sc, Ni, Cr and Mg/Mg+ΣFe ratio, suggesting it could be a more fractionated lava. Both these lavas have fractionated LREE and flat HREE patterns, with Yb slightly enriched relative to the elements Dy-Tm.

Three basic conclusions may be drawn from the data presented above:

(1) Because of its markedly higher La/Yb ratio, the mafic phonolitic tephrite is unlikely to yield more differentiated trachybasalts such as B25 by fractional crystallisation of any of the observed phenocryst assemblages, or of any other mineral assemblages found amongst the xenoliths. Such a situation would require bulk fractionates to have LREE distribution coefficients which were larger than those for the HREE. In view of the abundance of clinopyroxene and amphibole in the cumulate xenoliths and the preference of these phases for the heavier REE's, such a situation is unlikely.

(2) If a homogeneous source, with a chondritic, relative REE pattern was envisaged, then the high La/Yb ratio of B43 would suggest that garnet may be involved, either as a fractionating phase or as a residual

mineral after partial melting. The markedly lower La/Yb ratios of the other lavas for which REE data are available would then suggest this phase may not be involved in the evolution of the other lavas. However if a heterogeneous source is envisaged, such a conclusion is invalid as the patterns may be just reflecting source REE variation.

(3) The almost identical REE patterns for lavas B25 and the more differentiated B32, suggests that if the latter has differentiated from B25 by a fractional crystallisation process, then the bulk distribution coefficient for all REE's must be close to 1.

A model for point 3, above, was developed earlier in this chapter. In this least-squares mixing calculation, the mineral compositions from xenolith B24 (cpx, amphibole, plagioclase, magnetite, apatite) were used and yielded a satisfactory solution (table 9.15). The proportions of minerals required by this model are in fact very close to those of xenolith B24 (table 5.1). Thus, removal of 30.8% of an assemblage of 12% cpx, 46.7% amphibole, 28.5% plagioclase, 9.5% magnetite and 3.2% apatite, from trachybasalt B25, can yield a satisfactory approximation to B32.

The REE content predicted for trachybasalt/andesite B32, based on parent trachybasalt B25, was calculated using the model described above. Using the REE distribution coefficients given in table 9.1 (cpx- column 1, apatite- column 11), the resultant predicted REE trend calculated for the modelled B32 (figure 9.8) is very close to that observed. This then tends to lend support to the proposed fractional crystallisation scheme.

The relationship between the mafic phonolitic tephrite B43 and the less mafic lavas of the Sangeang Api series remains a problem. As already discussed, the higher $^{87}Sr/^{86}Sr$ ratios of this lava, the relatively high Rb, P_2O_5, Zr and La concentration and lower K/Rb ratio, compared with markedly less mafic lavas (e.g. B44, B38; table 5.4), which have lower Sc, Cr and Ni,

FIGURE 9.8

Calculated REE pattern of Sangeang Api ne-trachybasalt B32 compared with the REE pattern of B32 as analysed, using B25 as the parent liquid,based on the mixing model E,table 9.15 where trachybasalt B32 = 31% crystallisation of an assemblage ; Cpx 0.12,Amph 0.47,Plag 0.28,Mag 0.10, Apatite 0.03 from trachybasalt B25.Calculation of the REE pattern of B32 (est.) used the above mineral proportions,the Rayleigh fractionation expression ($\frac{cl}{co} = F^{(D-1)}$) and the REE distribution coefficients in table 9.1.

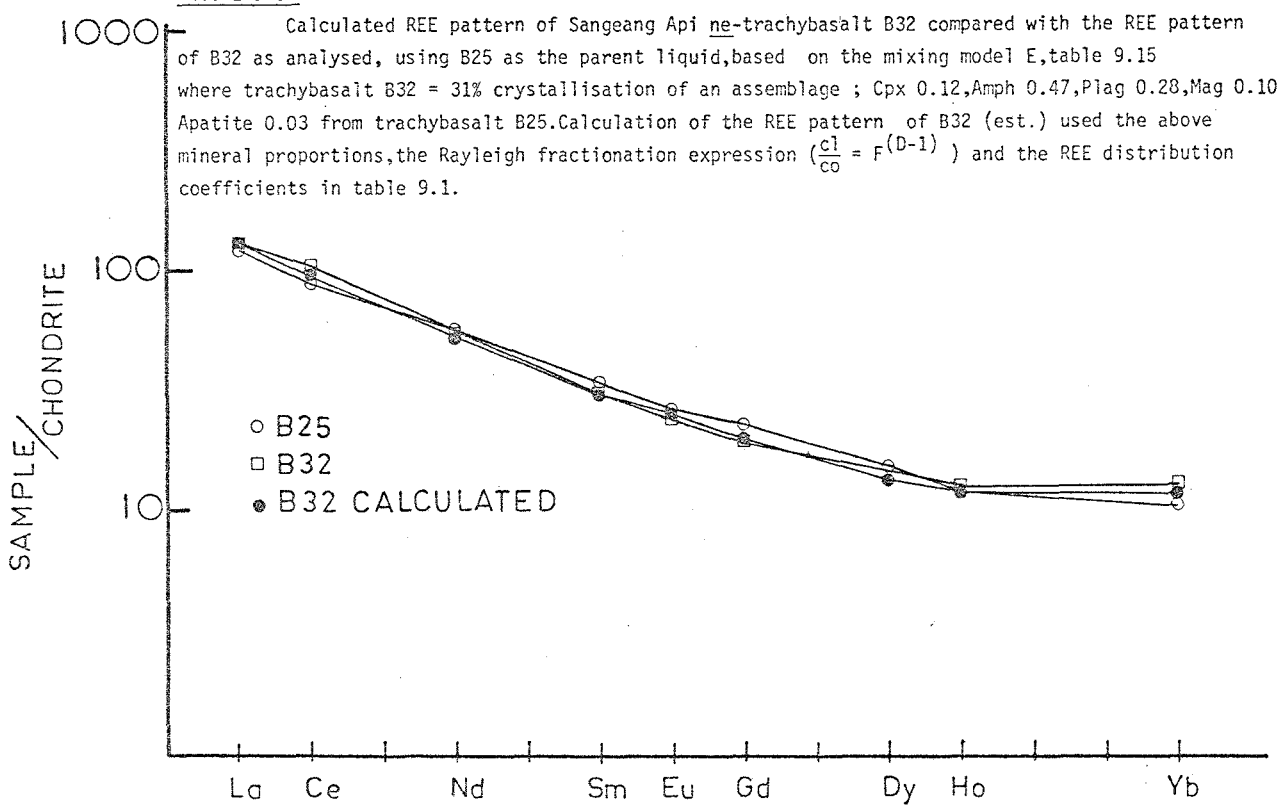

all suggest that there is not a direct fractional crystallisation relationship between B43 and many of the more differentiated Sangeang Api lavas. In addition, the highly fractionated REE pattern of B43, compared with that of the differentiated trachybasalt B25, also suggests that a connection by any fractional crystallisation process involving minerals present in either the lavas or xenoliths, is unlikely.

Island arc calcalkaline and high-K volcanic rocks typically have patterns resembling those from the Rindjani suite (i.e. with LREE's showing varying degrees of enrichment and rather flat middle-heavy REE chondrite-normalized patterns), but some volcanic rocks are reported with more fractionated REE patterns and high La/Yb ratios, for instance from basanitoids from Grenada in the Lesser Antilles (Shimazu and Arculus, 1973), from some andesites from the Southern Chilean Andes (Tupungato andesite, Lopez-Escobar et al., 1976) and from basaltic andesites, andesites and dacites from the Northern Chilean Andes and Peru (Thorpe et al., 1976; Noble et al., 1975). In each of these instances, melting of garnet peridotite is invoked as the ultimate source of the fractionated REE pattern with its high La/Yb ratio.

The difference between the REE pattern of the mafic phonolitic tephrite B43 and that of the less magnesium trachybasalt B25, is reminiscent of the difference between the REE patterns of alkali olivine basalts or basanites and tholeiites from the Tertiary-Quaternary basalts of S.E. Australia (e.g. Frey et al., 1978) or the Hawaiian nephelinite and alkali basalts or tholeiites (e.g. Schilling and Winchester, 1969; Sun and Hanson, 1975; Kay and Gast, 1973; Philpotts et al., 1971).

In these suites it has been suggested that the mantle source may have a similar composition, but that the different geochemistries of the erupted lavas is the result of varying degrees of melting and of variations in the residual mineral assemblages (e.g. Frey et al., 1978; Sun and Hanson, 1975; Kay and Gast, 1973). In the Sangeang Api suite however, the marked contrasts

in the REE patterns of different lavas, together with the variation in $^{87}Sr/^{86}Sr$ ratios of both the lavas and xenoliths, suggests that this source is also geochemically heterogeneous.

9.11 The Petrogenesis of the Sangeang Api Lava-Intrusive Suite: Conclusions

In short it is concluded that while the Sangeang Api lavas could have differentiated by fractionation of mineral assemblages represented in the mafic and ultramafic xenoliths and that these rocks could therefore represent cumulates, it is also likely that more than one primary magma was involved. Thus while the range of rock-types in the xenolith suite, from olivine clinopyroxenite, through amphibole-rich gabbro to amphibole-poor gabbro, and thence to the phenocryst assemblage of the lavas, does represent an idealised crystallisation sequence of a single magma batch, as a consequence of falling pressure and temperature, the actual suite of xenoliths erupted probably crystallised from several magma batches and as such are probably a composite group having recorded the eruption and passage of numerous injections of magma.

9.12 Differentiation of the Highly Undersaturated, K_2O-rich Suites from Soromundi and G. Sangenges

The question of how this group as a whole acquired their marked enrichment in K_2O and related elements is considered of great importance to the general problem of island arc petrogenesis and to the problems of the origin of potassium-rich suites elsewhere. These problems are dealt with in chapter 12.

As discussed in chapter 6, there are significant differences in the mineralogy of members of the leucitite suite from G. Sangenges and Soromundi. The latter contains abundant hydrous minerals (amphibole and phlogopite), while the former has mainly phenocrysts of olivine and clinopyroxene. Similarly, while the members of these suites from both volcanoes, have the

same general geochemical characteristics (high K, Rb, Sr contents, low K/Rb ratios and high K_2O/Na_2O ratios and relatively high $^{87}Sr/^{86}Sr$ ratios), they do have certain contrasting features. In particular, the G. Sangenges suite shows marked Ti- and total Fe-enrichment with decreasing MgO, a trend not observed in the Soromundi suite. This difference may relate to the fractionation of assemblages including amphibole, phlogopite and magnetite, from the Soromundi liquids, while those of G. Sangenges may largely comprise olivine and clinopyroxene.

The most abundant phenocryst/megacryst phase in all the lavas is clinopyroxene and the leucitite lavas from both volcanoes show trends of simultaneous depletion of CaO, Sc, Ni and Cr with decreasing MgO and of Al_2O_3 and Sr-enrichment with decreasing CaO, all features suggestive of clinopyroxene fractionation. They plot on the same Al_2O_3-CaO trend as the cpx-rich ankaramites from Rindjani (figure 6.5) which as already discussed, possibly differentiated by fractionation of a clinopyroxene-dominated, olivine-clinopyroxene assemblage. Although all of these lavas contain leucite either as phenocrysts, microphenocrysts or in the groundmass, there is no K_2O-depletion trend which is attributable to fractionation of this phase. This suggests that leucite crystallised late in the sequence after the lavas had acquired their compositional diversity.

Even though the lavas show some characteristics suggestive of some crystal fractionation, it is also apparent that much of their geochemical diversity is not attributable to this mechanism. Thus in the G. Sangenges leucitite suite, where olivine, clinopyroxene and, occasionally, magnetite are the sole phenocryst phases, incompatible elements such as K, Rb, Nb, Zr and P might be expected to show simple, negative covariation with MgO, for instance. This is not the case and the variation of these elements is often poorly correlated with those of other major elements. In both the Soromundi and

G. Sangenges suites, the situation exists where more mafic members of the suite may have higher concentrations of K_2O, P_2O_5, Rb, Zr and Nb than some less mafic and presumably more differentiated lavas of the same suite. This type of compositional diversity possibly arises from processes similar to those in the Sangeang Api suite where at least two primary magmas may have been involved, and even more strongly underlined by the contrast in composition between lavas of different volcanoes of this sector of the Sunda Arc. Aspects of this compositional diversity are discussed in detail in chapter 12.

9.13 Conclusions

The general conclusion of this chapter is that while fractional crystallisation is probably an important mechanism, and accounts for a large amount of the compositional diversity of lavas from individual volcanoes, it cannot account for all variation, either within single suites, or between suites from different volcanoes. This then implies that there are significant variations in the compositions of primary melts generated beneath this sector of the Sunda Arc.

The ramifications of the last conclusions are considered to be particularly important in the understanding of island-arc petrogenesis and are discussed in detail in chapter 12.

Table 9.17

Mineral Analyses used in Least-Squares Mixing Calculations

1. Model A, table 9.5, LB7 → LB1			
	CPXA	CPXB	OL
SiO_2	53.16	49.35	37.91
Al_2O_3	1.44	4.46	-
FeO	3.27	8.53	16.63
MgO	17.46	13.90	44.07
CaO	23.59	22.56	0.31
Na_2O	-	-	-
K_2O	-	-	-
P_2O_5	-	-	-
MnO	-	-	0.23
TiO_2	0.33	0.93	-

2. Model B, table 9.5, LB11 → 41621				
	OL	CPX	PLAG	MAG
SiO_2	38.87	50.67	47.78	-
Al_2O_3	-	3.95	33.20	4.93
FeO	17.82	6.64	0.71	77.23
MgO	42.81	14.56	-	3.66
CaO	0.23	22.90	17.71	-
Na_2O	-	-	1.60	-
K_2O	-	-	0.08	-
P_2O_5	-	-	-	-
MnO	0.28	-	-	0.41
TiO_2	-	0.87	-	9.89

3. Model C, table 9.5, LB11 → LB28				
	OL	AMPH	PLAG	MAG
SiO_2	38.63	51.21	38.97	46.70
Al_2O_3	-	1.59	14.59	33.86
FeO	14.77	9.74	11.81	0.53
MgO	46.21	15.09	13.87	0.52
CaO	0.27	21.20	12.94	16.25
Na_2O	-	-	2.70	2.08
K_2O	-	-	0.74	0.07
P_2O_5	-	-	-	-
MnO	-	0.53	-	-
TiO_2	-	0.42	2.37	-

4. Model D, table 9.7, 41632 → 41626			
	OL	CPX	PLAG
SiO_2	38.87	48.66	47.78
Al_2O_3	-	6.18	33.10
FeO	17.82	8.41	0.71
MgO	42.81	13.89	0.07
CaO	0.23	20.05	17.71
Na_2O	-	0.42	1.52
K_2O	-	-	0.08
P_2O_5	-	-	-
MnO	0.28	0.15	-
TiO_2	-	1.04	-

5. Model E, table 9.7 41676 → 41622					
	AMPH	CPX	PLAG	MAG	APAT
SiO_2	44.22	51.76	46.70	-	-
Al_2O_3	11.49	2.27	33.86	4.93	-
FeO	11.83	8.71	0.53	77.23	0.20
MgO	13.81	15.39	-	3.66	-
CaO	11.95	20.21	16.25	-	52.40
Na_2O	2.12	0.34	2.08	-	-
K_2O	0.77	0	0.07	-	-
P_2O_5	-	-	-	-	40.98
MnO	-	0.04	-	0.41	-
TiO_2	2.54	0.17	-	9.89	-

6. Model F, table 9.7, LB67 → 41687					
	OL	CPX	AMPH	PLAG	MAG
SiO_2	38.63	51.21	38.97	46.70	0.10
Al_2O_3	-	1.59	14.59	33.86	1.69
FeO	14.77	9.74	11.81	0.53	79.97
MgO	46.21	15.09	13.87	0.52	1.00
CaO	0.27	21.20	12.94	16.25	-
Na_2O	-	-	2.70	2.08	-
K_2O	-	-	0.74	0.07	-
P_2O_5	-	-	-	-	-
MnO	-	0.52	-	-	0.28
TiO_2	-	0.42	2.37	-	11.51

7. Model G, table 9.10, 41637 → 41672				
	OL	CPX	PLAG	MAG
SiO_2	36.87	51.76	52.11	0.10
Al_2O_3	-	2.27	29.59	1.69
FeO	26.42	8.71	0.54	79.97
MgO	35.79	15.39	0.06	1.00
CaO	0.22	20.21	12.79	-
Na_2O	-	0.34	4.18	-
K_2O	-	-	0.26	-
P_2O_5	-	-	-	-
MnO	0.67	0.04	-	0.28
TiO_2	-	0.17	-	11.51

8. Model H, table 9.10, 41622 → LB3				
	OPX	CPX	PLAG	MAG
SiO_2	52.94	51.76	55.43	0.10
Al_2O_3	1.63	2.27	27.86	1.69
FeO	17.51	8.71	0.49	79.97
MgO	24.96	15.39	0.05	1.00
CaO	1.53	20.21	11.28	-
Na_2O	0.05	0.34	5.14	-
K_2O	-	-	0.36	-
P_2O_5	-	-	-	-
MnO	0.18	-	-	0.28
TiO_2	0.07	0.17	0.09	11.51

9. Model I, table 9.10, 41622 → 41671				
	OPX	CPX	PLAG	MAG
SiO_2	52.94	51.76	55.43	0.13
Al_2O_3	1.63	2.27	27.86	0.61
FeO	17.51	8.71	0.49	80.93
MgO	24.96	15.39	0.05	0.95
CaO	1.53	20.21	11.28	-
Na_2O	0.05	0.34	5.14	-
K_2O	-	-	0.36	-
P_2O_5	-	-	-	-
MnO	0.18	-	-	0.23
TiO_2	0.07	0.17	0.09	12.23

Table 9.17 Continued

Mineral Analyses used in Least Squares Mixing Calculations

	10. Model A, table 9.11, T12 → T30				11. Model B, table 9.11, T30 → T32				12. Model C, table 9.11, T32 → T20			
	CPX	OL	PLAG	MAG	CPX	OL	PLAG	MAG	CPX	BIOT	PLAG	MAG
SiO_2	51.30	36.62	50.68	-	50.27	36.30	47.45	-	48.35	35.62	47.55	-
Al_2O_3	3.34	-	30.61	5.30	3.59	-	34.05	5.30	5.50	15.72	33.73	6.14
FeO	8.27	28.96	0.50	78.00	9.25	26.22	0.51	78.00	7.87	11.17	0.49	78.85
MgO	13.83	32.70	-	1.60	13.58	35.72	-	1.60	12.50	15.92	-	3.40
CaO	22.08	0.35	12.94	-	21.94	0.32	16.52	-	24.00	0.46	16.16	-
Na_2O	-	-	4.30	-	-	-	0.97	-	-	-	1.68	-
K_2O	-	-	0.66	-	-	-	0.14	-	-	10.53	0.22	-
P_2O_5	-	-	-	-	-	-	-	-	-	-	-	-
MnO	-	1.14	-	0.55	0.18	1.14	-	0.55	-	-	-	0.54
TiO_2	0.88	-	-	9.30	0.90	-	-	9.30	1.30	6.46	-	8.02

	13. Model A, table 9.13, B43 → B44	14. Model C, table 9.13, B43 → B38			15. Model D, table 9.15, B25 → B28				
	$B5^{(1)}$	OL	CPX	PLAG	MAG	CPX	AMPH	PLAG	MAG	APAT
SiO_2	48.42	39.90	52.54	46.78	-	49.57	38.95	45.09	-	-
Al_2O_3	4.24	-	2.23	34.22	7.42	4.65	14.95	35.41	5.44	-
FeO	8.16	11.63	3.73	0.59	77.14	8.12	12.40	0.36	82.00	0.20
MgO	17.50	47.70	16.15	-	4.81	13.17	13.23	-	3.23	-
CaO	20.55	0.35	24.00	17.06	-	23.41	12.62	18.64	-	52.40
Na_2O	0.22	-	-	0.85	-	-	2.09	0.32	-	-
K_2O	0.04	-	-	0.16	-	-	2.02	0.18	-	-
P_2O_5	0.01	-	-	-	-	-	-	-	-	40.98
MnO	0.14	-	-	-	-	-	-	-	0.39	-
TiO_2	0.59	-	0.50	-	7.16	0.83	2.47	-	5.62	-

	16. Model E, table 9.15, B25 → B32				
	CPX	AMPH	PLAG	MAG	APAT
SiO_2	49.67	38.95	45.09	-	-
Al_2O_3	4.65	14.95	35.41	5.44	-
FeO	8.12	12.40	0.36	82.00	0.20
MgO	13.17	13.23	-	3.23	-
CaO	23.41	12.62	18.64	-	52.40
Na_2O	-	2.09	0.32	-	-
K_2O	-	2.02	0.18	-	-
P_2O_5	-	-	-	-	40.98
MnO	-	-	-	0.39	-
TiO_2	0.83	2.47	-	5.62	-

Notes. (1) Bulk composition of olivine clinopyroxenite B4, also used in model B, table 9.13 (B43 → B38).

Chapter 10

NEAR LIQUIDUS PHASE RELATIONSHIPS IN BASALTIC AND ANDESITIC SYSTEMS AND THE DIFFERENTIATION OF ISLAND ARC MAGMAS

10.1 Introduction

This chapter is an introductory examination of the phase relationships implied by the results of the modelling procedures presented in chapter 9. These relationships are examined in the light of published experimental data, largely based on natural basaltic or andesitic systems, both saturated and undersaturated with water. The discussions presented have formed the basis for more detailed discussion in chapter 11, where the results of new experimental work are presented.

The calculations and discussions presented in chapter 9, together with information provided in chapters 3 to 7, suggest several fractionating assemblages are likely to be important. These either represented in the lavas as megacryst or phenocryst phases or inferred to have been present at depth, prior to eruption:

1. Clinopyroxene + olivine, where clinopyroxene >>olivine (Rindjani: ankarami some Sangeang Api lavas and olivine-clinopyroxenite xenoliths, leucitic lavas from Soromundi and G. Sangenges).
2. Olivine $\pm$ clinopyroxene (olivine >> clinopyroxene) (most mafic high-Al basalts from Rindjani). This assemblage shows gradation to assemblage 3 as does assemblage 1.
3. Plagioclase + clinopyroxene + olivine $\pm$ magnetite $\pm$ apatite (more differentiated Rindjani high-Al basalts, silica poor basaltic andesites, trachybasalts from Tambora and Sangeang Api).
4. Amphibole + plagioclase + magnetite $\pm$ clinopyroxene $\pm$ olivine $\pm$ apatite (some Sangeang Api trachybasalts, Sangeang Api gabbroic intrusives and inferred to have crystallised from Rindjani high-Al basalts to yield andesitic residual liquids).

5. Plagioclase + clinopyroxene + orthopyroxene + magnetite ± apatite (eruptive assemblage of Rindjani andesites, coexisting liquid being dacitic in composition).

Undersaturated parental basaltic liquids crystallising assemblages 1, 2 and 3 will yield undersaturated residual liquids of low MgO-trachybasalt, high-Al basalt, basaltic andesite, trachyandesite or hawaiite or mugearite-like composition. Only assemblage 4 may crystallise from an undersaturated parent melt and yield a *Q*-normative, differentiated, residual liquid. Assemblage 5 will only crystallise in a *Q*-normative bulk composition.

In the Rindjani suite, the transitions between different stable mineral assemblages, in particular, between the olivine + clinopyroxene ± plagioclase assemblages of many lavas with <53% SiO_2 and the hypothetical amphibole + magnetite ± plagioclase ± clinopyroxene ± olivine postulated to give rise to andesitic residual liquids and between this assemblage and the plagioclase + clinopyroxene + orthopyroxene + magnetite assemblage of the erupted andesites, has resulted in marked discontinuity and divergence in the liquid line of descent. Similarly the transition in the Tambora suite between the more plagioclase-poor trachybasalts with >4.5% MgO and the more plagioclase-rich trachybasalt-trachyandesites and also between the olivine-phenocryst bearing and amphibole-bearing lavas of the Sangeang Api suite, all represent a similar type of discontinuity. This type of discontinuous evolution has been noted in a number of island-arc and continental marginal calcalkaline suites (e.g. McBirney, 1969; amongst lavas of Central American volcanoes. Gorton, 1977; amongst suites from the New Hebrides.).

The contrasting inferred assemblages leading to the divergent evolution of the Rindjani basaltic lavas are reminiscent of those proposed by Green et al., (1974) in the derivation of an alkali olivine basalt-hawaiite-benmoreite series at low pressure (amphibole absent) and an associated series of hawaiites, mugearites and benmoreites derived at Pload >8 kbars, where amphibole is a postulated fractionate.

10.2 The P/T Stability Limits of Amphibole in Basaltic-Andesitic Liquids

A number of experimental studies have been undertaken in order to determine the stability field of amphibole in basaltic to andesitic systems and in particular to determine the conditions under which it achieves its highest thermal stability. Andesites appear to have erupted at relatively high temperatures (1020^{o}-$1110^{o}C$, for basaltic andesites from Paracutin; Zies, 1946; Wilcox, 1956) and it would appear therefore that amphibole should be stable to between 1020^{o} and $1100^{o}C$ to be an effective fractionating phase.

The stability of amphibole is likely to be affected by: 1. load pressure, 2. water vapour pressure 3. bulk composition of the system and possibly oxygen fugacity (Allen et al., 1975). In a study of the system pargasite + H_2O + CO_2 at pressures <8 kbars, Holloway (1973) found that at pressures <4 kbars, the upper stability temperature of amphibole decreased as the mole fraction of H_2O in the fluid phase decreased. At load pressures <4 kbars, there was a marked increase in the stability of amphibole as the mole fraction of H_2O in the fluid phase was decreased, reaching a maximum and then decreasing with further decrease in mole fraction H_2O. His results suggest that amphibole may be stable at quite high temperatures (up to $1090^{o}C$) at relatively low pressures, in relatively water poor systems. Holloway (1973) also showed that above 1-2 kbars pargasite disappeared by incongruently melting to olivine + clinopyroxene spinel + liquid, while at very low pressure it disappeared by a dehydration reaction to yield olivine + clinopyroxene + nepheline + anorthite + spinel + fluid.

Experimental studies on natural basaltic and andesitic compositions, under water saturated conditions, occasionally show amphibole to be on the liquidus, for instance: in the Hualalai alkali basalt at $1090^{o}C$, and 13 kbars and the Mt. Hood andesite over a wide pressure range at $950^{o}C$ (Allen et al., 1975). More often, however, the appearance of amphibole is preceded at higher temperatu by an interval of olivine and clinopyroxene crystallisation, between the liquidus and the amphibole-out curve (e.g. Irvine, 1972; Yoder, 1969). Early

olivine and clinopyroxene may then disappear by reaction once the amphibole stability field is reached (e.g. Holloway and Burnham, 1972). Plagioclase may also precede amphibole at very low pressures (<2.5 kbars) (e.g. Holloway and Burnham, 1972, Yoder, 1969).

A number of studies have demonstrated that in a basaltic composition, the residual liquid in equilibrium with amphibole, may be andesitic in composition. Cawthorn et al. (1973) demonstrated that amphibole appears in the hypersolidus assemblage of a series of undersaturated and oversaturated compositions from the Lesser Antilles, under water saturated conditions at 5 kbars, in the temperature range 1050-1025°C. They showed that residual liquids trended towards the more silica-rich members of the series. This also demonstrates that fractionation of *ne*-normative amphibole from *ne*-normative liquids may result in the production of *Q*-normative differentiates. Holloway and Burnham (1972) achieved similar results on an olivine tholeiite composition in the range 5-10 kbars, with $P_{H_2O} = P_{total}$ to $P_{H_2O} = 0.6\ P_{total}$, suggesting that high-A basalt liquid will coexist with olivine and clinopyroxene above the amphibole-out temperature (ca. 1050°C), andesitic to dacitic liquids coexist with amphibole + clinopyroxene + magnetite between 1000°C and 1050°C, and dacitic to rhyolitic liquid could coexist with amphibole + plagioclase + clinopyroxene + magnetite between 800°C and 900°C. In both these studies, olivine + clinopyroxene persist above the amphibole-out curve. The upper temperature stability limit of amphibole is likely to decrease with increasing silica activity of the melt (e.g. Allen et al., 1975, Green and Ringwood, 1968, Cawthorn et al. 1973), and is also likely to be partly dependent on the alkali content of the liquid (Cawthorn, 1976). The outlined studies suggest that amphibole is a potential fractionating phase in broadly basaltic to andesitic systems above about 4 kbars As the amphibole-out curve has a positive slope at low pressures, (e.g. Eggler and Burnham, 1973), an isothermal decrease in pressure will result in its breakdown, and subsequent re-equilibration of the liquid to an anhydrous plagioclase-pyroxene-magnetite assemblage, like that of the Rindjani andesites, is possible.

10.3 Plagioclase Crystallisation in Hydrous Systems

In addition to its effect on the stability of amphibole, water has a major effect on the stability of plagioclase relative to ferromagnesian phases in general. In the Mt. Hood andesite for instance, Eggler and Burnham (1973) found plagioclase on the anhydrous liquidus at 1250°C and 5 kbars, 100°C above the orthopyroxene-out curve, while under water-saturated conditions at the same pressure, orthopyroxene and plagioclase appear together on the liquidus at 950°C and at higher pressures plagioclase retreats well below the liquidus. Similarly in a range of compositions from basanitoid to andesite at 5 kbars, with $P_{H_2O} = P_{total}$, Cawthorn et al. (1973) found that plagioclase crystallised at about 925-950°C, well below the liquidus which ranged from 1125°C to 1050°C. Yoder (1969) also demonstrated the effective depression of the plagioclase liquidus temperature under conditions of increasing water pressure and interpreted these results to indicate a resultant shift in plagioclase composition towards more anorthitic compositions. This mechanism may account for the occurrence of extremely anorthite-rich plagioclase phenocrysts (xenocrysts?) in some Rindjani basalts and andesites as well as in the lavas of all other suites considered in this thesis as well as the Sangeang Api intrusive rocks. Such An-rich plagioclase is also noted from a number of other island arc lava suites (e.g. Aleutians, Marsh, 1976) as well as the plutonic blocks from the Lesser Antilles (Lewis, 1973). However, Yoder's (ibid) results in fact do not really demonstrate a change in the composition of the liquidus plagioclase for any given liquid composition, merely a shift of the plagioclase liquidus to lower temperatures with increasing P_{H_2O}. It may well be that P_{H_2O} does result in the precipitation of increasingly An-rich liquidus plagioclase, but this proposed behaviour has not as yet been convincingly demonstrated.

The suppression of the plagioclase liquidus at moderate pressures in water-bearing systems and the increased interval of amphibole, olivine and clinopyroxene crystallisation above the plagioclase liquidus, is likely to

account for many characteristic features of calcalkaline suites in general. Particularly their high Al and normative plagioclase contents and low MgO, Ni and Cr. Because even in water saturated systems, the plagioclase liquidus rapidly approaches the high-Al basalt-andesite liquidus at pressures <3 kbars (e.g. Yoder and Tilley, 1967, Eggler and Burnham, 1973), hydrous liquids of these compositions will precipitate plagioclase at shallow depths. At these low pressures, the amphibole-out curve rapidly retreats to low temperatures (e.g. Yoder and Tilley, 1962) and it would be unstable at the eruptive temperatures of the andesites.

10.4 Magnetite Crystallisation

As discussed, the relatively low Mg/Mg+Fe value of the calculated extract necessary to yield Rindjani andesites from postulated basaltic parents suggests that unless the amphibole has unusually high Fe content, then magnetite must also be a fractionated component. Experimental studies on the likely stability of magnetite in the andesitic compositions are in some conflict with this conclusion. Eggler and Burnham, (1973), for instance, found that at the QFM buffer, magnetite was not a liquidus phase in the Mt. Hood andesite under water saturated or under-saturated conditions at low pressures. Under water saturated conditions its stability field was rapidly diminished with increasing pressure, though with decrease in P_{H_2O}, its upper stability temperature increased above that at $P_{H_2O} = P_{total}$. At higher fO_2 values than the QFM buffer ilmenite appeared at higher temperatures than magnetite, a phase absent from natural andesites. Holloway and Burnham (1972), on the other hand, found magnetite in equilibrium with amphibole and clinopyroxene and andesitic liquid in an olivine tholeiite system at 1000-1050°C, at the NNO buffer (log $fO_2 \simeq -10$), suggesting that magnetite may be a potential fractionating phase at slightly higher fO_2 than those used by Eggler and Burnham, with $P_{H_2O} < P_{total}$. Osborn (1969) calculated that fO_2 values may reach 10^{-5}b at 1 kbar water pressure in shallow magma chambers, allowing magnetite fractionatio to yield calcalkaline differentiation trends. While Fudali (1965) and Eggler

and Burnham (1973) provide evidence disputing the likely existence of such high fO_2 values, the existence of magnetite in the St. Vincent cumulate nodules, suggests that it is in fact a stable phase. Powell (1978) calculates fO_2 values between the NNO and HMN buffers (ca. log $fO_2 \simeq$ -7.0 to -7.5 at 1100°C). It appears from the evidence provided by these nodules as well as the experiments of Holloway and Burnham (1973) and Eggler and Burnham (1973) that, as with the coexistence of plagioclase and amphibole, that magnetite stability is likely to be favoured by relatively low partial pressures of H_2O at 5-8 kbars, with fO_2 values slightly higher than the NNO buffer.

10.5 The Derivation of the Rindjani Dacites

Three factors are of major importance in the derivation of dacites from andesites:

1. The marked effect of pressure on the solubility of water in silicate melts (e.g. Burnham and Davis, 1974).
2. The inter-related effects of water concentration and load pressure on the liquidus temperature and composition of plagioclase.
3. The effect of water in reducing liquidus temperatures at moderate pressure.

The major effect of the pressure-dependence of water solubility in andesitic or basaltic liquids is on the slope and temperature of the liquidus. At a given concentration of water, a water-undersaturated composition has a positive liquidus slope (in terms of T and P). However because the solubility of water decreases exponentially at pressures less than about 2 kbars (e.g. Burnham and Davis, 1974) and is very low at pressures approaching 1 atmosphere, the liquidi of systems with even small amounts of water quickly intersect the water saturated liquidus as they rise. Any further rise than results in exsolution of water vapour and a consequent negative-sloped, curving liquidus path tending towards the near-anhydrous, 1 atmosphere liquidus temperature.

The Mt. Hood andesite, (Eggler and Burnham, 1973) has a 1 atmosphere liquidus temperature of nearly 1250°C, while with 4.7% H_2O, the water undersaturated liquidus at 10 kbars was about 1025°C.

In addition, increasing water concentration has a dramatic effect in suppressing the liquidus temperature of plagioclase at moderate pressures (e.g. Yoder, 1969). At low pressures however, irrespective of whether the liquid is water saturated or not, plagioclase becomes the liquidus phase.

Andesitic liquids may segregate from an amphibole-gabbro residue at 7-10 kbars., close to both the amphibole- and plagioclase-out curves (see chapter 11). Under these conditions plagioclase will be An-rich (e.g. Yoder, 1969). Crystallisation under these conditions will yield trend "A" on figure 9.3. On eruption to the low pressure region (<2 kbars.), amphibole will break down and the P-T course of the rising magma will take it into the region where the plagioclase-out curve moves to the liquidus and rapidly increasing temperatures and hence to a region of rapidly increasing crystallinity. Under these conditions the andesite liquid will precipitate abundant plagioclase, which will be more Ab-rich than that crystallised earlier. The rapid movement of andesitic liquids into this low pressure, water saturated field, where plagioclase is the liquidus phase and where the liquidus has a negative slope, is responsible for the re-equilibration of the residual liquid trend from that producing the less K_2O-enriched andesites, to that producing the high-K andesites and dacites (figure 9.3). This is a pressure-dependent "quenching" and is responsible for the discontinuity between the andesite and dacite fields.

An added complication may be considered, where the andesitic liquid (with 2-3% H_2O) is erupted to a shallow magma chamber, perhaps only 1-2 kms from the surface. In this case the liquid would become oversaturated with water. Very sudden vapour-pressure release is then to be expected on final eruption of the lava. The abrupt change in the plagioclase composition in the Rindjani andesites (An85-95 to An75-55) is then possibly a function of this sudden low of water pressure. Rapid growth of plagioclase during this violent degassing (boiling) is likely to result in the complex zonation of plagioclase observed, as well as the abrupt re-equilibration of the residual liquid to dacitic composition.

Fudali and Melson (1972), on the grounds of velocities of debris expelled during volcanic eruption, suggest that water vapour pressures as high as 5 kbars may be achieved in shallow magma chambers. Thus this rapid degassing of the system may be responsible for the discontinuous nature of the low-K_2O andesite and high K_2O andesite/dacite fields (cf. the "divergent type" volcanoes of McBirney, 1969).

The Rindjani dacites contain small needles of amphibole as microlites in the groundmass glass, apparently formed immediately before quenching. These suggest that the dacites were not completely dry on eruption. Eggler and Burnham's (1973) experiments suggest that under water saturated conditions, amphibole is stable at about 950°C at 1 kbar, while the water saturated solidus at this temperature lies at 0.5 kbars. Using the plagioclase geothermometer of Mathez (1976) and by considering coexisting groundmass plagioclase/coexisting glass equilibria, approximations of quench temperatures were obtained, both for a dry and 1 kbar water pressure-system (table 3.11). Temperatures so obtained are higher than 1000°C for a dry system and generally less than 900°C for 1.0 kbars P_{H_2O}. Temperatures calculated using coexisting groundmass opx-cpx pairs (Woods and Banno, 1973) (table 3.11), yield results in the range 900-1000°C, between the plagioclase values quoted above. This suggests that 0.5 kbars may be the approximate P_{H_2O} value from which the dacites were quenched at about 925°C. Under these conditions, according to the curves of Eggler and Burnham (1973), the lava may be expected to contain approximately 2.0% H_2O at eruption, which is close to that measured for the Paracutin andesite (Eggler, 1972).

10.6 Summary

1. It is possible that andesitic residual liquids differentiate from basaltic parents by fractionating amphibole + plagioclase ± clinopyroxene olivine + magnetite assemblages. This assemblage could crystallise from water undersaturated liquids at relatively low pressures (3-10 kbars).

Liquids were probably water undersaturated at least at >3 kbars. Temperatures were probably in the range 1000°C - 1080°C while oxygen fugacities were more oxidising than those of the NNO buffer.

2. Dacites result from the re-equilibration of andesitic magmas to low-pressure, plagioclase dominated phenocryst assemblages.
3. At depth, at temperatures above the amphibole-out temperature, basaltic parent liquids fractionate clinopyroxene and/or olivine ± plagioclase (at lower pressures or lower water contents) to yield low magnesian, relatively low silica high-Al basalts, trachybasalts or trachyandesites.

Chapter 11

EXPERIMENTAL MELTING OF HIGH-A1 BASALT

11.1 Introduction

In the preceding sections (chapters 9 and 10) it was concluded that *Q*-normative andesites of Rindjani are unlikely to represent primary melts of peridotite, but may be derived by fractional crystallisation from the *ne*- to *ol-hy*-normative high-A1 basalts.

Argued on the basis of trace element, K_2O and Mg/Mg+Fe variations, it was concluded that if the andesites are derived by fractional crystallisation of high-A1 basalts, then it is necessary that amphibole, plagioclase and magnetite have crystallised from the basalts, possibly accompanied by olivine and/or clinopyroxene.

As discussed in chapter 10, the optimum conditions for the crystallisation of these phases at, or close to, the liquidus of a basaltic parent magma, occurs within the relatively low pressure field (3-10 kbars). Liquids were probably water-undersaturated for most of their evolutionary course, at least at pressures >3 kbars. Temperatures were probably in the range 1000°C - 1080°C and oxygen fugacity was probably more oxidising than those of the NNO buffer (probably between the NNO and HMN buffer, and possibly closer to the latter).

It was also suggested that the crystallisation of different near-liquidus assemblages, one anhydrous and the other hydrous from high-A1 basaltic magmas, could yield different liquid lines of descent if they were fractionated. These producing on the one hand *hy*-to *ne*-normative "hawaiite" differentiates with high K_2O, low MgO and relatively low SiO_2, and on the other, andesite differentiates, of quartz-normative character, showing limited K_2O enrichment.

It is suggested that the more alkali-enriched trend, with less silica-enrichment, is the result of fractionation of an olivine-clinopyroxene-plagioclase (anhydrous) assemblage, while the less alkali-, more silica-enriched trend results from removal of an amphibole-bearing (hydrous) assemblage.

It was inferred that the anhydrous assemblage may bave crystallised at pressures less than ca. 3 kbars (i.e. where the amphibole-out curve retreats rapidly to low temperatures, figure 11.9) (cf. Green et al., 1974), and possibly at higher temperatures and/or lower P_{H_2O} conditions, where the temperature interval of olivine-clinopyroxene-plagioclase crystallisation betweer the liquidus and the amphibole-out curve would be larger.

11.2 Objectives

It was decided that if the models inferred from other petrological features, in particular, geochemical variations, were correct; (i.e.

(1) High-Al basalt = low MgO, high-Al basalt ("hawaiite") liquid + olivine + plagioclase + clinopyroxene ± magnetite

and

(2) High-Al basalt = andesite liquid + amphibole + plagioclase + clinopyroxene magnetite ± olivine ± apatite

- then it would be informative to investigate the liquidus phase relationships of such a possible parental basalt in the low to moderate pressure range (3-10 kbars), with small amounts of water present.

This would then allow the definition of the stability fields of principal hypersolidus, mineral phases as a function of T, P and $\%H_2O$. It would allow the determination of the compositions of the synthesised minerals and the comparison of these with those of the phenocrysts of the natural rocks, the determination of likely derivative liquid trends and the definition of the amphibole stability field.

Table 11.1 Summary of Experimental Run Conditions and Products.

Run Number	Temperature °C	Pressure (Kbars)	% H_2O	Capsule	Time (mins)	Run Products	Comments
T82	1000	5	2	$Ag_{50}Pd_{50}$	40	Cpx, Ol, Pl, Gl, QCpx	
T71	1040	5	2	$Ag_{75}Pd_{25}$	30	Cpx. Ol, Pl, Gl, Q Amph, QCpx	
T70	1100	5	2	$Ag_{75}Pd_{25}$	30	Cpx, Ol, Pl, Gl, Q Amph, QCpx	
T78	1110	5	2	$Ag_{50}Pd_{50}$	30	Ol, Gl	
T76	1120	5	2	$Ag_{50}Pd_{50}$	30	Gl	above liquidus
T75	1140	5	2	$Ag_{50}Pd_{50}$	30	Gl	above liquidus
T85	1000	10	2	$Ag_{50}Pd_{50}$	40	Amph, Pl, CrSp, Cpx?, Gl, Q Amph, QCpx	quench-rich, very fine grained
T84	1060	10	2	$Ag_{50}Pd_{50}$	30	Cpx, Pl, Sp, Gl, QCpx, Q Amph	quench-rich, very fine grained
T83	1100	10	2	$Ag_{50}Pd_{50}$	30	Cpx, Pl, Gl, Q Amph, QCpx	
T86	1140	10	2	$Ag_{50}Pd_{50}$	30	Cpx, Gl	
T87	1160	10	2	$Ag_{50}Pd_{50}$	30	Cpx, Gl	very close to liquidus
T150	980	5	5	$Ag_{50}Pd_{50}$	30	Amph, Gl	
T151	990	5	5	$Ag_{50}Pd_{50}$	30	Ol, Amph, Gl	
T131	1020	5	5	$Ag_{50}Pd_{50}$	30	Ol, Gl, Q Amph?	
T122	1060	5	5	$Ag_{50}Pd_{50}$		Ol, Gl, Q Amph	
T127	1075	5	5	$Ag_{50}Pd_{50}$	30	Ol, Gl	very close to liquidus
T125	1090	5	5	$Ag_{50}Pd_{50}$	30	Gl	above liquidus
T159	1030	10	5	$Ag_{50}Pd_{50}$	30	Amph, Gl, QCpx?	
T175	1065	10	5	$Ag_{50}Pd_{50}$	30	Cpx, Gl, Q? Amph	quench-rich
T152	1070	10	5	$Ag_{50}Pd_{50}$	30	Cpx, Gl, Q Amph	
T153	1090	10	5	$Ag_{50}Pd_{50}$	30	Cpx, CrSp, Gl	close to liquidus
T170	1050	7.5	8	$Ag_{50}Pd_{50}$	30	Cpx, Ol, CrSp, Gl	
T172	1070	7.5	8	$Ag_{50}Pd_{50}$	30	Gl	above liquidus
T177	1020	3	5	$Ag_{50}Pd_{50}$	30	Ol, Cpx, Pl, CrSp, Q Amph, Gl	
T174	1050	3	5	$Ag_{50}Pd_{50}$	30	Ol, Gl, V	Near vapour saturated liquidus amphibole quench on olivine
T173	1070	3	5	$Ag_{50}Pd_{50}$	30	Gl, V	water saturated, above liquidus

Notes: All runs performed with 15 mg charges

Abbreviations: Cpx-clinopyroxene, Ol-olivine, Pl-plagioclase, Sp-spinel, CrSp-Cr-spinel, Amph-amphibole, Gl-glass (quenched liquid), QCpx-Quench clinopyroxene, Q Amph-Quench amphibole, V-vapour.

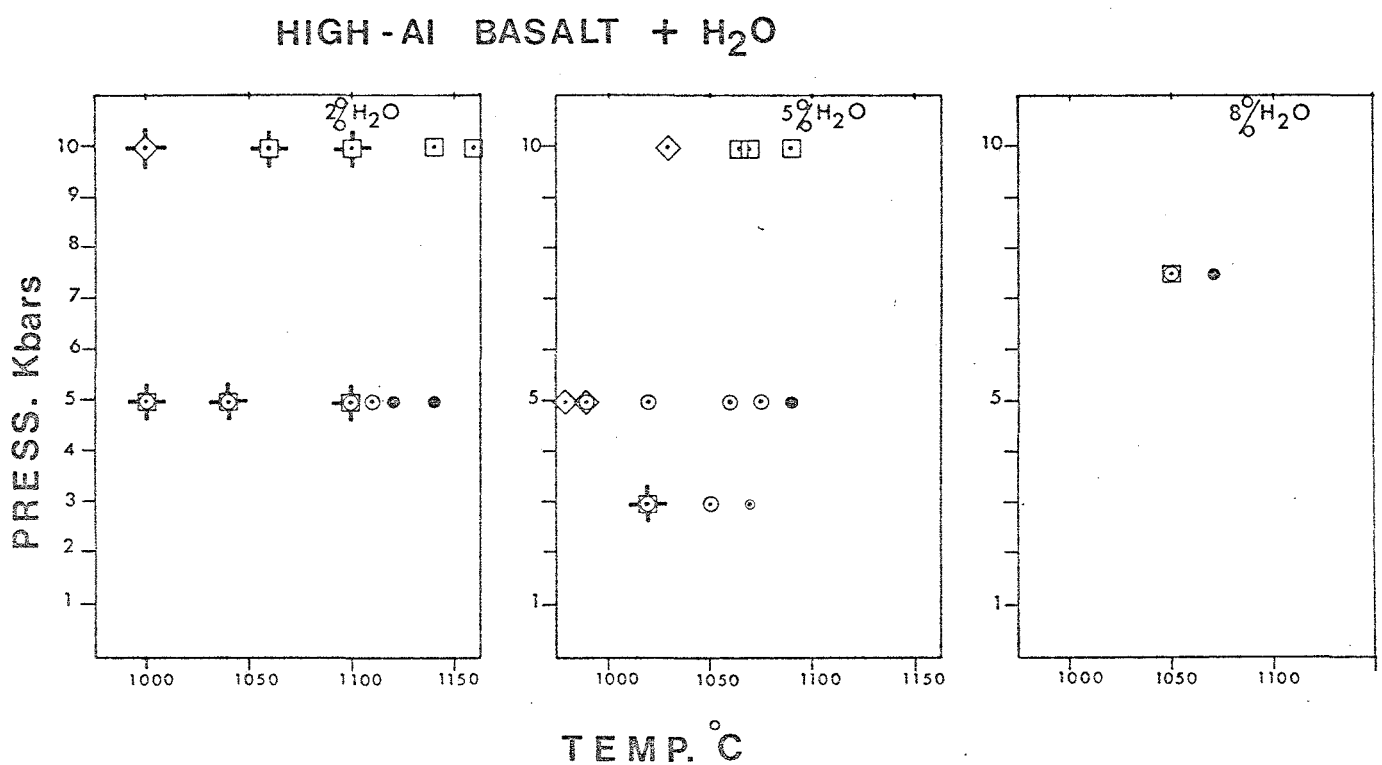

Figure 11.1

Phases crystallised in the experimental runs on glass composition 41632 (see table 11.9,col.1) at specified temperatures and water contents. The results of these experiments are also tabulated in table 11.1.

The experiments were carried out on alkali-olivine basalt 41632 (analysis given in table 3.13) which is a relatively Ni- and Cr-rich (71 and 219 ppm respectively) basalt with an Mg/Mg+ΣFe value of 0.52 ($Mg/Mg+Fe^{2+}$ = 0.60, or Mg/Mg + 0.85Fe = 0.55). The natural rock contains phenocrysts of olivine (Fo 82.5 to Fo 73), rare, relatively Al-rich, Cr-rich augite (Ca 44.9 Mg 42.0 Fe 13.1) and plagioclase (An 75 to An 92).

11.3 Experimental Methods

Methods used are essentially those of Green and Ringwood (1967) (and others), utilizing Boyd-England-type, piston-cylinder apparatus. Capsules employed were of Ag_{50} Pd_{50} and Ag_{75} Pd_{50} (table 11.1). 15 mg of sample were used with water added using a micro-syringe. The starting composition was prepared by fusing the natural rock and quenching it to glass, which was then finely ground under acetone. Details of experimental techniques are given in the appendix.

11.4 Experimental Results

Experimental runs were carried out between 3 and 10 kbars, with 2-8% H_2O. The run conditions and phases synthesised are summarised in table 11.1 and the phase relationships are summarised in figure 11.1.

The major features of these experiments may be summarised as follows:

(1) For both 2 and 5% H_2O, olivine is the liquidus phase at 5 kbars, with cpx only a few degrees below the liquidus with 2% H_2O, but many degrees below with 5% H_2O.

(2) With 2% H_2O at 5 kbars and 5% H_2O at 3 kbars (vapour saturated at the liquidus) olivine, cpx and plagioclase crystallise together close to the liquidus.

(3) With both 2 and 5% H_2O, at 10 kbars, cpx is the liquidus phase and olivine does not appear at all at this pressure.

(4) At 7.5 kbars with 8% H_2O, olivine and cpx both appear near the liquidus.

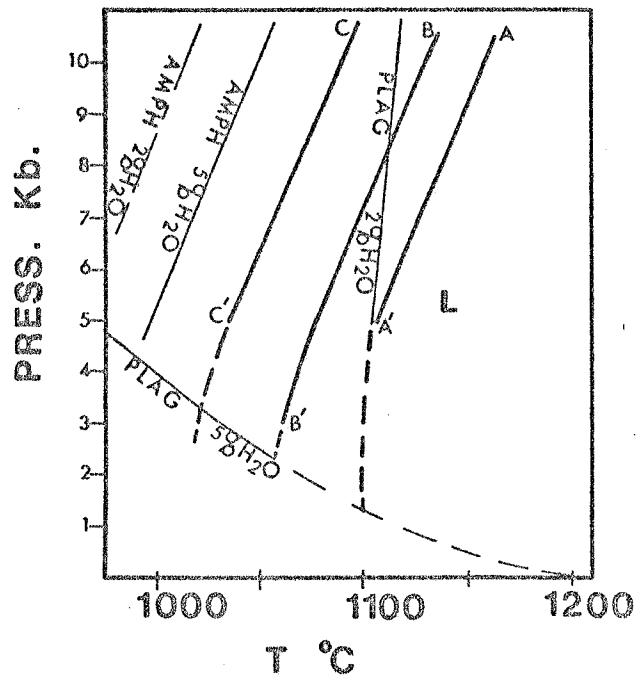

Figure 11.2

A summary of the main features of the experimental runs as described in figure 11.1. In particular, the relative positions of the liquidi are shown, illustrating their movement with variation in water content.

A-A' = liquidus with 2% H_2O

B-B' - " 5% H_2O

C-C' = " 8% H_2O

The amphibole and plagioclase liquidi are also shown for 2 and 5% H_2O runs.

Solid lines are experimentally determined phase boundaries, while dashed sections are projected extrapolations.

(5) Plagioclase stability is markedly affected by water content. With 2% H_2O at 5 kbars it appears ca. 15°C below the liquidus and is probably on the liquidus at 3 kbars. At 10 kbars (2% H_2O), plagioclase is still only ca. 90°C below the liquidus. At higher water contents the plagioclase liquidus retreats rapidly below the liquidus with increasing pressure. At 3 kbars with 5% H_2O (vapour saturated at the liquidus) it appears ca. 30°C below the liquidus, while at 5 kbars it appears at >100°C below the liquidus.

(6) Amphibole must appear at considerably less than 1000°C with 2% H_2O at 5 kbars (ca. 950°C?). The amphibole-out curve has a positive $\Delta P/\Delta T$ slope and is stable at ca. 1000°C at 10 kbars (with 2% H_2O). Under these conditions it coexists with plagioclase and possibly cpx, though these runs are very quench-rich and the cpx may not be an equilibrium phase.

(7) With 5% H_2O by comparison with 2% H_2O, the field of amphibole expands (to higher temperatures) and is also brought closer to the liquidus by the suppression of liquidus temperatures (figure 11.2). Amphibole crystallises at 1030°C at 10 kbars (with 5% H_2O), replaced by cpx and Cr-spinel at higher temperatures. At 5 kbars it is present alone at 980°C and with olivine at 990°C. The amphibole-out temperature at this pressure and water content (5%) is probably about 1000°C and possibly about 1040°C at 10 kbars. The absence of amphibole at 7.5 kbars, with 8% H_2O at 1050°C suggests that the upper stability temperature of amphibole is not a linear function of % H_2O and temperature at a given pressure, but may have a maximum with respect to % H_2O, as shown diagrammatically in figure 11.3. This behaviour is equivalent to that determined by Holloway (1973) as a function of mol. fraction of H_2O in the vapour phase.

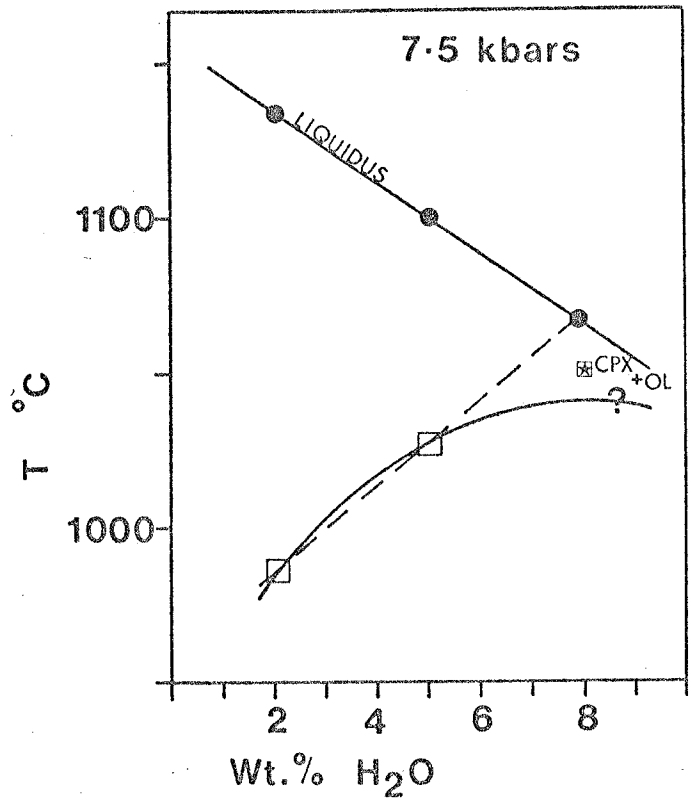

Figure 11.3

A representation of the amphibole-out curve and liquidus at 7.5 kb. as a function of temperature and water content. The spots represent the liquidus temperatures at 2 and 5% H_2O (projected from 5 and 10 kb. runs) and that with 8% H_2O (determined at 7.5kb.). The large squares similarly represent the projected amphibole liquidi with 2 and 5% H_2O . If the upper stability temperature of amphibole increased linearly with increasing water content, then it should be stable on the liquidus with 8% H_2O at 1060°C (dashed line). However runs at 7.5 kb. with 8% H_2O reveal Ol and Cpx to be liquidus phases, not amphibole , and in fact Ol and Cpx are present to temperatures markedly below the liquidus, suggesting that the rate of increase in the amphibole liquidus temperature decreases markedly with increasing water content above 5% at these pressures.

(8) All runs are undersaturated with respect to H_2O with 2% H_2O added and for 5 and 10 kbars runs with 5% H_2O. The runs with 5% H_2O have a vapour phase present at 3 kbars at and below the liquidus (1050°C). The runs at 7.5 kbars with 8% H_2O are also undersaturated with respect to H_2O.

(9) The liquidi all have positive $\Delta P/\Delta T$ slopes in the pressure range covered by the runs made (figure 11.2). There is a regular decrease in the liquidus temperature in the pressure interval 5-10 kbars of about 15°C/1% H_2O between 2 and 8% H_2O.

(10) Magnetite was not observed in any of the runs, in contrast to the experiments of Holloway and Burnham (1972) on the 1921 Kiluea tholeiite where magnetite was reported within 25°C of the liquidus. As discussed previously, magnetite was a necessary component in the evolution of the andesites from basaltic parents and its absence in these runs could be taken as possible evidence of higher fO_2 conditions in natural calcalkaline magmas. These runs are buffered by the furnace assemblage at fO_2 <NNO (Green, 1976), while Holloway and Burnham's (ibid) runs were buffered at the HMN buffer.

11.5 Mineral Chemistry

Microprobe analyses of representative mineral phases from the experimental runs are given in tables 11.2 - 11.6. The composition run in these experiments seemed very prone to rapid nucleation and growth of quench products on cooling, particularly in those runs at 10 kbars and at temperatures >100°C below the liquidus. The quench products were generally of Al-rich cpx of poor stoichiometry (table 11.7). The reported analyses (of ferromagnesian minerals) are those with the highest Mg/Mg+Fe values and best stoichiometry obtained from any given run. Mg/Mg+Fe values of amphibole, cpx and olivine are plotted against temperature in figure 11.4 and show regular decrease with decreasing temperature.

Table 11-2 Electron Microprobe Analyses of Experimental Phases - Clinopyroxene

Run No.	T82	T82	T71	T70	T84	T83	T86	T87	T159	T175	T153	T153	T170	T170	T177
Temperature (°C)	1000	1000	1040	1100	1060	1100	1140	1160	1030	1065	1090	1090	1050	1050	1020
Pressure (kb)	5	5	5	5	10	10	10	10	10	10	10	10	7.5	7.5	3
% H_2O	2	2	2	2	2	2	2	2	5	5	5	5	8	8	5
SiO_2	49.5	49.8	49.7	50.5	48.0	48.9	49.4	51.6	46.4	48.7	52.1	51.5	49.4	50.4	49.5
Al_2O_3	6.7	7.2	8.3	6.3	9.8	10.3	9.2	6.3	11.6	9.8	4.9	5.4	7.3	6.9	7.0
FeO	9.3	9.3	8.6	7.2	10.6	9.1	6.7	7.4	9.6	6.6	6.7	6.4	5.9	6.1	8.2
MgO	13.4	13.5	14.5	16.2	13.0	12.9	14.6	16.5	15.0	13.7	17.3	16.4	14.5	14.8	13.4
CaO	19.0	18.2	16.8	18.1	16.7	17.0	18.3	17.2	14.4	18.8	17.9	19.1	20.9	20.0	19.9
Na_2O	-	-	0.5	0.4	0.4	-	0.4	-	0.7	0.6	-	-	0.4	0.4	0.6
K_2O	0.1	0.2	0.1	-	0.1	0.1	0.1	-	0.4	-	-	-	-	-	-
TiO_2	I.5	1.4	1.0	0.8	1.1	1.3	0.7	0.6	1.5	1.1	0.5	0.6	0.9	0.7	1.2
MnO	-	-	-	-	-	-	-	-	-	-	-	-	-	-	-
Cr_2O_3	0.3	0.4	0.3	0.4	0.2	0.2	0.5	0.5	0.2	0.5	0.6	0.6	0.8	0.8	0.3
Total	99.8	99.9	99.8	99.9	99.9	99.8	99.9	100.1	99.8	99.8	100.0	100.0	100.1	100.1	100.1
100 Mg/Mg + Fe (mol.)	72.1	72.2	75.2	80.0	68.7	71.7	79.6	79.8	73.6	78.9	82.0	82.1	81.5	81.3	74.3
Number of Ions on the Basis of 6 Oxygens															
Si Z	1.836	1.842	1.824	1.848	1.779	1.792	1.804	1.877	1.711	1.783	1.897	1.880	1.817	1.845	1.831
Al	0.164	0.158	0.176	0.152	0.221	0.208	0.106	0.123	0.289	0.217	0.103	0.120	0.183	0.155	0.169
Al	0.129	0.152	0.185	0.120	0.206	0.241	0.201	0.148	0.214	0.205	0.105	0.111	0.132	0.142	0.137
Fe	0.288	0.287	0.263	0.222	0.328	0.279	0.205	0.226	0.296	0.201	0.205	0.195	0.181	0.185	0.254
Mg	0.744	0.745	0.794	0.886	0.721	0.708	0.797	0.892	0.827	0.756	0.936	0.890	0.795	0.805	0.736
Ca	0.756	0.719	0.663	0.710	0.663	0.668	0.716	0.669	0.571	0.736	0.697	0.747	0.821	0.786	0.787
Na X + Y	-	-	0.036	0.031	0.030	-	0.025	-	0.050	0.044	-	-	0.025	0.028	0.039
K	0.007	0.009	0.006	-	0.004	0.006	0.004	-	0.020	-	-	-	-	-	-
Ti	0.041	0.039	0.028	0.023	0.031	0.036	0.019	0.016	0.041	0.029	0.014	0.017	0.025	0.019	0.031
Mn	-	-	-	-	-	-	-	-	-	-	-	-	-	-	-
Cr	0.010	0.012	0.009	0.011	0.006	0.007	0.016	0.014	0.008	0.015	0.019	0.019	0.023	0.024	0.009
Z	2.00	2.00	2.00	2.00	2.00	2.00	2.00	2.00	2.00	2.00	2.00	2.00	2.00	2.00	2.00
X + Y	1.98	1.97	1.98	2.00	1.99	1.95	1.98	1.97	2.02	1.99	1.98	1.98	2.00	1.99	1.99
Mol. Proportions															
Ca	42.3	41.1	38.5	39.1	38.7	40.3	41.7	37.5	33.7	43.5	37.9	40.8	45.7	44.3	44.3
Mg	41.6	42.5	46.2	48.7	42.1	42.8	46.4	49.9	48.8	44.7	50.9	48.6	44.2	45.3	41.4
Fe	16.1	16.4	15.3	12.2	19.2	16.9	11.9	12.6	17.5	11.8	11.2	10.6	10.1	10.4	14.3
Ca/Ca + Mg (mol.)	0.504	0.491	0.455	0.445	0.479	0.485	0.473	0.428	0.408	0.493	0.427	0.456	0.508	0.494	0.517
Al^{vi}/Al^{iv}	0.78	0.951	1.05	0.79	0.93	1.16	1.03	1.21	0.74	0.94	1.01	0.93	0.72	0.92	0.81

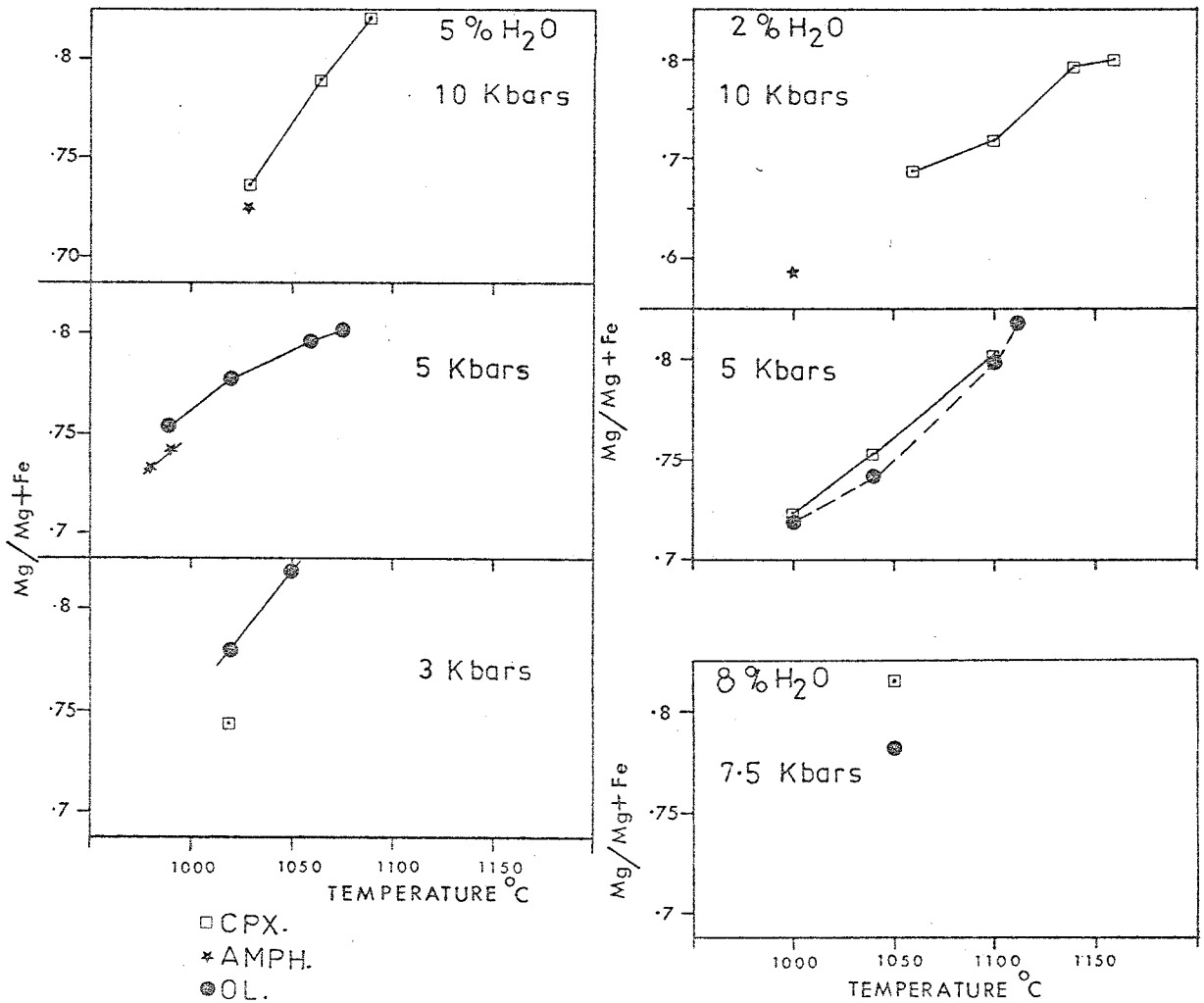

Figure 11.4

Mg/Mg+Fe variation with temperature for clinopyroxene, olivine and amphibole synthesised in these experiments.

Clinopyroxene, olivine and amphibole are plotted in figure 11.5, together with olivine and clinopyroxene compositions from the original lava 41632 and the field of reacted Ca-rich amphiboles from Rindjani andesites.

The liquidus olivine and cpx both have Mg/Mg+Fe values of about 0.81 - 0.82 and in the case of olivine, this value is similar to that of more magnesian phenocrysts in the natural lava.

1. Clinopyroxene

The analysed clinopyroxenes (table 11.2, figures 11.4, 11.5) are somewhat aluminous augites, with Mg/Mg+Fe values ranging from 0.69 to 0.82. CaO content is slightly lower than those of the natural basalt (figure 11.5 and table 3.3), though those from runs with higher water content (run T153, 10 kbar - 5% H_2O, T170, 7.5 kbars - 8% H_2O and T177, 3 kbars - 5% H_2O) do have similar compositions to analysed cpx from the starting basalt 41632 (e.g. compare with analyses 11 and 12, table 3.3). TiO_2 concentrations are in the range 0.5 - 1.5% and are generally in the range of the natural pyroxenes. TiO_2 shows a positive correlation with Al_2O_3 and both Al_2O_3 and TiO_2 show generalised trends of depletion with increasing temperature at any given water content and pressure.

2. Olivine

Analysed olivines (table 11.3, figure 11.5) range from Fo 81.9 to Fo 71.7 and fall well within the range of natural olivines from basalt 41632 (figure 11.5, table 3.6). The olivines have moderately high CaO concentrations and have MnO values in the range 0.2 to 0.4%. Assuming a K_D of 0.3 ($K_D = (Fe/Mg)^{ol}/(Fe/Mg)^{liq}$), the liquids in equilibrium with olivine have $Mg/Mg+Fe^{2+}$ values ranging from 0.57 to 0.43. K_D values for coexisting olivine-cpx pairs ($K_D = (Fe/Mg)^{ol}/(Fe/Mg)^{cpx}$) are close to 1 (table 11.8).

3. Amphibole

Synthesised amphibole is of calcium-rich hornblende/pargasite composition. Analyses are given in table 11.4 and plotted in 11.5. The compositions are

Table 11.3

Experimental Phases - Olivine

Run No.	T82	T71	T70	T78	T151	T131	Ti22	T127	T170	T177	T174
Temperature (°C)	1000	1040	1100	1110	990	1020	1060	1075	1050	1020	1050
Pressure (Kb)	5	5	5	5	5	5	5	5	7.5	3	3
% H_2O	2	2	2	2	5	5	5	5	8	5	5
SiO_2	36.9	38.2	37.9	38.6	37.4	38.2	38.3	38.7	37.9	40.4	39.3
FeO	25.7	23.8	19.1	17.3	22.7	20.6	19.1	18.5	20.3	19.5	16.9
MgO	36.6	38.2	42.2	43.3	39.1	40.3	41.8	41.9	41.1	38.4	43.1
CaO	0.3	0.4	0.4	0.4	0.4	0.4	0.4	0.4	0.3	1.2	0.3
TiO_2	0.3	0.1	-	0.1	0.1	0.2	-	0.1	-	0.1	-
MnO	0.4	-	0.2	0.3	0.3	0.2	0.2	0.3	0.4	0.3	0.3
TOTAL	100.2	100.7	99.8	100.0	100.1	99.9	99.8	99.9	100.0	99.9	99.9
$\frac{100\ Mg\ (mol)}{Mg + Fe}$	71.73	74.14	79.77	81.70	75.38	77.70	79.61	80.19	78.24	77.80	81.92
Number of ions on the basis of 4 oxygens											
Si	0.978	0.994	0.976	0.983	0.978	0.988	0.985	0.991	0.980	1.035	0.998
Fe	0.569	0.518	0.412	0.369	0.497	0.446	0.411	0.396	0.439	0.418	0.359
Mg	1.445	1.481	1.620	1.643	1.524	1.554	1.603	1.599	1.584	1.467	1.631
Ca	0.008	0.011	0.011	0.011	0.011	0.011	0.011	0.011	0.008	0.033	0.008
Ti	0.006	0.002	-	0.002	0.002	0.004	-	0.002	-	0.002	-
Mn	0.009	-	0.004	0.006	0.006	0.004	0.004	0.006	0.009	0.006	0.006
TOTAL	3.016	3.004	3.023	3.014	3.019	3.007	3.014	3.006	3.019	2.962	3.002
100 $Mg/Mg+Fe^{2+}$ of equilibrium liquids assuming Ol/liq KD*=0.3	43.2	46.2	54.2	57.3	47.9	51.1	53.9	54.8	51.9	51.2	57.6

*KD = $(Fe/Mg)^{Ol}$ / $(Fe/Mg)^{liq}$ = 0.3 (Roeder & Emslie, 1971).

Table 11.4

Experimental Phases - Amphibole

Run No.	T85	T85	T150	T150	T151	T159
Temperature °C	1000	1000	980	980	999	1030
Pressure (Kb)	10	10	5	5	5	10
$\%H_2O$	2	2	5	5	5	5
SiO_2	42.3	41.1	40.7	40.8	42.6	42.5
Al_2O_3	14.4	15.7	15.5	15.7	15.3	15.3
FeO	13.4	13.8	9.4	8.6	8.6	9.4
Fe_2O_3	-	-	0.3	1.7	-	-
MgO	10.7	10.6	14.0	13.9	13.9	13.9
MnO	-	-	-	-	-	-
TiO_2	2.4	2.7	2.3	2.5	2.6	2.2
CaO	11.4	10.5	11.0	11.4	11.5	11.6
Na_2O	1.5	1.9	1.9	1.6	1.8	1.6
K_2O	0.9	1.1	0.9	0.9	0.9	0.8
TOTAL	97.0	97.4	96.0	97.1	97.2	97.3
Tetrahedral Cations (230)						
Si	6.280	6.093	6.013	5.968	6.174	6.156
Al^{iv}	1.720	1.907	1.987	2.032	1.826	1.844
TOTAL	8.000	8.000	8.000	8.000	8.000	8.000
Octahedral Cations (320)						
Al^{vi}	0.791	0.827	0.717	0.680	0.787	0.775
Fe^{2+}	1.661	1.709	1.163	1.056	1.038	1.144
Fe^{3+}	-	-	0.029	0.184	-	-
Mg	2.361	2.348	3.090	3.020	3.009	3.000
Mn	-	-	-	-	-	-
Ti	0.268	0.305	0.256	0.272	0.278	0.238
TOTAL	5.081	5.189	5.255	5.211	5.112	5.157
M4 Site (230)						
Excess Oct.	0.081	0.189	0.255	0.211	0.112	0.157
Ca	1.817	1.674	1.745	1.789	1.794	1.800
Na	0.102	0.137	0.000	0.000	0.094	0.043
TOTAL	2.000	2.000	2.000	2.000	2.000	2.000
A Site (230)						
Na	0.321	0.394	0.556	0.442	0.420	0.419
K	0.174	0.212	0.175	0.183	0.157	0.147
TOTAL	0.495	0.606	0.731	0.625	0.577	0.566
Total Cations	15.495	15.606	15.731	15.625	15.577	15.566
Ca	31.11	29.21	28.95	29.57	30.71	30.28
Mg	40.44	40.97	51.27	49.92	51.52	50.47
ΣFe	28.45	29.82	19.78	20.50	17.77	19.25
100 Mg/Mg+ΣFe	58.70	57.87	72.16	70.89	74.35	72.4
100 $Mg/Mg+Fe^{2+}$			72.65	74.09		
BEST NAME	Parg.	Parg.	Parg.	Parg.	Parg.	Parg.

Notes: All analyses by electron microprobe. Low totals are due to unanalysed OH (+ F, Cl). Analyses recalculated according to the routine of Papike et al (1974), with Fe^{2+} estimated by this method:

Nomenclature (Parg. = pargasite) (Papike et. al., ibid)

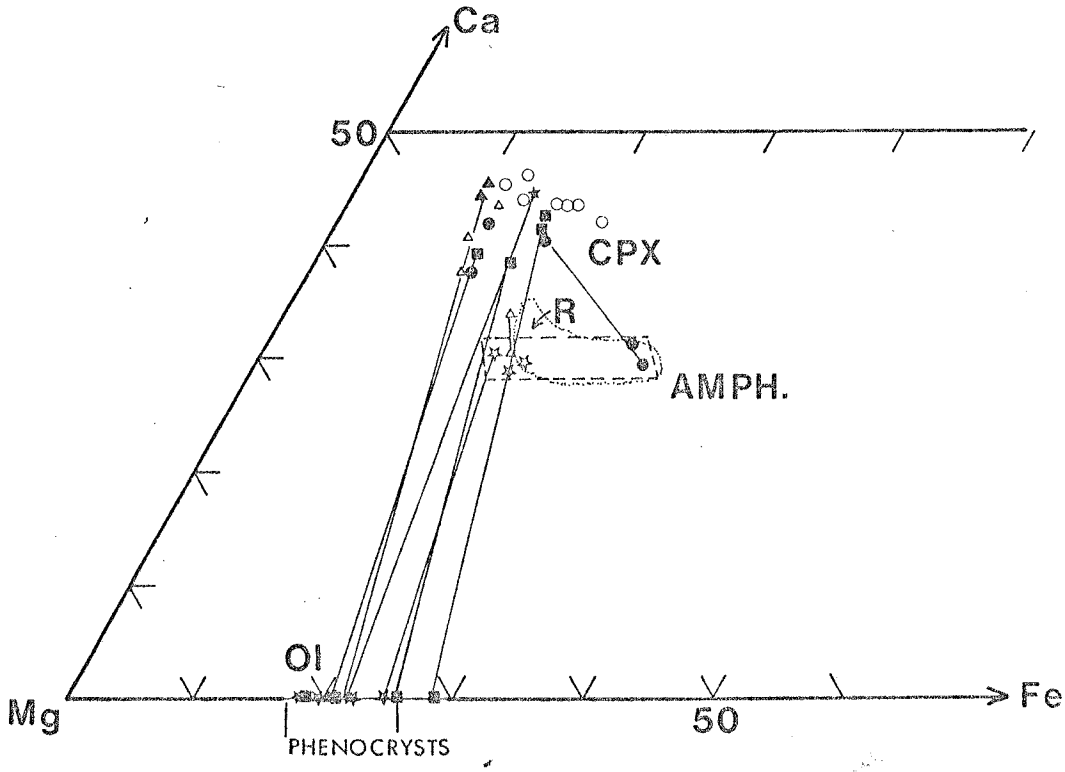

Figure 11.5

Compositional variation in synthesised Cpx,Olivine and Amphibole in terms of mol. proportion of Ca-,Mg- and Fe end members.Coexisting phases are connected by tie-lines.The symbols distinguish phases crystallised under the following conditions: ■ - 5kb./2%H_2O, ● -10kb./2%H_2O, △ -10kb./5%H_2O , ☆ -5kb./5%H_2O, ▲ -7.5kb./8%H_2O, ✱ -3kb./5%H_2O. For comparitive purposes, the compositions of phenocrysts from Rindjani basalt 41632 are also included.

○ - Cpx, olivine phenocrysts occupy the range indicated on the Mg-Fe axis, field R is that occupied by the reacted amphiboles from Rindjani andesites.

similar to those of the partially reacted calcic hornblendes from some of the andesite (table 3.10), and have high Al_2O_3 contents and low SiO_2. Mg/Mg+Fe values range from 0.74 to 0.58. The amphibole from run T151 (5 kbars, 5% H_2O, 990°C) has an Mg/Mg+Fe value of 0.74, very close to that of the coexisting olivine (Mg/Mg+Fe = 0.75).

The amphiboles have Na_2O concentrations ranging from 1.5 to 1.9% and K_2O from 0.8 to 1.1%. K_2O/Na_2O ratios are between ca. 0.5 to 0.6. Calculated coexisting liquids have slightly lower K_2O/Na_2O ratios (e.g. run T150, 980°C, 5 kbars and 5% H_2O, T159, 1030°C, 10 kbars and 5% H_2O, table 11.9). The ratio (Na_2O) liquid/(Na_2O) amphibole ≈2 and (K_2O) liquid/(K_2O) amphibole is <2 (ca. 1.5 - 1.7). Green (1976, 1973) also suggests that (Na_2O) liquid/(Na_2O) amphibole ≈2, but that (K_2O) liquid/(K_2O) amphibole is >2. The amphiboles also contain quite high concentrations of TiO_2 (2.2 - 2.7%) and suggest a (TiO_2) liquid/(TiO_2) amphibole factor of about 0.3.

4. Plagioclase

Plagioclase appears in those runs with 2% H_2O and at 3 kbars with 5% H_2O. The analysed plagioclases tend to show considerable variation within a single charge, particularly those at 10 kbars (table 11.5). In particular T84 (1060°C, 10 kbars, 2% H_2O) had plagioclase ranging from An 64.4 to An 88.7 (table 11.5) and those from run T85 (1000°C, 10 kbars, 2% H_2O) ranged from An 60.5 to An 93.8.

Synthesised plagioclase also often tends to show rather poor stoichiometry with cation totals (on the basis of 8 oxygens) generally falling in the range 4.958 to 4.986.

Anorthite content was calculated in three ways: 1. as mol. Ca/1, 2. as total mol. ($Al + Fe^{3+}$)-1 and 3. as mol. Ca/Ca+Na+K. In most instances the latter method yielded a considerably higher An content, suggesting that the analyses are Na-deficient. This may either be due to analytical error

Table 11.5 Analyses of Plagioclase Synthesised in Experimental Runs

Run No.	T70	T70	T71	T82	T82	T83	T84	T84	T85	T85	T177
Temp.	1100	1100	1040	1000	1000	1100	1060	1060	1000	1000	1020
Pressure - k.bars	5	5	5	5	5	10	10	10	10	10	3
$\%H_2O$	2	2	2	2	2	2	2	2	2	2	5
SiO_2	47.08	47.38	49.17	48.24	49.40	47.17	52.00	46.88	46.19	54.38	48.92
Al_2O_3	33.31	33.37	31.76	32.48	31.14	33.63	29.51	33.62	34.33	28.86	28.43
FeO											
MgO	0.50	0.36	0.33	0.33	0.83	0.0	0.51				2.89
CaO	17.36	17.10	15.57	16.05	14.63	16.99	12.63	17.17	18.00	11.30	13.12
Na_2O	0.88	0.94	2.10	1.66	2.31	1.13	3.59	1.12	0.65	3.56	2.91
K_2O	0.07	0.10	0.16	0.22	0.24	0.17	0.41	0.14	0.0	0.78	0.34
Fe_2O_3	0.87	0.69	0.76	1.01	1.64	0.90	1.08	1.06	0.83	1.11	3.38
STRUCT.											
Si	2.1610	2.1736	2.2519	2.2116	2.2579	2.1658	2.3711	2.1556	2.1243	2.4564	2.2578
Al	1.8007	1.8030	1.7131	1.7537	1.6763	1.8186	1.5848	1.8206	1.8596	1.5353	1.5453
Fe^{2+}											
Fe^{3+}	0.0300	0.0238	0.0261	0.03481	0.0563	0.0310	0.0370	0.03664	0.0287	0.0377	0.1173
Mg	0.0342	0.0246	0.0225	0.02254	0.0565		0.0346	0	0		0.1988
Ca	0.8538	0.8406	0.7641	0.7884	0.7165	0.8359	0.6171	0.8459	0.8870	0.5469	0.6488
Na	0.0783	0.0836	0.1865	0.1475	0.2047	0.1006	0.3174	0.0998	0.0579	0.3118	0.2604
K	0.0041	0.0058	0.0093	0.0128	0.0140	0.0100	0.0238	0.0082	0	0.0449	0.0200
TOTAL	4.962	4.955	4.9737	4.9716	4.9824	4.962	4.9860	4.9669	4.9576	4.9331	5.0485
An (Ca/1 basis)	85.4	84.06	76.41	78.84	71.65	83.59	61.71	84.59	88.70	54.69	64.88
An ($Al+Fe^{3+}-1$ basis)	83.07	82.68	73.92	78.85	73.26	82.17	62.18	85.67	88.83	57.30	66.26
An (Ca/Na+Ca+K basis)	91.19	90.38	79.60	83.10	76.61	88.31	64.39	88.68	93.87	60.52	69.82
Or	.43	.62	.97	1.35	1.49	1.05	2.48	0.86	0.0	4.97	2.15

(volatilisation of Na by the electron beam for instance) or may represent a real deficiency in the synthesised plagioclases.

These problems notwithstanding however, the analyses do suggest that the first crystallised plagioclase at both 5 and 10 kbars with 2% H_2O (1100^oC) are very Ca-rich (calcic bytownite-anorthite), which is in good agreement with the composition of plagioclase occurring as partially resorbed phenocrysts in the natural basalt 41632 (as well as in other basalts and andesites from this suite).

5. Spinel

Spinel is the only other phase recognised in the runs. One run contained aluminous spinel (T84, 1060^oC, 10 kbars, 2% H_2O table 11.6), a phase not recognised in any lavas of the Rindjani suite. Cr-spinel occurred in several runs at >5 kbars and compositions (table 11.6) are quite like those of some of the Cr-spinel inclusions in magnesium olivine phenocrysts/megacrysts from alkali olivine basalts (e.g. 41631, 41621, 41626, table 3.9).

11.6 Liquid Compositions and Chemistry

Determination of the composition of the equilibrium liquid coexisting with the crystallised phases in experimental runs is difficult (e.g. Green 1976, Nicholls and Ringwood, 1974; Cawthorn et al., 1973).

The direct analysis of interstitial glass is probably often unlike any liquid that may have been in equilibrium with near-liquidus crystals at the particular run conditions. This is largely due to the modification of the liquid by rapidly growing quench products during the cooling of the charge. These quench minerals were generally clinopyroxene or amphibole.

Quenched cpx has lower CaO, higher Al_2O_3 and is more Fe-rich than the equilibrium cpx. Quenched amphibole is generally more silica-rich and more Fe-rich than equilibrium amphibole (also see Green, 1976). Analyses of typical quench cpx and amphibole are given in table 11.7.

Table 11.6

Electron Microprobe Analyses of Experimental Run Products - Spinels

Run No.	T84	T85	T153	T170
Temperature (^{o}C)	1060	1000	1090	1050
Pressure (kb)	10	10	10	7.5
% H_2O	2	2	5	8
SiO_2	-	-	-	-
TiO_2	0.35	0.48	0.37	0.37
Al_2O_3	63.47	17.97	19.22	13.42
Cr_2O_3	0.97	39.90	45.12	47.53
Fe_2O_3 [1]	0.71	11.57	5.19	11.56
FeO	19.39	20.29	19.95	13.12
MnO	-	-	-	-
MgO	14.83	9.64	9.90	13.49
CaO	0.26	0.13	0.23	0.48
Total	99.98	99.98	99.98	99.97
	Number of ions on the basis of 32(O)			
Si	-	-	-	-
Al	15.600	5.447	5.767	4.036
Cr	0.160	8.108	9.078	9.584
Fe^{3+}	0.112	2.238	0.994	2.219
Ti	0.056	0.093	0.070	0.073
Mg	4.613	3.698	3.760	5.136
Fe^{2+}	3.385	4.366	4.252	2.803
Mn	-	-	-	-
Ca	0.058	0.036	0.065	0.134
Total	23.984	23.986	23.986	23.985
$Mg/Mg + Fe^{2+}$	0.577	0.459	0.469	0.640
Cr/Cr + Al	0.010	0.598	0.612	0.704
$Fe^{3+}/Cr+Al+Fe^{3+}$	0.007	0.142	0.063	0.142
Mol % U.Sp.	1.04	1.62	1.27	0.90

Notes: [1] Calculated by the method of Carmichael (1967).

Table 11.7 Analyses of typical quench-products from experimental runs

Phase	Amphibole	Clinopyroxene
Run No.	T175	T83
Temperature ^{o}C	1065	1100
Pressure (kbars)	10	10
$\%H_2O$	5	2
SiO_2	49.05	49.01
Al_2O_3	19.8	11.24
FeO	10.1	10.92
MgO	6.73	12.15
CaO	8.95	15.06
Na_2O	1.59	-
K_2O	1.12	0.23
TiO_2	1.62	1.18
TOTAL	98.97	99.79
Mg/Mg+ΣFe	54.3	66.48

The liquid compositions in the experiments were determined by two methods:

1. By direct microprobe analysis of glass from those charges in which there is relatively minor quench growth (generally those at low pressures and close to the liquidus) (table 11.10).
2. By calculation, in the case of runs which contain only one phase, based on the microprobe determination of the composition of that phase and the composition of the starting glass (table 11.9). The proportion of crystallisation was determined as follows: In the case of runs with olivine as the sole phase in equilibrium with the liquid,

the olivine-liquid K_D value of 0.3 (Roeder and Emslie, 1970) was assumed. The $Fe^{2+}/Fe^{2+} + Fe^{3+}$ ratio of the liquid at the liquidus was then calculated, knowing the MgO and total Fe content of the liquid (starting glass, table 11.9) and the liquidus olivine composition (Fo 82), by applying Roeder and Emslie's (ibid) $K_D = (Fe^{2+}/Mg)ol/(Fe^{2+}/Mg)$ liquid = 0.3). This also assumed that the liquidus olivine (Fo 82) constituted a negligible component of the charge very close to the liquidus and that the liquid in this case closely approximated the composition of the starting glass.

At temperatures below the liquidus where olivine was the sole phase, the % crystallisation was then determined by calculating the amount of the equilibrium olivine composition stable at that temperature which had to have crystallised from the starting composition to yield an equilibrium liquid FeO/MgO ratio such that the olivine/liquid K_D value of 0.3 was achieved.

For those runs with cpx or amphibole as the sole phase, the K_D cpx-liquid and K_D amphibole-liquid values were determined indirectly by first determining their equilibrium with olivine (whose K_D olivine-liquid is assumed to be 0.3) and from these inferring the cpx-liquid and amphibole-liquid Mg-Fe distributions relative to the olivine-liquid K_D.

Values for the olivine-cpx K_D $\left(K_D = \frac{(XMg^{ol})\ (XFe^{cpx})}{XFe^{ol})\ (XMg^{cpx})}\right)$ and olivine-amphibole K_D $\left(K_D = \frac{(XMg^{ol})\ (XFe^{amph.})}{(XFe^{ol})\ (XMg^{amph.})}\right)$ are given in table 11.8. The average ol-cpx K_D is close to 1, so it was assumed that the cpx-liquid K_D is the same as that for olivine (0.3). The olivine-amphibole K_D was slightly >1 and an accordingly higher amphibole-liquid K_D of 0.35 was adopted.

On the basis of these K_D values, the % crystallisation of those runs with only one of the phases, cpx, olivine or amphibole was calculated (table 11.9).

Table 11.8

Olivine-cpx and olivine-amphible K_D values for co-existing phases for experimental runs at 5 kbars

Run No.	Temp.(^oC)	Pressure (kb)	$\%H_2O$	Co-existing Phases	K_D
T70	1100	5	2	Ol-cpx	0.99
T71	1040	5	2	Ol-cpx	0.95
T82	1000	5	2	Ol-cpx	0.98
T151	990	5	5	Ol-amph	1.06

As the above method can only be applied in the situation where only one phase coexists with the liquid, the composition of liquids from charges where a number of phases coexist had to be inferred from electron microprobe analyses of glass (table 11.10). The proportion of crystallisation in these runs was then calculated on the basis of the enrichment of K_2O, assuming this component to be entirely resident in the melt (when amphibole is absent). The proportion of crystallisation of two run series at particular pressures and with particular water contents is plotted as a function of temperature in figure 11.6. The most significant factor is the rapid increase in the degree of crystallinity on the appearance of amphibole. This is a similar phenomenon to that illustrated by Holloway and Burnham (1972) in their experiments on an olivine tholeiite composition (compare figure11.6 with figure 6 from Holloway and Burnham 1972).

The large increase in the volume of liquid on the disappearance of amphibole suggests that amphibole is melting incongruently to yield liquid and either cpx (at 10 kbars) or olivine (5 kbars).

Table 11.9 Calculated Equilibrium Liquids in Some Experimental Charges

Run No.	Starting [1] Composition	[3] T78	T127	T122	T131	[4] T87	T86	T195	[5] T150
Temperature (°C)		1110	1075	1060	1020	1160	1140	1065	980
Pressure (kb)		5	5	5	5	10	10	10	5
% H_2O		2	5	5	5	2	2	5	5
SiO_2	50.00	50.04	50.29	50.42	50.67	49.87	50.06	50.17	53.37
Al_2O_3	17.85	17.92	18.30	18.50	18.86	18.81	18.74	18.96	18.69
Fe_2O_3	1.22 [2]	1.22	1.25	1.26	1.29	1.32	1.34	1.39	1.66
FeO	8.48	8.44	8.22	8.09	7.79	8.57	8.66	8.74	8.06
MgO	6.49	6.34	5.59	5.21	4.57	5.66	5.64	5.47	3.75
CaO	10.46	10.50	10.72	10.82	11.03	9.90	9.64	9.31	9.92
Na_2O	2.73	2.74	2.80	2.83	2.88	2.96	2.98	3.02	3.01
K_2O	1.27	1.28	1.30	1.32	1.34	1.37	1.40	1.44	1.39
TiO_2	1.13	1.13	1.15	1.17	1.18	1.17	1.17	1.14	0.71
P_2O_5	0.18	0.18	0.17	0.18	0.18	0.19	0.20	0.20	0.24
MnO	0.18	0.18	0.17	0.18	0.18	0.19	0.20	0.20	0.24
$Mg/Mg + Fe^{2+}$	0.5769	0.5723	0.5477	0.5391	0.5110	0.5423	0.5388	0.5289	0.4534
Coexisting phase		Ol	Ol	Ol	Ol	CPX	CPX	CPX	Amph
Mg/Mg + Fe		0.8170	0.8019	0.7961	0.7770	0.798	0.7956	0.7892	0.7218
% crystallisation		0.40	2.48	3.50	5.36	7.7	9.4	12.15	26.62
					C.I.P.W. Norm				
Q	-	-	-	-	-	-	-	-	1.86
C	-	-	-	-	-	-	-	-	-
or	7.51	7.56	7.68	7.80	7.92	8.10	8.27	8.51	8.21
ab	23.10	23.18	23.69	23.95	24.37	25.04	25.21	25.55	25.47
an	32.70	32.82	33.53	33.89	34.58	34.00	33.63	33.93	33.39
ne	-	-	-	-	-	-	-	-	-
di	14.26	14.33	14.63	14.77	15.05	10.85	10.04	8.40	11.15
hy	6.37	6.36	6.71	6.82	7.25	4.78	6.35	7.64	16.46
ol	11.58	11.24	9.15	8.13	6.11	12.51	11.74	11.20	-
mt	1.77	1.77	1.81	1.83	1.87	1.91	1.94	2.02	2.41
il	2.14	2.15	2.18	2.22	2.24	2.22	2.22	2.17	1.35
ap	0.32	0.32	0.33	0.33	0.34	0.34	0.35	0.36	0.43

Notes:

1 X.R.F. analysis of starting glass

2 Fe_2O_3/FeO ratio calculated on the basis of olivine-liquid K_D = 0.3 for the nearest liquidus olivine composition (Run T174, Ol Fo 81.92)

3 Liquid composition calculated by calculating the % crystallisation necessary to modify the starting composition Mg No. to that in equilibrium with the equilibrium olivine (K_D = 0.3). (Those runs with olivine as the sole hypersolidus phase, T78, T127, T122, T131)

4 Equilibrium liquids of runs with clinopyroxene as the sole crystallising phase (T87, T86, T175) calculated in the same way as 3, assuming a CPX-liq K_D of 0.3.

5 Liquid in equilibrium with amphibole as the sole liquidus phase (see text).

Table 11.10 Electron Microprobe Analyses of Glass from Experimental Runs [1]

Run No.	T78	T70	T71	T87	T85	T127	T131	T170
Temperature (°C)	1110	1100	1040	1160	1000	1075	1020	1050
Pressure (kb)	5	5	5	10	10	5	5	7.5
% H_2O	2	2	2	2	2	5	5	8
SiO_2	49.84	50.01	50.23	50.39	55.53	49.97	51.03	51.24
Al_2O_3	18.55	19.41	20.00	19.25	22.64	18.41	19.75	20.21
Fe_2O_3	0.07	1.13	2.64	1.56		0.33	1.82	1.57
FeO	8.95	8.00	7.56	8.23	6.82	8.91	7.46	8.17
MgO	6.73	5.31	3.65	5.48	1.66	6.07	4.38	4.95
CaO	10.10	9.71	8.47	9.66	8.03	10.23	9.65	9.04
Na_2O	2.82	3.20	3.74	2.37	2.59	2.86	2.90	2.60
K_2O	1.28	1.45	1.93	1.43	1.87	1.45	1.33	1.36
TiO_2	1.20	1.40	1.56	1.32	0.85	1.31	1.44	0.94
MnO	-	-	-	-	-	-	-	0.13
Mg/Mg+ΣFe	.5712	.1522	.3961	0.5031	0.3024	0.5452	0.4620	0.4790
$Mg/Mg+Fe^{2+}$	.5730	.5419	.4625	.5426		.5483	.5113	.5191
Coexisting phases	Ol	Ol,Cpx,Pl	Ol,Cpx,Pl	Cpx	Amph,Cpx?, Pl,Crsp.	Ol	Ol	Cpx,Ol,Crsp.
C.I.P.W. Norm								
Q	-	-	-	-	9.25	-	0.02	0.10
C	-	-	-	-	2.48	-	-	-
or	7.56	8.57	11.40	8.45	11.05	8.57	7.86	8.03
ab	23.86	27.07	31.74	20.05	21.92	24.20	24.54	22.00
an	34.18	34.32	32.09	37.67	37.87	33.12	36.95	39.47
ne	-	-	0.27	-	-	-	-	-
di	11.50	9.80	6.60	6.83	-	12.94	7.39	2.83
hy	3.30	1.99	-	20.16	15.59	2.38	17.41	23.32
ol	16.53	13.35	11.26	1.54	-	15.15	-	-
mt	0.10	1.64	3.83	2.26	-	0.48	2.64	2.27
il	2.28	2.66	2.96	2.51	1.61	2.49	2.73	1.78
ap	-	-	-	-	-	-	-	-

Notes: [1] Due to a number of factors discussed in the text calculated liquid compositions (table are regarded as more reliable than analysed ones.

Compositions of both calculated and analysed liquids are given in tables 11.9 and 11.10, together with C.I.P.W. norms. These compositions are plotted in the normative *ne-ol-di-hy-Q*-diagram (figure 11.7) together with the fields of the various groups of Rindjani lavas.

A number of features are of significance:

1. Those liquids which are in equilibrium with one or more minerals of the group: olivine, clinopyroxene, plagioclase, do not show very significant SiO_2-enrichment relative to the starting composition. They have compositions that are generally within the *ol-hy-di*-normative field (figure 11.7) with differentiation indices and normative plagioclase compositions somewhat like those of hawaiite (e.g. Coombs and Wilkinson, 1969) and resemble the more differentiated Rindjani (low MgO) high-Al basalts.
2. The fused glass used as the starting composition for all these experiments (analysis given in table 11.9) has lower Na_2O than the original rock from which this glass was prepared (41632) (2.73% Na_2O vs. 3.67% Na_2O). Apparently sodium must have been lost during the fusion process. Thus the starting composition (figure 11.7) is *hy*-normative whereas the natural lava is slightly *ne*-normative. If the starting composition were to have its higher Na_2O restored, its normative composition would then shift across the low pressure divide (Yoder and Tilley, 1962) and runs which crystallised combinations of clinopyroxene, olivine and plagioclase, would probably have retained liquid compositions within the *ne*-normative field.

   For this reason, the experiments are more directly applicable to the differentiation of those Rindjani basalts which are *hy*-normative (figure 11.7), like olivine basalt 41676 (table 3.12). This lava has a similar composition to 41632, but has slightly lower Na_2O content.

Figure 11.6

The calculated proportion of crystallisation of run series at specified temperatures.

In the case of those runs where equilibrium liquids were calculated (table 11.9), the proportions of crystallisation so yielded were used. In the other cases, (i.e. where analysed liquids had to be used), then the % crystallisation was determined by calculating the enrichment of incompatible or reasonably incompatible elements (K_2O, TiO_2, Na_2O) relative to their concentrations in the starting composition. The silica content of the most crystalline runs in each series is indicated. Particularly notable is the marked increase in crystallinity when amphibole appears.

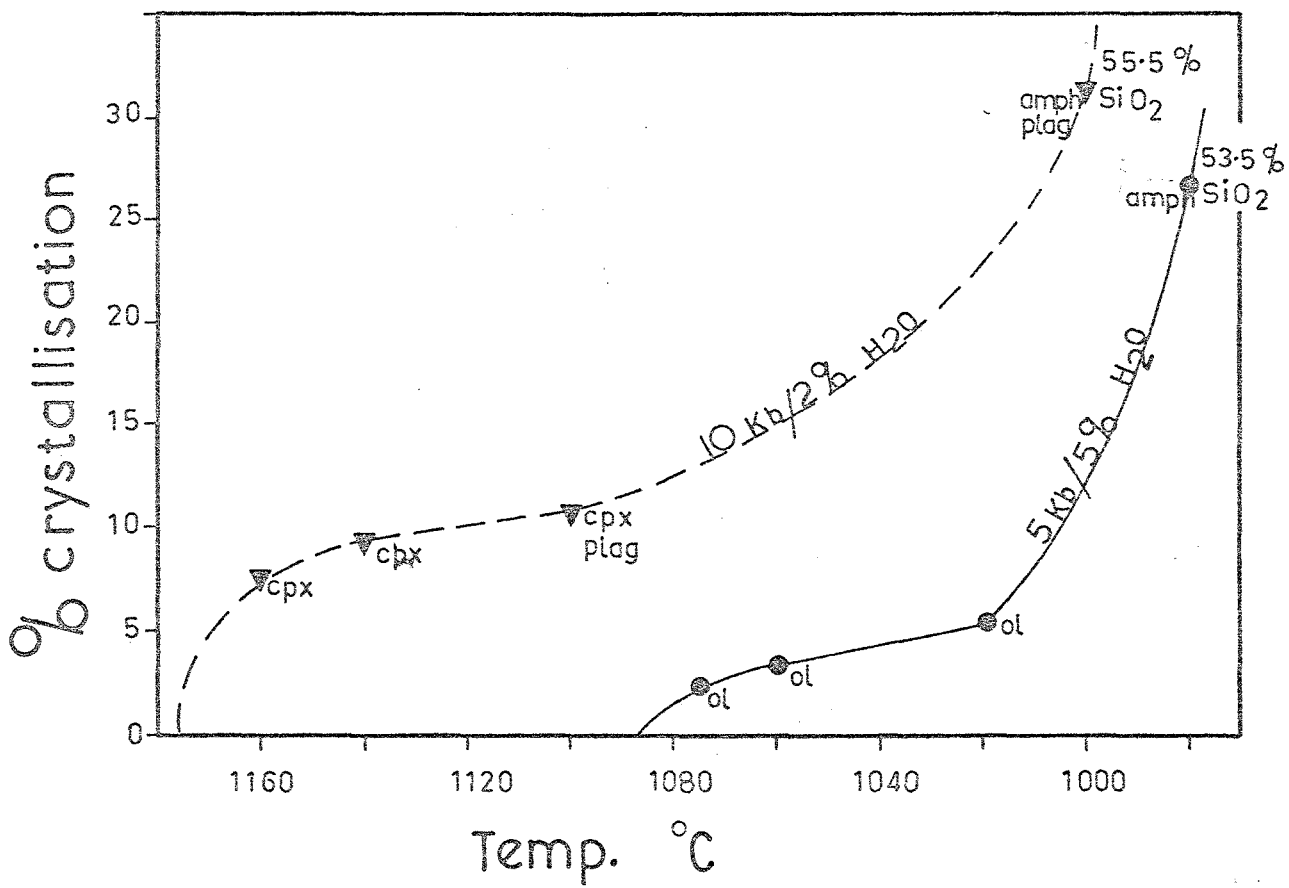
% crystallisation
0
5
10
15
20
25
30
1160
1120
1080
1040
1000
Temp. °C
cpx
cpx
cpx
plag
amph
plag
55·5 % Si O2
53·5 %
amph
Si O2
10 Kb/2 % H2O
5 Kb/5 % H2O
ol
ol
ol

3. In general the compositional variation of the liquid from amphibole-absent runs (i.e. 5 kbars with 2% H_2O 10 kbars with 2% H_2O at > ca. 1010°C, 5 kbars with 5% H_2O at > ca. 1000°C and at 3 kbars with 5% (H_2) is towards Al_2O_3 enrichment, MgO and Mg/Mg+Fe depletion and CaO depletion or enrichment depending on whether clinopyroxene or olivine is crystallising.

4. Runs in which amphibole occurs as an equilibrium phase have a greater degree of crystallinity and have liquids that are SiO_2-enriched, both relative to the starting composition and also to those runs where amphibole is absent. This applies both to the analysed interstitial glass compositions and to the calculated liquid compositions (tables 11.9 and 11.10).

Some of the liquids are *Q*-normative and resemble basaltic or low-silica andesites (e.g. T150, T159, table 11.9), or andesites (T85, table 11.10).

These liquids have inferred $Mg/Mg+Fe^{2+}$ values <0.5 and lower MgO, slightly lower CaO and markedly lower TiO_2 than the starting basalt composition.

The composition of liquids in equilibrium with amphibole in these runs tends to support the proposal that andesitic liquids may be derived by amphibole fractionation from basaltic parents, and support findings of similar studies by Cawthorn et al. (1973) and Holloway and Burnham (1972).

11.7 Discussion of the Results of the Experimental Study

The key factors in the differentiation of hydrous liquids at moderate pressures, illustrated by these experiments on the Rindjani basalt, are:

1. The marked suppression of liquidus temperatures by the addition of relatively small amounts of water.

Figure 11.7

Normative *ne-di-ol-hy-Q* diagram. Showing the normative compositions of calculated and analysed experimentally derived liquids, together with the fields of the various Rindjani lava groups.

The numbered fields represent the areas occupied by the following Rindjani lavas:

1. *ne*-normative, high-Al basalts and ankaramites.
2. *hy*-normative, high-Al basalts and basaltic andesites.
3. andesites.
4. dacites.

Point A (star) is the normative composition of the starting glass (table 11.9). Point B is the composition of the original rock, basalt 41632. Triangular symbols are calculated liquids, while squares represent analysed glasses. Open symbols (i.e. nos. 8 and 13) are from amphibole-bearing runs.

The numbered points represent liquids, either calculated or analysed, from the following runs.

		Run No. (see table 11.1)	Temp°C	Press. Kbar.	$\%H_2O$
	1	T78	1110	5	2
	2	T127	1075	5	5
	3	T122	1060	5	5
Calculated	4	T131	1020	5	5
Liquids	5	T87	1160	10	2
	6	T86	1140	10	2
	7	T195	1065	10	5
	8	T150	980	5	5
	9	T78	1110	5	2
	10	T70	1100	5	2
	11	T71	1040	5	2
Analysed	12	T87	1160	10	2
Liquids	13	T85	1000	10	2
	14	T127	1075	5	5
	15	T131	1020	5	5
	16	T170	1050	7.5	8

FIGURE 11.7

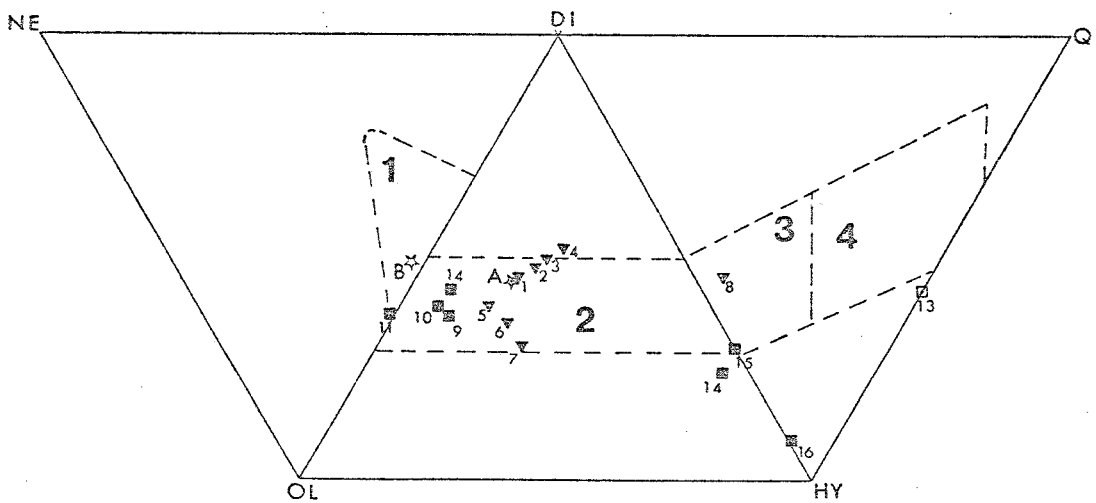

2. The rapid decrease in the liquidus temperatures of plagioclase with small increases in water content, a feature also discussed by Yoder (1969). With 2% H_2O the plagioclase-out curve has a steep positive slope, lying at 1100°C at 5 kbars and ca. 1110°C at 10 kbars. With 5% H_2O the plagioclase-out curve has a relatively shallow negative $\Delta P/\Delta T$ slope and retreats rapidly to lower temperatures with increasing pressure. It approaches the water saturated liquidus at slightly less than 3 kbars (ca. 1050°C), but lies at <980°C at 5 kbars.

3. The liquidus temperature of both cpx and olivine is much less markedly depressed by the addition of water than is that of plagioclase. This results in a much larger temperature interval of olivine (and/or cpx) crystallisation before the appearance of plagioclase (see figure 11.10). This factor alone is likely to have a marked effect on the nature of the differentiation path of hydrous liquids by comparison with that of anhydrous analogues. It is probably an important factor in the development of the geochemical character of calcalkaline suites. In particular this factor will lead to the production of normative-plagioclase enriched liquids with high Al_2O_3 and CaO, but with low MgO.

4. These experiments, on a high-Al basalt, also suggest that the field of cpx expands at the expense of olivine, with increasing pressure. This is a feature of most experimental studies of basaltic composition (e.g. Green and Ringwood, 1967, Thompson, 1977). In the case of this Rindjani basalt, olivine is alone on the liquidus at 5 kbars, coexists with cpx at 7.5 kbars and is absent at 10 kbars. The relatively aluminous, slightly *ne*-normative basalts from Rindjani appear to have fractionated olivine (for instance lava 41621 is nearly aphyric and has olivine as the main phenocryst phase) and then olivine-plagioclase-clinopyroxene, which is the crystallisation sequence at 5 kbars with 2% H_2O or 3 kbars with 5% H_2O.

The ankaramite lavas from west Lombok have clinopyroxene as an import phenocryst phase (>olivine). This may suggest that they have differentiated at and erupted from, greater depths than the olivine-dominated high-Al basalts. This behaviour may also be important to the differentiation of the Sangeang Api lavas with their cpx-rich cumulates.

5. The almost simultaneous appearance of olivine, clinopyroxene and plagioclase close to the liquidus at 5 kbars/2% H_2O and 3 kbars/5% H_2O is suggestive of a four-phase, low pressure cotectic (ol-cpx-plag-liquid). Under these conditions the existence of the low pressure divide (Yoder & Tilley, 1962) prevents the evolution of *hy*- or *Q*-normative differentiates from *ne*-normative parents (or visa versa). This assemblage closely matches the eruptive mineralogy of the Rindjani high-Al, basaltic lavas and basaltic andesites, as well as that of the trachybasalts from Tambora volcano.

11.8 *Amphibole Crystallisation*

The upper temperature stability limit of amphibole as a function of water content and pressure is obviously a question of vital interest if this phase is considered the key to the differentiation of andesites from basaltic parents.

The highest temperatures at which amphibole crystallised in these experiments was 1030°C at 10 kbars, with 5% H_2O. Amphibole was absent at 1065°C (cpx) at the same pressure and its breakdown temperature is presumably in the range 1030-1065°C. At 5 kbars with 5% H_2O, amphibole coexisted with olivine at 990°C and was present alone at 980°C, whereas olivine was present alone at 1020°C. Therefore the temperature of amphibole breakdown is likely to be about 1000°C.

Higher amphibole stability temperatures have been found in other basaltic compositions. Irving (1971), for instance, found amphibole at 1100°C at 13.5 kbars with 2% H_2O in a mugearite composition and Holloway and Ford (1975) synthesised fluoro-hydroxy pargasite at temperatures in excess of 1200°C in a vapour-absent system. Furthermore amphibole stability is also probably partly compositionally dependent. For instance, Cawthorn et al. (1973) found that amphibole crystallised at progressively higher temperatures from increasingly more mafic liquids, while Cawthorn (1976) also suggested that Na_2O concentration of the liquid may also have an effect on the initial crystallisation temperature of amphibole.

The main factor determining the feasibility of amphibole fractionation as a means of deriving andesites from basaltic parents is the maximum temperature at which amphibole is likely to be a stable hypersolidus phase. Temperatures at which andesites equilibrated with their phenocrysts are in some doubt, though they may be fairly high. Wilcox (1956) found, by direct measurement, that the maximum vent temperature of the erupting Paracutin andesite was 1070°C. This temperature is slightly higher than the experimentally determined maximum stability temperature of amphibole in this study. On the other hand, Gill and Till (1978), on the basis of coexisting oxide, plagioclase and pyroxene geothermometers, suggest that the Fijian, Namosi andesite was equilibrated at between 1000 and 1050°C which are in general agreement with temperatures yielded by coexisting pyroxenes and by plagioclase microphenocryst-glass pairs from Rindjani andesites (chapter 3). These factors suggest that andesite temperatures may be less than the maximum amphibole stability temperatures determined in this study and in any case there may be grounds for suggesting that amphibole may be stable to slightly higher temperatures than those found in these experiments on this particular basalt composition.

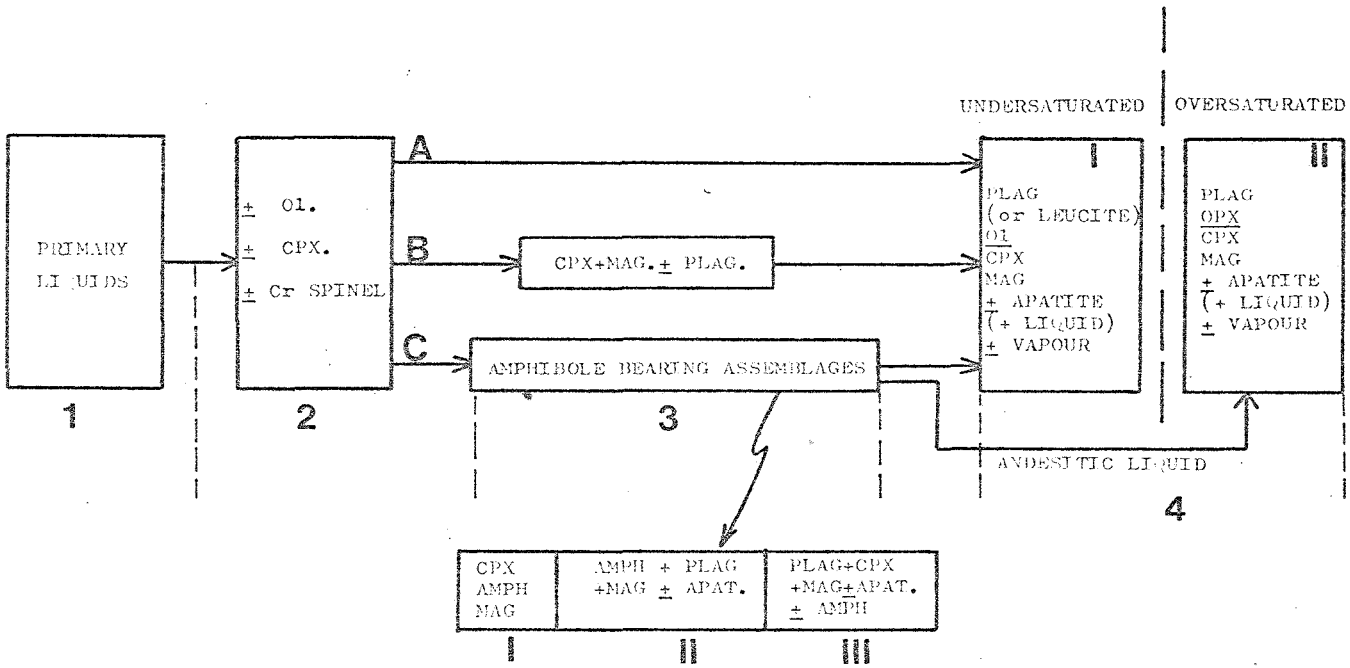

Figure 11.8

Flow chart summarising the crystallisation history of Sunda Arc lavas.As discussed in the text,the trend from left to right ,from stage 1 to 4 ,is one of decreasing temperature and/or pressure.The sequence from A to C is one of decreasing temperature and /or increasing water content.As discussed in chapter 12,the primary liquids yielding the range of lavas in this sector of the Sunda Arc show considerable compositional variation ,particularly in terms of their alkalinity. Thus initial parent melt composition will also affect the differentiation path.

Liquids in equilibrium with assemblage 4I will be somewhat alkaline,relatively MgO-poor,high-Al basalts,trachybasalts ,trachyandesites,leucitites,leucite tephrites,hawaiites or mugearites.The bulk compositions represented by assemblage 4II will andesitic,with residual liquid of dacitic composition.

In the P/T diagram figure 11.10,fields marked 1 to 4 are equivalent to those similarly marked in this flow chart.In figure 11.10 (A-D), trends a-b are equivalent to that represented by A in this diagram,while trend a-p-i is equivalent to trend 1-2-C-4 in this figure.

11.9 *Crystallisation Sequences and the Fractionation of Sunda Arc Magmas*

The flow chart presented in figure 11.8 summarises possible generalised evolutionary paths of magmas from this sector of the Sunda Arc as suggested by petrographic and geochemical data as well as modelling calculations presented earlier in this thesis.

Thus field 1 is that of the primary liquids, which as will be discussed in chapter 12, must encompass considerable diversity, ranging from the *ol-hy*-normative, relatively low K_2O parents of the least alkaline high-Al basalts from Rindjani, through the highly alkaline. undersaturated, *lc*-normative Soromundi and G. Sangenges leucitites. Field 2 is that of olivine, clinopyroxene or olivine + clinopyroxene-crystallisation, presumably close to the liquidus and is represented by ol- and or cpx-rich, feldspar- or feldspathoid-poo lavas represented in most of the suites described in this thesis. This may also represent the field of crystallisation of the Sangeang Api olivine-clinopyroxenite nodules.

Lavas may erupt directly with the olivine-clinopyroxene assemblage, or may take path A and crystallise a feldspar- or feldspathoid-bearing assemblage (4). In chapter 9 it was suggested that such a mechanism yielded the relatively K_2O-enriched, low MgO high-Al basalts from the Rindjani suite and possibly much of the variation within the Tambora suite.

As an alternative to A, path C passes through the field of amphibole crystallisation, including both plagioclase-bearing and plagioclase-free assemblages. In chapter 9 it was suggested that some of the Sangeang Api lavas had evolved along such a path and that the associated amphibole-rich xenoliths may have resulted from accumulation of assemblages so-crystallised. Furthermore if the calcalkaline andesites from Rindjani are the result of fractional crystallisation of high-Al basalts, then this path is critical to the evolution of andesite liquids.

If the primary liquid involved is markedly undersaturated, then assemblages crystallised in field 3 will give rise to those of field 4I as magmas approach eruption, while marginally undersaturated or *ol-hy*-normative parents may yield the *Q*-normative assemblage 4II following crystallisation of the amphibole-bearing assemblages.

The remainder of this chapter is concerned with the discussion of the relationship of idealised crystallisation sequences just outlined to the experimentally determined phase relationships.

11.10 Phase Relationships and Crystallisation Sequences

The main elements of the phase relationships determined in this study are summarised in figure 11.9 (A-D). The $\%H_2O$-dependent positions of the liquidus and the plagioclase- and amphibole-liquidi have been extrapolated from the available 2 and 5% H_2O data to create a series of four P/T diagrams each representing a 1% H_2O increment from 2-5% H_2O. The low pressure portion of the diagrams, together with the water-saturated liquidus is partly based on the 3 kb data from this study as well as the phase relationships of Yoder (1969) with additional data from Cawthorn et al. (1973) and Eggler and Burnham (1972).

Using the above series of diagrams those shown in figure 11.10 (A-D) were constructed, where the fields of crystallisation of those assemblages outlined in the flow chart (figure 11.8) are distinguished (1-4). A minimum temperature of $1000^{o}C$ is taken as a cut-off for these diagrams as for reasons already outlined, it is considered that andesites erupted at or above this temperature. The amphibole stability field is divided into two assemblages; a plagioclase-free assemblage (3I) and a plagioclase-bearing assemblage (3II), the latter is interpreted as the critical assemblage in the derivation of andesitic residual liquids, as well being equivalent to the assemblages in the Sangeang Api gabbroic xenoliths (e.g. B24, plate 5D).

Figure 11.9

The results of these experiments carried out with 2 and 5% H_2O have been extrapolated to yield phase diagrams with 1% H_2O increments from 2% to 5% H_2O. Relationships at low pressures are partly inferred, partly indicated by the relationships in the 3kbar/5% H_2O runs and partly taken from relationships indicated by experiments of Yoder (1969), Eggler and Burnham (1973) and others.

Line A-B-D is the liquidus. Point C represents the intersection of the water-saturated liquidus.

Line F-D is the water saturated plagioclase liquidus.

Line E-C-D is the water saturated liquidus.

Olivine and/or clinopyroxene are on the liquidus over the interval A-B.

Plagioclase becomes the liquidus phase at B.

Point X represents the highest temperature of amphibole-plagioclase coexistance.

FIGURE 11.9

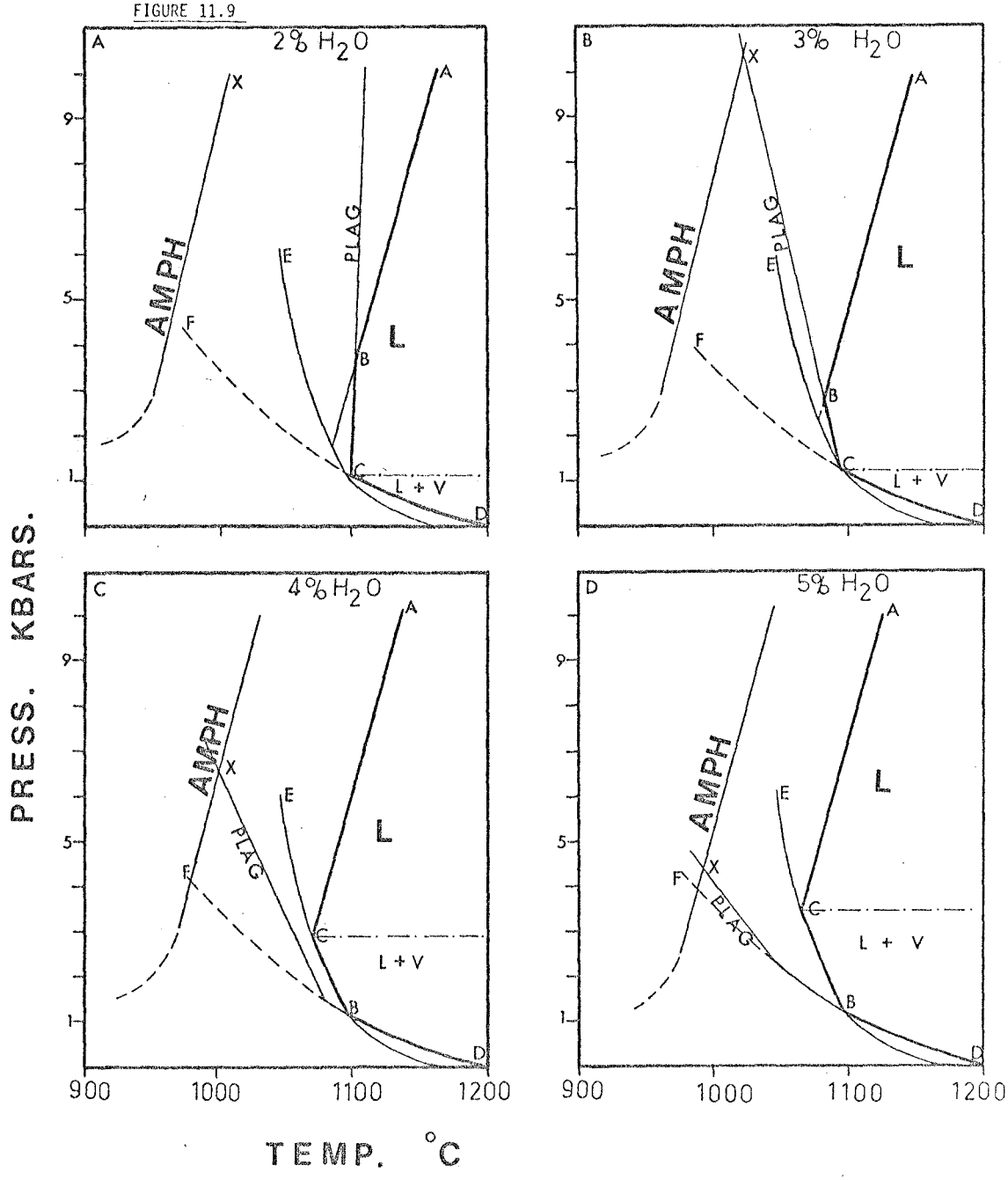
A
2% H_2O
B
3% H_2O
C
4% H_2O
D
5% H_2O
AMPH
PLAG
L
L + V
X
E
F
A
B
C
D
9
5
1
900
1000
1100
1200
PRESS. KBARS.
TEMP. °C

As discussed with respect to the flow chart shown in figure 11.8, there are two main pathways by which basaltic parental liquids may differentiate. Those following path A do not pass through the amphibole stability field and initially crystallise cpx and/or olivine-bearing assemblages. These magmas may erupt directly with this assemblage or may pass into the plagioclase stability field and crystallise a plagioclase-cpx-olivine assemblage prior to eruption. Such a path is shown by the trend a-b on figures 11.10 A-D. The increase in water content represented by these four diagrams (from 2% to 5%) expands the field in which cpx and/or olivine may fractionate, relative to the plagiophyric assemblages, thus compared with the 2% H_2O case, the system with 5% H_2O is more likely to differentiate more aluminous, normative plagioclase-enriched residual liquids.

On figure 11.10, the relative extent of the individual cpx and olivine fields are not differentiated, though data presented earlier in this chapter suggests that the olivine-cpx field (2) tends to be dominated by olivine at pressures <7.5 kbars and by cpx at higher pressures. In these experiments there is some suggestion that there may be a thin and diminishing field of olivine alone on the liquidus, perhaps up to 8 or 9 kbars. Over this pressure range there will also be a diminishing field where cpx and olivine coexist at temperatures slightly below the liquidus and at least in the upper pressure range of this region, at still lower temperatures, olivine disappears, apparently by reaction with the liquid. This field then being occupied by cpx alone, expanding to the liquidus at higher pressures (>9 kbars).

These conclusions are also supported by the experimental finding of Presnall (1966) on the join forsterite-diopside-iron oxide. Holloway and Burnham's (1972) experiments on the Kilauea tholeiite also show the same behaviour. Their determinations of modal proportion of olivine and cpx close to the liquidus (fig. 6, Holloway and Burnham, op. cit.) show olivine to be

modally dominant very close to the liquidus at 5 kbars, but at 50°C below this the proportion of olivine diminishes to a very minor role, in favour of cpx. At 8 kbars, olivine is never more than a minor constituent.

These details have a number of important implications with respect to the Sunda Arc lavas and mafic-ultramafic nodules. In the first place, the mafic, cpx-dominated assemblages, with minor olivine, of a number of lavas from several volcanoes (e.g. the ankaramites from Lombok), probably fractionated close to the liquidus at higher pressures than the olivine-dominated, high-Al basalts from Rindjani. If these cpx-rich lavas followed a cooling path, close- and subparallel to the liquidus, from about 10 kbars, then they may crystallise cpx first and then a cpx-dominated ol-cpx assemblage later, at slightly lower T and P. This would then account for the more magnesian composition of some Cr-diopside megacrysts compared with associated olivine.

Furthermore, if a relatively rapid cooling path from the liquidus at about 9 kbars is followed, then an initially relatively olivine-rich, olivine-cpx assemblage would crystallise, but would rapidly become more cpx-rich with cooling, until olivine disappeared altogether. The assemblage along this path would represent a series of increasingly olivine-poor olivine-clinopyroxenite cumulates analogous to some of those present in the Sangeang Api nodule suite. Petrographic evidence from the Sangeang Api xenoliths suggests that the disappearance of olivine is marked by the appearance of magnetite, yielding the magnetite clinopyroxenites. As already discussed, these experiments were buffered at fO_2 conditions slightly more reducing than those at the NNO buffer and no magnetite crystallised. Previous calculations suggested that andesite generation required magnetite precipitation, which then suggests that natural fO_2 values are more oxidising than those of these experiments (perhaps between the NNO and HMN buffers) which is in accord with calculations of Gill and Till (1978) and Powell (1978). Somewhat similar experiments of Holloway and Burnham (1972) yielded

magnetite within 50°C of the liquidus of the Kilauea tholeiite at the NNO buffer at 5 and 8 kbars and in view of this a hypothetical magnetite liquidus has been added to figure 11.10B as a predicted result of higher fO_2 values.

In the flow chart (figure 11.8) the major alternative to the crystallisation sequence discussed above (path A) is the path leading to the precipitation of amphibole-bearing assemblages (path C) between the olivine/clinopyroxene and low pressure plagiophyric assemblages. It is this path which is considered to be the key factor in the fractionation of andesitic differentiates and also in the generation of the Sangeang Api amphibole bearing cumulates.

Of particular importance to andesite generation in view of the calculations presented in chapter 9 is the field of amphibole + plagioclase crystallisation (field 3II in figure 11.10). Because of the opposite slopes of the plagioclase and amphibole liquidi and the rapid variation in the slope of the plagioclase liquidus with varying water content (figure 11.9 A-D), there is a marked maximum in the temperature of amphibole-plagioclase coexistence at any particular water content. With increasing water content above 3%, there is a steady decrease in this maximum temperature which also occurs at progressively lower pressures (figures 11.9, 11.10). By far the maximum extent of this field above 1000°C occurs in the system with 3% H_2O (figure 11.10B) where it extends to the highest temperatures between 9 and 10 kbars.

The above results have important implications for andesite generation. In particular they suggest that even though the amphibole-plagioclase field does extend to reasonably high temperatures, this field is still well below the liquidus. This suggests that a basaltic liquid cooling from its liquidus at about 10 kbars will crystallise olivine and clinopyroxene over a considerable temperature interval before it reaches the amphibole-plagioclase field. Furthermore such a path (e.g. path a-p, figure 11.10B) requires marked cooling at the 7-10 kbar pressure range. This suggests that to enter the

Figure 11.10

The major crystallisation fields from figure 11.9 are distinguished. Numbered fields are also equivalent to those in the flow chart, figure 11.8. 1 = liquid, 2 = olivine and/or cpx, 3I = amphibole $\pm$ olivine $\pm$ cpx without plagioclase, 3II = amphibole + plagioclase $\pm$ olivine $\pm$ cpx, 4 = plagioclase bearing assemblages without amphibole. 1000^{o}C is considered as the minimum temperature at which broadly basaltic-andesitic liquids are likely to evolve. The trends indicated are discussed in the text.

FIGURE 11.10

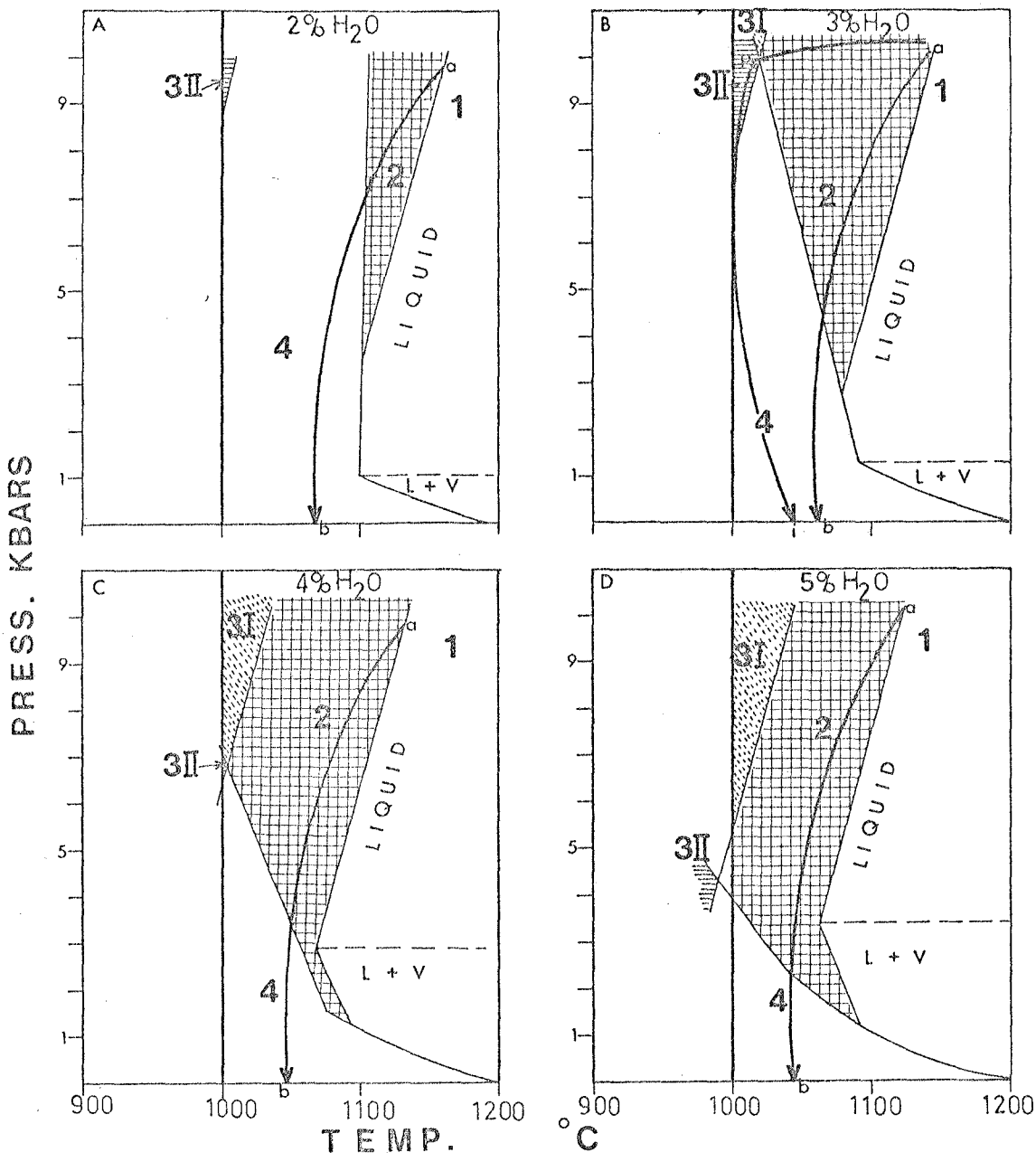
A
2% H_2O
B
3% H_2O
C
4% H_2O
D
5% H_2O
3I
3II
1
2
4
a
b
LIQUID
L + V
PRESS. KBARS
TEMP. °C
900
1000
1100
1200
1
5
9

amphibole-plagioclase field and hence differentiate an andesitic residual liquid a basaltic parent magna must be somehow impeded in its ascent and allowed to cool markedly in the 20-30 km depth range. The resultant residual liquid (andesite) must then be tapped and rise rapidly to the surface crystallising an increasingly plagioclase-rich phenocryst assemblage with a dacitic residual liquid. This path is illustrated on figure 11.10B (path a-p-i).

11.11 Conclusions

The main conclusions arising from these phase relationships, particularly considering the origin of andesite are:

1. Liquids are hydrous, but relatively water-poor. Conditions which optimise the extent of crystallisation of the critical amphibole-plagioclase field in P/T space occur with about 3% H_2O.
2. The amphibole-plagioclase field is of fairly restricted extent even at these most optimum conditions and temperatures >1000^{o}C and lies between 5 and 10 kb , with its highest temperature at about 8 kbars. These pressure conditions imply a depth in the range 20 to 30 km ., with maximum extent at about 25 km . In this part of the Sunda Arc, these depths approximate the depth to the base of the crust (Moho) (on seismic evidence, e.g. Curray et al., 1977).

The last conclusion may have major importance in the origin of andesites, considering the requirement that in order to enter the critical amphibole-plagioclase field to generate andesitic residual liquids, basaltic parent liquids must cool considerably below their liquidi at this depth (ca. 20 km .).

Thus it is possible that the base of the crust-mantle interface may represent a point where liquids rising from the mantle are in some way impeded in their ascent. In this way they may then be allowed to cool until they start to crystallise the amphibole-bearing assemblage. The

density contrast between the mantle and the lower crust is one factor which is likely to result in a marked decrease in the ascent-rate of basaltic magmas, originating in the mantle, once the less dense crust is reached. Other anisotropies present at the mantle/crust interface (e.g. phase transitions, temperature differences, compositional differences) may also markedly impede the ascending basaltic magma.

As pointed out earlier in this chapter, there is a dramatic increase in the proportion of crystallisation with cooling once the amphibole-field is reached. Similarly, calculations presented in chapter 9, suggest that the andesitic liquids are produced by about 40% crystallisation of this assemblage from a basaltic parent. Thus it is likely that any given volume of andesite erupted at the surface has also left behind an almost equivalent volume of amphibole-rich gabbro at the base of the crust. Thus the crust in island arcs may in fact be growing simultaneously both from the base downwards and the surface upwards.

This amounts to an underplating hypothesis and such models have been proposed in slightly different context, for instance by White (1979).

Several ramifications of this are likely to be important:

1. In young island arcs, where the crust is very thin ($\leq$15 km .), amphibole crystallisation at its base, may only occur at temperatures $<1000^{o}C$. Thus the production of andesitic liquids may be less common in these arcs. Such in fact is observed in such primitive arcs as the South Sandwich. Conversely, in those situations where the sub-arc crust is very thick, the opportunity for basaltic magmas to cool significantly at pressures in the range 7-10 kb and thus intersect the amphibole-plagioclase field, is probably enhanced. Thus in continental margins such as the Andean margin of South America, where the crustal base is at considerable depth, the relative abundance of andesitic lavas is considerably greater than in many oceanic arcs built on this oceanic crust.

2. As discussed previously, in order to reach the amphibole field, basaltic liquids must also cool through an interval of clinopyroxene and olivine crystallisation, from the liquidus. However, once the amphibole-field is reached, if these phases are carried with the liquid, they will react to yield amphibole (as illustrated by the alkali pyroxenites from Sangeang Api). Conversely however, the reverse process is possible, as illustrated by the partially fused amphibole-rich xenoliths from Sangeang Api (e.g. B7, plate 4B,D , table 5.4).

   If the amphibole-rich layer at the base of the crust, (formed by fractionation and accumulation from preceding basaltic magmas) is punctured, a new intrusion of high temperature magma, at least localised incongruent melting of the amphibole may occur. This may yield an olivine-clinopyroxene assemblage alkali-rich liquid. Such melt would occur in a high temperature, column-like core, marking the intrusion of the new basaltic liquid. Grading out from this core, the temperature would decrease to lower temperature, amphibole-bearing assemblages in the flanks. In this way diapiric intrusions may be mobilized with the high temperature olivine-clinopyroxenite core, marking the passage of the newly intruded column of basaltic liquid. This core would carry with it a lower temperature "mantle" of amphibole-rich rocks. This situation would then reproduce that observed in the Alaskan Zoned Ultramafic complexes. As already discussed the rock types represented in these have almost exact analogues amongst the nodules of Sangeang Api volcano.

3. The possibility that later high temperature basalt intrusions may produce localised incongruent melting of the postulated amphibole-rich zone (which may exist at the base of the crust after an arc has

had an extended previous history of andesitic eruptive activity) also has important implications for the genesis of alkaline lavas in island arcs.

Analyses of glass representing the product of incongruent melting of amphibole in some Sangeang Api xenoliths (chapter 5) indicate that partial melts of amphibole may be very alkaline in character, with high Na_2O and K_2O. Glasses analysed in chapter 5, are leucite- or even kalsilite-normative. Thus the possibility exists that some of the alkaline island arc lavas are in fact products of mixing of liquid formed by the incongruent melting of amphibole-rich residual material at the base of the crust, with mantle derived primary basalts.

Chapter 12

VARIATIONS IN PRIMARY MELT AND SOURCE COMPOSITIONS AND GENERAL MODELS FOR ISLAND ARC MAGMA GENERATION

12.1 Introduction

In chapter 9 it was argued that although a great deal of the compositional diversity found in the volcanic suites from the Lombok-Sumbawa sector of the Sunda Arc can be accounted for by fractional crystallisation, such an explanation is incapable of explaining all compositional variation. Thus, specific suites are in some cases composed of several groups of rocks not easily linked by any fractional crystallisation scheme. Furthermore, the gross compositional variations between adjacent volcanoes along the arc, is also not easily attributable to any fractional crystallisation scheme. This chapter therefore, examines the nature and origin of this 'residual' compositional diversity.

Included are: (a) consideration of the time-space relations commonly recognised in many arcs, (b) discussion of factors likely to result in compositional diversity and differences in primary magma composition, including variation in degree of partial melting of the source, and source heterogeneity, and (c) discussion of problems relating to the origin of alkaline lava suites in convergent plate regimes.

12.2 The Geochemical Nature of Between-Suite and Within-Suite Variation, Attributable to Differences in Primary Magma Composition.

(a) Within-suite variation

In chapter 9 it was found that individual lavas or groups of lavas within several suites from single volcano-complexes could not be modelled as components of any simple fractional crystallisation trend that might have related them to other lavas from the same suite. For example, the

ankaramite group from the Rindjani suite was found to be relatively too Sr-rich and in some cases, also K_2O- and Rb-rich to yield the slightly less mafic high-Al basalts. Furthermore, the high-Al basalt group encompassed a variety of lavas with varying K_2O and Rb concentrations, ranging from *ne*- to *ol*-,*hy*-normative types. It was found that the more mafic of the *ol*-*hy*-lavas of this group could possibly yield andesitic differentiates. Yet other, equally mafic, more undersaturated members of the group (e.g. 41632, table 3.13), actually had higher K_2O and LREE concentrations than many andesites and even if amphibole fractionation did occur, as postulated, these basalts could not represent liquids potentially parental to the andesites. Thus there appears to be some primary variation in liquids represented by the general high-Al basalt group from Rindjani, though some of the variation could also be due to fractional crystallisation of phases similar to analysed phenocryst assemblages.

The Sangeang Api group of lavas, with their significantly variable Sr-isotopic composition, provide even more marked evidence that more than one primary liquid was involved in the erupted lava suite. Thus, the most mafic lava of the suite (B43) has markedly more radiogenic Sr than many of the other less mafic lavas. It was also found that this rock had K_2O-, Rb-, Sr-, P_2O_5- and possibly Na_2O-concentrations which were up to 30% higher than would be predicted by extrapolation of the variation trends shown by slightly less mafic trachybasalts of the same suite. B43 also has a markedly different REE pattern than other lavas of the suite, with a LREE-enriched and HREE-depleted character, and the less fractionated REE patterns of the other lavas, which have markedly lower La/Yb ratios, could not be derived from this rock, by fractionation of any mineral assemblage represented either in the Sangeang Api xenoliths or as phenocrysts.

Finally, the very alkaline, undersaturated, leucite-bearing lavas from Soromundi and G. Sangenges, while showing some features consistent with differentiation by fractional crystallisation, particularly of cpx-dominated assemblages, also show variation in many of the LIL elements of a much greater magnitude than would result merely from the above mechanism.

It is suggested therefore that there is a significant component of geochemical variability amongst magmas erupted from individual volcanoes that existed before fractional crystallisation caused even further differentiation. The extent of this variability, however, is small compared with the variation between different volcanoes along the arc.

(b) Between-suite variation

In chapter 7, the volcanic rocks from the volcanoes studied from this sector of the Sunda Arc, were shown to fall into three groups. These groupings are justified both on petrographic and geochemical grounds.

1. A calcalkaline series: including the lavas from Rindjani volcano and the *Q*-normative group (3) from G. Sangenges.
2. A series of potassic, *ne*-normative trachybasalts and trachyandesites ("shoshonites"): this group including the lavas of Tambora and Sangeang Api volcanoes as well as the feldspathoid-free, *ne*-normative series (2) from G. Sangenges.
3. A highly undersaturated, feldspathoid-bearing (leucite), alkaline series: this composed of the Soromundi lavas and the feldspathoidal group (1) from G. Sangenges.

Geochemically these three groups are distinguished by variation in LIL-element concentrations, particularly K_2O and related trace elements. In terms of these elements, the sequence through the above groupings, from calcalkaline, through the *ne*-normative trachybasalt-trachyandesite ("shoshonite") group to the alkaline, feldspathoid-bearing one, is one of continuous enrichment. In this sense, variation between these groups is systematic.

Figure 12.1

K_2O v. SiO_2 variation of all lavas analysed in this thesis from the Lombok-Sumbawa sector of the Sunda arc (also including some basaltic andesites and andesites from Agung volcano on Bali).

The same symbols are used in all the variation diagrams in this chapter.

Group 1 - calcalkaline lavas

- ● - Agung volcano, Bali
- ○ - Rindjani volcano, Lombok.
- □ - *Q*-normative basaltic andesites and andesites from G. Sangenges, Sumbawa.

Group 2 - potassic, slightly undersaturated lavas, with groundmass K-feldspar, but only rare feldspathoid.

- X - Tambora (+ P. Satonda).
- ■ - Sangeang Api.
- ▲ - *ne*-trachybasalts from G. Sangenges.

Group 3 - highly undersaturated, leucite-bearing lavas.

- △ - Soromundi.
- + - G. Sangenges.

This diagram illustrates the marked distinction between the three groups of lavas and in particular the marked increase in slope of the K_2O-SiO_2 variation from the calcalkaline series to the feldspathoidal series.

Figure 12.1

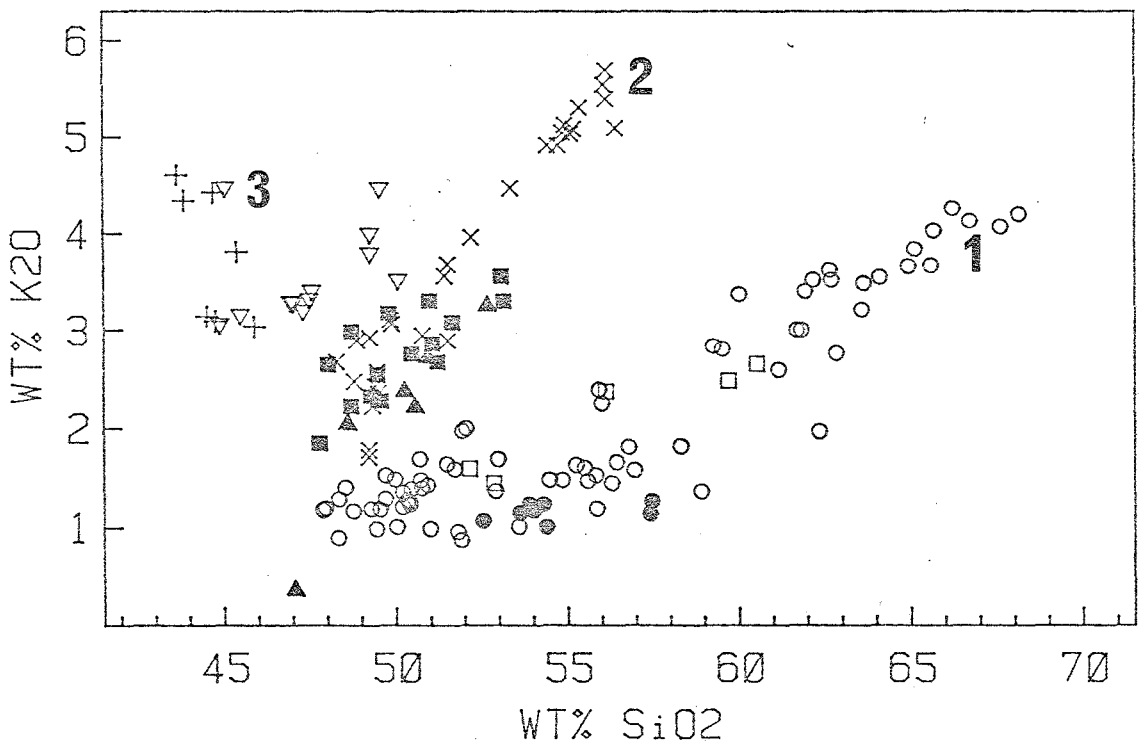

The compositional differences between these three series are illustrated by reference to the variation diagrams displayed in figures 12.1 - 12.5. By comparison with the calcalkaline group, the two more alkaline suites are distinguished by high concentrations of K_2O (figures 12.1 and 12.5A), Sr (800-2000 ppm) (figure 12.5B) and Rb (figure 12.2), lower, but variable K/Rb ratios and higher K_2O/Na_2O ratios, ranging from 0.5 to 2.0 (figures 12.3 and 12.4). Many of the leucite-bearing, very alkaline lavas are mafic with Mg/Mg+ΣFe values >0.6, as are some members of the second group, (for instance the phonolitic tephrite B43 from Sangeang Api). These mafic lavas are characterised by low Al_2O_3 (<15%), high Ca and Sc and moderately high Ni and Cr. In general, the members of the calcalkaline and trachybasalt-trachyandesite series have higher concentrations of Al_2O_3, are often more silica-rich or are components of trends which lead to more silica enrichment, have lower MgO and CaO and lower Mg/Mg+Fe values, by comparison with lavas of the very alkaline group. However, they also have lower Rb, Sr and higher K/Rb ratios.

Compared with the basaltic lavas of the calcalkaline series, the lavas of the two more alkaline series, in spite of their frequently higher MgO and Mg/Mg+Fe values, may have slightly lower Ni and Cr concentrations. Even though the lavas of the two alkaline groups have K_2O, Rb and Sr (and probably Ba) concentrations which are 3-10 times those of the calcalkaline group lavas, concentrations of TiO_2, P_2O_5, Zr and Nb are similar in members of all three series.

The most interesting geochemical feature is the progressive increase in the concentration of K_2O, Rb and Sr through the three suites, from the calcalkaline group to the highly alkaline group. Thus in the MgO-variation diagrams (figure 12.5 A, B, C) a series of echelon trends for K_2O, Rb and Sr result each suite showing overlapping MgO values, but with different

Figure 12.2

Rb v. SiO_2 variation of all lavas analysed from this sector of the Sunda arc. Symbols are the same as those in figure 12.1

The variation in Rb-concentration between the three series; 1. calcalkaline, 2. *ne*-trachybasalts and -trachyandesites and 3. leucite-bearing lavas, is illustrated and shows a similar pattern to the K_2O v SiO_2 variation in figure 12.1, with markedly increasing slope from field 1 to 3.

Figure 12.2

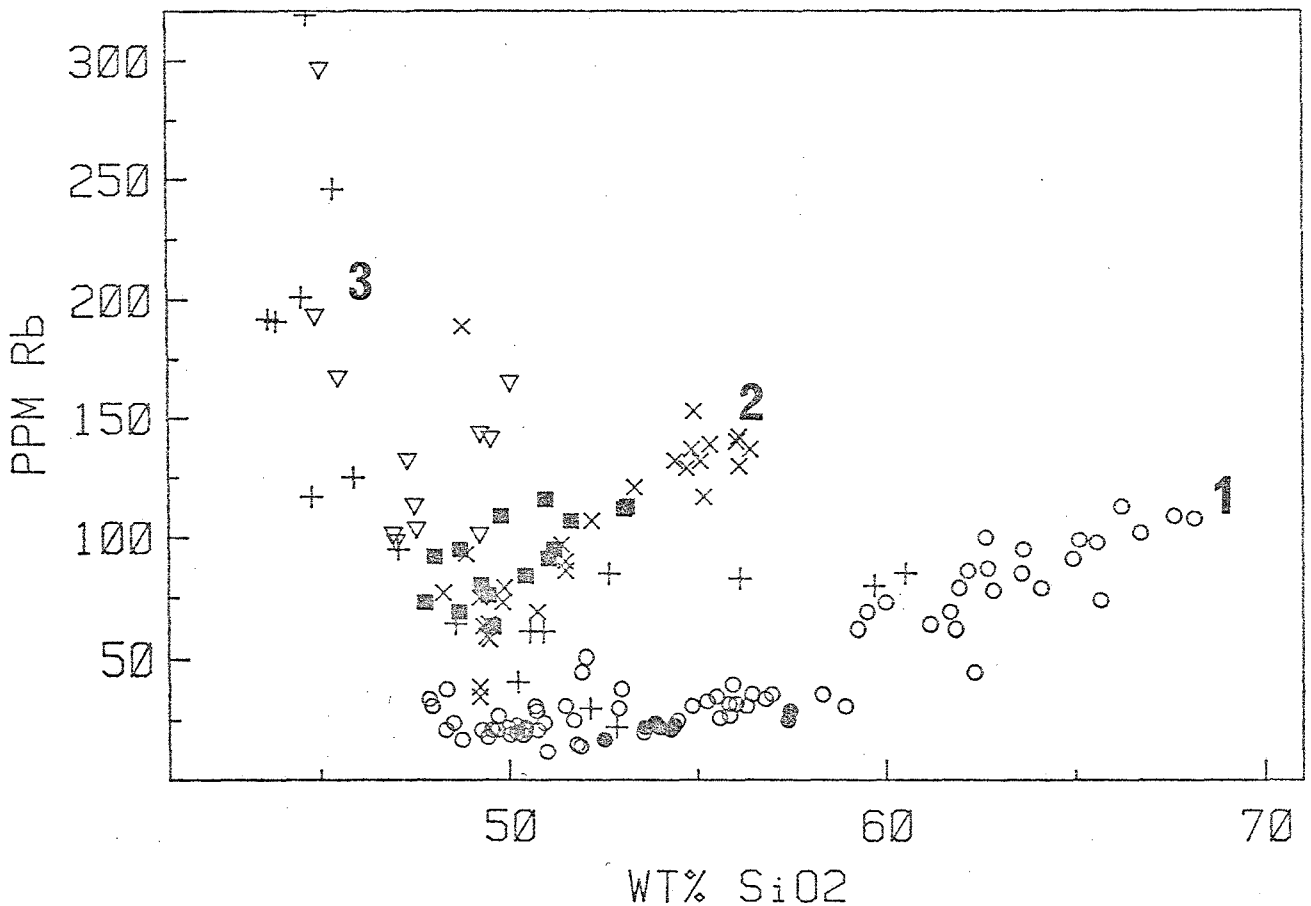

levels of enrichment of K_2O, Rb and Sr. Significantly, Zr, even though this is also usually considered as an "incompatible" element, does not show the same discrimination between the three series (figure 12.5D). The trachybasalts from Tambora, Sangeang Api and G. Sangenges for instance have about three times the Rb concentration of the calcalkaline basalts with similar MgO concentrations, yet have similar Zr concentrations.

This systemmatic variation through the three series outlined, is also illustrated by the progressive change in slope of the K_2O-SiO_2 and K_2O/Na_2O-SiO_2 variations (figures 12.1 and 12.3).

While each of the three suites show distinctive levels of enrichment of LIL elements, as discussed in chapter 8, they also each exhibit trends suggestive of fractional crystallisation. Thus general within-suite trends consist of K_2O, Rb, Zr, Nb and Na_2O enrichment with MgO depletion, while CaO, Fe, Ni, Cr and Sc all decrease. Sr and Al_2O_3 tend to show trends of continuous enrichment in the leucite-bearing suites, while in the calcalkaline and trachybasalt-trachyandesite suites, these elements are enriched until MgO diminishes to about 4% and then they start to decrease, as a consequence of the onset of plagioclase crystallisation (figure 12.5B).

The fact that many major elements tend to show overlapping ranges for each suite, as well as similar variation trends, suggests that there is no simple fractional crystallisation mechanism relating the calcalkaline and more alkaline suites. This also suggests that the levels of enrichment of K_2O, Sr and Rb were inherited prior to the differentiation of the more evolved lavas of each suite.

Sr-isotopic data and REE geochemistry also provide further distinctions between the lavas of the three defined suites. Some aspects of the Sr-isotope geochemistry of the lavas from this sector of the Sunda Arc have been discussed in chapter 7 and also by Whitford et al., (1979) and by Foden and

Figure 12.3

Variation of K_2O/Na_2O v. SiO_2 for all lavas analysed from this sector of the Sunda arc.

The symbols represent the same sample-groups as in figure 12.1, as do the three groups (1, 2 and 3). This plot illustrates the same pattern of variation as did the K_2O- and Rb-SiO_2 plots in figure 12.1 and 2 and illustrates the distinction between the three series and the relative increase in enrichment of K compared to Na through the series from Calcalkaline to Leucititic.

Figure 12.3

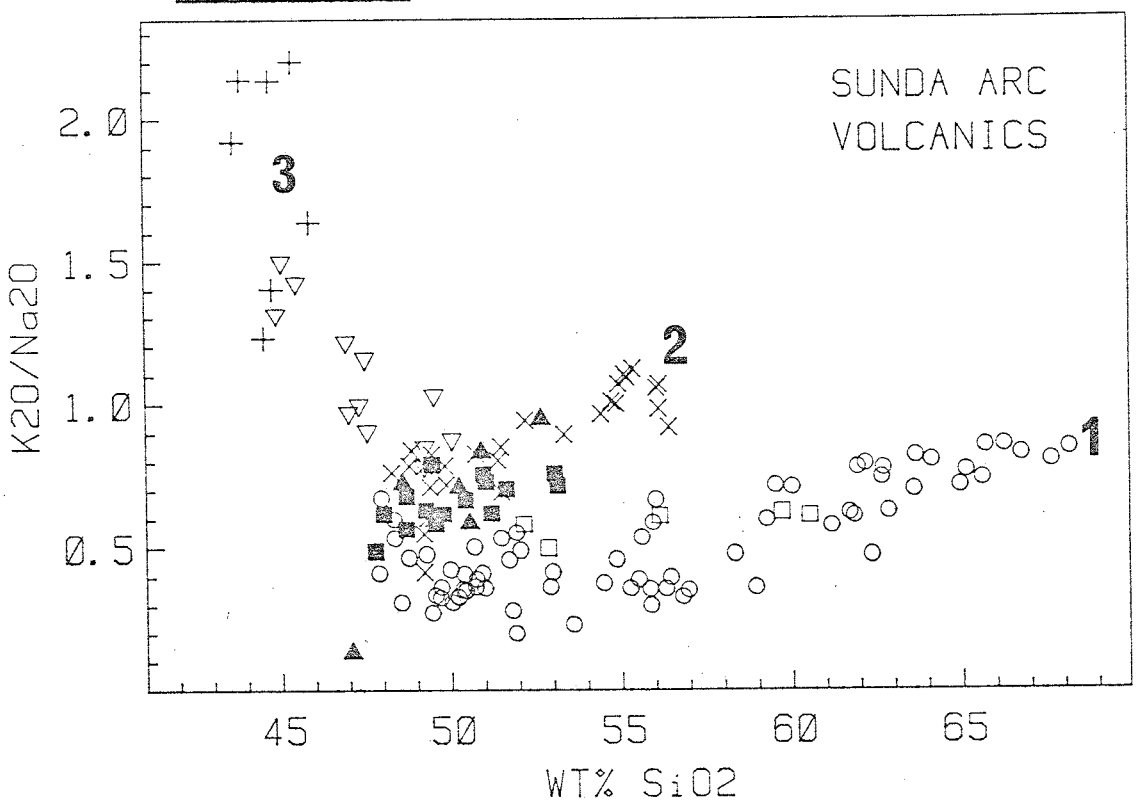
SUNDA ARC
VOLCANICS
K2O/Na2O
2.0
1.5
1.0
0.5
45
50
55
60
65
WT% SiO2
1
2
3

Varne (1980). The calcalkaline suite from Rindjani as well as the members of the trachybasalt-trachyandesite suite from Tambora, are characterised by relatively low, constant $^{87}Sr/^{86}Sr$ ratios, averaging 0.7039. Other members of the *ne*-normative, trachybasalt suite and members of the very alkaline, leucite-bearing suite, have higher and more variable $^{87}Sr/^{86}Sr$ ratios. The most mafic leucitites have the highest Sr-isotopic ratios (0.7053).

REE data are available for a few rocks from this sector of the arc (table 9.3 and 9.4, figures 9.1, 9.4 and 9.7). It appears that the lavas of the two more alkaline suites are LREE-enriched, as well as having higher total REE concentrations than the lavas of the calcalkaline suite. Analysed members of the calcalkaline suite have La/Yb ratios less than 10, while the more alkaline groups have ratios between 11 and 27. REE patterns are not available for any of the very alkaline, leucite-bearing lavas, though limited XRF data suggest that these have very high La concentrations (37-99 ppm) and may well have La/Yb ratios even higher than those lavas for which full REE patterns are available.

Many of the above features suggest that compositional variety embodied in the differences between the three groups defined, must relate to primary differences in the compositions of the magmas supplying each series. In this sense, the tendency for Sr to become increasingly radiogenic in the more alkaline lavas and for the $^{87}Sr/^{86}Sr$ ratios to become more variable in the undersaturated, potassic suites compared to the calcalkaline suites, is likely to be of particular importance.

In general it can possibly be argued that the geochemical variability seen within suites for instance between the ankaramites and high-Al basalts from Rindjani, is similar in character and perhaps in cause, to the much more obvious variability between different suites.

Figure 12.4

Variation of K/Rb ratio v. MgO and SiO_2 for all lavas analysed from this sector of the Sunda arc. The symbols represent the same sample-groups as in figure 12.1. The figures illustrate the gradual decrease in K/Rb ratio from the calcalkaline series (1) to the *ne*-trachybasalt-trachyandesite series (2) to the leucitite series (3).

Figure 12.4

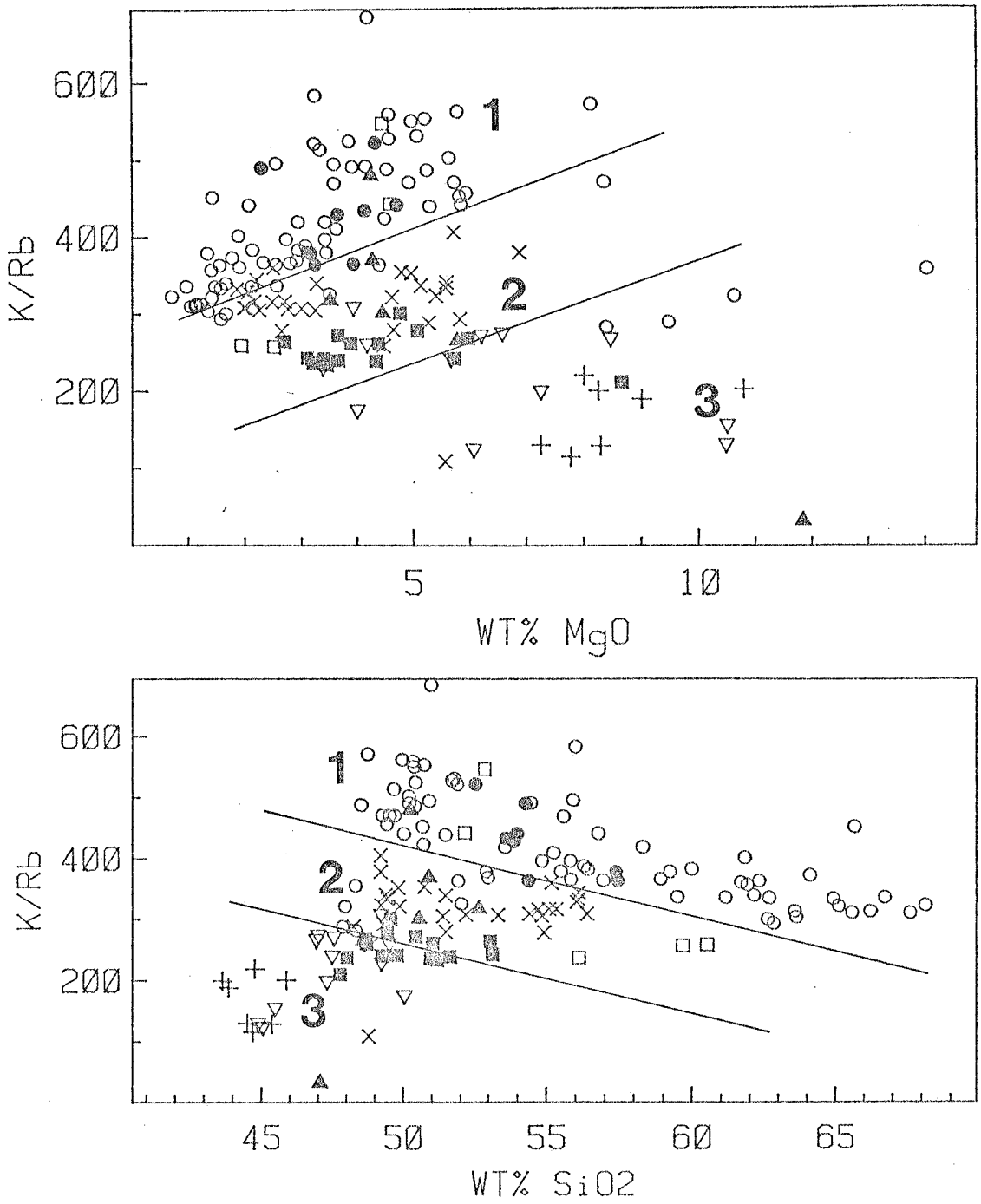
600
400
200
K/Rb
1
2
3
5
10
WT% MgO
600
400
200
K/Rb
1
2
3
45
50
55
60
65
WT% SiO2

Figure 12.5

The variation of K_2O, Rb, Sr and Zr v. MgO for all lavas analysed from the Lombok-Sumbawa sector of the Sunda arc. Symbols represent the same sample groups as in figure 12.1.

The variation of K_2O, Rb and Sr as shown in diagrams A, B and C exhibit similar patterns, as illustrated by the inset in figure B. There is a systematic enrichment of each of these LIL elements over the entire MgO range, from the calcalkaline series (1) to the *ne*-trachybasalt-trachyandesite series (2) to the leucitite series (3). The implication of the interpretation of the variation of these elements shown in the inset in B, is that the parental liquids to each series reflected the range of enrichment of these elements initially and that the subsequent fractionation of these maintained this distinction, with decreasing MgO (trend B). By contrast the Zr concentrations (fig. D) of each of these series is very similar and there does not appear to have been the enrichment of this incompatible element that is shown by the LIL group of the incompatible elements.

Figure 12.5

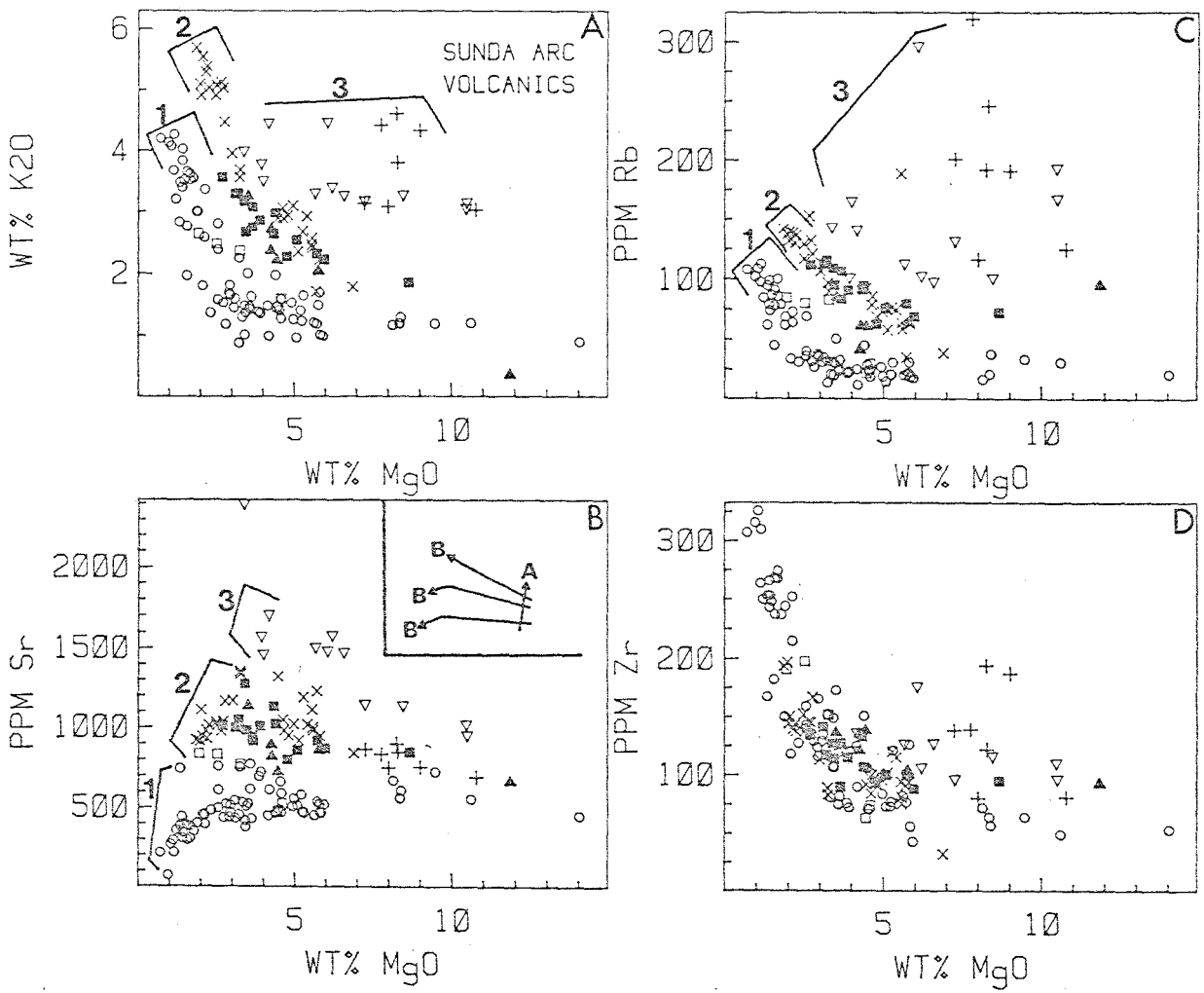
A
SUNDA ARC
VOLCANICS
WT% K2O
WT% MgO
B
PPM Sr
C
PPM Rb
D
PPM Zr
1
2
3
A
B

Figure 12.6

This figure illustrates the variation of the ratio of small, highly charged, incompatible or nearly incompatible trace elements or minor elements of the group, Ti, P, Zr and Nb over LIL-type incompatible elements (K or Rb).

The symbols are the same as those in figure 12.1. The diagrams distinguish two fields; CA - calcalkaline (and is the same as series 1 in the previous diagrams in this chapter) and A = alkaline (which includes both series 2 and 3 of the previous figures in this chapter ... leucitites and *ne*-trachybasalts and -trachyandesites).

The calcalkaline lavas all have higher ratios than the alkaline lavas suggesting that the process which led to the enrichment of the K-type LIL incompatible elements did not result in the same degree of enrichment of Ti, Zr, P and Nb. This suggests that either in this arc environment the elements of the Ti, Zr, P, Nb group are not incompatible with respect to source mineralogies, or that differences between the sources of the alkaline and calcalkaline series require real geochemical heterogeneity.

Figure 12.6

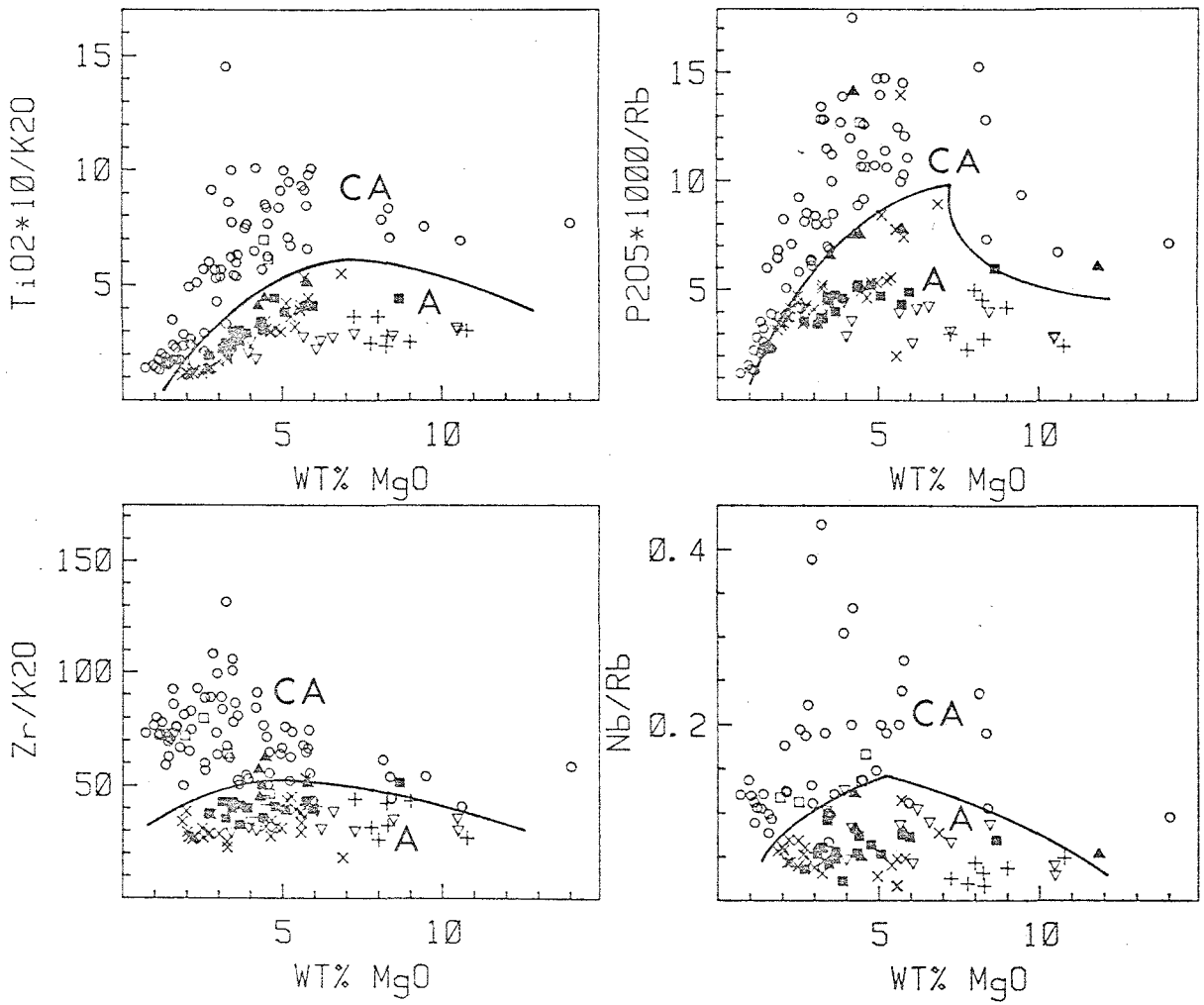
TiO2*10/K2O
15
10
5
CA
A
5
10
WT% MgO
P2O5*1000/Rb
15
10
5
CA
A
5
10
WT% MgO
Zr/K2O
150
100
50
CA
A
5
10
WT% MgO
Nb/Rb
0.4
0.2
CA
A
5
10
WT% MgO

12.3 *Compositional Affinities of the Volcanic Associations of Lombok and Sumbawa*

Volcanic rock series of broadly potassic character, with low to intermediate silica content, which range from strongly undersaturated types to slightly oversaturated varieties, have been described from a number of localities. These may be from within continental plates as described by Holmes and Harwood (1937), Bell and Powell (1969) and Ferguson and Cundari (1975) from the Birunga Province, by Nicholls and Carmichael (1969) from North America or from the Rhine Rift. They also occur in convergent plate volcanic arcs, as described from New Ireland, by Johnson et al. (1976), from Papua (Johnson et al., 1978), from Indonesia as described in this thesis and by Iddings and Morley (1915) and Brouwer (1938, 1943), from the Mediterranean (Keller, 1974; Appleton, 1972) and in the Andes, as described by James (1977). An important question then arises as to whether all these suites, from contrasting tectonic environments, have similar origins.

Joplin (1968) considered the potassic volcanic associations, ascribing mildly potassic varieties (K_2O - Na_2O), of oversaturated or mildly undersaturated character, to a shoshonitic association. These she considered characteristic of recently stabilised orogenic areas, also noting that members of the shoshonitic association often occurred in conjunction with more undersaturated leucitic lavas. On the basis of Joplin's original definition, the potassic *ne*-trachybasalts and trachyandesites from Tambora, Sangeang Api and G. Sangenges would be considered as shoshonites. More recently the term shoshonite has been restricted to potassic lavas from continental margin- and island-arcs. Many rocks so-termed are markedly less potassic and less undersaturated than the Sumbawan examples.

Jakes and White (1972), Gill (1970) and others, have discussed the shoshonites in terms of the spatial structure and temporal evolution of arcs and considered that this suite occurred at the greatest distance from the trench and late in the eruptive history of the arc.

The potassic volcanic associations of Indonesia have been frequently compared to two better-known volcanic areas: the Roman Region and the Birunga Province (Iddings and Morley (1915); Joplin, 1968). In all three areas there are volcanic associations that are closely associated in space and time, yet range in normative character from *Q*-, and *hy*-bearing to *ne*-bearing with K_2O/Na_2O ratios varying from >2 to 0.5 or less. The comparison between the suites of these three regions have also been discussed by Foden and Varne (1979).

The Roman Region (Washington, 1917) includes a group of highly potassic *ne*- and *lc*-normative, leucite-bearing lavas as well as less potassic suites including basalt, trachybasalt and latite (Joplin, 1968; Appleton, 1972; Cundari and Le Maitre, 1970). These two groups may be equivalent to the leucitite- and potassic *ne*-trachybasalt - *ne*-trachyandesite suites from Sumbawa. In both areas, enrichment in K is accompanied by enrichment in Sr and Rb. In both areas there is also a tendency for increasing K in the mafic rocks from the different associations to be accompanied by increase in initial $^{87}Sr/^{86}Sr$ ratios (Cox et al., 1976), although ratios from the Roman Region are generally higher than those from the Lesser Sunda Islands. In the Birunga Province, on the other hand, initial $^{87}Sr/^{86}Sr$ ratios in the more potassic mafic feldspathoidal lavas are lower ($\sim$0.705) than in the less potassic mafic feldspar-bearing lavas (0.707) and are even higher (0.711) in the rare *Q*- and *hy*-normative samples (Bell and Powell, 1969). With these suites as in the case of those from Lombok and Sumbawa, it seems obvious that

Table 12.1

TYPICAL POTASSIUM-RICH LAVAS FROM THE BIRUNGA AND TORO-ANKOLE REGIONS OF THE AFRICAN RIFT

*	1	2	3	4	5	6	7
SiO_2*	40.56	42.57	48.02	42.09	50.17	53.16	57.66
Al_2O_3	8.15	10.83	14.57	15.59	16.86	18.24	17.46
Fe_2O_3	5.04	4.96	2.91	3.47	2.99	2.10	3.42
FeO	5.40	7.65	7.32	8.63	7.02	6.07	4.12
MgO	18.15	9.16	7.47	4.74	4.36	2.46	1.94
CaO	11.39	14.39	9.33	10.77	8.65	6.40	4.30
Na_2O	1.08	1.98	2.79	4.61	2.89	3.61	4.32
K_2O	5.14	3.88	3.84	4.83	4.47	5.38	4.62
TiO_2	4.43	3.70	2.90	3.47	1.67	1.55	1.78
P_2O_5	0.37	0.71	0.64	1.50	0.73	0.66	0.21
MnO	0.28	0.14	0.18	0.26	0.17	0.18	0.16
H_2O^+	2.36	0.94	0.46	0.49	0.21	0.38	0.22
$Mg/_{Mg+\Sigma Fe}$	0.76	0.57	0.57	0.42	0.44	0.36	0.32
K_2O/Na_2O	4.75	1.96	1.37	1.05	1.54	1.49	1.07
Sc	22				17	8.5	
Rb	167	104	128	119	165	171	170
Sr	2004	1463	1190	1798	1109	1381	890
Zr	613	451	503	547	440	451	515
Nb	205	183	132	181	131	193	126
La	155				91	139	
Yb	0.91				2.35	2.80	
K/Rb	255	309	249	337	225	261	226
Rb/Sr	0.083	0.071	0.108	0.066	0.149	0.124	0.190
La/Yb	170				38.7	49.6	
$^{87}Sr/^{86}Sr$	0.7055	0.7053	0.7076	0.7046	0.7075	0.7070	0.7074

1. Leucite mafurite (C4007). Bunyaruguru.
2. Leucite anakaratrite (C999) Nyamunuka, Katwe-Kikorongo.
3. Leucite absarokite (C1906) Nyarubebsa II.
4. Olivine leucitite (S.45) Nyiragongo
5. Shoshonitic absarokite (C2794) Muhavura.
6. Banakite (C2799) Muhavura.
7. Trachyandesite (CV258) Sabinyo.

* Major elements have been normalized to 100% volatile-free, H_2O^+ value is pre-normalized.

Major element analyses are from those collated by Bell and Powell, (1969), from a number of original sources. Sample numbers refer to the original source (see Bell and Powell, 1969, pp. 551-552). Rb, Sr, $^{87}Sr/^{86}Sr$, Zr, Nb analyses are by Bell and Powell (ibid), while La, Yb, Sc analyses are from Mitchell and Bell, 1976, pp. 296-297.

any petrogenetic scheme invoking only partial melting of homogeneous peridotite upper mantle followed by crystal-liquid fractionation must encounter fatal difficulties when confronted by the evidence for isotopic variability.

In the volcanic associations of Lombok and Sumbawa it is plain that enrichment in K is accompanied by enrichment in Sr and Rb but not by enrichment in Ti or in Zr (figures 12.5 and 12.6). Similarly, neither Nb nor P show enrichment of the order of that shown by Rb (figure 12.6). In this respect there appears to be an uncoupling of the elements normally classed as "incompatible": the group of relatively small and highly charged ions tends not to be enriched whereas the LIL group in its enrichment pattern behaves as it does in the widely-distributed sodic-alkaline provinces.

The behaviour of Ti, Zr, Nb and to a lesser extent P, in this Indonesian suite are in marked contrast to that in the Birunga Province lavas. Typical analyses of some representative lavas from the Birunga province are given in table 12.1. In particular it can be seen from these that Nb and Zr concentrations in the Sumbawa alkaline rocks are very low by comparison. In fact Nb concentrations in the Indonesian examples are two orders of magnitude lower than the African examples and Zr concentrations are three to four times lower.

Ti and Zr are of course key elements in geochemical classifications of volcanic rocks according to tectonic setting. It has already been noted that trachybasalts from the Sumbawa potassic *ne*-trachybasalt - *ne*-trachyandesite association and basalts from the Rindjani basalt-andesite-dacite association are rich in Al_2O_3 (~18 wt.%) but poor in TiO_2 (~1 wt.%), compositional characteristics that typify volcanic rocks from island arcs and similar circumoceanic settings (Chayes, 1965). The Sumbawa leucitites also possess similar TiO_2 contents, although they are poorer in Al_2O_3.

Thus even the potassic associations from Sumbawa retain the island arc imprint. Potassic volcanic rocks from New Ireland, Papua New Guinea, are similarly rich in Al_2O_3 and poor in TiO_2, but unlike the Lesser Sunda Islands, are not associated with a Benioff zone although some centres were active as recently as the Pleistocene (Johnson et al., 1976). In contrast, TiO_2 contents of Birunga Province rocks are commonly greater than 3 wt.% (Bell and Powell, 1969; Holmes and Harwood, 1937). These observations add support to suspicions that the Roman Region vulcanicity is in some way related to an island arc or converging plate boundary setting (Ninkovich and Hays, 1973; Thompson, 1977).

It is noted, however, that Birunga rocks are generally more mafic than Roman rocks (Cundari and Le Maitre, 1970), and that leucitites from Nyiragongo, with MgO contents comparable with many Roman rocks, have TiO_2 contents that range down to 2 wt.% and tephrites down to 1.6 wt.% (Bell and Powell, 1969). Conversely a Roman Region clinopyroxene leucitite, selected as representative and interpreted on experimental grounds to be an upper mantle melt, is strikingly similar to Nyiragongo olivine leucitites and has 3.25% wt.% TiO_2, (Thompson, 1977). It is also noted that the Sumbawa potassic associations have K_2O/Na_2O ratios that range only up to 2, like the Birunga Province, whereas Roman Region leucite-bearing volcanics from Roccamonfina have K_2O/Na_2O ratios in the 2-4 range.

12.4 Volcanic Composition-Space-time Relations in the Lombok-Sumbawa Arc Sector, and the Generalized Island Arc Schema

Twenty-five years ago Rittman (1953) recognised that for any cross-section across the Indonesian orogenic belt, the calcalkaline character of magmas from active volcanoes decreased from the foredeep towards the hinterland. Further he also recognised that the calcalkaline character of lavas

of any single volcano decreased with time. Since then, the Sunda Arc system has come to be regarded as one of the classic examples of an arc showing well-defined correlation between the composition of erupted lavas (particularly of K_2O content) and the depth to the underlying Benioff Seismic Zone (e.g. Hutchison, 1975, 1976; Hatherton and Dickinson, 1969; Whitford and Nicholls, 1976; Nielson and Stoiber, 1973). More recently however Foden and Varne (1980) have pointed out that, at least in the Lombok-Sumbawa sector of the arc, such a relationship is not defined by the compositions of lavas from the volcanoes of Quaternary and Recent ages.

In the last decade, the island arc concept that has developed within the plate tectonic model assigns the volcanic rocks to three magmatic associations: a tholeiite association, a calcalkali association, and an alkali association (e.g. Kuno, 1950; Jakes and White, 1969; Ringwood, 1974).

The tholeiite association is dominantly basalt and basaltic andesite, silica-rich volcanic rocks are rare, and it displays an iron-enrichment trend. Arcs where most of the volcanic activity has been assigned to this association, like Tonga and South Sandwich, are believed to represent an early stage of arc evolution (Baker, 1968) characterized by fast subduction rates (Miashiro, 1972), whereas the calc-alkali association, dominated by andesite and with a silica-enrichment trend, is believed to typify more evolved arcs like the Lesser Antilles, the Aleutians and the Sunda Arc, where subduction rates may be slower.

The alkali association is not well defined: it includes both silica-oversaturated and undersaturated suites, some of them peralkaline. In the volcanic island arc schema the alkali association is the culmination of two magmatic evolutionary sequences, one temporal and the other spatial, just as Rittman (1953) first argued for the Sunda Arc.

In the temporal magmatic sequence of the arc schema, the tholeiite association is considered to develop early, followed by the calc-alkali association, and later (finally?) by the alkali association.

The spatial magmatic sequence of the arc schema places the tholeiite association near the trench where the Benioff zone is shallow, the calc-alkali association over intermediate Benioff zone depths (100-200km) farther from the trench, and the alkali association farthest from the trench where the Benioff zone earthquakes are deepest.

This concept of three volcanic island arc magmatic associations that increase in alkalinity away from the trench is "still the cornerstone of generalized schemes for the spatial compositional variation of island arc magmas", although it is currently being shown to be inadequate (Arculus and Johnson, 1978), and is commonly expressed as a "k-h" relationship (Whitford and Nicholls, 1976; Ninkovich and Hays, 1972; Nielson and Stoiber, 1973; Hatherton and Dickinson, 1969), where the content of K_2O at some specified SiO_2 content in a volcanic series is taken as a measure of alkalinity ($\underline{K}$), and correlated with depth to underlying Benioff zone ($\underline{h}$). Not only are K and related trace elements like Rb, Ba, Sr, Pb and Cs supposed to increase with increasing $\underline{h}$, but so also are Th, U, the light REE, Th/U, K/Na, Rb/Sr, La/Yb and possibly also Ti and Zr (Arculus and Johnson, 1978).

The Sunda Arc is one of the type localities for this volcanic composition-space variation. Hutchison (1975, 1976) recently used multiple linear regression analysis to relate the K, Sr and Rb contents of Sunda arc volcanics to their SiO_2 contents and depths to Benioff zone. Two solutions to Hutchison's K_2O-SiO_2-$\underline{h}$ expression for the Sunda Arc as a whole are plotted for comparison with our data for Rindjani, Tambora and Sangeang Api (figure 12.7). It is plain that the Rindjani basalt-andesite-dacite suite ($\underline{h}$ = 165 km) conforms quite well with volcanic composition-space relationship of the whole

Sunda Arc. Equally plainly, the Tambora suite ($\underline{h}$ = 180 km) and the Sangeang Api suite ($\underline{h}$ = 190 km) are far more potassic than would be predicted. Whitford and Nicholls (1976) derived K_{55} values from a similar set of data, and also compiled earlier interpretations of Sunda Arc volcanic composition-space relationships: Rindjani, and also the Balinese centres to the west, again behave as would be predicted by the schema but Tambora and Sangeang Api do not.

The failure of the volcanic island arc schema to explain the volcanic composition-space relationships in the Bali-Lombok-Sumbawa sector of the Sunda Arc seems to extend to the temporal sequence. Although the volcanic stratigraphy is not well known, it is evident that the highly potassic and undersaturated leucitite association was erupted from centres that became extinct in the early Quaternary and that the present-day activity in this arc sector is less potassic.

While it is not disputed that there is tendency for potassium-rich volcanoes to be located over deep parts of the Benioff zone: Batu Tara (Brouwer, 1938) is one good example from the Sunda Arc. However it is emphasized that the active potassic centres of Sumbawa are flanked to the west by active volcanoes of the basalt-andesite-dacite association, and that all the volcanoes are underlain by Benioff zone depths in the range 150-190 km . Hutchison (1976) and Nielson and Stoiber (1973) both comment that even if the potassium content of the magmas is determined by the depth at which melting occurs, by inference the Benioff zone, then some other factor or factors must also play an important role in controlling magmatic compositions. One of these additional factors may perhaps be the age of onset of volcanism (Carmichael et al., 1974) the relatively potassium-poor Isu-Bonin arc was initiated 25-50 m.y. ago, whereas the relatively potassium-rich Java sector of the Sunda Arc was initiated 150-175 m.y. ago. However, the Lombok-Sumbawa sector of the Sunda Arc is young, yet potassic.

Figure 12.7

K_2O v SiO_2 variation of all lavas analysed in this thesis from the Lombok-Sumbawa sector of the Sunda arc. Symbols represent the same sample groups as in figure 12.1.

The 200 and 165 kilometer lines represent solutions to Hutchison's (1976) regression relating K_2O-SiO_2 and Benioff Zone depth (h) based on all Sunda arc data available to him.

This figure illustrates that while the Rindjani suite (h =165-170 km) does conform to the general K_2O-Benioff Zone depth relationship and has K_2O concentrations appropriate to its height above the Benioff Zone, Tambora (h = 180 km) and Sangeang Api (h = 190 km) are markedly more potassic than predicted from the Sunda arc data in general. The leucitic suite are even more potassic and while Soromundi and G. Sangenges volcanoes presently are situated less than 200 km above the Benioff Zone, they are now inactive, having become dormant in the late Quaternary, so that it is not possible to be absolutely sure of their h values during their period of activity, though it does seem unlikely that they were above a very much deeper Benioff Zone.

Figure 12.7

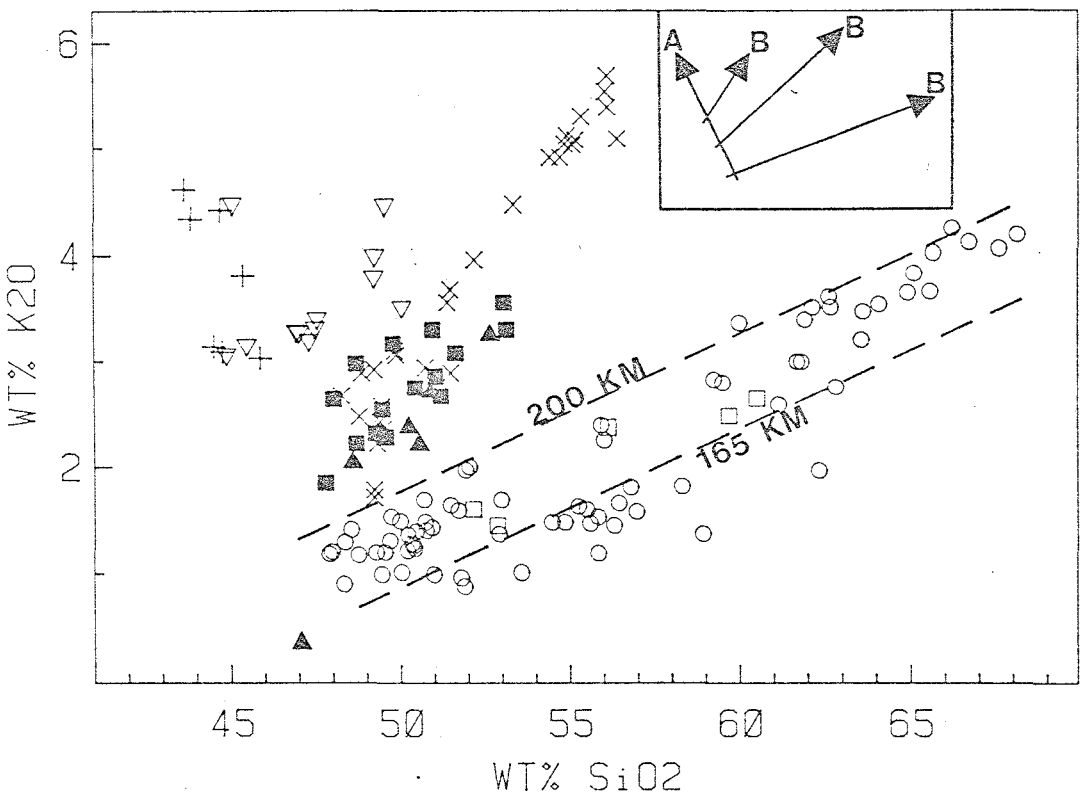

It is concluded that there is no compelling tectonic evidence for suggesting that the richness in potassium of the Sumbawa volcanics results from partial melting at much greater pressures of the same source material that yields the Rindjani basalt-andesite-dacite association to the west. Similarly, the Benioff zone relationships in the arc sector offer little support for zone refining and mantle scavenging potassium-enrichment mechanisms that rely solely on path-length of mantle traversed by ascending melt (e.g. Ninkovich and Hays, 1972; Harris, 1957; Best, 1975). It is noted, however, that Hamilton's (1974) Benioff zone contours suggest a fairly abrupt steepening in dip of the Benioff zone beneath Sumbawa at depths of about 200-300 km, and that although deep-focus earthquakes (≈600 km) occur north of Sumbawa there is an apparent gap in seismic activity in the 300-500 km depth range (Cardwell and Isacks, 1978).

It has also been suggested that alkaline rocks in island arcs may be sited on fracture zones that provide pathways for melts to rise from mantle regions that are normally not tapped (Delong et al., 1975). The examples cited are apparently sodic alkaline rocks, but the notion could apply to the Sumbawa situation: Audley-Charles' (1975) postulated Sumba fracture system could provide such pathways.

12.5 The Variation in Primary Melt Geochemistry

As the Benioff Zone lies at a similar depth beneath all the volcanoes of this section of the arc, then it appears that compositional differences between the lavas of these adjacent volcanoes cannot be attributed to differences in pressure-(depth) dependent phase relationships in the down-going slab, or in the overlying mantle. Neither can these differences be attributed to mantle scavenging or zone refining models (e.g. Ninkovich and Hays, 1972; Best, 1975), which depend on the length of mantle traversed, the thickness of the mantle-wedge being the same for each volcano.

In considering the origin of both island arc and continental potassic suites, models must account for three particular features common to both these groups:

1. The extreme enrichment of LIL elements in mafic, apparently "primary" leucititic lavas.
2. The variation in the levels of concentrations of these LIL elements in coeval suites of lavas, often erupted from closely adjacent volcanoes.
3. The variability of Sr isotopic composition and the general more radiogenic Sr of potassium-rich suites in general (e.g. Bell and Powell, 1969).

These factors suggest at least two stages in the evolution of compositional diversity amongst erupted suites in this sector of the Sunda Arc, as well as in similar suites from non-arc regions cited previously. The first of these causes enrichment of K, Rb, Sr and related elements in the primary melts supplying each series and possibly reflects variation in the source. The second results in the compositional variation within each series, and is probably one of fractional crystallisation that results in the depletion of MgO, CaO, Fe, Cr, Ni and Sc, enrichment of K_2O, Na_2O, Rb, Zr, and Nb trends of initial enrichment followed, in suites, by depletion of Al_2O_3, TiO_2, P_2O_5 and Sr. These two trends are illustrated as insets in figures 12.5B and 12.7 (trends A and B). This type of behaviour is analogous to that described by Appleton (1972) from suites showing differing levels of potassium enrichment from the Roman Province of Italy.

The key to the origin of the potassium-rich lavas and the diversity of suites from these provinces, would appear to be the nature of this first stage (A). In general this variation must either reflect variations in conditions of fusion of a source, or compositional variations in that source. If the latter is the case, then it implies at its simplest that heterogeneities have either developed by differentiation within the same general

source, or by the enrichment of this source by addition of components from a separate reservoir. Models which lead to differentiation of a single source include; the formation and segregation of small amounts of partial melt or various type of zone refining or mantle scavenging, while models requiring separate sources amount to mixing hypotheses. It is felt that evidence from the lavas from the Lombok-Sumbawa sector of the Sunda Arc supports the latter situation, the necessity for a two (at least) source mechanism resting on two factors:

1. The variation in Sr-isotopic composition between the calcalkaline and alkaline suites and the isotopic variability within the alkaline group itself.
2. The differences in the degree of enrichment of <u>different</u> incompatible elements between the various suites and between the calcalkaline and alkaline suites in particular.

Sr isotopic evidence either allows the alkaline leucitites to have originated from a source with Sr of mixed origin, the separate initial sources having Sr of different $^{87}Sr/^{86}Sr$ ratio, or by disequilibrium partial melting of a source with heterogeneous segregations of high Rb/Sr ratio and of significant and variable age (possibly phlogopite).

The relative behaviour of different incompatible elements however lends further insight to this problem of source character. The systematic enrichment of K, Rb and Sr (figure 12.5A-C), increasing Rb/Sr and K/Sr ratios and decreasing K/Rb ratios from the calcalkaline suite through the *ne*-trachybasalts and -trachyandesites, to the leucitites, suggests that the leucitites are enriched in these elements in the order Rb>K>Sr relative to the calcalkaline suite and that the *ne*-trachybasalt-trachyandesite group are intermediate between these two extremes.

While it is conceivable that these variations may be due to some combination of varying partial melting in the presence or absence of phlogopite and/or amphibole, the behaviour of incompatible elements of the

group Ti, P, Zr and Nb (figure 12.5D and figure 12.6) are more problematic. Bulk distribution coefficients of these elements with the possible exception of Ti are likely to be less than 1 for any combination of likely mantle minerals (ol, cpx, opx, garnet, amphibole, phlogopite, spinel). Therefore, if the high K_2O, Rb, Sr and LREE contents of the leucitites relative to the calcalkaline basalts, is the result of either small degrees of partial melting, mantle scavenging, zone refining, or remelting of segregations of early melts, then P, Zr and Nb should also show similar orders of enrichment. In fact, as illustrated by figures 12.5D and 12.6 the calcalkaline suite has markedly higher ratios of Ti, P, Nb and Zr to Rb and K (and Sr) than the alkaline lavas. This suggests that the source yielding the alkaline lavas has been supplied with additional K, Rb and Sr from a separate source, compared with its counterpart for the calcalkaline lavas and that the progressive enrichment through the three series described from this sector of the arc suggest a variable or progressive source enrichment.

This is further illustrated by the Rb-Zr variations shown in figure 12.8. As both these elements are incompatible, they are likely to show linear covariation during fractional crystallisation, plotting as lines which tend to extrapolate through the origin, with positive slopes, the magnitude of which depends on the initial Rb/Zr ratio of the parental liquid (except in the case of mica crystallisation, in which case the Rb/Sr ratios would be expected to decrease). In figure 12.8, the calcalkaline lavas from the Rindjani and the trachybasalts and trachyandesites from Tambora and Sangeang Api, show reasonable straight-line variations which would extrapolate through the origin, the former group having lower Rb/Zr ratios and hence a steeper slope. The leucitic lavas however, show very large variations in Rb content with relatively small Zr variation. As many

Figure 12.8

Variation of Zr v. Rb for all lavas analysed in this thesis from the Lombok-Sumbawa sector of the Sunda Arc.

Trend A-B illustrates the variation in Rb-Zr in the most magnesian members of each suite (symbols refer to the same samples as in figure 12.1) and show that while there is a very large variation (increase) in the concentration of Rb from the most mafic calcalkaline lavas (near A) to the most undersaturated leucitites (near B), this trend is accompanied by only very slight increase in Zr. Trends X, Y and Z show the variation of Rb and Zr within the more differentiated members of each suite (differentiation which is at least partly attributable to fractional crystallisation) and which shows that less mafic lavas from any single volcano tend to have similar Rb/Zr ratios to their most mafic members (parents ?). This suggests that at least during fractionation, Rb and Zr had similar and low, distribution coefficients.

This then suggests that the variation of Rb/Zr ratio between the mafic members of each suite (increasing from the calcalkaline lavas to the leucitites) either reflects marked differences in the distribution coefficients for Rb and Zr in the sources of the calcalkaline and leucitite suites, or that the leucitite source must have been relatively Rb-enriched compared to the calcalkaline source.

Figure 12.8

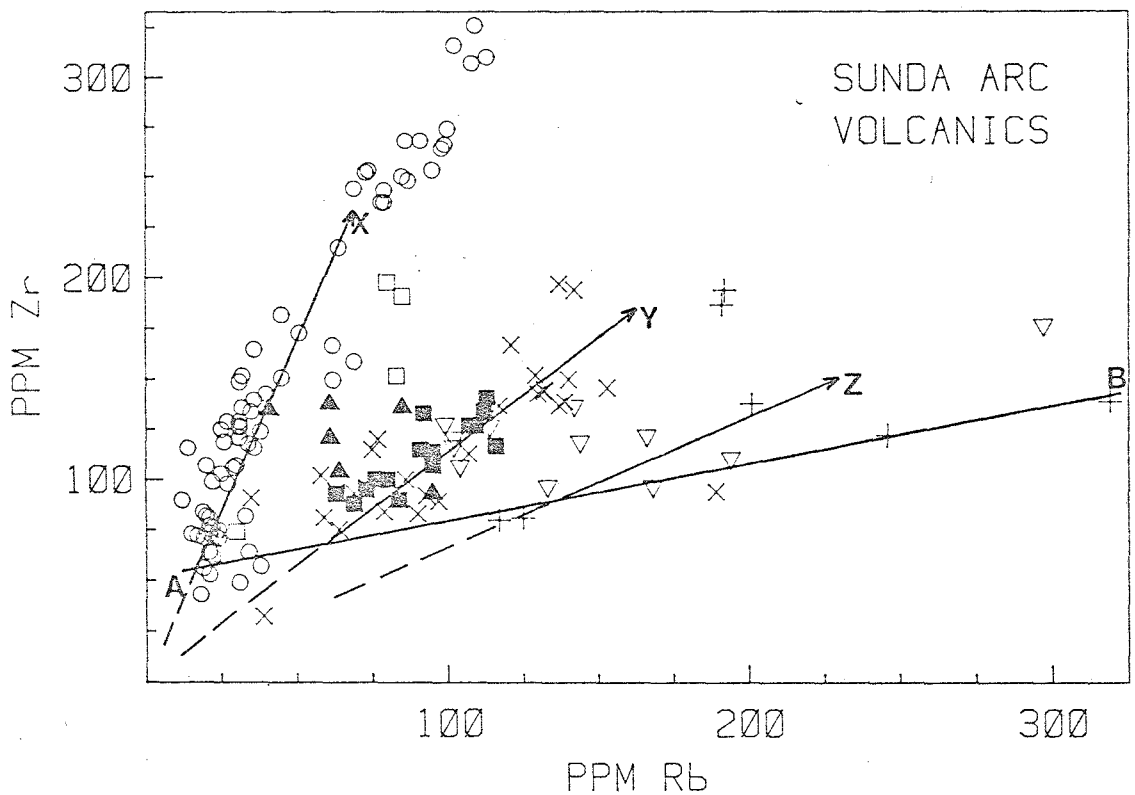
SUNDA ARC
VOLCANICS
PPM Zr
PPM Rb
300
200
100
100
200
300
A
X
Y
Z
B

of the leucitites have high Mg/Mg+Fe values (often >0.6), it seems likely they are relatively unfractionated. This then suggests that the variation in Rb/Zr ratio amongst many of the leucitic lavas is a primary feature and reflects variation in the source. This suggests a heterogeneous source, with a large variation in Rb content. The Rb-Zr variation trend of the leucitites extrapolates through the more mafic (low Rb, Zr) members of the other alkaline and calcalkaline suites and it may be suggested that this trend represents the variation of these elements in the primary liquids formed by partial melting of a source variably enriched in a Rb-rich component. Melting of a slightly enriched source yields calcalkaline liquids in the region of A in figure 12.8, while highly enriched source yields leucititic liquids in the region of B. Intermediate degrees of enrichment yields the less alkaline suites. Fractional crystallisation of primary liquids formed along this line A-B, would then show variation along lines passing through this line and the origin (as shown by the suites from Rindjani, Tambora and Sangeang Api).

These factors are compatible with models for the generation of potassium-rich lavas proposed by Lloyd and Bailey (1975), Appleton (1972) and Cox et al. (1977). They suggest that these lavas result from the partial fusion of mantle altered or metasomatised, by alkali-, LREE-, Sr^{87}-rich fluids or liquids. Lloyd and Bailey (1975) further amplified this general concept, by suggesting that the very potassic lavas resulted from partial melting of mantle metasomatised within the P/T field of phlogopite stability and more sodic varieties from regions of amphibole stability.

12.6 The Composition of Sources Yielding the Lavas from the Lombok-Sumbawa Sector of the Sunda Arc

In chapter 9 it was argued that the lavas, and in particular, the more mafic lavas, from this sector of the Sunda Arc, had a number of geochemical,

and some mineralogical features which were inconsistent with derivation by partial melting of either subducted oceanic lithosphere, or the oldest, Miocene crust of this region. Thus partly by process of elimination, this line of argument in fact only leaves the mantle wedge between the Benioff Zone and the base of the crust, beneath the arc, as the source for the liquids erupted as lavas in this sector of the arc. This was implied to be a peridotite source region, though there is no "concrete" evidence for this (for instance, no lherzolite nodules erupted by calcalkaline volcanoes from island arcs, have ever been reported).

Thus the situation is, that while it is strongly suspected that the primary magmas supplying the island arc volcanoes, at least in this sector of the Sunda Arc, are of mantle origin, there is no real evidence as to mantle mineralogy or geochemistry. If this mantle is not of the commonly accepted spinel or garnet lherzolite with olivine about Fo90, which represents the source for many intraplate, basalt-dominated volcanic provinces, then any constraints which might exist for the recognition of primary magmas are weakened. This in turn means that arguments about the extent to which fractional crystallisation must have been involved in the production of more differentiated lavas, may also be faulty. For instance, if the mantle was not as magnesian or as olivine-rich as generally assumed, then andesites with low Mg/Mg+Fe may indeed be potential direct mantle derivatives. With presently available data such a model is difficult to evaluate because of the very fact that if the composition of the mantle is unknown, then the composition of the liquids it can produce must be equally unknown. Nicholls' (1974) and others' model of a mantle modified by the intrusion of pyroxenite diapirs, themselves produced by melting above the Benioff Zone, which may provide silicic melts and water, is perhaps an example of the type of process

which can profoundly modify the typical lherzolitic mantle. The precise geochemical character of liquids formed by later stage melting of these diapirs would be very difficult to predict with any confidence.

Perhaps the best approach is to assume the lavas have fractionated from primary melts derived from a "typical" olivine-rich peridotite mantle and on this basis: (a) take, for instance, one of the more mafic high-Al basalts from the Rindjani calcalkaline suite and reverse the assumed fractional crystallisation scheme to yield a composition which, on the grounds of $Mg/Mg+Fe^{++}$ ratio and Ni content, might be a potential primary melt for a peridotite mantle source; (b) calculate the trace element content of such a hypothetical melt; (c) assume a simple peridotite source mineralogy and a "reasonable" degree of melting and on this basis calculate the trace element content of such a source. How reasonable this model is could be judged by comparison with sources calculated for suites from non-arc environments. It would then be possible to use this source to evaluate whether or not the leucitites could be derived from a similar source. While such a series of assumptions, arguments and calculations are unlikely to prove whether or not the lavas of this sector of the arc are derivatives of peridotite mantle, they will allow some estimation of the geochemical composition and compositional variation of such a source, if indeed it is the correct one.

In chapter 9 (section 9.6-2) it was shown that the *ne*-normative, high-Al basalts from Rindjani are not unlike alkali-olivine basalt-hawaiite lavas from many intraplate basalt provinces. Also, while these Rindjani lavas are not likely to be primary mantle melts, there is evidence that olivine-dominated fractionation has occurred. Thus a close approximation to Frey, Green and Roy's (1978), lherzolite-bearing, primary alkali olivine basalt,

Table 12.2

Calculated Trace Element Concentration of a Possible Peridotite Source to Rindjani Basalt 41632 Compared with that Capable of Yielding a Victorian Alkali Basalt

	A	x chond.	B	x chond.
La	2.60	8.26	2.43	7.7
Ce	5.76	7.08	5.12	6.3
Nd	3.22	5.39	2.75	4.6
Sm	0.69	3.64	0.80	4.2
Eu	0.223	3.10	0.29	4.1
Gd	0.697	2.69	-	-
Tb	-	-	0.14	2.95
Dy	0.699	2.15	-	-
Ho	0.153	2.10	0.19	2.65
Yb	0.547	2.63	0.57	2.75
Y	3.84	1.92	5.25	2.62
U	0.21		0.13	
Th	0.66		0.34	
Hf	0.46		0.36	
Ba	102		41.4	
Cs	0.02		-	
Rb	2.01		3	
Sv	50.0		74	
Zr	8.49		18	
Ni	4363		1603	
Sc	29.5		23.5	
% K_2O	0.129		0.129	
% P_2O_5	0.027	0.056		
% TiO_2	0.18		0.3-0.4	

A. A potential peridotite source capable of yielding the calculated primary melt whose composition is given in table 9.8 (41632 + 20% (.8 Ol + .2 cpx)) by 12% partial melting. Mantle mode: .15 cpx, .25 opx, .60 Ol. Melt proportions: 0.5 cpx, .25 opx, .25 ol.

B. A peridotite source which yields Frey et al's (1978) primary alkali basalt (69-1036) (table 9.8) by their 11% partial melt model leaving a residue of 63% olivine, 22.5% Opx, 9.5% Cpx, 5% Garnet.

Notes: Composition A was calculated using the trace element concentrations of Col. A, table 9.8 and utilizing equation 15 of Shaw (1970) ("batch melting") - $\frac{Cl}{Co} = \frac{1}{Do + F(1-P)}$. Distribution coefficients are given in table 9.1 (cpx col. 1, opx col. 4, ol col. 6). K_2O was calculated using the same K_D as Rb, while P_2O_5 was calculated using those of Sr. TiO_2 was calculated using the same distribution coefficients as for the HREE.

69-1036, from Mt. Frazer, Victoria, was achieved by addition of 20% of an assemblage of 80% olivine and 20% cpx. The major and trace element composition of this calculated possible primary liquid were given in table 9.8, together with values from the Victorian example and the REE patterns are plotted in figure 12.9.

The similarity of the calculated primary liquid and the lherzolite-bearing, Victorian example are possible empirical evidence that the Rindjani basalt may have originated by melting of a relatively typical peridotite source.

The most significant differences between the two compositions are the markedly lower TiO_2, P_2O_5 and Zr concentrations in the composition calculated from the island arc basalt, these being less than half the concentrations in the Victorian basalt. In addition Ba is twice as abundant in the composition calculated from the island arc basalt. Ba enrichment relative to the LREE is apparently a characteristic feature of island arc lavas (e.g. Sun and Hanson, 1976), as are the low Ti, Zr and P concentrations.

Taking this calculated "primary melt" composition, assuming a simple mantle assemblage (60% olivine, 25% opx and 15% cpx) and using Shaw's (1970) "batch melting" equation, the trace element composition of a possible peridotite mantle which could yield the trace element concentrations of the hypothetical parent magma to basalt 41632, by 12% partial melting, was calculated. It was assumed that the phases contributed to the liquid in the proportions; cpx 50%, olivine 25% and opx 25%. Distribution coefficients used in this calculation are given in table 12.2 and 9.1 and the resultant trace element concentrations are given in table 12.2 together with the concentrations of the same elements required to yield Frey et al.'s (1978) alkali olivine basalt 69-1036, by their preferred 11% partial melt model.

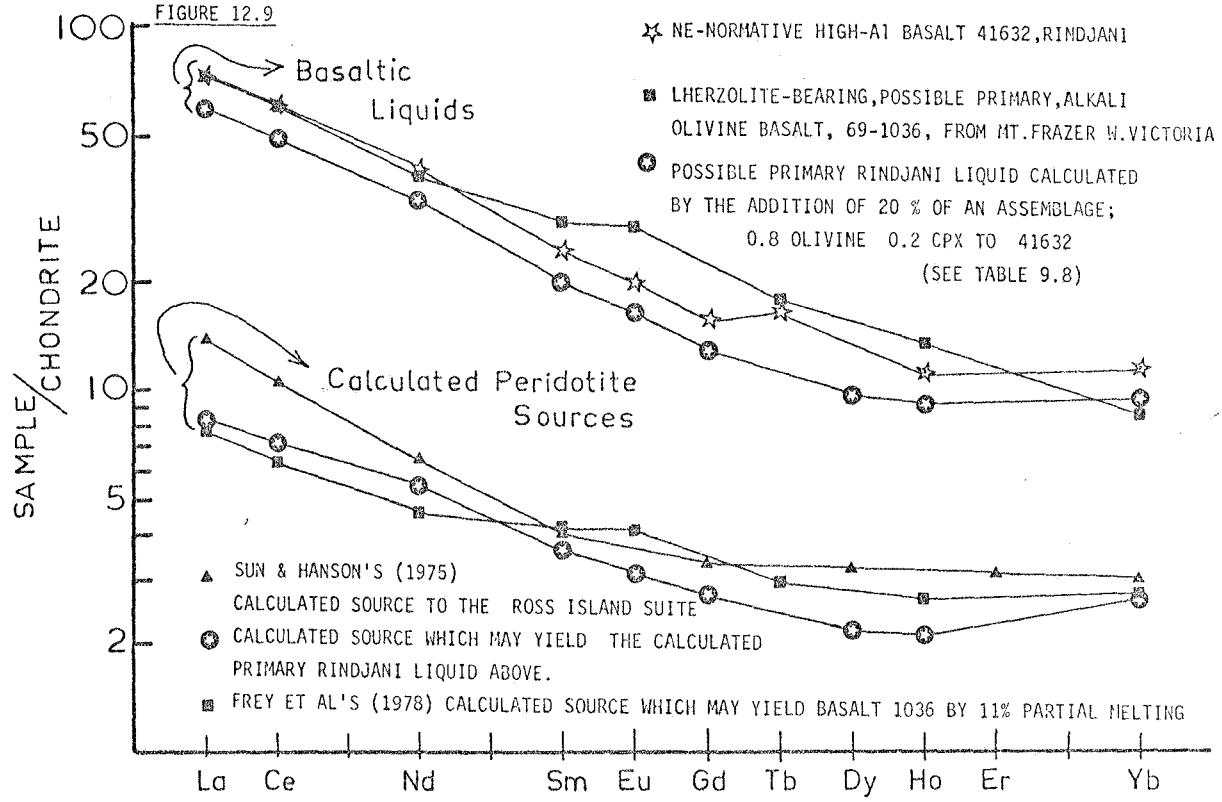

FIGURE 12.9

REE patterns of Rindjani ne-normative High-Al basalt 41632 (☆),the possible primary liquid calculated from this (◎) by the addition of 20% (0.8 Ol 0.2 Cpx, see table 9.8) and one of Frey et al (1978) possible primary alkali olivine basalts (69-1036) from Mt.Frazer W.Victoria (■).

Also shown are possible (calculated) peridotite sources which may yield the above basalt liquids and the Ross Island basanitoids (Sun and Hanson,1975)..The possible source to the Rindjani basalt (◎) was calculated from the calculated primary liquid above assuming 12% partial melting,a mantle assemblage comprising 0.15 cpx,0.25 opx and 0.6 ol,melting in the proportions 0.5 cpx,0.25 opx, 0.25 ol,using Shaw's (1970) "batch melting" equation (15) and the distribution coefficients in table 9.1 (see table 12.2). Frey et al's(1978) source was calculated using an 11% partial melt of a mantle leaving a residue composed of 63% olivine,22.5% opx,9.5% cpx and 5% garnet.

The REE patterns (figure 12.9) for both these sources are very similar, in both cases having about 8x chondritic LREE and 2-3 x chondritic HREE concentrations. Such a mantle REE pattern has also been proposed by Sun and Hanson (1975) as a source for the Ross Island basanitoids and their calculated pattern is also included in figure 12.9. This type of relatively "fertile" mantle is also implied by Varne and Graham's (1971) data on the hornblende lherzolite nodule from Ataq.

There is reasonable similarity between the calculated mantle trace element contents of this hypothetical island arc source and that for the Victorian basalt. In particular, K_2O, Rb, Sr, REE and Sc concentrations are very similar. Again, however, TiO_2, Zr and P_2O_5 concentrations are much lower. Ti was calculated using distribution coefficients similar to those of the HREE, following the suggestion of Sun and Hanson (1975), and the resultant source has 0.18% TiO_2, which is half that calculated to be present in the source to the Victorian basalts. Perhaps significantly, Frey et al. (1978) point out that the 0.3-0.4% TiO_2 required to yield the Victorian basalts is markedly less than the 0.7% required to yield the Hawaiian basalts. Zr distribution coefficients are not well known though this element is generally taken to be incompatible with respect to olivine, pyroxenes, plagioclase, garnet and spinel. Frey et al. (1978) suggest that Zr has a bulk distribution coefficient of about 0.05 with respect to their mantle mineralogies. McCallum and Charette (1978) determined D(Zr) cpx/liq. = 0.05-0.22, which is consistent with the bulk distribution factor quoted above, and this figure was used to calculate the Zr concentration in table 12.2. However even if the Zr distribution coefficient for cpx/liquid was taken to be as high as that of the HREE, ≈0.7, then this would still only yield a mantle with about 13 ppm Zr using this model, which is still very markedly less than the 18 ppm required to yield the Victorian basalt.

In view of this it would appear, assuming a peridotite mantle source is correct, unless some unknown phase which has a Zr distribution coefficient considerably >1 is residual after melting, that the source yielding island arc lavas must be Zr-deficient relative to source regions supplying intraplate volcanoes. The same may also apply to Ti, P and Nb.

The main conclusion from these calculations, apart from the reservations mentioned above, is that they do allow a relatively typical peridotite-type mantle to yield arc basalts of the type represented by 41632. This approach was extended a step further by considering the capacity of such a mantle as that just calculated, to yield the very alkaline leucite-bearing volcanics from Sumbawa.

Factors discussed in section 12.5 suggested that:

1. either the source for the leucitites is enriched in Rb, K and Sr but not in Zr, Ti, Nb or P, relative to that of the calcalkaline lavas, or
2. that the bulk distribution coefficients must be markedly different during the fusion and segregation of the leucitite melts from their source compared with the situation for the calcalkaline melts (i.e. the Ti, Zr, Nb and P group of elements must be retained in the leucitite source to a much greater extent than the calcalkaline source and the relative enrichment of K, Rb and Sr in the former group then being due to smaller degrees of partial fusion). This in turn implies that the source is mineralogically heterogeneous, while the first suggestion implied geochemical heterogeneity. Perhaps the most reasonable suggestion would be a combination of both of the above.

An approximate estimate of the parental melt to the leucitite series was achieved by averaging the compositions of all members of this series from Soromundi and G. Sangenges which had Mg/Mg+Fe values >0.61. The

concentration of Rb, Sr, Zr, K_2O, TiO_2 and P_2O_5 in this average composition is given in table 12.3, together with the concentrations of these elements calculated for the hypothetical parent magma to the Rindjani calcalkaline basalt 41632. The ratios of these elements (leucitite/calcalkaline parent) are also given and indicate an order of enrichment $Rb>K_2O>Sr>P_2O_5>Zr>TiO_2$, actual enrichment factors ranging from 9.2 to about 1.

If the leucitites result from melting of the same hypothetical peridotite source as calculated to yield the calcalkaline basalt 41632, then the 2 ppm Rb of this source would require that the leucitites, with an average of 147 ppm Rb, must have originated by 0.3% partial melting. This assumes the same low distribution coefficients used in calculating the source to the Rindjani basalt. At such small proportions of melting it may be reasonable to assume that a Rb-bearing phase like phlogopite may be present in the residue, which in turn would result in a higher bulk Rb distribution coefficient. This would then mean that the 0.3% partial melt figure quoted above is in fact a maximum. Such small amounts of partial melting seem highly improbable as the chance of such a small amount of liquid escaping from the source must be very small. Furthermore even if the highest D(Zr) cpx/liq value of 0.22 determined by McCallum and Charette (1978) is adopted, the 0.3% partial melt figure calculated from the Rb concentration, still yields a melt with 200 ppm Zr if the same Zr concentration as that calculated for the calcalkaline source is used. This is twice the Zr concentration of the leucitite. It would therefore appear that at least with respect to the Rb concentration of their respective sources, that the leucitite source must be Rb-enriched with respect to the calcalkaline source.

In the previous section the lack of enrichment of Zr relative to Rb, Sr and K_2O was taken to indicate that either Zr had a similar concentration in the source of both the leucitite- and calcalkaline-series, or that the

Table 12.3

Comparison of the Average Mafic Leucitite Composition and the Calculated Rindjani, high-Al Basalt Primary Melt

	A	B
SiO_2	45.79	48.47
Al_2O_3	12.06	14.63
FeO_T	10.74	10.75
MgO	10.05	12.15
CaO	14.17	8.65
Na_2O	2.27	2.94
K_2O	3.14	0.97
TiO_2	0.95	0.92
P_2O_5	0.45	0.20
MnO	0.18	0.16
Mg/Mg+Fe	0.64	0.70
Rb	147	16
Sr	957	365
Zr	102	67
Y	21	16.5
Sc	45	33
Nb	7	-

A. Average of the four most mafic leucitites from G. Sangenges and G. Soromundi (S23, Si17, Si16, Si6).

B. Calculated primary, parental magma to Rindjani high-Al basalt 41632 (table 9.8).

Average leucitite/41632 parent.

Rb	9.2
K_2O	3.2
Sr	2.6
P_2O_5	2.2
Zr	1.5
Sc	1.4
Y	1.3
TiO_2	1.03

Note: FeO_T = total Fe as FeO.

ratio of for instance Rb/Zr is the same in both sources, but that bulk distribution coefficients for Zr must be much higher in the leucitite source.

Assuming the first hypothesis, then the Zr concentration of the average leucitite (table 12.3) is about 1.5 times that of the calculated calcalkaline source. Thus if the sources of both series are assumed to have the same concentration of Zr (9 ppm) and if the same distribution coefficients as used to calculate the Rindjani source are used, then this suggests that the leucitites resulted from about 7% partial melting. This seems a much more reasonable figure than that based on Rb (<0.3%). If the 7% melting figure is taken as reasonable, then this implies that such a source must have 11.4 ppm Rb to yield the 147 ppm Rb concentration in the average leucitite. This is about 6x the concentration of Rb calculated for the calcalkaline source and assumes the same distribution coefficients. Again these distribution coefficients are probably a lower limit and if a minor (~1%) Rb-bearing phase (e.g. phlogopite) is residual in the source and assumed to have a Rb K_D of about 3-4, then such a source would require about 16 ppm Rb to yield the leucitite liquid with 147 ppm Rb. The other LIL elements, K and Sr, show less marked enrichment than Rb in the leucitite series lavas and on the basis of the above model would also be enriched in the leucitite source compared with Zr, but less so than Rb.

These models demonstrate that:

1. The trace element geochemistry of calcalkaline, high-Al basalts from Rindjani, is not inconsistent with an origin involving partial melting of olivine-rich two pyroxene peridotite mantle, which has trace element concentrations similar to that which might yield slightly undersaturated basalts in non-arc tectonic regimes. It would appear however that unless some hypothetical phase remaining in the residue after melting

has taken place, retains Ti, Zr, Nb and P, that this source must be depleted in these elements relative to source mantles in other non-arc provinces.

2. It also appears that the same hypothetical mantle source is unable to yield the calcalkaline basalts and the much more LIL element enriched leucitites. The latter group require a source which is enriched in Rb, Sr and K relative to the calcalkaline one, but may have approximately the same concentrations of Zr, Ti, P and Nb.

In general it must be conceded that point 1 above is not real proof that the lavas have originated by melting of a lherzolitic mantle and merely allows the possibility. However it seems likely that point 2 is valid whatever the source. Furthermore the previously described differences in Sr-isotopic composition between the calcalkaline and leucitite suites, the latter being more radiogenic, may also be evidence of geochemical heterogeneity and also support the implied relatively Rb-enriched character of the leucitite source.

If the calculations suggest that the leucitites have resulted from melting of a source which, relative to that which yielded the calcalkaline series, has been enriched in LIL elements, then the *ne*-normative, trachy-basalt, -trachyandesite suites which form an intermediate series between the calcalkaline- and leucitite series may have resulted from melting of a source which has undergone an intermediate degree of enrichment. Further, as discussed in chapter 9 and in section 12.2 (this chapter), some compositional variation within suites from individual volcanoes is not attributable to fractional crystallisation. Lava B43 from the Sangeang Api suite was found to have LIL element concentrations about 30% higher than levels predicted on the basis of other major element concentrations as well as

having a more fractionated REE pattern and more radiogenic Sr. It is possible therefore that this type of variation is also attributable to the same factors which yield the larger-scale, between-suite variation. If the lavas erupted by an individual volcanoe over a relatively short time span are tapping source regions which themselves are variably enriched in LIL elements, then this tends to suggest that mantle heterogeneities are of small scale.

If this model of a mantle source region, variably enriched in certain trace- and minor-elements, is correct, it is interesting to speculate on the likely nature of the island arc source prior to its apparent secondary enrichment. Does the calcalkaline series, for instance, result from melting of the "normal" mantle beneath the arc? or has the source for this series also undergone some enrichment? Furthermore what is the source of the apparently, Rb-, K- and Sr-rich, Ti-, Zr-, Nb- and P-poor component, which has brought about this enrichment process? These problems are speculated upon in the final section of this chapter.

12.7 The Origin of Primary Geochemical Diversity in the Context of the General Arc Model

The results of this study yield several important conclusions:

1. The concentrations of K_2O and related elements in coeval island arc suites need not correlate with the depth to the active Benioff Zone, or be related to the stage of temporal evolution of a particular arc.
2. Geochemical differences between calcalkaline lavas and more alkaline types, ranging from *ne*-trachybasalts through to mafic leucitites, reflect actual differences in the composition of the mantle source region. Certain LIL elements are selectively enriched and this fact together with the differences in the isotopic composition of Sr, suggests a two source mechanism rather than one invoking differentiation within a single source.

3. Compositions of the leucititic lavas from Sumbawa are very like those from continental rift localities and this comparison is further enhanced by the occurrence, in both situations, of discrete suites of volcanics showing varying degrees of undersaturation and alkalinity, suggesting that some petrogenetic process may be common to both environments.

4. While potassium-rich suites from convergent plate boundaries and continental rifts do have common features, those of the latter group maintain their arc character in having much lower concentrations of Ti, Zr, Nb and P.

Several questions arise from these conclusions:

(i) If the lavas in this sector of the Sunda Arc are in fact derived by partial melting of a peridotite source which is heterogeneous with respect to LIL elements, Sr isotopic composition and possibly LREE, Th and U, to what extent is the composition of this mantle due to the introduction of these elements and what is the "normal" abundance of these elements in the source prior to the development of heterogeneities?

(ii) What is the source of the introduced elements and by what means are these introduced?

(iii) If the type of compositional variation seen between adjacent volcanoes in this sector of the Sunda Arc is equivalent to the across-arc, Benioff Zone-correlated variation seen in other arcs, then why is there an apparent uncoupling of this relationship in this sector of this arc?

(iv) If the apparent low abundance of Zr, Ti, Nb and P in the hypothetical peridotite source is real, what is its origin?

The general concept of a mobile, incompatible element-enriched, "fluid" or melt, with trace element concentrations similar to olivine melilite, kimberlite or carbonatite, has been invoked in a number of studies as a significant contributor to peridotite sources yielding alkaline basalt suites. Such a component has been recognised in lherzolite nodules from continental basalt suites (Frey and Green, 1974) and has also been invoked as a source of mantle heterogeneities required to account for the range of basalt-types (olivine tholeiite to olivine melilitite) from the same suites (Frey et al., 1978); Lopez-Escobar et al. (1977). If such a component is being supplied to the source of the island arc volcanic rocks, then the problem is, what is the geometry of the total system? How is this component being supplied and to what extent does its supply determine the time-space-volcanic composition relationship recognised in many arcs?

Sun and Hanson (1975a) and others suggest that the MORB series is derived from melting of shallow level, depleted mantle, while more alkaline ocean island volcanoes tap a more "fertile" mantle source beneath this. They suggest that the type of mantle convective system in the oceanic basins maintains this geometry. However, as Gill (1976) points out, differences between ocean ridge tholeiites and more alkaline ocean island basalts are similar to differences between lavas which in the "typical" island arc, occur close to, and further away from, the trench. He suggests that while it is likely that these lavas are of mantle origin, the presence of the subduction zone isolates the mantle wedge, beneath the island arc, from the active convection cell of the ocean basin. Gill (ibid) therefore implied that the island arc situation would now allow the tapping of Sun and Hanson's (1975a) two reservoirs. Gill (1976) went on to suggest that arc magmas acquire their compositional diversity by different degrees of fusion and

as a result of the presence of different residual mineral assemblages. It has already been argued in earlier sections of this chapter however, that it is more likely that compositional differences in erupted suites relate to real source heterogeneities. At the same time, however, it seems likely that the geometry of the arc-mantle wedge-Benioff Zone system and its relatively small scale compared with the broad ocean basins, place doubt on the applicability of Sun and Hanson's (1975a) mechanism, even though the end result and general two-reservoir concept may be the same.

To arrive at a solution to the problem of how a two source model may be fitted to the island arc situation, requires knowledge of the origin of the arc itself and in particular, the origin and nature of the mantle wedge, effectively "trapped" on the continental side of the Benioff Zone.

This sector of the Sunda Arc, as discussed in chapter 2, is probably formed on thin, oceanic-type crust. Evidence was also presented in chapter 2, that the segment of the Sunda Arc-trench system to the east of eastern Java, is probably no older than Miocene and prior to this an earlier (Mesozoic?) arc system may have been active along a belt from Sumatra and western Java, northwards to Kalimantan and Sulawesi. This suggests that the area to the north of the present-day Lombok-Flores segment of the Sunda Arc, may have, up until the Miocene, been on the ocean-ward side of the then trench. The present trench-arc system, might then have developed, extending in a more easterly direction from the west Java segment of the older arc, stranding a fragment of oceanic crust and upper mantle, on the southern edge of which, Lombok and Sumbawa were to become established.

Jurassic-Cretaceous sea floor is currently undergoing subduction beneath this sector of the arc and if the above scenario is correct, then the islands of Lombok and Sumbawa must be overlying Jurassic ocean crust.

How an arc becomes established in the first place, is not well understood. It may be considered to result from initial buckling and downwarping of oceanic crust near to a continental margin, followed by fracturing and underthrusting. The mantle on the continental side of the trench would then be the same as the upper mantle of the ocean basins, and may well represent the same source region that yielded the MORB series at the ridge, having migrated to its present position as a consequence of sea floor spreading. If this were the case then the source region of island arc lavas is likely to have some of the geochemical and mineralogical characteristics of the depleted MORB source. The island arc tholeiite series (e.g. Jakes and Gill, 1970) is an example of an arc suite having geochemical features consistent with derivation from an incompatible element-depleted source such as that of the ocean ridge tholeiites.

Mid-ocean ridge tholeiites are considered to have formed by relatively large amounts of melting of depleted peridotite, at shallow depths (e.g. Green, 1971), leaving a refractory harzburgite residue. The geochemistry of MORB (e.g. Sun et al., 1978) reflects a source which has low concentrations of LIL elements as well as other incompatible elements, such as Ti, Zr, Nb, P and LREE. If such a mantle does in fact represent that "stranded" on the continental side of the Benioff Zone, beneath island arcs, then the low Ti, Nb, Zr and P concentrations of island arc lavas in general, could reflect the low abundances of these elements in the source which is the same as that which yielded ocean ridge basalts at the spreading centres.

Of course, in the state that this source left the ocean ridge, it would be quite incapable of yielding any island arc series with the possible exception of the arc tholeiites. It is interesting to consider such a source in the light of the conclusion reached earlier in this chapter, that at

least relative to the calcalkaline source, the source yielding the alkaline lavas in this arc is probably relatively enriched in LIL elements. In view of the very refractory, depleted nature of the MORB-type source suggested above, it would also be necessary to conclude that the calcalkaline arc series, must also represent the products of a re-enriched source and that in its "natural state", the mantle beneath the island arc must only have trace element concentrations capable of yielding the island arc tholeiite series.

In summary, this model implies that refractory, depleted, harzburgite is delivered to the site of the island arc by ocean floor spreading, where it becomes isolated from the convective system operating in the ocean basin. This peridotite would have very low concentrations of LIL elements, Ti, Zr, Nb and P as well as a LREE-depleted character. Once isolated as the mantle wedge beneath the island arc it would be supplied with small amounts of LIL element-and LREE-rich liquid, which would systematically "rejuvenate" the refractory peridotite, enabling it to then yield the range of calcalkaline and more alkaline island arc lavas. A similar model has been proposed by Green (1976) Lopez Escobar et al., (1977). The component enriching the arc source region would be supplied from depth and would have the greatest effect on the deepest zones of the subarc mantle. In this sector of the Sunda Arc, seismic evidence (Cardwell and Isacks, 1978) suggests that between the trench and the zone of active volcanoes, the dip of the Benioff Zone is very shallow, while further from the trench it becomes near-vertical, plunging to nearly 700 km. Thus mantle zones overlying the very deep Benioff Zone might be relatively easily supplied with the "enriching component", while the narrow wedge closer to the trench would be more effectively shielded by the subducting slab.

If this "enriching component" is assumed to be of kimberlitic affinity, supplied from depths of the order of 700 km, then it may have left residual minerals including: garnet, perovskite, ilmenite, rutile, sphene and apatite, which may retain Ti, P,, Nb, Zr and the HREE. Thus while the mantle becomes enriched in the LIL elements, it retains its depleted character with respect to the elements mentioned above.

A possible explanation of the fact that in the Sumbawa-Lombok sector of this arc, both calcalkaline and highly alkaline lavas have erupted from adjacent volcanoes at similar height above the Benioff Zone, may be a direct tapping of the alkaline reservoir by some large scale fracture or fault. In support of this model as a general mechanism for the generation of alkaline suites in island arcs, is the observation of Delong et al. (1975), that a number of arc-alkaline suites are associated with cross-arc structures. It has been suggested that some form of transcurrent fracture has dislocated the Sunda Arc between the eastern end of Sumbawa and Flores island, because there is an apparent offset in the line of active volcanoes between these two islands (Audley Charles', 1975, "Sumba Fracture"). This hypothetical fracture may then represent a conduit, tapping the source of the alkaline liquids and allowing their access to shallow regions of the mantle adjacent to the fracture.

If the general arc case, where increasing alkalinity occurs both with time and distance from the trench, results from systematic alteration of the mantle by the proposed alkali-rich component, then it is possible that the Benioff Zone itself actually represents the conduit for the transport and delivery of this component.

This hypothesis is supported by calculations performed by Ito (1978), who suggests that the slip zone between the descending slab and the overlying mantle is in fact a low-viscosity, low density liquid layer, which tends to flow upwards along the mantle-slab interface. He also suggests that at

depth in the asthenosphere, any separate liquid phase adjacent to the slab, may be drawn into the slip zone and then move upwards. He also suggested that the dissipation of gravitational energy at the bottom of the downward edge of the slab may produce local melting, this liquid again rising up the slip zone. By these means, both a possible source of the products of small amounts of partial fusion and a means by which they may be supplied to the mantle at shallower depths and closer to the trench, are provided.

It is possible then, that the alkali-rich melt phase in the slip-zone, may both move up the slab and percolate vertically into the overlying mantle, the latter situation probably being favoured by a decrease in dip of the slab. Where upward percolation takes place, alteration of the overlying mantle is likely, as the alkali-rich liquid reacts with olivine and pyroxene to yield mica- and hornblende-peridotite. This altered mantle may then in turn melt to yield the lavas eventually erupted at the surface. In this way, the largest amounts of the alkali-rich component would be supplied to the mantle overlying the deepest parts of the Benioff Zone, with progressively smaller amounts reaching the shallower regions, hence yielding progressively less enriched mantle towards the shallower Benioff Zone regions. It is possible, then, as suggested previously, that completely unenriched mantle would yield the arc tholeiite series on partial melting and that the spectrum of all other arc-suites, from calcalkaline through to the highly undersaturated alkaline varieties, are derived from initially depleted mantle with varying amounts of newly introduced alkaline component.

In fact this mechanism may not be very different to the situation in continental rifts. In both situations dislocations of the crust and upper mantle allow the tapping of kimberlite-like melts from depth. In the rift situation, these may produce alteration of the higher levels of the mantle as suggested by Lloyd and Bailey (1975), this later melting to yield a range of lavas of differing alkalinity, or the kimberlitic material may

erupt directly to form kimberlite pipes or carbonatitic volcanoes. The main differences between this situation and that in the island arc are that, the "fault" (= Benioff Zone) is inclined in the latter case while the rifts are bounded by near-vertical faults, so that in the arc situation, the alkaline component is effectively "sieved" through the overlying mantle wedge and has much less chance of being delivered directly to the surface and secondly the mantle underlying the rifts does not have the initially depleted character of that under the arcs, thus accounting for differences in Ti, Zr, Nb and P between the two situations.

Chapter 13

CONCLUSIONS

13.1 Summary

Most of the main results and conclusions have already been summarised in previous chapters, and it is not proposed to repeat them here. These summaries appear in sections 2.4, 3.5, 5.7, 8.9, 9.5, 9.7, 9.11, 9.13, 10.6, 11.12 and 12.7. The petrographic features of the rocks of the five volcanoes studied are summarized in chapter 7.

Stated briefly, the most important conclusions of this study are:

1. Magmas erupted from volcanoes in the Lombok-Sumbawa sector of the Sunda arc seem to be derived mainly from melting of the mantle wedge above the Benioff Zone and there is little participation of material from the downgoing slab or the lower crust beneath the arc, although water may be derived from dehydration of the slab.
2. If this mantle wedge beneath the arc is of peridotite composition dominated by forsteritic olivine (Fo 90), then most of the lavas from the five volcanoes studied are fractionated (with the possible exception of some leucitites).

Fractional crystallisation is probably an important mechanism in the generation of much of the compositional diversity found within suites from individual volcanoes. However some of the variation found within some suites must also be due to variation in primary melt composition. Likewise fractional crystallisation cannot account for compositional variation between the different suites erupted by adjacent volcanoes in this sector of the arc. Thus the differences between the three recognised suites (1. the calcalkaline suite, 2. the *ne*-trachybasalt-trachyandesite suite and 3. the leucitite suite) also require variation in primary melt composition.

3. If the mantle is of a more iron-rich composition then a greater range of the erupted lavas may be primary melts, but the available data do not allow this possibility to be accurately evaluated.

4. Where recognised, fractionation trends are largely attributable to crystallisation in the low pressure region (<10kb) corresponding to uppermost mantle and crustal depths.

5. Primary basaltic liquids were probably hydrous, with perhaps 2-3% H_2O, and the crystallisation behaviour of water-bearing melts is probably responsible for a large part of the distinctive character of island arc magmatism, particularly that of the calcalkaline suite. Thus the MgO-, Ni- and Cr-poor and Al_2O_3-, CaO- and plagioclase-rich character of many island arc lavas can be explained as the result of the effect of water in retarding the precipitation of plagioclase relative to clinopyroxene and olivine until very low pressures.

6. The Rindjani suite is typical of the calcalkaline suites of many island arcs. Calculations suggest that the high-Al basalts could be derived from primary melts of mantle origin by olivine-clinopyroxene fractionation, and that variation within the group of high-Al basalts could arise from fractionation of their plagioclase-olivine-clinopyroxene phenocryst assemblages. Fractionation of this phenocryst assemblage could not yield andesitic differentiates.

The compositional variation within the Rindjani andesites cannot be reproduced by fractional crystallisation of their plagioclase-clinopyroxene-orthopyroxene-magnetite phenocryst assemblages. The dacites however may have been liquids in equilibrium with this phenocryst assemblage.

If the andesites are derived from basaltic parents like the associated high-Al basalts by fractional crystallisation, then they may have resulted from crystallisation of an amphibole-plagioclase-magnetite-dominated assemblage.

Phase relationships in the high-Al basalt-water system place constraints on the conditions of andesite formation. Optimum conditions under which the assemblage amphibole-plagioclase-magnetite may coexist, closest to the basalt liquidus, occur with 3% H_2O, between 6 and 10 kbars and with an fO_2 between that of the NNO and HMN buffers. Under these conditions this assemblage may coexist up to about 1050-1060^oC. This is still likely to be 50^oC below the basalt liquidus and to yield andesitic differentiates, mantle derived parent basalts must cool markedly in the pressure-range 6-10 kbars, a depth corresponding to the probable depth to the Moho in this sector of the Sunda arc.

Under the above conditions andesitic residual liquids may form from basaltic parents in equilibrium with an amphibole-plagioclase-magnetite assemblage. These may then rise and crystallise the observed plagioclase-rich phenocryst assemblages at lower pressures. At very shallow depths, water saturat may occur, resulting in explosive eruption, during which segregation of the small amounts of siliceous residual liquid could take place to yield the dacites. If the parental basaltic liquids do not cool sufficiently at depth to enter the amphibole stability field, they will fractionate ol-cpx and then plag-cpx-ol assemblages to yield the range of ankaramites and high-Al basalts.

These results imply that those island arcs that are growing as a result of andesitic eruption at the surface are simultaneously growing downwards as a result of accretion of equivalent volumes of hornblende gabbro at their bases. This also implies that the total bulk composition of the arc continues to be basaltic, even where andesites are the dominant extrusive magma composition.

7. The K_2O content of coeval island arc suites need not show a positive correlation with the depth to the Benioff Zone, neither need the very K_2O-rich lavas occur late in the history of a given arc.

This suggests that in arcs where the depth to the Benioff Zone does show a significant correlation with the K_2O content of the lavas, this relationship must be an indirect one and that the K_2O content of the lavas is probably not determined by pressure-dependant phase relationships either in the down-going slab or the overlying mantle.

8. Geochemical differences between suites in the Lombok-Sumbawa sector of this arc, particularly in terms of variation in K, Rb and Sr, imply that marked geochemical heterogeneity exists in the mantle source region. This factor together with the systematic variation of these elements through the three suites distinguished in this arc sector, together with the Sr-isotopic variation, tends to suggest that a two (or more) end-member mixing or contamination event is responsible for the source heterogeneity. In such a case, the variation in the relative proportion of end-members results in the variation in the degree of alkalinity of the erupted suites.

9. Relative to suites from other tectonic environments all of these from this sector of the Sunda Arc have low concentrations of Ti, Zr, Nb and P. These show little variation between the different suites in spite of the large variation in the concentration of the LIL group of the incompatible elements.

Calculations show that even if the residue/liquid distribution coefficients for this group of elements, in the mantle source are anomalously high, this group of elements must still be relatively depleted by comparison with their concentrations in non-arc mantles. The K-, Rb- and Sr-enrichment process apparently did not produce enrichment of these small, highly charged ions, generally grouped with them as "incompatible elements".

10. If between-suite variation in K_2O- and related element concentration reflects variations in the concentrations of these elements in the source mantle, this then suggests that in arcs where a K_2O-Benioff Zone depth correlation does exist, the concentration of K_2O and related elements may systematically increase in the magma source region above successively greater Benioff Zone depths. Yet it has also been concluded that the relationship between K_2O content of the lavas and the Benioff Zone depth is an indirect one and therefore it is unlikely that the actual source of the K_2O-rich component is the Benioff Zone itself. A possible explanation of these factors is that the Benioff Zone represents a conduit along which the K_2O-rich component moves upwards from depth and from which is supplied to the overlying mantle. This rate of supply diminishes with decreasing Benioff Zone depth.

11. In the Sumbawa sector of this arc, the above situation may have been disturbed by the presence of some major cross-arc fault (possibly the hypothetical "Sumba Fracture") which passes across the arc between Sumbawa and Flores and has produced some possible relative northwards movement of Sumbawa and may have acted as more direct conduit which allowed the K_2O-rich component and more direct access to shallower regions of the mantle and effectively destroyed the "normal" correlation with Benioff Zone depth.

12. It is possible that, in those arcs where they occur, members of the arc tholeiite suite represent the products of melting of the source-region before the introduction of the K_2O-rich component. This suggests that the "normal" sub-arc mantle may be a very refractory, incompatible element-depleted peridotite. It is suggested that the source mantle beneath island arcs may have already yielded a basalt melt fraction

elsewhere, perhaps at an accretionary margin and then have reached its present position by sea floor spreading, becoming isolated from the mantle convection system of the ocean by the development of the subduction zone. Once isolated, this wedge of depleted peridotite is gradually "rejuvenated" by the introduction of the LIL element rich component. This component apparently does not contain significant concentrations of Ti, Zr, Nb, Hf and P; the low concentrations of these elements in the island arc lavas is a feature inherited from the prior depletion of the sub-arc mantle.

13. The mafic and ultramafic intrusive rocks from Sangeang Api may at least in part have a cumulate origin and the succession from olivine clinopyroxenite to hornblende gabbro does represent a possible crystallisation sequence with falling temperature and/or pressure. The compositional variation of the Sangeang Api lavas can be interpreted as resulting from fractional crystallisation of assemblages represented in the nodule suite. However variation in $^{87}Sr/^{86}Sr$ isotopic ratios in both the intrusives and extrusives suggests that the nodules probably record a more complex sequence of events than simple crystallisation of a single magma batch.

The marked similarity of the Sangeang Api nodules and the rock types represented in the Alaskan-type zoned ultramafic complexes, particularly in terms of their mineral assemblages and mineral compositions, suggests that these ultramafic bodies may be formed in an island arc environment.

Irvine (1973, 1974) suggested that the Alaskan bodies were formed by precipitation from relatively alkaline, mafic magmas like those erupted by Sangeang Api volcano.

The assemblages present in the Sangeang Api nodule-suite are also like those inferred to have crystallised from the calcalkaline magmas to yield the sequence of basalts and andesites from basaltic parents, though the assemblages precipitated from the less alkaline calcalkaline

liquids may differ in detail. For instance the amphiboles may be less potassic, phlogopite may be rare or absent and orthopyroxene may occur. These are features that distinguish the nodule suites of the Lesser Antilles volcanoes (e.g. Lewis, 1973, Wills, 1974) from the Alaskan and Sangeang Api assemblages.

14. The occurrence of very refractory megacrysts or xenocrysts, often in a partially reacted state in many lavas from this sector of the Sunda Arc, may have important bearing on the nature of the mantle source. These include: 1. olivine with Cr-spinel inclusions from Rindjani as magnesian as Fo 93; 2. Cr-diopside with very low Al, Ti and Na contents and 100Mg/Mg+Fe values up to 93 from Rindjani ankaramites, the Sangeang Api phonolitic tephrites and Soromundi leucitites, and; 3. the occurrence of very anorthitic plagioclase (up to An 93) from many of the lavas of all the volcanoes studied.

The very mafic character of the olivine and diopside tends to support an ultramafic peridotite source. The very refractory character of the Cr-diopside is also interesting in the light of the wide range of alkalinity shown by the lavas in which they occur. Thus if the Soromundi leucitite had resulted from a smaller degree of partial melting then the Rindjani ankaramite, then it would be expected that its residual clinopyroxene would be relatively enriched in Al, Ti and Na compared with that in the more extensively melted source. Instead of which, not only is the clinopyroxene of both rock types the same, but it is also of such a refractory composition that it can only be compared with that of the most depleted, high-temperature alpine-type peridotite. Not a source which is in any way likely to yield highly undersaturated leucitite lavas. This then tends to support the previously cited hypothesis that the island arc is underlain by refractory peridotite which may have already yielded a

liquid component, possibly at the mid-ocean ridge and that much of the character of the island arc magma suites is derived from re-enrichment of this depleted source.

The hypothesis is possibly further supported by the marked similarity of the abovementioned refractory phases to megacrysts of almost identical composition from oceanic tholeiites from a number of localities (e.g. Donaldson and Brown, 1977).

The problem of the very anorthitic nature of the plagioclases of island arc rocks is one of the major problems of island arc petrogenesis. Donaldson and Brown (1977) and others have found plagioclase xenocrysts of similar composition in oceanic tholeiites and these may indicate a depleted source with an unusually high Ca/Na ratio. Such an explanation may apply to the island arc situation, though the effects of high water pressure (e.g. Yoder, 1969) have also been invoked. As discussed in chapter 11 however, the presently available experimental data does not unequivocally support this theory. It is undoubtedly true that the liquidus temperature of plagioclase crystallisation is markedly reduced by increasing water pressure, however this only indicates that the first plagioclase to appear does so at decreasing temperatures as water pressure rises and it has yet to be demonstrated that the actual composition of this plagioclase also becomes more calcic (i.e. that there is a gradual distortion of the plagioclase liquidus-solidus loop as the water pressure rises). Yet the extremely calcic composition of the plagioclase in the Sangeang Api gabbroic nodules and in the nodules from the Lesser Antilles (Lewis, 1973) associated with liquids of "normal" Ca/Na ratio does tend to suggest that liquids in the island arc environment do crystallise anomalously calcic plagioclase. Furthermore the clinopyroxenes in general are also commonly

relatively Na-poor compared to non-arc counterparts and there may therefore be a case for suggesting that Na is distributed more strongly in favour of the melt during island arc magmatism. This is perhaps one of the key areas for future experimentation relating to problems of island arc petrogenesis.

REFERENCES CITED

Allen, J.C., Boettcher, A.L., Marland, G., 1975. Amphiboles in andesite and basalt: I. Stability as a function of P-T-fO_2. *Amer. Mineral., 60,* 1069-1085.

Allen, J.C., Boettcher, A.L., 1971. The stability of amphiboles in basalts and andesites at high pressures. *Geol. Soc. America Abs. with Programs, 3,* 490.

Anderson, A.T., 1974. Evidence for a picritic, volatile-rich magma beneath Mt. Shasta, California. *J. Pet., 15,* 243-267.

Aoki, K., 1970. Petrology of kaersutite-bearing ultramafic and mafic inclusions in Iki Island, Japan. *Contrib. Mineral. Petrol. 25,* 270-283.

Aoki, K. and Kushiro, I., 1968. Some clinopyroxene from ultramafic inclusions in Dreiser Weiher, Eifel. *Contrib. Mineral. Petrol. 18,* 326-337.

Appleton, J.D., 1972. Petrogenesis of potassium-rich lavas from the Roccamonfina volcano, Roman Region, Italy. *J. Petrol. 13,* 425-56.

Arculus, R.J., 1976. Geology and geochemistry of the alkali basalt-andesite association of Grenada, Lesser Antilles island arc. *Geol. Soc. Amer. Bull., 87,* 612-624.

Arculus, R.J. and Curran, E.B., 1972. The genesis of the calc-alkaline rock suite. *Earth and Planetary Sci. Letters, 15,* 255-263.

Arculus, R.J., Johnson, R.W., 1978. Criticism of generalized models for the magmatic evolution of arc-trench systems. *Earth Planet. Sci. Lett. 39,* 118-126.

Arculus, R.J., S.E. Delong, R.W. Kay, C. Brooks and S.S. Sun, 1977. The alkalic rock suite of Bogoslof Island, Eastern Aleutian Arc, Alaska. *Jour. of Geology, 85,* 177-186.

Arth, J.G., 1976. Behaviour of trace elements during magmatic processes - a summary of theoretical models and their applications. *J. Res. U.S. Geol. Surv. 4,* 41-47.

Audley-Charles, M.G., 1975. The Sumba fracture: a major discontinuity between eastern and western Indonesia. *Tectonophysics 26,* 213-228.

Baker, P.E., 1968. Comparative volcanology and petrology of the Atlantic island-arcs. *Bull. Volcan., 32,* 189-206.

Baxter, A.N., 1978. Ultramafic and mafic nodule suites in shield-forming lavas from Mauritius. *Jl. Geol. Soc. Lond., 135,* 565-581.

Becker, H.J., 1977. Pyroxenites and hornblendites from the maar-type volcanoes of the Westeifel, Federal Republic of Germany. *Contrib. Mineral., 65,* 45-52.

Bell, K., Powell, J.L., 1969. Strontium isotope studies of alkalic rocks: the potassium-rich lavas of the Birunga and Toro-Ankole regions, east and central equatorial Africa. *J. Petrol. 10,* 536-72.

Ben-Avraham, Z., Emery, K.O., 1973. Structural framework of the Sunda Shelf. *American Assoc. Petrol. Geol. Bull., 57,* 2328-2366.

Best, M.G., 1975. Migration of hydrous fluids in the upper mantle and potassium variation in calc-alkaline rocks. *Geology, 3,* 429-432.

Best, M.G., 1975. Amphibole-bearing cumulate inclusions, Grand Canyon, Arizona, and their bearing on silica-undersaturated hydrous magmas in the upper mantle. *J. Petrol., 16,* 212.

Best, M.G., 1974. Mantle-derived amphibole in xenoliths in alkalic basaltic lavas. *J. Geophys. Res., 79,* 2107.

Best, M.G., 1970. Kaersutite-peridotite inclusions and kindred megacrysts in basanitic lavas, Grand Canyon, Arizona. *Contrib. Mineral. Petrol., 27,* 25.

Binns, R.A., 1969. High-pressure megacrysts in basanitic lavas near Armidale, New South Wales. *Am. J. Sci., 267-A, 33-49.*

Binns, R.A., Duggan, M.B., Wilkinson, J.F.G., 1970. High pressure megacrysts in alkaline lavas from north eastern New South Wales. *Am. J. Sci., 269,* 132-168.

Boettcher, A.L., 1973. Volcanism and orogenic belts - the origin of andesites. *Tectonophysics, 17,* 223-240.

Bowen, N.L., 1928. "The Evolution of the Igneous Rocks", *Princeton University Press, Princeton, N.J.*

Brooks, C., James, D.E. and Hart, S.R., 1976. Ancient lithosphere: its role in young continental volcanism. *Science, 193,* 1086-1094.

Brouwer, H.A., 1943. Leuciethoudende en leucietvrije gesteenten van den Soromandi op het eiland Soembawa. *Ned. Akad. van Wet., Afd. Nat. 52, 6,* 303-307.

Brouwer, H.A., 1938. Leucite rocks of the active volcano Batoe Tara (Malay Archipelago). *Proc. K.N.Ac. Wet. Amsterdam, 42, 1,* 23-29.

Bryan, W.B., Finger, L.W., and Chayes, F., 1969. Estimating proportions in petrographic mixing equations by least-squares approximation. *Science, 163,* 426-427.

Cardwell, R.K., Isacks, B.L., 1978. Geometry of the subducted lithosphere beneath the Banda Sea in eastern Indonesia from seismicity and fault-plane solutions. *J. Geophys. Res., 83,* 2825.

Carmichael, I.S.E., 1967. The iron-titanium oxides of sialic volcanic rocks and their associated ferromagnesian silicates. *Contrib. Mineral. Petrol., 14,* 36-64.

Carmichael, I.S.E., 1967. The mineralogy and petrology of the volcanic rocks from the Leucite Hills. Wyoming. *Contrib. Mineral. Petrol., 15,* 24-66.

Carmichael, I.S.E., 1964. The petrology of Thingmuli, a Tertiary volcano in eastern Iceland. *J. Petrol., 5,* 435-460.

Carmichael, I.S.E., Turner, F.J., Verhoogen, J., 1974. Igneous Petrology. McGraw-Hill, New York, 739pp.

Carswell, D.A., 1975. Primary and secondary phlogopites and clinopyroxenes in garnet lherzolite xenoliths. *Phys. Chem. Earth, 9,* 417.

Carter, D.J., Audley-Charles, M.G., Barber, A.J., 1976. Stratigraphical analysis of island arc - continental margin collision in eastern Indonesia. *J. Geol. Soc. Lond., 132,* 179-198.

Cawthorn, R.G., 1976. Melting relations in part of the system CaO-MgO-Al_2O_3-SiO_2-Na_2O-H_2O under 5kb. pressure. *J. Petrol., 17,* 44-72.

Cawthorn, R.G., Curran, E.B., Arculus, R.J., 1973. A petrogenetic model for the origin of the calc-alkaline suite of Grenada, Lesser Antilles. *J. Petrol., 14,* 327-337.

Cawthorn, R.G., O'Hara, M.J., 1976. Amphibole fractionation in calc-alkaline magma genesis. *Amer. Jl. Sci., 276,* 309-329.

Chapman, N.A., 1976. Inclusions and megacrysts from undersaturated tuffs and basanites, East Fife, Scotland. *J. Petrol., 17,* 472.

Church, S.E. and Tilton, G.R., 1973. Lead and strontium isotopic studies in the Cascade Mountains: bearing on andesite genesis. *Bull. Geol. Soc. Am., 84,* 431-454.

Colley, H., and Warden, A.J., 1974. Petrology of the New Hebrides: *Geol. Soc. Amer. Bull., 85,* 1635-1646.

Coombs, D.S., Wilkinson, J.F.G., 1969. Lineages and fractionation trends in undersaturated volcanic rocks from the East Otago Volcanic Province (New Zealand) and related rocks. *J. Petrol., 10,* 440-501.

Cox, K.G., Hawkesworth, C.J., O'Nions, R.K., Appelton, J.D., 1976. Isotopic evidence for the derivation of some Roman Region volcanics from anomalously enriched mantle. *Contrib. Mineral. Petrol. 56,* 173-180.

Cross, W., 1897. Igneous rocks of the Leucite Hills and Pilot Butte, Wyoming. *Am. J. Sci., 4,* 115-141.

Cundari, A., Le Maitre, R.W., 1970. On the petrogeny of the leucite-bearing rocks of the Roman and Birunga volcanic regions. *J. Petrol., 11,* 33-47.

Curray, J.R., Shor, G.G., Raitt, R.W., Henry, M., 1977. Seismic refraction and reflection studies of crustal structure of the eastern Sunda and western Banda arcs. *J. Geophys. Res., 82,* 2479-2489.

Dawson, J.B., Powell, D.G., Reid, A.M., 1970. Ultrabasic xenoliths and lava from the Lashaine Volcano, Northern Tanzania. *J. Petrol., 11,* 519-548.

Dawson, J.B., Smith, J.V., 1973. Alkalic pyroxenite xenoliths from the Lashaine Volcano, Northern Tanzania. *J. Petrol., 14,* 113-31.

Deer, W.A., Howie, R.A., and Zussman, J., 1966. An introduction to the rock forming minerals. Longmans, London.

Delong, S.E., Hodges, F.N., Arculus, R.J., 1975. Ultramafic and mafic inclusions, Kanaga Island, Alaska and the occurrence of alkaline rocks in island arcs. *J. Geology 83,* 721-736.

Donaldson, C.H., Brown, R.W., 1977. Refractory megacrysts and magnesium-rich melt inclusions in spinel in oceanic tholeiites: indications of magma mixing and parental liquid composition. *Earth. Planet. Sci. Lett., 37,* 81-89.

Donnelly, T., Rogers, J.J.W., Pushkar, P. and Armstrong, R.L., 1971. Chemical evolution of igneous rocks of the eastern West Indies: an investigation of throium, uranium and potassium distributions, and lead and strontium isotopic ratios. *Geol. Soc. Am. Mem., 130,* 181-224.

Eggler, D.H., 1972. Amphibole stability in H_2O-undersaturated calc-alkaline melts. *Earth Planet. Sci. Lett., 15,* 28-34.

Eggler, D.H., Burnham, C.W., 1973. Crystallisation and fractionation trends in the system andesite-H_2O-CO_2-O_2 at pressures to 10kb. *Geol. Soc. America Bull., 84,* 2517-2532.

Ehrat, H., 1929. Die tatigen vulkane des G. Api (Sangean) Bei Bima, Niederlandisch - Indien. *Z.f. Vulkan, 12,* 8-14.

Ellis, D.J., 1976. High pressure cognate inclusions in the Newer volcanics of Victoria. *Contrib. Mineral. Petrol., 58,* 149-180.

Evans, B.W., and Wright, T.L., 1972. Composition of liquidus chronite from the 1959 (Kilauea Iki) and 1965 (Makaopuhi) eruptions of Kilauea volcano, Hawaii. *Am. Mineral., 57,* 217-230.

Ewart, A., 1976. Mineralogy and chemistry of modern orogenic lavas - some statistics and implications. *Earth Planet. Sci. Lett., 31,* 417-432.

Ewart, A., Bryan, W.B., Gill, J.B., 1973. Mineralogy and geochemistry of the younger volcanic islands of Tonga, S.W. Pacific. *J. Petrol., 14,* 429-465.

Ewart, A., Bryan, W.B., 1973. The petrology and geochemistry of the Tongan Islands. In: *The Western Pacific: Island Arc, Marginal Seas, Geochemistry (P.J. Coleman, ed.) pp 508-522. Nedlands: Univ. of W. Australia Press.*

Ewart, A., Stipp, J.J., 1968. Petrogenesis of the volcanic rocks of the central North Island, New Zealand, as indicated by a study of $^{87}Sr/^{86}Sr$ ratios, and Sr, Rb, K, U and Th abundances. *Geochim. Cosmochim. Acta, 32,* 699-735.

Ewart, A. and Taylor, S.R., 1969. Trace element geochemistry of the rhyolitic volcanic rocks, Central North Island, New Zealand. Phenocryst data. *Contr. Mineral. Petrol., 22,* 127-146.

Faune, G., Hurley, P.M., 1963. The isotopic composition of strontium in oceanic and continental basalts. *J. Petrol., 4,* 31-50.

Ferguson, A.K., Cundari, A., 1975. Petrological aspects and evolution of the leucite bearing lavas from Bafumbira, S.W. Uganda. *Contra. Mineral. Petrol., 50,* 25-46.

Findlay, D.C., 1969. Origin of the Tulameen ultramafic-gabbro complex, Southern British Columbia: *Canadian J. Earth Sci., 6,* 399-425.

Fitch, T.J., 1972. Plate convergence, transcurrent faults and internal deformation adjacent to southeast Asia and western Pacific. *J. Geophys. Res., 77,* 4432-4460.

Fitch, T.J., 1970. Earthquake mechanisms and island arc tectonics in the Indonesian-Philippine region. *Bull. Seismological Soc. Amer., 60,* 565-591.

Fitch, T.J., Hamilton, W., 1974. Reply to discussion on a paper by Fitch, T.J. *J. Geophys. Res., 79,* 4982-5..

Fitch, T.J., Molnar, P., 1970. Focal mechanisms along inclined earthquake zones in the Indonesian-Philippine region. *J. Geophys. Res., 75,* 1431-1444.

Flower, M.F.J., 1973. Evolution of basaltic and differentiated lavas from Anjouan, Comores archipelago. *Contrib. Mineral. Petrol., 38,* 237-260.

Flynn, R.T., Burnham, C.W., 1978. An experimental determination of rare earth partition coefficients between a chloride containing vapor phase and silicate melts. *Geochim. Cosmochim. Acta., 42,* 685-702.

Foden, J.D., Varne, R., 1980. The petrology and tectonic setting of Quaternary-Recent volcanic centres of Lombok and Sumbawa, Sunda Arc. *Chemical Geology, 30,* 201-226.

Frechen, J., 1963. Kristallisation, mineralbestand, mineralchemismus und forderfolge der mafitite vom Dreiser Weiheir in der Eifel. *N.J. Mineral. Monatsh., 9-10,* 205-225.

Frey, F.A., Green, D.H., and Roy, S., 1978. Integrated models of basalt petrogenesis: A study of quartz tholeiites to olivine melilitites from south eastern Australia utilizing geochemical and experimental petrological data. *J. Petrol., 19,* 463-513.

Frey, F.A., Prinz, M., 1978. Ultramafic inclusions from San Carlos, Arizona: Petrologic and geochemical data bearing on their petrogenesis. *Earth Planet. Sci. Lett., 38,* 129-176.

Frey, F.A., Green, D.H., 1974. The mineralogy, geochemistry and origin of lherzolite inclusions in Victorian basanites. *Geochim. Cosmochim. Acta., 38,* 1023.

Frisch, T., and Schminke, H.U., 1969. Petrology of clinopyroxene-amphibole inclusions from the Rogue Nablo volcanics, Gran Canaria, Canary Islands. *Bull. Vol., 33,* 1073-88.

Fudali, R.F., Melson, W.F., 1972. Ejecta velocities, magma chamber pressure and kinetic energy associated with the 1968 eruption of Arenal volcano. *Bull. Volc., 35,* 381-401.

Gast, P.W., 1968. Trace element fractionation and the origin of tholeiitic and alkaline magma types. *Geochim. Cosmochim. Acta., 32,* 1057-1086.

Gast, P.W., 1967. Isotopic geochemistry of volcanic rocks. In: Basalts (H.H. Hess and A. Poldervaart eds.) Vol. 1., 325-358. New York: John Wiley.

Gill, J.B., 1978. Role of trace element partition coefficients in models of andesite genesis. *Geochim. Cosmochim. Acta, 42,* 709-724.

Gill, J.B., 1976. Evolution of the mantle. Geochemical evidence from alkali basalt. Comment. *Geology, 4,* p. 625.

Gill, J.B., 1974. Role of underthrust oceanic crust in the genesis of a Fijian calc-alkaline suite. *Contr. Mineral. Petrol., 43,* 29-45.

Gill, J.B., 1970. Geochemistry of Viti Leru, Fiji, and its evolution as an island-arc. *Contrib. Mineral. Petrol., 27,* 179.

Gill, J.B., and Till, A., 1978. Petrology and geochemistry of Namosi andesites and dacites, Fiji. Abstract: International Geodynamics Conference, Western Pacific and Magma Genesis, Japan, March, 1978.

Gill, J.B., and Compston, W., 1973. Strontium isotopes in island arc volcanic rocks, in Coleman, P. ed., The western Pacific-Island arcs, marginal seas, geochemistry: Perth, Western Australia Univ. Press., 483-496.

Gledhill, A. and Baker, P.E., 1973. Strontium isotope ratios in volcanic rocks from the South Sandwich Islands. *Earth Planet. Sci. Lett., 19,* 309-372.

Gorton, M.P., 1977. The geochemistry and origin of quaternary volcanism in the New Hebrides. *Geochim. Cosmochim. Acta., 41,* 1257.

Green, D.H., 1976. Experimental testing of "equilibrium" partial melting of peridotite under water-saturated, high-pressure conditions. *Can. Mineralogist, 14,* 255-268.

Green, D.H., 1973. Experimental melting studies on a model upper mantle composition at high pressure under water-saturated and water-undersaturated conditions. *Earth Planet. Sci. Lett., 19,* 37-53.

Green, D.H., 1971. Compositions of basaltic magmas as indicators of conditions of origin: applications to oceanic volcanism. *Phil. Trans. R. Soc. London, Ser. A., 268,* 707-25.

Green, D.H., and Ringwood, A.E., 1967. The genesis of basaltic magmas. *Contr. Mineral. Petrol., 15,* 103-190.

Green, D.H., Edgar, A.D., Beasley, P., Kiss, E., and Ware, N.G., 1974. Upper mantle source for some hawaiites, mugearites and beumoreites. *Contr. Mineral. Petrol., 48,* 33-43.

Green, T.H., 1972. Crystallisation of calcalkaline andesite under controlled high pressure hydrous conditions. *Contr. Min. Pet., 34,* 150-166.

Green, T.H., and Ringwood, A.E., 1968. Genesis of the calcalkaline igneous rock suite. *Contr. Min. Pet., 18,* 105-162.

Greenland, L.P., 1970. An equation for trace element distribution during magmatic crystallisation. *Am. Mineral., 55,* 455-465.

Hamilton, W., 1979. Tectonics of the Indonesian region. U.S.G.S. Prof. Paper 1078 (in press).

Hamilton, W., 1978. Tectonic map of the Indonesian region. Map 1-875-D, (miscellaneous investigations series), U.S. Geol. Survey.

Hamilton, W., 1977. Subduction in the Indonesian region. In: Island Arcs, Deep Sea Trenches and Back-Arc Basins. Ed. M. Talwan; and W.C. Pitman III. A.G.U. Washington D.C., 15-31.

Hamilton, W., 1974. Earthquake map of the Indonesian region. Map 1-875-C, Miscellaneous investigations series, U.S. Geol. Survey.

Hamilton, 1973. Tectonics of the Indonesian region. *Bull. Geol. Soc. Malaysia, 6,* 3-10.

Harris, P.G., 1957. Zone refining and the origin of potassic basalts. *Geochim. Cosmochim. Acta., 12,* 195-208.

Harris, K.L., and Nicholls, I.A., 1978. An experimental study of the partitioning of selected rare earth elements between garnet, clinopyroxene, amphibole and liquids of andesitic and basaltic composition. *Geochim. Cosmochim. Acta.* (in press).

Hart, S.R., and Brooks C., 1977. The geochemistry and evolution of the early Precambrian mantle. *Contrib. Mineral. Petrol., 61,* 109-128.

Hatherton, T., Dickinson, W.R., 1969. The relationship between andesitic volcanism and seismicity in Indonesia, the Lesser Antilles and other island arcs. *J. Geophys. Res. 74,* 5301-5310.

Hedervari, P., 1978. New seismicity maps of the Indonesian region. *Abstract. Int. Geodynamics Conf., "Western Pacific and Magma Genesis".*

Hedge, C.E., 1966. Variations in radiogenic strontium found in volcanic rocks. *J. Geophys. Res., 71,* 6119-6126.

Hedge, C.E., Hildreth, R.A., Henderson, W.T., 1970. Strontium isotopes in some Cenozoic lavas from Oregon and Washington. *Earth Planet. Sci. Lett., 8,* 434-438.

Hedge, C.E., Knight, R.J., 1969. Lead and strontium isotopes in volcanic rocks from northern Honshu, Japan. *Geochem. J., 3,* 15-24.

Heltz, R.T., 1973. Phase relationships of basalts in their melting range at P_{H_2O} = 5kb at a function of oxygen fugacity. *J. Petrol., 14,* 249-302.

Heming, R.F., 1977. Mineralogy and proposed P-T paths of basaltic lavas from Rabaul Caldera, Papua New Guinea. *Contrib. Mineral. Petrol., 61,* 15-33.

Holloway, J.R., 1973. The system pargasite - H_2O-CO_2: A model for melting of a hydrous mineral with a mixed-volatile fluid. I. Experimental results to 8 kbar. *Geochim. Cosmochim. Acta, 37,* 651-666.

Holloway, J.R., Ford, C.E., 1975. Fluid-absent melting of the fluorodroxy amphibole pargasite to 35 kilobars. *Earth Planet. Sci. Lett., 25,* 44-48.

Holloway, J.R., Burnham, C.W., 1972. Melting relations of basalt with equilibrium water pressure less than total pressure. *J. Petrol., 13,* 1-29.

Holmes, A., Harwood, H.F., 1937. The volcanic area of Bufumbira. *Mem. Geol. Surv. Uganda 3,* Pt. 2, 1-300.

Hunerwadel, F.M., 1921. Die eruptivgesteine von nord mittel Sumbawa. *Doctoral thesis,* Basel.

Hurlbut, C.S., Griggs, D.T., 1939. Igneous rocks of the Highwood Mountains, Montana. Pt. 1. The Laccoliths. *Bull. Geol. Soc. Am., 50,* 1043-1112.

Hurley, P.M., Hughes, H., Faure, G., Pinson, W.H., Fairbairn, H.W., 1962. Radiogenic strontium - 87 Model of continent formation. *J. Geophys. Res., 67,* 5315.

Hurley, P.M., Fairbairn, H.W. and Pinson, W.H., 1966. Rb-Sr isotopic evidence in the origin of potash-rich lavas of Western Italy. *Earth Planet. Sci. Lett., 5,* 301-306.

Hutchison, C.S., 1976. Indonesian active volcanic arc: K, Sr and Rg variation with depth to the Benioff Zone. *Geology, 4,* 407-8.

Hutchison, C.S., 1975. Correlation of Indonesian active volcanic geochemistry with Benioff zone depth. *Geologie en Mijnbouw, 54,* 157-168.

Iddings, J.P., Moreley, E.W., 1915. Contributions to the petrography of Java and Celebes. *J. Geol. 23,* 231-245.

Irvine, T.N., 1974. Petrology of the Duke Island Ultramafic Complex, South-eastern Alaska. *Geol. Soc. Amer. Mem., 138.*

Irvine, T.N., 1973. Bridget Cove volcanics, Juneau area, Alaska: possible parental magma of Alaskan-type ultramafic complexes. *Carnegie Inst. of Wash. Yearbook, 72,* 478-491.

Irvine, T.N., 1967. Chromian spinal as a peterogenetic indicator, Part 2, Petrologic applications, *Can. J. Earth Sci., 4,* 71-103.

Irvine, T.N. and Findlay, T.C., 1972. Alpine type peridotite with particular reference to the Bay of Islands igneous complex. *Publ. Can. Dept. Energ. Mines Resources Earth Phys. Branch., 42,* 97-129.

Irving, A.J., 1978. A review of experimental studies of crystal/liquid trace element partitioning. *Geochim. Cosmochim. Acta., 42,* 743-771.

Irving, A.J., 1974. Pyroxene-rich ultramafic xenoliths in the Newer basalts of Victoria, Australia. *N. Jb. Miner. Abh., 120,* 147-167.

Irving, A.J., 1971. Geochemical and high pressure experimental studies of xenoliths, megacrysts and basalts from south-eastern Australia. *Unpublished Ph.D. thesis, Aust. National Univ. Canberra.*

Irving, A.J., Green, D.H., 1972. Experimental study of phase relationships in a high-pressure mugearitic basalt as a function of water content. *Geol. Soc. Am. Abstracts with Programs,* pp. 550-551.

Isacks, B., Oliver, J. and Sykes, L.R., 1968. Seismology and the new global tectonics. *J. Geophys. Res., 73,* 5855.

Ito, K., 1978. Ascending flow between the descending lithosphere and the overlying asthenosphere. *J. Geophys. Res., 83,* 262-268.

Jackson, E.D., 1969. Chemical variation in coexisting chromite and olivine in chromitite zones of the Stillwater Complex., *Econ. Geol. Monogr., 4,* 41-71.

Jakeš, P., Gill, J., 1970. Rare earth elements and the island arc tholeiitic series. *Earth Planet. Sci. Lett., 9,* 17-28.

Jakeš. P., White, A.J.R., 1972. Major and trace element abundances in volcanic rocks of orogenic areas. *Geol. Soc. Am. Bull., 83,* 29-4.

Jakeš, P., White, A.J.R., 1971. Composition of island arcs and continental growth. *Earth Planet. Sci. Letts., 12,* 224-230.

Jakeš, P., White, A.J.R., 1969. Structure of the Melanesian Arcs and correlation with distribution of magma types. *Tectonophysics, 8,* 223-236.

James, D.E., 1977. Magmatic and Seismic evidence for subduction of the Nazca plate beneath central Peru. *Carnegie Yearbook, 76.*

James, D.E., Brooks, C., Cuyubama, A., 1976. Andean Cenozoic Volcanism: Magma genesis in the light of strontium isotopic composition and trace element geochemistry. *Geol. Soc. Amer. Bull., 87,* 592-600.

Johnson, R.W., Smith, I.E.M., Taylor, S.R., 1978. Hotspot volcanism in St. Andrews Strait, Papua New Guinea: geochemistry of a Quaternary bimodal rock suite. *B.M.R. Jl. Aust. Geol. Geophyr. 3, 1,* 55-70.

Johnson, R.W., Wallace, D.A., Ellis, D.J., 1976. Feldspathoid-bearing, potassic rocks and associated types from volcanic islands off the coast of New Ireland, Papua New Guinea: a preliminary account of geology and petrology. *In: "Volcanism in Australasia:* ed. R.W. Johnson, 297-316. Elsevier Amsterdam.

Joplin, G.A., 1968. The shoshonite association: a review. *J. Geol. Soc. Aust. 15,* 275-294.

Katili, J.A., 1975. Volcanism and plate tectonics in the Indonesian Island arcs. *Tectonophys. 26,* 165-188.

Katili, J.A., 1973. On fitting certain geological and geophysical features of the Indonesian island arc to the new global tectonics. In: The Western Pacific: island arcs, marginal seas, geochemistry. Ed. P.J. Coleman, pp 287-305. Perth: University of Western Australia Press.

Katili, J.A., Soetadi, R., 1971. Neotectonics and seismic zones of the Indonesian Archipelago. *Roy. Soc. N.Z. Bull., 9,* 39-45.

Katsui, Y., Niida, K., Yamamoto, M. and Nemoto, S., 1978. Genesis of calcalkaline andesite from Oshima - Oshima and Ichinomegata volcanoes, North Japan. Abstracts: Inter. Geodynamics Conf., Western Pacific and Magma Genesis., Japan.

Katsui, Y., Nickimura, S., Masuda, Y., Kurasawa, H. and Fujimaki, J., 1974. Petrochemistry of the Quaternary volcanic rocks of Hokkaido, north Japan. *Japanese Soviet seminar on Geodynamic Project.*

Kay, R.W., Sun, S.S., and Lee-Hu, C.-N., 1978. Pb and Sr isotopes in volcanic rocks from the Aleutian Islands and Pnibilof Islands, Alaska. *Geochim. Cosmochim. Acta., 42,* 263-273.

Kay, R., and Gast, P.W., 1973. The rare earth content and origin of alkali-rich basalts. *J. Geol., 81,* 653-682.

Kay, R., Hubbard, N.J., and Gast, P.W., 1970. Chemical characteristics and origin of oceanic ridge volcanic rocks. *J. Geophys. Res., 75,* 1585-1613.

Keller, J., 1974. Petrology of some volcanic rock series of the Aeolian Arc, Southern Tyrrhenian Sea: calcalkaline and shoshonitic associations. *Contr. Mineral. Petrol., 46,* 29-47.

Kelsey, C.H., 1963. Calculation of the C.I.P.W. norm. *Min. Mag., 34,* 276-282.

Kesson, S. and Price, R.C., 1972. The major and trace element chemistry of kaersutite and its bearing on the petrogenesis of alkaline rocks. *Contr. Mineral. Petrol., 35,* 119-124.

Klerkx, J., Deutsch, S., Pichler, H., and Zeil, W., 1977. Strontium isotopic composition and trace element data bearing on the origin of Cenozoic volcanic rocks of the central and southern Andes. *J. Volcanol. Geothermal Res., 2,* 49-71.

Kudo, A.M., Weill, D.F., 1970. An igneous plagioclase thermometer. *Contrib. Mineral. Petrol., 25,* 52-65.

Kuno, H., 1950. Petrology of Hakone Volcano and the adjacent areas, Japan. *Bull. Geol. Soc. Am., 61,* 957-1020.

Kuno, H., 1959. Origin of Cenozoic petrographic provinces of Japan and surrounding areas. *Bull. Volc., 20,* 37.

Kuno, H., 1966. Lateral variation of basalt magma across continental margins and island arcs. *Bull. Volcanol., 29,* 195-222.

Kuno, H., 1968. Origin of andesite and its bearing on the island arc structure. *Bull. Volcanol., 32,* 141-176.

Kuno, H., 1969. Mafic and ultramafic nodules in basaltic rocks of Hawaii. *Geol. Soc. Am. Mem., 115,* 189-234.

Kushiro, I., 1960. Si-Al relations in clinopyroxenes from igneous rocks. *Am. J. Sci., 258,* 548-554.

Kushiro, I., 1972. Effect of water on the composition of magmas formed at high pressures. *J. Petrol., 13,* 311-334.

Larson, R.L., 1975. Late Jurassic sea-floor spreading in the eastern Indian Ocean. *Geology, 3,* 69-71.

Le Bas, M.J., 1962. The role of aluminium in igneous clinopyroxenes with relation to their parentage. *Am. J. Sci., 260,* 267-288.

Leeman, W.P., Scheidegger, K.F., 1977. Olivine/liquid distribution coefficients and a test for crystal-liquid equilibrium. *Earth Planet. Sci. Lett., 35,* 247-257.

Le Maitre, R.W., 1969. Kaersutite-bearing xenoliths from Tristan da Cunha. *Min. Mag., 37,* 185-197.

Le Pichon, X., 1968. Sea-floor spreading and continental drift. *J. Geophys. Res., 73,* 3661-3705.

Lewis, J.F., 1973. Petrology of ejected plutonic blocks of the Soufriere volcano, St. Vincent, West Indies. *J. Petrol., 14,* 81-112.

Lewis, 1973. Mica pyroxenite inclusions in limburgite - Hopi Buttes. *Brigham Young University., 20,* 191-225.

Lloyd, F.E., Bailey, D.K., 1975. Light element metasomatism of the continental mantle: the evidence and consequences. *Phys. Chem. Earth, 9,* 389.

Loney, R.A., Himmelberg, G.R., and Coleman, R.G., 1971. Structure and petrology of the alpine-type peridotite at Burro Mountain, California, U.S.A. *J. Pet., 12,* 245.

Lopez-Escobar, L., Frey, F.A., Vergara, M., 1977. Andesites and high-Al basalts from the central-south Chile high andes: Geochemical evidence bearing on their petrogenesis. *Contr. Mineral. Petrol., 63,* 199-228.

Macdonald, G.A., Katsura, T., 1964. Chemical composition of Hawaiian lavas. *J. Petrol., 5,* 82-133.

Magaritz, M., Whitford, D.J., James, D.E., 1978. Oxygen isotopes and the origin of high $^{87}Sr/^{86}Sr$ andesites. *Earth Planet. Sci. Lett., 40,* 220-230.

Marsh, B.D., 1976. Some Aleutian andesites: their nature and source. *J. Geol., 84,* 27-45.

Mathez, E.A., 1973. Refinement of the Kudo-Weill plagioclase thermometer and its application to basaltic rocks. *Contr. Mineral. Petrol., 41,* 61-72.

Matrais, I. bin, Pfeiffer, D., Stach, L.W., Sukardi, R., 1972. Hydrogeology of the island of Lombok (Indonesia). *Seri Hidrogeologi 2, Geol. Surv. Indonesia, Bandung,* 23pp.

McBirney, A.R., 1969. Compositional variations in Cenozoic calcalkaline suites of Central America. *Oregon Dept. Geol. Mineral Indust. Bull., 65,* 185-189.

McCallum, I.S., Charette, M.P., 1978. Zr and Nb partition coefficients: Implications for the genesis of marine basalts, KREEP and sea floor basalts. *Geochim. Cosmochim. Acta., 42,* 859-871.

Meijer, A., 1976. Pb and Sr isotopic data bearing on the origin of volcanic rocks from the Mariana island arc system. *Bull. Geol. Soc. Am., 87,* 1358-1369.

Mertzmann, S.A., 1977. The petrology and geochemistry of the Medicine Lake volcano, California. *Contrib. Mineral. Petrol., 62,* 221-249.

Minster, J.B., Jordan, T.H., Molnar, P., Haines, E., 1974. Numerical modelling of instantaneous plate tectonics. *Geophys. J. Roy. Astron. Soc., 36,* 541-576.

Mitchell, R.H., Bell, K., 1976. Rare earth element geochemistry of Potassic lavas from the Birunga and Toro-Ankole regions of Uganda, Africa. *Contr. Mineral. Petrol., 58,* 293-303.

Murali, A.V., Leeman, W.P., Ma, M.-S., Schmitt, R.A., (1979). Evaluation of fractionation and hybridization models for Kilauea. Eruptions and probable mantle source of Kilauea and Mauna Loa tholeiitic basalts, Hawaii. *J. Pet.* (in press).

Miyashiro, A., 1972. Metamorphism and related magmatism in plate tectonics. *Amer. J. Sci., 272,* 629-656.

Mysen, B.O., Boettcher, A.L., 1975. Melting of a hydrous mantle: II. Geochemistry of crystals and liquids formed by anatexis of mantle peridotite at high pressures and high temperatures as a function of controlled activities of water, hydrogen and carbon dioxide. *J. Petrol., 16,* 549-593.

Mysen, B.O., Kushiro, I. (and Nicholls, I. and Ringwood, A.E.), 1974. A possible mantle origin for andesitic magmas: Discussion of a paper by Nicholls and Ringwood. *Earth Planet. Sci. Lett., 21,* 221-229.

Nash, W.P., Wilkinson, J.F.G., 1971. Shonkin Sag laccolith, Montana: pt. II, Bulk rock geochemistry. *Contrib. Mineral. Petrol., 33,* 162-170.

Nash, W.P., Wilkinson, J.F.G., 1970. Shonkin Sag laccolith, Montana: pt. I, Mafic minerals and estimates of temperature, pressure, oxygen fugacity and silica activity. *Contrib. Mineral. Petrol., 25,* 241-269.

Neumann van Padang, M., 1951. Catalogue of the active volcanoes of the world including solfatara fields. Pt. 1. Indonesia. *International Volcanological Assoc., Napoli.,* 271pp.

Nicholls, I.A., 1974. Liquids in equilibrium with peridotitic mineral assemblages at high water pressures. *Contr., Mineral., Petrol., 45,* 289-316.

Nicholls, I.A., Whitford, D.J., 1976. Potassium-rich volcanic rocks of the Sunda island arc, Java, Indonesia. *Abst. 25th I.G.C. Vol. 1,* p. 58.

Nicholls, I.A., and Whitford, D.J., 1976. Primary magmas associated with Quaternary volcanism in the western Sunda arc. In: Johnson, R.W. (ed). *Volcanism in Australasia, Elsevier,* 77-90.

Nicholls, I.A., Ringwood, A.E., 1972. Production of silica-saturated tholeiitic magmas in island arcs. *Earth Planet. Sci. Lett., 17,* 243-246.

Nicholls, I.A., Ringwood, A.E., 1973. Effect of water on olivine stability in tholeiites and the production of silica-saturated magmas in the island-arc environment. *J. Geol., 81,* 285-300.

Nicholls, J., Carmichael, I.S.E., 1969. A commentary on the Absarokite-Shoshomite-Banakite series of Wyoming, U.S.A. *Schweiz. Mineral. Petro. Mitt., 49, 1,* 47-64.

Nielson, D.R., Stoiber, R.E., 1973. Relationship of Potassium content in andesitic lavas and depth to the seismic zone. *J. Geophys. Res. 78,*6887-6892.

Ninkovich, D., Hays, J.D., 1972. Mediterranean island arcs and origin of high potash volcanoes. *Earth Planet. Sci. Lett., 16,* 331-345.

Noble, D.C., Bowman, H.R., Herbert, A.J., Silverman, M.L., Heropoulos, C.E., Fabbi, B.P. and Hedge, C.E., 1975. Chemical and isotopic constraints on the origin of low-silica latite and andesite from the Andes of central Peru. *Geology, 3,* 501-504.

Osborn, E.F., 1969. Experimental aspects of calc-alkaline differentiation, in McBirney, A.R., ed., *Proceedings of the Andesite Conference. Oregon, Dept. Geol. Min. Ind. Bull., 65,* 33-42.

Osborn, E.F., 1959. Role of oxygen pressure in the crystallisation and differentiation of basaltic magma. *Am. Jour. Sci., 257,* 607-647.

Page, R.W., Johnson, R.W., 1974. Strontium isotope ratios of Quaternary volcanic rocks from Papua, New Guinea. *Lithos, 7,* 91-100.

Papike, J.J., Cameron, K.L., Baldwin, K., 1974. Amphiboles and pyroxenes: Characterization of other than quadrilateral components and estimates of ferric iron from microprobe data. *Geol. Soc. Am. Abstr. with Programs, 6,* 1053.

Pe, G.G., Gledhill, A., 1975. Strontium isotope ratios in volcanic rocks from the southeastern part of the Helenic arc. *Lithos, 8,* 209-214.

Peacock, M.A., 1931. Classification of igneous rock series. *J. Geol., 39,* 54-67.

Petroeschevsky, W.A., 1949. A contribution to the knowledge of the Gunung Tambora (Sumbawa) *Tijdschr. Kon. Ned. Aardv. Gen. 66.* 688-703.

Philpotts, J., Martin, W., Schnetzler, C.C., 1971. Geochemical aspects of some Japanese lavas: *Earth Planet. Sci. Lett., 12,* 89-96.

Philpotts, J., Schnetzler, C., 1970. Phenocrysts - matrix partition coefficients for K, Rb, Sr and Ba with applications to anorthosite and basalt genesis. *Geochim. Cosmochim. Acta., 34,* 307-322.

Powell, M., 1978. Crystallisation conditions of low-pressure cumulate nodules from the Lesser Antilles island arc. *Earth Planet. Sci. Lett., 39,* 162-172.

Presnall, D.C., 1966. The join forsterite-diopside-iron oxide and its bearing on the crystallisation of basaltic and ultramafic magmas. *Am. J. Sci., 264,* 753-809.

Pushkar, P., Steuber, A.M., Tomblin, J.F., Julian, G.M., 1973. Strontium isotope ratios in volcanic rocks from St. Vincent and St. Lucia, Lesser Antilles. *J. Geophys. Res., 78,* 1279-1287.

Pushkar, P., 1968. Strontium isotope ratios in volcanic rocks of three island arc areas. *J. Geophys. Res., 73,* 2701-2713.

Ringwood, A.E., 1974. The petrological evolution of island arc systems. *Geol. Soc. London Jour., 130,* 183-204.

Ritsema, A.R., 1954. The seismicity of the Sunda Arc. *Indonesian Jl. Nat. Sci. 1-2-3.*

Rittmann, A., 1953. Magmatic character and tectonic position of the Indonesian volcanoes. *Bull. Volc., 14,* 45-58.

Roeder, P.L., Emslie, R.F., 1970. Olivine-liquid equilibrium. *Contr. Mineral. Petrol., 29,* 275-289.

Rose, W.I., Anderson, A.T., Woodruff, L.G., Bonis, S.B., 1978. The October 1974 basaltic tephra from Fuego volcano: Description and history of the magma body. *J. Volc. Geotherm. Res., 4,* 3-53.

Ruckmick, J.C., Noble, J.A., 1959. Origin of the ultramafic complex at Union Bay, southeastern Alaska. *Bull. Geol. Soc. Am., 70,* 981-1018.

Sato, H., 1977. Nickel content of basaltic magmas: identification of primary magmas and a measure of the degree of olivine fractionation. *Lithos., 10,* 113-121.

Schainer, J.F., Yoder, H.S., 1960. The nature of residual liquids from crystallisation with data on the system nepheline-cliopside-silica. *Am. J. Sci., 258A,* 273-283.

Schilling, J., Winchester, J., 1969. Rare earth contribution to the origin of Hawaiian lavas. *Contr. Mineral. Pet., 23,* 27-37.

Scholl, D., Marlow, M., MacLeod, N., Buffington, E., 1976. Episodic Aleutian Ridge igneous activity; implications of Miocene and younger submarine volcanism west of Buldir Island (175.9^{o}E). *Bull. Geol. Soc. Am., 87,* 547-554.

Shaw, D.M., 1970. Trace element fractionation during anatexis. *Geochim. Cosmochim. Acta., 34,* 331-40.

Shimazu, N., Arculus, R.J., 1975. Rare earth element concentration in a suite of basanitoids and alkali olivine basalts from Grenada. Lesser Antilles. *Contrib. Mineral. Pet., 50,* 231-240.

Sigurdsson, H., Tomblin, J.F., Brown, G.M., Holland, J.G., Arculus, R.J., 1973. Strongly undersaturated magmas in the Lesser Antilles island arc. *Earth Planet. Sci. Lett., 18,* 285-295.

Simkin, T., Smith, J.V., 1970. Minor-element distribution in olivine. *J. Geol., 78,* 304-325.

Sorensen, H., 1974. The Alkaline Rocks, ed. H. Sorensen, J. Wiley and Sons, pp 622. London, 1974.

Stanton, R.L., Bell, J.D., 1969. Volcanic and associated rocks of the New Georgia Group, British Islands Protectorate. *Overseas Geol. Min. Res. (G.B.). 10,* 113-145.

Stern, C.R., 1974. Melting products of olivine tholeiite basalt in subduction zones. *Geology, 4,* 227-230.

Stern, C.R., Wiley, P.J., 1973. Melting relations of basalt-andesite-rhyolite-H_2O and a pelagic red clay at 30 kb. *Contr. Mineral. Petrol., 42,* 313-323.

Stewart, D.C., 1975. Crystal in calc-alkaline andesites as breakdown products of high-Al amphiboles. *Contrib. Mineral. Petrol., 53,* 195-204.

Sudradjat, A., 1975. Reconnaissance geologic map of Sumbawa, West Nusa Tenggara. Geol. Surv. Indonesia, Ministry of Mines.

Sun, S.S., Nesbitt, R.W., Sharaskin, A.Y., 1979. Geochemical characteristics of mid-ocean ridge basalts. *Earth Planet. Sci. Lett.,* (in press, 1979).

Sun, S.S., Hanson, G.N., 1976. Evolution of the mantle: Geochemical evidence from alkali basalt: Comment and Reply. *Geology, 4,* 625-631.

Sun, S.S., Hanson, G.N., 1975. Evolution of the mantle: Geochemical evidence from alkali basalt. *Geology, 3,* 297-302.

Sun, S.S., Hanson, G.N., 1975. Origin of Ross Island basanitoids and limitations upon the heterogeneity of mantle sources for alkali basalts and nephelinites. *Contr. Mineral. Petrol., 52,* 77-106.

Sun, C.-O., Williams, R.J., Sun, S.S., 1974. Distribution coefficients of Eu and Sr for plagioclase-liquid and clinopyroxene-liquid equilibria in oceanic ridge basalts: an experimental study *Geochim. Cosmochim. Acta., 38,* 1415-1433.

Taylor, S.R., 1969. Trace element chemistry of andesites and associated calcalkaline rocks. *Oregon Dept. Geol. Mineral Indust. Bull., 65,* 43-63.

Taylor, H.P., Jr., Noble, J.A., 1969. Origin of magnetite in the zoned ultramafic complexes of southeastern Alaska, in "*Magmatic Ore Deposits,*" *H.D.B. Wilson, ed. Econ. Geol. Monogr., 4,* 209-230.

Thompson, R.N., 1977. Primary basalts and magma genesis III. Alban Hills, Roman Comagmatic Province, Central Italy. *Contrib. Mineral. Petrol., 60,* 91-108.

Thompson, R.N., 1975. Primary basalts and magma genesis. II. Snake Plain, Idaho, U.S.A. *Contrib. Mineral. Petrol., 52,* 213-232.

Thornton, C.P., Tuttle, O.F., 1960. Chemistry of igneous rocks: pt. 1 Differentiation Index. *Am. J. Sci., 258,* 664-684.

Thorpe, R.S., Potts, P.J., Franeis, P.W., 1976. Rare earth data and petrogenesis of andesite from the North Chilean Andes. *Contr. Mineral. Petrol., 54,* 65-78.

Upton, B.G.J., Wadsworth, W.J., 1972. Peridotitic and gabbroic rocks associated with the shield-forming lavas of Reunion. *Contrib. Mineral. Petrol., 35,* 139-158.

Van Bemmelen, R.W., 1949. The geology of Indonesia. *The Hague: Government Printing Office.*

Varne, R., 1977. On the origin of spinel lherzolite inclusions in basaltic rocks from Tasmania and elsewhere. *J. Petrol., 18,* 1-23.

Varne, R., Graham, A.L., 1971. Rare earth abundances in hornblende and clinopyroxene of a hornblende lherzolite xenolith: Implications for upper mantle fractionation processes. *Earth Planet. Sci. Lett., 13,* 11-18.

Warden, A.J., 1970. Evolution of Aoba Caldera Volcano, New Hebrides. *Bull. Volc., 34,* 107-140.

Washington, H.S., 1917. Chemical analyses of igneous rocks. *Prof. Pap. U.S. geol. Surv. 99.*

White, A.J.R., 1979. An underplating model for the formation of the lower crust. Abst. in *Crust and Upper Mantle of Southeast Australia. Bureau of Mineral Resources, Geology and Geophysics, Record 1979/2,* p. 96.

Whitford, D.J., 1975. Geochemistry and petrology of volcanic rocks from the Sunda Arc, Indonesia. Ph.D. thesis, R.S.E.S., Australian National Univ.

Whitford, D.J., 1975. Strontium isotopic studies of the volcanic rocks of the Sunda arc, Indonesia, and their petrogenetic implications. *Geochim. Cosmochim. Acta., 39,* 1287-1302.

Whitford, D.J., Foden, J.D., Varne, R., 1978. Sr-isotope geochemistry of calc-alkaline and alkaline lavas from the Sunda Arc in Lombok and Sumbawa, *Indonesia. Carnegie Inst. D.T.M. Yr. bk.* 77.

Whitford, D.J., Jezek, P.A., 1979. Origin of late-Cenozoic lavas from the Banda arc, Indonesia: Trace element and Sr-isotope evidence. *Contrib. Mineral. Petrol., 68,* 141-150.

Whitford, D.J., Compston, W., Nicholls, I.A., Abbott, M.J., 1977. Geochemistry of Late Cenozoic lavas from eastern Indonesia: the role of subducted sediments in petrogenesis. *Geology, 5,* 571-575.

Whitford, D.J., Nicholls, I.A., 1976. Potassium variation in lavas across the Sunda arc in Java and Bali. In: *Johnson, R.W. (ed.). Volcanism in Australasia, Elsevier,* 63-76.

Wilcox, R.E., 1956. Petrology of Paracutin volcano, Mexico. *U.S. Geol. Surv. Bull., 965-C,* 281-353.

Wilkinson, J.F.G., 1975. Ultramafic inclusions and high-pressure megacrysts from a nephelinite sill, Nandewar Mountains, northeastern New South Wales, and their bearing on the origin of certain ultramafic inclusions in alkaline volcanic rocks. *Contrib. Mineral. Petrol., 51,* 235.

Wilkinson, J.F.G., Binns, R.A., 1977. Relatively iron-rich lherzolite xenoliths of the Cr-diopside suite: A guide to the primary nature of anorogenic tholeiitic andesite magmas. *Contrib. Mineral. Petrol., 65,* 199-212.

Wills, K.J.A. The geological history of southern Dominica and plutonic nodules from the Lesser Antilles. Ph.D. thesis, University of Durham.

Wilshire, H.G., Shervais, J.W., 1975. Al-augite and Cr-diopside ultramafic xenoliths in basaltic rocks from western United States. *Phys. Chem. Earth., 9,* 257.

Wilshire, H.G., Schwarzman, E.C., Trask, N.J., 1971. Distribution of ultramafic xenoliths at 12 north American sites. *U.S. Geol. Survey Interagency Report.* Astrogeology 42.

Wood, B.J., Banno, S., 1973. Garnet-orthopyroxene and orthopyroxene-clinopyroxene relationships in simple and complex systems. *Contr. Mineral. Petrol., 42,* 109-124.

Yagi, K., Onuma, K., 1967. The join $CaMgSi_2O_6$-$CaTiAl_2O_6$ and its bearing on the titanaugites. *J. Fac. Sci. Hokkaido Univ., 8,* 463-483.

Yoder, H.S., Tilley, C.E., 1962. Origin of basaltic magmas. An experimental study of natural and synthetic rock systems. *J. Petrol., 3,* 342-532.

Yoder, H.S., jr., 1969. Calcalkaline andesites: experimental data bearing on the origin of their assumed characteristics, in McBirney, A.R., ed., Proceedings of the Andesite Conference: *Oregon, Dept. Geol. Mineral Indust. Bull., 65,* 77-89.

Zielinski, R.A. and Frey, F.A., 1970. Gough Island: Evaluation of a fractional crystallisation model. *Contrib. Mineral. Petrol., 29,* 242-254.

Zies, E.G., 1946. Temperature measurements at Paracutin volcano. *Am. Geophys. Union Trans., 27,* 178-180.

Appendix 1

SAMPLE CATALOGUE

NOTES: 1. Samples are cited in the same order as they appear in the whole-rock analysis tables in the body of the thesis and in the CIPW norm table (appendix 2).

2. Abbreviations are as follows:

(i) Island; L - Lombok

S - Sumbawa

(ii) Volcano Complex;

R - Rindjani, G.S. - G. Sangenges, T - Tambora (P.S. - P. Satonda), S - Soromundi, S.A. - Sangeang A

(iii) Phenocrysts;

Ol - olivine, Cpx - clinopyroxene, Opx - orthopyroxene, Pl - plagioclase, Mg - magnetite,

B - biotite, A - amphibole, Ph - phlogopite, Lc - leucite, Apat - apatite, K - alkali feldspar.

3. Phenocrysts are listed in decreasing order of abundance. Percentage phenocryst figure is an approximate estimate and the reader should refer to the modal analysis tables of typical examples of each petrographic group of rocks from each volcano given in chapters 3, 4, 5 and 6.

Sample No. Used in Text	Univ. of Tas. Tasmania Geol. Dept. No.	Rock Types	Phenocrysts	% Phenocrysts	Island	Volcano Complex	Locality	Co-ordinates (° 'E, ° 'S)
LB8	48001	ankaramite	Cpx,Ol,Pl,Mg	55	L	R	Tandjung Village, W. Lombok	116°08'E, 8°21'S
LB7	48002	ankaramite	Cpx,Ol,Pl	45	L	R	" "	" "
LB9	48003	ankaramite	Cpx,Pl,Ol,Mg	55	L	R	" "	" "
LB1	48004	ankaramite	Cpx,Pl,Ol,Mg	50	L	R	" "	" "
LB11	48005	ankaramite	Pl,Cpx,Ol	55	L	R	" "	" "
LB10	48006	ankaramite	Cpx,Ol,Pl	15	L	R	" "	" "
LB67	48007	high-Al basalt	Pl,Ol,Cpx,Mg	40	L	R	Pohgading River, East Lombok	116°36'E, 8°34'S
41676	41676	high-Al basalt	Pl,Cpx,Ol,Mg	50	L	R	10km East of Mataram, Narmarda Area	116°10'E, 8°33'S
LB47	48008	high-Al basalt	Pl,Cpx,Ol,Mg	40	L	R	Djangkok River, nr. Endut Village	116°11'E, 8°32'S
41621	41621	high-Al basalt	Ol,Pl,Cpx	8	L	R	North of Swela Village, East Lombok	116°32'E, 8°28'S
LB68	48009	high-Al basalt	Pl,Ol,Cpx,Mg	40	L	R	Pohgading River, East Lombok	116°36'E, 8°34'S
41632	41632	high-Al basalt	Pl,Ol,Cpx,	18	L	R	3km South of G. Pusuk	116°32'E, 8°26'S
LB51	48010	high-Al basalt	Pl,Cpx,Ol,Mg	30	L	R	Djangkok River, Endut	116°11'E, 8°32'S
LB65	48011	high-Al basalt	Pl,Cpx,Ol,Mg,A	60	L	R	Pohgading River, East Lombok	
41631	41631	high-Al basalt	Pl,Ol,Cpx,Mg	25	L	R	3km South of G. Pusuk	116°32'E, 8°26'S
41624	41624	high-Al basalt	Pl,Cpx,Ol,Mg	40	L	R	Between Swela and Pasagan Villages	116°32'E, 8°27'S
LB71	48012	high-Al basalt	Pl,Ol,Cpx	25	L	R	Pohgading River, East Lombok	116°36'E, 8°34'S
41623	41623	high-Al basalt	Pl,Ol,Cpx	10	L	R	Between Swela and Pasagan Villages	116°32'E, 8°27'S
LB25	48013	high-Al basalt			L	R	Bentak, West Lombok	116°05'E, 8°25'S
LB64	48014	high-Al basalt	Pl,Cpx,Opx,Ol,Mg	30	L	R	Pohgading River, East Lombok	116°36'E, 8°34'S
LB19	48015	high-Al basalt	Pl,Cpx,Mg,A	40	L	R	Between Pamenang and Bentak, W. Lombok	116°05'E, 8°24'S
41626	41626	high-Al basalt	Pl,Ol	10	L	R	Pasagan Village	116°28'E, 8°27'S
41692	41692	high-Al basalt	Pl,Cpx,Ol,Mg	40	L	R	Kopang Area, Central Lombok	116°23'E, 8°38'S
41635	41635	high-Al basalt	Pl,Cpx,Mg,Ol	60	L	R	5km S. Sembulan Village	116°32'E, 8°24'S
41651	41651	high-Al basalt	Pl,Ol,Mg,Cpx	50	L	R	North Lombok	116°28'E, 8°17'S
41658	41658	high-Al basalt	Pl,Ol,Mg,Cpx	30	L	R	" "	" "

Sample No. Used in Text	Univ. of Tasmania Geol. Dept. No.	Rock Types	Phenocrysts	% Phenocrysts	Island	Volcano Complex	Locality	Co-ordinates (° 'E, ° 'S)
LB26	48016	high-Al basalt			L	R	Bentak, West Lombok	116°05'E, 8°27'S
41643	41643	high-Al basalt	Pl,Ol,Mg	50	L	R	5km N. Sembulan Village	116°31'E, 8°21'S
41678	41678	high-Al basalt	Pl,Ol,Cpx,Mg	50	L	R	Narmarda Area, 15km E. of Mataram	116°10'E, 8°33'S
41683	41683	High-Al basalt	Pl,Cpx,Ol,Mg,A	60	L	R	Renggung River, Kopang, Central Lombok	116°21'E, 8°37'S
41634	41634	low silica andesite	Pl,Cpx,Ol,Mg	50	L	R	South of Sembulan Village	116°32'E, 8°25'S
41684	41684	low silica andesite	Pl,Cpx,Ol,Mg	60	L	R	Renggung River, Kopang, Centra. Lombok	116°21'E, 8°37'S
41632	41637	low silica andesite	Pl,Cpx,Ol,Mg	50	L	R	South of Sembulan Village	116°33'E, 8°24'S
LB61	48019	low silica andesite	Pl,Cpx,Mg,Ol	45	L	R	Wagegesang River, Southern flank of Rindjani	116°20'E, 8°35'S
41647	41647	low silica andesite	Pl,Cpx,Opx,Mg	55	L	R	Between Bawah Nau and Sajang	116°30'E, 8°20'S
41622	41622	low silica andesite	Pl,Cpx,Opx,Mg,Apat	38	L	R	Between Swela and Pasagan Villages	116°32'E, 8°28'S
41627	41627	low silica andesite	Pl,Cpx,opx,Mg	75	L	R	Pasagan Village	116°28'E, 8°27'S
41625	41625	low silica andesite	Pl,Cpx,Opx,Mg,Ol	50	L	R	" "	" "
41687	41687	low silica andesite	Pl,Cpx,Opx,Mg,Ol	45	L	R	Renggung River, South of Kopang	116°20'E, 8°38'S
LB6	48018	andesite	Pl,Cpx,Opx,Mg,Apat	55	L	R	Tangung, W. Lombok	116°08'E, 8°21'S
LB29	48019	high-K, high-Sr andesite	Pl,Cpx,Opx,Mg	50	L	R	Pusik Pass, W. Lombok	116°05'E, 8°30'S
LB28	48020	" "	Pl,Cpx,Opx,Mg	50	L	R	" "	" "
41646	41646	andesite	Pl,Cpx,Opx,Mg,Apat	55	L	R	Between Sembulan and Bawah Nau	116°30'E, 8°21'S
41644	41644	andesite	Pl,Cpx,Ol,Mag	45	L	R	South of Bawah Nau Village	116°30'E, 8°22'S
41688	41688	andesite	Pl,Cpx,Opx,Mg,Ol	40	L	R	Renggung River, South of Kopang	116°20'E, 8°38'S
41636	41636	andesite	Pl,Cpx,Opx,Mg	67	L	R	South of Sembulan Village	116°33'E, 8°24'S
LB42	48021	andesite	Pl,Cpx,Opx,Mg,Apat	45	L	R	Djangkok river nr. Endut Village	116°12'E, 8°33'S
LB41	48022	andesite	Pl,Cpx,Opx,A,Apat	50	L	R	" "	" "
41675	41675	dacite	Pl,Cpx,Opx,Mg	45	L	R	Narmarda Area	116°10'E, 8°34'S
LB12	48023	high-K, high-Sr andesite	Pl,A,Cpx,Mg,Apat	45	L	R	Between Penamang and Bentak, W. Lombok	116°05'E, 8°24'S
LB22	48024	" "	Pl,Cpx,Mg,Apat	45	L	R	Bentak, W. Lombok	116°05'E, 8°26'S
41676	41672	high-K andesite	Pl,Cpx,Ol,Mg,B	20	L	R	Narmarda Area	116°10'E, 8°34'S
LB55	48025	high-K andesite			L	R	Wagegesang River	116°20'E, 8°35'S
LB69	48026	high-K andesite	Pl,A,Cpx,Mg	10	L	R	Pohgading River	116°36'E, 8°31'S
LB4	48027	high-K andesite	Pl,Cpx,Mg,Opx	25	L	R	Tangung, W. Lombok	116°08'E, 8°21'S
LB3	48028	high-K andesite	Pl,Cpx,Opx,Mg	10	L	R	" "	" "
41668	41668	high-K andesite	Pl,Opx,Cpx,Mg	35	L	R	Narmada Area	116°10'E, 8°34'S
LB2	48029	dacite	Pl,Cpx,Ol,Mg	5	L	R	Tangung, W. Lombok	116°08'E, 8°21'S
41645	41645	dacite	Pl,Cpx,Opx,Mg,A	50	L	R	South of Bawah Nau Village	116°30'E, 8°22'S
41691	41691	dacite	Pl,Opx,Mg,Cpx,Apat	30	L	R	Kopang Area, Central Lombok	116°23'E, 8°38'S
41650	41650	dacite	Pl,A,Opx,Mg,Cpx	40	L	R	South of Desanjar	116°27'E, 8°16'S
LB60	48030	dacite			L	R	Wagegesang River	116°20'E, 8°35'S
LB48	48031	dacite	Pl,Opx,Cpx,Mg,Apat	30	L	R	Djankok River, Endut	116°12'E, 8°33'S
LB43	48032	dacite	Pl,A,Mg,Apat	3	L	R	" "	" "
LB49	48033	dacite	Pl,A,Mg	3	L	R	" "	" "

Sample No. Used in Text	Univ. of Tasmania Geol. Dept. No.	Rock Types	Phenocrysts	% Phenocrysts	Island	Volcano Complex	Locality	Co-ordinates (° 'E, ° 'S)
41677	41677	dacite	Pl,A,Mg	10	L	R	Namada Area	116°10'E, 8°34'
41671	41671	dacite	Pl,A,Mg	3	L	R	" "	" "
41638	41638	dacite	Pl,A,Mg,Cpx,Opx	10	L	R	Near Sembulan Village	116°33'E, 8°24'
41641	41641	dacite	Pl,A,Mg,B	11	L	R	North of Sembulam Village	116°31'E, 8°20'
41664	41664	dacite	Pl,A,B,Mg	5	L	R	Namada Area	116°10'E, 8°34'
41639	41639	dacite	Pl,A,Mg	6	L	R	Sembulan Village	116°33'E, 8°24'
PS8	48034	ne-trachybasalt	Cpx,Pl,Ol,Mg	50	S	PS	Satonda Island, 5km N.W. of Kananga Village	117°45'E, 8°05'
PS2	48035	ne-trachybasalt	Pl,Cpx,Ol,Mg	50	S	PS	" "	" "
PS4	48036	"	"		S	PS	" "	" "
PS7	48037	"	"		S	PS	" "	" "
PS3	48038	"	"		S	PS	" "	" "
T12	48039	"	Cpx,Pl,Ol,Mg	25	S	T	400 meters from Tambora Summit on N.W. flank	117°58'E, 8°13'
T17	48040	"	Cpx,Pl,Ol,Mg	25	S	T	" "	" "
T9	48041	"	Pl,Cpx,Ol,Mg	3	S	T	" "	" "
T8	48042	"	Cpx,Pl,Mg,Ol	35	S	T	" "	" "
T21	48043	"	Pl,Cpx,Ol,Mg	50	S	T	" "	" "
T2	48044	"	Pl,Cpx,Ol,Mg	35	S	T	" "	" "
T18	48045	ne-trachybasalt	Pl,Cpx,Ol,Mg	35	S	T	400 meters below Tambora Summit	117°58'E, 8°13'
T3	48046	"	Pl,Cpx,Ol,Mg	50	S	T	" "	" "
T30	48042	"	Pl,Cpx,Ol,Mg	40	S	T	N.W. Summit plateau, 2800 meters	117°59'E, 8°14'
T13	48048	"	Pl,Cpx,Ol,Mg,B	70	S	T	450 meters below Tambora Summit	117°58'E, 8°13'
T5	48049	"	Pl,Cpx,Ol,Mg	50	S	T	" "	" "
T26	48050	"	Pl,Cpx,Ol,Mg	35	S	T	Summit plateau	117°59'E, 8°14'
T10	48051	ne-trachybasalt	Pl,Cpx,Ol,Mg	35	S	T	N.W. side, 400 meters below summit	117°58'E, 8°13'
T27	48052	"	Pl,B,Cpx,Mg	10	S	T	Summit plateau (N.W.)	117°59'E, 8°14'
T36	48053	"	Pl,B,Cpx,Mg	15	S	T	"	" "
T32	48054	"	Pl,Cpx,B,Mg	10	S	T	"	" "
T31	48055	"	Pl,Cpx,B,Mg	15	S	T	"	" "
T11	48056	"	Pl,Cpx,Ol,Mg	20	S	T	N.W. side 400 meters below summit	117°58'E, 8°14'
T25	48057	"	Pl,B,Cpx,Mg	5	S	T	Summit Plateau, N.S.W side	117°58'E, 8°15'
T23	48058	"	Pl,B,Cpx,Mg	10	S	T	" "	" "
T43	48059	"	Pl,Cpx,B,Mg	10	S	T	" "	" "
T29	48060	"	Pl,Cpx,B,Mg,Apat	8	S	T	" "	" "
T41	48061	"	Pl,Cpx,B,Mg,Apat	8	S	T	" "	" "
T20	48062	"	Pl,Cpx,Mg,Lc	25	S	T	N.W. side 400 meters below summit	117°58'E, 8°13'
T28	48063	Alkali gabbro (Shonkinite)	Pl,Cpx,K,Ol,Mg, Apat,B		S	T	Summit Plateau	117°59'E, 8°14'
T33	48064	"	Pl,Cpx,B,Mg,Ol,K, Apat		S	T	"	" "
T4	48065	"	Pl,Cpx,Ol,K,B,Mg		S	T	N.W. side 450 metres below summit	117°57'E, 8°13'

Sample No. Used in Text	Univ. of Tasmania Geol. Dept. No.	Rock Types	Phenocrysts	% Phenocrysts	Island	Volcano Complex	Locality	Co-ordinates (^{o} 'E, ^{o} 'S)
T6	48066	Alkali gabbro (Shonkinite)	Pl,B,Cpx,K,Mg		S	T	N.W. side 450 meters below Summit	117^{o}57'E, 8^{o}13'
B43	48067	phonolitic tephrite	Cpx,Ol,Mg	35	S	SA	S.W. coast, 1953 lahar	119^{o}01'E, 8^{o}13'
B44	48068	"	Cpx,Pl,Ol,Mg	40	S	SA	" "	" "
B39	48069	ne-trachybasalt	Pl,Cpx,Ol,Mg	30	S	SA	" "	" "
B38	48070	"	Cpx,Pl,Ol,Mg	40	S	SA	" "	" "
B31	48071	"	Pl,Cpx,Mg,Ol	45	S	SA	" "	" "
B29	48072	phonolitic tephrite			S	SA	" "	" "
B25	48073	"	Pl,Cpx,Mg,B,A	25	S	SA	S.W. Coast, 1911 lava flow	119^{o}02'E, 8^{o}15'
B34	48074	ne-trachybasalt	Pl,Cpx,A,Mg,B	35	S	SA	S.W. Coast, 1953 lahar	119^{o}01'E, 8^{o}13'
B36	48075	"	Pl,Cpx,Mg,B,A	50	S	SA	" "	" "
B35	48076	"	Pl,Cpx,A,Mg,Apat	35	S	SA	" "	" "
B28	48077	"	Pl,Cpx,A,Mg,B	35	S	SA	" "	" "
B27	48078	phonolitic tephrite	Pl,Cpx,A,Mg	35	S	SA	S.W. Coast 1911 lahar	119^{o}02'E, 8^{o}14'
B18	48079	ne-trachybasalt	Cpx,Pl,Ol,Mg,B	20	S	SA	S.W. Coast, 1953 lahar	119^{o}01'E, 8^{o}13'
B42	48080	"	Pl,Cpx,Mg,B,A	35	S	SA	" "	" "
B32	48081	"	Pl,Cpx,Mg	20	S	SA	" "	" "
B23	48082	olivine clinopyroxenite	Cpx,Ol,Ph		S	SA	S.W. Coast 1911 lahar	119^{o}02'E, 8^{o}14'
B5	48083	"	Cpx,Ol,A,Ph		S	SA	" "	" "
B4	48084	"	Cpx,A,Ol,Ph		S	SA	S.W. Coast 1953 lahar	119^{o}01'E, 8^{o}13'
B2G	48085	magnetite clinopyroxenite			S	SA	Xenolith in trachybasalt boulder, 1953 lahar	" "
B13	48086	alkali pyroxenite	Cpx,Ph,A		S	SA	cobble, 1911 lahar, S.W. coast	119^{o}02'E, 8^{o}14'
B22	48087	"	Cpx,Mg,A,Pl		S	SA	" "	" "
B25	48088	magnetite clinopyroxenite	Cpx,Mg,Pl,A		S	SA	xenolith in 1911 lava flow, S.W. coast	119^{o}02'E, 8^{o}15'
B2H	48089	"	Cpx,Pl,Mg		S	SA	xenolith in trachybasalt boulder, 1953 lahar	119^{o}01'E, 8^{o}12'
B24	48090	hornblende gabbro	A,Pl,Cpx,Mg,Apat		S	SA	cobble 1911 lahar, S.W. coast	119^{o}03'E, 8^{o}15'
B7	48091	"	A,Pl,Cpx,Mg		S	SA	xenolith in trachybasalt boulder, 1911 lahar	119^{o}02'E, 8^{o}15'
B11	48092	"	Pl,Cpx,Mg,A		S	SA	cobble, 1953 lahar (near village)	119^{o}01'E, 8^{o}12'
B10	48093	"	Pl,Cpx,Mg,A		S	SA	cobble, 1993 lahar, S.W. coast	" "
B8	48094	"	Pl,Cpx,A,Mg		S	SA	cobble, 1911 lahar, S.W. coast	119^{o}02'E, 8^{o}14'
B9	48095	olivine clinopyroxenite	Cpx,Ol,Ph		S	SA	S.W. coast, 1953 lahar	119^{o}01'E, 8^{o}12'
B29	48096	magnetite clinopyroxenite	Cpx,Mg		S	SA	cobble, 1911 lahar, S.W. coast	119^{o}03'E, 8^{o}15'
B2D	48097	"	Cpx,Mg		S	SA	xenolith trachybasalt boulder, 1953 lahar	119^{o}01'E, 8^{o}12'

Sample No. Used in Text	Univ. of Tasmania Geol. Dept. No.	Rock Types	Phenocrysts	% Phenocrysts	Island	Volcano Complex	Locality	Co-ordinates (° 'E, ° 'S)
B1A	48098	magnetite clinopyroxenite	Cpx,Mg,Pl		S	SA	xenolith trachybasalt boulder, 1953 lahar	119°01'E, 8°12'
B2E	48099	"	Cpx,Mg,Pl		S	SA	" "	" "
B28	48100	"	Cpx,Mg,Pl		S	SA	cobble, 1911 lahar, S.W. coast	119°03'E, 8°15'
B2A	48101	"	Cpx,Mg,Pl		S	SA	xenolith in trachybasalt boulder 1953 lahar	119°01'E, 8°12'
B20	48102	hornblende clinopyroxenite	Cpx,A,Mg		S	SA	S.W. coast, 1911 lahar	119°02'E, 8°14'
B21	48103	alkali clinopyroxenite	Cpx,A		S	SA	" "	" "
B16	48104	"	Cpx,A,Mg,Ph		S	SA	cobble, 1911 lahar, S.W. coast	" "
B6B	48105	"	Cpx,Mg,A,Pl		S	SA	cobble, 1953 lahar, S.W. coast	119°01'E, 8°12'
B15	48106	"	Cpx,Pl,Ph,Mg,A		S	SA	" "	" "
B14	48107	"	Cpx,Pl,Mg,A		S	SA	cobble, 1911 lahar, S.W. coast	119°02'E, 8°13'
B1B	48108	hornblende gabbro	A,Pl,Cpx,Mg		S	SA	xenolith in trachybasalt boulder, 1953 lahar	119°01'E, 8°12'
B14f	48109	"	Pl,Cpx,A,Mg		S	SA	cobble, 1911 lahar, S.W. coast	119°02'E, 8°13'
B17	48110	"	Pl,Cpx,A,Mg		S	SA	" "	" "
B6A	48111	"	Pl,Cpx,A,Mg		S	SA	cobble, 1953 lahar, Near village	119°01'E, 8°12'
B27X	48112	"	Pl,Cpx,A,Mg		S	SA	S.W. coast, 1911 lahar	119°03'E, 8°15'
S3	48113	Olivine leucitite	Cpx,Ol,Mg	65	S	GS	All G. Sangenges samples were	Between
S23	48114	"	Cpx,Ol,Mg	35	S	GS	taken from the west branch	117°12'E, 8°30'
S21	48115	"	Cpx,Lc,Mg,Ol	35	S	GS	of Barang Ree river, which drains	117°10'E, 8°32'
S27	48116	"	Cpx,Ol,Mg	20	S	GS	northwards directly from the summit	" "
S22	48117	"	Cpx,Ol,Mg,Lc	45	S	GS	of Sangenges.	" "
S17	48118	leucitite	Cpx,Mg,Ol	25	S	GS	All samples were taken from up-stream	" "
S19	48119	Olivine leucitite	Cpx,Ol	25	S	GS	of B. Puti village (117°12'E, 8°30'S)	" "
S9	48120	leucite tephrite	Cpx,Ol,Mg	20	S	GS	for a distance of 8km.	" "
S8	48121	ne-trachybasalt	Pl,Cpx,Ol,Mg	70	S	GS	" "	" "
S28	48122	"	Pl,Cpx,Ol,Mg	60	S	GS	" "	" "
S5	48123	"	Pl,Cpx,Ol,Mg	35	S	GS	" "	" "
S16	48124	"	Pl,Cpx,Mg	60	S	GS	" "	" "
S1	48125	"	Pl,Cpx,K,Mg	75	S	GS	" "	" "
S10	48126	basaltic andesite	Pl,Cpx,Mg	35	S	GS	" "	" "
S11	48127	"	Pl,Cpx,Mg,Ol	70	S	GS	" "	" "
S26	48128	hornblende andesite	Pl,Cpx,A,B,Apat	35	S	GS	" "	" "
S15	48129	"	Pl,Cpx,A,Mg	35	S	GS	" "	" "
S7	48130	"	Pl,Cpx,A,Mg	25	S	GS	" "	" "
S12	48131	hornblende gabbro	Pl,A,Cpx,Mg		S	GS	" "	" "
Si17	48132	madupite	Cpx,Ph,Mg	50	S	S	Outcrop, ESE of Soromundi	118°37'E, 8°20'
Si16	48133	"	Cpx,Ph,Mg	50	S	S	" "	" "

Sample No. Used in Text	Univ. of Tasmania Geology Dept. No.	Rock Types	Phenocrysts	% Phenocrysts	Island	Volcano Complex	Locality	Co-ordinates (° 'E, ° 'S)
Si6	48134	leucite lamproite	Cpx,Ph,Mg,Ol	35	S	S	East flank of Soromundi	118°35'E, 8°18'
Si13	48135	"	Cpx,Ol,Mg,Ph	25	S	S	" "	118°36'E, 8°18'
Si11	48136	"	Cpx,Mg,Ph,Pl	40	S	S	" "	" "
Si14	48137	leucitite	Cpx,Lc,Mg	45	S	S	" "	" "
Si10	48138	leucite lamproite	Cpx,Lc,Mg	40	S	S	" "	" "
Si12	48139	"	Cpx,A,Ph,Mg	45	S	S	" "	" "
Si15	48140	leucite tephrite	Cpx,Lc,Mg	65	S	S	ESE of Soromundi	118°37'E, 8°19'
Si3	48141	"	Pl,Cpx,Mg	75	S	S	eastern flank of Soromundi	118°38'E, 8°20'
Si1	48142	"	Pl,Cpx,Mg,A,Ph	45	S	S	" "	" "
Si9	48143	"	Cpx,Pl,Lc,Mg	45	S	S	near summit of Soromundi	118°34'E, 8°17'
Si18	48144	hornblende clinopyroxenite	Cpx,A,Apat,Mg,Ph		S	S	S. Sai river	118°39'E, 8°21'

APPENDIX 2. C.I.P.W. Norms

C.I.P.W. Norms were calculated by computer (Burroughs, B6700), using the method of Kelsey (1963). Analyses were recalculated on an anhydrous basis before the norm calculation and FeO was arbitrarily set on the basis of Fe^{2+} = 0.85 Fe. Samples in this table appear in the same order and sequence as they appear in the major- and trace-element analyses tables in the main body of the thesis.

Sample No.	*Q*	*C*	*or*	*ab*	*an*	*lc*	*ne*	*di*	*hy*	*ol*	*cs*	*mt*	*hm*	*il*	*ap*	*pf*	Area (Km²) Table
LB8	-	-	5.33	8.41	19.33	-	2.32	40.92	-	19.82	-	2.22	-	1.31	0.36	16.05	3.12
LB7	-	-	7.10	11.86	26.05	-	1.74	30.63	-	18.11	-	2.46	-	1.57	0.49	20.70	"
LB9	-	-	6.95	12.83	22.68	-	6.10	30.18	-	16.33	-	2.49	-	1.69	0.76	25.88	"
LB1	-	-	7.65	25.73	27.19	-	2.55	26.15	-	15.86	-	2.51	-	1.72	0.65	25.93	"
LB11	-	-	7.03	18.29	24.22	-	1.50	29.69	-	14.28	-	2.47	-	1.87	0.65	26.82	"
LB10	-	-	6.90	16.77	25.73	-	2.42	28.87	-	14.43	-	2.52	-	1.76	0.62	26.09	"
LB67	-	-	5.88	26.35	32.36	-	2.23	13.70	-	14.82	-	2.30	-	1.91	0.47	34.45	"
41676	-	-	5.97	27.41	32.14	-	-	12.84	3.87	12.90	-	2.46	-	1.88	0.54	33.38	"
LB47	-	-	10.01	27.80	26.96	-	0.33	15.59	-	14.11	-	2.36	-	2.11	0.75	38.14	"
41621	-	-	8.78	27.26	27.46	-	1.26	14.99	-	14.64	-	2.49	-	2.39	0.75	37.38	"
LB68	-	-	7.04	25.48	30.06	-	2.43	15.95	-	14.07	-	2.41	-	2.07	0.50	34.95	3.13
41632	-	-	7.16	28.79	29.34	-	1.24	14.15	-	14.23	-	2.35	-	2.15	0.60	37.20	"
LB51	-	-	9.69	26.06	28.38	-	-	14.77	9.30	6.59	-	2.36	-	2.09	0.78	35.75	"
LB65	-	-	8.25	30.07	29.76	-	0.03	13.16	-	13.82	-	2.31	-	1.88	0.73	32.36	"
41631	-	-	7.29	28.65	28.01	-	0.52	17.36	-	12.89	-	2.49	-	2.23	0.57	36.46	"
41624	-	-	5.68	28.78	32.41	-	-	9.46	15.18	3.85	-	2.33	-	1.83	0.49	36.46	"
LB71	-	-	7.44	25.94	33.05	-	-	12.52	7.54	8.29	-	2.40	-	2.18	0.66	33.38	"
41623	-	-	9.02	25.59	25.12	-	5.36	16.62	-	12.64	-	2.53	-	2.44	0.69	39.97	"
LB25	-	-	7.57	27.33	33.58	-	1.56	13.92	-	11.64	-	2.13	-	1.51	0.57	36.45	"
LB64	-	-	9.41	29.33	29.63	-	-	11.28	8.03	7.15	-	2.31	-	2.32	0.55	36.75	"
LB19	-	-	8.36	18.86	24.28	-	10.52	22.45	-	10.07	-	2.57	-	2.25	0.64	37.75	3.14
41626	-	-	8.74	29.76	25.88	-	2.45	15.80	-	11.89	-	2.46	-	2.39	0.74	40.96	"
41692	-	-	11.64	30.19	27.15	-	-	11.87	4.86	8.96	-	2.28	-	2.12	0.95	41.83	"
41635	0.31	-	5.87	23.17	38.60	-	-	9.76	17.62	-	-	2.28	-	1.91	0.49	29.35	"
41651	-	-	8.01	29.64	33.07	-	2.72	9.43	-	12.24	-	2.19	-	1.97	0.75	40.37	"
41658	-	-	8.19	32.62	35.39	-	0.35	4.41	-	14.18	-	2.23	-	1.98	0.67	41.16	"
LB26	-	-	8.43	29.26	38.91	-	-	6.92	3.10	9.38	-	1.90	-	1.46	0.64	37.69	"
41643	-	-	7.70	26.67	32.32	-	3.70	14.17	-	10.28	-	2.40	-	2.13	0.65	38.07	"
41678	-	-	11.82	32.11	25.61	-	1.30	13.85	-	10.14	-	2.27	-	2.07	0.83	45.24	"
41683	-	-	5.18	36.87	27.14	-	-	14.79	1.47	9.15	-	2.54	-	2.44	0.43	42.04	3.15
41634	-	-	8.11	31.76	29.57	-	-	10.14	14.50	1.07	-	2.35	-	2.01	0.50	39.87	"
41684	-	-	5.96	36.68	26.95	-	-	13.83	9.13	2.85	-	2.16	-	1.91	0.55	42.64	"
41637	-	-	9.96	34.25	29.66	-	-	9.06	7.27	5.23	-	2.18	-	1.82	0.57	44.22	"
LB61	0.85	-	8.75	33.08	27.08	-	-	9.65	16.10	-	-	1.99	-	1.82	0.70	42.68	"
41647	4.96	-	8.77	27.20	33.72	-	-	4.00	17.04	-	-	1.99	-	1.74	0.58	40.94	"
41622	2.62	-	9.43	34.61	27.27	-	-	6.66	15.02	-	-	2.01	-	1.73	0.65	46.66	"
41627	4.63	-	7.04	33.54	26.22	-	-	12.46	11.44	-	-	2.08	-	2.07	0.53	45.21	"
41625	2.76	-	9.06	36.15	25.71	-	-	8.94	13.00	-	-	2.02	-	1.75	0.62	47.97	"
41687	-	-	9.64	38.27	22.64	-	-	11.72	12.73	0.44	-	1.95	-	1.96	0.66	47.91	"

Sample No.	Q	C	or	ab	an	lc	ne	di	hy	ol	cs	mt	hm	il	cp	DI	Analysis Table No.
LB6	7.72	-	8.66	23.26	33.51	-	-	6.74	15.89	-	-	1.94	-	1.67	0.62	39.64	3.16
LB29	4.62	-	13.30	28.51	28.36	-	-	6.28	14.74	-	-	1.80	-	1.42	1.00	46.42	"
LB28	1.79	-	14.11	34.41	28.01	-	-	5.63	12.27	-	-	1.61	-	1.32	0.87	50.30	"
41646	3.69	-	9.84	35.29	25.22	-	-	7.97	13.81	-	-	1.97	-	1.68	0.55	48.82	"
41644	-	-	10.69	46.27	21.40	-	-	7.26	9.47	0.82	-	1.73	-	1.70	0.67	56.96	"
41688	3.74	-	9.34	37.72	25.-0	-	-	9.56	10.70	-	-	1.75	-	1.70	0.50	50.80	"
41636	10.56	-	8.12	31.89	29.26	-	-	3.76	12.90	-	-	1.67	-	1.32	0.52	50.57	"
LB42	4.12	-	8.56	34.16	27.03	-	-	9.02	13.15	-	-	1.87	-	1.49	0.61	46.84	"
LB41	7.62	-	10.73	32.25	25.67	-	-	8.30	11.82	-	-	1.63	-	1.48	0.52	50.60	"
41675	14.08	-	11.65	35.25	22.19	-	-	5.34	8.20	-	-	1.34	-	1.31	0.64	60.98	"
LB12	7.16	-	16.53	33.05	20.38	-	-	9.52	10.02	-	-	1.52	-	1.14	0.68	56.75	3.17
LB22	4.53	-	16.70	39.88	24.60	-	-	3.03	8.43	-	-	1.22	-	1.00	0.52	61.21	"
41672	4.75	-	19.91	40.13	17.01	-	-	4.42	9.89	-	-	1.35	-	1.70	0.86	64.79	"
LB55	8.66	-	15.30	38.05	19.38	-	-	6.80	8.78	-	-	1.27	-	1.20	0.59	62.01	"
LB69	8.32	-	17.73	41.51	16.18	-	-	1.93	10.70	-	-	1.33	-	1.35	0.95	67.57	"
LB4	9.18	-	20.11	36.92	22.28	-	-	2.01	7.10	-	-	0.91	-	1.06	0.42	66.21	"
LB3	8.71	-	17.74	40.74	15.50	-	-	2.81	10.39	-	-	1.39	-	1.63	1.11	67.19	"
41668	9.32	0.36	20.83	37.60	20.93	-	-	-	8.47	-	-	0.88	-	1.15	0.48	67.75	"
LB2	8.74	-	21.38	41.09	12.20	-	-	3.56	9.22	-	-	1.35	-	1.55	0.93	71.21	"
41645	11.92	-	16.31	37.24	17.39	-	-	7.25	6.94	-	-	1.28	-	1.26	0.43	70.94	"
41691	9.64	-	20.83	38.32	19.79	-	-	1.63	7.31	-	-	0.89	-	1.10	0.49	68.80	3.18
41650	12.44	0.12	18.99	38.63	18.71	-	-	-	8.29	-	-	1.03	-	1.23	0.57	70.06	"
LB60	12.58	-	21.00	37.35	15.94	-	-	1.26	9.02	-	-	1.02	-	1.19	0.64	70.93	"
LB48	12.69	-	20.60	35.86	20.78	-	-	0.15	7.51	-	-	0.85	-	1.09	0.47	69.15	"
LB43	13.31	-	23.80	39.82	11.88	-	-	1.02	7.53	-	-	0.90	-	1.17	0.57	76.93	"
LB49	11.76	-	22.69	42.19	12.24	-	-	0.92	7.50	-	-	0.90	-	1.19	0.61	76.64	"
41677	11.16	-	21.65	43.25	11.71	-	-	1.81	7.71	-	-	0.95	-	1.24	0.52	76.07	"
41671	13.25	-	21.72	41.91	12.36	-	-	1.29	6.79	-	-	0.93	-	1.24	0.52	76.88	"
41638	13.92	-	24.39	42.19	9.67	-	-	2.58	4.90	-	-	0.79	-	1.19	0.38	80.49	"
41641	12.75	-	25.20	41.95	11.17	-	-	0.30	6.44	-	-	0.76	-	1.07	0.36	79.90	"
41664	15.22	-	24.06	42.78	8.98	-	-	1.47	5.33	-	-	0.72	-	1.09	0.36	82.07	"
41639	16.40	-	24.80	42.00	8.49	-	-	2.06	4.12	-	-	0.71	-	1.12	0.31	83.20	"
2. Tambora																	
PS8	-	-	10.54	19.43	26.73	-	4.36	19.50	-	14.47	-	2.29	-	1.87	0.83	34.33	4.1
PS2	-	-	13.15	19.56	24.94	-	6.22	17.11	-	13.71	-	2.35	-	1.86	1.12	38.95	"
PS4	-	-	14.28	19.39	26.42	-	5.09	15.87	-	13.64	-	2.34	-	1.89	1.09	38.77	"
PS7	-	-	15.17	19.79	27.41	-	3.53	14.36	-	14.29	-	2.37	-	1.92	1.18	38.48	"
PS3	-	-	13.89	19.37	23.45	-	7.40	18.27	-	12.21	-	2.40	-	1.87	1.15	40.66	"
T12	-	-	15.80	12.33	25.38	-	9.37	19.68	-	12.20	-	2.45	-	1.84	0.99	37.49	4.2
T17	-	-	14.61	15.66	27.51	-	5.92	18.00	-	13.18	-	2.41	-	1.62	0.90	36.20	"
T9	-	-	17.09	14.81	26.36	-	7.73	17.06	-	11.59	-	2.41	-	1.68	1.09	39.63	"
T8	-	-	10.08	20.04	23.70	-	7.93	20.74	-	12.28	-	2.35	-	1.73	1.17	38.05	"

Sample No.	Q	C	or	ab	an	lc	ne	di	hy	ol	cs	mt	hm	il	ap	DI	Analysis Table No.
T21	-	-	17.26	14.86	22.81	-	9.02	18.49	-	12.47	-	2.35	-	1.77	0.99	41.14	4.2
T2	-	-	18.30	16.24	22.38	-	9.26	17.37	-	11.57	-	2.23	-	1.75	0.92	43.80	"
T18	-	-	18.11	16.12	21.58	-	10.74	18.03	-	10.60	-	2.19	-	1.71	0.93	44.97	"
T3	-	-	17.35	21.32	23.41	-	4.72	16.20	-	12.08	-	2.32	-	1.76	0.88	43.38	"
T30	-	-	21.02	19.24	25.77	-	9.84	12.56	-	7.59	-	1.57	-	1.28	1.15	50.10	"
T13	-	-	17.08	22.73	19.59	-	6.75	18.79	-	10.31	-	2.18	-	1.66	0.94	46.56	"
T5	-	-	21.76	19.97	27.29	-	9.00	9.63	-	8.47	-	1.52	-	1.26	1.11	50.73	4.3
T26	-	-	23.42	21.09	24.26	-	7.84	11.38	-	8.04	-	1.68	-	1.28	1.04	52.34	"
T10	-	-	26.40	23.73	19.67	-	10.04	8.54	-	7.74	-	1.46	-	1.21	1.22	60.17	"
T27	-	-	29.05	28.10	17.31	-	7.12	6.13	-	8.41	-	1.50	-	1.08	1.34	64.26	"
T36	-	-	29.79	28.56	17.04	-	7.63	4.91	-	8.05	-	1.43	-	1.26	1.35	65.98	"
T32	-	-	29.75	29.64	18.32	-	4.83	4.41	-	9.06	-	1.44	-	1.31	1.27	64.22	"
T31	-	-	30.26	28.48	17.27	-	6.51	4.61	-	8.91	-	1.45	-	1.28	1.26	65.25	"
T11	-	-	29.02	25.69	18.34	-	9.41	7.43	-	6.44	-	1.37	-	1.13	1.19	64.12	4.4
T25	-	-	31.30	29.38	17.65	-	5.77	3.77	-	8.26	-	1.42	-	1.24	1.24	66.45	"
T23	-	-	30.01	29.70	18.08	-	5.25	4.34	-	8.64	-	1.42	-	1.27	1.30	64.97	"
T43	-	-	31.84	31.36	15.71	-	6.17	3.36	-	7.98	-	1.29	-	1.15	1.14	69.38	"
T29	-	-	30.06	33.52	14.34	-	7.24	4.09	-	7.26	-	1.28	-	1.14	1.08	70.63	"
T41	-	-	32.76	29.87	13.85	-	7.89	4.69	-	7.31	-	1.32	-	1.16	1.16	70.53	"
T20	-	-	33.65	27.80	10.37	-	11.49	7.57	-	5.67	-	1.27	-	1.15	1.06	72.94	"
T28	-	-	15.27	13.58	25.20	-	7.91	19.66	-	13.18	-	2.46	-	1.97	0.79	36.76	"
T33	-	-	9.14	19.62	24.94	-	-	24.09	3.66	12.53	-	3.02	-	2.20	0.82	28.76	"
T4	-	-	19.31	16.89	26.27	-	6.92	14.66	-	11.10	-	2.07	-	1.67	1.13	43.12	"
3. Sangeang Api																	
B43	-	-	10.94	2.67	13.12	-	15.94	43.09	-	9.42	-	2.27	-	1.54	1.03	29.55	5.3
B44	-	-	13.10	10.99	19.50	-	12.05	29.77	-	9.68	-	2.40	-	1.72	0.81	36.14	"
B39	-	-	13.70	14.64	20.60	-	8.90	26.40	-	10.66	-	2.46	-	1.81	0.83	37.25	"
B38	-	-	15.03	16.42	24.80	-	5.83	21.63	-	11.14	-	2.45	-	1.85	0.86	37.28	"
B31	-	-	13.47	18.10	22.37	-	8.14	22.31	-	10.43	-	2.49	-	1.93	0.78	39.70	"
B29	-	-	17.59	9.78	20.40	-	14.80	24.33	-	8.02	-	2.23	-	1.71	1.13	42.17	"
B25	-	-	15.59	10.73	24.54	-	13.77	20.72	-	9.50	-	2.32	-	1.73	1.11	40.09	"
B34	-	-	16.92	22.12	25.33	-	5.99	15.31	-	9.70	-	2.05	-	1.59	1.00	45.04	"
B36	-	-	18.21	22.94	21.37	-	7.59	16.31	-	9.02	-	2.06	-	1.51	1.02	48.73	"
B35	-	-	16.28	19.84	25.23	-	8.11	16.96	-	8.93	-	2.11	-	1.60	0.95	44.23	"
B28	-	-	15.74	23.63	25.19	-	6.89	15.10	-	8.87	-	2.01	-	1.51	1.02	46.31	"
B27	-	-	18.77	14.20	20.16	-	15.80	19.20	-	7.26	-	2.00	-	1.43	1.21	48.77	"
B18	-	-	19.51	18.61	23.23	-	9.89	16.82	-	7.46	-	1.95	-	1.54	1.02	48.01	"
B42	-	-	19.53	27.11	20.45	-	6.43	14.72	-	7.64	-	1.82	-	1.40	0.92	53.07	"
B32	-	-	21.02	25.72	20.86	-	7.56	13.77	-	7.04	-	1.77	-	1.31	0.95	54.31	"
B23	-	-	-	-	6.75	0.46	1.50	46.43	-	38.24	3.28	2.55	-	0.75	0.02	1.96	5.4
B5	-	-	-	-	10.45	0.19	1.02	66.27	-	16.42	2.55	1.97	-	1.11	0.02	1.20	"
B4	-	-	-	-	10.42	0.23	1.80	76.50	-	6.79	1.51	1.59	-	1.13	0.02	2.04	"
B2G	-	-	-	-	12.33	0.32	1.69	56.59	-	17.81	5.87	3.18	-	2.18	0.05	2.02	"

Sample No.	Q	C	or	ab	an	lc	ne	di	hy	ol	cs	mt	hm	il	ap	DI	Analysis Table No.
B13	-	-	-	-	13.01	24.65	3.78	6.04	-	38.07	9.46	2.36	-	2.61	0.02	28.43	5.4
B22	-	-	-	-	17.76	0.70	2.93	39.09	-	23.01	9.90	3.89	-	2.67	0.05	3.63	"
B25	-	-	-	-	14.95	1.30	5.61	33.53	-	27.14	9.93	4.53	-	2.92	0.09	6.91	"
B2H	-	-	-	-	25.68	0.33	3.45	34.00	-	22.30	7.50	3.82	-	2.50	0.45	3.77	"
B24	-	-	-	-	39.26	3.96	4.94	9.97	-	24.91	5.83	3.33	-	2.95	4.94	8.90	"
B7	-	-	-	-	40.11	2.80	6.36	12.90	-	25.02	6.10	3.65	-	2.94	0.12	9.16	"
B11	-	-	-	-	49.07	1.03	3.79	10.38	-	22.86	6.57	3.86	-	2.40	0.05	4.82	"
B10	-	-	-	-	48.32	0.75	3.59	26.00	-	13.86	2.74	2.98	-	1.72	0.05	4.34	"
B8	-	-	-	-	47.66	1.97	4.54	8.27	-	22.87	6.60	3.43	-	2.49	2.22	6.50	"
4. G. Sangenges																	
S3	-	-	2.16	4.11	11.92	-	10.04	53.54	-	12.65	-	2.55	-	1.69	1.36	16.31	6.1
S23	-	-	-	-	13.10	14.03	8.50	42.07	-	14.71	2.59	2.55	-	1.73	0.73	22.53	"
S21	-	-	-	-	8.34	20.12	9.30	31.25	-	16.66	7.23	2.95	-	2.06	1.92	29.42	"
S27	-	-	-	-	15.87	17.66	7.95	39.20	-	11.99	0.97	2.78	-	1.99	1.62	25.60	"
S22	-	-	-	-	9.86	21.36	10.98	27.69	-	16.34	6.84	2.85	-	2.03	2.07	32.34	"
S17	-	-	-	-	15.46	14.34	10.10	39.99	-	12.25	1.31	3.05	-	2.13	1.39	24.44	"
S19	-	-	-	-	13.69	20.47	9.48	33.50	-	13.30	2.95	2.84	-	2.07	1.74	39.95	"
S9	-	-	-	-	15.58	14.56	11.69	38.61	-	11.62	1.25	3.11	-	2.17	1.44	26.25	"
S8	-	-	12.05	17.51	27.51	-	3.42	20.17	-	13.58	-	2.61	-	1.98	1.18	32.98	6.2
S28	-	-	13.07	24.69	27.05	-	3.90	14.87	-	11.31	-	2.19	-	1.86	1.08	41.66	"
S5	-	-	16.02	22.32	26.33	-	2.82	17.24	-	10.31	-	2.21	-	1.69	1.09	41.16	"
S16	-	-	14.01	23.43	29.16	-	2.60	14.18	-	11.25	-	2.20	-	1.84	1.37	40.04	"
S1	-	-	19.23	27.04	25.17	-	1.06	13.78	-	8.87	-	1.90	-	1.65	1.33	47.32	"
S10	1.19	-	9.45	23.29	35.13	-	-	4.55	21.49	-	-	2.28	-	1.85	0.76	33.94	6.3
S11	2.10	-	8.57	24.63	32.82	-	-	6.98	20.02	-	-	2.33	-	1.92	0.65	35.30	"
S26	1.98	-	13.98	32.84	26.81	-	-	7.80	13.11	-	-	1.62	-	1.13	0.74	48.60	"
S15	8.06	-	14.64	33.62	24.93	-	-	5.11	10.72	-	-	1.27	-	0.94	0.72	56.33	"
S7	7.49	-	15.46	36.13	21.00	-	-	6.24	10.02	-	-	1.51	-	0.87	0.69	59.08	"
S12	-	-	-	-	46.03	2.29	5.27	16.34	-	20.81	1.49	3.42	-	2.87	1.50	7.56	6.3
5. Soromundi																	
Si17	-	-	-	-	13.08	14.63	10.11	40.01	-	15.20	1.35	2.63	-	1.84	1.17	24.74	6.4
Si16	-	-	-	-	12.75	14.21	10.67	37.66	-	16.33	2.51	2.71	-	1.86	1.31	24.86	"
Si6	-	-	9.89	-	14.93	7.47	12.39	38.63	-	11.44	-	2.49	-	1.77	1.00	29.75	"
Si13	-	-	12.77	-	14.20	4.83	14.68	39.43	-	8.82	-	2.49	-	1.78	1.02	32.26	"
Si11	-	-	20.14	1.59	16.30	-	16.31	29.85	-	10.57	-	2.51	-	1.71	1.04	38.04	"
Si14	-	-	-	-	13.83	20.76	13.64	34.44	-	9.38	1.46	2.71	-	1.94	1.67	34.40	"
Si10	-	-	17.51	-	17.62	1.45	15.43	32.01	-	10.53	-	2.52	-	1.72	1.02	34.43	
Si12	-	-	19.61	2.37	21.12	-	11.81	29.59	-	10.05	-	2.61	-	1.78	1.09	33.79	
Si15	-	-	26.42	3.56	12.76	-	17.91	28.39	-	6.00	-	2.18	-	1.58	1.22	47.90	
Si3	-	-	20.82	13.58	19.07	-	10.96	21.97	-	8.42	-	2.30	-	1.75	1.15	45.36	"
Si1	-	-	22.45	7.11	15.02	-	18.27	25.37	-	6.94	-	2.24	-	1.55	1.08	47.82	
Si9	-	-	23.63	6.77	15.42	-	17.78	25.44	-	5.70	-	2.21	-	1.60	1.47	48.18	"
Si18	-	-	-	-	16.97	3.07	3.83	33.13	-	24.31	7.39	4.43	-	2.65	4.28	6.90	

Appendix 3

MAJOR AND TRACE ELEMENT ANALYTICAL TECHNIQUES

Major- and trace-element determinations was largely performed using X-ray fluorescent spectrographic methods based on those of Norrish and Hutton (1969) and Norrish and Chappell (1967), at the Geology Department, University of Tasmania.

1. Sample Preparation

Rock samples of between 0.5 and 2.0 kg. weight were chosen for analysis. These were cleaned of all weathered surfaces and initially broken into large fragments with a geological hammer. The sample was then reduced to fragments of 105 mm or less, in a jaw crusher. This crush was then quartered by passing through a stainless steel sample splitter several times to reduce the sample for final grinding to about 200-500 gms. The sample was then ground in a tungsten-carbide swing-mill, in 150 gm lots. Batches of powder from each sample so produced were then recombined and thoroughly mixed.

With the exception of W, C and Co, the contamination of the sample during crushing and grinding is negligible.

Fused lithium borate glass discs were prepared for major element analysis using the method of Norrish and Chappell (1967). The flux was prepared in bulk prior to the analysis of each batch of samples, the mixture comprising; lithium tetraborate - 38.0 gm, lithium carbonate - 29.6 gm and lanthanum oxide - 13.2 gm. This mixture was fused and quenched to a glass coarsely crushed to inhibit the take-up of water from the atmosphere.

Each disc was then prepared from 1.5 gm of the above flux, 0.02 gm of sodium nitrate and 0.28 gm of sample (rock powder). The discs were prepared from unignited rock powders which had been dried at 150^{o}C and loss on ignition was determined separately.

Table A3-1

Instrumental settings for x-ray fluorescent analysis of Major elements

Philips PW1410, Vacuum Spectrograph

Element	Si	Ti	Al	Fe	Mg	Ca	K	P	Mn	Na
Tube	Cr	Cr	Cr	Cr	Cr	Cr	Cr	Cr	Au	Cr
Crystal	P.E.	LiF200	P.E.	LiF200	A.D.P.	LiF200	P.E.	P.E.	LiF200	K.A.P.
Collimator(1)	C	F	C	F	C	F	F	C	F	C
Tube Voltage (KV)	50	35	50	50	50	45	45	50	50	50
Tube Current (ma)	45	12	45	45	45	18	30	50	30	50
Counter E.H.T.(V)	1550	1610	1550	1560	1550	1560	1560	1560	1560	2520
Peak (^{o})	108.79	86.17	144.9	57.45	136.6	113.08	50.17	89.1	62.95	54.2
Background(2) count rate	99 c/s	100 c/s	50 c/s	81 c/s	7 c/s	100 c/s	70 c/s	11 c/s	90 c/s	24 c/s
Analytical Line	Kα	Kα	Kα	Kα	Kα	Kα	Kα	Kα	Kα	Kα
Counter(3) Gas	F+D+V P10	F+D+V P10	F+D+V P10	F+D+V P10	F+D+V P10	F+D+V P10	F+D+V P10	F+D+V P10	F+D+V P10	F+D+V P10
Channel Height(V)	2.10	3.55	2.5	3.6	3.35	2.55	3.0	3.75	2.7	3.0
Lower Level (V)	2	2	2	1	1	1	1	1	2.5	2

Notes: (1) C = coarse, F = Fine; (2) Background determined at peak position for all elements except Na on a pure SiO_2 (+ flux) disc or in the case of SiO_2 on a flux disc. (3) F = Gas Flow Proportional Counter; D = Automatic Discriminator; V = vacuum.

All analyses done on fused glass discs except Na which was determined on pressed powder pellets.

Boric acid - backed, pressed pills were prepared after the method of Norrish and Chappell (1967) for analysis of trace elements and Na. Pills were made with 5-6 gm of rock powder as this was the minimum amount of powder required to yield an apparent infinite thickness for Kα radiation of some of the heavier trace elements (e.g. Nb).

2. Major Element Analysis

The discs and pills were analysed using a Philips PW1410 vacuum spectrograph. Instrumental settings for major elements are given in table A3-1. All major elements were determined on the fused glass discs except for Na which was determined on pressed pills. Backgrounds were determined on the peak setting of the element in question using 100% SiO_2 discs. The SiO_2 background was determined on a pure reagent blank disc. Background for Na was taken off-peak and methane gas was used to eliminate interference from the escape peak of K $K\alpha$ radiation from the K.A.P. crystal and to reduce backgrounds.

Counting times were 50 seconds (peak) except for SiO_2, MgO and Na_2O where 100 seconds (peak) was used. Every Na sample was counted for background as well (50 seconds).

Matrix corrections were made on nominal percentage readings from the XRF using the method of Norrish and Hutton (1969) to yield true percentage values.

Standards prepared from Tasmanian igneous rocks (mainly Jurassic dolerite, TAS DOL-1) and calibrated against international standards, were used as "working standards" with known nominal percentage compositions. Discs of several of these were prepared at the same time as the unknown samples, from the same batch of flux. These were checked against international standards and during runs on unknown samples, were counted once every fifth sample to minimise the effects of instrumental drift.

Table A3-2

Instrument Settings for X-ray fluorescent analysis of trace elements

Philips PW1410, Vacuum Spectrograph

Element	Tube	KV	mA	Coll.	Vacuum	Counter	Crystal	Angle	Background	Counting Time	Comments
Scandium ($K\alpha_1$)	Cr	50	50	coarse	Yes	gfpc	LiF200	97.67	96^o	20, 20	Correction for Ca interface made.
Chromium ($K\alpha_1$)	Au	50	50	fine	yes	gfpc	LiF200	69.34	$\pm 1^o$	50, 50, 50	None metalic holders used, correction for $V_{K\beta}$ interference
Nickel ($K\alpha_1$)	Au	50	30	fine	no	gfpc + scint.	LiF200	48.65	49.65^o	50, 50	With 3.0 volt window
Rubidium ($K\alpha_1$)	Mo	50	30	fine	no	scint.	LiF200	38.00	$\pm 0.6^o$	20, 20, 20	determined simultaneously with Y
Strontium ($K\alpha_1$)	Au	60	40	fine	no	scint.	LiF220	35.87	$\pm 0.7^o$	20, 20, 20	determined simultaneously with Zr.
Zirconium ($K\alpha_1$)	Au	60	40	fine	no	scint.	LiF220	32.17	$\pm 1.0^o$	20, 20, 20	Correct for Sr $K\beta$ interference
Niobium ($K\alpha_1$)	Mo	50	30	fine	no	scint.	LiF220	30.45	$\pm 0.5^o$	100, 100, 100	5 gram sample
Lanthanum ($L\alpha_1$)	Cr	50	50	coarse	yes	gfpc	LiF220	138.7	$\pm 1^o$	100, 100, 100	2.5 volt window

Notes: All determinations made on pressed powder pellets. gfpc = gas flow proportional counter

Scint. - scintillation counter.

3. Trace Element Analysis

The instrumental settings used during trace element determination in this study are given in table A3-2. The mass absorption coefficients for the trace elements were calculated from the known major element composition of each sample using the method of Champion et al. (1968).

Trace elements were determined on boric acid - backed pressed pills. Analytical lines and background positions (see table A3-2) were chosen to minimise the effects of interfering peaks and sloping backgrounds. Where interferences were unavoidable (e.g. Sr Kβ on Zr Kα and Rb Kβ on Y Kα) then the extent of interference was measured and corrected for.

Artificial standards were used, largely prepared by mixing measured amounts of trace elements with spec. pure quartz. These standards were checked both for linearity between standards of different concentration of the same element and against international standards (making appropriate correction for the mass absorption of the radiation of the element in question by the silica matrix of the standard).

4. FeO Determinations

FeO was determined on some Rindjani lavas. Samples were dissolved using an HF-H_2SO_4 dissolution and Fe^{2+} was determined using the method of Reichen and Fahey (1962).

In this method, the Fe^{2+}-bearing solution reacts with iodine monochloride in excess HCl. The free iodine thus liberated is titrated against a standard solution of potassium iodate using CCl_4 as an indicator.

The main problem with the method is that there is likely to be some oxidation of Fe^{2+} during the dissolution. This is minimised by digesting the sample cold, overnight.

Table A3-3

Analysed FeO values from Rindjani lavas

Sample No.	Wt% FeO	Wt% Fe_2O_3	Fe^{2+}/Fe^{3+}	$Fe^{2+}/\Sigma Fe$
41632	6.44	3.48	2.05	0.67
41631	4.53	6.30	0.80	0.44
41623	7.26	3.45	2.33	0.70
41626	4.80	5.91	0.90	0.47
41635	3.98	5.59	0.79	0.44
41678	5.68	3.83	1.64	0.62
41634	5.93	4.14	1.59	0.44
41684	6.32	2.82	2.48	0.71
41647	5.82	2.39	2.69	0.73
41643	5.86	4.34	1.49	0.60
41683	4.93	6.01	0.91	0.48
41622	4.79	3.72	1.43	0.59
41646	5.06	3.30	1.70	0.63
41637	5.97	3.31	2.00	0.67
41627	4.03	4.84	0.92	0.48
41625	4.82	3.79	1.41	0.58
41688	4.88	2.57	2.10	0.68
41636	3.90	3.27	1.32	0.57
41672	3.41	2.30	1.88	0.62
41644	5.53	1.68	3.65	0.79
41668	2.52	1.19	2.35	0.70
41677	2.96	1.04	3.13	0.76
41645	4.21	1.15	4.03	0.80
41675	3.68	2.00	2.03	0.67
41650	3.4	1.13	3.15	0.77
41641	1.67	1.64	1.13	0.53
41671	2.25	1.76	1.42	0.59
41664	2.65	0.34	8.55	0.89
41638	2.34	0.98	2.65	0.73
41639	1.95	1.13	1.91	0.66

NOTES: FeO determined by iodometric titration. Fe_2O_3 calculated from XRF determination of ΣFe as Fe_2O_3 - Fe as FeO. Fe^{2+}/Fe^{3+} and $Fe^{2+}/\Sigma Fe$ are atomic Wt% ratios.

The results of these determinations are given in table A3-3. The ratios Fe^{2+}/Fe^{3+} and $Fe^{2+}/\Sigma Fe$ are quite variable, even between otherwise nearly identical samples (e.g. basalts 41632 and 41631). This tends to suggest that the lavas may have undergone partial and variable oxidation during eruption and thus the analysed ratios may not be truly indicative of the Fe^{2+}/Fe^{3+} ratios of the liquids at depth.

It is perhaps significant that the dacites (e.g. 41664, 41638 and 41677) which are predominantly glassy and may have quenched more quickly have higher Fe^{2+}/Fe^{3+} ratios and this may also support the hypothesis that the more crystalline andesites and basalts have undergone some oxidation.

For the above reasons, in the main body of the thesis, Mg/Mg + ΣFe ratios are discussed more commonly and for the purposes of the CIPW norm calculation (appendix 2) an arbitrary $Fe^{2+}/\Sigma Fe$ ratio of 0.85 was adopted.

Appendix 4

MINERAL ANALYSIS USING THE ELECTRON MICROPROBE

Analyses of minerals reported in this thesis were all carried out using electron microbeam techniques. Most were carried out on the JEOL JXA-50A instrument in the Central Science Laboratory at the University of Tasmania, though in addition, a few were done on the JEOL JXA-5 probe at Melbourne University and some on the TPD probe at R.S.E.S., A.N.U.

The JEOL JXA-50A instrument at the University of Tasmania, on which most of the analyses were performed, has two crystal spectrometers for wave length dispersive analysis and an EDAX energy dispersive system using a Li-drifted Si crystal detector. The latter system is integrated with an on-line NOVA computer. This automatically processed the data from the EDAX multichannel analyser, performed all the necessary corrections and printed the final analysis as well as the structural formula (based on a previously specified number of oxygens) on a teletype. Because of its speed and convenience, this sytem was used almost exclusively in favour of the wave length dispersive system.

Corrections made are based on the procedure of Reed and Ware (1975) for those corrections specifically applicable to the energy dispersive analysis system, in addition to the standard Z (atomic number), A (absorption) F (fluorescence) (e.g. Springer, 1976) corrections. Corrections specifically related to the energy dispersive system dealt with problems of peak overlap, pulse pile-up, system dead-time, escape peaks generated in the Si (Li) detector and absorption in the Be window and allowed the calculation of a background continuum, which was subtracted from the analysed spectrum.

Analyses were performed using an accelerating voltage of 15 kV, a beam current of 3.0 nA, take-off angle of 29.5^{o}, and an energy range of 0-16 kev. Background points were taken at 2.3 kev and 9.87 kev and Ni_2Si or pure Cu standards were used to calibrate the gain and zero of the multichannel analyser.

Analyses were performed on polished thin sections, either as small discs or as short rectangular slides. These were coated with carbon in an evacuated volatilization chamber.

The instrument was calibrated initially against pure metal or simple compound standards and then against a range of minerals of known compositions. Calibration was routinely checked during any series of analyses by analysis of a Cr-diopside from Delegate, N.S.W. The beam current was monitored by the insertion of a Faraday cup.

Appendix 5

EXPERIMENTAL TECHNIQUES

Experiments were performed using a piston-cylinder type apparatus very similar to that described by Boyd and England (1960) and general techniques are very similar to those of Boyd and England (1960, 1963) and Green and Ringwood (1967a, 1967b).

1. Capsules

Capsules were fabricated from Ag-P d (Ag50-Pd50 and Ag75-Pd25, see table 11.1) tubing. Lengths of tubing about 1.5 cm long were cut and one end sealed by welding with a fine-flame oxy-acetylene welding torch. The tube was then dried and weighed and the required amount of water was added using a microsyringe. The capsule was reweighed and the appropriate amount of sample was added (ca. 15 mgm) and lightly packed-down. The capsule was again re-weighed and then the top was gradually flattened, from the open-end down to the top of the sample. The capsule was re-weighed to ensure no water had been squeezed out and the top cold-sealed by trimming off a thin sliver. The top of the capsule was then quickly sealed using a fine-tipped electric arc welder and the flattened section was folded over.

2. Run Assembly

The capsule containing the sample was fitted into boron nitride spacers which into a graphite (furnace) tube with a graphite plug at the base. The thermocouple was welded from Pt-Pt10% Rh wires passed through a ceramic sheath. This was fitted down the hollow bore of the upper spacer in the graphite tube, resting on a thin porcelain disc over the sample capsule. A crushable alumina insert fitted around the top of the thermocouple sheath. The graphite furnace assembly fitted in a lead-sheathed, talc tube of the same diameter as the piston (0.5") and this was capped in the cylinder, by a stainless steel plug with a pyrophyllite collar.

3. Run Techniques

Runs were made under "piston-in" conditions and pressure readings incorporated a correction of about -10% to account for the effect of friction (Green et al., 1966).

Runs were performed on fused glass samples, finely ground under acetone and dried, with 2, 5 and 8% H_2O added as described earlier.

Pressure was applied at temperatures less than that chosen for the run in question until a pressure a few hundred bars less than the run pressure was reached. The temperature was then increased and the pressure allowed to rise until both run-temperature and -pressure were simultaneously reached. Run times (table 11.1) were kept short (ca. 30 minutes) to minimise the effects of Fe-loss to the capsule.

4. Run Product Analysis

After the run was completed, the capsule was opened and the charge broken up into fragments. Some of these were retained for microprobe analysis and XRD determination and some were crushed more finely and mounted in oil and microscopic identification of phases present made.

Microprobe analysis of crystals and glass from runs was carried out using a JEOL JXA-50A electron microprobe/SEM with an EDAX (Si(Li)) energy-dispersive X-ray detection system. The combined SEM facility allowed a secondary electron image of variably magnified areas of the charge to be examined facilitating the location of suitable crystals for analysis and the accurate location of the electron beam. Glass areas were analysed using a reduced area scan-mode to limit specimen damage and Na volatilisation.

References Cited in the Appendices

Boyd, F.R., England, J.L., 1963. Effect of pressure on the melting of diopside, Ca Mg Si_2O_6, and albite, Na Al Si_3O_8, in the pressure range up to 50 kilobars. *J. Geophys. Res., 68,* 311-322.

Boyd, F.R., England, J.L., 1960. Apparatus for phase-equilibrium measurements at pressures up to 50 kb and temperatures up to 1750°C. *J. Geophys. Res., 65,* 741.

Green, D.H., Ringwood, A.E., 1967a. An experimental investigation of the gabbro to eclogite transformation and its petrological applications. *Geochim. Cosmochim. Acta., 31,* 767-833.

Green, D.H., Ringwood, A.E., 1967b. The genesis of basaltic magmas. *Contrib. Mineral. Petrol., 15,* 103-190.

Green, T.H., Ringwood, A.E., Major, A., 1966. Friction effects and pressure calibration in a piston-cylinder apparatus at high pressures and temperature. *J. Geophys. Res., 71,* 3589-3594.

Kelsey, C.H., 1963. Calculation of the CIPW Norm. *Min. Mag., 34,* 276-28.

Norrish, K., Hutton, J.T., 1969. An accurate X-ray spectrographic method for the analysis of a wide range of geological samples. *Geochem. Cosmochim. Acta., 33,* 431-455.

Norrish, K., Chappell, B.W., 1967. X-ray fluorescent spectrography. In: Physical Methods in Determinative Mineralogy. Ed. J. Zussman. Academic Press, London.

Reed, S.J.B., Ware, N.G., 1975. Quantitative electron microprobe analysis of silicates using energy dispersive X-ray spectrometry. *J. Petrol., 16,* 499-519.

Reichen, L.E., Fahey, J.J., 1962. An improved method for the determination of ferrous oxide in rocks and minerals including garnet. *Geol. Surv. Amer. Bull.* 1144-B.

Springer, G., 1976. Correction procedures in electron-probe analysis. In: A Short Course in Microbeam Techniques, Ed. D.G.W. Smith., Mineral., Assoc. Canada., Edmonton.